Intensive Quenching Systems:
Engineering and Design

100%

Part Cracking / Distortion

CONVENTIONAL

INTENSIVE

0%

Cooling Rate

N.I. Kobasko, M.A. Aronov, J.A. Powell and G.E. Totten

Intensive Quenching Systems: Engineering and Design

N. I. Kobasko, M. A. Aronov, J. A. Powell, and G. E. Totten

ASTM Stock Number: MNL64

Photocopy Rights

Foreword

THIS PUBLICATION, *Intensive Quenching Systems: Engineering and Design,* was sponsored by Committee D02 on Petroleum Products and Lubricants. This is Manual 64 in ASTM International's manual series.

Contents

Preface

From 1964 to 1999, one of the authors of this volume, Dr. Nikolai Kobasko, worked at the Thermal Science and Engineering Institute of the National Academy of Sciences of Ukraine in Kyiv. At the institute, there were approximately 1,200 scientists and engineers working in all areas of thermal science: heat conduction, radiation, thermal dynamics, and fluid dynamics. In addition to the thermal sciences, Dr. Kobasko placed a heavy emphasis on metallurgical science and physics, as demonstrated in his book *Steel Quenching in Liquid Media Under Pressure*, published in 1980.

The present book, *Intensive Quenching Systems: Engineering and Design*, is an attempt to knit together three disciplines: thermal sciences, metallurgy, and physics. The cross-pollination of these disciplines shows the fundamental correlations that exist between metallurgical processes and the underlying thermal science. These correlations form the foundation for more recent computer modeling of the complex physical interactions that happen in the heat-treating process.

Why is it important to read our book?

Knowing the fundamentals of the quenching processes, the reader will be able to solve the following problems:

1. Calculating the cooling time (for dwell time in the intensive quench for speed of conveyors, etc.) that will provide an optimal quenched layer after intensive quenching of steel parts
2. Creating beneficial high compressive residual stresses at the surface of steel parts, even when they are through-hardened
3. Using the benefits of the "steel superstrengthening" phenomenon to make higher-power-density parts
4. Developing synergies between the benefits from high compressive residual stresses and the superstrengthening phenomenon to increase the fatigue life and service life of steel parts significantly
5. Improving the environmental conditions in a factory by switching from oil and polymer quenching to clean, fast intensive quenching in plain water—thereby allowing the incorporation of the heat-treating processes into the part manufacturing cell
6. Optimizing distortion control in the quenching of steel parts

In essence, this book is intended for use by both metallurgists and mechanical engineers to assist them in their work designing and implementing quenching systems. A critical component of any quench system is the quenchant. This book is an effort to break down the quenching process into many smaller, manageable increments and to examine the dynamics present at surface of the part, as well as how each phase of the quench and each phase in the material will affect the end result.

This book will also be useful for undergraduate and postgraduate students who are interested in learning more about generalized equations for calculating the cooling time of any configuration of steel parts and the duration of the transient nucleate boiling process. Both generalized equations create a basis for quench system engineering design.

We will show that it is much easier to evaluate the generalized Biot number (value of Bi_V) than to determine the Grossmann factor H (see Chapters 6 and 13). The use of the generalized Biot number will allow the designer to get the quenching process quickly into the proper "neighborhood," from where more sophisticated finite element and computation fluid dynamics (CFD) modeling (or actual part trials) can fine-tune the process to its proper "home."

The book examines the use of intensive water quenching, IQ processes, to achieve the desired mechanical properties in steel parts made with steel alloys of lower hardenability (and presumably less expensive). Higher cooling rates and the higher hardenability of the intensive quench process also means that the carburization processing time can be reduced (or eliminated). Since less carbon content is needed in the carbon gradient, intensive quenching in water can achieve the same hardness profile as oil-quenching a part that has been carburized to a deeper total case.

In particular, this book discusses the development of high compressive stresses on the part's surface, both during quench cooling ("current" compressive stress) and as residual compressive stress, through the establishment of a very high ("intensive") cooling rate, applied uniformly through the martensite transformation range, and the control of distortion. The beneficial effects of these compressive stresses on a part's properties are also discussed. In addition, the authors examine the relationship between hardness (and the corresponding tensile strength, yield strength, and ductility) and the management of residual stress profiles in the hardened layer of the part to increase the fatigue life of the hardened part.

Introduction

This ASTM manual, *Intensive Quenching Systems: Engineering and Design*, contains 13 chapters. The primary focus of this book is on highly forced heat transfer–that is, intensive quenching (IQ) processes. Particular attention is paid to the replacement of relatively expensive alloyed steels with less expensive carbon steels for machine parts subjected to normal operating conditions. The use of carbon steels with increased strength properties instead of alloyed steels will provide opportunities for cost savings related to the reduction of alloying elements such as tungsten, nickel, molybdenum, chromium, and others. In addition, IQ processes, which are based on water and aqueous solutions, provide an excellent and environmentally friendly alternative to petroleum quenching compositions. These various advantages are accomplished through the use of the newly developed IQ processes described herein.

Chapter 1 describes contemporary approaches of obtaining high-strength materials. High-temperature and low-temperature thermomechanical treatments are discussed, and alternative methods of creating high-strength materials by intensive quenching are considered. The primary focus of this chapter and of the manual as a whole is to describe the attainment of high-strength materials by intensive quenching within the martensite range. It is emphasized that the combination of high-temperature and low-temperature thermomechanical treatments with accelerated cooling within the martensite range significantly increases a part's mechanical and plastic material properties. It is shown that in some cases even intensive quenching of low-carbon alloy steels by itself may increase yield strength by 15 % and impact strength by 250 %. Intensive quenching results in additional material strengthening and creation of high surface compressive residual stresses–both of which increase the service life of steel parts. IQ process technology is inexpensive and beneficial.

Chapter 2 is a study of transient nucleate boiling during quenching of steel, which includes the self-regulated thermal process. The main purpose of this chapter is to describe the utilization of the duration of transient nucleate boiling as a basis for designing quenching processes. The generalized equation for the calculation of the duration of transient nucleate boiling relative to the creation of IQ methods is discussed. Calculation and experimental results correlate well. These processes are explained and illustrated by many practical examples used in the heat-treating industry.

Chapter 3 shows that the cooling capacity of quenchants can best be characterized by the critical heat flux densities and heat transfer coefficients during the three phases of cooling:

1. film boiling process
2. nucleate boiling process
3. single-phase convection

A new and preferred technique for determining the critical heat flux densities is described.

Chapter 4 presents the criteria (dimensionless dependencies) for the calculation of convective heat transfer coefficients with respect to steel quenching in directed water streams and intensive jets. The primary focus is on intensive quenching of steel parts in water flow, and calculation examples are provided. It is shown that very intensive quenching of splined cylindrical specimens in pressurized water jets prevents crack formation and increases surface hardness. The results can be used for process and equipment design and can be combined with other information provided throughout this text to optimize quenching of steel parts.

Chapter 5 describes the generalized equation for calculation of the cooling time for bodies of arbitrary shape, based on regular thermal condition theory. The generalized equation can be used for designing manufacturing processes and calculation of conveyor speeds for quenching systems. This information is obtained from simplified and rapid calculations and is required during the initial stages of design of heat-treating and quenching systems for steel parts. The equation makes it possible to calculate the ideal critical size of steel parts of low-hardenability steels to provide an optimal quenched layer and residual stress distribution. The equation may also be used for the design of two-step interrupted intensive quenching and two-step quenching processes combined with cryogenic treatment. Comparison of the generalized equation with various analytical solutions and calculation accuracy is discussed.

Chapter 6 describes Kondratjev form factors (K), which are used in the generalized equations described throughout this book. Also discussed are three methods for their determination: analytical, numerical, and experimental, which have been developed for practical use. The results provided here can be used for creating databases of Kondratjev form factors suitable for use with different part geometries. Throughout this discussion, there are literature references to the development and use of Kondratjev numbers. Finally, the determination of average heat transfer coefficients using standardized probes is discussed.

Chapter 7 describes the distribution of transient and residual stresses during steel quenching. It has been established that high compressive stresses are formed at the surface of parts quenched under conditions of intensive cooling. It has also been shown that there exists an optimal depth of the hardened layer where compressive stresses reach their maximum value. The results introduced in this chapter were used for the creation of three intensive quenching methods designated IQ-1, IQ-2, and IQ-3. Due to high residual compressive stresses at the surface, the service life of steel parts has been significantly increased.

Chapter 8 describes the characteristics of steel quenching under pressure. It has been shown that for conditions where the Biot number Bi approaches infinity, it is possible to control the surface temperature during nucleate boiling. This expands the potential for low-temperature thermomechanical treatment (LTMT) and steel quenching in water under pressure. Illustrations of the implementation of such processes are provided. High-temperature thermomechanical treatment (HTMT) is widely used for the mass production of rebars. Information provided in this chapter suggests the possibility of combining HTMT with LTMT and intensive quenching to reduce production costs and increase service life. In addition, these new technologies are environmentally friendly.

In Chapter 9, it is shown that intensive cooling within the martensite range results in additional strengthening

("superstrengthening") of a material, with simultaneous improvement of its plastic properties. This phenomenon is observed when the cooling rate within the martensite range is higher than a critical value. There is also a different point of view, according to which very fast cooling above the martensite start temperature results in additional strengthening of metals due to "freezing of vacancies" formed during heating. Both hypotheses are presented in this chapter. The mechanism of additional improvement of the material's mechanical properties is explained, as well.

Five intensive steel quenching methods, designated IQ-1 through IQ-5, are discussed in Chapter 10, and illustrations of their application are provided. IQ processes result in the creation of high compressive residual stresses at the surface of steel parts and small tensile residual stresses at the core. Such an optimal residual stress distribution created by intensive cooling within the martensite range significantly increases the mechanical properties of a material and improves its plastic properties. Examples of the use of simplified calculations are provided to aid in the design and application of intensive quenching processes.

Chapter 11 describes the calculation of conveyor speed for various kinds of conveyors and devices. These results are particularly of interest for designers dealing with industrial line construction.

Chapter 12 presents the rich experience of the use of IQ methods in the United States and other countries. It has been shown that, compared to traditional oil quenching, the service life of steel parts after intensive quenching increases by 1.5 to 2 times, or even more in some cases.

The final chapter analyzes heat flux densities and heat transfer coefficients obtained by solving heat conduction inverse problems. Current methods of solving inverse heat conduction problems are described. These methods are needed to study the initial period of the quenching process and to determine the cooling characteristics of different types of quenchants. The need for many industries to develop standardized probes and methods for the quenchant cooling capacity evaluation on the basis of solving inverse heat conduction problems is discussed.

Nikolai I. Kobasko, PhD, FASM

Dr. Kobasko received his Ph.D. from the National Academy of Sciences of Ukraine. He is a leading expert on quenching and heat transfer during the hardening of steels. He was the Head of the laboratory of the Thermal Science Institute of the National Academy of Sciences of Ukraine. He is Director of Technology and Research and Development for IQ Technologies, Inc., Akron, Ohio and President of Intensive Technologies, Ltd, Kyiv, Ukraine. The aim of both companies is material savings, ecological problem-solving, and increasing service life of steel parts. He is an ASM International Fellow (FASM).

Dr. Kobasko is the author and co-author of more than 250 scientific and technical papers, several books and more than 30 patents and certificates. He received the Da Vinci Diamond Award and Certificate in recognition of an outstanding contribution to thermal science. Dr. Nikolai Kobasko was Editor-in-Chief and Co-Editor of the WSEAS Transactions on Heat and Mass Transfer; and is currently a member of the Editorial Board for the International Journal of Mechanics (NAUN) and the Journal of ASTM International (JAI).

Dr. Michael A. Aronov

Dr. Aronov received his B. S. and Masters degrees in Thermal Science and Fluid Dynamics from the St. Petersburg Polytechnic Institute in Russia. Dr. Aronov received his Ph.D. degree in Thermal Science and Engineering from the Institute of Metallurgical Thermal Engineering also in Russia. He is the Chief Executive Officer of IQ Technologies, Inc. of Akron, Ohio.

Dr. Aronov has 37 years of experience in the field of heat and mass transfer, combustion, and thermodynamics in industrial, commercial, and residential heat transfer systems. He has extensive experience in experimental research, mathematical modeling of heat and mass transfer in combustion forging, and heat treating furnaces and quenching machinery. Dr. Aronov also has extensive experience in the design and development of heating and cooling systems for forging and heat-treating applications. Dr. Aronov has published more than 70 technical papers and has ten patents, four of which are related to different types of quenching equipment and technology.

Joseph A. Powell

Joseph A. Powell received his B.S. in Industrial Management from the University of Akron, and was granted a Juris Doctorate from the University of Akron School of Law. Mr. Powell is President, and a principal of IQ Technologies Inc, and of Akron Steel Treating Company (AST), a family business, in Akron, Ohio.

Mr. Powell is a founding member of the Heat Treating Network part of the Metal Treating Institute, a member of the Akron Chapter of ASM, the ASM/Heat Treating Society, and the ASM Quenching and Cooling Committee. He is also a member of the Metal Treating Institute (MTI), an associate member of the National Tooling & Machining Association (NTMA), and the Summit County Machine Shop Group.

Mr. Powell has a patent for "Variable Cooling Rate Quench Media, Cooling Rate Monitoring System and Real Time Computerized Control System for the Quenching of Metals during Heat Treatment or other Controlled Cooling or Solidification Operations."

George E. Totten, Ph.D., FASM

George E. Totten received his B.S. and Masters degrees from Fairleigh Dickinson University in New Jersey and his Ph.D. from New York University. Dr. Totten is past president of the International Federation for Heat Treating and Surface Engineering (IFHTSE) and a fellow of ASM International, SAE International, IFHTSE, and ASTM International. Dr. Totten is a Visiting Research Professor at Portland State University, Portland, Oregon, and he is also president of G.E. Totten and Associates LLC, a research and consulting firm specializing in thermal processing and industrial lubrication problems.

Dr. Totten is the author, coauthor, or editor of over 500 publications, including patents, technical papers, book chapters, and books and sits on several journal editorial boards, including the Journal of ASTM International.

1

Thermal and Metallurgical Basics of Design of High-Strength Steels

N. I. Kobasko[1]

1.1 INTRODUCTION

The objective of heat treatment of metals is the creation of high-strength materials by heating and quenching. It is often recommended that alloy and high-alloy steels should be through-hardened in petroleum oils or high concentrations of aqueous polymer solutions and plain carbon, and that low-alloy steels should be quenched in water. Petroleum oils are used to reduce quench cracking and distortion of steel parts during the through-hardening process. For this reason, slow cooling is used, and expensive alloy elements provide through-hardening. Oil quenching is most often performed at low to moderate temperatures with generally acceptable thermal gradients in the cross-sections of steel parts.

To increase the strength of parts, engineers often utilize high-temperature or low-temperature thermomechanical treatment. Typically, the potential use of intensive steel quenching methods for alloy and high-alloy steel grades is not considered, because it is a widely accepted point of view that alloy steels should be quenched very slowly within the martensite range; this is commonly stated in various manuals and handbooks on heat treatment of steels. In this book, the problem of the creation of high-strength materials and minimizing quench is addressed by the intensification of heat transfer within the martensite range. So, what was previously discouraged is now used to achieve high-strength materials while minimizing distortion.

To obtain a fundamental understanding of the physics of processes occurring during intensive quenching of alloy and high-alloy steels, the regularities involved in the quenching of high-alloy steels will now be discussed. One of the factors exhibiting a significant effect on part distortion is the formation of high thermal gradients in the cross-sections during quenching.

This book describes a new approach in the quenching technology of alloy and high-alloy steel grades [1], which consists of the following:
- Intensive quenching is performed throughout the entire quenching process, including the martensite temperature range.
- Intensive quenching is interrupted when an optimal thickness of the outer quenched layer is formed.
- Intensive quenching results in the creation of high compressive stresses at the surface of parts during the through-hardening process.
- Intensive quenching within the martensite temperature range creates a high dislocation density, resulting in improvement of material strength.

- During intensive quenching, dislocations are "frozen" and are not accumulated at the grain boundary, which improves the plastic properties of the material.
- The creation of high dislocation density and high compressive stresses within the surface layers increases the service life of steel parts.
  Intensive quenching provides the following benefits:
- Uses less expensive steels instead of more expensive alloy and high-alloy steel grades
- Increases the hardness of the quenched surface by HRC 2−5, which in some cases provides for the elimination of carburizing or a reduction of carburizing time
- Minimizes quench distortion
- Maximizes labor productivity
- Reduces the number of manufacturing operations
- Replaces expensive and flammable quench oils
- Provides for an environmentally friendly quenching process
  Factors affecting the strength and service life of steel parts will be considered in this book.

Intensive quenching provides additional opportunities for high- and low-temperature thermomechanical treatment. The first opportunity is the potential use of intensive quenching of forged parts immediately after forging (direct forge-quenching). The second is the delay of martensitic transformations with further low-temperature thermomechanical treatment; this is of particular importance since intensive quenching within the martensitic range is equivalent to low-temperature thermomechanical treatment, which significantly simplifies the manufacturing process. Detailed information about high- and low-temperature thermomechanical treatments is provided later in this chapter.

As stated above, material strengthening may be achieved with intensive quenching and thermomechanical heat treatment to achieve high strength and high plasticity. Both approaches require process optimization to prevent quench crack formation and to minimize distortion during rapid quenching. This can be done by delaying transformation of austenite into martensite during intensive quenching. Due to the discovery of an unconventional phenomenon—that intensive quenching prevents crack formation, decreases distortion, and increases mechanical properties of the materials—new opportunities are now available for heat treaters [1−3].

These problems are discussed in detail in many chapters of this book. Chapter 2 contains a discussion of the so-called self-regulated thermal process, which controls the temperature field and microstructure formation when the heat transfer coefficient approaches infinity. This is obvious since at

---

[1] IQ Technologies, Inc., Akron, Ohio, and Intensive Technologies Ltd., Kyiv, Ukraine

very large Biot numbers (Bi), that is, as Bi → ∞, the surface temperature of steel parts is equal to the bath temperature. Temperature field and microstructure formation control as Bi → ∞ is discussed in Chapters 2 and 8. Application of these quench process designs shows how agitated water using jets and other means of controlling fluid flow can be used to replace quench oils for agitated water for quenching alloy steels. This issue is discussed in Chapter 4.

When the Biot number approaches an infinite value, the heat transfer coefficient is very high, which means that there will be significant temperature gradients inside the component. Intensive quench process design to accommodate the thermal stresses that are formed is discussed in Chapter 7, where it is shown that during the intensive quenching process, the formation of high surface compressive residual stresses is used to prevent crack formation and increase service life.

It is also known that distortion can be decreased by providing uniform cooling around the quenched surface. When steel parts are quenched in water, localized bubbles due to steam formation appear around the surface, which significantly deforms the temperature field and, as a result, causes nonuniform microstructure transformation, resulting in unacceptably large distortions. To decrease distortion, localized film boiling must be eliminated, which will provide more uniform cooling. This is accomplished by optimizing the first critical heat flux density, which minimizes distortion. The critical heat flux densities and methods of their optimization are discussed in Chapter 3.

To prevent quench cracking during intensive quenching, it is important to provide compressive current and residual stresses at the surface of steel parts. This can be done by interruption of the intensive quenching process at a process- and material-specific time to provide an optimal quenched layer. The solution to this problem is described in Chapters 5, 6, and 7.

Maximum compressive stresses at the surface of steel parts and very fast cooling of the optimized quenched layer provide additional strengthening (superstrengthening) of steel, which will result in increased service life. This issue is discussed in Chapter 9.

In Chapters 10, 11, and 12, new methods of quenching are considered, and their benefits are shown using many examples from the industry. Along with designing processes to achieve highly strengthened materials, new methods of simplified calculations are developed. Using CFD (computational fluid dynamics) modeling and analysis based on solving inverse problems (IP), the correctness and accuracy of various intensive quenching processes are discussed. Thus, the ideas presented in Chapter 1 can be widely extended.

This is the first book in which thermal science and heat treatment of materials are discussed together. To increase the applications of new quenching methods, several standards should be developed to facilitate the design of intensive quenching technological processes. More information connected with the intensive quenching processes and thermomechanical heat treatment is available in [4–6].

1.2 FACTORS AFFECTING STRENGTH AND SERVICE LIFE OF STEEL PARTS

The engineering strength of machine parts depends on the grain size of the material and dislocation density. Fig. 1 shows the correlation of strength versus the number of defects (dislocation density). With respect to the crystal
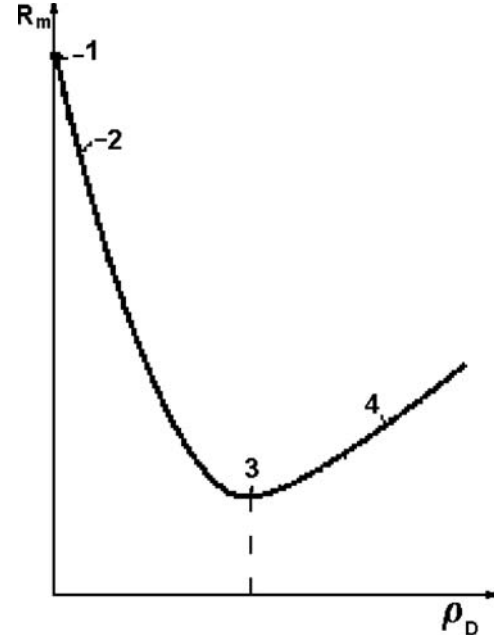
Fig. 1—Ultimate strength versus dislocation density in metal [1,3]: 1, theoretical strength; 2, strength of whiskers; 3, pure nonhardened metals; 4, alloys hardened by hammer, heat treatment, and thermomechanical treatment.

structure and interatomic forces, the theoretical strength of the material can be determined by the following equation:

$$\tau_{theor} \approx \frac{G}{2\pi}, \tag{1}$$

where G is the shear modulus.

The theoretical value of strength is greater by 100 to 1,000 times the actual strength. There are two ways to increase strength:
1. create metals and alloys that are free of defects, or
2. increase the dislocation density,

as well as reducing the grain size and creation of fine carbides to impede movement of dislocations.

The minimum strength is determined by the critical dislocation density. The dislocation density in annealed metals is between 10^6 cm^{-2} and 10^8 cm^{-2}. Currently, crystals have been obtained that do not contain dislocations. In practice, materials whose composition consists of soft metallic matrices reinforced with filamentary crystals which are free of defects.

When the dislocation density of a material increases, strength is increased as [7–9]:

$$\sigma_\tau = \sigma_0 + k_1 Gb\sqrt{\rho_D}, \tag{2}$$

where σ_0 is transverse stress before deformation (after annealing); k_1 is strengthening factor depending on the kind of lattice and alloy composition; and b is Burger's vector.

Grain boundaries are efficient barriers for the movement of dislocations in metals. The finer grain, the higher the metal strength. The dependence of yield limit upon the grain size is described by the Hall-Petch equation [10].

$$\sigma_T = \sigma_0 + K_y d^{-1/2}, \tag{3}$$

where d is grain diameter; σ_0, and K_y (strength factor) are constant for every metal.

Eqs 2 and 3 are the bases for all methods of hardening metals and alloys: strain hardening, steel quenching, and other treatments.

The following dependence has been established between tensile strength and grain size [6]:

$$\sigma_B = \sigma_0 + K_B d^{-1/2}. \qquad (4)$$

Tensile strength determines maximum loading capacity of a part and is one of the basic characteristics of a metal that determines its use. Theoretical aspects of the structural sensitivity of the strength are considered in [11].

Tension tests with constant strain rate (ε) show that the strain force P during the process of plastic deformation at first increases and then decreases. The *engineering tensile strength* is a stress at the time when the maximum is reached on the curve of P versus strain:

$$\frac{dP}{d\varepsilon} = 0. \qquad (5)$$

It is also important to take into account–in addition to the yield strength, fracture strength, and tensile strength– fatigue characteristics of the materials, such as fatigue limit. Metal that is subjected to alternate loadings fails at stresses that are much lower than the yield strength. The accumulation of distortions in the lattice and development of cracks under the action of repeated or alternating stresses is called *fatigue*.

The maximum stress that does not cause failure under infinitely large number of alternating loadings is the *fatigue limit*. Fatigue limit is a very important characteristic of the material. For example, it is possible to increase the fracture strength of wire up to 350 kg f/mm^2, while, at the same time, the fatigue limit for experimental samples remains at the level of 30–40 kg f/mm^2. It is assumed that the main cause of maintaining the endurance at low level while the fracture strength increases is embrittlement [11].

Tempering of strained steel increases its cyclic strength. The optimal temperature of tempering cold-drawn wire for increasing the endurance strength is 150–200°C (300–390°F), which corresponds to the maximum development of aging processes. The cyclic strength increases due to the release of residual stresses at tempering and strain aging, which exhibits unfavorable effects [11].

The experience of using high-strength materials has shown that machine constructions or parts often exhibit brittle failure suddenly at stresses less than the yield strength. For this reason, to provide the reliability of constructions, in addition to high yield strength and high fracture strength, the material must exhibit high resistance to brittle failure. For the determination of the resistance to brittle failure, impact tests are often performed. The impact strength A_f has two components: $A_f = A_b + A_p$, where A_b is the energy of the deformation before the buildup of the crack, and A_p is the energy of the crack propagation. At the brittle fracture, A_p is approximately zero. At ductile fracture or semibrittle fracture, the value of A_p is the main characteristic of the metal viscosity. Some metals are susceptible to brittle fracture when the temperature decreases. This phenomenon was called *cold brittleness*.

Machine parts are subjected to gradual destruction due to many other phenomena and processes of fatigue as well: wear, corrosion, and so on. Resistance to these kinds of destruction determines the service life of machine parts and

constructions. These issues are considered in detail in works of Ivanova, Troschenko [12–14], and others.

The most efficient method with active effect upon the structure of the material is plastic deformation of supercooled austenite, which is implemented by means of thermomechanical treatment [15,16]. This treatment yields a fine-grain austenite structure. Methods of thermomechanical treatment can be applied to steels during the time when supercooled austenite is sufficiently stable so that decomposition of austenite in the intermediary range, which is important as for the thermomechanical treatment, does not occur.

When designing the thermomechanical treatment, the extent of deformation and time of maintaining a constant temperature must be chosen so that the grains become as fine as possible, which, according to Eqs 3 and 4, results in strengthening of the material. The temperature of deformation must be selected so that dynamic or collective recrystallization does not result in grain growth. It has been established that while the temperature of deformation increases, the period of recrystallization decreases.

The effects of the above-mentioned factors on the strength and duration of the service life of steel parts are closely connected with heating and cooling of the metal. Therefore, the study of thermal and physical processes occurring during heat treatment of steel parts is of practical importance.

1.3 ROLE OF PHASE TRANSFORMATIONS DURING STEEL STRENGTHENING
1.3.1 Diffusion Transformations of Supercooled Austenite

The heat treatment process consists of heating steel to the austenitizing temperature and then cooling it by a particular pathway to achieve the desired properties. In Fig. 2, the crosshatched region is the area of optimal temperatures of heating for hypoeutectoid (carbon content < 0.8 %) and hypereutectoid (carbon content > 0.8 %) steels. Heating steel parts above temperatures indicated in Fig. 2 is undesirable, because higher temperatures result in increased austenite grain growth, which leads to decreased mechanical properties. Also, at high temperatures, oxidation and decarburization of the steel occurs. The total heating time prior to
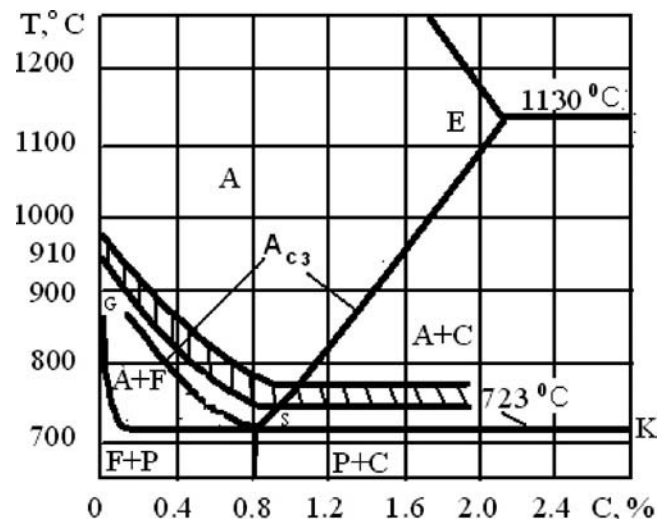

Fig. 2—Austenitizing temperature versus carbon content in steel (A, austenite; F, ferrite; P, pearlite; C, carbon content in % or cementite).

quenching consists of time τ_i of heating to optimal temperature and holding (soaking) time $\tau_â$ prior to the start of the quenching process [15]:

$$\tau_{total} = \tau_i + \tau_â. \tag{6}$$

Maintaining the total time at temperature prior to quenching is necessary for completing phase transformations and equalization of phase composition due to diffusion processes, which become slower with increasing alloy content. These issues are considered in detail in [17–19].

During the steel transformation process, ferrite-pearlite mixes into austenite of hypoeutectoid steels and the grain size becomes finer–which, according to Eqs 3 and 4, results in the strengthening of material. The rate of grain refinement increases with superhigh rates of heating and cooling of metal. The first is achieved by surface heating of metal by induction heating, and the second by the intensification of heat transfer during quenching (intensive quenching). During intensive quenching, austenite is supercooled and its transformation occurs not on the GSK (see Fig. 2) line but at a lower temperature up to martensite start temperature, which depends on the content of carbon.

Depending on the cooling rate, different phases are formed, which are determined by TTT (time-temperature transformation) and CCT (continuous cooling transformation) diagrams (Fig. 3). The characteristic critical point is thermal hysteresis, which becomes apparent during heating and cooling of metals and alloys. The greater the supercooling of austenite, the finer the grain size. During grain refinement, the energy is consumed for the formation of the interface between the new and old phases. The total change in free energy of the system during the formation of a new phase ($\Delta\Phi$) is [20]:

$$\Delta\Phi = -V\Delta f_V + S\sigma, \tag{7}$$

where V is a volume of new phase; S is a surface area of new phase particles; Δf_V is difference of free energy for one unit of volume; and σ is surface tension.

For ball-shaped nucleating centers, Eq 7 becomes:

$$\Delta\Phi = -\frac{4}{3}\pi r^3 n\Delta f_V + 4\pi r^2 n\sigma \tag{8}$$

where n is the quantity of particles of a new phase; and r is a radius of particles. As the size of particles of a new phase increases, the first term of Eq 8 increases in proportion to volume, and the second term increases in proportion to the surface area. For small particles, the second term of Eq 8 prevails, and for large particles, its first term prevails.
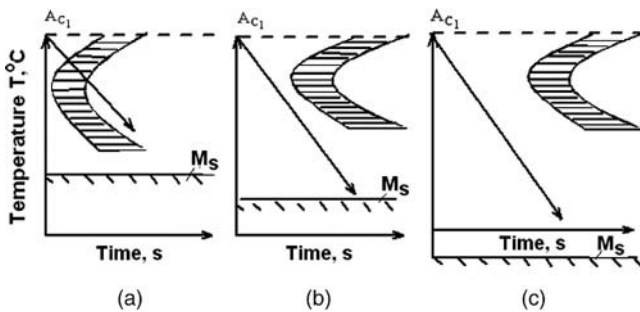

Fig. 3—Chart of isothermal decomposition of austenite for three classes of steels [14]: (a) pearlite; (b) martensite; (c) austenite.

Therefore, there exists a critical particle size determined by the following condition:

$$\frac{d\Delta\Phi}{dr} = 0, \tag{9}$$

or

$$r_{cr} = 2\sigma/\Delta f_V. \tag{10}$$

This means that the new phase, when in equilibrium with the old phase, should be in a more dispersed state when the temperature is lower.

This approach is used in the practice when intensively cooled to room temperature melted materials provide fine microstructures and even nanomicrostructures [21].

The transformation starts with the formation of nucleating centers, and then crystals grow, at a rate depending on the supercooling temperature, until they collide. Using the Kolmogorov mathematical relationship for steel transformation, the dependence of the phase volume transformation to transformation time, when the center formation rate is constant and their growth rate is linear, is obtained from this equation [20]:

$$V(\tau) = V_0\left[1 - \exp\left(-\frac{\pi nC^3\tau^4}{3}\right)\right], \tag{11}$$

where V_0 is initial volume occupied by the "mother phase"; $V(\tau)$ is the volume of the new phase that is appearing with time τ; n is the number of new crystallization centers; and C is the rate of crystal growth. Eq 11 is related to the diffusion processes of supercooled austenite transformation, which occurs during pearlite formation. In the case where metal cools at a rate exceeding a critical value, the austenite is supercooled to the temperature at which the diffusion-free process of transformation from austenite into martensite occurs. Thus, during diffusion transformation in steel, the grain size becomes finer with increasing supercooling of the initial phase, and that results in steel strengthening.

1.3.2 Diffusion-Free Transformation in Steel

As discussed earlier, during the austenite–pearlite transformation, the leading role is played by carbon diffusion, and during the austenite–martensite transformation, only the lattice is reorganized without a change in the concentration of reacting phases. Martensite is a hard solution of carbon in α-iron with the same concentration in the initial austenite. Since the solubility of carbon in α-iron is about 0.01 %, the martensite is a supersaturated hard solution that results in a tetragonal crystal structure [22–25].

The lattice parameters of martensite and austenite and the ratio of tetragonal structure for the martensite lattice versus the carbon content of carbon steel are shown in Fig. 4.

The transformation of austenite into martensite has shear cooperative character, and the martensite crystals in steel are formed almost instantly, disregarding the temperature for about one ten-millionth of a second. Thus, Gulyaev [22] notes that every plate is formed during the time interval of about 1×10^{-7} s, and the entire portion of plates, consisting of hundreds of thousands of crystals, in 1×10^{-3} s, and afterward the transformation stops. During further cooling, the transformation resumes as a result of the formation of new portions of martensite, and so on [22,23]. The specific volume of martensite is much greater than the specific volume of the initial phase of austenite, and therefore the formation of martensite plates results in the appearance of
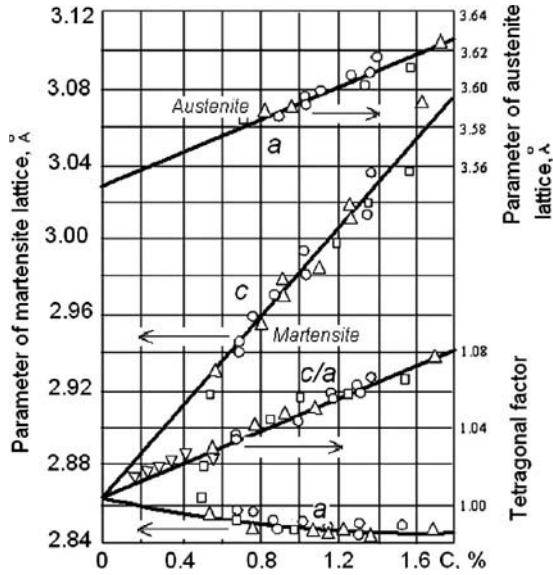
Fig. 4—Lattice parameters of martensite and austenite, and tetragonal ratio of martensite lattice versus the carbon content of carbon steel.

inner stresses due to pulling-apart forces. Actually, the specific volume of different structural components of phases can be determined by the following empirical equations [1]:

for ferrite:

$$V_\alpha = 0.12708 + 5.528 \times 10^{-6}T; \qquad (12)$$

for austenite:

$$V_\gamma = 0.12282 + 8.56 \times 10^{-6}T + 2.25 \times 10^{-3}C; \qquad (13)$$

for martensite:

$$V_i = 0.12708 + 4.45 \times 10^{-6}T + 2.79 \times 10^{-3}C; \qquad (13a)$$

and for carbide (Fe₃C):

$$V_{\hat{e}} = 0.13023 + 4.88 \times 10^{-6}T, \qquad (14)$$

where C is the mass concentration of carbon, and T is the temperature in °C.

At room temperature, the specific volume of martensite is greater than the specific volume of austenite by about 4 %. It has been established that martensite transformation is the main phase transformation in a solid body. Martensite transformation in steels is a complicated process where a number of martensite phases are formed that differ from each other by properties and lattice. Depending on the composition and heat treatment, four martensite phases–ε', ε, χ', and α_i (Fig. 5)–can be formed in steel. X-ray studies have shown that the martensite transformations typically follow the sequence [23]:

$$\gamma \rightarrow \varepsilon' \rightarrow \varepsilon \rightarrow \chi' \underset{\rightarrow}{\overset{\rightarrow}{}} \alpha_i,$$

where: $\rightarrow$ and $\underset{\rightarrow}{\overset{\rightarrow}{}}$ indicate cooling and heating correspondingly.

Intermediary martensite structures ε' and ε with low energy defects are observed in such steel alloys as iron-manganese-carbon. In carbon steels and the majority of alloy steels with a high energy of packing defects, there are no such structures, and transformations are indicated by the scheme [23]:

$$\gamma \rightarrow \chi' \underset{\rightarrow}{\overset{\rightarrow}{}} \alpha_M \text{ or } \gamma \rightarrow \alpha_i.$$
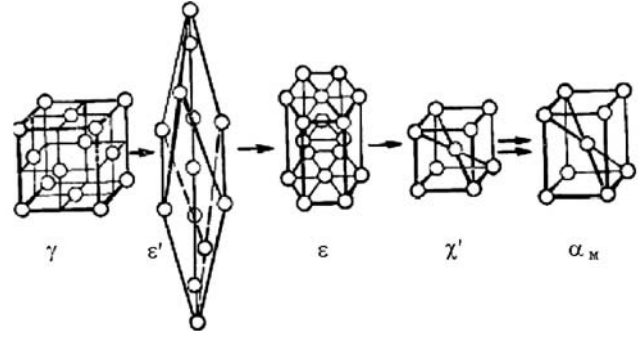
Fig. 5—Lattices of martensite phases in steel [23].

Information about phase transformations occurring in steels during heat treatment and cooling capacity of quenchants are available in [24–28].

Transformation of supercooled austenite into martensite occurs over a specific temperature range, as indicated in Fig. 6.

The start (M_S) and finish (M_F) temperatures of martensite transformations for a steel of a given composition are constant when cooling rates are not large. Experimentally, it has been shown that, for relatively low cooling rates, M_S is constant if the transformation temperature of austenite into martensite under such conditions is cooling-rate independent and only the transformation kinetics are affected. Below point M_C in Fig. 7, slower cooling results in a greater degree of transformations. Here, M_C is the temperature at the middle of martensite range that doesn't depend on the cooling rate of transformation. When the temperature decreases below the M_C temperature, the slow cooling delays the transformation processes. In this range of temperatures, intensive cooling results in more complete transformation. Above M_C, slow cooling results in martensite transformation, and martensitic transformation is inhibited because of the processes of stabilization.

When cooling rate increases, the M_S temperature can change. Thus, for steel having 0.5 % carbon, it has been
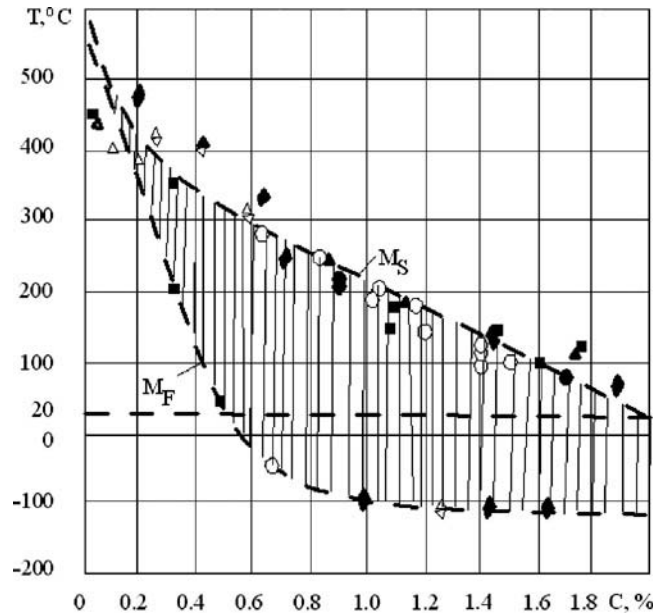
Fig. 6—Martensite start temperature (M_S) and martensite finish temperature (M_F) versus content of carbon in steel.
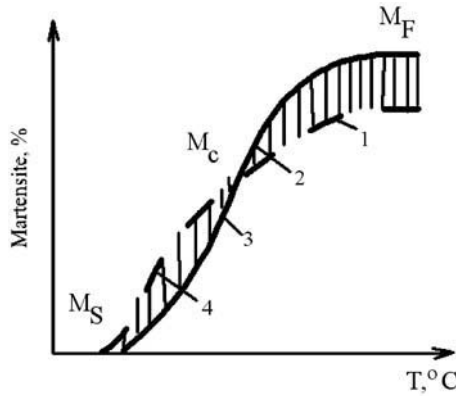
Fig. 7—Martensite curve for intensive and slow cooling within the range of martensite transformations: 1 – slow cooling; 2 – reduction of martensite due to stabilization; 3 – intensive cooling; 4 – increase in martensite due to isothermal transformation.

Fig. 9—Martensite start temperature point for a medium carbon steel (1) and high carbon alloy steel (2) versus grain size [1,23].

shown that M_S was 370°C and remained the same until a cooling rate of 660 °C/s, and when the cooling rate exceeded 16,500 °C/s, the M_S increases almost linearly to 460°C; as the cooling rate is increased further, the M_S again remains constant, as shown in Fig. 8. Increasing the total carbon content shifts this curve to the area of lower temperatures [29,30]. Ansell et al. [29] reported that the dependence of the position of martensite point M_S on cooling rate is due to the mechanism of athermal stabilization of austenite.

The character of the dependence of the position of the martensite point for a number of steels versus austenite grain size is shown in Fig. 9 [23]. Reducing the austenite grain size from 200−300 μm to 20−30 μm results in the reduction of M_S for medium-carbon steel from 328°C to 303°C. In this case, the initial rate of transformation increases. It has also been established that high pressures do not significantly change the initial martensite start temperature. For this reason, pressure has not been used in practice for the control of phase transformations. Using moderate pressures (up to 20 $\times$ 10^5 Pa), it is possible to control the required surface temperature of parts to be quenched in order to slow down or speed up the transformation process of austenite into martensite for highly forced heat transfer. This is important relative to the development of new methods of steel strengthening.

There are two types of martensitic transformations: isothermal and athermal, both of which exhibit specific kinetic

Fig. 8—Temperature of martensite start versus cooling rate [29]: 1, Fe – C – 0.5 % C; 2, Fe – C – 0.7 % C.

and morphological properties. Kurdyumov [31,32] notes that, in different steels and ferrous alloys, martensite transformation can occur either with an outburst—when, during a very short time, a significant number of martensite phases are formed—or isothermally, which occurs if cooling stops and the process is performed for a relatively long time and gradually stops. For these cases, the morphology and substructure of martensite crystals are different, which is observed by transmission electronic microscopy (TEM) [31,32].

The explosion character of martensite transformations results in the formation of a high density of dislocations in steel. Thus, the study of hardened carbon steels containing 0.28 and 0.4 % carbon has exhibited one martensite needle containing a dislocation lattice formed by series of straight parallel dislocations. In this case, the dislocation density is 10^{11} cm^{-2} and greater [30,33]. In high-carbon steels containing 0.98−1.4 % carbon, a dislocation lattice was also found. However, the dislocation density was so large that it is difficult to distinguish them even under high magnification.

The probability of self-tempering in high-carbon steels after quenching is lower because of the lower M_S temperature. Therefore it is difficult to explain the increase in the dislocation density by the possibility of self-tempering of martensite. This effect is likely due to the increase in specific volume of martensite plates, which results in more intensive processes of plastic strain of untransformed austenite, leading to a higher dislocation density. Indeed, in low-carbon steels, the lower specific volume of martensite and higher M_S lead to a relatively low dislocation density of about 10^{11} cm^{-2}. It has been noted that, for these steels, one should expect greater redistribution and annihilation of dislocations formed at martensite transformation, resulting in the reduction of their density [30].

These data show that diffusion-free martensite transformations are efficient means for forming high dislocation density in steel, which results in significant improvement of strengthening properties.

1.4 HIGH-TEMPERATURE THERMOMECHANICAL TREATMENT (HTMT)

Various thermomechanical treatments of steel are widely used in practice. The most widespread methods are high-temperature thermomechanical treatment (HTMT) and low-temperature

Fig. 10—Time of isothermal transformation versus temperature for different steel grades: (a) steel 30 (0.29 % C), heating to 1,000°C; (b) steel 60 (0.62 % C), heating to 900°C; (c) steel U9 (0.88 % C), heating to 780°C.

thermomechanical treatment (LTMT). The conditions required to perform thermomechanical treatment and cooling are determined based on the CCT and TTT diagrams for the steel alloy of interest.

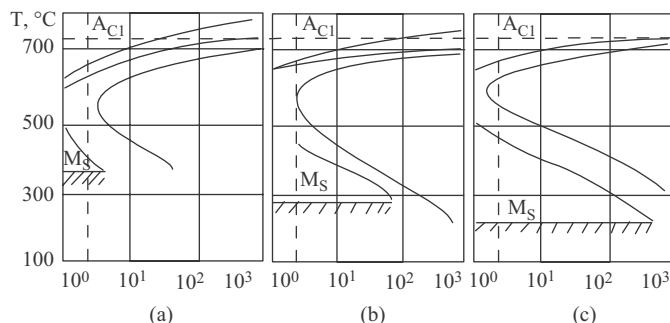CCT and TTT diagrams are invaluable. For example, they are used for the calculation of optimal conditions to cool steel parts. CCT and TTT diagrams are also used to select quenching processes, determine steel hardenability, and calculate residual stresses. Typically, kinetics of isothermal transformations of supercooled austenite are presented as coordinates of transformation temperature versus isothermal soaking times required to provide a given degree of decomposition. Fig. 10 shows TTT diagrams for steels with different carbon contents. Fig. 11 shows CCT diagrams for selected steel grades.
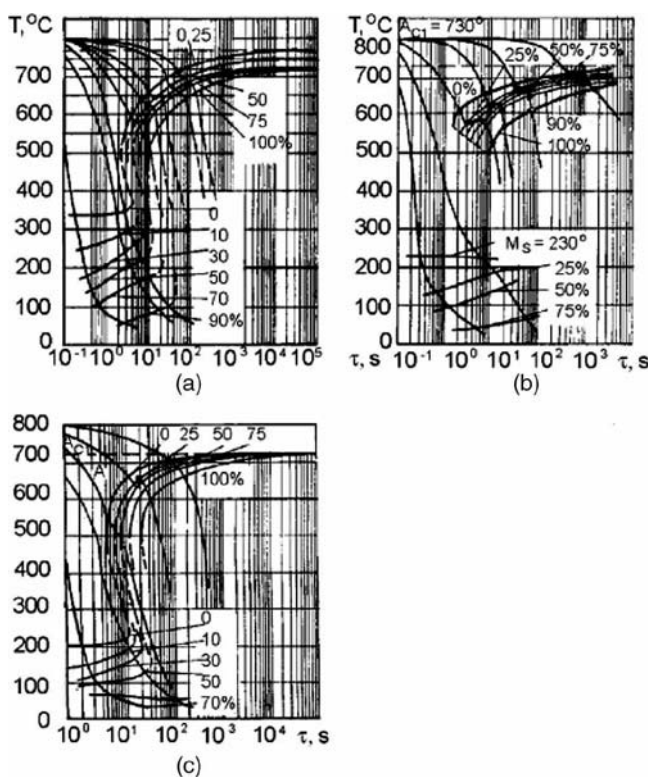

Fig. 11—CCT diagrams: (a) steel 45 (AISI 1045); (b) steel U8 (AISI 1080); (c) steel U12 (AISI W1).

Thermomechanical treatment consists of heating, deformation, and cooling (in various sequences), resulting in the formation of high density dislocation imparted by plastic deformation [15,24,26]. The particular process to be used must provide the optimal and most efficient method of plastic deformation and the best scheme of joint implementation of heat treatment and plastic deformation. Classification of different schemes of thermomechanical treatment, their analysis, and generalization based on experimental studies have been reported by Bernshtein [15].

LTMT consists of heating steel to a temperature above A_{C3} and then cooling it at a rate greater than the critical cooling rate to the temperature range of high stability of supercooled austenite, holding at this temperature, deformation of supercooled austenite within the range of its high stability, and further quenching (the A_{C3} temperature in hypoeutectoid steel is the temperature at which transformation of ferrite into austenite is completed upon heating). Supercooling is necessary for suppressing the recrystallization process. The HTMT process consists of austenitizing, deformation, quenching, and final operation of low-temperature tempering.

The principal difference of HTMT from heat treatment after rolling or forging is the suppression of the recrystallization process during HTMT, where a specific structural state is formed with the higher dislocation density and the position with respect to the formation of branched sub-boundaries. HTMT improves the plastic properties of a material, and LTMT improves its strength properties. HTMT eliminates the development of reversible temper brittleness within the dangerous range of tempering, produces higher impact strength at room and low temperatures, increases the impact strength by 1.5 to 3 times, significantly reduces the ductile−brittle transition temperature (DBTT), and decreases the potential for crack formation during heat treatment.

LTMT is preferably applied for high-alloy steels having 1−7 % chromium, 1−5 % nickel, and other alloys. When performing LTMT on carbon wire (steel U7A [AISI 1070], U10A [AISI W1]), highly complex mechanical properties (R_m up to 3,000 MPa) are obtained. For steel 40KhS (AISI 5140), the fracture strength S_k was 2,400 MPa; at the same time after conventional heat treatment for the same hardness, the fracture strength was 1,550 MPa. It has been established that in some cases due to LTMT, impact strength increases, the inclination for temper embrittlement is not reduced, and there is no effect on the temperature of transition from viscous destruction to brittle destruction. It has also been reported that the amount of retained austenite increases in the case of LTMT [15].

One mechanism for improving strength characteristics of steel after LTMT is the formation of a high density of dislocations in austenite. The interaction of dislocations with carbon atoms in martensite is another mechanism of steel strengthening due to LTMT. Japanese investigators have noted that, in the process of LTMT, the dislocation density formed reaches values of $10^{12}–10^{13}$ cm^{-2}, resulting in higher strength [33].

The presence of carbides in steel provides obstacles to the movement of dislocations [26]. Bernshtein has noted that the most universal explanation of the nature of steel strengthening during LTMT focuses on the changes in the dislocation structure of austenite during its deformation and further transfer of these changes to martensite. However,

even this mechanism is not comprehensive, because it is not possible to explain the changes in mechanical properties of steel during tempering after LTMT without considering carbide reactions in some steels [15,16].

HTMT may be used in conjunction with intensive quenching of forgings. Forgings are usually annealed, and forging heat is rarely used in practice, resulting in higher manufacturing costs. Moreover, the opportunity for additional strengthening by utilizing this heat to conduct HTMT is typically lost. The potential of utilizing forging heat with HTMT to provide additional strengthening will now be considered based on previously published work of Bernshtein [15,16].

High-temperature thermomechanical steel treatment is the process of heating to the temperature of stable austenite, at which time the steel is deformed and immediately quenched to obtain martensite (Fig. 12). The final conventional operation is low-temperature tempering. The deformation temperature for HTMT is normally above the A_{C3}. A combination of hot pressure treatment of steel with heat treatment has been studied, but primarily from the point of view of reducing costs for repeated heating due to quenching or normalization.

The principal difference between HTMT and rolling heat treatment lies in the creation of conditions of high-temperature plastic deformation and subsequent quenching under which the development of the recrystallization process is suppressed and a structural state is created that is characterized by a higher density of dislocations and their location with the creation of branched sub-boundaries. This process also produces distinctive mosaic properties of steel after HTMT. With respect to the probable orientational effect of substructure elements upon the final steel structure after quenching, it is important to select the optimal kind of deformation for thermomechanical treatment for each part.

When comparing HTMT and LTMT, it is often emphasized that it is difficult to prevent the development of recrystallization at high temperatures, and due to this, it is necessary to make some special improvements in technology. To obtain a high complex of mechanical properties, it is necessary to achieve not only the high specific density of dislocations but also their optimal configuration (distribution). Grange and Mullhauser established that the higher the temperature of austenitizing is, the slower the process of recrystallization after the plastic deformation becomes [34]. This fact is of great importance for HTMT. It is also well known that the process of recrystallization depends on the degree of deformation (see Fig. 13). The effect of the initial grain size (heating temperature) upon the recrystallization time is shown in Fig. 14.

When using HTMT, one cannot always suppress the recrystallization processes completely, either because conditions of technology do not allow quenching immediately after the deformation or due to higher temperatures at which the plastic deformation occurs. To what extent does the process of partial recrystallization during treatment result in the reduction of the effect of strengthening in the case of HTMT?

It has been shown that it is necessary to suppress recrystallization completely to obtain the best result from HTMT [15–17]. However, partial recrystallization during earlier

Fig. 13—Time necessary for full recrystallization at various degrees of 51V60 steel deformations with heating at 2,200°F (1,200°C), rolling at 1,700°F (930°C), and recrystallization at 1,400–1,800°F (760–1,000°C) [15].

Fig. 12—Scheme of high-temperature thermomechanical steel treatment (HTMT).
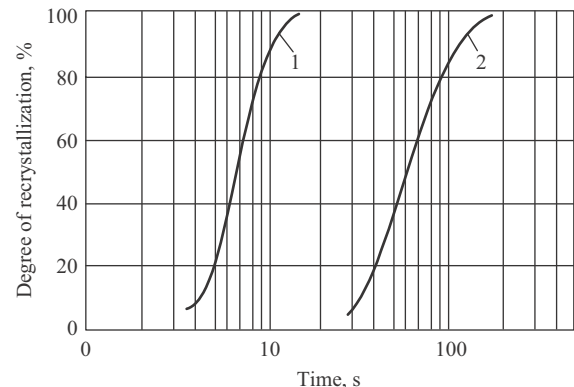
Fig. 14—The effect of the initial grain size (heating temperature) upon the recrystallization for AISI 51B60 steel at 1,500°F (820°C): 1, after heating at 927°C, grain size ASTM 7; 2, after heating at 1,200°C, grain sizes ASTM 4–5 [34].

stages results in an insignificant reduction in strengthening. It has been established that the initial stages of recrystallization exhibit a positive influence upon not only plasticity but also fatigue strength. As for recrystallization, there is an accompanying reduction in the yield limit [15].

1.4.1 Influence High-Temperature Thermomechanical Treatment Parameters on Mechanical Properties of Steels

In laboratory experiments and industrial tests of HTMT, different methods of deformation have been used: rolling of rods, strips, or bands; forging; closed and open stamping; extrusion; pressing with a pressing lathe; dragging; torsion; high-speed deformation (by explosion). The methods that proved to be the most effective are rolling, stamping, and forging. For HTMT, the steel grades used in the countries of the former USSR are: 40 (AISI 1040), 45 (AISI 1045), U9 (AISI 1090), 40Kh (AISI 5140H), 40KhN (AISI 3140), 30KhGSA (AISI 5130), 50KhG (AISI 5150), 60S2 (AISI 9260), 55KhGR (AISI 5155H), 65G (AISI 1566), ShKh15 (AISI 52100), 9Kh (AISI L2), and P18 (AISI T1), among others.

Reduction of the deformation temperature (and its approach to the A_{C3} temperature) always exhibits a favorable effect on the increase in strength due to HTMT. However, it is necessary to consider the slower recrystallization processes as the austenitizing temperature increases. Therefore, it is advisable to austenitize at high temperatures and to deform at temperatures close to the A_{C3} temperature.

The effect of HTMT on the fracture strength S_k and plasticity for steel 30KhGSA (AISI 5130) in the case of tension at −320°F (−195°C) is shown in Fig. 15.

The most significant improvement of mechanical properties is achieved in the case of HTMT with a relatively low degree of deformation (25−40 %). Further increase in the degree of deformation does not yield an additional increase in strength, and changes in plastic characteristics reach the stage
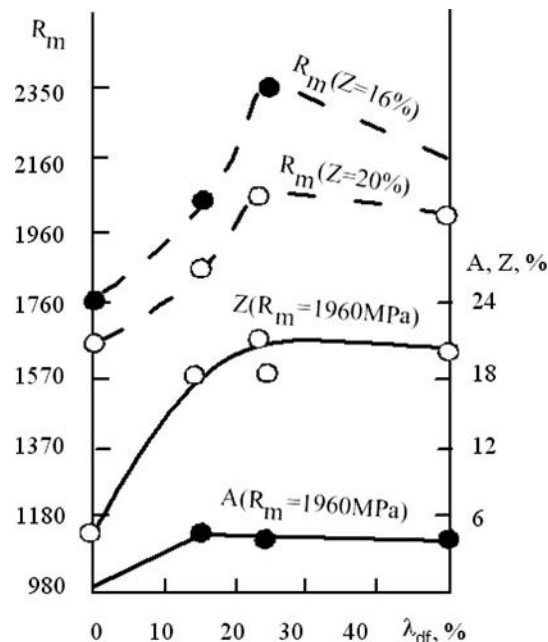
Fig. 16—Strength (while the plasticity is constant) and plasticity (while the strength is constant) versus degree of deformation for steel 55KhGR (AISI 5155) in the case of high-temperature thermomechanical treatment [15].

of saturation even at 40−50 %. The latter values of deformation degree are the limits advisable for HTMT (see Fig. 16).

The effect of carbon on strength in the case of HTMT is analogous to the effect of conventional heat treatment: strength increases with carbon content. Although plasticity is known to decrease with increasing carbon content, with HTMT this tendency occurs to a lesser extent. Brittle fracture occurs sooner than expected if the carbon content is high. The optimal carbon content for steel subjected to conventional heat treatment is about 0.4 %; for steel subjected to HTMT, it is about 0.5 %. In the case of vacuum steel melting and if steel is made of especially pure charge materials, this limit value is shifted higher since the plastic strength increases.

The advantage of HTMT is that higher values of plasticity are obtained up to a maximum carbon content of about 0.6 %. In this case, the shear strength is high, and it is possible to obtain a high strength of martensite when the carbon content is high (see Fig. 17) [15].

The effect of carbon appears in the fixation of dislocation structure of strengthened austenite and also in changes in dislocation structure of austenite during plastic deformation for thermomechanical treatment (increase in the dislocation density and changes in the character of dislocation distribution). The addition of carbon exhibits a drastic effect on the increase in dislocation density of steel subjected to HTMT.

1.4.2 Machine-Construction Steels

At United States Steel Laboratories, Grange and his colleagues [34] investigated the application of HTMT for steels possessing the following compositions:

A. 0.26 % carbon, 0.52 % nickel, 1.32 % chromium, 1.0 % molybdenum, 0.35 % vanadium
B. 0.57 % carbon, 1.16 % nickel, 1.07 % chromium, 0.26 % molybdenum
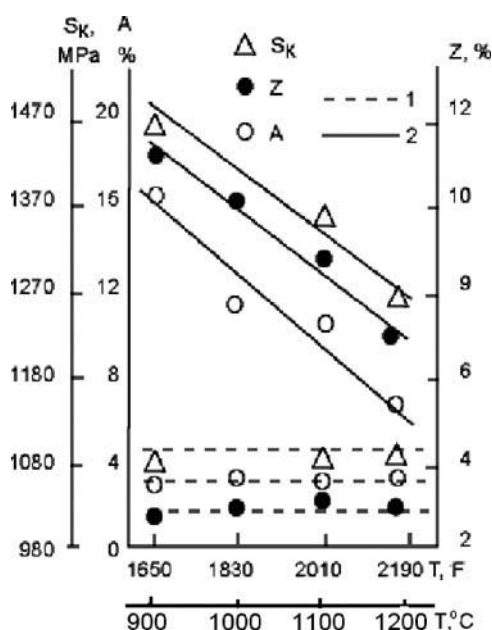C. 0.87 % carbon, 4.95 % nickel, 2.07 % manganese

Fig. 15—Effect of high-temperature thermomechanical treatment upon the break strength S_k and plasticity for steel 30KhGSA (AISI 5130) in the case of tension at −320°F (−195°C): 1, conventional heat treatment; 2, thermomechanical treatment [15].
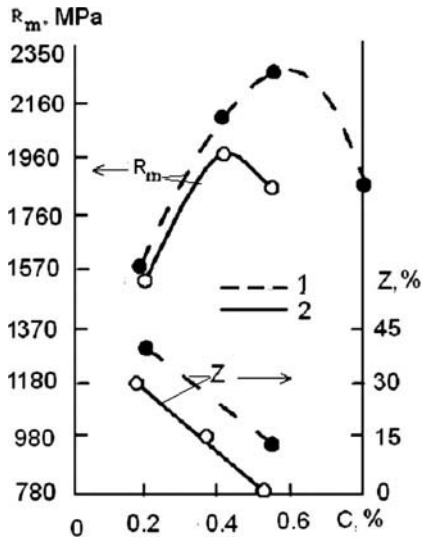
Fig. 17—R_m and Z versus carbon content: 1, high temperature thermomechanical treatment; 2, conventional quenching [15].

D. 0.41 % carbon, 1.90 % nickel, 0.82 % chromium, 0.28 % manganese
E. 0.25 % carbon, 0.59 % nickel, 0.73 % chromium, 0.27 % vanadium

It has been shown by investigations that mechanical and plastic properties of machine construction steels increase after high-temperature thermomechanical treatment [34].

Kula and Lapata [35] studied 4340 steel (0.39 % carbon, 1.75 % nickel, 0.8 % chromium, 0.23 % molybdenum) during open melting and showed that HTMT resulted in significant strengthening (increasing the yield limit by 25 %). In this case, plasticity and viscosity in the high-strength state are very high [34,35] and the temperature where cool fracture occurs decreases, and there is a decreased potential for fracture during tempering (see Fig. 18). The correlation among values of strength, plasticity, and viscosity on longitudinal and transverse samples after HTMT is the same as after conventional heat treatment; impact strength after HTMT

Fig. 18—The scheme of low-temperature thermomechanical treatment.

significantly increases, especially in low-temperature tests, in the area of threshold of brittleness.

There is essential improvement of properties of steel 4340 after HTMT at 1,550°F (845°C), with 75 % pressing out, even in the quenched state (without tempering): while the yield limit after conventional heat treatment is 1,370 MPa, after HTMT it goes up to 1,770 MPa. This is probably connected with the increase in the plastic strength due to the high-temperature thermomechanical treatment. The authors of [15,36,37] have made the conclusion that HTMT can be successfully applied for the production of strips, sheets, and wire.

1.5 LOW-TEMPERATURE THERMOMECHANICAL TREATMENT (LTMT)

Low-temperature thermomechanical treatment (LTMT) is shown schematically in Fig. 18. To perform low-temperature thermomechanical heat treatment, it is necessary to super-cool austenite to 400−500°C, where it should be deformed to a certain degree that has the designation λ_{df}. Transformation at this time should be delayed, and supercooled austenite should be stable. For this purpose, as a rule, high-alloy steels are strengthened by this method. This is an expensive process that is rather complicated to perform. It will be shown here that intensive quenching can replace both low-temperature and high-temperature thermomechanical treatment.

The process of LTMT requires a delay of the transformation of austenite into martensite during quenching. This is especially important when applying intensive quenching. During intensive quenching, the surface temperature decreases rapidly to the bath temperature, while temperature at the core remains very high. Immediately at the surface, a brittle martensitic layer is formed, which precludes mechanical deformation (see Fig. 19(a)).

To successfully design a low-temperature thermomechanical treatment, it is necessary to delay transformation of austenite into martensite during the intensive quenching process (see Fig. 19(b)). This may be accomplished by utilizing the self-regulated thermal process (to be described in detail in subsequent chapters of this text) [38,39]. It is known that a delay of the transformation of austenite into martensite can be fulfilled by using appropriate pressure or water salt solutions [1,38].

Until now, LTMT has been used for high-alloy steels, where supercooled austenite remains when cooling at a low rate up to 400−500°C. Unfortunately, this cannot be performed for low-alloy and plain carbon steels. That is why LTMT is not widely used in practice.

1.6 THE USE OF THERMOMECHANICAL HEAT TREATMENT

The steel grade 30KhN2MA (AISI 4330), with a chemical composition of 0.27−0.34 % carbon, 0.3−0.6 % manganese, 0.17−0.37 % silicon, 1.25−1.65 % nickel, 0.6−0.9 % chromium, 0.2−0.3 % molybdenum, 0.05 % titanium, and less than 0.3 % copper is widely used in the industry. The mechanical properties of steel 30KhN2MA (AISI 4330) after conventional heat treatment and thermomechanical treatment with the deformation in the area of stable and metastable austenite are presented in Table 1. Table 1 shows that ultimate strength R_m, after $\lambda_{df} = 70$, increases by 11 % compared with the conventional heat treatment. Similar results are provided in Table 2 for 40KhNM steel. Note that in all cases, after the thermomechanical treatment or conventional quenching, the
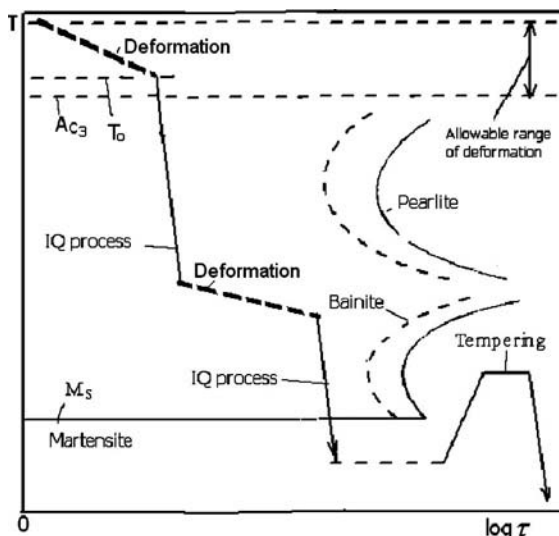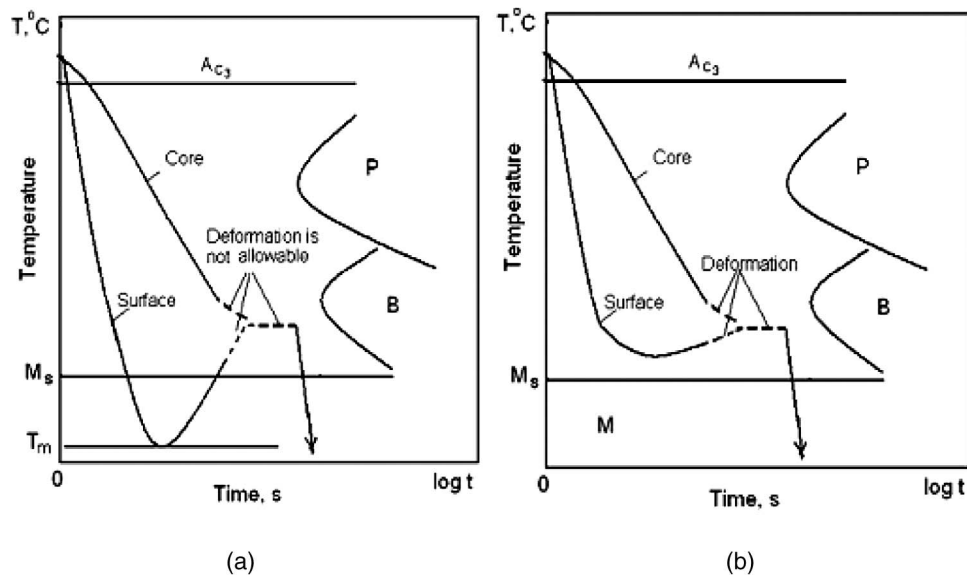
Fig. 19—Scheme of incorrect (a) and correct (b) low-temperature thermomechanical heat treatment (LTMT).

final operation was tempering at 210°F (100°C) for 4 hours. More information connected with the degree of deformation and tempering temperature is provided in Table 3.

It is important to compare HTMT after oil and water quenching because of the difference in cooling rate. As follows from Table 1, after thermomechanical treatment in water, tensile strength increased by 4.6 % when deformation was 85 % and by 20 % when deformation was 70 %. This means that a high degree of deformation decreases the effect of HTMT. Obviously, there exists an optimal degree of plastic deformation for the HTMT process where the effect is maximal. Final conclusions can be made after analyzing more experimental data. However, it is worth keeping in mind that combining thermomechanical treatment with the intensive quenching can provide improvement of mechanical properties of more than 20 %. Such tendency is clearly seen from Table 1.

There is an improvement of 4340 steel properties after high-temperature thermomechanical treatment at 1,550°F (845°C) with 75 % deformation even just after quenching (without tempering).

Data given in Table 2 show that HTMT facilitates the attainment of high mechanical properties. In addition, the LTMT (which also possesses significant process difficulties) has an advantage over HTMT for high strength only for chrome-nickel steel with 0.4 % carbon. For steel with lower carbon content, like 30KhN2M steel, the increase in the strength after high-temperature and low-temperature thermomechanical treatment was almost the same. Advantages of thermomechanical treatment relative to conventional heat treatment regarding plastic strength in high-strength conditions has also been shown [40–43].

It should be noted that cooling from the austenitizing temperature to the metastable area, when applying LTMT, must be sufficiently rapid to avoid the formation of ferrite and, after deformation, the cooling should be fast enough to prevent the formation of bainite (see Fig. 20(a)). The strength achieved as a result of LTMT increases as the deformation temperature is decreased, presumably because of the greater strain hardening induced in the austenite. In any case, the temperature chosen should be low enough to avoid recovery and recrystallization, but high enough to prevent bainite from forming during the deformation. The amount of deformation is a most important variable. One of the most significant trends is that, for many steels, the ductility actually increases with increasing deformation, although this

TABLE 1—Mechanical properties of steel 30KhN2MA (GOST 4543 (71) or approximately AISI 4330) after conventional heat treatment and thermomechanical treatment with the deformation in the area of stable and metastable austenite [15]

Treatment	In water			In oil		
	R_m (MPa)	Z (%)	A (%)	R_m (MPa)	Z (%)	A (%)
Thermomechanical treatment from 1,650°F (900°C) with λ_{df} =85 %	2,007	9.8	5.7	1,919	9.9	6.3
Conventional heat treatment from 1,650°F (900°C)	1,864	9.3	5.3	1,777	10.0	7.0
Thermomechanical treatment at 1,020°F (550°C), λ_{df} =70 %	2,060	9.2	5.7	1,716	10.4	7.4
Note: Composition of 30KhN2MA steel: 0.27–0.34 C; 0.3–0.6 Mn; 0.17–0.37 Si; 0.6–0.9 Cr; 1.25–1.66 Ni; 0.2–0.3 Mo; $<=$ 0.1 Al; $<=$ 0.3 Cu; $<=$ 0.05 Ti.						

TABLE 2—Mechanical properties of steel 40KhNM (AISI 4140) after conventional heat treatment and thermomechanical heat treatment (TMT) [15]

Heat	Treatment	R_m (MPa)	Z (%)	A (%)
I	TMT at 1,650°F (900°C), $\lambda_{df} = 85$ %, oil quenching	2,416	9.8	5.8
	Conventional oil quenching from 1,470°F (800°C)	2,243	9.7	6.3
II	TMT at 1,020°F (550°C) (in salt), $\lambda_{df} = 81$ %, oil quenching	2,629	9.6	7.3
	TMT at 1,020°F (550°C) (in air furnace), $\lambda_{df} = 81$ %, oil quenching	2,586	9.9	7.4
	Many-stage oil quenching from 1020°F (550°C)	2,261	4.3	3.9

Note: Composition of 40KhNM steel: 0.38–0.45 C; 0.50–0.80 Mn; 0.17–0.37 Si; 0.80–1.20 Cr; 0.15–0.25 Mo.

only becomes significant at deformations above 30 % reduction in thickness.

As might be expected, steels subjected to heavy deformation during LTMT exhibit very high dislocation densities (up to 10^{13} cm^{-2}), formed partly during deformation and partly during the shear transformation to martensite [42]. The deformation is usually carried out in the temperature range (500−600°C) in which alloy carbides would be expected to precipitate, so it is not surprising that fine alloy carbide dispersions have been detected by dark field electron microscopy [30,42].

On transforming deformed austenite to martensite, it is likely that at least part of the dislocation substructure, together with the fine carbide dispersion, is inherited by the martensite (see Fig. 20b). The martensite plate size has been shown to be very substantially smaller than in similar steels given a straight quench from the austenitizing temperature [42,43].

Several factors must contribute to strength, because no one mechanism can fully account for the high degree of strengthening observed. However, it seems likely that the major contributions are from the very high dislocation density and the fine dispersion of alloy carbides associated with the dislocations [43]. It should also be added that the fine precipitate particles can act as dislocation multiplication centers during plastic deformation. The martensitic transformation is an essential part of the strengthening process, as it

TABLE 3—Mechanical properties of steel 55KhGR (AISI 5155H) with respect to conditions of thermomechanical treatment and tempering [15]

| Tempering temperature	Degree of deformation, λ_{df} (%)	R_m (MPa)	$R_{p0.2}$ (MPa)	A (%)	Z (%)	HRC
210°F (100°C)	0	1,759	—	0	4.5	59.5
	15	1,666	—	0.9	8.5	51.0
	25	1,803	—	—	—	63.0
	50	2,391	—	2.25	13.8	62.0
	75	2,068	—	—	—	62.0
390°F (200°C)	0	1,749	—	0	5.9	59.0
	15	2,293	1,779	—	8.9	58.5
	25	2,352	1,745	—	14.0	59.0
	50	2,352	1,725	5.6	18.0	58.5
	75	2,254	1,705	2.5	9.0	59.0
480°F (250°C)	15	2,107	1,808	2.57	13.0	53.0
	25	2,107	1,835	4.6	20.0	53.0
	50	2,097	1,825	3.2	19.0	53.5
	75	2,068	1,797	4.0	21.0	55.0
570°F (300°C)	0	1,833	—	2.0	9.5	43.8
	15	2,019	1,735	3.7	14.0	50.0
	25	2,029	1,803	5.0	25.0	51.0
	50	1,960	1,725	4.12	24.0	52.0
	75	1,989	—	3.20	22.0	53.7
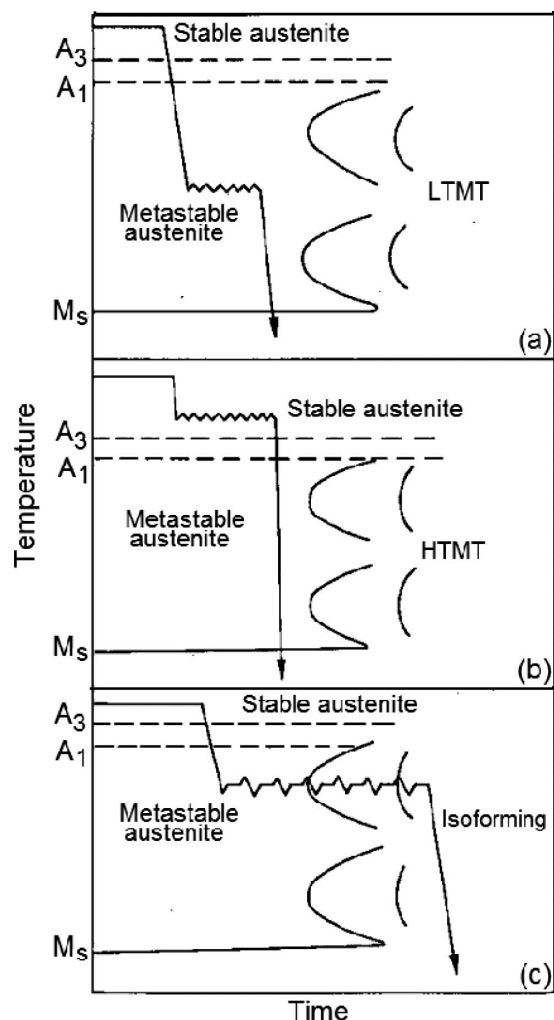
Fig. 20—Schematic diagrams of thermochemical treatments: (a) ausforming low-temperature mechanical treatment; (b) high-temperature mechanical treatment; (c) isoforming transformation [43].

substantially increases the dislocation density and divides each deformed austenite grain into a large number of martensitic plates, which are much smaller than those in conventional heat treatments. It is also likely that these small plates have inherited fine dislocation substructures from the deformed metastable austenite [42,43].

One can expect that combining HTMT with LTMT leads to a significant increase in the mechanical and plastic

properties of a material. The scheme of the combined process is shown in Fig. 18. To support this, examine the data presented in Table 4. When applying LTMT (35 % deformation) combined with the quenching in oil for martensite, tensile strength is 2,550 MPa and elongation is 8 %; the scheme of such a process is shown in Fig. 20(a). When applying HTMT (35 % deformation) combined with the quenching in oil for martensite, tensile strength is 2,500 MPa and elongation is 7.5 %; this process is shown in Fig. 20(b). However, prevention of martensite transformation (see Fig. 20(c) and Table 4 bottom) decreases the mechanical properties of steel. For example, when applying isoforming transformation, the tensile strength is only 1,370 MPa and elongation is 5 %. This conclusion is very important for developing high-strength materials based on the self-regulated thermal process that is considered in Chapter 2. Especially, that is related to improvement of tools made of alloy high-carbon steels where the martensite start temperature is within 120–180°C. This kind of steel process, shown in Fig. 20(a), can be easily performed providing fast cooling both in the pearlite and martensite ranges. Draper [44] came to the conclusion that HTMT and tempering steel at 200°C makes possible an increase in the erosion resistance of the steel by more than five times.

The influence of HTMT involved approximately 20–60 % deformation in the temperature range of about 1,000–1,150°C and conventional quenching of W-Mo-V high-speed steel was investigated by the authors of [15,45]. The HTMT—comprising austenitizing at 1,190°C, drop forging at approximately 1,000–1,150°C, and tempering at 540°C—may be employed for making particular tools from 12−0−2+C high-speed steel. The authors of [45] underlined that the method can be recommended for the manufacture of parts of gear-cutting hobs. It is possible also to use HTMT for parting-off tools and other high-speed steel tools of simple geometrical shapes. The method, with deformation by hot rolling, is suitable for the manufacture of twist drills, rebars which are usually hot rolled [43,65].

The positive effect of HTMT (rolling at 1,650°F/900°C after cooling from 2,200°F/1,200°C at the rate of 1.5 °C/min and 20–30 % deformation and with the further tempering at 390°F/200°C, 705°F/375°C, 1,020°F/550°C, and 1,200°F/650°C) upon the impact strength for 30KhGSA steel is shown in Fig. 21. After tempering at 390°F (200°C) and 705°F (375°C), the number of impacts before fracture increased by a factor of three, while after tempering at 1,020°F (550°C) and 1,200°F (650°C) the number of impacts increased only by a factor of 1.5. Due to HTMT, brittle

TABLE 4—Results of tests with chrome-nickel-molybdenum steel of 50KhN4M after thermomechanical treatment in different conditions (after austenitizing at 1650°F/900°C) [15]

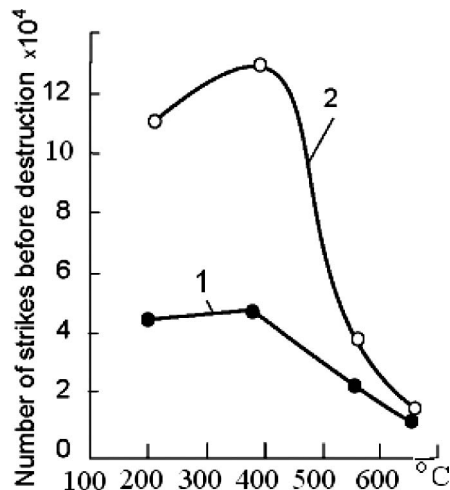| Deformation temperature	Degree of deformation (%)	Next treatment	R_m (MPa)	R_p (%)	A (%)	Z (%)	a_k (J/cm^2)
—	—	Oil quenching	2,350	1,720	6	9	20
1,650°F (900°C)	90		2,650	1,860	9	22	20
1,650°F (900°C)	35		2,500	1,670	7.5	17	35
930°F (500°C)	35		2,550	1,720	8	18	30
1,650°F (900°C)	35	Isothermal heat treatment	2,060	1,470	5	8	15
930°F (500°C)	35		1,370	980	5	14	20

Fig. 21—The number of impacts until the fracture of specimens made of 30KhGSA (AISI 5130H) steel versus the tempering temperature in the case of (1) conventional heat treatment and (2) thermomechanical treatment. Rolling is at 1,650°F (900°C) after cooling from 2,200°F (1,200°C) at the rate of 1.5 °C/min and with 25–30 % deformation [15].

fracture between grains in the zone of advanced development of cracking was suppressed. After HTMT, a crack exits within the body of the grain (the same as after tempering in the brittleness zone); after conventional heat treatment, the crack was observed between boundaries of austenite grains.

The effect of HTMT upon the structure and properties of 50KhN4M steel was also investigated [15,18]. Samples of 20 by 20 by 65 mm were deformed up to 80 % (see Fig. 22) in a hydraulic press at 1,650°F (900°C), and then some samples were immediately quenched in oil and others were heat-treated isothermally for 2 hours at a bath temperature of 610°F (320°C). After high-temperature and low-temperature thermomechanical treatment, the steel was tempered at 210°F (100°C). Table 3 shows that HTMT provides high strength and plasticity. For a relatively low deformation degree (35 %), properties after HTMT and LTMT are almost the same. Some reduction of values of the yield limits after HTMT with 10–30 % deformation (and also the change in the plasticity) is probably connected with non-monotonous changes in the amount of residual austenite (see Fig. 22), which reaches the maximum at low degrees of deformation in the case of HTMT.
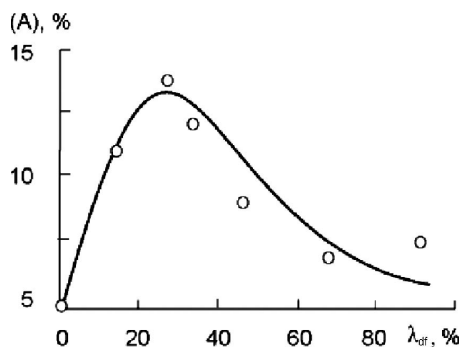

Fig. 22—Effect of the deformation degree upon the amount of residual austenite for 50KhN4M steel. Cooling after deformation is at 1,650°F (900°C) in oil [15].

For 55KhGR (AISI 5155H) steel, it has been established that HTMT produces a stable strengthening effect. Thus, conducting high-temperature short-time tempering at 1,110°F (600°C) for 30 minutes with hardness 32–34 HRC after HTMT and then quenching after short-time heating (4 minutes at 1,620°F/880°C in salt bath, oil cooling) and tempering at 480°F (250°C), the properties achieved will exceed those obtained immediately after HTMT and tempering at the same temperature.

1.7 THERMOMECHANICAL TREATMENT OF SPRING STEELS AND SOME CHARACTERISTICS OF THE PROCESS

Spring steel is a low-alloy, medium-carbon steel with a high yield strength. This allows objects made of spring steel to return to their original shape despite significant bending or twisting. Silicon is the key component to most spring steel alloys. An example of a spring steel used for cars would be AISI 9255 or Russian steel 55S2, containing 1.5–1.8 % silicon, 0.70–1.00 % manganese, and 0.52–0.60 % carbon. Most spring steels (as used in cars) are hardened and tempered to about 45 HRC [46,47]. The thermomechanical heat treatment of spring steels increases their quality significantly.

The effect of the deformation degree after HTMT is shown in Table 5. An increase in mechanical properties is still achieved after HTMT with 25 % deformation (with the use of hot rolling) [15,48].

HTMT for steels of 55S2, 55S2Kh, and 55S2M grades eliminated fragile fracture and significantly improved the mechanical properties (see Figs. 23 and 24 and Tables 6 and 7). While the deformation degree increases up to 50 %, strength does not significantly increase, and the further increase to 75 % deformation results in decreased strength, which may be connected with more intensive development of recrystallization processes in the steel that is highly deformed.

It appears that HTMT reduces the strength-lowering effect of tempering [10]. For example, high-temperature thermomechanical treatment of steel and subsequent tempering within the range of 400–750°F (200–400°C) increases the fracture strength by 340–390 MPa and the yield strength by more than 390–490 MPa compared to steel subjected to conventional heat treatment. It is believed that maintaining high mechanical properties after HTMT with the increase in the tempering temperature is related to the stability within the thin structure formed.

Shukyarov and Paisov [48] established that after high-temperature thermomechanical treatment of 55S2 steel alloyed with chromium, molybdenum, tungsten, and vanadium, the ultimate strength and yield strength are increased by 150–300 MPa and the plasticity is increased 1.5 to 3 times. It is said that the higher the austenization temperature (900–1,050°C), the higher the plasticity after tempering at 350–400°C.

An important conclusion can be made concerning the recrystallization process of deformed austenite. The recrystallization of the steel occurs comparatively rapidly in the process of HTMT. With an increasing degree of deformation and temperature, the process of recrystallization increases, too, and is accelerated. When 55S2 steel is alloyed with chromium, molybdenum, and vanadium, the rate of recrystallization decreases four to ten times. That favors the use of HTMT for parts of considerable size [48].

Figs. 25 and 26 show that for a steel grade having 0.59 % carbon and 2.62 % silicon, when subjected to HTMT with 70 %

TABLE 5—Effect of the deformation degree in the case of high-temperature thermomechanical treatment upon mechanical properties of 55S2 steel (AISI 9255) (with tempering at 480°F/250°C, austenitizing temperature 1,760°F/960°C) [15,48]

Steel grade	λ_{df} (%)	R_m (MPa)	R_p (MPa)	A (%)	Z (%)
55S2 (AISI 9255)	Usual	Fragile fracture			
	25	2,256	2,010	5	10
	50	2,276	2,020	7	9
	75	2,158	1,982	6	10
55S2Kh	Usual	Fragile fracture			
	25	2,433	2,207	9	18
	50	2,492	2,266	9	18
	75	2,453	2,246	10	19
55S2M	Usual	Fragile fracture			
	25	2,394	2,178	8	25
	50	2,472	2,256	7	20
	75	2,423	2,207	8	27
55S2V	0	2,158	1,942	4	10
	25	2,453	2,246	13	26
	50	2,550	2,286	10	24
	75	2,472	2,256	12	25
55S2FM	Usual	2,256	2,040	5	12
	25	2,472	2,256	9	18
	50	2,531	2,286	8	18
	75	2,492	2,266	9	20

deformation at 1,740°F (950°C) for one pass, the fracture strength increases up to 2,350–2,450 MPa and fatigue limit increases more than 300 MPa. For the same high-temperature thermomechanical treatment with the same deformation, but for *two* passes, it is 2,650–2,700 MPa. Fatigue stress test data for steel having 0.62 % carbon and 2.16 % silicon are given in Fig. 26. The limit strength for the steel used in Fig. 26 after conventional heat treatment is very low.

1.8 COMBINING THERMOMECHANICAL TREATMENT WITH THE INTENSIVE QUENCHING PROCESS COULD BE VERY BENEFICIAL

There are not enough data providing the impact of intensive quenching combined with the thermomechanical treatment (TMT) process on mechanical properties of a material. This is because the TMT process is used mostly for alloy steels to make low-temperature thermomechanical treatment reliable. As a rule, alloy steels are quenched in oil.

Let's compare the mechanical properties of AISI 5140 steel with those of AISI 1040 steel, both subjected to TMT. The AISI 5140, after TMT, was quenched in oil; the AISI 1040 was quenched in water. The martensite start temperature for both steels was about 350°C. The heat transfer

coefficient of oil within a range of temperature of 100–350°C is 300 W/m²K, and the heat transfer coefficient within the same interval for water is about 4,000 W/m²K due to the boiling process, which occurs above 100°C. This means that the cooling rate within the martensite range differs significantly between the two.

The equation for cooling rate evaluation, depending on heat transfer coefficients, is well known [1,49]:

$$v = \frac{abKn}{D^2}(T - T_m), \qquad (15)$$

where v is the cooling rate in °C/s; a is the thermal diffusivity of a material in m²/s; b is the coefficient depending on the configuration of steel parts; Kn is the Kondratjev number (a dimensionless value); D is size (diameter or thickness) in m; T is temperature in °C; and T_m is bath temperature in °C.

For a cylindrical 10-mm specimen, when quenching in oil (300 W/m²K) and water (4,000 W/m²K), the Kondratjev numbers are 0.05 and 0.4 [1]. According to Eq 15, the cooling rate within the martensite range in cold agitated water is eight times faster than with the still oil.

Let's see how the mechanical properties of alloy steels, subjected to TMT and quenched in oil, differ from the
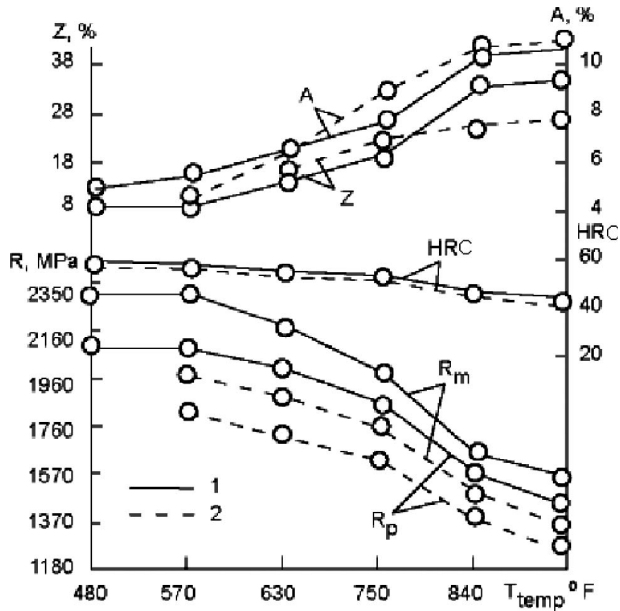
Fig. 23—Mechanical properties of 55S2 steel upon tempering temperature after high-temperature thermomechanical treatment (deformation degree of 50 % and austenitizing at 1,760°F/960°C): 1, high-temperature thermomechanical treatment; 2, conventional heat treatment [15].

mechanical properties of plain carbon steel, subjected to TMT and quenched in cold water. It is well known that alloying increases the mechanical properties of steel considerably, depending on the content of the alloying elements [50]. The chemical composition of steels AISI 1040, AISI 5140, and 40KhN is presented in [51].
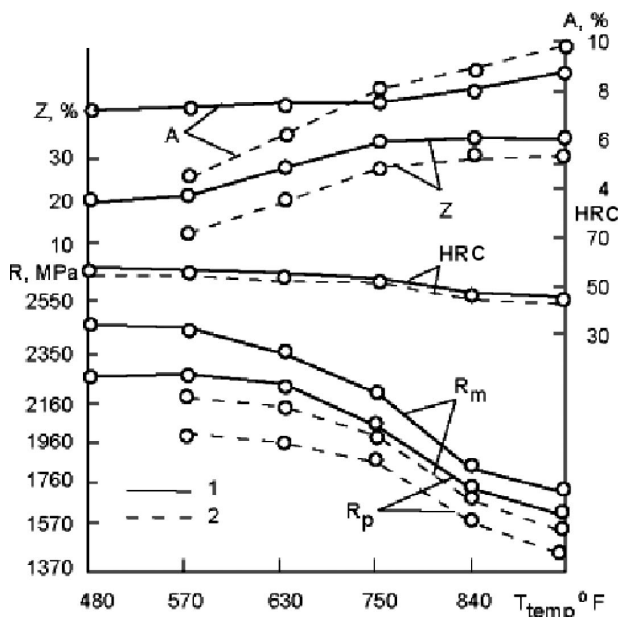

Fig. 24—Mechanical properties of 55S2V steel versus tempering temperature after high-temperature thermomechanical treatment (deformation degree of 50 % and austenitizing at 1,760°F/960°C): 1, high-temperature thermomechanical treatment; 2, conventional heat treatment [48].

The data in Table 8 are averages for tests with three, five, or more specimens. The deviation of stress values is within 2–3 %. In all cases, heating at a constant temperature before quenching is for 10 minutes. Below the lines, the data correspond to conventional heat treatment in oil. The data above the line correspond to properties obtained by high-temperature thermomechanical treatment.

The mechanical properties of AISI 1040 steel subjected to HTMT and quenched in cold water have more advantages as compared with AISI 3140 steel subjected to HTMT and quenched in oil (see Tables 8 and 9).

For example, the yield strength of AISI 1040 steel (see Table 9) after TMT with quenching in water and tempering at 600°C is 883 MPa. The yield strength of AISI 5140 steel (see Table 9) after TMT with quenching in oil and tempering at 600°C is 804 MPa. The elongation of AISI 1040 steel after TMT with quenching in water and tempering at 600°C is 17 %; the elongation of AISI 5140 steel after TMT with quenching in oil and tempering at 600°C is 16.5 %. This comparison shows that yield strength of AISI 1040 steel is better by 10 % compared with AISI 5140 steel quenched in oil during the TMT process.

As is seen from Table 10, AISI 5140 steel contains 0.8–1.1 % chromium and about 0.3 % Ni. Instead of that, its yield strength is less by 10 % than that of AISI 1040 steel quenched in water. The same tendency remains for AISI 5140 steel that was additionally alloyed with 0.63 % tungsten. In this case, the alloyed steel yield strength was 863 MPa and elongation was 16 %. However, plain carbon steel that went through the TMT process but was quenched in water has a yield strength of 883 MPa and elongation of 17 % (see Tables 8 and 9). It looks like it is possible to save 1 % chromium, 0.3 % nickel, and 0.6 % tungsten by combining TMT with accelerated cooling within the martensite range.

To be sure that conclusion is correct, the author [15] compared mechanical properties of AISI 5140 steel quenched in oil with those of the same steel quenched intensively in water. More information on intensive quenching is provided in [52]. It appears that intensively quenched AISI 5140 steel has better mechanical properties, especially impact strength, which is increased 1.5 to 2 times (see Table 11). It follows also that the higher the martensite start temperature is, the higher are the mechanical properties of steel. For example, yield strength after intensive quenching of AISI 4118 steel is 14 % higher and the impact strength increases 2.4 times [52]. With increasing martensite start temperature, the cooling rate within the martensite range, according to Eq 15, increases in direct proportion to the increased temperature. There is no doubt that a high cooling rate within the martensite range can increase the mechanical properties of steel significantly. This issue is discussed in detail in Chapter 9.

1.9 THE PROBLEMS ARISING DURING STEEL HEAT TREATMENT
It follows from the above discussion that, for increasing the strength properties, service life, and reliability of steel parts, it is necessary to minimize grain size to the extent possible and to form a high density of dislocations. This is achieved by thermomechanical treatment and intensification of heat transfer processes during phase transformations, and as a result, austenite is cooled to lower temperatures so that finer structure is formed. This is related to diffusion processes. The intensification of heat transfer processes in the range of

TABLE 6—Tempering effect upon mechanical properties of 55S2M steel for high-temperature thermomechanical treatment and conventional heat treatment [48]

Tempering	R_m (MPa)	R_p (MPa)	A (%)	Z (%)	Tempering	R_m (MPa)	R_p (MPa)	A (%)	Z (%)
480°F (250°C)	2,472[a] F.F.[b]	2,256 F.F.	7 F.F.	20 F.F.	750°F (400°C)	2,220 2,000	2,080 1,860	7.5 8	33 27
570°F (300°C)	2,472 2,158	2,256 1,962	7 4	22 12	840°F (450°C)	1,870 1,700	1,760 1,610	8 9	34 28
660°F (350°C)	2,354 2,109	2,217 1,923	7.5 6	27 20	930°F (500°C)	1,750 1,550	1,640 1,450	9 10	34 28

Notes:
[a] Above the line are properties in the case of high-temperature thermomechanical treatment (λ_{df} = 50 %); below the line are properties in the case of conventional heat treatment.
[b] F.F. = fragile fracture.

TABLE 7—Fracture strength for 55S2M steel after tempering [15,48]

Heat treatment	$R_{p0.005}$ (MPa) after tempering at:				
	570°F (300°C)	660°F (350°C)	750°F (400°C)	840°F (450°C)	930°F (500°C)
High-temperature thermomechanical treatment	1,372	1,500	1,509	1,548	1,450
Conventional heat treatment	1,303	1,333	1,362	1,352	1,176
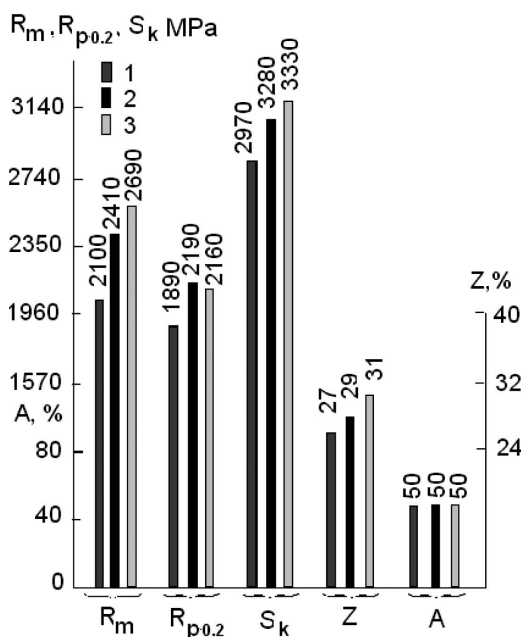
Fig. 25—Mechanical properties for steel having 0.59 % C and 2.62 % Si after treatment in different conditions: 1, without deformation, quenching at 1,740°F (950°C), and tempering at 390°F (200°C) for 1 hour; 2, deformation at 70 % for one pass, quenching from 1,740°F (950°C), and tempering at 390°F (200°C) for 1 hour; 3, deformation at 70 % for two passes, quenching from 1,560°F (850°C), and tempering at 390°F (200°C) for 1 hour [15,48].
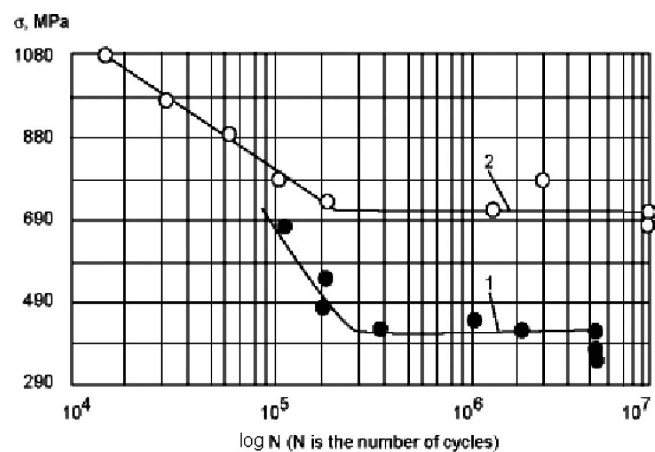
Fig. 26—Fatigue strength for steel samples having 0.62 % C and 2.16 % Si after treatment in different conditions: 1, without deformation, quenching from 1,740°F (950°C), and tempering at 570°F (300°C) for 1 hour; 2, 85 % deformation for two passes, quenching from 1,740°F (950°C), and tempering at 570°F (300°C) for 1 hour [10,42].

martensite transformations is related to the propensity for quench cracking, distortion, and unfavorable distribution of residual stresses. For this reason, it is often recommended that quenching should be performed intensively in the pearlite or intermediary areas, and slowly within the martensite range.

TABLE 8—Mechanical properties of 40Kh (AISI 5140) and 40KhN (AISI 3140) steel in the case of different treatment

Steel grade	Processing conditions	R_m (MPa)	R_p (MPa)	A (%)	Z (%)
40KhN	TMT, λ_{df} = 40 %, oil quenching from 1,650°F (900°C), tempering at 1,200°F (650°C) for 1.5 h	<u>927</u> 785	<u>795</u> 613	<u>16</u> 23	<u>65</u> 55
40KhN +0.3 % Mo	Same	<u>1,069</u> 868	<u>956</u> 716	<u>16</u> 22	<u>58</u> 63
40KhN +0.63 % W	Same	<u>996</u> 834	<u>863</u> 633	<u>16</u> 21	<u>63</u> 63.5
40Kh	Improvement, cool riveting (λ = 35 %), oil quenching from 1,560°F (850°C), tempering at 750°F(400°C) for 1.5 h	<u>1,432</u> 1,207	<u>1,418</u> 1,158	<u>17</u> 10	<u>47</u> 44
40Kh	Same, tempering at 930°F (500°C)	<u>1,118</u> 1,010	<u>1,015</u> 873	<u>11.5</u> 14	<u>51.5</u> 45
40Kh	Same, tempering at 1,110°F (600°C)	<u>917</u> 829	<u>804</u> 746	<u>16.5</u> 17	<u>68</u> 60

Note: The data above the line correspond to properties in the case of high-temperature thermomechanical treatment, and data below the line correspond to properties in the case of normal (conventional) heat treatment.

TABLE 9—Mechanical properties of AISI 1040 steel for heavy rolling with 19-mm diameter in the case of high-temperature thermomechanical treatment and conventional heat treatment

Tempering	R_m (MPa)	$R_{p0.2}$ (MPa)	A (%)	Z (%)	a_k (J/cm^2)
390°F (200°C)	<u>1,972</u> 1,422	<u>1,570</u> 1,246	<u>7.0</u> 2.0	<u>40.0</u> 16.0	<u>35</u> 30
570°F (300°C)	<u>1,766</u> 1,628	<u>1,472</u> 1,511	<u>7.5</u> 7.0	<u>39.0</u> 35.0	<u>30</u> 40
750°F (400°C)	<u>1,373</u> 1,177	<u>1,226</u> 1,099	<u>8.5</u> 8.5	<u>53.0</u> 50.0	<u>80</u> 85
930°F (500°C)	<u>1,324</u> 1,001	<u>1,177</u> 883	<u>11.0</u> 12.0	<u>55.0</u> 60.0	<u>105</u> 120
1,110°F (600°C)	<u>991</u> 785	<u>883</u> 667	<u>17.0</u> 16.0	<u>60.0</u> 60.0	<u>130</u> 200

Note: The data above the line correspond to properties in the case of high-temperature thermomechanical treatment, and data below the line correspond to properties in the case of normal (conventional) heat treatment.

TABLE 10—Chemical composition of 40 (AISI 1040), 40Kh (AISI 5140), and 40KhN (AISI 3140) steels [51]

Steel	C	Mn	Si	Cr	Ni	Mo	Cu	Al	Ti
AISI 1040 (40)	0.37–0.45	0.50–0.80	0.17–0.37	0.25 max	0.25 max	—	0.25 max	—	—
AISI 5140 (40Kh)	0.34–0.44	0.50–0.80	0.17–0.37	0.8–1.1	0.3 max	—	0.3 max	—	—
AISI 3140 (40KhN)	0.38–0.43	0.50–0.80	0.17–0.37	0.45–0.75	1.0–1.4	0.15 max	0.3 max	$\leq$ 0.1	$\leq$ 0.05

There are many quenchants that possess these properties. Among them are aqueous polymer solutions, various kinds of oils with additives that intensify the process of cooling at high temperatures, and others. Unfortunately, for most quenchants, reducing cooling rates within the martensite range also reduces cooling rates at high temperatures, which relates to the reduction of hardenability of steel parts. For increasing the depth of the hardened layer and

TABLE 11—Mechanical properties at the core of conventional (oil) and intensively quenched steels [52]

Steel	Quench	Tensile strength (MPa)	Yield strength (MPa)	Elongation (%)	Reduction (%)	Impact strength (J/cm^2)
40Kh	In oil	780	575	21	64	113
40Kh	Intensive	860	695	17	65	168
AISI 4118	In oil	755	630	18	74	70
AISI 4118	Intensive	920	820	15	68	170

improving the strengthening of parts, it becomes necessary to use alloy and high-alloy steels. The majority of machine parts are made of high-alloy steels, not because plain carbon steels do not provide sufficient strength and reliability in service but because of the potential for quench cracking during quenching; it is impossible to provide sufficiently high hardness of the parts after quenching.

For parts of complicated configuration or parts prone to quench cracking during intensive quenching, it is necessary to use alloy steels and to quench in oils. Therefore, elimination of quench cracks during the intensification of heat transfer processes in the area of martensite transformations is an extremely important practical problem.

It is noted in [2,53] that increasing the cooling rate within the martensite range initially increases the probability of quench cracking to a maximum value, but above this cooling rate, the probability for quench cracking approaches zero. It is suggested that this is based upon the transformation of austenite into martensite and that the effect on the reduction of quench cracking is caused by a high cooling rate within the martensite range. For every steel grade, there is a critical cooling rate within the martensite range beyond which quench cracking is minimized and strengthening properties increase [2,53].

An analogous observation of reducing the probability of quench cracking when the cooling rate within the martensite range increases is that quench cracking is related to the non-uniformity of cooling at the surface during quenching [54]. If uniform cooling of the surface for highly forced heat transfer is facilitated, then there will be no quench cracks, because favorably distributed structural and thermal stresses will be formed in a part to be quenched. However, the intensification of heat transfer processes within the martensite range—that is, cooling steel parts at the rate exceeding a critical value—results in very high strengthening of material. It is believed that intensification of heat transfer processes within the martensite range is equivalent to low-temperature thermomechanical treatment. Indeed, when the cooling rate within the martensite range increases, less time is required for the process of the transformation of austenite into martensite; as a result, the transformation has a character of an explosion. Since the specific volume of martensite is greater than the specific volume of the initial phase of austenite (see curves of Figs. 16 and 17), the plastic deformation of supercooled austenite formed between martensite plates will occur. When the transformation has an explosive character, avalanche formation of dislocations takes place, and they are frozen by rapid cooling to low temperatures. Aspects of explosion phenomena and processes connected with freezing dislocations have been highlighted by Ivanova [9,12].

It is also well known that low-temperature thermomechanical treatment of some steels increases the endurance limit to 1,100–1,200 MPa. It has been calculated that steel can be deformed at a dislocation density not exceeding 10^{13} cm^{-2} [7]. It is possible that, in some cases, with the explosive character of transformations and avalanche formation of dislocations, their density can reach very high values, which must result in very large increases in the complex of mechanical properties of the material. Thus, the intensification of heat transfer processes within the martensite range starting with an alloy-specific critical cooling rate reduces quench cracking and improves the strengthening properties of the material.

On the other hand, intensive cooling creates high compressive residual stresses at the surface of steel parts, which prevents crack formation, too [55,56].

Currently in Ukraine and Russia, the technology of heat treatment of semi-axles of automobiles at a high cooling rate within the martensite range is in use [4,55]. As a result, high-alloy steels have been replaced with steels having lower alloy content, and the service life of semi-axles has been increased, resulting in substantial manufacturing cost reductions [1,4]. In the case of conventional quenching in water, aqueous solutions and electrolytes are used during nucleate boiling where the temperature of the surface of a part to be quenched typically remains high for a relatively long time just above saturation temperature of water. Within this range of temperatures, steel transformations, such as martensitic transformation, are delayed because the temperature of the surface during nucleate boiling typically varies within the range of 110–130°C, while the temperature in the core of the steel part can vary within the range of 300–860°C (see Chapter 2) [1,4]. When the transformation of supercooled austenite into martensite is delayed, stabilization of supercooled austenite is observed and the material loses strength due to self-tempering, annihilation and fixing dislocations by carbon atoms and other alloy elements occurs, and, as a result, the material becomes fragile. During nucleate boiling, the highest thermal and structural stresses are obtained. Depending on the degree of the transformation of austenite into martensite in a part to be quenched, quench cracks can occur due to thermal stress formation.

Shteinberg [57] has reported that quench cracks are formed only if a part to be quenched contains more than 50 % martensite. For low-carbon and medium-carbon steel grades (see Fig. 6), at temperatures of 110–130°C, more than 50 % martensite is formed, and therefore, during water quenching of steels such as 40Kh and 45, there exists a substantial propensity for quench cracking. To avoid these unfavorable phenomena, it is necessary to change the boiling temperature of

the quenchant so that during the process of nucleate boiling, when parts are quenched in underheated liquid, no more than 50 % martensite is formed. This can be achieved by using various additives to increase the boiling temperature or by changing the pressure acting on the quenching media. In this way, the boiling temperature of the quenching can be controlled by controlling the pressure with respect to the temperature field of a part to be quenched to speed up or slow down the transformation of austenite into martensite. It is important in this approach that the temperature field of a part to be quenched and, therefore, the process of phase transformations can be controlled when heat transfer is highly forced, that is, when the Biot number approaches infinity (heat transfer and Biot numbers will be discussed in detail in subsequent chapters in the book).

Many quenching methods are available to vary the heat transfer coefficient in different temperature ranges and control phase transformation processes. This approach does not solve this problem completely, because reducing the heat transfer coefficient α requires the application of high-alloy steels, and increasing α results in an abrupt reduction of the surface temperature, at which more than 50 % martensite is formed, which is connected with the danger of quench cracking. Therefore, changes in the quenchant boiling temperature by means of changing pressure or applying additives is the preferred methodology to control the temperature field of parts to be quenched when the heat transfer is highly forced.

The intensification of heat transfer processes within the martensite range and regulation of the surface temperature by pressure result in decreasing the probability of quench cracking and improving the strengthening properties of steel, and thereby allow the use of plain carbon steels instead of expensive alloy steel grades. Delaying the transformation of austenite into martensite by means of pressure until the finish of nucleate boiling, and then cooling a part

within a martensite range at a rate exceeding a critical value, avoids quench cracking and increases the material strength.

The service life and reliability of service of steel parts are affected also by residual stresses in hardened steel parts. These can be surface tensile or compressive stresses. Tensile stresses are formed during the work with external loads, which reduces the service life of parts. If the stresses at the surface are compressive, then tensile stresses appear in internal layers, which can cause the formation of cracks or chipping, as observed, for example, at the service of carburized parts. In connection with this, the most favorable distribution of residual stresses is when stresses at the surface are compressive and tensile stresses are in the core [58,59]. Since residual stresses during quenching are formed mainly because, during phase transformations, kinematic changes (superplasticity) occur, the change in pressure acting on the quenchant can delay phase transformation and also control the value of residual stresses [1,60].

Therefore, the quenching problem is also a problem of the control of residual stresses to facilitate a favorable distribution on cross-sections of a part, which will increase the service life of steel parts. For solving these important problems, it is necessary to calculate temperature fields and residual stresses formed at quenching. These issues are considered in more detail in [4,61,62].

1.10 SELECTED CURRENT PROCESS EXAMPLES

A *rebar*, or reinforcing bar, is a common steel bar, often used in reinforced concrete and reinforced masonry structures. It is usually formed from low-carbon steel and is given ridges for better mechanical anchoring into the concrete (see Fig. 27(a)). It can also be described as reinforcement or reinforcing steel [63–65]. The resulting reinforced concrete or other material is an example of a composite material. The ASTM Standard Specification A706/A706M-96b for low-alloy-steel deformed

(a)

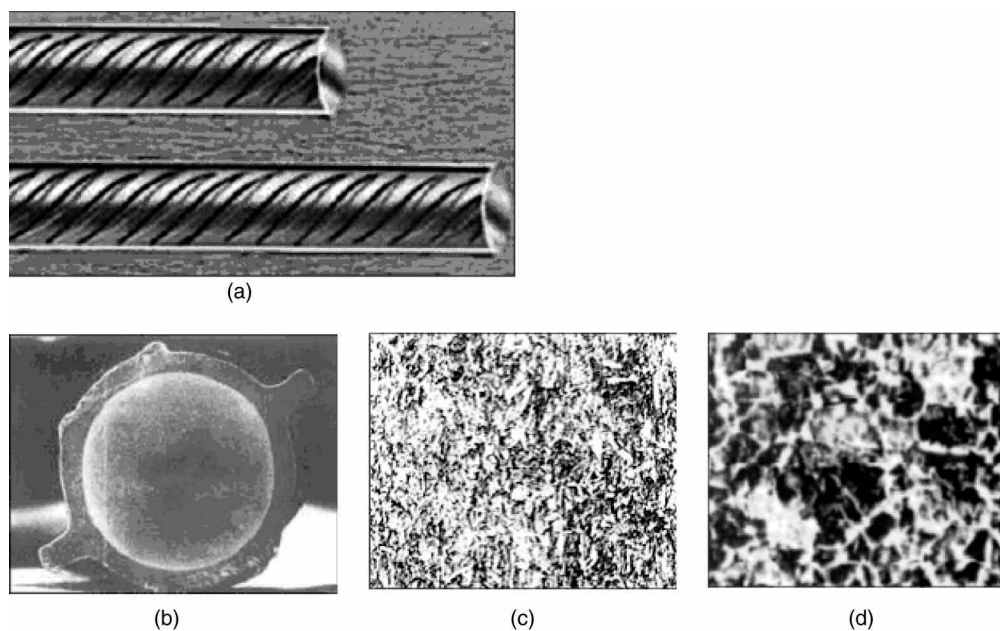(b)   (c)   (d)

Fig. 27—Use of the thermomechanical treatment combined with the interrupted intensive quenching for mass production of rebars [65]: (a) thermomechanically treated rebars; (b) microstructure through section of bar where a hardened layer is seen clearly; (c) tempered martensite in hardened layer; (d) ferrite-pearlite at the core of bar.

Fig. 28—High plastic and bending properties of rebars are achieved by combining thermomechanical treatment with the intensive quenching [65].

TABLE 12—Comparison of mechanical properties of rebars subjected to conventional treatment and thermomechanical treatment (TMT) combined with the interrupted intensive quenching process [65]

Rebar quality	Grade	Yield strength (MPa), min	UTS (MPa), min	Elongation (%), min
Conventional	Fe−500	500	545	14.5
TMT bars	Fe−500	550	630	18

and plain bars for concrete reinforcement can be found in [63]. The rebar should have high mechanical properties, fine microstructure (see Figs. 27c, 27d), and high plastic and bending properties (see Fig. 28).

A production process in bar mills where, directly after the last rolling stand, the bar passes through the cooling system that provides a short and intensive cooling of the surface is described in [64,65]. Since the reduction in temperature occurs at a rate higher than the critical rate for martensite quenching, the surface layer of the rebar is converted to a hardened structure forming a shell (see Fig. 27(b)), while the core remains austenitic, which then transforms to a ferrite-pearlite structure (see Fig. 27(d)) upon further cooling. The shell or rim of the bar possesses a fine tempered martensite structure (see Fig. 27(c)). Mechanical properties of the bar material are significantly improved compared with conventional manufacturing, as shown in Table 12 [65]. Note that the yield strength and ultimate strength are simultaneously improved, and increased plastic properties are also obtained (see Table 12 and Fig. 28). In addition, the bending properties of the rebars are considerably improved relative to those obtained by the conventional process of manufacturing [64,65].

It should be noted that optimizing the thermomechanical treatment and intensive quenching process and combining them together can significantly improve the existing mechanical and plastic properties of rebars and other products [66,67].

It has been shown that intensive quenching can produce many improvements for steel materials [68,69]. If material is subjected to thermomechanical treatment and intensively quenched, mechanical properties will be improved further than is shown in this chapter. More detailed information on interrupted intensive quenching for achieving optimal hardened layer in steel parts can be found in [68]. To successfully apply thermomechanical treatment combined with the intensive quenching in practice, further careful investigations are

needed in the field of heat transfer control during quenching and its mathematical descriptions [70,71].

1.11 SUMMARY

1. It is established on the basis of analyzing high-temperature thermomechanical treatment (HTMT) and low-temperature thermomechanical treatment (LTMT) that combining thermomechanical treatment with accelerated quenching significantly increases the mechanical and plastic properties of materials.
2. When correctly used, LTMT can be effectively applied to high-carbon steels by adjusting the surface temperature of steel parts during the self-regulated thermal process.
3. In some cases, intensive quenching of low-carbon alloy steels increases yield strength by 15 % and impact strength by 250 %. Intensive quenching results in additional material strengthening and creation of high surface compressive residual stresses. Both factors increase the service life of steel parts.
4. Combining HTMT, LTMT, and optimized intensive quenching, it is possible to manufacture high-strength materials using plain carbon steels.
5. It makes sense to optimize thermomechanical treatment and intensive quenching processes and combine them for mass production of rebars, tubes, fasteners, tools, and others products.
6. The optimal temperature for thermomechanical treatment is 900−930°C and optimal deformation is 25−35 %.
7. The high-strength materials are based on the formation of high dislocation density in material and formation of fine grains (microstructure). This can be done by very fast cooling within the martensite range, which seems to be equivalent to LTMT (see Chapter 9).

References

[1] Kobasko, N. I., *Steel Quenching in Liquid Media Under Pressure*, Naukova Dumka, Kyiv, 1980.
[2] Kobasko, N. I., and Prokhorenko, N. I., Effect of the Quenching Rate on the Formation of Cracks in Steel No. 45, *Metal Science and Heat Treatment*, Vol. 6, No. 2, 1964, pp. 104−105.
[3] Kobasko, N. I., Effect of Structural and Thermal Stresses upon Crack Formation at Steel Quenching, *Proceedings of the All-Union Conference on Increasing Productivity and Economy of Heating Furnaces*, Dnepropetrovsk, Ukraine, December 1967, pp. 26−27.
[4] Kobasko, N. I., Intensive Steel Quenching Methods, *Quenching Theory and Technology*, 2nd Ed., Liščić, B., Tensi, H. M., Canale, L. C. F., and Totten, G. E., Eds., CRC Press, New York, 2010.
[5] Kobasko, N. I., Morhuniuk W. S., and Ushakov, B. K., Design of Steel-Intensive Quench Processes, *Steel Heat Treatment: Equipment and Processes Design*, 2nd Ed., Totten, G. E., Ed., CRC Press, New York, 2007, pp. 193−237.
[6] Kobasko, N. I., The Steel Superstrengthening Phenomenon, Part 2, *Int. J. Microstructure and Materials Properties*, Vol. 3, No. 4/5, 2008, pp. 526−547.
[7] Ivanova, V. S., and Gordienko, L. K., *New Ways of Increasing Metal Strengthening*, Nauka, Moscow, 1964.
[8] Oding, I. A., Ivanova, V. S., Burdukskiy, V. V., and Geminov, V. N., *Theory of Yield and Long Durability of Metals*, Metallurgizdat, Moscow, 1959.
[9] Ivanova, V. S., Role of Dislocations in Strengthening and Failure of Metals, Nauka, Moscow, 1965.
[10] Prokhazka, Ya., Ways of Increasing the Yield of Metals and Alloys, *MiTOM* No. 10, 1973, pp. 65−72.
[11] Gridnev, V. N., Meshkov, Yu. A., Oshkaredov, S. P., and Chernenko, N. F., *Technological Basics of Electrical Heat Treatment of Steel*, Naukova Dumka, Kyiv, 1977.

[12] Ivanova, V. S., *Strength of Metals at Cyclic Loads,* Nauka, Moscow, 1967.

[13] Ivanova, V. S., and Terentiev, V. F., *Nature of Fatigue of Metals,* Metallurgiya, Moscow, 1975.

[14] Troschenko, V. T., *Methods of the Study of Metal Resistance to Distortion and Failure at Cyclic Loads,* Naukova Dumka, Kyiv, 1974.

[15] Bernshtein, M. L., *Termomekhanicheskaya obrabotka metallov i splavov* (Thermomechanical treatment of metals and alloys), 2 Vols., Moscow, Metallurgiya, 1968.

[16] Wikipedia, Thermomechanical Processing, http://en.wikipedia.org/wiki/Thermomechanical_processing, and other sections.

[17] Smith, J. L., Russol, G. M., and Bhatia, S. C., *Heat Treatment of Metals,* 2 Vols., Alkem Publishing Unit, Singapore, 2009.

[18] Gulyaev, A. P., *Metal Science,* Metallurgiya, Moscow, 1977.

[19] Shepelyakovskii, K. Z., *Machine Surface Strengthening by Quenching with Induction Heating,* Mashinostroenie, Moscow, 1972.

[20] Vol'nov, I. N., The Use of Kolmogorov's Kinetic Equations for the Description of Crystallization of Alloys, *Metal Science and Heat Treatment,* Vol. 42, No. 6, 2000, pp. 207−210.

[21] Kobasko, N. I., Secondary Intensive Cooling of Melted Materials for Getting Their Fine Microstructures, *Proceedings of the 6th IASME/WSEAS International Conference on Heat Transfer, Thermal Engineering and Environment (HTE '08),* Rhodes, Greece, August 20−22, 2008, pp. 539−542.

[22] Gulyaev, A. P., and Petunin, E. V., *Metalographic Studies of the Transformations of Austenite into Martensite,* Mashgiz, Moscow, 1952.

[23] Lysak, L. I., and Nikolin, B. I., *Physical Basics of Heat Treatment of Steel,* Tekhnika, Kyiv, 1975.

[24] Degarmo, E. P., Black, J. T., and Kohser, R. A., *Materials and Processes in Manufacturing,* 9th Ed., John Wiley & Sons, New York, 2003.

[25] Totten, G. E., Funatani, K., and Xie L., *Handbook of Metallurgical Process Design,* Marcel Dekker, New York, 2004.

[26] Callister, D. W. Jr., *Materials Science and Engineering: An Introduction,* 6th Ed., John Wiley & Sons, New York, 2003.

[27] Totten, G. E., and Howes, M. A. H., *Steel Heat Treatment Handbook,* Marcel Dekker, New York, 1997.

[28] Totten, G. E., Bates, C. E., and Clinton, N. A., *Handbook of Quenchants and Quenching Technology,* ASM International, Materials Park, OH, 1993.

[29] Ansell, I. S., Donachie, S. I., and Messler, R. W., The Effect of Quench Rate on the Martensitic Transformation in Fe-C Alloys, *Met. Trans.,* No. 2, 1972, pp. 2443−2449.

[30] Petrov, Yu. N., *Defects and Diffusion-Free Transformation in Steel,* Naukova Dumka, Kyiv, 1978.

[31] Kurdyumov, G. V., On Behavior of Carbon in Hardened Steel, *DMM,* Vol. 24, No. 5, 1967, pp. 909−917.

[32] Kurdyumov, G. V., Martensitic Transformations (Survey), *Metalophysics,* Vol. 1, No. 1, 1979, pp. 81−91.

[33] Yukio, H., Motozo, N., and Shigeharun, K., One Consideration on the Strengthening Mechanism of Steel, *Bull. Fac. Educ. Kanazawa Univ., Nat. Sci.,* No. 23, 1974, pp. 35−43.

[34] Grange, R. A., and Mitchell, I. B., *Metals Engineering Quarterly,* (No. 1), 1961, p. 41.

[35] Kula, E. B., and Lapata, S. L., *Trans. ASM,* Vol. 215, 1959, p. 73.

[36] Petrova, S. N., Sadovskyi, V. D., and Sokolkov, E. N., *Steel Strengthening,* Metallurgizdat, Moscow, 1960, p. 111.

[37] Reed-Hill, R. et al., *Physical Metallurgy Principles,* 3rd Ed., PWS Publishing, Boston, 1991.

[38] Kobasko, N. I., Self-Regulated Thermal Processes During Quenching of Steels in Liquid Media, *International Journal of Microstructure and Materials Properties,* Vol. 1, No. 1, 2005, pp. 110−125.

[39] Kobasko, N. I., Steel Superstrengthening Phenomenon, *Journal of ASTM International,* Vol. 2, No. 1, 2005.

[40] Toshiaki T., Grain Refinement by Thermomechanical Treatment of Gear and Bearing Steel for Automobile Applications, *Netsu Shori* (Journal Code: G0963A), Vol. 45, No. 6, 2006, pp. 358−362.

[41] Omotoyinbo, J. A., Oborunniwo, O. E., Ogunlare, O., and Ohwole, O. O., Strengthening of Alloy Steels by High Temperature Thermomechanical Treatment, *Journal of Applied Sciences Research,* Vol. 2, No. 8, 2006, pp. 484−485.

[42] Mazanec, K., and Mazancova, E., *Physical Metallurgy of Thermomechanical Treatment of Structural Steels,* Cambridge International Science Publishing, Cambridge, England, 1997.

[43] Cast Steel: Low and High Temperature Thermomechanical Treatments, *Key to Metals,* http://steel.keytometals.com/Articles/Art108.htm.

[44] Draper, J., *Modern Metal Fatigue Analysis,* EMAS, Warrington, England, 2008.

[45] Degarmo, E. P., Black, J. T., and Kohser, R. A., *Materials and Processes in Manufacturing* (9th ed.), Wiley, New York, 2003, p. 388.

[46] Shukyarov, R. I., and Paisov, I. V., Effect of Thermomechanical Treatment and Alloying on the Structure and Properties of Silicon Spring Steels, *Metal Science and Heat Treatment,* Vol. 8, No. 9, 1966, pp. 736−738.

[47] Gavranek, V. V., and Filippova, Z. K., The Stability of the Influence of High Temperature Thermomechanical Working on the Properties of 1Kh12VNMF Steel, *Metal Science and Heat Treatment,* Vol. 14, No. 2, 1972, pp. 128−130.

[48] Shukyarov, R. I., and Paisov, I. V., Effect of Thermomechanical Treatment and Alloying on the Structure and Properties of Silicon Spring Steels, *Metal Science and Heat Treatment,* Vol. 8, No. 9, 1966, pp. 736−738.

[49] Kobasko, N. I., Morhuniuk, W. S., and Dobrivecher, V. V. Control of Residual Stress Formation and Steel Deformation During Rapid Heating and Cooling, *Handbook of Residual Stresses and Deformation of Steel,* Totten, J., Howes, M., and Inoue, T., Eds., ASM International, Materials Park, OH, 2002.

[50] Dowling, Norman E., *Mechanical Behavior of Materials,* 2nd Ed., Prentice-Hall, Upper Saddle River, New Jersey, 1998.

[51] *Worldwide Guide to Equivalent Irons and Steels,* 4th Ed., Mack, W. C., Coordinating Ed., ASM International, Materials Park, OH, 2000.

[52] Aronov, M. A., Kobasko, N. I., Powell, J. A., and Young, J. Y., Practical Application of Intensive Quenching Technology for Steel Parts and Real Time Quench Tank Mapping, *Proceedings of 19th ASM Heat Treating Society Conference,* Cincinnati, OH, November 1−4, 1999.

[53] Kobasko, N. I., On New Ways of Steel Hardening Based on Intensification of Heat Transfer Within the Martensite Range, *Izvestiya AN USSR, Metals,* No. 1, 1979, pp. 146−153.

[54] Bogatyrev, Yu. M., Shepelyakovskii, K. Z., and Shklyarov, I. N., Effect of Cooling Rate upon Crack Formation at Steel Quenching, *MiTOM,* No. 4, 1967, pp. 15−22.

[55] Kobasko, N. I., Current and Residual Stresses During Quenching of Steel Parts, *Finite Elements,* Mastorakis, N. E., and Martin, O., Eds., WSEAS Press, Athens, 2007, pp. 86−99.

[56] Liščić, B., Tensi, H. M., and Luty, W., *A Handbook "Theory and Technology of Quenching,"* Springer-Verlag, Berlin, 1992, pp. 367−389.

[57] Shteinberg, M. M., *Heat Treatment of Steel,* Metallurgizdat, Moscow, 1945.

[58] Kobasko, N. I., Optimized Quenched Layer for Receiving Optimal Residual Stress Distribution and Superstrengthened Material, *3rd WSEAS International Conference on Applied and Theoretical Mechanics,* Spain, December 14−16, 2007, pp. 168−174.

[59] Freborg, A. M., Ferguson, B. L., Aronov, M. A., Kobasko, N. I., and Powell, J. A., Intensive Quenching Theory and Application for Impacting High Residual Surface Compressive Stresses in Pressure Vessel Components, *J. Pressure Vessel Technology,* Vol. 125, No. 2, 2003, pp. 188−195.

[60] Kobasko, N. I., Steel Quenching in Liquid Media Under Pressure, *Proceedings of the 4th WSEAS International Conference on Heat and Mass Transfer,* Gold Coast, Queensland, Australia, January 17−19, 2007, pp. 98−103.

[61] Kobasko, N. I., Energy Efficient and Eco-Friendly Intensively Quenched Limited Hardenability Low Alloy Steels, *Journal of ASTM International,* Vol. 6, No. 1, 2009.

[62] Kobasko, N. I., Quench Process Optimization for Receiving Super Strong Materials, *WSEAS Transactions on Systems,* Vol. 4, No. 9, September 2005, pp. 1394−1401.

[63] ASTM Standard Specification A706/A706M-96b for Low-Alloy-Steel Deformed and Plain Bars for Concrete Reinforcement.

[64] Gayal, J., Latest Developments on Steel Front, *Science Tribune,* January 28, 1999, http://www.tribuneindia.com/1999/99jan28/science.htm.

[65] Evo Tech Pvt Ltd., Thermomechanical Treatment for Reinforcement Bars Opening Up New Vistas, http://rajmarkan.tripod.com.

[66] U.S. Patent No. 6,458,226, Process for the Thermomechanical Treatment of Steel, filed on July 20, 1999, published on July 20, 2002.

[67] Nazarenko, V. R., Yankovskii, V. F., Dolginskaya, M. A., and Yakovenko, M. P. Damascus Steel: Myths and Reality, *Metal Science and Heat Treatment,* Vol. 34, No. 6, 1992, pp. 402−410.

[68] Kobasko, N. I., Quenching Apparatus and Method for Hardening Steel Parts, U.S. Patent No. 6,364,974 B1, April 2, 2002.

[69] Kobasko, N., Aronov, M., Powell, J., and Totten, G., One More Discussion: "What Is Intensive Quenching Process?", *Journal of ASTM International,* Vol. 6, No. 1, 2009.

[70] Vergana-Hernandez, H. J., and Hernandez-Morales, B., A Novel Probe Design to Study Wetting Kinematics During Forced Convective Quenching, *Experimental Thermal and Fluid Science,* Vol. 33, No. 5, 2009, pp. 797−807.

[71] Liščić, B., Heat Transfer Control During Quenching, *Materials and Manufacturing Processes,* Vol. 24, 2009, pp. 879−886.

2

Transient Nucleate Boiling and Self-Regulated Thermal Processes

N. I. Kobasko[1]

2.1 INTRODUCTION

The investigation of transient nucleate boiling is of great importance since knowledge of the laws of nucleate boiling processes are used to control phase transformations in metals. It is especially related to martensite transformations where the martensite start temperature M_S is comparable to the boiling temperature of the boundary liquid layer. Since the self-regulated thermal process has been introduced, which is the main part of transient nucleate boiling where wall temperature changes very slowly and is supported at approximately the same level up to the start single-phase convection, it makes sense to use this discovery to control phase transformation in steel. It is necessary to develop a generalized equation for determination of the duration of transient nucleate boiling process.

Note that pressure can shift boiling temperature to the martensite start temperature M_S, which may be used to control martensite phase formation. This is possible when the self-regulated thermal process is established. However, in practice, it is always difficult to determine the duration of transient nucleate boiling. This chapter describes a generalized equation for the determination of the time of transient nucleate boiling and the self-regulated thermal process, which do not differ significantly from each other. Calculation results obtained using the generalized equation agree well with the experimental data.

The generalized equation has been used to create intensive steel quenching technologies designated as IQ-1, IQ-2, and IQ-3 (see Chapter 10) and for proving the steel super-strengthening phenomenon (see Chapter 9). This chapter starts with the survey of nucleate boiling parameters and finishes with the practical application of the generalized equation for intensive technologies development.

2.2 BUBBLE PARAMETERS AND DYNAMICS

During intensive steel quenching, nucleate boiling and one-phase convection prevail, and therefore it is important to study their regularities. When IQ-2 technology is implemented, nucleate boiling prevails. With IQ-3 technology, the one-phase convection prevails, and there is neither film boiling nor nucleate boiling. The regularities of nucleate boiling processes are discussed in [1−7].

The inner characteristics (bubble dynamics) of the boiling process will be considered first. During the boiling process, the bubble departure diameter d_0 on a heated metal surface at atmospheric pressure is about 2.5 mm. When the pressure increases, value of d_0 decreases. Some parameters–bubble departure diameter, bubble release frequency, and vapor bubble growth rate–are presented in Tables 1 and 2.

When austenitized steels are immersed into a cold quenching bath, at the time of immersion, a boundary liquid boiling layer is formed. The boundary liquid layer is heated to the saturation (boiling) temperature, and at the same time the surface is intensively cooled. Then the liquid at the boundary layer starts to boil and a certain heat flux density is reached, which depends on the shape and size of the part to be quenched and the thermal conductivity of the material. Depending on the heat flux density, film boiling may occur or may be absent. If there is no film boiling, transient nucleate boiling is established where the heat flux density is reduced exponentially. It is important to determine the effect of heat flux density variation on the inner characteristics of boiling, in particular, multiplication of $d_0 f$. This multiplication $(d_0 f)$ is called vapor bubble growth rate and designated by $\overline{W}''$, that is,

$$\overline{W}'' = d_0 f. \tag{1}$$

Tolubinsky [1] showed that the effect of heat flux density varied by four or five times with the average value of $\overline{W}''$.

The average vapor bubble growth rate $\overline{W}''$ is affected by pressure. Fig. 1 shows the relationship of $\frac{\overline{W}''}{W''_{0.1}}$ versus pressure. The value of $W''_{0.1}$ is vapor bubble growth rate at normal pressure; W'' is the vapor bubble growth rate at a higher pressure. As the pressure increases, the ratio of $\left(\frac{W''}{W''_{0.1}}\right)$. abruptly decreases (see Fig. 1).

It is of practical interest to understand the effect of aqueous salt solution concentrations on the inner characteristics of the nucleate boiling process, including the bubble dispatch diameter, dispatch frequency, and their multiplication, the steam bubble growth rate W''. Experimental results obtained with boiling solutions of sodium chloride (NaCl) and sodium carbonate (Na_2CO_3) at normal pressure are presented in Table 3.

Table 3 shows that in the case of boiling of high-concentration solutions of sodium chloride and sodium carbonate, the vapor bubble growth rates are the same as for water. Vapor bubble growth rate for boiling aqueous solutions is determined by properties of the solvent (water) and its vapor pressure and is only very weakly affected by properties of the dissolved substances, viscosity, and Prandtl number of the solution [1]. Therefore, the value of W'' for boiling aqueous solutions can be considered to be equal to W'' for boiling water.

Unfortunately, there are no data for optimal concentrations of aqueous solutions (10−12 %) where the most

---

[1] *IQ Technologies, Inc., Akron, Ohio, and Intensive Technologies Ltd., Kyiv, Ukraine*

TABLE 1—Bubble departure diameter and bubble release frequency versus pressure [1]						
		Pressure (MPa)				
Substance	Boiling parameters	0.02	0.05	0.08	0.1	
Water at 100°C (212°F)	d_0 (mm)	13.3	5.4	2.9	2.3	
	f (Hz)	22	43	66	67	
	$d_0 f$ (m/s)	0.293	0.232	0.192	0.154	
Aqueous sugar solution at 100°C (212°F) (70–72 %)	d_0 (mm)	8.3	3.7	2.2	2.0	
	f (Hz)	31	55	79	76	
	$d_0 f$ (m/s)	0.257	0.204	0.174	0.152	
Note: d_o is diameter of bubble in mm; f is frequency of bubble in Hertz; $d_0 f$ is vapor bubble growth rate in m/s						

TABLE 2—Effect of pressure upon the average vapor bubble growth rate $\overline{W}''$ at the saturation point [1]

Pressure (MPa)	0.1	0.2	0.3	0.4	1.0
$\overline{W}''$ (m/s)	0.155	0.0775	0.059	0.0465	0.022

TABLE 3—Comparison of parameters of boiling process for water and aqueous salt solutions at normal pressure

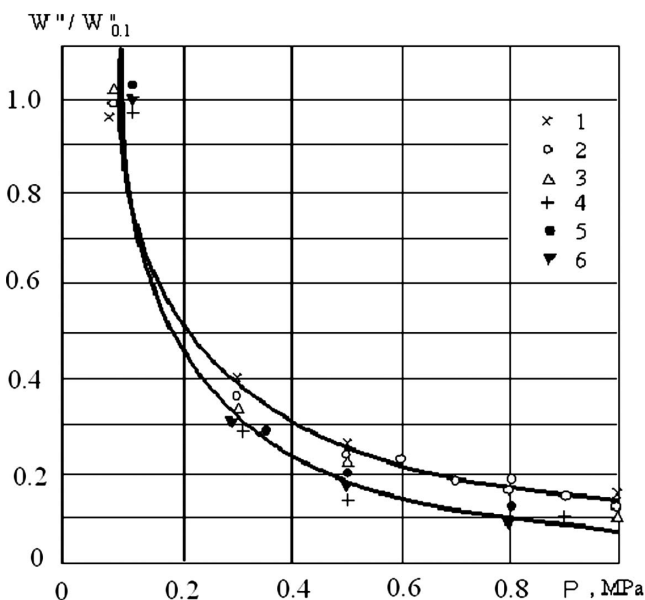| Substance	d_0 (mm)	f (Hz)	W'' (m/s)
Water	2.5	62	0.155
25 % NaCl solution	2.4	64.5	0.155
29 % Na_2CO_3 solution	2.4	65	0.156

Fig. 1—Effect of pressure upon the average vapor bubble growth rate at boiling of water (1–3) and ethyl alcohol (4–6) on the surface of different materials: 1 and 4, permalloy; 2 and 5, brass; 3 and 6, copper [1].

uniform intensive cooling is achieved. For these concentrations, the effect can be determined from the double electric layer, which changes the surface tension of liquid at the surface layer [2].

2.2.1 Surface Properties

The material surface properties, to some extent, affect the average value bubble departure diameter d_0 and bubble release frequency f (see Table 4). However, while d_0 changes, corresponding changes occur in the opposite direction with respect to the bubble release frequency f.

In numerous experiments [1], it has been noted that for the overwhelming majority of vapor bubbles formed at that surface, greater frequency corresponds to lower departure diameter at which the value of W'' is kept constant. Therefore, the average value of $\overline{W}'' = d_0 f$ is a characteristic value for a liquid and its vapor.

Thus far, we have introduced some parameters for boiling water and aqueous solutions related to vapor bubble departure diameter, bubble release frequencies, and average vapor bubble growth rate W''. It is also of practical interest to evaluate overheating of the boundary liquid layer. The effect of temperature on the thickness of the boundary layer at constant heat flux densities was first reported by Jacob and Fritz [1]. Typical profiles of temperature distributions are presented in Fig. 2, which shows that there is no large overheating of the liquid within the thickness of the boundary layer.

Oscillations (pulsations) of the temperature in the boundary layer are also important [1,3]. When the total temperature difference is $T_{Sf} - T_S = 9K$, the amplitude $T_{max} - T_{min}$ of temperature oscillations in this layer achieves is $\geq 5K$. Fig. 3

TABLE 4—Effect of heated surface material on bubble departure diameter and release frequency in the case of boiling water at normal pressure

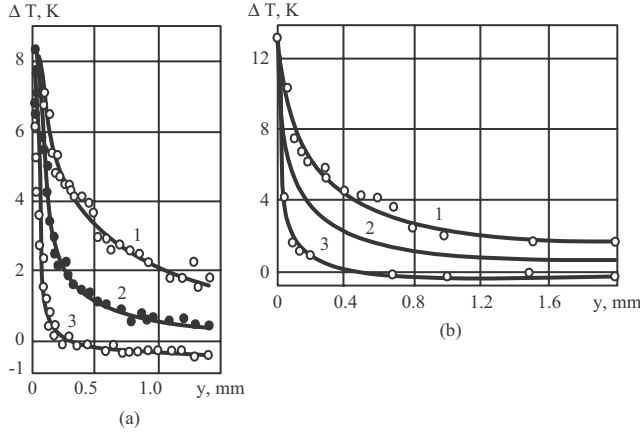| Material	d_0 (mm)	f (Hz)	W'' (m/s)
Permanite	2.5	61	0.153
Brass	2.3	67	0.157
Copper	2.8	56	0.157
Average	2.5	62	0.155

Fig. 2—Temperature profile at the boundary water boiling layer: 1, maximum; 2, average; and 3, minimum values of overheating [4].

illustrates changes of temperature and temperature oscillations by thickness y of a water boundary layer.

Temperature oscillations are caused by growth of the bubbles [1,4]. When nucleate boiling of liquid occurs, large temperature oscillations also occur at the heat transfer surface and at boundary layer of the boiling liquid. Temperature oscillations of the heated surface when boiling occurs at single centers are shown in Fig. 4.

Overheating in the boundary layer is greater when the heat flux is moving to the boiling liquid. When the liquid overheat $\Delta T = T_{Sf} - T_S$ increases, the number of nucleating centers also increases.

According to Tolubinsky [1], the number n of nucleating sites increases in direct proportion to the cube of the temperature difference:

$$n_s \sim \Delta T^3. \qquad (2)$$

It is also well known that the average heat flux density during nucleate boiling, too, is proportional to the cube of temperature difference:

$$q \sim \Delta T^3. \qquad (3)$$

Tolubinsky has reported that the average heat flux density per one nucleating center, in the case of full nucleate boiling, is constant [1]:

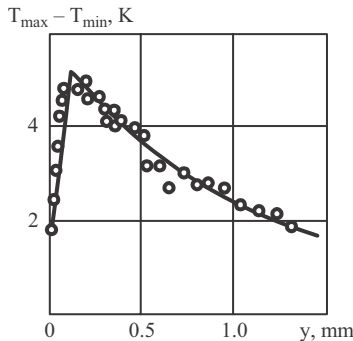$$q_0 = \frac{q}{n} \cong const. \qquad (4)$$

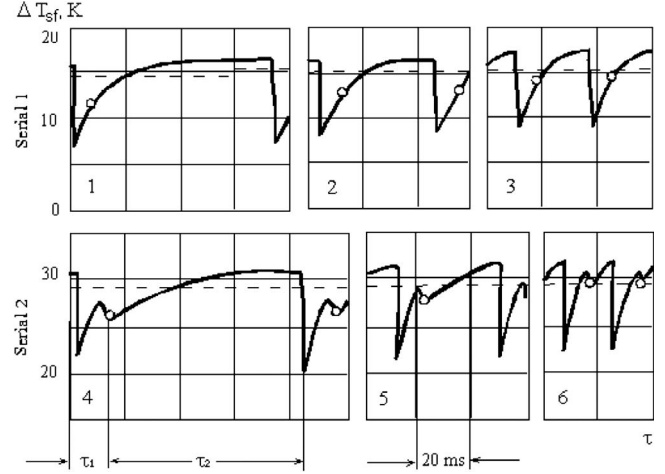Fig. 3—Amplitude of liquid temperature oscillations ($T_{\max} - T_{\min}$) in the boundary liquid layer [4].

Fig. 4—Oscillations of the surface temperature in the case of boiling at single centers: 1, q = 0.25 MW/m²; 2, q = 0.30 MW/m²; 3, q = 0.43 MW/m²; 4, q = 0.46 MW/m²; 5, q = 0.65 MW/m²; 6, q = 0.88 MW/m². The dashed line indicates the surface overheating average in time surrounding the nucleating center [1].

This is the basis for the ($d_0 f$) of bubble departure diameter d_0 and bubble release frequency f, which has been obtained from the experiments and is the main value for heat transfer evaluation during nucleate boiling process.

As the heat flux density q increases, overheat $\Delta T = T_{Sf} - T_S$ of the boundary layer also increases, and new nucleating centers are activated. Average characteristics d_0, f, and $\overline{W}''$ are reasonably stable with respect to changing heat flux density and contribute to the average vapor bubble growth rate, which does not depend on q.

It is customary to consider that the measure of heat transfer intensity during boiling is given by

$$\alpha\left(\frac{W}{m^2 K}\right). \qquad (5a)$$

The coefficient α is:

$$\alpha = q/\Delta T, \qquad (5b)$$

where q is the heat flux density (W/m²); and ΔT is wall overheat in (K).

This expression for α follows from the heat transfer equation for boiling, written in the form of Newton's law of cooling. The value of α is called a *heat transfer coefficient*. However, during convection, it is assumed that ΔT is the difference between the temperature of a wall and the quenchant temperature. During boiling, this is a difference between the surface temperature of a body and the saturation (boiling) temperature of the quenchant. The heat transfer coefficient is the quantity of heat removed from a unit of a surface area per one degree.

It is important to relate the heat flux density during boiling to the difference $\Delta T = T_{Sf} - T_S$, instead of difference $\Delta T = T_{Sf} - T_m$, as it is done during the convection, where T_{Sf} is the temperature of a wall (a surface to be cooled); T_S is a saturation temperature; and T_m is the temperature of the medium (quenchant). Therefore, formation of nucleating centers depends on the overheat of a boundary layer, which is determined by:

$$R_{cr} \cong \frac{2\sigma T_S}{r^* \rho'' \Delta T}, \qquad (6)$$

where:

R_{cr} is a critical size of a bubble which is capable to grow and function;

σ is surface tension (N/m);

T_S is a saturation (boiling) temperature (K);

r^* is latent heat of evaporation (J/kg);

ρ'' is vapor density (kg / m^3); and

$\Delta T = T_{Sf} - T_m$ is wall overheat.

Active nucleating centers are the basic carriers that remove heat from a surface and transfer it to a cooler bath, as explained by Dhir [2, p. 372]: After initiation, a bubble continues to grow (in a saturated liquid) until forces cause it to detach from the surface. After departure, cooler liquid from the bulk fills the space vacated by the bubble, and the thermal layer is re-formed. When the required superheat is attained, a new bubble starts to form at the same nucleation site. Bubble dynamics include the processes of growth, bubble departure, and bubble release frequency, which includes time for reformation of the thermal layer (induction period). The bubble acts like a pump, removing hot liquid from the surface and replacing it with cooler liquid. This mechanism is the essential factor causing the high intensity of heat transfer during boiling, and the bath temperature essentially has no effect [1,2]. Therefore, it is necessary for the heat flux density during boiling to relate to a difference of $T_{Sf} - T_S$, but not to $T_{Sf} - T_m$, which can lead to large errors since

$$T_{Sf} - T_S << T_{Sf} - T_m.$$

These calculations were conducted at the saturation temperature of a liquid. However, it is important to determine the effect of underheat on the inner characteristics of the boiling process. *Underheat* is defined as a difference in temperatures between the saturation temperature and the bath temperature (bulk temperature):

$$\Delta T_{uh} = T_S - T_m. \tag{6}$$

The effect of underheat on the maximum diameter $d_{\max}$ of bubbles and their departure frequency f, and also on the average vapor bubble growth rate $\overline{W}''$ during boiling of underheated water at normal pressure, is shown in Fig. 5.

From Fig. 5, when underheating increases, the bubble departure diameter decreases and the release frequency increases. The average growth rate of vapor bubbles also increases. All of these facts are probably also true for partial nucleate boiling. Shock boiling and developed nucleate boiling close to transition boiling have, as yet, not been exhaustively studied.

When pressure increases, the bubble departure diameter, bubble release frequency, and average vapor bubble growth rate decrease (see Fig. 6).

These characteristics will be used for the computation of temperature fields during steel quenching.

Tolubinsky obtained the following generalized equation for the calculation of a heat transfer coefficient during nucleate boiling:

$$Nu = 75K^{0.7} \, Pr^{-0.2}, \tag{7}$$

where:

$Nu = \frac{\alpha}{\lambda} \sqrt{\frac{\sigma}{g(\rho'-\rho'')}}$ is the Nusselt criterion (number);
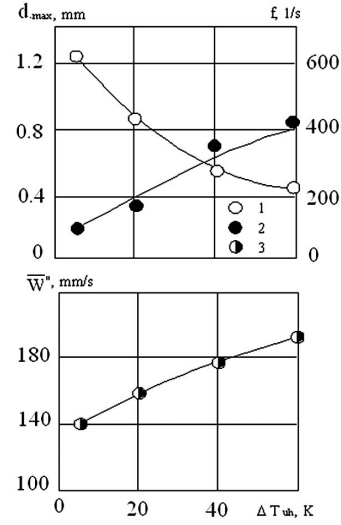
$Pr = \frac{v}{a}$ is the Prandtl number;

Fig. 5—The effect of underheat upon the maximal diameter $d_{\max}$ (1), bubble release frequency f (2), and average vapor bubble growth rate $\overline{W}''$ (3) at boiling of underheated water (P = 0.1 MPa) [1].

α is the heat transfer coefficient during nucleate boiling (W/m^{2}K);

λ is the heat conductivity of the liquid (W/mK);

σ is the surface tension (N/m);

g is gravitational acceleration (m/s^2);

ρ' is liquid density (kg/m^3);

ρ'' is vapor density (kg/m^3);

q is heat flux density (W/m^2);

r^* is latent heat of evaporation (J/kg);

W'' is vapor bubble growth rate (m/s);

v is kinematic viscosity (m^2/s); and

a is thermal diffusivity of liquid (m^2/s).

In the expanded form, Eq 7 can be rewritten as follows:

$$\frac{\alpha}{\lambda}\sqrt{\frac{\sigma}{g(\rho'-\rho'')}} = 75 \cdot \left(\frac{q}{r^*\rho''w''}\right)^{0.7}\left(\frac{a}{v}\right)^{0.2}. \tag{8}$$
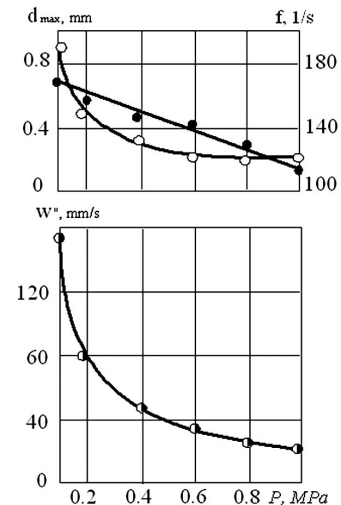

Fig. 6—The effect of pressure upon bubble parameters at boiling of underheated water (ΔT_{uh} = 20K): solid dots indicate bubble departure frequency; open dots show bubble departure diameter; lower graph plots vapor bubble growth [1].

No.	Authors	Equation	Coefficient β at pressure of 1 bar	Source
1.	V. P. Isachenko, V. A. Osipova, and A. S. Sukomel	$\alpha = 3q^{0.7}p^{0.15}$	3	[6]
2.	D. A. Labuntsov	$\alpha = \dfrac{3.4p^{0.18}}{1 - 0.0045p}\, q^{2/3}$	3.41	[5]
3.	D. A. Labuntsov	$\alpha = b\left(\dfrac{\lambda^2}{v\sigma T_S}\right)^{1/3} q^{2/3}$, $b = 0.075\left[1 + 10\left(\dfrac{\rho''}{\rho' - \rho''}\right)^{2/3}\right]$	3.39	[5]
4.	S. S. Kutateladze	$\alpha = \beta q^{0.673}$	4.3	[7]

TABLE 5—Equations obtained by different authors for the computation of heat transfer coefficients α during nucleate boiling and value β

Note: α is the heat transfer coefficient in W/m²K; q is heat flux density in W/m²; p is pressure in bars; β is the coefficient of the equation $\alpha = \beta q^n$; λ is the heat conductivity of liquid in W/mK; ρ'' is vapor density in kg/m³; ρ' is liquid density in kg/m³; σ is surface tension in N/m; v is kinematic viscosity of liquid in m²/s; and T_s is saturation temperature in K.

Therefore, the heat transfer coefficient during nucleate boiling is easily determined from:

$$\alpha = 75\lambda\left[\frac{g(\rho' - \rho'')}{\sigma}\right]^{0.5}\left(\frac{a}{v}\right)^{0.2}\left(\frac{1}{r^*\rho''w''}\right)^{0.7}\cdot q^{0.7}. \quad (9)$$

At constant temperature and constant pressure, the physical properties of the cooling medium are constant. Therefore, Eq 9 becomes:

$$\alpha = Cq^{0.7}, \quad (10)$$

where:

$$C = 75\lambda\left[\frac{g(\rho' - \rho'')}{\sigma}\right]^{0.5}\left(\frac{a}{v}\right)^{0.2}\left(\frac{1}{r^*\rho''w''}\right)^{0.7}.$$

From Eq 10, it follows that the heat transfer coefficient during nucleate boiling is proportional to the heat flux density to a power of 0.7. These results will now be compared with the results of other authors.

It is well known that, during nucleate boiling, the relationship between α and q can be presented as an exponential function with the exponent of about 2/3:

$$\alpha = cq^{2/3}. \quad (11)$$

Accordingly, the function ΔT of q is determined from:

$$\Delta T = \frac{1}{c}q^{1/3}, \quad (12)$$

or

$$q = c^3(\Delta T)^3. \quad (13)$$

Thus, the heat flux density is proportional to the temperature difference (wall overheat) raised to the third power. It follows that insignificant overheating of a boundary layer results in a sharp increase of heat flux density, and insignificant reduction of the overheat of the boundary layer, conversely, sharply reduces the heat flux density. Therefore, during nucleate boiling, the surface temperature does not change significantly.

The equation for the determination of the heat transfer coefficient during nucleate boiling when water is heated to the saturation temperature is [5]:

$$\alpha = \frac{3.4\, p_S^{0.18}}{1 - 0.0045\, p_S}\, q^{2/3}, \quad (14)$$

where p_S is pressure in bar and q is heat flux density in W/m².

These results illustrate the similarity between the Tolubinsky equation (Eq 10) and Eqs 11 and 14. According to Tolubinsky, the exponent is equal to 0.7 [1]. It should be noted that the heat transfer coefficient during nucleate boiling is determined with accuracy of ±25 % [1].

In general, a correlation has been established between the heat transfer coefficient and the heat flux density that can be written as $\alpha = \beta q^n$. These types of correlations are presented in Table 5. The value β and thermal properties are provided by Tables 6, 7, and 8.

Using these data, the boundary conditions to be used for steel quenching may be determined. It is known that boundary conditions of the third kind can be presented as:

$$\lambda\frac{\partial T}{\partial r}\bigg|_{r=R} + \alpha(T_{Sf} - T_S) = 0, \quad (15)$$

where:
λ is the thermal conductivity of steel; and

$\dfrac{\partial T}{\partial r}$ is a gradient of temperature at the surface.

TABLE 6—Coefficient β (the coefficient of the equation $\alpha = \beta q^n$) versus pressure

Equation number	Pressure (MPa)				
	0.1	0.2	0.3	0.4	1.0
No. 2 from Table 5	3.41	3.890	4.20	4.44	5.39
No. 1 from Table 5	3	3.329	3.537	3.693	4.238

Note: Atmospheric pressure is equal to 0.1013 MPa.

TABLE 7—Physical properties of water

T (°C)	$P \cdot 10^{-5}$ (Pa)	ρ (kg/m³)	c_p (kJ/kgK)	λ(W/mK)	$a \cdot 10^8$ (m²/s)	$\mu \cdot 10^6$ (Pa·s)	$v \cdot 10^6$ (m²/s)	$\beta' \cdot 10^4$ (1/K)	$\sigma \cdot 10^4$ (N/m)	Pr
0	1.013	999.9	4.212	0.560	13.2	1,788	1.789	−0.63	756.4	13.5
10	1.013	999.7	4.191	0.580	13.8	1,306	1.306	+0.70	741.6	9.45
20	1.013	998.2	4.183	0.597	14.3	1,004	1.996	1.82	726.9	7.03
30	1.013	995.7	4.174	0.612	14.7	801.5	0.805	3.21	712.2	5.45
40	1.013	992.2	4.174	0.627	15.1	653.3	0.659	3.87	696.5	4.36
50	1.013	988.1	4.174	0.640	15.5	549.4	0.556	4.49	676.9	3.59
60	1.013	983.1	4.179	0.650	15.8	469.9	0.478	5.11	662.2	3.03
70	1.013	977.8	4.187	0.662	16.1	406.1	0.415	5.70	643.5	2.58
80	1.013	971.8	4.195	0.669	16.3	355.1	0.365	6.32	625.9	2.23
90	1.013	965.3	4.208	0.676	16.5	314.9	0.326	6.95	607.2	1.97
100	1.013	958.4	4.220	0.684	16.8	282.5	0.295	7.52	588.6	11.75
110	1.43	951.0	4.233	0.685	17.0	259.0	0.272	8.08	569.0	1.60
120	1.98	943.1	4.250	0.686	17.1	237.4	0.252	8.64	548.4	1.47
130	2.70	934.8	4.266	0.686	17.2	217.8	0.233	9.19	528.8	1.35
140	3.61	926.1	4.287	0.685	17.2	201.1	0.217	9.72	507.2	1.26
150	4.76	917.0	4.313	0.684	17.3	186.4	0.203	10.3	486.6	1.17
160	6.18	907.4	4.346	0.681	17.3	173.6	0.191	10.7	466.0	1.10
170	7.92	897.3	4.380	0.676	17.2	162.8	0.181	11.3	443.4	1.05
180	10.03	886.9	4.417	0.672	17.2	153.0	0.173	11.9	422.8	1.03
190	12.55	876.0	4.459	0.664	17.2	144.2	0.165	12.6	400.2	0.965
200	15.55	863.0	4.505	0.658	17.0	136.4	0.158	13.3	376.7	0.932

Note: P is pressure in Pa; ρ is liquid density in kg/m³; c_p is specific heat capacity of liquid in kJ/(kgK); λ is heat conductivity of the liquid in W/mK; Pr = v/a is the Prandtl number; v is kinematic viscosity in m²/s; a is thermal diffusivity of liquid in m²/s; μ is dynamic viscosity in Pa·s; and β' is the coefficient of volume expansion.

TABLE 8—Properties of water vapor at the saturation temperature

T (°C)	$P \cdot 10^{-5}$ (Pa)	ρ'' (kg/m³)	r^* (kJ/kg)	c_p (kJ/kgK)	$\lambda \cdot 10^2$(W/mK)	$a \cdot 10^8$ (m²/s)	$\mu \cdot 10^6$ (Pa·s)	$v \cdot 10^6$ (m²/s)	Pr
100	1.013	0.598	2,256.8	2.135	2.372	18.58	11.97	20.02	1.08
110	1.43	0.826	2,230.0	2.177	2.489	13.83	12.46	15.07	1.09
120	1.98	1.121	2,202.8	2.206	2.593	10.50	12.85	11.46	1.09
130	2.70	1.496	2,174.3	2.257	2.686	7.072	13.24	8.85	1.11
140	3.61	1.966	2,145.0	2.315	2.791	6.130	13.54	6.89	1.12
150	4.76	2.547	2,114.3	2.395	2.884	4.728	13.93	5.47	1.16
160	6.18	3.258	2,082.6	2.479	3.012	3.722	14.32	4.39	1.18
170	7.92	4.122	2,049.5	2.583	3.128	2.939	14.72	3.57	1.21
180	10.03	5.157	2,015.2	2.709	3.268	2.339	15.11	2.93	1.25
190	12.55	6.397	1,978.8	2.856	3.419	1.872	15.60	2.44	1.30
200	15.55	7.862	1,940.7	3.023	3.547	1.492	15.99	2.03	1.36

Note: ρ'' is density of vapor in kg/m³; r^* is latent heat of evaporation in kJ/kg; other units defined in notes for Table 7.

To determine the heat transfer coefficient during nucleate boiling, Tolubinsky's equation (Eq 8) is substituted into Eq 15. In this case, boundary conditions of Eq 15 will be set in the following form:

$$\left[\frac{\partial T}{\partial r} + \frac{\beta^m}{\lambda}(T - T_S)^m\right]\Bigg|_{r=R} = 0, \qquad (16)$$

where $m = 3.33$ for Tolubinsky's equation and $m = 3$ for the Labuntsov equation [5]. In the boundary conditions of Eq 16, the value of β has the following form:

$$\beta = \frac{75\lambda'(\rho' - \rho'')^{0.5}g^{0.5}}{\sigma^{0.5}(\rho''r^*\overline{w}'')^{0.7}\Pr^{0.2}}. \qquad (17)$$

(Table 6 presents values of β for different equations.) Eq 17 was obtained from Tolubinsky dimensionless correlation by the replacement of q with

$$\alpha(T_{Sf} - T_S).$$

It is possible to do this procedure using Eq 11:

$$\alpha = c\left[\alpha(T_{Sf} - T_S)\right]^{2/3}$$

or

$$\frac{\alpha}{c} = \alpha^{2/3}(T_{Sf} - T_S)^{2/3}.$$

It follows that:

$$\alpha = c^3(T_{Sf} - T_S)^2. \qquad (18)$$

Substituting the found value (from Eq 18) to boundary conditions of the third kind in Eq 15:

$$\frac{\partial T}{\partial r}\Bigg|_{r=R} = \frac{c^3}{\lambda}(T_{Sf} - T_S)^3 = 0. \qquad (19)$$

Thus, the boundary conditions during nucleate boiling are given by:

$$\frac{\partial T}{\partial r}\Bigg|_{r=R} + \frac{\beta^m}{\lambda}(T_{Sf} - T_S)^m = 0, \qquad (20)$$

where $3 < m < 3.33$.

It is very important to determine these boundary conditions, since it is practically impossible to measure the surface temperature during nucleate boiling because:

1. There is little change of temperature within the limits of accuracy of measurement results with respect to the change of heat flux density that affects the intensity of steel cooling.
2. While the accuracy of experimental measurements increases, there are other difficulties associated with the fluctuation of surface temperatures during nucleate boiling. In this case, it is necessary to use a statistical approach, which consumes additional expense and time.
3. During transition boiling, local film boiling occurs, which complicates three-dimensional problems for determination of heat transfer coefficients.

Therefore, the statement of boundary conditions based on careful study of parameters and dynamics of bubbles during nucleate boiling is of significant practical interest for solving problems of transient heat conductivity. It is also important to have boundary conditions for the determination of time transient nucleate boiling.

In the boundary conditions of Eq 16, most important is value β, which depends on physical properties of the quenching medium. Tables 7 and 8 provide physical properties of a liquid and vapor, depending on temperature.

The vapor bubble growth rate depends on pressure and underheat of the liquid medium. Tolubinsky's empirical correlation for the determination of vapor bubble growth rate at higher pressures is:

$$\frac{W''}{W''_{0.1}} = \left(\frac{\rho_{0.1}}{\rho''}\right)^{2.3+0.5\lg\frac{P}{P_{cr}}}, \qquad (21)$$

where:
W'' is bubble growth at current pressure;
$W''_{0.1}$ is bubble growth rate at normal pressure;
$\rho''_{0.1}$ is vapor density at normal pressure (kg/m³);
ρ'' is vapor density at current pressure (kg/m³);
ρ_{cr} is critical pressure; and
P is the pressure at which the steam bubble growth rate is determined.

2.3 HEAT TRANSFER DURING STEEL QUENCHING

Typically, steel parts are quenched in cold quenchants, and for intensive quenching it is assumed that there is no film boiling. This condition is achieved by reducing the quenchant temperature, using aqueous salt solutions at optimal concentrations, and creation of intensive jets and water flow during quenching.

Consider the process of quenching when a part is immersed into a cold quenchant. At the time of immersion into the cold quenchant, a boundary boiling layer is formed and its formation can be divided into several stages:

1. During the first stage, the cold liquid is heated to the saturation temperature. The surface of a metal at this time is cooled significantly, and the surface temperature drops rapidly.
2. During the second stage, the boundary layer is overheated, and nucleating centers of vapor formation are created. At the surface layer of the metal, a significant temperature gradient is established.
3. During this last stage, the surface of the metal becomes completely covered by tiny vapor bubbles (shock boiling starts). Additional cooling of the steel can proceed by different pathways.

If vapor bubbles have completely covered the surface of metal and heat flux density inside of the heater increases, then film boiling begins. The maximum heat flux density at which there is transition of bubbles in a continuous vapor film is called the *critical heat flux density*. If the heat flux density is less than the critical value, then, after the formation of a boundary liquid boiling layer, nucleate boiling is established. If the heat flux density is close to the critical value, then the transition mode of boiling is initiated, where localized vapor films are formed on the surface; this is undesirable, since it is associated with nonuniform hardness distribution and distortion.

Critical heat flux densities are considered in detail in Chapter 3. There are actually two critical heat flux densities. The first is a transition from nucleate boiling to film boiling. The second is a transition from full film boiling back to nucleate boiling. Between the first and second critical heat flux densities, there is a well-known correlation [6,7]:

$$\frac{q_{cr1}}{q_{cr2}} \approx 0.2, \qquad (22)$$

where:

q_{cr1} is the first critical heat flux density (W/m^2); and
q_{cr2} is the second critical heat flux density (W/m^2).

This dependence is very important and widely used for the computation of temperature fields for steel quenching in liquid media.

In most cases, steel parts are heated up to the austenization temperature of the steel, higher than A_{C3} temperature. In this case, the temperature field is uniform, since all points within the part are at the furnace temperature T_0. Upon immersion into the cold quenchant, the boundary liquid layer is formed. When compared to the duration of quenching process, the formation of the boundary layer is very short, and its duration in many cases can be neglected. What is most important is not the time for formation of the boundary liquid boiling layer, but the process of further cooling that can proceed with or without film boiling. These processes are completely different, and their development depends on events during the initial period of time. Therefore, the study of the processes occurring at the initial period of time are extremely important.

Assume that there is no film boiling and the main cooling process is nucleate boiling followed by single-phase convection. The mathematical model for computation of the temperature fields for steel quenching when there is no film boiling and nucleate boiling prevails has the form:

$$C\rho\frac{\partial T}{\partial r} + div(\lambda\,grad\,T) = 0, \qquad (23)$$

$$\left[\frac{\partial T}{\partial r} + \frac{\beta^m}{\lambda}(T - T_S)^m\right]_S = 0, \qquad (24)$$

$$T(r,0) = T_0. \qquad (25)$$

Boundary conditions in Eq 24 can be also obtained using approximate equations (see Table 5). At the establishment of single-phase convection, these boundary conditions are the normal boundary conditions of the third kind:

$$\left[\frac{\partial T}{\partial r} + \frac{\alpha_{conv}}{\lambda}(T - T_m)\right]_S = 0. \qquad (26)$$

Initial conditions include temperature distribution of the cross-section after nucleate boiling, which can be shown as:

$$T(r, \tau_{nb}) = \varphi(r), \qquad (27)$$

where:

α_{conv} is the heat transfer coefficient during convection;
r is a radius of a cylinder or a sphere, and $r = x$ for a plate;
τ_{nb} is time of transient nucleate boiling;
$\phi(r)$ is the temperature field of the cross-section at the time of completion of nucleate boiling; and
T_m is bulk temperature.

It should be noted that $T_m < T_S$, where T_S is a saturation temperature of the quenchant in a boundary liquid layer.

The time of transition from nucleate boiling to the single-phase convection is determined from:

$$q_{nb} \cong q_{conv}, \qquad (28)$$

where:

q_{nb} is the heat flux density at the conclusion of nucleate boiling; and
q_{conv} is heat flux density at the beginning of convection.

For the approximate analytical solution of this problem, a method of variational calculus will be used [8]. The process of cooling is divided into two stages. The first stage is an irregular thermal process. Minimizing functions are built on the basis of laws of calculus of variations. The solution found will satisfy Eqs 23 and 24. The method of solving this problem is described below [9–12].

2.4 ANALYTICAL SOLUTION TO THERMAL PROBLEMS RELATED TO STEEL QUENCHING
2.4.1 Statement of the Problem

In the process of heating and cooling of steel parts (heat treatment technology), new structures and mechanical properties of material are formed [1,13]. The selection of optimal conditions for heat treatment of metals is impossible without the computation of temperature fields, which are necessary to predict structural and thermal stresses. When there is a wide range of different parts being heat-treated, the use of numerical methods is even more difficult because of the time and expense involved, especially for parts with a complex configuration. In these cases, approximate solutions are often utilized. Therefore, it is important to develop approximate analytical methods to facilitate the calculations of temperature fields encountered during quenching.

The mathematical model describing the heat transfer during quenching is [8]:

$$C_V(T)T_\tau = div[\lambda(T)\vec{\nabla}T] + q_V(T), \quad \tau > 0, \qquad (29)$$

$$T(x,0) = f(x), \quad x \in D, \qquad (30)$$

$$\left[\lambda(T)\frac{\partial T}{\partial\vec{n}} + F(T)\right]_S = 0, \quad x \in S, \qquad (31)$$

where:

$C_V(T)$ is volumetric heat capacity;
$\lambda(T)$ is thermal conductivity;
$\vec{n}$ is outer normal;
S is the surface surrounding area D;
$q_V(T)$ is the density of internal heat sources; and
$F(T)$ is the heat flux density at the surface.

The system of equations 29–31 describes both heating and cooling processes. During heating, $F(T)$ is a total heat flux density due to processes of radiation, convection, and heat transfer and during cooling, processes of boiling and convection.

2.4.2 Statement of the Variational Problem

The variational problem equivalent to problem of Eqs 29–31 is a universal approach [9,10] that is used in nonequilibrium thermodynamics for the description of quasi-linear processes of heat transfer. For the heat transfer processes discussed here, the function will be:

$$I<T> = \int_0^\tau d\tau \int_V \left\{[C_V(T)T_\tau - q_V(T)]\right.$$

$$\times \int_f^T \lambda(T)dT - \frac{1}{2}\lambda^2(T)(\vec{\nabla T})^2\bigg\}dV$$

$$- \int_0^\tau d\tau \int ds \int_f^T F(T)\lambda(T)dT$$

$$+ \int_V dV \int_f^{T_0} C_V(T_0)[T_0 - f(x)]\lambda(T_0)dT_0 \longrightarrow \min \qquad (32)$$

Here $T_0 = T(x, \tau = 0)$. The first two integrals in Eq 32 take into account differential equation 29 and boundary conditions from Eq 31, and the last integral is the initial condition of Eq 30 [8].

2.4.3 Algorithms to Obtain Approximate Solutions

The process of cooling is divided into two steps. During the first step (irregular thermal condition), the temperature distribution is:

$$\vartheta(r, \tau) = \vartheta_0 - (\vartheta_0 - \vartheta_{sf})\left(1 - \frac{r}{\xi}\right)^n, \qquad (33)$$

where:
$\vartheta = T - T_s$;
$\vartheta_0 = T_0 - T_s$; and
ξ is depth of temperature penetration during the first step of cooling.

During the second step (regular thermal condition), the temperature distribution is:

$$\vartheta(r, \tau) = \vartheta_c - (\vartheta_c - \vartheta_{sf})\left(1 - \frac{r}{R}\right)^n, \qquad (34)$$

where:
$\vartheta = T - T_s$;
$\vartheta_c = T_c - T_s$;
$\vartheta_{sf} = T_{sf} - T_s$; and
T_{Sf} is surface temperature and T_S is saturation (boiling) temperature.

The duration of the irregular thermal condition can be approximated by [8,17]:

$$\tau_{ir} \approx B\frac{R^2}{a}, \qquad (35)$$

where B depends on Biot number and configuration of a body (see Fig. 7).

Kobasko and Zhovnir [8] used existing theories [9–13] and the variational method, including Eqs 32, 33, and 34, to develop a simplified method for the calculation of temperature field distribution during quenching of canonical bodies: plates, cylinders, and spheres. More information on transient boiling processes during quenching can be found in [13–26]. From these data, the following equation may be derived for calculation of the duration of transient nucleate boiling [27]:

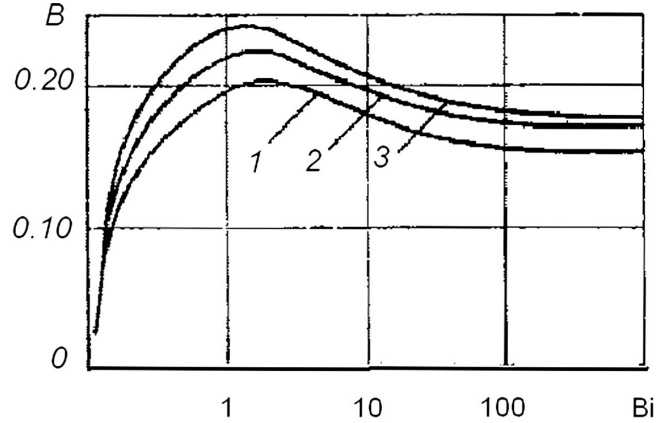$$\tau = \left[\Omega + b\ln\frac{\vartheta_I}{\vartheta_{II}}\right]\frac{K}{a}, \qquad (36)$$

Fig. 7—Value B versus Biot number Bi: 1, plate; 2, cylinder; 3, sphere [8].

where $b = 3.21$;

$$\vartheta_I = \frac{1}{\beta}\left[\frac{2\lambda(\vartheta_0 - \vartheta_I)}{R}\right]^{0.3}; \qquad (37)$$

$$\vartheta_{II} = \frac{1}{\beta}[\alpha_{conv}(\vartheta_{II} + \vartheta_{uh})]^{0.3}; \text{ and} \qquad (38)$$

$$\beta = \frac{75\lambda'(\rho' - \rho'')^{0.5}g^{0.5}}{\sigma^{0.5}(\rho''r^*\overline{W}'')^{0.7}\text{Pr}^{0.2}}. \qquad (39)$$

Eq 36 provides a generalized dependence for the determination of the time of transient nucleate boiling including the self-regulated thermal process [27].

Table 9 shows the duration of transient nucleate boiling for cylindrical test specimens (probes) of 20, 30, and 50-mm diameters. Cooling time was calculated using Eqs 36–39. Austenitizing temperature was 860°C. The quenchant (a water-salt solution) temperature was 20°C. The saturation (boiling) temperature of the quenchant was 120°C. From the equations above, the minimum value of β was 3 and the maximum value was 7.36. For these calculations, an average thermal conductivity and thermal diffusivity used were:

$$\lambda = 22\frac{W}{mK} \text{ and } a = 5.36 \cdot 10^{-6}\frac{m^2}{s}.$$

Comparison of the calculated results with the experimental data is shown in Fig. 8 [8].

Eqs 36–39 are the basis for the creation of new intensive steel quenching technologies. Along with the calculation of the

TABLE 9—Analytical calculation of transient nucleate boiling duration and temperature at the core of cylindrical specimens at the beginning and at the end of the self-regulated thermal process

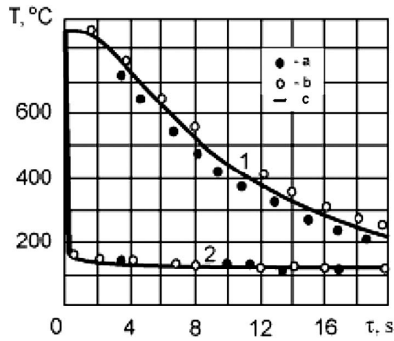| Dia (mm)	Nucleate boiling duration, τ_{nb} (s)	Core temperature when boiling starts, T_C^I (°C)	Core temperature when boiling ends, T_C^{II} (°C)
20	18.3	849	162
30	29	850	165
50	70.8	—	—

Fig. 8—Temperature versus time for the surface and center of a cylinder 20 mm in diameter: 1, temperature at the core; 2, temperature at the surface; a, experiment; b, analytical solution; c, numerical solution.

duration of nonstationary nucleate boiling, it is possible to evaluate the temperature at the core of steel parts. Using the same approach, an equation was determined for the core temperature:

$$\vartheta_c = \vartheta_{sf} + \frac{\beta^m R}{n\lambda}\vartheta_{sf}^m. \qquad (40)$$

Here $n = 2$ and $m = 10/3$ or 3.333.

To perform these calculations, the physical properties of the liquid quenchants must be known. To calculate the time of transient nucleate boiling, it is necessary to start with the calculation of factor β, using these fluid properties. For water, the value β is provided in Tables 6 and 7. In addition, values of ϑ_I and ϑ_{II} are calculated iteratively. According to Tolubinsky and Dhir [1,2], wall overheat cannot be significant because the heat flux density is proportional to overheat to the cubic power (or greater). The value of ϑ_I is within the range of 10−15°C and depends on the shape and the sizes of steel parts being quenched.

The value of ϑ_I is wall overheat at the beginning of the self-regulated thermal process, and ϑ_{II} is wall overheat at the end of this process. The first step of the iterative calculation is to select any value from the range discussed above. The closer the selected value is to the true value, the less steps will be required for the exact calculation of ϑ_I and ϑ_{II}. Table 6 shows that the most reliable value is $\beta = 7.36$.

Using this value of β, the overheat temperature at the beginning and at the end of nucleate boiling will be estimated, and the values of ϑ_I and ϑ_{II} will be determined using Eqs 37 and 38 for cylinders and spheres of different sizes. Cylinders are cooled from a temperature of 860°C. The average heat conductivity λ is 22 W/mK, and average thermal diffusivity a is $5.6 \cdot 10^{-6}$ m^2/s. The average convection heat transfer coefficient in slightly circulating water at a temperature of 20°C is equal to 1,000 W/m^{2}K. Using these initial data, values ϑ_I and ϑ_{II} for cylinders of diameter 20, 50, and 100 mm have been calculated and are shown in Table 10. The change in wall overheat is within the range of the error of the thermocouple in measuring the surface temperature.[2] The time of transient nucleate boiling is sufficient for developing new intensive quenching technologies, especially IQ-2 processes (see Chapter 10).

Table 10 shows the number of iterations that are necessary for the calculations of ϑ_I and ϑ_{II} by Eqs 37 and 38. The

initial value for ϑ_I is 20, and for ϑ_{II} is 5. Using a well-known approach, after two or three iterations, the exact results are obtained, which are presented in Table 9.

As seen in Table 10, the surface temperature during nucleate boiling does not change significantly, which is quite typical for very large steel parts. Thus, during quenching of cylinders of 100-mm diameter, the wall temperature is maintained almost constant for a relatively long time (138 s), changing only 2°C from 106.16°C to 104.1°C (see Tables 10 and 11).

Impact of the value β on transient nucleate boiling duration and wall superheat according to the generalized equation (Eq 36) is shown in Table 12.

It should be noted that the duration of the self-regulated thermal process was considered when developing processes for interrupted cooling to monitor conveyor speeds and also is used for developing the new quenching processes [28,29]. Self-regulated thermal processes were investigated using noise control systems [28], which are based on depicting specific frequencies of bubble oscillations responsible for the nucleate boiling process. Acoustic measurement can be used

TABLE 10—Values of ϑ_I and ϑ_{II} for cylinder-shaped samples quenched from 860°C in water at 20°C

Diameter (mm)	ϑ_I	ϑ_{II}	Number of iterations for ϑ_I	Number of iterations for ϑ_{II}
20	12.25	4.1	2	2
50	9.32	4.1	2	2
100	6.16	4.1	3	2

Note: $\vartheta_I = T_I - T_S$ and $\vartheta_{II} = T_{II} - T_S$, where T_I is overheat at the beginning of nucleate boiling; T_S is saturation temperature; and T_{II} is overheat at the end of nucleate boiling.

TABLE 11—Time τ_{nb} of transient nucleate boiling during quenching cylinder-shaped steel parts in conventional water at 20°C from a temperature of 860°C

Diameter (mm)	20	50	100
τ_{nb} (s)	12	60	138

TABLE 12—Impact of the value β on transient nucleate boiling duration and wall superheat according to the generalized equation (Eq 36)

β	τ_{nb} (s)	ϑ_I	ϑ_{II}
3	22.34	24.0	10.8
4.3	22.53	17.35	7.46
5	22.72	15	6.39
7.36	22.95	10.2	4.30

---

[2] Accurate calculations requite accurate temperature-time data. This means that the actual temperature at the point of interest must be measured with minimum time lag. The most significant contributors to a time-lag problem are thermocouple size and materials of construction and the contacts between the thermocouple and the specimen (or probe) on which the temperature is being measured. The problem is discussed by Liscic [13] and Totten, Tensi, and Stich [15].

to investigate boiling processes, especially shock and boiling. This issue is discussed in Chapter 3. The noise control system can be used for monitoring quenching technologies including IQ processes [30–32].

Self-regulated thermal processes were also investigated by using a noise control system [33–36]. Having experimental data achieved on the basis of the noise control system and temperature–time data recorded by thermocouples, it is possible to solve correctly the inverse problem (IP) [37,38].

2.5 THE SELF-REGULATED THERMAL PROCESS

Previously, it was shown that during nucleate boiling, high values of heat transfer coefficients are obtained due to the large growth rate of vapor bubbles and their relatively large surface area. It is of interest to determine values of heat transfer coefficients during nucleate boiling depending on wall superheat $\Delta T = T_{Sf} - T_S$. Such calculations can be performed if heat flux density q is taken as $q = \alpha_{nb}\left(T_{Sf} - T_S\right)$. During nucleate boiling, the heat transfer coefficient is very high, several times greater than natural convection. Therefore, the surface temperature of a steel part decreases very rapidly when approaching the boiling temperature; at that point, it decreases very slowly and is maintained above the saturation temperature.

This is proven by considering experimental data obtained previously by French [26], who investigated the behavior of the surface temperature of steel and copper spheres of 38.1-mm diameter that were heated to 875°C and cooled in cold water, boiling water, and water saturated with various gases. The temperature–time cooling curve results are presented in Figs. 9 and 10.

As shown in Fig. 9, steel spheres quenched in cold flowing water exhibit no film boiling. The surface temperature of the sphere decreases rapidly to approximately 100°C and then remains at the boiling temperature of the quenchant. The temperature at the center of the sphere did not vary significantly. It is also seen that the formation of a boundary boiling layer and appearance of active bubbles occurs within only 0.5 seconds. The core temperature of a sphere cools 875°C to 200°C over 28 seconds. Therefore, when there is no
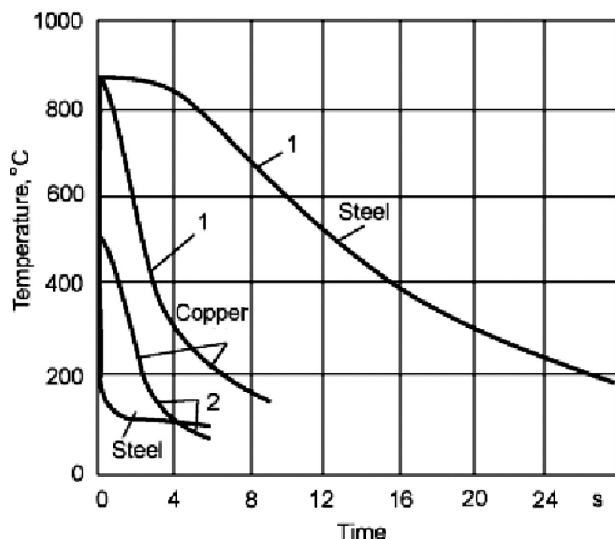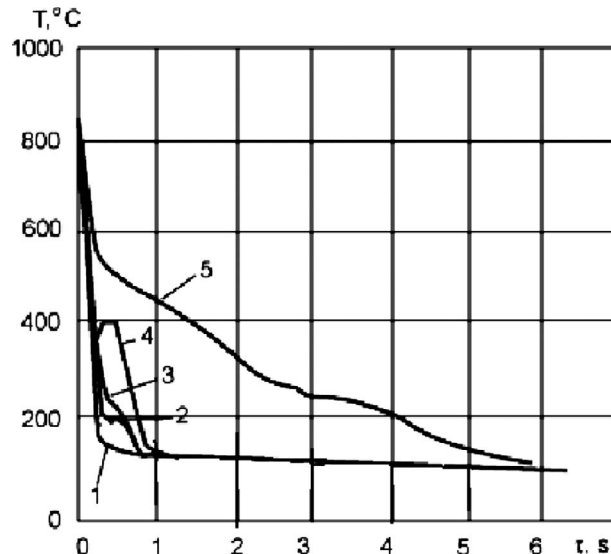
Fig. 10—Temperature at the surface versus time for a steel sphere of 38.1-mm diameter, quenched from 875°C in water of room temperature, saturated with various gases [26]: 1, tap water containing small amount of salts (simply metal ions from hard water); 2, boiled water; 3, water saturated with oxygen; 4, water saturated with air; 5, water saturated with carbonic gas.

film boiling, the first stage of the formation of a boundary boiling layer requires only approximately 2 % of the total cooling time. After the formation of a boundary boiling layer and establishment of the nucleate boiling, the surface temperature does not change significantly and is maintained at the boiling temperature of the quenchant.

When quenching spheres in water saturated with gases, film boiling is clearly observed (see curves 4 and 5 in Fig. 10).

Film boiling is observed when cooling copper spheres because the heat conductivity of copper is much greater than that of steel. The film boiling can be eliminated if the steel and copper spheres are cooled in intensive water jets. In this case, there will be a fast formation of a boundary boiling layer, and then, during nucleate boiling, the surface will be maintained at the boiling temperature of the quenchant.

Lykov, citing Yaryshev's work, explained this unusual character of change in temperature of a surface during quenching by associating the change of average surface temperature with the generalized Biot number (Bi_V) [12]:

$$\frac{\overline{T}_{Sf} - T_S}{\overline{T}_V - T_S} \geq \frac{1}{Bi_v^2 + 1.437Bi_V + 1} = \left(Bi_v^2 + 1.437Bi_V + 1\right)^{-0.5}, \quad (41)$$

where:
$\overline{T}_{Sf}$ is an average value of temperature with respect to area of a surface of a part to be cooled;
$\overline{T}_V$ is an average value of temperature with respect to volume of a part to be cooled;
T_S is a saturation temperature of a quenchant; and
Bi_V is a generalized Biot number, given by:
 $Bi_V = \frac{\alpha}{\lambda}K\frac{S}{V}$,
 (in this case, it is necessary to consider the heat transfer coefficient during nucleate boiling where $\alpha = \alpha_{nb}$);
λ is a heat conductivity of steel (W/m K);
K is a Kondratjev form factor (m^2) (see Chapter 6);
S is surface area (m^2); and
V is volume (m^3).

Fig. 9—Temperature at the surface and in the core versus time for steel and copper balls of 38.1-mm diameter, quenched from 875° C in water at room temperature (French's experiment [26]): 1, core; 2, surface.

Since, during the nucleate boiling, the heat transfer coefficient is very high:

$$\alpha_{nb} >> \alpha_{conv}, \tag{42}$$

which is especially true for cooling in a lightly agitated or nonagitated quenchant. From Eq 42, it follows that:

$$Bi_{V_{mu}} >> Bi_{V_{conv}}.$$

In Eq 41, when there is no film boiling and the nucleate boiling is established, the generalized Biot number Bi_V approaches infinity. When the $Bi_V \to \infty$, according to Eq 41,

$$\frac{\overline{T}_{Sf} - T_S}{\overline{T}_V - T_S} \to 0.$$

When this occurs, T_{Sf} approximates T_S, which means that during transient nucleate boiling, the surface temperature of a part is maintained at the boiling temperature.

If the surface temperature T_{Sf} is less than saturation temperature T_S, then nucleate boiling stops and a single-phase convection is established where $\alpha_{conv} << \alpha_{nb}$. When the value of α_{conv} is small, the generalized Bi_V number is also small, and according to Eq 41, at $Bi_V \to 0$,

$$\frac{\overline{T}_{Sf} - T_S}{\overline{T}_V - T_S} \to 1, \text{or} \overline{T}_{Sf} \approx \overline{T}_V.$$

This means that equalization of the temperature field occurs on cross-sections of parts and that the surface temperature must increase. It follows that, during nucleate boiling, the surface temperature is maintained at T_S and cannot be lower than T_S while boiling is in progress and condition $\alpha_{conv} << \alpha_{nb}$ is satisfied.

Thus, the self-regulation of heat flux density–which depends on the size and shape of parts to be hardened, the thermal conductivity of the material, and the initial temperature of the heated part–depends on the austenization temperature. Self-regulation occurs during transient nucleate boiling. The time of transient nucleate boiling is determined by Eqs 36–38. Therefore, the time of the self-regulated thermal process also is determined by Eq 36; however, it is less–approximately one second, as compared with the complete duration of the nucleate boiling process.

During full film boiling, there is no self-regulated process because the temperature field is more uniform on cross-sections of parts to be hardened. and at the time when film boiling starts, the temperature gradient may be insufficient for the occurrence of the self-regulation process. This was illustrated with experiments utilizing plate-shaped, cylindrical, and spherical test specimens [25,33]. The time of the self-regulated thermal process was determined by Eq 36, which was compared with the results obtained by numerical solution and from experimental data which are presented in Table 13.

2.6 EXPERIMENTAL DETERMINATION OF THE TIME OF THE SELF-REGULATED THERMAL PROCESS

The determination of the time of nonstationary nucleate boiling or the self-regulated thermal process is a difficult problem. Thus far, three experimental methods of determining the time of nonstationary nucleate boiling are known [27,30,31,33]. These methods include:
- Character of change in temperature of surface of the part [13,27]
- Visual monitoring [13,28]
- Recording sound effects [30,31,35]

During the self-regulated thermal process, a certain character of change in the temperature of the surface of a part is observed. During nucleate boiling, the surface temperature is maintained at approximately the boiling temperature of the quenchant. When the convection cooling process occurs, the surface temperature decreases significantly.

Using the first approach, the duration of the self-regulated thermal process can be determined if the convective heat transfer coefficient α_{conv} is sufficiently large. In this case, the transition from nucleate boiling to single-phase convection is clearly observed. However, it should be noted that the first method is less accurate than the other two methods. To measure the exact temperature at the surface and the duration of nucleate boiling using thermocouples is still a difficult problem. Most suitable for such measurement is a Liscic-Nanmac probe [13].

The second method involves visual monitoring and demands considerable time, material consumption, and cost [13,28]. However, at present, with the availability of high-speed video, the cost of such experiments has significantly decreased. The technique includes observing the appearance and disappearance of the vapor bubbles or moving of the wetting front [13].

The third method, recording of sound effects, is the most promising, although a great deal of work and understanding of the sound effects that are observed during the nucleate boiling is required [30,31,35]. In the subsequent

TABLE 13—Time of the self-regulated thermal process when cooling a test specimen of AISI 304 steel from 850°C in a 12 % aqueous solution of CaCl₂				
		Time of self-regulated thermal process (s)		
Sample shape	Thickness or diameter (mm)	Eq 36	Numerical calculation	Experiment
Plate	20	25	28	—
Cylinder	10	3.54	3.7	3.8
	30	24.4	22.5	23
Sphere	20	7.9	7	—
Note: Experimental studies are described in more detail in [27].				

discussion, a brief description of the methodology used to record sound (acoustic) effects will be provided, related to the occurrence and growth of vapor bubbles.

At the time of bubble generation, their size (diameter) is less than the critical value and bubbles are very small. Accordingly, the frequency of their oscillations will be characteristically high. Upon the establishment of advanced nucleate boiling, the bubble diameter increases, their dispatch frequency becomes stable, and therefore their oscillation frequencies are also stable. The only difference is that at greater heat flux densities, the intensity of sound effects will be higher, since more bubbles participate during boiling. While heat flux increases, the quantity of bubbles per surface area also increases, and their growth rate $W'' = d_0 f$ remains essentially constant. By recording the sound effects during nucleate boiling, it is possible to precisely determine the time of nonstationary nucleate boiling or the time of the self-regulated thermal process.

When a heated steel part or standard test specimen (or a probe) is initially immersed into the quenchant, the heat flux is sufficiently high that full film boiling arises. In this case, a continuous steam film is formed around the part or probe, which separates the liquid (the quenchant) from the heated surface. Thus, the oscillation of a film is observed with much smaller frequency than when bubbles first appear or for bubbles during nucleate boiling.

By comparison of the frequencies, the duration of film and nucleate boiling can be estimated. It is even possible to record the first stage of bubble generation, since they fluctuate at high frequencies that can be easily recorded [29,36]. It was possible to make such investigations because noise sounds were subdivided into 200 channels [36].

It has been established that each mode of boiling possesses corresponding characteristic frequencies of sound effects that lie within the range of 1−20 kHz. To record these oscillations, a sound analyzer [30] was used, connected through an amplifier to the sensor (hydrophone) used to measure the sound effects emitted during the quenching process. The sensor gauge is constructed of a piezoelectric element that responds to acoustic oscillations. The range of acoustic oscillations of 1−20 kHz was separated into 200 channels. Each channel recorded frequencies over a range of 100 Hz. The integrated intensity of sound fluctuations was also measured. The chart of experimental measurements is shown in Fig. 11. Studies in this area are described in more detail in [29,36].

Results of some experimental measurements are shown in Fig. 12. Fig. 12(a) illustrates the cooling process for a Kh18N9T (AISI 304) cylindrical test probe of 20-mm diameter. The temperature was measured at the center of a sample (curve 1) and at the surface (curve 2). After heating to 850°C, cooling was conducted in a concentrated aqueous solution of calcium chloride ($CaCl_2$) with a density of $\rho = 1{,}320$ kg/m^3 and temperature of 40°C. Integrated acoustic oscillations intensity was measured using an analyzer and the device shown in Fig. 11. The function of integrated intensity of sound effects versus time is shown in Fig. 12(b).

It is possible to select three characteristic acoustical regions during the cooling process. During the first region (I), an increase in acoustic oscillations intensity is observed; during the second region (II), the sound is attenuated; and during the third region (III), an increase in the integrated intensity of acoustic oscillations is once again observed, completely fading away when convection starts. It should be noted that in the third region during the time of maximum
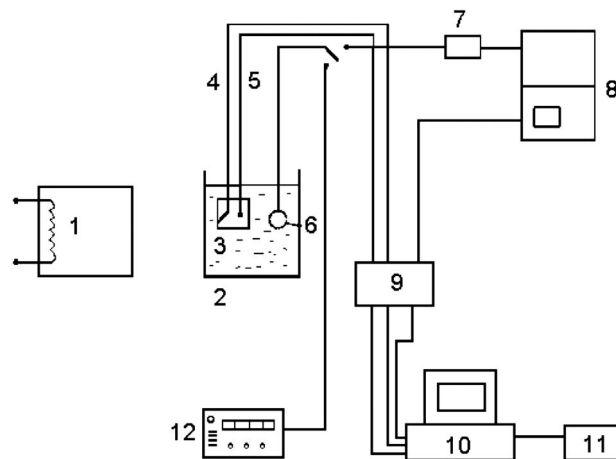

Fig. 11—Simplified schematic illustration of the experimental apparatus used for acoustical measurements [29,30].

acoustic oscillations intensity, there is no appreciable change in the surface temperature. From beginning to end of the full nucleate boiling, the temperature gradually decreases, which, in this case, is at the level of the boiling temperature of a boundary liquid layer (about 120°C).

We can give the following explanation to the character of change in intensity of the sound effects shown in Fig. 12(b). When a cylindrical sample is immersed into an aqueous solution of calcium chloride during Region I, a boundary boiling layer is formed, and liquid boils with the formation of numerous bubbles, resulting in an increase in sound intensity. In Region II, a localized steam film is formed, which decreases the intensity of acoustic oscillations. In Region III, the full nucleate boiling is observed and the sound intensity increases as the localized steam film is replaced with numerous bubbles. After 16 seconds, the
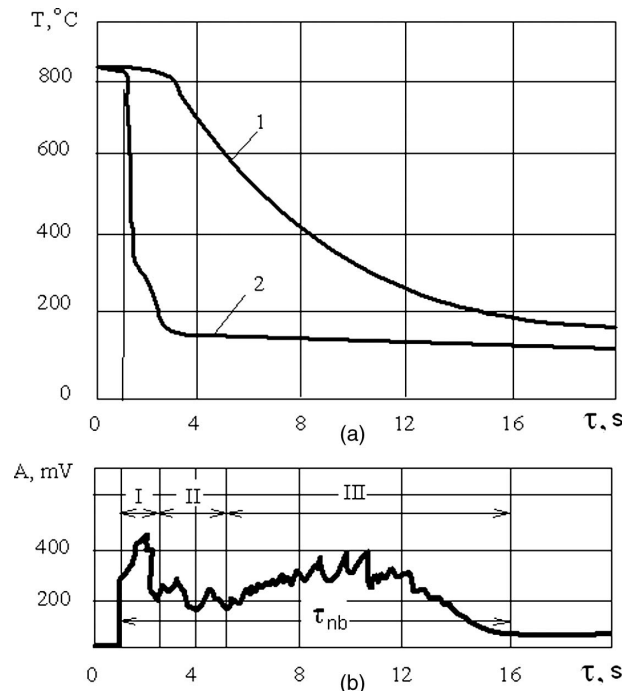

Fig. 12—Temperature–time curve of a cylinder-shaped probe (a) and noise intensity (b) during quenching from 860°C in an aqueous solution of $CaCl_2$: 1, center; 2, surface [29,30].

sound effects ceased because the nucleate boiling process ended and convection was established.

The duration of transient nucleate boiling will now be estimated using Eq 36 and then compared with the experimental data. The following initial conditions were used:

$T_0 = 850°C$;
$T_S = 120°C$;
$\vartheta_0 = T_0 - T_S = 850°C - 120°C = 730°C$;
$\lambda = 22$ W/mK;
$a = 5.36 \times 10^{-6}$ m^2/s;
$R = 0.01$ m; and
$\alpha_{conv} = 427$ W/m^{2}K.

Using these data and Eq 36, the time of transient nucleate boiling τ_{nb} is equal to 15.5 s. Experimentally, it was determined to be approximately 16 s, which agrees reasonably well with the calculated result. The computational result is less by 0.5 s because the existence of shock boiling and possible localized vapor films were considered [36].

A portable device has been developed for recording sound effects directly in a production quench tank so that similar computations can be performed in the heat treating shop [29–31]. The results of calculations of the time of the self-regulated thermal process and time of sound effects for pins of various diameters are shown in Table 14. Experimental and computational results are in excellent agreement for these parts of simple configuration. If parts possess a more complicated configuration consisting of thin and thick sections, it is difficult to determine the time of nonstationary nucleate boiling precisely, since thin sections are cooled much faster, while the quenching process (and noise associated with this portion of the overall cooling) continues for thicker sections. However, using Eq 36, it is still possible to estimate with sufficient precision the *average* time of the self-regulated thermal process, which coincides with nonstationary nucleate boiling.

2.7 DISCUSSION

Boiling is a phase change process in which vapor bubbles are formed either on a heated surface or in a superheated liquid layer adjacent to the heated surface. Dhir [2] reported that heat flux on polished surfaces varies with wall superheat approximately as:

$$q \propto \Delta T^m, \tag{43}$$

where m has a value between 3 and 4. This means that wall superheat ΔT during quenching of steel parts does not change significantly with a change of q. This process was investigated by French [26] by quenching a steel ball 38.1 mm in diameter in cold water containing a small amount of salts and making calculations of the duration of the self-regulated thermal process and the surface temperature at the beginning and end of the quenching process.

In this study, the steel ball was heated to 875°C and then cooled in water at 20°C containing mineral salts. For these calculations, the following input data were used:

$T_0 = 875°C$;
T_m (bath temperature) = 20°C;
T_S (saturation temperature) = 100°C;
$\alpha_{conv} = 1,200$ W/m^{2}K;
$\lambda = 22$ W/mK; and
$R = 0.01905$ m.

Overheat ΔT at the beginning and at the conclusion of the self-regulated thermal process can be evaluated from Eqs 36–38, where:

K is Kondratjev form factor in m^2 (see Chapter 6);
a is the thermal diffusivity of steel (m^2/s);
λ is the thermal conductivity of steel (W/mK);
T_0 is the initial temperature (°C);
T_I is the initial temperature of the surface at the beginning of nucleate boiling (°C);
T_{II} is the temperature of the surface at the end of nucleate boiling (°C);
$\vartheta_0 = T_0 - T_S$;
$\vartheta_I = T_I - T_S$;
$\vartheta_{II} = T_{II} - T_S$;
$\vartheta_{uh} = T_S - T_m$;
α_{conv} is convective heat transfer coefficient (W/m^{2}K); and
$\beta = 7.36$ [3].

Overheat at the beginning of the self-regulated thermal process can be evaluated using Eq 37:

$$\vartheta_I = \frac{1}{7.36}\left[\frac{2 \times 22 \times (775 - \vartheta_I)}{0.01905}\right]^{0.3} = 10.2°C,$$

and overheat at the end of the process can be evaluated using Eq 38:

$$\vartheta_{II} = \frac{1}{7.36}[1,200 \times (775 + \vartheta_{II})] = 4,3°C.$$

The duration of the self-regulated thermal process is then calculated from Eq 36:

$$\tau_{nb} = \left[0.48 + 3.21\ln\frac{10.2}{4.3}\right]\frac{36.77 \times 10^{-6}}{5.36 \times 10^{-6}} = 22.4s.$$

Here $K = \dfrac{R^2}{\pi^2} = 36.77 \times 10^{-6}m^2$ which is the Kondratjev form factor for a ball of 38.1-mm diameter. The thermal diffusivity of steel is $a = 5.36 \times 10^{-6}$ m^2/s. From these calculations, the surface temperature during the self-regulated thermal process changes from 110.2°C to 104.3°C and its duration is 22.4 s. If an average temperature of (110.2°C + 104.3°C)/2 = 107.25°C is used, the difference between the actual temperature and the average temperature is ±2.7 % This difference decreases as the diameter increases, which means that the simplified approach provided by Eq 36 can be used. This is important, since it provides a practice approach for heat treaters to delay the transformation of austenite into martensite during the intensive quenching process and facilitates the development various customized quenching processes.

2.7.1 Quench Process Investigations Performed by French

Quenching is a very old technology. Ancient experienced heat treaters–blacksmiths–had their own specialized know-how for quenching products, evaluating the duration of transient nucleate boiling (although they probably didn't recognize this particular physical process in this way). The key element of heat treating was to transfer quenched products from one quenchant to another at the end of nucleate boiling. The duration of nucleate boiling was evaluated simply by the noise and small vibrations the blacksmiths felt in their hands. Only experienced heat treaters could do this job, and they were highly respected in ancient societies. Nowadays, heat treating may be completely automated, and production lines are equipped with the conveyors, robots, and various kinds of hardware and software.

TABLE 14—Comparison of the time of the self-regulated thermal process measured experimentally with computational results obtained using Eq 36 for cooling conducted in an optimal concentration of a cold aqueous solution of $CaCl_2$

Type of pin	Steel grade	Time of nucleate boiling (s)	Calculation by Eq 36 (s)
M10 × 50	AISI 5140	4.4	4.0
	AISI 5136	4.4	
	20KhN3A	4.3	
	SAE 4130	4.4	
	AISI E9310	4.3	
M12 × 100	AISI 5140	6.0	6.0
	AISI 5136	6.1	
	20KhN3A	6.0	
	SAE 4130	6.2	
	AISI E9310	5.9	
M16 × 130	AISI 5140	10.0	10.0
	AISI 5136	10.2	
	20KhN3A	10.1	
	SAE 4130	10.3	
	AISI E9310	9.4	
M20 × 180	AISI 5140	14.9	15.0
	AISI 5136	15.0	
	20KhN3A	14.9	
	SAE 4130	15.1	
	AISI E9310	14.7	
M24 × 120	AISI 5140	20.9	21.0
	AISI 5136	21.0	
	20KhN3A	20.9	
	SAE 4130	21.2	
	AISI E9310	20.8	
M27 × 240	AISI 5140	28.0	28.0
	AISI 5136	28.3	
	20KhN3A	28.1	
	SAE 4130	28.4	
	AISI E9310	27.5	
M30 × 190	AISI 5140	31.9	32.0
	AISI 5136	32.3	
	20KhN3A	32.0	
	SAE 4130	32.8	
	AISI E9310	31.7	

Note: Composition of 20KhN3A steel: 0.17–0.24 C; 0.3–0.6 Mn; 0.17–0.37 Si; 0.6–0.9 Cr; 2.75–3.15 Ni; < 0.15 Mo; < 0.1 Al; < 0.03 Ti
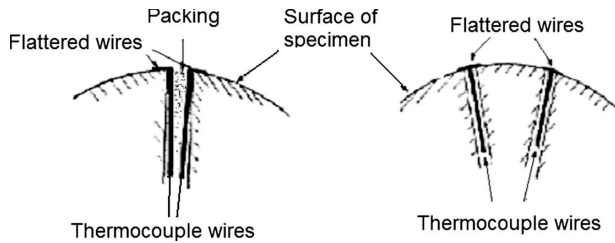
Fig. 13—Depiction of how thermocouples were arranged and accurately flattened to the wall of spheres and polished by French [26].

One of the serious investigations of quenching processes was performed by French in 1926–1930 [26]. At the time, he prepared and utilized unbelievably accurate spheres, cylinders, and plates, which were instrumented with thin thermocouples. Spheres were made from steel and copper. Fig. 13 shows how accurately spheres were prepared for investigations.

The experimental results from French's studies are summarized in Table 15, which shows that during quenching of the spheres in a cold 5 % water alkaline solution, film boiling is absent. Also, independently of size of sphere, the wall temperature decreases very quickly from 975°C to 150°C within one second, which would seem impossible. However, using computational methodology, such as finite element analysis, it is possible to solve this heat transfer problem as an inverse problem (IP). Details and methods of solving the inverse problem are provided in Chapter 13.

A regularization method for solving an IP problem was developed by Tikhonov [37]. This method was used and further developed by various authors [38–42]. Some results of computations using the software IQLab [40] are shown in Figs. 14 and 15. Fig. 14 shows that the heat flux density is very high at the very beginning of the quenching process and varies smoothly as the process proceeds. Fig. 15 shows that the maximum heat transfer coefficient (more than 200,000 W/m^2K) is achieved at the time of 2 seconds. Furthermore, the heat transfer coefficient decreases exponentially and reaches 30,000 W/m^2K within 20 seconds after immersion.

To be sure that these large values are reliable, the critical heat flux densities were determined (see Chapter 3, Section 3.4). The results of these calculations are shown in Table 16 for the critical heat flux densities for water and aqueous salt solutions and alkaline solutions.

TABLE 15—Time required for the surface of steel spheres of different sizes to cool to different temperatures when quenched from 875°C (1,605°F) in 5 % NaOH-water solution at 20°C and moving at 3 feet per second (0.914 m/s), according to French [26]

| Average size	Time (s)							
	700°C	600°C	500°C	400°C	300°C	250°C	200°C	150°C
1/4 inch (6.35 mm)	0.025	0.030	0.033	0.040	0.06	0.10	0.21	1.05
	0.025	0.040	0.050	0.063	0.12	0.23	0.42	0.67
	0.030	0.040	0.043	0.050	0.09	0.13	0.23	0.36
	0.027	0.037	0.043	0.051	0.09	0.15	0.29	0.69
1/2 inch (12.7 mm)	0.033	0.040	0.050	0.053	0.07	0.11	0.15	0.43
	0.035	0.038	0.046	0.060	0.09	0.13	0.22	0.49
	0.032	0.050	0.073	0.090	0.11	0.14	0.32	0.92
	0.016	0.043	0.050	0.083	0.17	0.24	0.35	0.65
	0.020	0.040	0.060	0.077	0.10	0.15	0.26	0.53
	0.028	0.042	0.058	0.071	0.11	0.15	0.26	0.60
1 inch (25.4 mm)	0.035	0.040	0.045	0.060	0.08	0.10	0.15	0.40
	0.050	0.050	0.080	0.083	0.11	0.19	0.40	1.20
	0.028	0.040	0.045	0.064	0.14	0.21	0.34	0.71
	0.020	0.020	0.050	0.086	0.19	0.32	0.32	0.99
	0.033	0.042	0.055	0.074	0.13	0.21	0.35	0.82
2.5 inches (63.5 mm)	0.025	0.040	0.060	0.065	0.08	0.10	0.29	0.65
	0.020	0.030	0.040	0.050	0.07	0.13	0.25	0.80
	0.030	0.043	0.070	0.100	0.15	0.20	0.31	0.52
	0.020	0.040	0.075	0.120	0.19	0.23	0.35	0.84
	0.020	0.043	0.080	0.130	0.21	0.28	0.39	0.56
	0.023	0.039	0.065	0.093	0.14	0.19	0.32	0.59
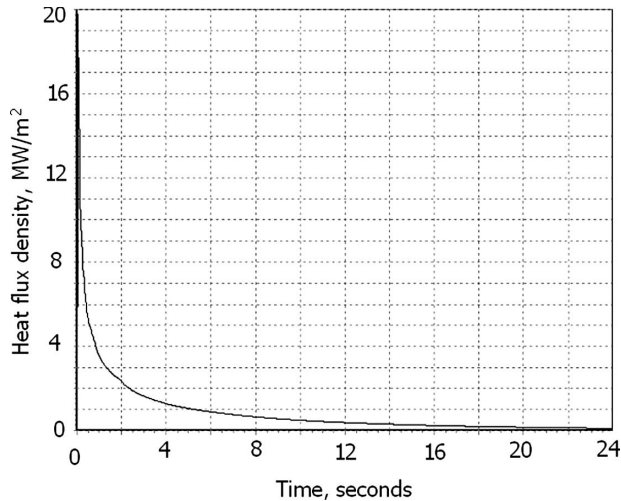
Fig. 14—Heat flux density versus time for a sphere 38.1 mm in diameter quenched from 875°C in a 5 % NaOH-water solution at 20°C.

Quenchant at 20°C	Critical heat flux densities, q_{cr1} (MW/m²)
12 % NaCl water solution	13
5 % NaOH water solution	15
12 % NaOH water solution	15–16
Water	6.9–7.0

TABLE 16—The first critical heat flux density for water and water salts and alkaline solutions at 20°C

Note that the first critical heat flux density is maximal heat flux when nucleate boiling changes by film boiling. These problems (shock boiling and critical heat flux densities) are discussed in Chapter 3.

It has been shown that the maximum critical heat flux densities in water-salt solutions can reach 9−15 MW/m² [27]. From the maximum critical heat flux, it is possible to calculate the maximum heat transfer coefficients during nucleate boiling when quenching. If overheat is 50K, the heat transfer coefficient during quenching in an aqueous alkaline solution can be:

$$\alpha_{nb} = \frac{q_{max}}{T_W - T_S} = \frac{15 \times 10^6 W/m^2}{50K} = 300,000 \frac{W}{m^2 K}.$$

For water, a lower value is obtained because of the lower first critical heat flux density:

$$\alpha_{nb} = \frac{q_{max}}{T_W - T_S} = \frac{6.9 \times 10^6 W/m^2}{50K} = 138,000 \frac{W}{m^2 K}.$$
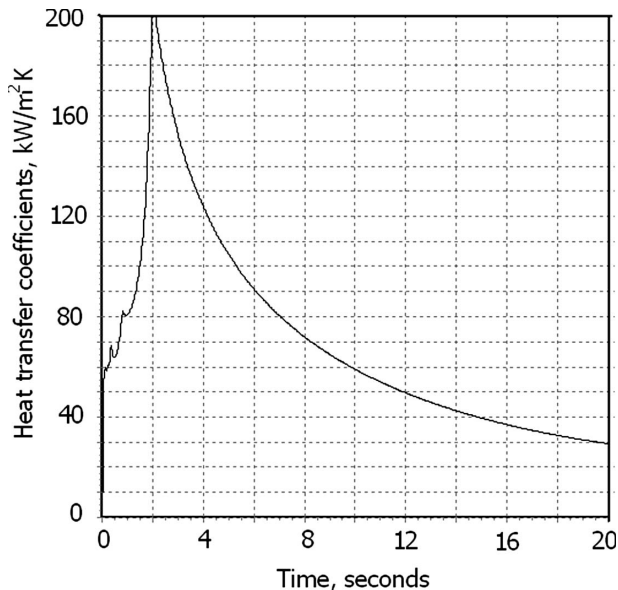
Fig. 15—Shock and nucleate boiling heat transfer coefficients versus time for a sphere of 38.1 mm in diameter quenched from 875°C in a 5 % aqueous NaOH solution at 20°C.

It should be noted that Tolubinsky and Kutateladze underlined many times that maximal overheat is within 10 to 30°C [1,7]. During immersion of steel parts heated to 800−1,000°C into cold liquid, due to very big gradient of temperature, overheat can be more than 30°C.

From Fig. 14, in one second the heat flux density decreases to 3 MW/m² where the self-regulated thermal process is already established. At that time, the wall overheat is 10.2K and the heat transfer coefficient is:

$$\alpha_{nb} = \frac{q_{max}}{T_W - T_S} = \frac{3 \times 10^6 W/m^2}{10.2K} = 294,000 \frac{W}{m^2 K}.$$

Due to the very high heat transfer coefficient during nucleate boiling, the surface temperature of steel parts during quenching decreases immediately to a temperature close to the saturation temperature. Further surface temperature changes very slowly until the boiling process is completed. This phenomenon is designated as the self-regulated thermal process [33].

Many equations, including the equations of Labuntsov (see Table 5), should provide approximately equivalent values of the heat transfer coefficients, especially for water at atmospheric pressure. According to Labuntsov, at $\Delta T = 10$K, α is approximately 8,400 W/m²K. Such a big difference can be explained by highly forced processes and existing boiling sites on the surface of steel parts; there is no need to spend energy to grow them from the very beginning.

The heat transfer coefficients calculated using the equations from Table 5 are rather low as compared with the heat transfer coefficients during quenching. One cannot say that Labuntsov's equations are not true. All of equations in Table 5 are true for the conditions for which they were developed–most commonly for electrically heated wires and different elements placed into boiling liquids. It should be noted that experiments of Labuntsov and others were very precisely performed; however, in many cases they don't coincide with the results derived from the quenching processes.

During *quenching*, heat flux density radically decreases from the high temperature where shock boiling exists. During *heating* of thin specimens, heat flux density slowly increases when the liquid is approximately at the boiling temperature. These processes (quenching and heating) are absolutely different. During quenching, the wall temperature decreases very quickly to the initial temperature of the self-regulated thermal process ϑ_I and then decreases very slowly until reaching the value ϑ_{II}. For a cylinder of 100-mm diameter, the wall temperature during the self-regulated thermal process, which is equal to 138 s, changes from 106.16°C to 104.1°C. It is possible to use an average temperature of

105.1°C (see Eq 44) and average temperature differ from real temperature only ±3 % (see Eqs 37 and 38)

$$T_{sf} = T_S + \overline{\xi}_0 \approx const, \qquad (44)$$

where:
T_{sf} is the surface (wall) temperature of a body;
T_S is the saturation temperature; and
$\overline{\xi}_0 = \overline{T}_{sf} - T_S$ is average wall overheat.

Such a simplified approach is more reliable than heat transfer coefficient calculations. The self-regulated thermal process, in many cases, starts immediately after immersion of a steel part into the quenchant if film boiling is absent.

It is unusual to consider that full film boiling could be absent during quenching from 800°C to 900°C in cold water salt solutions. Usually, it is assumed that three modes of heat transfer will exist: film boiling, nucleate boiling, and convective heat transfer. Evidence for the absence of film boiling include:

- Prior to boiling, cold liquid should be heated to the saturation temperature, and during this time, the wall temperature of the steel part decreases significantly because the specific heat of water and aqueous salt solutions is rather high [27].
- When quenching in water and aqueous salt solutions, a double electrical layer is established between wall and liquid, which eliminates film boiling [27,43] (see Chapter 3, Section 3.5).
- Recent studies show that initial heat flux density, moving from wall to liquid at the very beginning of immersion, is a finite value that is often less than the first critical heat flux density [34,39].
- CFD (computational fluid dynamics) modeling has shown that during quenching in agitated water, the temperature of the boundary layer remains below saturation temperature [39].
- It has been discovered that shock boiling increases the critical heat flux density and wall superheat [31,36].
- Acoustical analyses have provided evidence that film boiling is absent [29,30].

These factors have been effectively used since 1968 in heat-treating industries [20,31,32,42]. An important discussion was published in 1976 in which the self-regulated thermal process was considered [44,45]. The primary issue there was whether vapor bubbles can affect quenching processes. As seen from Figs. 14 and 15, during immersion of steel parts into a cold quenchant, heat flux and heat transfer coefficients are huge, which is a result of the behavior of the small bubbles formed during boiling in cold liquids. Types of boiling processes are presented in Fig. 16 [2].

The presence of bubbles in a quenching system:
- can be seen,
- can be heard,
- can be felt due to tiny vibrations of thin steel parts during quenching,
- can be measured by noise control systems, and
- can be calculated.

More information is provided [2] (see Fig. 16).

The Labuntsov [5] equation works well when we approach the scheme shown in Fig. 16 from the left side. However, the quenching processes should be considered from the opposite upper side, where at the beginning shock boiling is observed (see Fig. 17).

Shock boiling during quenching in cold liquids, according to French, is very short-lived (see Table 15). Independently
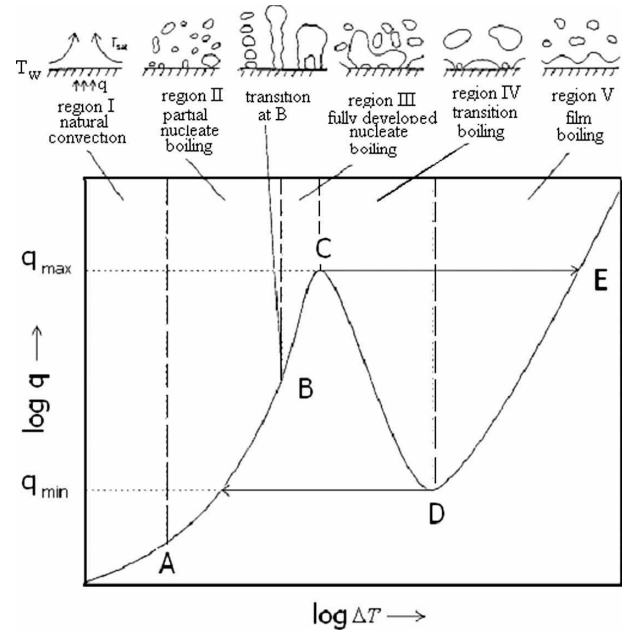
Fig. 16—Typical boiling curve, showing qualitatively the dependence of the wall heat flux, q, on the wall superheat, ΔT, defined as the difference between the wall temperature, T_w, and the saturation temperature, T_S, of the liquid. Schematic drawings show the boiling process in five regions, designated I–V, illustrated and discussed in [2], including the transition points A–E.

of the size of the steel part, the duration of shock boiling is less than one second. Based on these facts, the generalized analytical equation (Eq 36) was achieved to calculate the duration of transient nucleate boiling and the self-regulated thermal process [27]. The difference between transient nucleate boiling and the self-regulated thermal process is less than one second.

2.7.2 Why Is It Important to Study Shock Boiling?
The initial stage of the formation of nucleate boiling requires much more careful attention to understand the
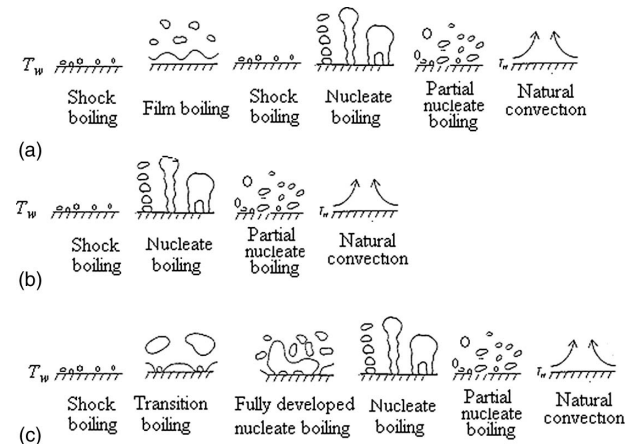

Fig. 17—Scheme showing three possible ways of evolution of the boiling processes: (a) conventional quenching where film boiling exists; (b) intensive quenching in water-salt solutions of optimal concentration where film boiling is completely absent; (c) quenching of large steel parts in cold, slightly agitated water where film boiling is absent, but transition boiling exists.

shock boiling phenomenon [44−47]. There is a need to develop a theoretical approach for explaining the absence of film boiling during immersion of heated steel parts into cold liquids [27,38,41].

The duration of the first stage is very short, probably due to shock boiling, which removes a huge amount of heat from the heated surface. Let us analyze experimental data of French [26]. At quenching of steel spheres 38.1 mm in diameter from a temperature of 875°C in cold water containing some salts, the first stage takes only 0.5 s, whereas the time of the self-regulated thermal process calculated by Eq 36 is 22−23 s. The average convection heat transfer coefficient was equal to 1,200 W/m^{2}K. Thus, the duration of the first stage equates to only 2 %. During this insignificant time, the boundary liquid layer is heated to the temperature of boiling, and then is overheated to $\Delta T = T_{Sf} - T_S$, where formation of tremendous nucleating centers occur. It takes only 0.5 s for all these complicated processes.

Despite the insignificant duration of the first stage, its careful study is of practical interest. Using special additives effecting surface tension, one can control processes occurring in the boundary liquid layer at the initial period of time [27,38,41].

Really, when considering Eq 6 connecting the critical size of bubbles with the surface tension σ (in N/m), one can see the essential effect of the surface tension of a liquid on the critical size of a bubble. The smaller the critical size of a bubble, the more bubbles can arise in a unit of surface area. Finally, it will affect the first critical heat flux density, which causes film boiling processes "to be or not to be."

For intensive quenching technologies, film boiling is undesirable and should be suppressed completely. Therefore, it is very important to have special additives that considerably increase the first critical heat flux density $q_{cr.1}$.

Because the initial period of the formation of a boundary boiling liquid layer has been poorly studied, it is important to plan ways that could help to start such investigations. In our opinion, the analysis of sound effects that occur at the formation of a boundary boiling liquid layer has good prospects. One of the most promising studies is the analysis of many channels, each responsible for a certain frequency range of the sound oscillations of vapor bubbles. This makes it possible to draw important conclusions about the first stage of quenching [29−31].

The sound analysis of the initial stage should also be accompanied by visual examination using a high-speed camera-recorder. It is also important to make accurate measurements of the surface temperature and duration of the first stage at quenching of samples or steel parts. For this purpose, one can use the well-known Liscic-Nanmac probe [13]. The probe measures temperatures at the surface and at a distance of 1.5 mm from the surface precisely enough by means of special, very exact thermocouples with a thickness of 0.025 mm.

The combination of visual examination with exact measurement of temperature at the surface and the appropriate analysis of sound effects through many channels can lead to a profound understanding of the phenomena that are observed at the time of immersing parts to be quenched into the cold quenchant. On the other hand, it is important to acquire statistical data related to the character of changes in surface temperature, which sharply reduces from the initial value (temperature of austenization) up to the saturation temperature of the quenchant.

Having such statistical data, it is possible to calculate precisely the heat transfer coefficients for the first stage of intensive cooling, that is, the forming and boiling up of a boundary liquid layer. In some cases, these data can be used as boundary conditions of the first kind.

Measurement of the surface temperature of parts at nucleate boiling, as already mentioned, is quite a difficult problem. Here it is more expedient to measure the time of transient nucleate boiling using sound effects. This will allow proceeding to boundary conditions of the first kind, since the computation of temperature fields by such an approach will be very accurate.

For the determination of the time of nonstationary nucleate boiling, it is important to know a convection heat transfer coefficient. For its determination, one can use techniques described in [29,30,36].

These issues have been discussed in more detail in [27,31] and applied in practice [48−51].

2.7.3 The Self-Regulated Thermal Process Is Widely Used in Practice

The self-regulated thermal process is widely used in practice [31,51]. It can be also used to manufacture extremely high-strength materials with plain carbon steels by applying high-temperature thermomechanical treatment (HTMT) or low-temperature thermomechanical treatment (LTMT).

To make the LTMT process possible, it is necessary to supercool austenite to 400−500°C, where it should be deformed to certain degree. Transformation during this time should be delayed, and supercooled austenite should be stable. For this purpose, as a rule, high-alloy steels, which allow such procedure, are used. Using the self-regulated thermal process, one can extend the possibilities of LTMT for plain carbon steels, and especially for high-carbon steels [27]. The LTMT process requires the delay of transformation of austenite into martensite during quenching, particularly when applying intensive quenching. The problem is that, during intensive quenching, the temperature at the surface of a steel part drops rapidly to saturation temperature, while the temperature at the core remains very high. Immediately at the surface, a brittle martensitic layer is formed, which precludes the process of mechanical deformation. To make the LTMT process possible, one should delay the transformation of austenite into martensite during intensive quenching—which can be done by using the self-regulated thermal process. As is already known, delay of the austenite-to-martensite transformation can be achieved by using appropriate pressure or water-salt solutions [27].

At present, LTMT has been used for high-alloy steels where supercooled austenite remains stable at low cooling rate to 400−500°C. Unfortunately, this cannot be done for low-alloy and plain carbon steels. That is why LTMT is not widely used in practice. Our investigation extends the possibility of using HTMT and LTMT in combination with intensive quenching [27]. In such a way, high-strength materials can be achieved that are as strong as Damascus steel. This concept was discussed in detail in Chapter 1.

2.8 LIST OF SYMBOLS

a thermal diffusivity (m^2/s)
Bi conventional Biot number (dimensionless)
Bi_V generalized Biot number (dimensionless)
C, c numerical factors
c_p specific heat capacity (kJ/kgK)

d_o bubble departure diameter

f bubble release frequency (Hz)

g gravitational acceleration (m/s^2)

$K = \dfrac{q}{\rho''' r^* W''}$ Tolubinsky number (dimensionless)

K Kondratjev form factor (m^2)

Kn Kondratjev number (dimensionless)

n_s nucleation sites density (m^{-2})

p pressure (Pa)

q heat flux density (W/m^2)

r coordinates (m)

r^* latent heat of evaporation (J/kg)

R_{cr} critical radius of a bubble (m)

S surface area (m^2)

T temperature (K or °C)

T_S saturation temperature (K or °C)

T_c core temperature (K or °C)

T_m medium (bulk) temperature (K or °C)

V volume (m^3)

W'' vapor bubble growth rate (m/s or mm/s), $= d_o f$

x coordinates (m)

α heat transfer coefficient (W/m^{2}K)

β parameter depending on properties of liquid and vapor

β' volumetric expansion (1/K)

ϑ_I wall superheat at the beginning of self-regulated thermal process

ϑ_{II} wall superheat at the end of self-regulated thermal process

ϑ_c $T_c - T_S$

λ thermal conductivity (W/mK)

μ dynamic viscosity (kg/m·s)

v kinematic viscosity (m^2/s)

ρ liquid density (kg/m^3)

ρ'' vapor density (kg/m^3)

σ surface tension (N/m)

τ time (s)

2.9 SUMMARY

1. The generalized equation for the determination of the duration of transient nucleate boiling has been obtained, which includes the self-regulated thermal process. This equation is a basis for development of intensive steel quenching methods.

2. The generalized equation is verified by experiments and is widely used for the development of quenching recipes when designing the above-mentioned technologies.

3. Wall overheat during the self-regulated thermal process changes very slowly and can be derived from the equation: $\alpha_{nb} = \beta q^m$, where $\beta = 7.36$ and $m = 10/3$.

4. Equations of Labuntsov and other authors, which were established on the basis of heating thin wire immersed into boiling liquid, can be used only qualitatively, not quantitatively, for designing of quenching processes.

5. During the self-regulated thermal process, one can consider surface temperature as a constant value, that is, $T_{sf} = T_S + \dfrac{\vartheta_I + \vartheta_{II}}{2}$, and use this approach for simplified temperature field calculations with an accuracy of ±3 %.

6. During quenching of steel parts in cold water salt solutions of optimal concentration, film boiling is absent. The initial stage of quenching includes shock boiling, which is not widely and deeply investigated yet.

7. During quenching of real machine components, including massive rollers and rotors, heat flux density after establishing the self-regulated thermal process is less than $q = 0.1q_{cr1}$, and therefore partial boiling is observed and Tolubinsky investigations are very useful here.

8. Taking into account characteristics of the self-regulated thermal process, it is possible using plain water instead of oils when quenching alloy and high-alloy steels, which improves environment conditions significantly.

9. The self-regulated thermal process extends the possibility of high-temperature and low-temperature thermomechanical heat treatments to the manufacture of very high-strength materials using plain carbon steels.

10. Further special investigations are needed here, which can be successfully done by an international team [52].

11. There is a need to develop standards for intensive quenching technologies and to publish books for heat treaters and engineers to explain the new discovered processes.

References

[1] Tolubinsky, V. I., *Heat Transfer at Boiling*, Naukova Dumka, Kyiv, 1980.

[2] Dhir, V. K., Boiling Heat Transfer, *Annu. Rev. Fluid Mech.*, Vol. 30, 1998, pp. 365–401.

[3] Yagov, V. V., Nucleate Boiling Heat Transfer: Possibilities and Limitations of Theoretical Analysis, *Heat and Mass Transfer*, Vol. 45, 2009, pp. 881–892.

[4] Markus, B. D., and Dropkin, D., Experimental Study of Temperature Profiles in Overheated Boundary Layer over Horizontal Surface at Nucleate Boiling in Great Volume, *Proc. of American Society of Eng. Mech.*, Series S, Vol. 87, No. 3, 1965, pp. 14–34.

[5] Labuntsov, D. A., Physical Fundamentals of Power Engineering, *Selected Works on Heat Transfer, Hydrodynamics and Thermodynamics*, MPEI, Moscow, 2000.

[6] Isachenko, V. P., Osipova, V. A., and Sukomel, A. S., *Heat Transfer*, Energoizdat, Moscow, 1981.

[7] Kutateladze, S. S., *Heat Transfer at Condensation and Boiling*, Mashgiz, Moscow, 1952.

[8] Kobasko, N. I., and Zhovnir, H. I., Analytical Method of Solving Thermal Problems for Steel Quenching, *Visnyk of Academy of Sciences of Ukrainian SSR*, No. 12, 1979, pp. 41–50.

[9] Diarmati, I., *Non-equilibrium Thermal-Dynamics*, Mir, Moscow, 1974.

[10] Lienhard IV, J. H., and Lienhard V, J. H., *A Heat Transfer Textbook*, 3rd Ed., Phlogiston Press, Cambridge, Massachusetts, 2005.

[11] Lavrentiev, M. A., and Lyusternik, L. A., *Course of Variational Calculus*, Gosizdat, Moscow, 1950.

[12] Lykov, A. V., *Theory of Heat Conductivity*, Vysshaya Shkola, Moscow, 1967.

[13] Liščič, B., Tensi, H. M., and Luty, W., *Theory and Technology of Quenching*, Springer-Verlag, Berlin, 1992.

[14] Michlin, S. G., *Numerical Implementation of Variational Methods*, Nauka, Moscow, 1966.

[15] Totten, G. E., Tensi, H. M., and Stich, A., Temperature Measurement Accuracy in Cooling Curve Analysis, *Heat Treat Progress*, Vol. 2, No. 4, 2002, pp. 45–49.

[16] Kobasko, N. I., Computer Analysis of Thermal Processes During Quenching of Steel, *Metal Science and Heat Treatment*, Vol. 18, No. 10, 1976.

[17] Kondratjev, G. M., *Regular Thermal Mode*, GITL, Moscow, 1952.

[18] *Thermal and Physical Properties of Materials*, Vargraftik, N. B., Ed., Gosenergoizdat, Moscow, 1956.

[19] Kobasko, N. I., and Kostanchuk, D. M., Calculation of the Cooling Capacity of Quenching Media by Using the Characteristics of the Boiling Process, *Metal Science and Heat Treatment*, Vol. 15, No. 10, 1973.

[20] Kobasko, N. I., Thermal Processes in Quenching of Steel, *Metal Science and Heat Treatment*, Vol. 10, No. 3, 1968.

[21] Kobasko, N. I., Effect of Pressure on Quenching of Steel, *Metal Science and Heat Treatment,* Vol. 20, No. 1, 1978.

[22] Kobasko, N. I., Intensification of the Quenching Process in Steel, *Metal Science and Heat Treatment,* Vol. 12, No. 2, 1970.

[23] Kobasko, N. I., Methods of Preventing Distortion and Crack Formation at Quenching of Steel Parts, *Metal Science and Heat Treatment,* No. 4, 1973, p. 12.

[24] Kobasko, N. I., Methods of Increasing the Steel Durability on the Basis of Extending the Possibilities of Low-Temperature Thermomechanical Heat Treatment, *Technology and Organization of Production,* No. 2, 1977, p. 72.

[25] Kobasko, N. I., Self-Regulated Thermal Process at Steel Quenching, *Promyshlennaya Teplotekhnika,* Vol. 20, No. 5, 1998, pp. 10–14.

[26] French, H. J., *The Quenching of Steels,* American Society for Steel Treating, Cleveland, OH, 1930.

[27] Kobasko, N. I., *Steel Quenching in Liquid Media Under Pressure,* Naukova Dumka, Kyiv, 1980.

[28] Kobasko, N. I., and Timchenko, N. P., Cinematographic Investigations of the Cooling Process of Alloys in Aqueous Polymeric Solutions, *Metal Science and Heat Treatment,* Vol. 28, No. 10, 1986, pp. 729–734.

[29] Povsten, S. G., Kobasko, N. I., Moskalenko, A. A., and Tyltin, A. A., On the Use of Monitoring Noise Effects for Realization of New Steel Quenching Methods, *Proc. of the 7th International Congress on Heat Treatment,* December 11–14, 1990, Moscow.

[30] Moskalenko, A. A., Kobasko, N. I., Protsenko, L. M., and Rasumtseva, O. V., Acoustical System Analyses: The Cooling Characteristics of Water and Water Salt Solutions, *Proceedings of the 7th IASME/WSEAS International Conference on Heat Transfer, Thermal Engineering and Environment (HTE '09),* Moscow, August 20–22, 2009, pp. 117–122.

[31] Kobasko, N. I., Transient Nucleate Boiling as a Law of Nature and a Basis for Designing of IQ Technologies, *Proceedings of the 7th IASME/WSEAS International Conference on Heat Transfer, Thermal Engineering and Environment (HTE '09),* Moscow, August 20–22, 2009, pp. 67–75.

[32] Kobasko, N. I., Quenching Apparatus and Method for Hardening Steel Parts, U.S. Patent No. 6,364,974 BI, April 2, 2002.

[33] Kobasko, N. I., Self-regulated Thermal Processes During Quenching of Steels in Liquid Media, *IJMMP,* Vol. 1, No. 1, 2005, pp. 110–125.

[34] Kobasko, N. I., What Is Duration of Non-stationary Nucleate Boiling and Thermal Equilibrium During Quenching of Steel Parts? *Proceedings of the 6th IASME/WSEAS International Conference on Heat Transfer, Thermal Engineering and Environment (HTE '08),* Rhodes, Greece, August 20–22, 2008, pp. 529–533.

[35] Ravnic, F., and Grum, J., Detection and Processing of Sound Signals in Steel Quenching, *Defectoskopie* (Brno), Vol. 11, No. 4–6, 2008, pp. 283–294.

[36] Kobasko, N. I., Moskalenko, A. A., Totten, G. E., and Webster, G. M., Experimental Determination of the First and Second Critical Heat Flux Densities and Quench Process Characterization, *Journal of Materials Engineering and Performance,* Vol. 6, No. 1, 1997, pp. 93–101.

[37] Tikhonov, A. N., and Glasko, V. B., Application of Regularization Method in Non-Linear Problems, *Jour. of Comp. Math. and Math. Physics,* Vol. 5, No. 3, 1965.

[38] Kobasko, N. I., and Guseynov, Sh. E., Initial Heat Flux Densities and Duration of Non-stationary Nucleate Boiling During Quenching, *Proceedings of the 5th WSEAS International Conference on Heat and Mass Transfer (HMT '08),* Acapulco, Mexico, January 25–27, 2008, pp. 104–109.

[39] Krukovskyi, P., Kobasko, N., and Yurchenko, D., Generalized Equation for Cooling Time Evaluation and Its Verification by CFD Analysis, *Journal of ASTM International,* Vol. 6, No. 5, 2009.

[40] Dobryvechir, V. V., Kobasko, N. I., Zotov, E. N., Morhuniuk, W. S., and Sergeyev, Yu. S., *Software IQLab* (commercially available from Intensive Technologies Ltd., Kyiv, Ukraine, www.itl.kiev.ua).

[41] Guseynov, Sh. E., and Kobasko, N. I., On One Nonlinear Mathematical Model for Intensive Steel Quenching and Its Analytical Solution in Closed Form, *Proceedings of the 5th WSEAS International Conference on Heat and Mass Transfer (HMT '08),* Acapulco, Mexico, January 25–27, 2008.

[42] Kobasko, N., Aronov, M., Powell, J., and Totten, G., One More Discussion: "What Is Intensive Quenching Process?", *Journal of ASTM International,* Vol. 6, No. 1, 2009.

[43] Frenkel, Ya. I., *Kinetic Theory of Liquids,* Nauka, Leningrad, 1975.

[44] Trayanov, G. G., Discussion of Articles by Kobasko N. I. on Thermal Processes During Quenching of Steel, *Metal Science and Heat Treatment,* Vol. 18, No. 7, 1976, pp. 601–602.

[45] Kobasko, N. I., Thermal Processes During Quenching of Steel (Reply to G. G. Trayanov), *Metal Science and Heat Treatment,* Vol. 18, No. 7, 1976, pp. 602–607.

[46] Kobasko, N. I., Methods of Overcoming Self-deformation and Cracking During Quenching of Metal Parts, *Metal Science and Heat Treatment,* Vol. 17, No. 4, 1975.

[47] Aronov, M. A., Kobasko, N. I., and Powell, J. A., Basic Principles, Properties and Metallurgy of Intensive Quenching, SAE Technical Paper Series, No. 2002-01-1338, 2002.

[48] Aronov, M. A., Kobasko, N. I., and Powell, J. A., Practical Application of Intensive Quenching Process for Steel Parts, *Proceedings of the 20th Heat Treating Conference,* St. Louis, 2000.

[49] Aronov, M. A., Kobasko, N. I., Powell, J. A., Wallace, J. F., and Schwam, D., Practical Application of the Intensive Quenching Technology for Steel Parts, *Industrial Heating,* April 1999, pp. 59–63.

[50] Kobasko, N. I., Worldwide Use of Intensive Quenching, in *Heat Treating: Proceedings of the 21st Conference,* Shrivastava S. and Specht, F., Eds., 2001, ASM International, Materials Park, OH, pp. 164–172.

[51] Kobasko, N. I., Aronov, M. A., Powell, J. A., Canale, L. C. F., and Totten, G. E., Improved Production of Automotive Parts by Intensive Quench Processing, *La Metallurgia Italiana,* No. 2, 2006, pp. 13–22.

[52] Kobasko, N. I., Database for Cooling Capacities of Various Quenchants to Be Developed with the Modern Computational and Experimental Techniques, 2006, www.worldses.org/projects/Heat_and_Mass_Transfer.doc.

3

Critical Heat Flux Densities and Characteristics of Heat Transfer During Film Boiling

N. I. Kobasko,[1] M. A. Aronov,[1] and J. A. Powell[1]

3.1 USING CRITICAL HEAT FLUX DENSITIES TO OPTIMIZE AND MAINTAIN QUENCH SYSTEMS

A common approach to determining if a quenchant will harden a particular alloy is to examine its cooling curve (time–temperature) and compare it to the TTT (time-temperature-transformation) diagram for the alloy of steel to be quenched. Cooling curves for liquid quenchants are generated by using a standard Ø12.5 × 60 mm Inconel alloy probe [1−5].

When using this approach, one should remember that the cooling curve for the actual part will differ from the cooling curve as determined by the quench probe. This is because the heat transfer conditions during quenching depend on the geometry and dimensions of the part being quenched. For example, the boiling process may take place during quenching of the probe, yet be absent when quenching a real part. Since the part and the probe cooling curves may differ significantly, the selection of a proper quenchant for a specific part may not be accurate if using only the standard quench cooling curve. Nevertheless, the use of cooling curves generated from the standard probe is effective when comparing different quenchants to each other or tracking quenchant quality changes over time.

This chapter discusses a different concept for evaluating the cooling capacity of quenchants other than just the standard cooling curves. This concept is based on the use of *critical heat flux densities*–parameters characterizing the boiling process for a particular quenchant. As will be shown, knowledge of the critical heat flux densities of the quenchant may be considerably more helpful for heat treaters and metallurgists. Unlike cooling curves, data on a quenchant's critical heat flux densities allow the heat treater to provide the optimal conditions for achieving the desired hardness and to enhance distortion control for any part under any quenching conditions. Furthermore, as with quench cooling curves, the critical heat flux densities may be used for quality control to assure that the quenchant's optimal quenching characteristics are maintained over time. Finally, knowledge of critical heat flux densities will provide for more accurate computer simulations of the quenching processes of specific parts and specific alloys. To define critical heat flux densities, let us first consider the modes of heat transfer during quenching in a liquid media [6−9].

When quenching in a vaporizable liquid (e.g., oil, polymer/water, brine, or water), four modes of heat transfer are typically encountered at the interface of the hot part and the quenchant (the boundary conditions). In order of their occurrence upon cooling of austenitized steel, these modes of heat transfer are:

- Shock boiling
- Full film boiling
- Nucleate boiling
- Convective heat transfer

3.1.1 Shock Boiling

The first stage of quenching, which occurs immediately upon immersion of hot steel into a vaporizable liquid quenchant, is "shock" boiling. Although most reviews on the quenching process address film boiling, nucleate boiling, and convection cooling, shock boiling is rarely considered. This initial stage of cooling occurs over a very short period of time: the relatively cold quenchant is flowing along the hot steel's surface while the part is being immersed into the quench [10]. The quenchant temperature in the boundary layer rises up very fast to a boiling temperature due to the very large temperature difference between the hot surface of the part and the quenchant. For example, a surface layer of a water-salt solution is heated to the boiling temperature in about a tenth of a second [6].

The modes of heat transfer during this short period of time are the following: First, there is convection heat transfer. Then nucleate boiling begins, with the formation of small vapor bubbles, followed very quickly by larger bubbles that grow in size and number until they detach from the part's surface, forming a "vapor blanket" of film boiling around the hot part. The formation of the vapor blanket over the entire part surface is the end of the shock boiling mode, and the beginning of the second mode of heat transfer during quenching, full film boiling.

In spite of the fact that shock boiling occurs over a very short period of time, we must consider the shock boiling process as very important, since it sets into motion all the subsequent modes of heat transfer that directly affect the remainder of the quench process and, therefore, all of the part's properties "as quenched."

The initiation of boiling on a part's surface depends on many factors, including:

1. The thermal and physical properties of the liquid and material being quenched–for example, the specific heat capacity, heat conductivity, density and quenchant surface tension, and quenchant viscosity

---

[1] IQ Technologies, Inc., Akron, Ohio, and Intensive Technologies Ltd., Kyiv, Ukraine

45

2. The quenchant agitation rate relative to the various part surfaces
3. Quenchant temperature
4. Surface temperature
5. Surface roughness
6. The part's orientation angle relative to the top of the liquid bath and direction of quench flow
7. Convective heat transfer at the interface of the part and the liquid

3.1.2 Full Film Boiling

After a very short period of shock boiling, the second mode of heat transfer from the cooling part to the liquid quenchant is "full film" boiling. The heat transfer rate when full film boiling first occurs defines the first critical heat flux density, q_{cr1} (note that the "density" of the "critical heat flux" indicates the amount of energy transferred from a given area, e.g., from 1 m^2). During full film boiling, the surface is fully engulfed by a vapor blanket (in the case of water, this vapor blanket is steam; in the case of oil, it is vaporized oil). The heat flux (that is, the heat passing through the part surface) slowly decreases as the part's surface and core are cooling. Eventually the heat flux becomes insufficient to support full film boiling on the part surface. The film boiling process then becomes unstable and erratic. The vapor blanket begins to collapse in some areas of the part surface, quickly re-form in other areas, and then collapse again, until the nucleate boiling process initiates. These nonuniform heat transfer conditions along the part surface areas (during the transition from the film boiling process to the more uniform nucleate boiling process), along with the changes in volume of the steel (during phase change from austenite to martensite), are the major contributors to part distortion (or cracking) during quenching.

When the vapor blanket starts to collapse, the quenchant begins contacting the part surface directly (and the "wetting process" starts). Note that the temperature of the part surface at this period of time should not be associated with the Leidenfrost temperature [7,8]. This is because the surface temperature of the part being quenched can differ from the values of the Leidenfrost temperature due to dissimilar conditions of heat transfer when quenching the part and during the procedure used for Leidenfrost temperature determination.

The duration of film boiling depends on many factors, including part shape and size, quenchant media, physical properties, part and quenchant temperatures, and quenchant agitation. Film boiling can last from a few seconds to tens of seconds on the same part [9,10]. For example, inside of a blind hole, film boiling will proceed for a longer time than in the area on the outer surface of the part where the agitation is greater. Also, film boiling typically occurs for a longer period of time on the bottom surface of the part due to the inhibition of bubbles leaving that surface and rising to the top of the tank.

3.1.3 Nucleate Boiling

Fig. 1 presents qualitatively the change of the heat flux from the surface of a part during quenching. This is basically a Nukiyama boiling curve [9] in reverse. Note that typical boiling curves presented in technical literature were obtained for heat transfer conditions in boilers during a *heating* cycle, while we are considering the *quenching* process, when the part surface temperature changes from high values to lower ones.
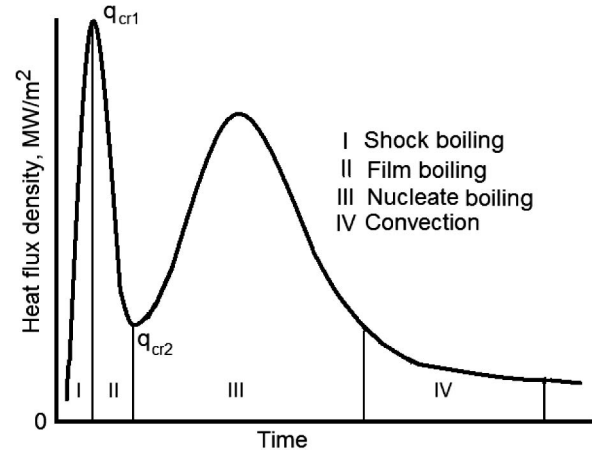
Fig. 1—Scheme of heat transfer modes during quenching of steel parts.

When the heat flux from the part can no longer support the film boiling mode, there is a shift to the nucleate boiling mode of heat transfer (see Fig. 1). The second critical heat flux density, q_{cr2}, occurs when the film boiling vapor blanket fully collapses, and nucleate boiling heat transfer takes the place of film boiling.

Nucleate boiling is characterized by a very high rate of heat extraction (a high heat transfer coefficient) at the surface of the part due to the formation each second of a large number of tiny bubbles over the part surface. The absence of the film blanket allows more of the surface to be exposed to the liquid phase of the quenchant and not the gaseous vapor phase. Therefore, as soon as the nucleate boiling mode of heat transfer starts, the heat flux from the part surface begins increasing (see Fig. 1).

In addition to being a fast mode of heat transfer, nucleate boiling is a more stable and more uniform mode of cooling. Compared to film boiling, there is usually less part distortion associated with the nucleate boiling mode. As with film boiling, the actual duration of nucleate boiling around the part depends on many factors, such as part shape and size, the quench medium's physical properties, temperature, and agitation.

Fig. 2 presents qualitatively the change of the part surface temperature (T_w) during quenching. During nucleate boiling, the part's surface temperature drops almost to the
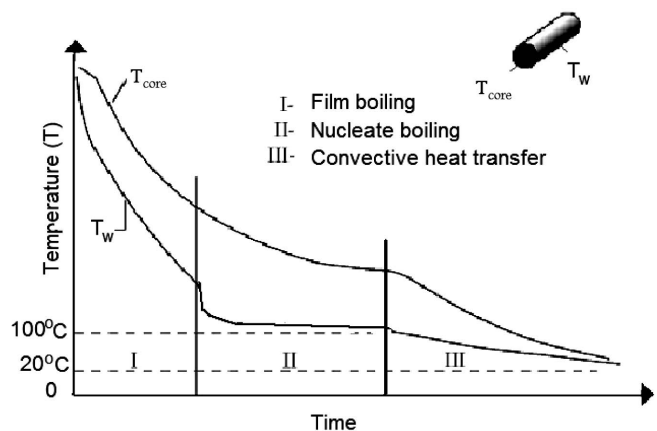

Fig. 2—Typical curves of cooling of the surface (T_w) and the core (T_{core}) during quenching of steel parts in agitated warm water.

water boiling temperature (in water, T_w is about 105–110°C). This plateau in the part surface temperature during the entire nucleate boiling mode (see phase II in Fig. 2) makes this cooling phase stable–a "self-regulated thermal process," as we have called it–once it is established [6]. As nucleate boiling continues, the part is getting colder, and the heat flux from the surface decreases. At some point in time, the heat flux from the part cannot support the nucleate boiling mode, and the last phase of the quench commences as convection cooling (phase III in Fig. 2).

3.1.4 Convective Heat Transfer
After nucleate boiling ceases, the surface temperature decreases from slightly above the boiling temperature of the quenchant down to the bulk fluid temperature. Convection cooling is a characterized by a much slower cooling rate than either film boiling or the nucleate boiling (see Fig. 1). Convection cooling is also more uniform along the surface of the part. Heat treaters appreciate the convection mode of quenching for its uniform cooling, since only minimal distortion occurs during this process. (This is why the gas quenching usually provides less distortion than a vaporizable liquid quench.)

3.1.5 Importance of Critical Heat Flux Densities
The critical heat flux densities q_{cr1} and q_{cr2} are inherent properties of any vaporizable quenchant. As mentioned above, the first critical heat flux density (q_{cr1}) is the *maximum* amount of thermal energy coming out of a unit of surface area needed to create film boiling in the given liquid over a hot surface area. The more "resistant" a liquid is to boiling when heat is applied, the higher the liquid's q_{cr1} is. The more resistant a quenchant is to boiling, the more likely it is to quench a part uniformly (with no film boiling), thus yielding less distortion. Also, with greater resistance to boiling, there is less likelihood of a "slack quench"–a quench that is sufficiently slow to produce spotty or lower than optimum as-quenched hardness for a given steel alloy.

On the other hand, the second critical heat flux density (q_{cr2}) is the *minimum* amount of heat energy necessary to support film boiling over the given surface area. In other words, q_{cr2} is the point at which the surface of the hot part has cooled sufficiently to allow the collapse of the vapor blanket, the end of film boiling, and the beginning of nucleate boiling over this same area.

Note that neither q_{cr1} nor q_{cr2} depends on the size of the steel part or the thermal properties of a material being quenched. These two parameters are inherent properties of the quenchant. In general, the greater the value of q_{cr1}, the less likely it is that the film boiling process will take place. The values for q_{cr1} do rise with agitation rates. The greater the agitation, the longer the amount of time needed for the liquid to reach the boiling temperature over a given hot area. If the agitation is sufficiently intensive, there will be little or no film boiling. Using violent agitation of the water quenchant to eliminate film boiling is one of the fundamental principles of intensive quenching.

The values of q_{cr1} can be used for determining an optimal concentration of soluble substances in water. Said another way, providing the maximum values of critical heat flux densities will result in minimization or even elimination of film boiling and the nonuniformity of cooling associated with it. The practical value of the elimination or minimization of film

boiling is to minimize part distortion from nonuniform cooling for a given liquid quenching system. When the heat flux from the part surface is equal to q_{cr1}, transition boiling can be observed. In this period of time, on the part surface, both the film boiling and nucleate boiling processes can take place locally, which may result in nonuniform part hardening and excessive part distortion.

3.1.6 Using a Silver Probe to Determine Critical Heat Flux Density
A spherical or cylindrical silver probe can be used to determine the cooling curve for a given liquid quenchant. Silver is used as the probe material because of its relatively high heat conductivity. Therefore, when a thermocouple is embedded at the geometric center of a silver probe, the temperature at the core will be approximately equivalent to the probe surface temperature.

As shown in Table 1, the heat conductivity of silver does not vary significantly within the temperature interval of 100–700°C. The average value of heat conductivity in the temperature range of 100–600°C is 371 W/mK. For comparison, the heat conductivity of austenitic stainless steel at these temperatures is 20 W/mK.

First, the silver probe is heated to 850°C (typically in the range of the austenitizing temperature for the steel parts that would be quenched in the liquid). After the probe reaches thermal equilibrium, it is immediately immersed into the liquid quenchant of interest. The quenchant may or may not be agitated. A cooling curve (cooling time vs. probe core temperature) is recorded, and the data are used to calculate the heat flux from the probe over time [2–5]. At present, a standardized Inconel 600 probe of Ø12.5 mm is used to provide cooling curves analysis [1–5].

Examination of the heat flux values calculated from the probe thermocouple data will show a sharp increase of the heat flux at some point in time. This heat flux represents the second critical heat flux density, q_{cr2} (see Fig. 3). As described above, q_{cr2} is the point when film boiling ends and (the faster and more uniform cooling) nucleate boiling becomes the primary cooling mode at the surface of the probe. To find the first critical heat flux density, q_{cr1}, the following experimental correlation between q_{cr2} and q_{cr1} is used [12–17]:

$$5q_{cr2} = q_{cr1}.$$

By repeating the above test procedures at different quench bath temperatures and agitation rates, the highest q_{cr1}–the point at which the quench bath is most resistant to film boiling–can be calculated. The highest q_{cr1} should correspond to the optimal quenching parameters (the temperature, and, to a lesser extent the agitation rate) that will produce the least amount of quench distortion in the parts

λ (W/mK)	Temperature (°C)							
	0	100	200	300	400	500	600	700
Steel	—	17.5	18	19.6	21	23	24.8	26
Silver	410	392	372	362	362	366	374	—

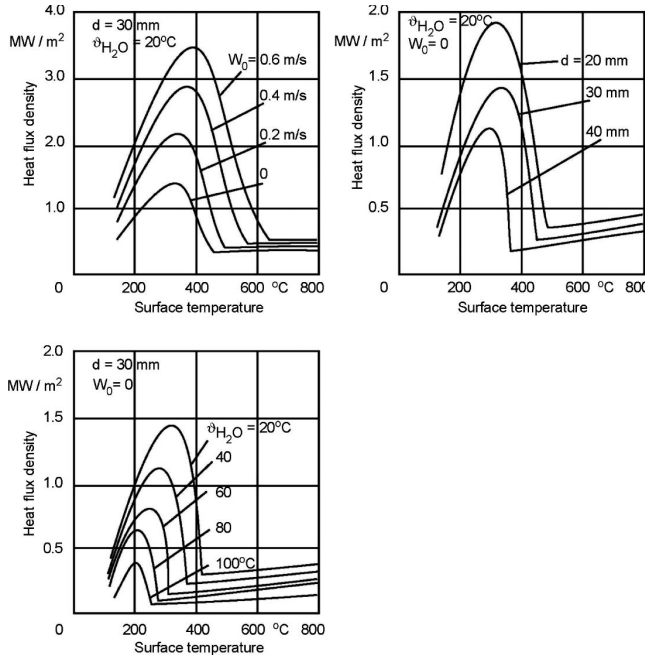**TABLE 1—Heat conductivity λ (W/mK) for nickel and silver versus temperature**

Fig. 3—Heat flux density for immersion quenching of nickel spheres in water baths as a function of the surface temperature, compared to the changes in bath temperature, sphere diameter, and flow velocity as variables [11].

being quenched. The first critical heat flux density q_{cr1} is affected by a combination of various physical properties, including oil viscosity, boiling point, chemical composition, and so on.

The operation of the quench tank at the highest q_{cr1} point (for a given quenchant) will assure that the onset of nucleate boiling will occur at the highest part surface temperature. In addition, it will mean less time under film boiling conditions, and therefore less nonuniform part cooling, and will provide more quenching time in the more uniform and faster nucleate boiling mode. Thus, the shorter the film boiling time and the longer the time that the part is cooled under nucleate boiling conditions, the more effective (fast and uniform) the quench cooling will be for a given liquid quenchant. Generally, with any quenchant, the more rapid the quenching cooling rate, the better the physical properties of the part will be after the quench: higher hardness, deeper hardness, better tensile strength, and greater ductility after part tempering.

Unfortunately, quenchant cooling curves (time−temperature curves) obtained at the core of standard probes for various quenchants reveal very little about what will happen to *actual* parts in *actual* quench tank conditions. However, unlike quench cooling curves, the knowledge of critical heat flux densities for a given quenchant, and the operation of the quench tank system at its maximum critical heat flux densities, q_{cr1} and q_{cr2}, will provide the heat treater with an optimized quenching process for that system and assure optimal hardness and lower distortion for all parts quenched in that system.

3.2 DETERMINATION OF Q_{CR1} UNDER FREE CONVECTION CONDITIONS

In this section, the boiling process on the part surface during cooling in the quench bath, with no force convection (that is, no agitation), is considered in detail. The technique

for determining of the critical heat flux densities q_{cr1} and q_{cr2} is described.

There are two approaches to explaining the mechanisms of the end of the film boiling process, when the vapor blanket starts collapsing on the part surface at the end of the full film boiling mode of heat transfer (see Fig. 1). The first is based on the fact that high intensity of heat transfer for nucleate boiling is maintained until the bubble filling (population) on the heated surface reaches a limit. The critical heat flux density corresponds to the upper limit of the number of nucleating sites formed on the heated surface. The correctness of such a concept is proved by experimental results [12], showing that when the heat transfer critical point is approached, a bi-phase layer (vapor bubbles and liquid) at the heated surface still exists.

The second approach is based on the consideration of the boiling collapse as a hydrodynamic phenomenon [13,14]. According to this idea, the heat transfer critical point occurs when the access of the liquid to a heated surface ceases, and steady film boiling is established–that is, when the liquid is pushed off and away from the heated surface by a continuous vapor layer.

A generalized correlation for the critical heat flux density q_{cr1} has been obtained by Kruzhilin [15] using dimensionless similarity parameters (a theory of similarity) according to the first approach discussed above. Tolubinsky et al. [12] developed this approach and obtained the following relationship for the calculation of the first critical heat flux density:

$$q_{cr1} = 7r^* \sqrt{af\rho'\rho''}, \qquad (1)$$

where:
q_{cr1} is the first critical heat flux density (W/m^2);
r^* is heat of vapor formation (J/kg);
a is thermal diffusivity of liquid (m^2/s);
f is a frequency of dispatch of vapor bubbles (Hz);
ρ' is density of liquid (kg /m^3); and
ρ'' is density of vapor (kg/m^3).

The second approach for the determination of q_{cr1} is based on the hydrodynamic theory of the heat transfer crises suggested by Kutateladze [13,14]. His notion of the boiling critical point is described by the hydrodynamic process only. The following equation for the first critical heat flux density was obtained:

$$q_{cr1} = kr^* \sqrt{\rho''} \sqrt[4]{g\sigma(\rho' - \rho'')}, \qquad (2)$$

where:
$k \approx 0.14$;
g is gravitational acceleration (m/s^2); and
σ is surface tension (N/m).

Eq 2 is true at the saturation temperature (boiling point) of a liquid. A cold liquid exhibits higher values of critical heat flux densities. This is illustrated by the "underheating" concept. Underheating is defined as a difference between temperature of saturation (boiling) and temperature of a quench bath, that is:

$$\vartheta_{uh} = T_S - T_m,$$

where:
ϑ_{uh} is the underheating of a cooling liquid;
T_S is saturation temperature; and

T_m is the temperature of the medium.

The first critical heat flux density increases as the underheating of a liquid increases and is determined by [12,13,16]:

$$q_{cr1}^{u.h} = q_{cr1}\left[1 + 0.065\left(\frac{\rho'}{\rho''}\right)^{0.8}\frac{Cp\,\vartheta_{u.h}}{r^*}\right], \qquad (3)$$

where:
$q_{cr1}^{u.h}$ is the first critical heat flux density of the cold liquid (quenchant); and
Cp is the specific heat capacity of the liquid, kJ/(kg°C).

The transition from film boiling to nucleate boiling is called the second critical point of the heat transfer at boiling. This transition exhibits as a critical point because, during the destruction of the vapor film and return to nucleate boiling, the heat transfer rate sharply increases and the surface temperature decreases. The temperature overheat corresponds to the minimum heat flux (at the end of film boiling, see Fig. 1).

The value of the second critical heat flux density q_{cr2} during boiling of the saturated liquid is less than q_{cr1}. The interrelationship between the first and second critical heat flux densities is expressed by [6,17]:

$$\frac{q_{cr2}}{q_{cr1}} \approx 0.2. \qquad (4)$$

Let's consider in more detail some of the factors affecting critical heat flux densities–in particular, the redundant pressure above the quench bath. When the pressure increases, the critical heat flux density also increases, as shown in Fig. 4.

To avoid the formation of the vapor blanket during steel quenching, it is necessary to reduce the temperature of the quenchant and, if possible, to increase the pressure above the surface of the quench bath. In those cases when it is impossible to reduce the quenchant temperature, it is useful to improve the liquid agitation rate–increased agitation may increase critical heat flux densities by several times.

Production quenching systems are usually equipped with propellers or pumps providing for liquid agitation in

Fig. 4—Comparison of dependence $q_{cr1} = q_{cr1}(P)$ computed by Eq 1 with experimental results [12,18,19] for water.

the quench bath. Under forced agitation conditions, the critical heat flux densities, described above, depend also on the quenchant circulation velocity. When the circulation velocity increases, the critical heat flux density increases, as well. Therefore, according to [17], for some liquids, the increase in speed of circulation from 1m/s to 5m/s increases q_{cr1} by 2.6 times.

3.3 TECHNIQUE OF DETERMINING CRITICAL HEAT FLUX DENSITIES UNDER TRANSIENT HEAT TRANSFER CONDITIONS

The idea of the proposed method is to measure the second critical heat flux density q_{cr2} using a silver probe and then to calculate the first critical heat flux density q_{cr1} using Eq 4 above. Measuring of q_{cr2} is done under full film boiling conditions on the probe surface. The silver spherical probe of 20-mm diameter is used to maintain full film boiling [10,19,20]. In later studies, it has been shown that the standard probe should be cylindrical, as shown in Fig. 5 [2,21].

The probe should have rounded ends to minimize the quenchant flow disturbance and for better uniformity of cooling of the probe [2,21,22]. Also, at the area where the thermocouple is placed, the heat transfer coefficient is more uniform along the probe surface as compared to the spherical probe when there is a quenchant flow vortex downstream of the probe.

The heat flux density is proportional to thermal conductivity, that is,

$$q = -\lambda\frac{\partial T}{\partial r},$$

at the time of immersion of a standard silver sample into the quenchant. Full film boiling is always observed on the probe surface, because the thermal conductivity of silver is 18 times greater than that of steel (see Table 1 above), and therefore, heat flux densities from the probe surface will be 18 times greater.

In the studies described below, cylindrical and spherical probes were used. In the majority of cases, experimental data were obtained from 20-mm-diameter spherical silver probes. However, for future work, preference should be given to cylindrical probes for the reasons stated above. Fig. 6 shows some experimental results (cooling rates) obtained with heated silver spherical probe immersion in water at different water temperatures [19,20].

There is no shock boiling shown here because the thermocouple at the core of the sample cannot detect shock boiling since it lasts only a very short time. Only a noise sensing system can detect the shock boiling mode [10].

Fig. 6 shows that water temperature and agitation rate significantly affect the cooling rate of spherical silver probes. From these data, the critical heat flux densities are estimated for nonagitated water at 20°C. The second critical heat flux density q_{cr2} can be calculated with the following equation:

$$q_{cr2} = \alpha_{FB}(T_{cr2} - T_S), \qquad (5)$$

where:
α_{FB} is a heat transfer coefficient under film boiling conditions (W/m²K);
T_{cr2} is a critical temperature of the surface that is in transition from film to nucleate boiling; and
T_S is the saturation temperature (for water at atmospheric pressure, $T_S = 100$°C).

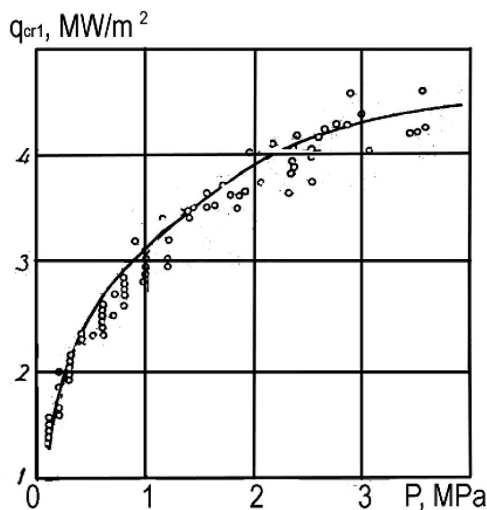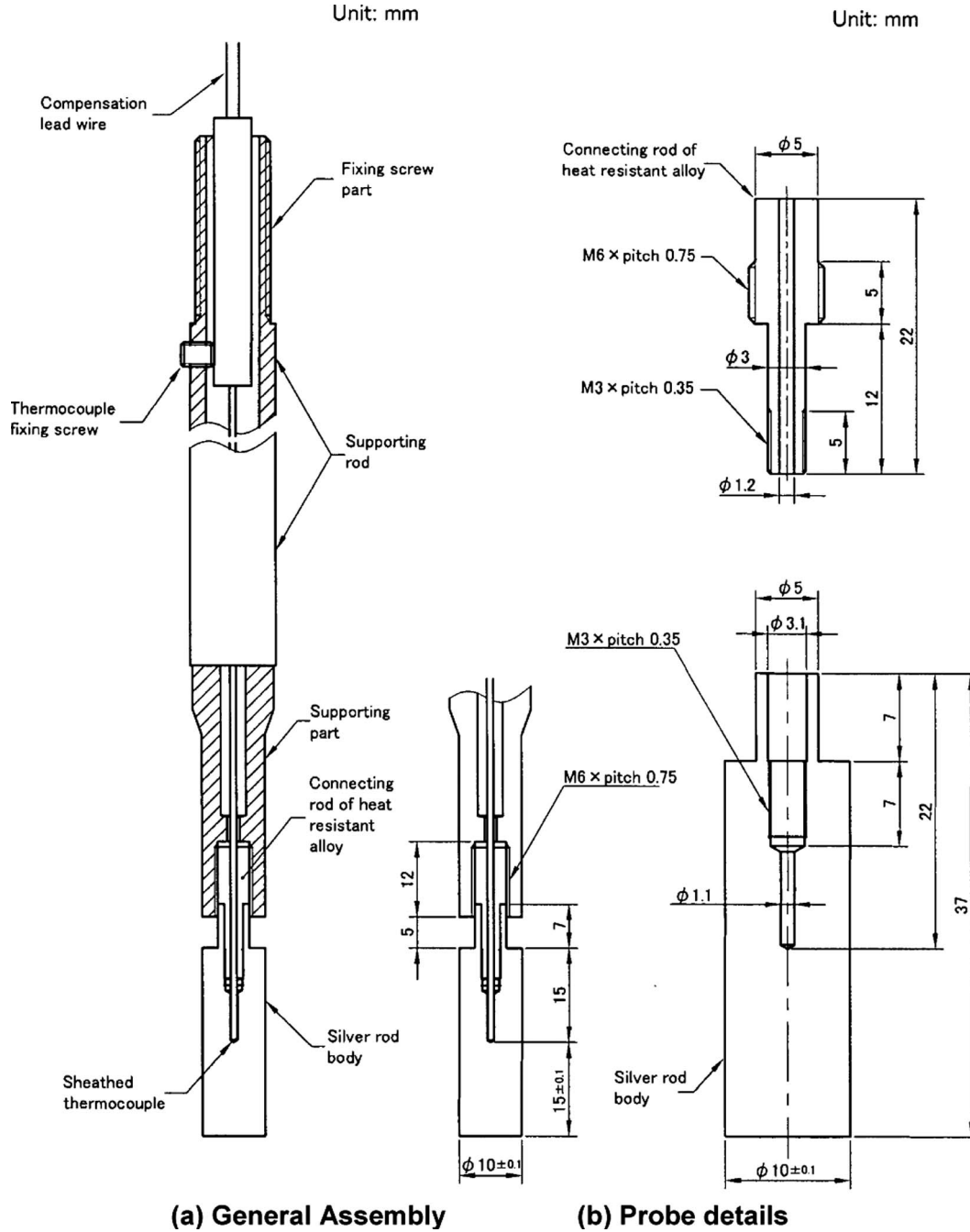**(a) General Assembly**   **(b) Probe details**

Fig. 5—The silver cylindrical probe and general probe assembly for measuring critical heat flux densities [2].

The heat transfer coefficient at the time of transition from film boiling to nucleate boiling can be determined from [21,23]:

$$v = m(T_{cr2} - T_S), \qquad (6)$$

where v is cooling rate of silver sphere and m is given by:

$$m = \frac{\alpha_{FB}\,\psi\,S}{c\rho\,V}.$$

For the calculation of m:
ψ is the criterion of temperature nonuniformity throughout the part cross-section;
c is the specific heat capacity of the material (silver);
ρ is the density of the material;

S is the surface area (m^2); and
V is the volume (m^3).

For low Biot numbers, the value of the temperature nonuniformity ψ is approximately 1, since the temperatures in the part's core and surface are almost equal, due to the very high heat conductivity of silver. For silver, $c\rho$ is calculated as follows:

$$c\rho = \frac{\lambda}{a} = \frac{362}{0.141 \cdot 10^{-3}} \approx 2567.376.$$

The term α_{FB} is calculated as follows:

$$\alpha_{FB} = \frac{R}{3} \cdot \frac{2,567,376 \times 173}{320} = 4627\,\text{W/m}^2\text{K}.$$
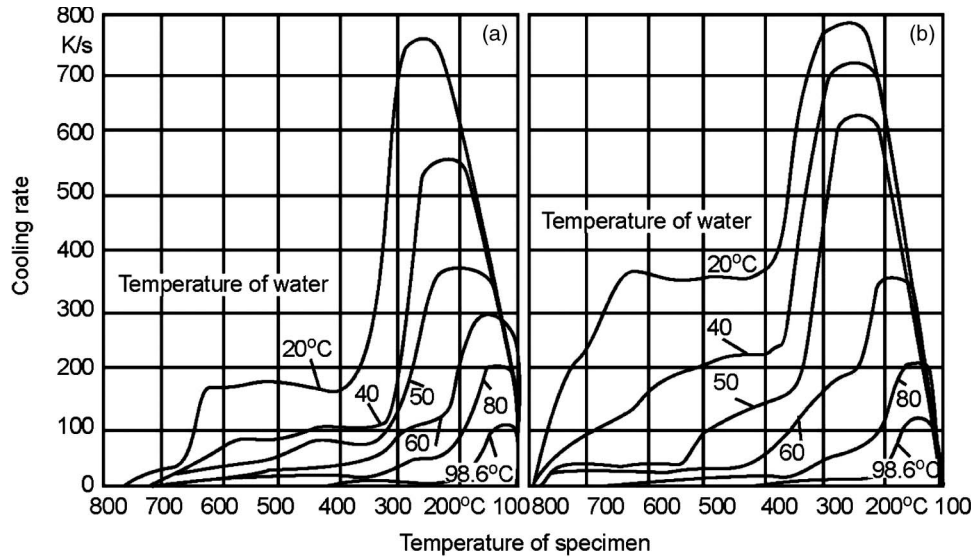
Fig. 6—Cooling rates of a silver spherical probe of 20-mm diameter after immersion in still water at different temperatures (a) and in water circulating at the rate of 0.25 m/s (b) [19,20].

Thus, q_{cr2} = 4,627 × 320 ≈ 1.48 MW/m². Taking into account a known ratio between q_{cr2} and q_{cr1} (see Eq 4):

$$q_{cr1} = \frac{1.48 MW/m^2}{0.2} = 7.4 MW/m^2.$$

These results are within 25% of the data shown in Table 2. The value of the first critical flux density obtained by Tolubinsky's equation for the same condition is 5.9 MW/m² (see Eqs 1 and 2). The calculation results can be considered satisfactory as a first approximation, given that the cooling rate was recorded at the center of the spherical probe while the surface temperature was unknown at the time of transition from film boiling to nucleate boiling.

Similar calculations were performed for quenching of a heated spherical silver probe in 40°C water. For the specified conditions, the cooling rate at the center of the sphere was v = 105°C/s, and transition from film boiling to nucleate boiling was observed at 473°C. The calculated heat transfer coefficient was α = 2,436 W/m²K and q_{cr2}, in this case, was equal to 908,600 W/m² or 0.909 MW/m². Taking into account the heat flux ratio (Eq 4):

$$q_{cr1} \approx \frac{0.909}{0.2} \approx 4.54 \, MW/m^2.$$

This value for the first critical heat flux density is much closer to the values shown in Table 2. From Eq 2 (Kutateladze), water at 40°C should exhibit a value of q_{cr1} of

approximately 4.40 MW/m², and from Eq 1 (Tolubinsky), the value for q_{cr1} would be about 4.72 MW/m². The average value from the above calculations is 4.56 MW/m², which falls between these two figures.

Therefore, using a silver probe, it is possible to determine critical heat flux densities of a liquid quenchant with relatively good accuracy. However, it is necessary to eliminate a shortcoming connected with the inaccurate measurement of the surface temperature when using a standard probe. To overcome this error, the following equation is used:

$$\frac{\overline{T}_{Sf} - T_S}{\overline{T}_V - T_S} = (Bi_v^2 + 1.437 Bi_v + 1)^{-0.5}.$$

The average surface temperature is then equal to:

$$\overline{T}_{Sf} = (\overline{T}_V - T_S)(Bi_v^2 + 1.437 Bi_v + 1)^{-0.5} + T_S.$$

By substitution of this result into Eq 5, the final expression for the determination of the second critical heat flux density is:

$$q_{cr2} = \alpha_F(\overline{T}_V - T_S)(Bi_v^2 + 1.437 Bi_v + 1)^{-0.5}. \quad (7)$$

In view of the interrelationship between the two critical heat flux densities (see Table 3 and Eq 4), the equation for the first critical heat flux density in the final form is:

$$q_{cr1} = 5\alpha_F(\overline{T}_V - T_S)(Bi_v^2 + 1.437 Bi_v + 1)^{-0.5}. \quad (8)$$

The average probe temperature can be determined by applying heat conductivity theory [24], where various analytical solutions of nonstationary heat conduction problems are described in detail with regard to heating and cooling for various bodies. Let us now consider examples of such analytical solutions for an infinite plate, an infinite cylinder, and a sphere. Assume that the coordinate origin is at the center of the subject shapes. For a plate, the average integrated temperature $\overline{T}_V$ is [24,25]:

$$\overline{T}_V(\tau) = \frac{1}{V} \int_V T(x, \tau) dv = \frac{1}{R} \int_0^R T(x, \tau) dx, \quad (9)$$

where $2R$ is the plate thickness.

TABLE 2—The first critical heat flux density q_{cr1} (MW/m²) versus underheating at normal atmospheric pressure for water

Equation	Underheating (°C)					
	0	20	40	60	80	100
Tolubinsky (Eqs 1 and 3)	1.27	2.40	3.57	4.72	5.90	7.06
Kutateladze (Eqs 2 and 3)	1.185	2.25	3.33	4.40	5.50	6.60

TABLE 3—Summary of reported values for the ratio of q_{cr2}/q_{cr1} as a constant [10]

Author(s)	q_{cr2}/q_{cr1} constant	Reference
V. I. Tolubinsky	0.05	[11], p. 237
S. S. Kutateladze	0.2	[12]
V. P. Isachenko, V. A. Osipova, and A. S. Sukomel	0.2	[16], p. 281
V. K. Koshkin, E. K. Kalinin, and J. A. Dreytser	0.2	[25], p. 287
N. I. Kobasko, A. A. Moskalenko, and G. E. Totten	0.204–0.207	[5], p. 94

The average temperature of the infinite cylinder is:

$$\overline{T}_V(\tau) = \frac{2}{R^2} \int_0^R r\, T(r, \tau)dr, \qquad (10)$$

and the average temperature of a sphere is:

$$\overline{T}_V(\tau) = \frac{3}{R^3} \int_0^R r^2\, T(r, \tau)dr. \qquad (11)$$

Substituting in Eqs 9–11, analytical solutions for the temperature fields for each of these shapes can be obtained. These analytical solutions for the average temperatures $\overline{T}_V(\tau)$ are given in the form of infinite series. Then, equating the average temperature $\overline{T}_V$ with the analytical solution $T(r, \tau)$, one can calculate the coordinates where the thermocouple should be located. For example, for an infinite cylinder, the thermocouple should be placed at the distance of $R/2$ from the axis. Moreover, recording the average temperature $\overline{T}$ at a point of $R/2$ significantly simplifies the measurement of q_{cr2}.

Practically, an "infinite" cylinder can be defined as a cylinder with the length more than four times greater than the diameter, that is, $\frac{\ell}{2R} \geq 4$. Thus, to measure critical heat flux densities q_{cr1} and q_{cr2}, it is better to use cylindrical probes made of silver (which provides full-film boiling) in which the thermocouple junction is located at the distance of $R/2$ from the axis.

Let us address one more issue related to the size of the silver probe. The probe size is an important factor because the heat flux density from the probe surface under transient heat transfer conditions depends on probe diameter. Probe diameter is especially critical during the nucleate boiling process, where the surface temperature rarely decreases below the quenchant boiling point. Note that the smaller the diameter of the probe, the greater the temperature gradient in the probe surface layer, and hence the greater the heat flux densities. When the probe surface temperature experiences a sharp decrease during nucleate boiling, the heat flux density is approximately inversely proportional to the section size. To confirm this point, refer to Fig. 3, where the effect of the section size upon the heat flux density is shown for cooling of spherical nickel probes in water at 20°C. As seen, different maximum heat flux densities for different

section sizes are observed. During cooling of a nickel probe of 20-mm diameter in water at 20°C, the maximum heat flux density is equal to 1.8 MW/m^2, while cooling a nickel ball of 40-mm diameter produces a maximum heat flux density of 1.15 MW/m^2.

As shown, when cooling the smaller diameter probe, the maximum heat flux density was greater by almost 1.6 times. Thus, for measurements of critical heat flux densities, it is important to use small probes, because this provides the condition $q > q_{cr1}$ and consequently the existence of the full film boiling mode of heat transfer on the probe surface. Up to now, reducing the section sizes of probes has been problematic due to such problems as an accuracy of the thermocouple placement in a small probe and measurement precision.

Thus far, the most suitable probe for measurements of critical heat flux densities is a cylindrical probe of Ø10 mm described in the Japanese Industrial Standard (JIS) K 2242 [26]. It can be used as reported, or it can be improved by placing the thermocouple junction at the distance of $R/2$ from the axis, and the ends of the cylindrical sample can be made rounded. These modifications make it possible to obtain more accurate measurements of the first and second critical heat flux densities.

3.4 EXPERIMENTAL MEASUREMENTS OF CRITICAL HEAT FLUX DENSITIES

Critical heat flux densities have been measured for some aqueous polymer quenchants that are widely used in the former Soviet Union, in particular polymer quenchant PK-2. Fig. 7 presents the results of q_{cr2} versus *underheating* of the quenchant (as defined in Section 3.2 above) with respect to saturation temperature [10,27]. A linear dependence of q_{cr2} and underheating is observed. As seen, the greater the underheating, the higher the value of q_{cr2}. This experimental finding agrees with Eqs 3 and 4, which correlate values of the critical heat flux density and underheating ($\vartheta_{uh} = T_S - T_m$).

Fig. 8 presents results for q_{cr2} versus the concentration of polymer PK-2. As the quenchant concentration increases, the second critical heat flux density decreases exponentially. These results indicate that the probability of the existence of the full-film boiling increases as the concentration increases.

Another question arises regarding the methodology used for determining critical heat flux densities and the relationship of these values to intensive quenching. However, it only matters that there exist optimal concentrations of aqueous solutions of any substances for which maximum values of the first and second critical heat flux densities can be
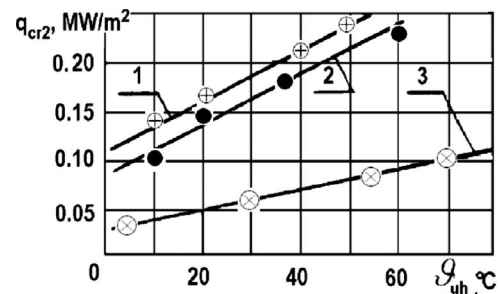

Fig. 7—Effect of underheating ϑ_{uh} on the second critical heat flux density q_{cr2} for polymer PK-2 and polyacrylamide: 1, polymer PK-2, results obtained using a spherical silver probe; 2, polymer PK-2, cylindrical silver probe; 3, polyacrylamide [27].
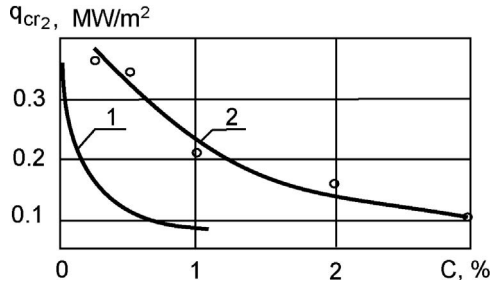
Fig. 8—Second critical heat flux density q_{cr2} versus the concentration of aqueous polymer solutions: 1, polyacrylamide; 2, polymer PK-2 [27].

Fig. 9—Schematic of the effect of ionic forces upon the surface layer of a solution.

achieved. By measuring critical heat flux densities at various concentrations of substances–in particular, salt solutions in water–it is possible to determine the optimal concentration where q_{cr1} reaches its maximum value and the quenching process has the most intensity and highest uniformity. Thus, the intensive quenching process can be optimized by selecting the salt concentrations where the q_{cr1} is at its highest value.

3.5 OPTIMAL CONCENTRATIONS OF AQUEOUS SALT SOLUTIONS

In production conditions, it is very important to optimize the concentrations of aqueous salt solutions as a way of providing more intensive and more uniform quenching of steel parts, for less part distortion during quenching. On the other hand, some salts can also be used as "oxygen attractors," to prevent the corrosion of steel parts and the quenching system.

The optimization of aqueous salt solutions is achieved by controlling the ionic charge that is present at the interface of the quenchant and the metal surface. A phenomenon was described by Frenkel [28], where the hot metal at high temperatures loses free electrons and the surface of the metal part becomes positively charged. Upon immersion of the positively charged metal into the electrolyte (aqueous salt solution), the negative ions in the salt solution are attracted to the metal surface, and a capacitor is formed, one side positively charged and the other side negatively charged, and there is a boiling liquid boundary layer (bubbles) in between on which the electric field acts.

Frenkel explains that, in the electric field that is formed, negative ions are attracted to the interface of liquid and metal, as shown in Fig. 9. Subsequently, a series of negative ions presses on neighbors in front of them and pushes them aside. Due to the electrical forces, there is a change in the surface tension of the ionized solution. Because the surface tension σ influences the first critical heat flux density (see Eq 2), the electric forces will affect the potential for film boiling.

As the salt concentration increases, the quantity of charge carriers also increases, up to an optimal concentration of the salt solution that provides the maximum critical heat flux density. At higher salt concentrations, the number of charge carriers decreases relative to the water-salt solution of optimal concentration because of the appearance of the double electrical layer at the metal−electrolyte interface [27,29]. The difference in adsorption forces acting on the positive and negative ions at the surface of metal causes ions of the same sign to accumulate. As a result, the metal obtains the opposite charge. Therefore, surface tension and a contact potential increase the metal−electrolyte interface, and the electrical double layer acts as a capacitor.
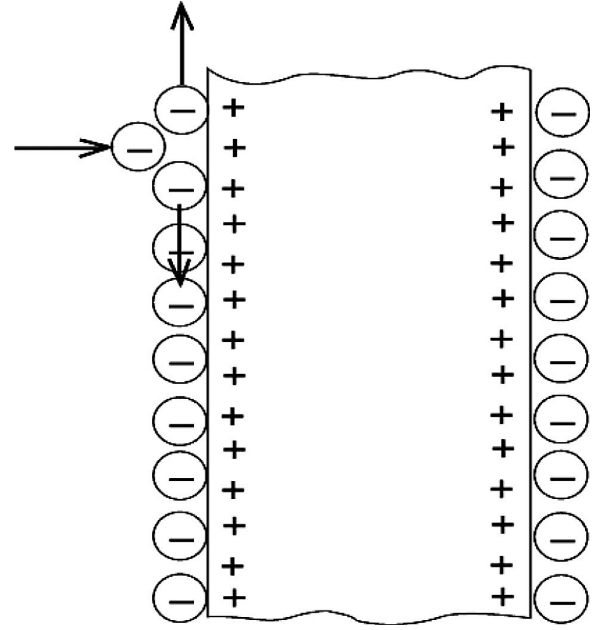
The capacity of such a capacitor depends on the dielectric penetrability of the liquid and the radius of the ion atmosphere of the electrical charge, which is equal to $\varepsilon_0 D\chi$, where ε_0 is the dielectric vacuum constant, D is the dielectric penetrability, and χ is the inverse radius of the ionic atmosphere. Carriers of the charges in the liquid (ions) are attracted by electrical interaction to the metal−liquid interface. Because the range of the action of these forces is significant, the layer of liquid molecules adjacent to the metal surface is under the pushing action of the second layer of molecules, so that the surface tension decreases by:

$$\Delta\sigma = \frac{1}{2}\varepsilon_0 D\chi\varphi_0^2 \qquad (12)$$

where:
$\Delta\sigma$ is the variation of the surface tension;
φ_0 is the difference of potentials between metal and electrolyte; and
ε_0 is the dielectric vacuum constant.

It is believed that the potential increase at the metal−liquid interface does not depend on the properties of the liquid and is determined by the nature of the metal only. The order of the potential increase is determined by:

$$\varphi_0 = \frac{9Ze}{10^{-9}r}, \qquad (13)$$

where:
r is the distance between neighbor atoms in the cubic lattice (for one-valence cuprum $\varphi_0 = 5.676$V);
Z is the valence; and
e is the charge of an electron.

Variations $\Delta\sigma$ with respect to the concentration of electrolytes in water have been analyzed [29]. It is well known that the inverse radius of an ionic atmosphere χ increases as the number of dissociated molecules increases. The
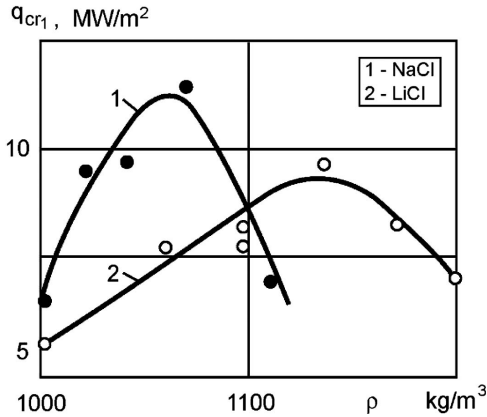
Fig. 10—First critical heat flux density q_{cr1} versus the concentration of NaCl and LiCl in water [27].

dielectric penetrability D of solution decreases as the concentration increases, as:

$$D = D_0 - 2\delta C, \qquad (14)$$

where:
D_0 is dielectric penetrability of distilled water;
δ is a coefficient of changes in dielectric penetrability depending upon the concentration; and
C is the concentration of electrolyte.

Therefore, there is an optimal concentration of electrolytes, where the maximum change in the coefficient of the surface tension is reached. That is why the critical heat flux density has an optimal value (see Fig. 10).

The existence of the optimal concentration of salt with regard to the heat transfer coefficients during nucleate boiling has not been fully resolved. Average (effective) values of heat transfer coefficients for aqueous solutions of sodium chloride (NaCl) and sodium hydroxide (NaOH) versus their concentrations (see Fig. 11) are calculated in [1] and [30]. These experiments were conducted with cylindrical probes of 10-mm diameter, made of stainless steel Kh18N9T (AISI 304).

Fig. 11 shows that the average heat transfer coefficient achieves maximum values at the concentration of 10–12 % sodium hydroxide in water, and then decreases. There are various explanations for this behavior:
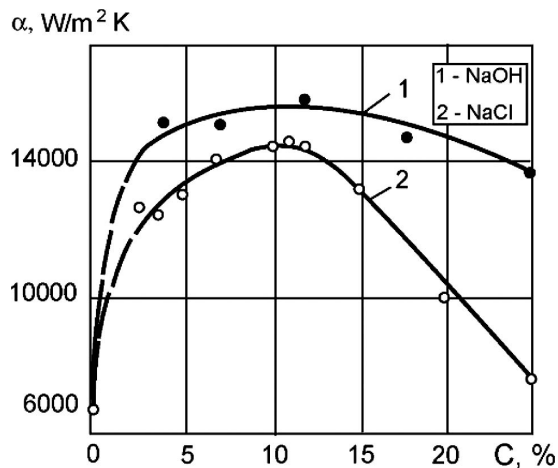
1. At low or high salt concentrations, localized steam films on the surface of the probe are observed during cooling because of the lower q_{cr1}. Localized steam films disappear at the optimal concentration, and therefore, the average heat transfer coefficient is at its maximum at this concentration.
2. Heat transfer coefficients during nucleate boiling at optimal concentrations increase due to the change in the surface tension caused by the existence of the attraction present in the ionic layer.

This issue should finally be clarified by more experimentation. However, it is most important to understand that an optimal concentration exists, at which the critical heat flux densities are maximized. This effect makes it possible to develop new salt quenchant solutions that may considerably intensify the effectiveness and uniformity of the steel quenching process. Some studies have shown that it is possible, using the proper salts, to not only increase cooling rates but also minimize surface corrosion [1].

3.6 CHARACTERISTICS OF HEAT TRANSFER DURING FULL FILM BOILING

During the full film boiling process, the heat transfer coefficients depend only on physical properties of the liquid and its vapor, and not on the material. This is confirmed by work conducted earlier by Moreaux and Beck [31] using cylindrical silver probes of 16-mm diameter and 48-mm length. The ends of the cylindrical probes were rounded. Some probes were covered with nickel, and others with heat-insulated material, and all met the previously described requirements concerning shape and size.

Fig. 12 presents cooling curves at the center of a cylindrical probe quenched in water at different temperatures with and without a nickel coating. The probes were heated to 850°C and quenched in nonagitated warm and hot water [31]. A full film boiling process was observed when the liquid was at its saturation temperature ($\vartheta_{uh} = 0$). From these data, the value of the average heat transfer coefficient may be determined by applying the theory of regular thermal conditions [23]. For this purpose, the value m (using the tabulated data obtained from Fig. 12) will be used. For each

Fig. 11—Average heat transfer coefficients versus the concentration of NaCl and NaOH in water at 20°C [27,30].
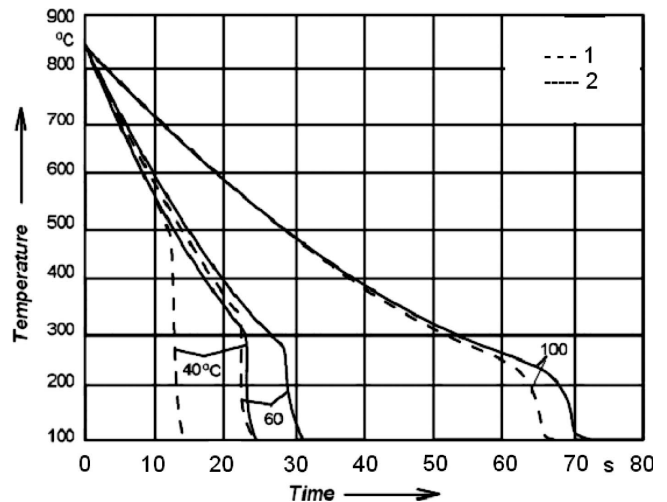
Fig. 12—Cooling curves for quenching in water at: 40°C, 60°C, and 100°C using: 1, silver cylindrical probes 16 mm in diameter coated with nickel of 10 μm thickness; 2, silver probes without coating [31].

heat transfer mode, the cooling factor m is calculated as:

$$m = \frac{\ln(T_1 - T_S) - \ln(T_2 - T_S)}{\tau_2 - \tau_1}. \qquad (15)$$

Knowing the value m permits the calculation of the Kondratjev number Kn from:

$$Kn = \frac{m}{m_\infty}, \qquad (16)$$

where:
$m_\infty = \frac{a}{K}$, which is true when $Bi \to \infty$;
α is the thermal diffusivity of silver (on average, 141×10^{-6} m^2/s);
$K = 75.08 \times 10^{-6}$ m^2; and therefore

$$m_\infty = \frac{141 \times 10^{-6} m^2/s}{75.08 \times 10^{-6} m^2} = 1.878 s^{-1}.$$

According to the Kondratjev theory of regular heat conduction conditions [23]:

$$Kn = \psi Bi_V = \frac{Bi_V}{\sqrt{Bi_V^2 + 1.437 Bi_V + 1}} \qquad (17)$$

and

$$Bi_V = \frac{\alpha}{\lambda} K \frac{S}{V}.$$

where:
α is the heat transfer coefficient in W/m^{2}K;
λ is heat conductivity in W/mK;
K is the Kondratjev form factor in m^2;
S is surface area in m^2; and
V is volume in m^3.

Using experimental data from Fig. 12 and Eqs 15–17, one can obtain a value for Kn of 0.0134 and for Bi_V of 0.0136.

Now, heat transfer coefficient can be calculated from:

$$Bi_V = \frac{\alpha}{\lambda} K \frac{S}{V} = 0.0136.$$

Here ratio S/V and Kondratjev form factor K for the finite cylinder are calculated as:

$$\frac{S}{V} = \frac{2(Z + R)}{RZ};$$

and

$$K = \frac{1}{\frac{5.784}{R^2} + \frac{\pi^2}{Z^2}},$$

where R is the radius and Z is the height of the finite cylinder.

$$\alpha_{FB} = 0.0136 \frac{\lambda V}{KS} = 0.0136 \frac{\lambda \cdot RZ}{K \cdot 2(Z + R)}. \qquad (18)$$

Here for the silver probe:
$\lambda = 371.3$ W/mK;
$R = 0.008$ m;
$Z = 0.048$ m; and
$K = 75.08 \times 10^{-6}$ m^2.

Substituting these values into Eq 18, we obtain a value of 219 W/m^{2}K for α_{FB}. This result agrees well with Eq 19 [32]:

$$\alpha_{FB} = 0.25 \left(\frac{\lambda'' C_p'' g(\rho' - \rho'')}{v''} \right)^{\frac{1}{3}}, \qquad (19)$$

where λ'' is the heat conductivity of vapor (W/mK);
C_p'' is the specific capacity of vapor (J/kgK);
g is the acceleration of gravity, 9.81 m^2/s;
ρ' is the density of the liquid, (kg/m^3);
ρ'' is the density of the vapor, (kg/m^3); and
v'' is the kinematical viscosity of the vapor (m^2/s).

By substituting into Eq 19 the following values:
$\lambda'' = 0.02372$ W/mK;
$C_p'' = 2,135$ J/kgK;
$g = 9.81$ m/s^2;
$\rho' = 958.4$ kg/m^3;
$\rho'' = 0.598$ kg/m^3;
$v'' = 20.02 \times 10^{-6}$ m^2/s,
the heat transfer coefficient is calculated as shown:

$$\alpha_{FB} = 0.25 \sqrt[3]{\frac{5.63 \times 10^{-4} \times 2135 \times 9.81 \times 982.5}{20.02 \times 10^{-6}}} \approx 208\,\text{W/m}^2\text{K}.$$

Comparison of the calculated result with the experimental data shows that the difference is

$$\varepsilon \approx \frac{(219 - 208)100\%}{219} \approx 5\%,$$

which is in very good agreement since the dispersion of heat transfer coefficients is within the range of 20 % [12]. It has been reported that heat transfer coefficients during full film boiling could be 300 W/m^{2}K [32,33]. According to published data [33], the film boiling heat transfer coefficient is equal to 140 W/m^{2}K during cooling of the chromium-nickel steel cylindrical specimen (15 mm in diameter and 45 mm in length) in water at 97°C.

The experimental data shown in Fig. 12 may be used to calculate the heat transfer coefficient during cooling of a cylindrical silver probe in water at 60°C [31], where, according to Eq 15, $m = 0.0453$. As in the previous example $m_\infty = 1.878$ s^{-1}, and therefore, the Kondratjev number is equal to

$$Kn = \frac{0.0453}{1.878} = 0.024.$$

Using $Kn = 0.024$, the generalized Biot number Bi_V is 0.0245. The heat transfer coefficient during cooling of the cylindrical silver probe of 16-mm diameter in water at 60°C is equal to 394 W/m^{2}K. The heat transfer coefficient calculated by Eq 19 is 208 W/m^{2}K. The difference between experiment and calculation is:

$$\varepsilon \approx \frac{(394.3 - 208)100\%}{394.3} \approx 47\%.$$

When the water temperature decreases down to 40°C or 20°C, the cooling rate increases, because during cooling of silver probes in cold water, the film boiling heat transfer coefficient may be 2,000 W/m^{2}K or greater, which differs by an order of magnitude from the data calculated by Eq 19. This phenomenon is explained as follows.

When the quenchant temperature decreases, the vapor film becomes unstable, oscillation of the vapor film is observed, and the underheated (to a saturated temperature) liquid intermittently contacts the surface of the probe. As a result, the average heat transfer coefficient increases, since this value is dependent on the frequency of the vapor film oscillations and the total area of coverage of the contacting liquid. The stability of the vapor film may be determined from Fig. 13 [31].
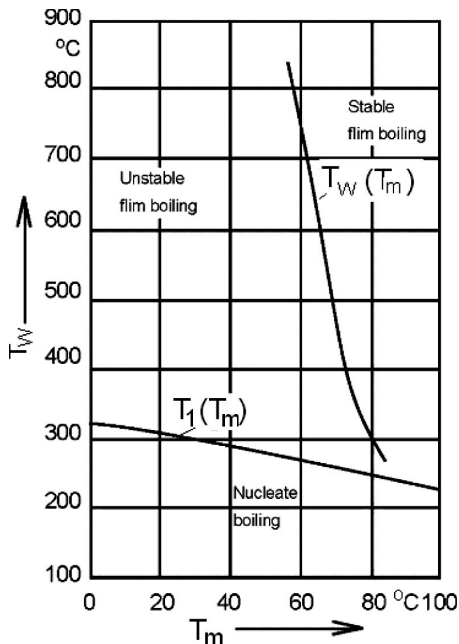
Fig. 13—Stability diagram of film boiling in water with a silver probe. T_W is the wall temperature of the probe; T_m is the water temperature [31]; and $T_1(T_m)$ is the lowest temperature for the film boiling–nucleate boiling transition.

From Fig. 13, the vapor film is most stable if the water temperature is greater than 80°C. If the water temperature is 20–40°C, the vapor film is unstable throughout the entire cooling process due to the oscillating contact with the heated surface.

This can be illustrated by analysis of sound effects that are observed during the oscillation of a vapor film. Some results related to this issue are published in [5], where the multichannel analysis of sound effects is described.

Fig. 14 illustrates the spherical silver probe used to study unstable film boiling. The 20-mm-diameter spherical silver probe was prepared by casting the probe from the molten silver with a type K chromel-alumel thermocouple inserted through a 1.5-mm stainless steel sheath, with the thermocouple tip precisely located at the geometric center before casting. After casting, the silver surface was properly ground. The spherical shape of the probe and the high surface finish were selected to ensure a uniform heat transfer
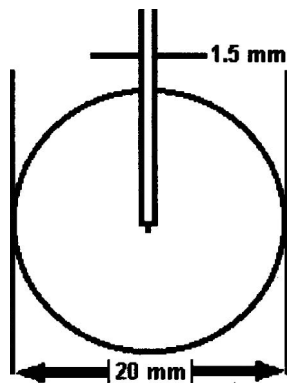
Fig. 14—Schematic of the cast silver spherical probe used for investigation of unstable film boiling.
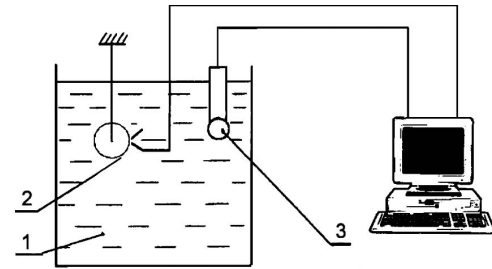
Fig. 15—Quenching system and apparatus placement: 1, quenchant to be studied; 2, spherical silver probe of 20-mm diameter; 3, sensor for recording acoustic effects.

throughout the whole quenching process. The high thermal conductivity of silver provides high heat flux densities.

Sound effects were determined using a sound sensor, and the signal was transmitted through an amplifier to the sound analyzer and computer for data processing (see Fig. 15).

The quenching experiments were conducted by the immersion of the heated spherical probe into a cylindrical stainless tank containing 15 kg of the quenchant, as shown in Fig. 15. (Experiments have also been successfully conducted using a 3L cylindrical glass beaker.) As depicted, a microphone was strategically placed near the silver probe surface to acoustically monitor the quenching process. The signal width was 0 to 20,000 Hz. However, to detect a relatively narrow characteristic signal frequency for nucleate boiling, the total signal width was divided into 100-Hz bands over 200 channels.

Fig. 16 provides a comparative illustration of the thermal and acoustical data obtained. Note that the temperature–time
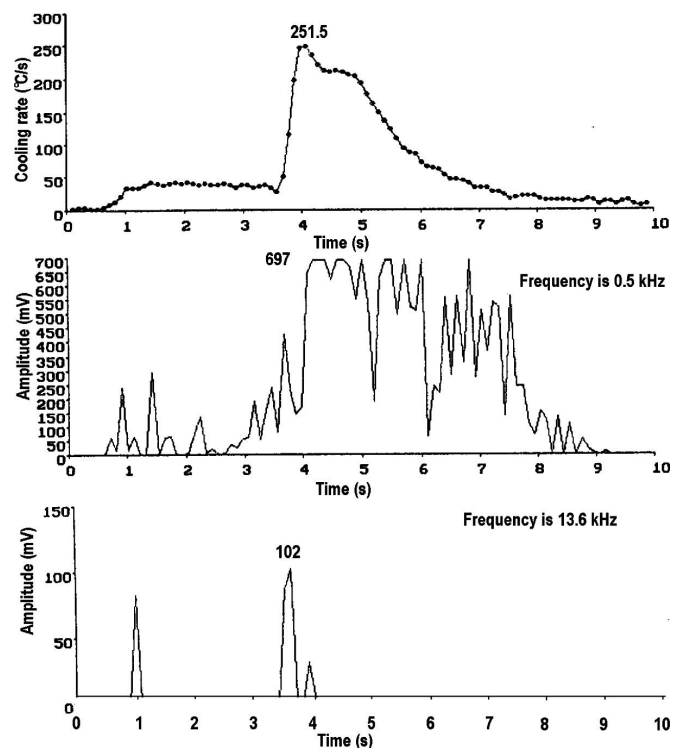
Fig. 16—Temperature–time, broadband, and narrowband quenching data [10].

data show that even the very sensitive silver probe did not detect the initial shock-boiling process characterized by q_{cr1}.

Since it has been shown experimentally that, during full film boiling, the heat transfer coefficient remains unchanged as the surface temperature changes, the average heat transfer coefficient can be used for the film boiling stage.

From Fig. 16, it is evident that, at a frequency of 0.5 kHz, there are appreciable sound effects from the oscillation of a vapor film, which increase upon full nucleate boiling. At a frequency of 13.6 kHz, only two sound spikes were observed, which were connected with the formation and growth of nucleating centers. Initially, vapor bubbles were very small, and the oscillation frequency was much higher than during nucleate boiling.

The first spike is due to the formation of nucleating centers that merged and created a vapor film. The energy connected with the oscillation of nucleating centers has passed to the oscillatory energy of a vapor film. The second spike is connected with the destruction of a vapor film and repeated formation of nucleating centers, which then have grown and begun to oscillate with less frequency.

The channel at frequency 13.6 kHz does not detect sound effects at the established nucleate boiling frequency (see Fig. 16). Thus, the analysis of sound effects confirms the oscillation of a vapor film in the area of unstable film boiling, and the sharp increase of the heat transfer coefficient in this boiling process is due to periodic contact (oscillation) of a cold liquid to the heated surface.

Film boiling possesses other interesting and important features. During film boiling in aqueous solutions, especially in aqueous polymer quenchants exhibiting inverse solubility, polymer coatings that exhibit low heat conductivity form at a hot metal surface. This coating considerably reduces the heat flux density from the surface to the quenchant. In this case, the transition from film boiling to nucleate boiling occurs at a higher temperature of the heated surface [31] (see Fig. 12) since the liquid water is effectively kept away from the hot part surface by the insulating layer of the polymer.

3.7 SOME SPECIAL CHARACTERISTICS OF FILM BOILING

Until now, only the characteristics of nucleate and film boiling have been discussed. The assumption has been that one process follows and subsequently replaces the other. According to this assumption, the entire surface of a test probe is fully covered by either a vapor blanket (film boiling) or bubbles (nucleate boiling), and the film boiling mode of heat transfer is replaced by the nucleated boiling mode instantly over the entire surface of the probe, which in turn is followed by single-phase convection heat transfer.

However, all three above heat transfer modes (full film boiling, nucleate boiling, and single-phase convection) may actually occur on the probe surface simultaneously [34–38]. Cinematographic investigations have shown that, during cooling of alloys in aqueous polymeric solutions, areas experiencing the sequence of full film boiling–nucleate boiling–single-phase convection can move along the probe surface at a certain speed [34]. A picture of the sequence of movement of the nucleate-to-film-boiling front is presented in Fig. 17 [39].

This phenomenon–where full film boiling (FB) is followed by nucleate boiling (NB) along the part's cooling surface–is observed when the probe has sharp or thin ends. For example, let us consider the quenching of a cone-shaped
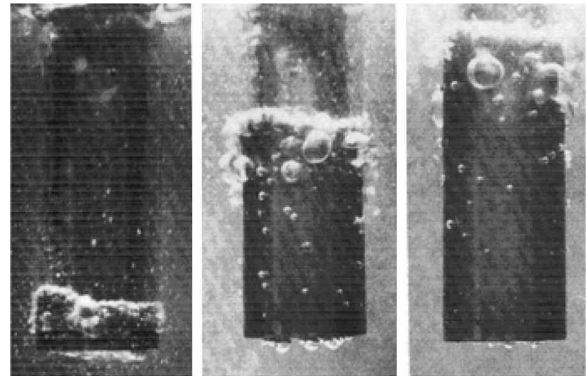
Fig. 17—Wetting process of a cylindrical Cr-Ni steel sample (45 mm in diameter and 45 mm long) being quenched in water of 60°C without agitation [39].

cylindrical probe. At the beginning of the quench, the entire probe surface is covered by a vapor blanket. The thin end of the probe cools faster, transitioning to the nucleate boiling mode of heat transfer. With time, the area covered by the bubbles moves up, pushing the vapor blanket along the probe axis, in a manner similar to that seen in Fig. 17 [34–39].

More information on the four modes of heat transfer and critical heat flux densities can be found in the literature [40,41]. Further careful studies with direct visual monitoring of the described movement of FB–NB boundaries have been performed [42]. Especially promising is combining visual monitoring with the use of electrical conductivity data to characterize quenchants [43].

During quenching of steel parts, a periodic replacement of film boiling with nucleate boiling, and vice versa, can be also observed on the part's surface, for example, when quenching parts in a water-polymer solution with inverse solubility. As mentioned in Section 3.6, a soluble, heat-insulated layer forms at the metal surface during quenching (see Fig. 18).

The soluble polymer layer, having low heat conductivity, decreases an initial heat flux density from the part's surface. If the established heat flux density is less than the first critical heat flux density (q_{cr1}), the nucleate boiling mode of heat transfer will take place. During nucleate boiling, the cold water–polymer solution touches the part surface, dissolving the polymer heat-insulating layer. In the areas of the part surface where the polymer layer is removed, the heat flux density from the surface increases sharply, and film boiling resumes, causing reestablishment of the polymer layer. This process continues while the part has enough thermal energy to support this phenomenon. More detailed information on the cooling capacity of different quenchants is available in [44–46].

When quenching parts intensively, the film boiling process should be fully eliminated. To eliminate film boiling from the very beginning of the quench, the following condition must always be satisfied:

$$q < q_{cr1},$$

where q is the initial heat flux density from the part surface.

This condition can be achieved if the quenchant is agitated vigorously enough to provide a sufficiently high q_{cr1}. If $q < q_{cr1}$, nucleate boiling will occur simultaneously over the entire surface, and parts will be cooled uniformly and intensively. The part distortion will be minimized, and a uniform and high hardness of the part will be obtained. When q is
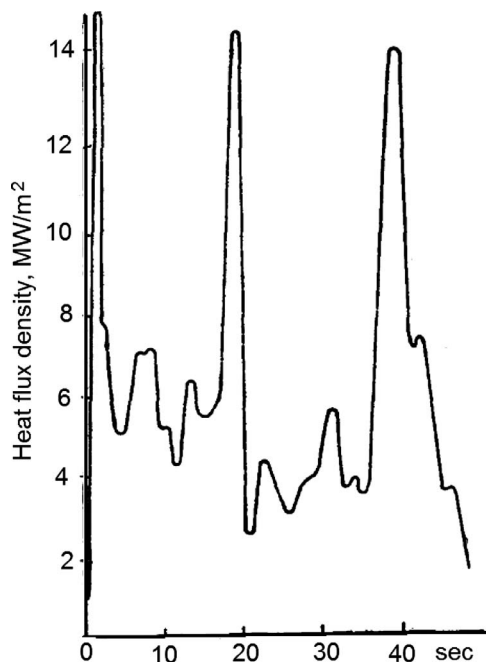
Fig. 18—Periodic changes versus time of heat flux density during quenching of a cylindrical probe made of AISI 304 steel in 0.1 % water solution of polyetilenoxide at 20°C (probe diameter 20 mm, length 80 mm, initial temperature 850°C). Periodic changes are explained by multiple transitions from film boiling to nucleate boiling [44–46].

close to q_{cr1}, a formation of a local vapor blanket may be observed, which may cause:

• Nonuniform hardness of the hardened surface
• Significant part distortion or even cracking
• Lower part performance characteristics

3.8 METHOD FOR DETAILED EVALUATION OF DIFFERENT MODES OF HEAT TRANSFER DURING QUENCHING

As we know, film boiling, nucleate boiling, and convection heat transfer take place during quenching of steel parts. All three types of heat transfer may be present on the part surface at the same time. Moreover, the surface areas experiencing different modes of heat transfer can move relative to each other or can periodically replace each other during the quench. Fig. 18 illustrates this effect.

To evaluate the heat transfer characteristics for different heat transfer scenarios correctly, it is necessary to have data on both the surface temperature and core temperature of the probe during cooling. Using a probe with only one thermocouple placed in its center allows for determining only average values of heat transfer characteristics. In other words, the thermocouple installed in the probe center is not sensitive enough to react to possible fast changes of different modes of heat transfer on the probe surface.

Special methods such as the Tensi method [33,43] and Liščić method [41] can be used for detailed evaluation of heat transfer during quenching of steel parts. For example, the Tensi method allows the measurement of electrical conductance between a heated probe and a quenchant, which is dependent on the mode of heat transfer on the probe surface [37,39,40].

As shown, measurements of electrical conductance can be used to quantitatively determine the change in the wetting behavior during the quenching process. During film boiling, a vapor blanket having low heat conductivity insulates the hot part from the quenchant. Under these conditions, the electrical conductance between the metal and the counter electrode is low. When the vapor blanket surrounding the probe collapses, nucleate boiling begins, resulting in the appearance of localized wetting on the probe surface. The wetting development is indicated by an increase of electrical conductance, with the increase proportional to the amount of surface wetted. When the probe surface is completely wetted, the electrical conductance is at its highest value.

The electrical conductance measuring apparatus is illustrated in Fig. 19. The apparatus uses a cylindrical probe of 15-mm diameter and 45-mm length made of chromium-nickel stainless steel. The electrical conductance data were recorded using a two-channel multiplex system having a scanning range between 60 µs and 10 ms and a maximum of 24,000 data points, which corresponds to a measuring time period of 120 s for two channels. One channel recorded temperature versus cooling time data using the procedures described in ASTM D6200 and ISO 9950 for unagitated quenchants or ASTM D6482 for agitated quenchants. The second channel simultaneously collected electrical conductance data [33].

The following four possible scenarios of heat transfer on the probe surface were considered in [33] and [43]:

a. Full film boiling and nucleate boiling are present at the same time on the probe surface. The area of nucleate boiling moves up along the probe surface replacing film boiling.

b. First, film boiling takes place throughout the entire probe surface area. At a certain point in time, nucleate boiling instantaneously replaces film boiling, and then convection heat transfer replaces nucleate boiling.

c. Some local areas of the probe surface are covered by the vapor blanket, while at the same time, other areas experience nucleate boiling. These local areas do not move.

d. The boiling process takes place on some local areas of the probe surface. Film boiling and nucleate boiling appear periodically in these areas, replacing each other.

Measurement results for electrical conductivity and temperature at the center of the probe for the above heat transfer conditions are shown in Fig. 20. Note that (a), (b), (c),
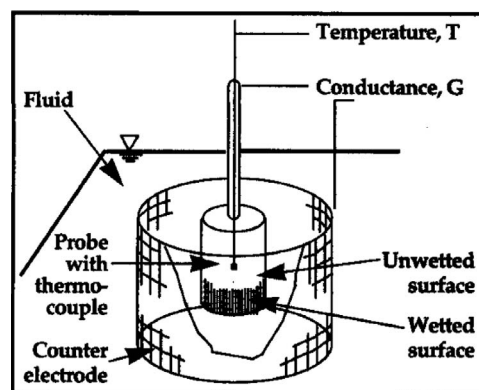
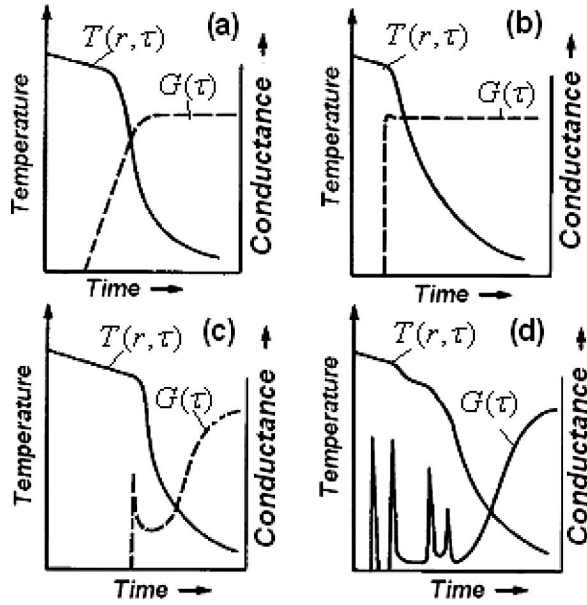**Fig. 19**—Electrical conductivity between a part to be quenched and quenchant [33,43].

Fig. 20—Electrical conductivity and temperature at the center of the probe [33,43].
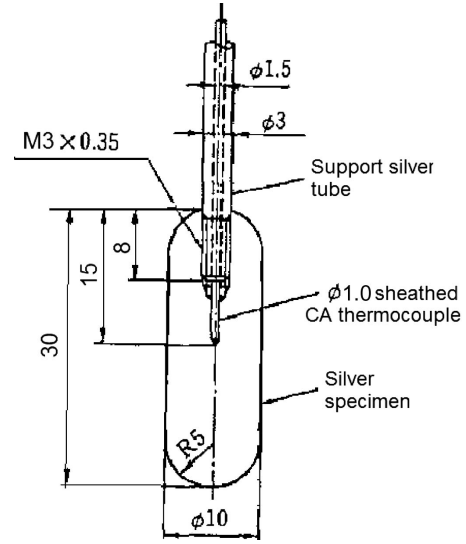

Fig. 21—Shape and dimensions of silver cylindrical probe with the rounded ends that is recommended for evaluations of critical heat flux densities [55].

and (d) on the figure correspond to the above four heat transfer scenarios.

Fig. 20 shows that temperature measurements alone provide only limited information regarding actual part quenching processes, and they are insufficient to adequately characterize hardening of steel. However, the characterization of the quenching process based on measuring the electrical conductivity is valuable additional information to conventional cooling curve analysis. It can also provide insight into the nature of the wetting processes and their uniformity (or lack thereof) that are impossible to observe from analysis of only cooling curve data. As is known, nonuniformity of wetting during quenching can result in a "spotty" or "slack" quench, with excessive part distortion. This is why the critical heat flux densities could be useful in heat-treating practice. More information on critical heat flux densities and heat transfer modes is provided in [39,47−56].

3.9 DISCUSSION

It has been shown that, during quenching of steel, heat transfer coefficients can reach 200,000 W/m^{2}K or more when shock boiling ends [57]. This means that a standard probe for critical heat flux evaluation should be rather small and made of high-conductivity material to provide equivalence of T_{sf} and T_{core} during testing of quenchants. This condition is satisfied if the Biot number Bi is less than 0.2.

The smallest cylindrical silver probes were tested by Narazaki and colleagues [55,56]. Fig. 21 shows the silver cylindrical probe with round ends as tested in [55]. This probe is suitable for critical heat flux evaluation. To demonstrate this, let us calculate the Biot number for a silver probe, presented in Fig. 20, when the heat transfer coefficient is equal to 200,000 W/m^{2}K:

$$Bi = \frac{\alpha}{\lambda}R = \frac{200,000 W/m^2 K}{362 W/mK} \times 0.005 m = 2.76.$$

Here, the heat conductivity for silver at 400°C is equal to 362 W/mK (see Table 1) and the radius is equal to 0.005 m (see Fig. 21). This calculation shows that during shock boiling

a large difference between surface temperature and core temperature will be observed.

At the end of film boiling, the heat transfer coefficient is approximately 4,000 W/m^{2}K and Bi is now:

$$Bi = \frac{\alpha}{\lambda}R = \frac{4,000 W/m^2 K}{362 W/mK} \times 0.005 m = 0.055.$$

Since, when evaluating critical heat flux densities, only film boiling heat transfer coefficients are used, the condition $Bi < 0.2$ will always be satisfied. This means that the surface temperature T_{sf} during testing will be equal to core temperature T_{core} of the probe only at the end of film boiling. So, the probe presented in Fig. 21 can be used for critical heat flux evaluation. The rounded ends of the cylinder will provide the second type of heat transfer mode and accurate estimations of critical heat flux densities.

It is important to keep in mind that, upon immersion of a steel part into the quenchant, the initial heat flux density q can be much greater than, about the same as, or much less than q$_{cr1}$. In the first case, q >> q$_{cr1}$, full film boiling is observed. Transition boiling is observed when q ≈ q$_{cr1}$. Then, in the last case, q << q$_{cr1}$, film boiling is absent and heat transfer is by nucleate boiling. Each of these three cases will produce different values of $\alpha = f(T_{sf})$ versus surface temperature. Therefore, there is no unique interrelationship of the heat transfer coefficient α as a function of surface temperature.

Special attention should be paid to the method of evaluation of heat transfer coefficients. In practice, quenchants are tested using standard probes, for example, a silver sphere or cylindrical probes made of Inconel 600. The thermocouples are located at the geometric center. It is assumed that a temperature field in a section of the silver probe is uniform, that is, $Bi \le 0.2$. This assumption was confirmed by calculation of the heat transfer coefficient from:

$$\alpha = \frac{q}{T_W - T_m}, \tag{20}$$

where q is a heat flux density on the surface; T_w is the wall temperature; and T_m is temperature of the quenchant. This

is a generally accepted approach for film and nucleate boiling heat transfer evaluation. However, film and nucleate boiling heat transfer coefficients should be determined from the following ratio:

$$\alpha = \frac{q}{T_W - T_s}, \tag{21}$$

where T_s is saturation (boiling) temperature of the quenchant. This means that in reality heat transfer coefficients during film and nucleate boiling are much higher than as accepted in practice.

Let us illustrate the above using the following example. Let $T_w = 110°C$; $T_s = 100°C$; and $T_m = 20°C$. If α is calculated by Eq 20, we find:

$$\alpha_1 = \frac{q}{110^oC - 20^oC} = \frac{q}{90^oC};$$

however, if the calculation is performed using Eq 21, then:

$$\alpha_2 = \frac{q}{110^oC - 100^oC} = \frac{q}{10^oC}.$$

Now consider by how much α_2 differs from α_1 by dividing one by the other:

$$\frac{\alpha_2}{\alpha_1} = \frac{q}{10^oC} : \frac{q}{90^oC} = 9.$$

In this example, α_2 is nine times greater than α_1, which means that using silver probes during testing, subsequent miscalculations of values of heat transfer coefficients are underestimated and will differ from the true values by almost an order of magnitude. Therefore, even though it would appear that the Biot number Bi is less than 0.2, in fact it is actually around 2, and the center temperature of a silver ball differs from the surface temperature. Therefore, it is impossible to make a unique function $\alpha = f(T_{sf})$ by measuring the temperature at the core of the testing probe and assuming that $T_{sf} = T_{core}$.

3.10 SUMMARY

1. The methodology for determination of critical heat flux densities in transient conditions of heat transfer for quenching processes has been developed. It was affirmed that the ratio q_{cr2}/q_{cr1} is approximately 0.2 in transient conditions of heat transfer, which considerably facilitates experimental determination of critical heat flux densities.
2. A simple technique to determine the maximum values of critical heat flux densities is suggested, which provides a method for determining the optimal concentrations of soluble substances in quench water to reduce distortion and increase uniformity of the quench. Determination of the maximum values of critical heat flux densities is of practical value for maintaining existing quenching systems, as well as the development of new quenchants and the implementation of intensive quenching methods.
3. The first and second critical heat flux densities, q_{cr1} and q_{cr2}, are inherent characteristics for all vaporizable liquid quenchants. Determination of the highest critical heat flux density for a given quenchant, and maintaining the quench bath at that temperature, will optimize the quench system for all the parts quenched in that system, while minimizing distortion and maximizing

as-quenched part properties. Knowledge of the highest critical heat flux density for a given vaporizable liquid quenchant will allow more direct comparisons between the performances of different quenchants, regardless of the geometry of the parts being quenched. In addition, this information will assist in making more accurate computer simulations of heat-treating processes.
4. Testing for and tracking of the critical heat flux densities q_{cr1} and q_{cr2} may be used as a quality assurance tool to assure optimal quenching performance is being maintained.
5. A silver cylindrical probe 10 mm in diameter, with rounded ends, is the best probe for critical heat flux evaluation.

References

[1] Totten, G. E., Bates, C. E., and Clinton, M. A., *Handbook of Quenchants and Quenching Technology,* ASM International, Materials Park, Ohio, 1993, pp. 69−128.

[2] ASTM Standard D7646-10: Standard Test Method for Determination of Cooling Characteristics of Aqueous Polymer Quenchants for Aluminum Alloy by Cooling Curve Analysis, *Annual Book of ASTM Standards,* ASTM International, West Conshohocken, PA, in press.

[3] ASTM Standard D6200-97: Standard Test Method for Determination of Cooling Characteristics of Quench Oils by Cooling Curve Analysis, *Annual Book of ASTM Standards,* ASTM International, West Conshohocken, PA, 2001.

[4] ASTM Standard D6482-99: Standard Test Method for Determination of Cooling Characteristics of Aqueous Polymer Quenchants with Agitation (Tensi Method), *Annual Book of ASTM Standards,* ASTM International, West Conshohocken, PA, 2000.

[5] ASTM Standard D6549-00: Standard Test Method for Determination of Cooling Characteristics of Quenchants by Cooling Curve Analysis with Agitation (Drayton Unit), *Annual Book of ASTM Standards,* ASTM International, West Conshohocken, PA, 2000.

[6] Kobasko, N. I., *Steel Quenching in Liquid Media Under Pressure,* Naukova Dumka, Kyiv, 1980.

[7] Leidenfrost, J. G., On the Fixation of Water in Diverse Fire, *International Journal of Heat and Mass Transfer,* Vol. 9, 1966, pp. 1153−1166.

[8] Walker, J., Boiling and the Leidenfrost Effect, *Fundamentals of Physics,* 3rd Ed., David Holliday and Robert Resnick, Eds., John Willey & Sons, New York, 1988, pp. E10-1 through E10-6.

[9] *Hemisphere Handbook of Heat Exchanger Design,* Hewitt, G. F., Coordinating Ed., Hemisphere, New York, 1990, pp. 2.7.1−2.8.1.

[10] Kobasko, N. I., Moskalenko, A. A., Totten, G. E., and Webster, G. M., Experimental Determination of the First and Second Critical Heat Flux Densities and Quench Process Characterization, *Journal of Materials Engineering and Performance,* Vol. 6, No. 1, 1997, pp. 93−101.

[11] Jeschar, R., Specht, E., and Köhler, Chr. Heat Transfer During Cooling of Heated Metallic Objects with Evaporating Liquids, *Theory and Technology of Quenching,* Liščić, B., Tensi, H. M., and Luty, W., Eds., Springer-Verlag, Berlin, 1992, pp. 248−340.

[12] Tolubinsky, V. I., *Teploobmen pri kipenii* (Heat transfer at boiling), Naukova Dumka, Kyiv, 1980.

[13] Kutateladze, S. S., *Fundamentals of Heat Transfer,* Academic Press, New York, 1963.

[14] Kutateladze, S. S., Hydrodynamic Crisis Model of Heat Transfer in Boiling Liquid at Free Convection, *Journal of Engineering Physics,* Vol. 20, No. 11, 1950, pp. 1389−1392.

[15] Kruzhilin, G. N., Heat Transfer from a Horizontal Plate to Boiling Liquid at a Free Convection. *Doklady AN USSR,* Vol. 58, No. 8, 1947, pp. 1657−1660.

[16] Incropera, F. P., and DeWitt, D. P., *Fundamentals of Heat and Mass Transfer,* John Wiley & Sons, New York, 1981.

[17] Isachenko, V. P., Osipova, V. A., and Sukomel, A. S., *Teploperedacha* (Heat transfer), Energomash, Moscow, 1981.

[18] Morozov, V. T., Study of Termination of Nucleate Boiling at Immersed Surface, *Crisis of Boiling and Temperature Mode of Evaporative Surfaces of Heati*ng, Vol. 58, TsKTI, Leningrad, pp. 64−77.

[19] Petrash, L. V., *Zakalochnye Sredy* (Quenchants), Mashgiz, Moscow, 1959.

[20] Luty, W., Types of Cooling Media and Their Properties, *Theory and Technology of Quenching*, Liščić, B., Tensi, H. M., and Luty, W., Eds., Springer-Verlag, Berlin, 1992, pp. 248−340.

[21] Kobasko, N. I., A Method for Evaluation of Critical Heat Flux Densities, *Proceedings of the 5th IASME/WSEAS Int. Conference on Heat Transfer, Thermal Engineering and Environment,* Athens, Greece, August 25−27, 2007, pp. 153−159.

[22] Mayinger, F., Thermo- and Fluid-Dynamic Principles of Heat Transfer During Cooling, *Theory and Technology of Quenching,* Liščić, B., Tensi, H. M., and Luty, W., Eds., Springer-Verlag, Berlin, 1992, pp. 41−72.

[23] Kondratjev, G. M., *Regulyarnyi Teplovoy Rezhim* (Regular thermal mode), Gostekhizdat, Moscow, 1954.

[24] Lykov, A. V., *Theory of Heat Conductivity,* Vysshaya Shkola, Moscow, 1967.

[25] Koshkin, V. K., Kalinin, E. K., Dreitser, G. A., and Yarho, S. A., *Nestatsionarnyi Teploobmen* (Non-stationary heat transfer), Mashinostroyenie, Moscow, 1973.

[26] Japanese Industrial Standard Silver Probe, JIS K 2242-1997.

[27] Kobasko, N. I., Quenching Media, *Metal Science and Heat Treatment,* Vol. 23, 1989, pp. 127−166.

[28] Frenkel, Ya. I., *Kinetic Theory of Liquids, Selected Works,* Vol. 3, Academy of Sciences of the USSR, Moscow, 1959.

[29] Fedorov, V. I., Kovalenko, G. V., and Kostanchuk, D. M., On the Issue of Boiling Up a Liquid on a Metal Surface, *IFZh,* Vol. 32, No. 1, 1977, pp. 18−23.

[30] Kobasko, N. I., Thermal Processes at Quenching, *Metal Science and Heat Treatment,* No. 3, 1968, pp. 2−6.

[31] Moreaux, F., and Beck, G., Effect of Workpiece Surface Properties on Cooling Behavior, *Theory and Technology of Quenching,* Liščić, B., Tensi, H. M., and Luty, W., Eds., Springer-Verlag, Berlin, 1992, pp. 182−207.

[32] Mikheev, M. A., and Mikheeva, I. M., *Basics of Heat Transfer,* Energy, Moscow, 1977.

[33] Tensi, H. M., Wetting Kinematics, *Theory and Technology of Quenching,* Liščić, B., Tensi, H. M., and Luty, W., Eds., Springer-Verlag, Berlin, 1992, pp. 208−219.

[34] Kobasko, N. I., and Timchenko, N. P., Cinematographic Investigations of the Cooling Process of Alloys in Aqueous Polymeric Solutions, *Metal Science and Heat Treatment,* Vol. 28, No. 10, 1986, pp. 729−734.

[35] Kobasko, N. I., Fedorov, V. I., Timchenko, N. P., and Morhuniuk, W. S., Dynamics of the Basic Modes of Heat Transfer at Quenching, *The 5th International Congress of Heat Treatment of Materials,* Budapest, 1986, Vol. 3, pp. 1852−1859.

[36] Kuenzel, Th., Einfluss der Widerbenetzung auf die allotrope Modification saenderung tauchgekuehlter Metallkoerper (in German), Dr.-Ing. dissertation, Technical University of Munich, 1986.

[37] Tensi, H. M., Stitzelberger, J. P., Künzel, Th., and Stich, A., Wetting Kinematics and Influence on the Metallurgical Structures, Final DFG-Report (Contract Number Te 65/27-1, 2). Deutsche Forschungsgemeinschaft, Bonn, 1989.

[38] Timchenko, N. G., Fedorov, V. I., and Kobasko, N. I., Dynamics of Change of the Basic Modes of Heat Transfer During Cooling at Quenching, *Promteplotekhnika,* Vol. 9, No. 3, 1987, pp. 57−60.

[39] Tensi, H. M., Stich, A., and Totten, G. E., Fundamentals About Quenching by Submerging, *Proceedings of the International Heat Treating Conference: Equipment and Processes,* Schaumburg, IL, April 18−20, 1994, pp. 243−251.

[40] Totten, G. E., Bates, C. E., and Clinton, M. A., *Handbook of Quenchants and Quenching Technology,* ASM International, Materials Park, OH, 1993, pp. 69−128.

[41] Liščić, B., Critical Heat-Flux Densities, Quenching Intensity and Heat Extraction Dynamics During Quenching in Vaporizable Liquids, *Proceedings of the 4th International Conference on Quenching and the Control of Distortion,* Beijing, May 20−23, 2003, pp. 21−28.

[42] Vergana-Hernandez, H. J., and Hernandez-Morales, B., A Novel Probe Design to Study Wetting Front Kinematics During Forced Convective Quenching, *Experimental Thermal and Fluid Science,* Vol. 33, No. 5, 2009, pp. 797−807.

[43] Totten, G. E., and Tensi, H. M., Using Conductance Data to Characterize Quenchants, *Heat Treating Progress,* Vol. 2, No. 5, 2002, pp. 39−42.

[44] Krivoshei, F. A., Solution of Inverse Problems of Heat Transfer Based on the Method of Statistical Regularization, author's abstract of doctoral thesis (in Russian), Institute of Thermal Science and Engineering of the National Academy of Sciences of Ukraine, Kyiv, 1993.

[45] Kobasko, N. I., and Krivoshei, F. A., On the Mechanism of Temperature and Heat Flow Oscillations in Cooling Metallic Specimens in Aqueous Solutions of Polymers, *Dokl. Akad. Nauk Ukr.,* No. 11, 1994, pp. 90−94.

[46] Kobasko, N. I., Current State of the Problem and Principal Criteria to Evaluating the Cooling Capacity of Quenching Media, *Metal Science and Heat Treatment,* Vol. 38, Nos. 1−2, 1996, pp. 49−55.

[47] Kobasko, N. I., Technological Aspects of Quenching, *Metal Science and Heat Treatment,* Vol. 33, No. 4, 1991, pp. 253−263.

[48] Tolubinsky, V. I., Ostrovskiy, J. N., Kobasko, N. I., and Spivakov, Ju. A., Intensity of Heat Transfer and Limit Heat Flux Densities at Boiling Water Solutions of Polyacrylamide, *Promteplotekhnika,* Vol. 6, No. 2, 1984, pp. 3−6.

[49] Kobasko, N. I., Ostrovskiy, Ju. N., and Pisarev, V. B., Crisis of Heat Transfer at Boiling Mixes of Water-Liquid Glass with Regard to Processes of Quenching, *Technology and Organization of Production,* No. 4, 1980, DR No. 2047.

[50] Kobasko, N. I., and Kostanchuk, D. M., Estimation of Cooling Capacity of Quenchants, *Metal Science and Heat Treatment,* No. 10, 1973, pp. 21−27.

[51] Kobasko, N. I., and Kasyanova, M. D., Study of Some Features of Non-stationary Heat Transfer at Quenching, *Teplofizika i Teplotekhnika,* No. 33, 1977, pp. 67−71.

[52] Ganiev, R. F., Malyshev, P. A., Dobkin, F. S., Kobasko, N. I., Ostrovskiy, Ju. N., and Pisarev, V. E., Experimental Study of the Effect of Vibration upon Crisis of Heat Transfer at Boiling a Liquid, *Applied Mechanics,* Vol. 13, No. 9, 1977, pp. 127−130.

[53] Kobasko, N. I., Moskalenko, A. A., Deyneko, L. N., and Dobryvechir, V. V., Electrical and Noise Control Systems for Analyzing Film and Transient Nucleate Boiling Processes, *Proceedings of the 7th IASME/WSEAS International Conference on Heat Transfer, Thermal Engineering and Environment (HTE '09),* Moscow, August 20−22, 2009, pp. 101−105.

[54] Moskalenko, A. A., Kobasko, N. I., Protsenko, L. M., and Rasumtseva, O. V., Acoustical System Analyzes the Cooling Characteristics of Water and Water Salt Solutions, *Proceedings of the 7th IASME/WSEAS International Conference on Heat Transfer, Thermal Engineering and Environment (HTE '09),* Moscow, August 20−22, 2009, pp. 117−122.

[55] Narazaki, M., Fuchizawa, S., Kogawara, M., and Inaba, M., Effects of Surface Oxidation on Cooling Characteristics During Quenching of Heated Metals in Subcooled Water, *Tetsu-to-Nagane (J. Iron Steel Inst. Jpn.),* Vol. 79, No. 5, 1993, pp. 583−589.

[56] Narazaki, M., Totten, G. E., and Webster, G. M., Hardening by Reheating and Quenching, *Handbook of Residual Stress and Deformation of Steel,* Totten, G., Howes, M., and Inoue, T., Eds., ASM International, Materials Park, OH, 1992, pp. 248−295.

[57] Kobasko, N. I., Transient Nucleate Boiling as a Law of Nature and a Basis for Designing of IQ Technologies, *Proceedings of the 7th IASME/WSEAS International Conference on Heat Transfer, Thermal Engineering and Environment (HTE '09),* Moscow, August 20−22, 2009, pp. 67−75.

4

Convective Heat Transfer

N. I. Kobasko[1]

4.1 BASIC CONCEPTS

The basic concepts of heat transfer are discussed in detail in other texts on the subject, such as [1]. In this chapter, information on convective heat transfer will be provided to illustrate how convection can be used to intensify quenching processes, especially the widely used water flow and water jets.

Convection heat transfer is a process of heat transfer occurring between a surface of a solid body and a fluid, where heat transfer occurs by the simultaneous action of heat conductivity and convection. Convection takes place in liquids and gases where particle movement is possible. There are two kinds of movement: natural and forced. Natural movement, also called free movement or *natural convection*, is due to a change of the fluid density with temperature in a gravitational field. Forced movement or *forced convection* occurs under action of external devices, for example, a pump or propeller.

Intensity of convection is characterized by a heat transfer coefficient α_{conv}, which is defined from the Newton-Riemann equation $Q = \alpha_{conv}(T_{sf} - T_m)S$. This equation can be rewritten as:

$$\alpha_{conv} = \frac{Q}{(T_{sf} - T_m)S}, \qquad (1)$$

where:
Q is heat flux in W/m^2;
T_{sf} is surface temperature;
T_m is quenchant temperature; and
S is surface area in m^2.

The heat transfer coefficient can be defined as the quantity of heat transferred per unit time per unit area of a surface when the difference of temperatures between the surface S and liquid equals 1 degree [1,2]. Eq 1 is often unreasonably applied to film and nucleate boiling, which causes confusion with respect to basic concepts. For example, during film and nucleate boiling, for Eq 1, $T_{sf} - T_m$ is used instead of a difference of temperatures $T_{sf} - T_s$, and here $T_{sf} - T_m \gg T_{sf} - T_s$, because T_s is much closer to T_{sf} than T_m.

Processes of heat transfer are fully related to conditions of fluid movement. There are two basic types of flow: laminar (Fig. 1(a)) and turbulent (Fig. 1(b)). In laminar mode, the flow is a quiet stream. For the turbulent mode, fluid movement is in disorder or vortical. Fluid movement is defined as vortical if the fluid moves around in a circle or a helix, or if it tends to spin around some axis (whirling). The transition from a laminar flow into turbulent flow occurs at critical value defined by the Reynolds number:

$$Re_{cr} = \frac{\omega_{cr}d}{v} = 2100,$$

where:
ω is the speed of movement of a fluid [1,2];
d is a characteristic dimension of the channel; and
v is the kinematic viscosity of a liquid.

Laminar flow conditions occur up to Re = 10, and flow is fully turbulent from Re $\geq$ 2,100.

As for convection, there are both natural and artificial forms of turbulence. The former is established naturally. The second is caused by the presence in a stream of any barriers, turbulizing grates, or other disturbances.

In the laminar and turbulent streams, there are stabilization zones, at the end of which streams are stabilized (see Fig. 2). For a laminar stream, the stabilization zone length l_H depends on the diameter of the tube and the Reynolds number, in this relationship:

$$l_H = 0.05dRe.$$

For a turbulent stream, the stabilization zone length l_H depends mainly on the diameter of the tube, and is given by:

$$l_H = 15d.$$

The process of heat transfer is complex, and the heat transfer coefficient is a complex function of various variables describing this process. Generally, the heat transfer coefficient is a function of the fluid flow ω, shape ϕ, the dimensions $\ell_1, \ell_2, ... \ell_n$, and temperature and physical properties of the liquid: thermal conductivity λ, specific thermal capacity C_p, density ρ, and viscosity μ, that is:

$$\alpha_{conv} = f\left(\omega, T_m, T_{sf}, \lambda, C_p, \rho, \mu, \phi, \ell_1, \ell_2 ...\right). \qquad (2)$$

The following solutions are now applied as quenchants: water, oils, aqueous polymer solutions, aqueous salt solutions, and others. To establish concrete dependences such as Eq 2, it is necessary to solve a closed system of differential equations with corresponding conditions of uniqueness.

4.2 DIFFERENTIAL HEAT TRANSFER EQUATIONS
4.2.1 Heat Transfer Equations

Many handbooks provide the Fourier-Kirchhoff differential equation. It establishes a correlation between time τ and spatial changes in temperature at any point of the moving medium and has the following form [1,2]:

$$\frac{DT}{d\tau} = a\left(\frac{\partial^2 T}{\partial x^2} + \frac{\partial^2 T}{\partial y^2} + \frac{\partial^2 T}{\partial z^2}\right) \qquad (3)$$

where:

$$\frac{DT}{d\tau} = \frac{\partial T}{\partial \tau} + \omega_x \frac{\partial T}{\partial x} + \omega_y \frac{\partial T}{\partial y} + \omega_z \frac{\partial T}{\partial z}.$$

---

[1] *IQ Technologies, Inc., Akron, Ohio, and Intensive Technologies Ltd., Kyiv, Ukraine*
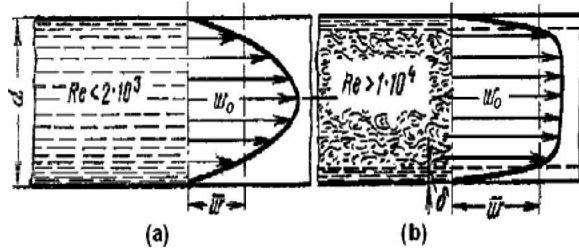
Fig. 1—Distribution of liquid flow velocity in a cross-section of a tube during laminar (a) and turbulent (b) movement.

The equation is used in this form to study the process of heat conductivity in moving liquids.

4.2.2 Equation of Movement

The differential *equations of movement* of the liquid medium are the Navier-Stokes equations in which the three-dimensional statement of problems has the following form:

$$\rho \frac{\partial \omega_x}{\partial \tau} + \rho \left(\omega_x \frac{\partial \omega_x}{\partial x} + \omega_y \frac{\partial \omega_x}{\partial y} + \omega_z \frac{\partial \omega_x}{\partial z} \right)$$
$$= \rho g_x - \frac{\partial p}{\partial x} + \mu \left(\frac{\partial^2 \omega_x}{\partial x^2} + \frac{\partial^2 \omega_x}{\partial y^2} + \frac{\partial^2 \omega_x}{\partial z^2} \right) \quad (4)$$

$$\rho \frac{\partial \omega_y}{\partial \tau} + \rho \left(\omega_x \frac{\partial \omega_y}{\partial x} + \omega_y \frac{\partial \omega_y}{\partial y} + \omega_z \frac{\partial \omega_y}{\partial z} \right)$$
$$= \rho g_y - \frac{\partial p}{\partial y} + \mu \left(\frac{\partial^2 \omega_y}{\partial x^2} + \frac{\partial^2 \omega_y}{\partial y^2} + \frac{\partial^2 \omega_y}{\partial z^2} \right); \quad (4a)$$

$$\rho \frac{\partial \omega_z}{\partial \tau} + \rho \left(\omega_x \frac{\partial \omega_z}{\partial x} + \omega_y \frac{\partial \omega_z}{\partial y} + \omega_z \frac{\partial \omega_z}{\partial z} \right)$$
$$= \rho g_z - \frac{\partial p}{\partial z} + \mu \left(\frac{\partial^2 \omega_z}{\partial x^2} + \frac{\partial^2 \omega_z}{\partial y^2} + \frac{\partial^2 \omega_z}{\partial z^2} \right). \quad (4b)$$

All terms of these equations have the dimension of force per unit volume, for example, N/m^3. They are used for both laminar and turbulent movement. The first equation (4) is a projection of resultant forces onto the x-axis, and the second and third equations (4a and 4b) are projections of resultant forces to the y- and z-axes, respectively. These equations are obtained based on the second law of mechanics, according to which resultant force is equal to the product of mass of element ρdV by its acceleration $\frac{D\omega_x}{d\tau}$.
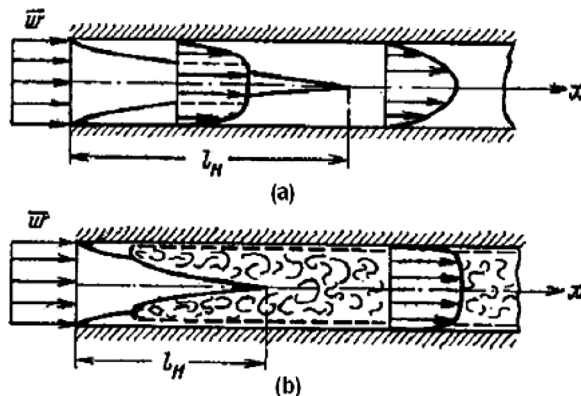
Fig. 2—Hydrodynamic stabilization of liquid flow in a tube during laminar (a) and turbulent (b) movement of liquid: l_H is the required tube length to make the liquid stream stable.

The Navier-Stokes equations (Eqs 4, 4a, and 4b) can be rewritten in vector form as:

$$\rho \frac{d\vec{\omega}}{d\tau} = \rho \vec{g} - \nabla p + \mu \nabla^2 \vec{\omega}. \quad (4c)$$

This doesn't take into account liquid density ρ as a function of temperature, however. In reality,

$$\rho = \rho_0 (1 - \beta \vartheta),$$

where:
ρ_0 is the density of the liquid at room temperature;
β is the volumetric expansion coefficient; and
$\vartheta = T - T_m$, with T_m being initial temperature (usually fluid temperature at room condition).

If we take this relationship into account, Eq 4c can be rewritten as [2]:

$$\frac{d\vec{\omega}}{d\tau} = -\vec{g}\beta\vartheta - \frac{1}{\rho}\nabla p + \nu \nabla^2 \vec{\omega}. \quad (4d)$$

4.2.3 Equation of Continuity

Because in the equation of movement a new unknown variable, pressure p, appeared, the number of unknown variables in Eqs 3 and 4d is greater than the number of equations–that is, the system is not closed. To obtain a closed system, it is necessary to attach to the available equations one more equation, the *equation of continuity*, which is deduced on the basis of the law of conservation of mass and has the following form:

$$\frac{\partial \rho}{\partial \tau} + \frac{\partial(\rho \omega_x)}{\partial x} + \frac{\partial(\rho \omega_y)}{\partial y} + \frac{\partial(\rho \omega_z)}{\partial z} = 0. \quad (5)$$

This equation for incompressible liquids becomes simpler– because $\frac{\partial \rho}{\partial \tau} = 0$ since the density for incompressible liquids is constant–and reduces to:

$$\frac{\partial \omega_x}{\partial x} + \frac{\partial \omega_y}{\partial y} + \frac{\partial \omega_z}{\partial z} = 0. \quad (6)$$

4.2.4 Boundary Conditions

The system of differential equations for processes of convection covers an uncountable set of heat transfer processes. In order to separate from these one concrete case, it is necessary to attach to the system of differential equations some boundary conditions, that is, *conditions of uniqueness*.

Conditions of uniqueness consist of:
- the geometrical conditions describing the shape and the sizes of the system in which the process proceeds;
- the physical conditions describing physical properties of the quenchant and body;
- the boundary conditions describing characteristics of the process at the boundaries of the body; and
- the time conditions describing characteristics of the process in time.

When such conditions of uniqueness for some concrete case are set, they, together with the system of differential equations, make the concrete mathematical description of the differential process possible.

Even when there are such precise statements, it is impossible to solve analytically the resulting systems of equations, and their numerical solution encounters numerous difficulties, in particular, when it is necessary to have generalized

results. These difficulties are overcome by the use of the similarity theory, which is based on the following. All the differential equations specified above are reduced to a dimensionless form, and through simple transformations, dimensionless complexes are obtained which consist of constant values used in differential equations. These dimensionless complexes are called *numbers of similarity* or *criteria*.

The first theorem of the theory of similarity establishes the connection between constants of similarity and allows the identification of the specified numbers of similarity. In general form, the theorem is formulated so that processes similar between themselves have identical numbers of similarity.

On the basis of the second theorem of similarity, the dependence between the variables describing any process can be presented as dependence between numbers of similarity K_1, K_2,..., K_n:

$$f(K_1, K_2, ..., K_n) = 0. \tag{7}$$

And at last, the third theorem of similarity states that those processes are similar when conditions of uniqueness are similar and the numbers of similarity composed of the values used in conditions of uniqueness have identical numerical values.

Thus, the theory of similarity makes it possible, without integrating differential equations, to obtain from them numbers of similarity, and with the use of experimental data, to establish the equations of similarity that are valid for all processes similar to the given one. The theory of similarity does not give a general solution, but it does provide a generalization of the experimental data that will be valid within the restrictions made in the experiments conducted.

4.3 THE EQUATION OF SIMILARITY FOR PROCESSES OF NATURAL CONVECTION HEAT TRANSFER

The process of natural convection arises because of the difference in density of the heated and cold particles of a quenchant. The equation of similarity for processes of natural convection heat transfer establishes a connection between the Nusselt number Nu, Grashof number Gr, and Prandtl number Pr and has the form as follows:

$$Nu = f(Gr, \text{Pr}). \tag{8}$$

These factors are further defined as:

$$Nu = \frac{\alpha \ell}{\lambda};$$

$$Gr = g\beta\Delta T \frac{\ell^3}{\nu^2}; \text{ and}$$

$$\text{Pr} = \frac{\nu}{a},$$

where:
α is the heat transfer coefficient at convection (W/m^{2}K);
ℓ is a characteristic geometrical dimension (m);
λ is the heat conductivity of the quenchant (W/mK);
g is gravitational acceleration, 9.81 m^2/s;
β is the volumetric expansion coefficient of the quenchant;
ΔT is the temperature change (°C);
ν is kinematic viscosity (m^2/s); and
a is the thermal diffusivity of the quenchant (m^2/s).

The Nusselt number is a dimensionless number and is the ratio of convective to conductive heat transfer across

(normal to) the boundary between the surface being cooled and the fluid. The conductive component of this ratio is measured under conditions approaching those of a motionless (unagitated) fluid. A Nusselt number within Re < Re$_{cr}$ = 2,000 is characteristic of laminar flow. Larger Nusselt numbers in the range of 2,000−10,000 are indicative of turbulent flow.

The Grashof number is a dimensionless number that corresponds to the approximate ratio of the buoyancy to viscous forces acting on a fluid in natural convection. Lower Grashof numbers indicate that the boundary layer is laminar, and higher Grashof numbers, that the boundary layer is turbulent. The transition from laminar to turbulent flow occurs in the range between 10^8 and 10^9 for natural convection.

The Prandtl number is a dimensionless number that provides an approximation of the ratio of momentum diffusivity (kinematic viscosity) and thermal diffusivity. A small Prandtl number indicates that heat diffuses quickly relative to the velocity (momentum). Typical Prandtl numbers are 0.7−0.8 for gases such as air, approximately 1.8 for water at 20°C (see Table 2 later in the chapter), and 100−40,000 for engine oil.

The temperature factor of volumetric expansion β characterizes the relative change in volume with change in temperature by 1°C (at constant pressure):

$$\beta = \frac{1}{V}\left(\frac{\partial V}{\partial T}\right)_{p=const}$$

where V is specific volume in m^3/kg.

According to the theory of similarity, for similar processes, the determined numbers of similarity must be identical. During convection, the determined number is Nusselt number Nu, describing the intensity of the process of convection:

$$Nu = \frac{\alpha \ell}{\lambda},$$

where:
α is the heat transfer coefficient at convection (W/m^{2}K);
ℓ is a characteristic geometrical dimension (m); and
λ is the heat conductivity of the quenchant (W/mK).

For Prandtl numbers within the range 1−10, it is possible to use a simple dependence for the determination of number Nu with quite high accuracy, which has the form as follows [3]:

$$Nu = 0.13(Gr\,\text{Pr})^{\frac{1}{3}}. \tag{9}$$

For convenience of calculations, the dimensionless dependence of Eq 9 can be reduced to the form

$$\alpha_{conv} = \lambda\left(\frac{g\beta\Delta T}{a\nu}\right)^{\frac{1}{3}}, \tag{10}$$

from which it follows that the convection heat transfer coefficient for the considered conditions of cooling does not depend on the size of parts to be quenched.

Example 4.1
Calculate a heat transfer coefficient for natural convection at the time of transition from nucleate boiling to a single-phase convection in water. This would occur approximately when the temperature of the surface of a part to be quenched is equal to 100°C. Consider a cylindrical sample of 30-mm diameter and 200-mm length that is cooled from

875°C in still water at 10°C. The thermal and physical properties of water at 10°C are:

$\lambda = 0.580$ W/mK;
$\beta = 0.7 \times 10^{-4}$ 1/K;
$v = 1.306 \times 10^{-6}$ m²/s;
$g = 9.81$ m/s²;
$a = 13.8 \times 10^{-6}$ m²/s; and
$\Delta T = 100°C - 10°C = 90°C$.

Substituting these values into Eq 10, we get:

$$\alpha_{conv} \approx 0.58 \left(\frac{9.81 \times 0.7 \times 10^{-4} \times 90}{13.8 \times 10^{-6} \times 1.306 \times 10^{-6}} \right)^{\frac{1}{3}} \approx 875 \, \text{W/m}^2 \, \text{K}.$$

Thus, at the time of transition from nucleate boiling to a single-phase convection, the heat transfer coefficient during cooling in still water at 10°C is approximately equal to 875 W/m²K. It is similarly possible to calculate α_{conv} for other temperatures of water that may be used as a quenching medium. The results of calculations are provided in Table 1.

Table 1 shows that with an increase of water temperature, the convection heat transfer coefficient increases despite a reduction of the temperature difference $\Delta T = T_{sf} - T_m$. This is due to a change in the thermal and physical properties of water with the change of its temperature (see Table 2).

Such behavior of water when used as a quenchant surely affects the duration of nonstationary nucleate boiling or of the self-regulated thermal process, which is the same. Table 3 presents the results of calculations of time τ_{nb} versus temperature of water using equations obtained in Chapter 2. Table 3 shows that the duration of nucleate boiling is reduced to 22 % with increasing water temperature. These facts should be considered in process design.

4.4 SIMILARITY OF PROCESSES OF HEAT TRANSFER DURING FORCED CONVECTION

4.4.1 Calculation of Convection Heat Transfer Coefficients in Water Flow

Usually, intensive steel quenching is conducted in intensive water flow or jets, or controlled sprayer cooling. That is why it

TABLE 2—Prandtl number Pr and volumetric expansion β versus temperature of water

Water temperature (°C)	Prandtl number	$\beta \times 10$ (1/K)
10	9.45	0.7
20	7.03	1.82
30	5.45	3.21
40	4.36	3.87
50	3.59	4.49

is very important to provide a detailed description of dimensionless equations of similarity that can be easily used for process design. Similarity of forced convection heat transfer processes is described by equations of similarity as follows:

$$Nu = f(\text{Re}, \text{Pr}). \tag{11}$$

Whether it is a directed stream of water or another quenchant, or forced sprayer cooling, the criteria discussed above (Reynolds Number Re = wD/v and Prandtl Number Pr = v/a) are necessarily present in these equations.

Cooling of parts in ring channels, since such systems are most often used in practice and have a direct relation to intensive quenching, will now be considered (see Fig. 3(a)).

The similarity of directed streams of a liquid in ring channels of any cross-section shape has the form of Eq 11 and has been described in detail in [4, 5]. In the generalized form, the equation of similarity is as follows:

$$\overline{Nu} = 0.021 \, \text{Re}^{0.8} \cdot \text{Pr}^{0.43} (\text{Pr}_m / \text{Pr}_{sf})^{0.25} \cdot \varepsilon_l, \tag{12}$$

where:
Pr_m is the Prandtl number for a quenchant far from the surface; and
Pr_{sf} is the Prandtl number for a quenchant near a surface to be quenched.

TABLE 1—Heat transfer coefficient at natural convection versus temperature of water and temperature of a surface of a part to be quenched

Part surface temperature (°C)	Convection heat transfer coefficient (W/m²K)				
	Water temperature 10°C	Water temperature 20°C	Water temperature 30°C	Water temperature 40°C	Water temperature 50°C
100	875	1,283	1,622	1,780	1,884
90	841	1,227	1,541	1,675	1,749
80	804	1,165	1,450	1,555	1,590
70	764	1,097	1,346	1,413	1,389
60	719	1,018	1,222	1,234	1,102
50	667	925	1,068	980	—
40	606	808	848	—	—
30	530	642	—	—	—
20	420	—	—	—	—
10	334	—	—	—	—

TABLE 3—Duration of the self-regulated thermal process versus temperature of water for a steel sample of 30 mm in diameter cooled from 875°C

Water temperature (°C)	10	20	30	40	50
τ_{nb} (s)	31	27.6	25.6	24.9	24.4

For pipes of round section, the equivalent diameter d_{eq} is equal to the geometrical diameter d. Coefficient ε_1 takes into account changing of the average value of heat transfer along the pipe. If $\ell/d > 50$, then $\varepsilon_e = 1$; ℓ is the length of the pipe, and d is the equivalent diameter. Here, the characteristic temperature is the average temperature of a quenchant far from a surface to be quenched, and the characteristic dimension is equivalent diameter d_{eq}, equal to four times multiplied areas of the cross-section of the ring channel divided by its full wetted perimeter u, disregarding which part of this perimeter participates in the heat transfer (see Eq 13):

$$d_{eq} = \frac{4S}{u}, \qquad (13)$$

where:
S is the area of cross-section of the channel; and
u is the full perimeter of the channel.

Example 4.2
For a simple tube, equivalent diameter d_{eq} is equal to the inner diameter of the tube:

$$d_{eq} = \frac{4S}{u} = \frac{4 \times \pi R^2}{2\pi R} = 2R = D.$$

Example 4.3
For a ring channel (see Fig. 3(a)), equivalent diameter d_{eq} is equal to the inner diameter D of the cooling chamber minus the diameter d of the round steel part:

$$d_{eq} = \frac{4S}{u} = \frac{4 \times (\pi R^2 - \pi r^2)}{2\pi R + 2\pi r} = \frac{4\pi \times (R - r) \times (R + r)}{2\pi \times (R + r)}$$
$$= 2R - 2r = D - d.$$

Table 4 presents results of calculations of the correction $\left(\dfrac{\mathrm{Pr}_m}{\mathrm{Pr}_{sf}}\right)^{0.25}$ for water at various temperatures, and also for various wall temperatures. Such data are necessary for the calculation of process conditions during steel quenching in
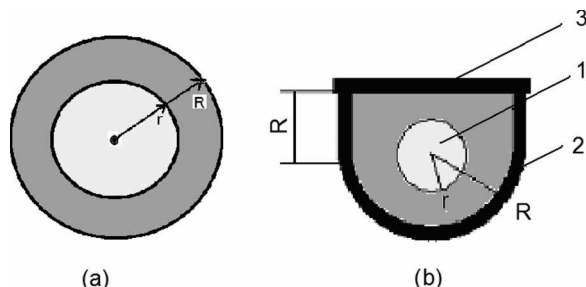
Fig. 3—Cross section of round (a) and U-shaped (b) quench chambers for truck semi-axles: 1, semi-axle of 60-mm diameter; 2, U-shaped chamber consisting of a half-cylinder of 40-mm radius and additional side walls R of 40-mm height; 3, cover of the chamber.

water under pressure. Increasing pressure increases the boiling temperature of a boundary liquid layer, and therefore the temperature of a wall increases and the specified correction has essential effect in Eq 12. Although Table 4 shows this effect, it is not significant. The primary effect on the correction is caused by the water temperature, which affects its viscosity and therefore the Prandtl number Pr_m over the length of a pipe. If $\ell/d > 50$, then $\varepsilon_e = 1$. At $\ell/d < 50$, it is necessary to take into account the effect of a thermal initial spot [2]. Values of ε_e are presented in Table 5.

It should be emphasized once more that Eq 12 is applicable to channels of any cross-section shape—round, square, rectangular, ring—and for all conventional liquids when the Reynolds number Re is between 1×10^4 and 1×10^6 and the Prandtl number Pr is in the range 0.6 to 2,500. Eq 12 is also valid for channels of complex cross-sections—in particular, when there are one or several pipes of small diameter in a pipe with a larger diameter. The multiplier $(\mathrm{Pr}_m/\mathrm{Pr}_{sf})^{0.25}$ represents the correction for the dependence of physical properties of a quenchant (mainly viscosity) upon temperature. Depending on the direction of heat flux, this correction can be either greater or less than one. More detail on single-phase convection is presented in [1,6].

Example 4.4
To better understand the application of the equation of similarity (Eq 12), consider the problem of determining the convection heat transfer coefficient at the time of transition from nucleate boiling to single-phase convection for truck semi-axles

TABLE 4—Correction $\left(\dfrac{\mathrm{Pr}_m}{\mathrm{Pr}_{sf}}\right)^{0.25}$ versus pressure and temperatures of water at the time of transition from nucleate boiling to a single-phase convection

Water temperature (°C)	Pressure (MPa)	$\left(\dfrac{\mathrm{Pr}_m}{\mathrm{Pr}_{sf}}\right)^{0.25}$	Average correction
20	0.10	1.42	1.54
	0.20	1.48	
	0.27	1.51	
	0.36	1.54	
	0.48	1.57	
	0.62	1.59	
	0.79	1.61	
	1.0	1.62	
40	0.10	1.23	1.36
	0.20	1.31	
	0.27	1.34	
	0.36	1.36	
	0.48	1.39	
	0.62	1.41	
	0.79	1.43	
	1.0	1.43	

TABLE 5—Values of dependence $\varepsilon_\ell = f(^\ell/_d, \text{Re})$ at the turbulent mode									
	$^\ell/_d$								
Re	1	2	5	10	15	20	30	40	50
1×10^4	1.65	1.50	1.34	1.23	1.17	1.13	1.07	1.03	1.00
2×10^4	1.51	1.40	1.27	1.18	1.13	1.10	1.05	1.02	1.00
5×10^4	1.34	1.27	1.18	1.13	1.10	1.08	1.04	1.02	1.00
1×10^5	1.28	1.22	1.15	1.10	1.08	1.06	1.03	1.02	1.00
1×10^6	1.14	1.11	1.08	1.05	1.04	1.03	1.02	1.01	1.00

of 60-mm diameter, quenched by water flow at 8 m/s in the quenching U-tube shown in Fig. 3(b). The length of the semi-axles is 0.8 m. The average pressure in the chamber is 0.143 MPa. The first step in this calculation is to determine the equivalent diameter of the cross-section of the chamber using Eq 13.

The surface area of cross-section of the chamber (see Fig. 3(b)) is equal to

$$4S = 4\left[\frac{\pi R^2}{2} + (2R \times R)\right] - 4\pi r^2$$
$$= 2(\pi + 4)R^2 - 4\pi r^2 = 11.54 \times 10^{-3} \, m^2.$$

The full wetted perimeter U is equal to:

$$U = \frac{2\pi R}{2} + 4R + 2\pi r = (\pi + 4)R + 2\pi r = 0.474 \, \text{m}.$$

Therefore, equivalent diameter d_{eq} is equal to:

$$d_{eq} = \frac{4S}{U} = \frac{11.54 \times 10^{-3} m^2}{0.474 m} = 0.0243 m.$$

The ratio of the length of the chamber ℓ to equivalent diameter d_{eq} is:

$$\varepsilon = \ell/d_{eq} = \frac{0.8}{0.00411} \approx 195,$$

and therefore, $\varepsilon_\ell = 1$, as ℓ/d_{eq} is much greater than 50.

The next step is to calculate the temperature factor $\left(\frac{\text{Pr}_m}{\text{Pr}_{sf}}\right)^{0.25}$. The water temperature in the quench chamber is 20°C. The wall temperature at a pressure of 0.143 MPa is approximately 110°C. At these specified temperatures, $\text{Pr}_m = 7.03$ and $\text{Pr}_{sf} = 1.60$ [1]. Therefore:

$$\left(\frac{\text{Pr}_m}{\text{Pr}_{sf}}\right)^{0.25} = 1.45.$$

With regard to these calculations, the dimensionless Eq 12 is now written as:

$$\bar{N}u = 0.03 \, \text{Re}^{0.8} \, \text{Pr}^{0.43} \qquad (14)$$

At a water temperature of 20°C:

$$\text{Pr}^{0.43} = 2.31, \text{Re} = \frac{8m/s \times 0.0243}{1.006 \times 10^{-6} m^2/s} = 193240,$$

$$\text{Re}^{0.8} = 16,939, \text{ and}$$

$$\bar{N}u = 0.03 \times 16939 \times 2.31 = 1174.$$

Since

$$\bar{N}u = \frac{\alpha}{\lambda} d_{eq},$$

or, rewritten,

$$\bar{\alpha}_{conv} = \frac{\bar{N}u\lambda}{d_{eq}},$$

it follows that

$$\bar{\alpha}_{conv} = \frac{1174 \times 0.597 W/m \, K}{0.0243 \, m} = 28505 W/m^2 K.$$

This cooling process is very intensive quenching, because the Biot number $Bi = \frac{\bar{\alpha}_{conv}}{\lambda}R$ for semi-axle 60 mm in diameter (that is, radius R = 0.03 m), using a heat conductivity of steel $\lambda = 22\frac{W}{mK}$, is equal to:

$$Bi = \frac{28505 W/m^2 K \times 0.03 m}{22 W/mK} = 39,$$

which is equivalent to $Bi \to \infty$.

To evaluate the intensity of this type of quenching, it makes sense to calculate the Kondratjev number Kn, which according to [13] is equal to 0.95. Very intensive quenching begins when Kn reaches 0.8.

4.4.2 Spray Cooling

Having considered characteristics of heat transfer during water-flow cooling in channels, let's consider now spray cooling. In most cases, sprayer cooling represents a rather simple device consisting of two hollow finite cylinders, one of them inserted into the other in a parallel way, and both sealed at the end faces. Here, the inner hollow cylinder has nozzles, which can be of different diameters and located at the generatrix[2] of the cylinder in many different ways (see Fig. 4), square or hexagonal. The character of the positions of slots in the sprayer is shown in Fig. 5. The spray system itself is shown in Fig. 6. Typical pressure in this system is up to 0.9 MPa [13].

The average heat and mass transfer coefficients for impinging flow from regular (square or hexagonal) arrays of round nozzles (ARN) may be calculated as described in [7−9] with an accuracy of ±15 %. The generalized dimensionless equation has the following form:

$$\bar{N}u = K_1 K_2 \text{Re}^{\frac{2}{3}} \text{Pr}^{0.42}, \qquad (15)$$

---

[2] A *generatrix* is defined as a geometric element that may be moved to generate a line, surface, or solid. This term is sometimes referred to as a *generator*.
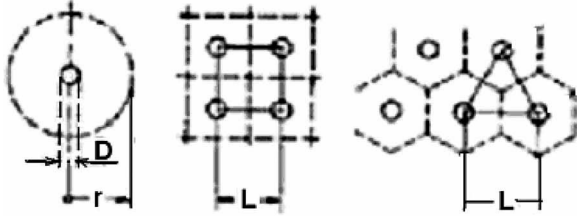
Fig. 4—Character of the positions of round holes in the sprayer [9].

where:

$$K_1 = \left[1 + \left(\frac{H/D}{0.6}\sqrt{f}\right)^6\right]^{-0.05};$$

$$K_2 = \frac{\sqrt{f}(1 - 2.2\sqrt{f})}{1 + 0.2(H/D - 6)\sqrt{f}};$$

$$f = \frac{(\pi/4)D^2}{A_{square(hexagon)}};$$

D is the diameter of a nozzle in the sprayer;

H is a distance from a nozzle (aperture) to the surface to be quenched; and

A is the area of the square, hexagon.

Dimensionless numbers K_1 and K_2 are connected to the geometry and arrangement of nozzles with respect to the surface to be quenched. The Reynolds number Re is related to the speed of the quenchant at the beginning of the outlet from a nozzle, and the Prandtl number Pr characterizes physical properties of the quenchant. The dimensionless equation of similarity (Eq 15) is valid within the boundaries of the following values and given parameters:

- $2000 \leq \text{Re} \leq 100000$
- $0.004 \leq f \leq 0.04$
- $2 \leq \dfrac{H}{D} \leq 12$

Example 4.5

Calculate the heat transfer coefficient during cooling of cylindrical bodies in a sprayer. Assume that the cylindrical steel sample possesses a diameter of 60 mm and a height of 160 mm and will be cooled in the sprayer illustrated in Fig. 6, where the inner diameter is 80 mm and height is 200 mm. Over the circle of the sprayer, 25 nozzles of 2-mm diameter are drilled, and over the height 20 nozzles are drilled. The total number of nozzles in the sprayer is $20 \times 25 = 500$. The temperature of the water supplied from the pump is 20°C. The speed of water at the outlet from a nozzle (aperture) is 8 m/s. The task is to determine the convection heat transfer coefficient for the sprayer.
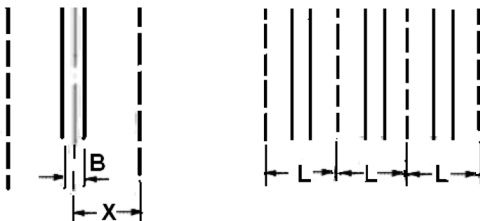
Fig. 5—Character of the positions of slots in the sprayer [9].
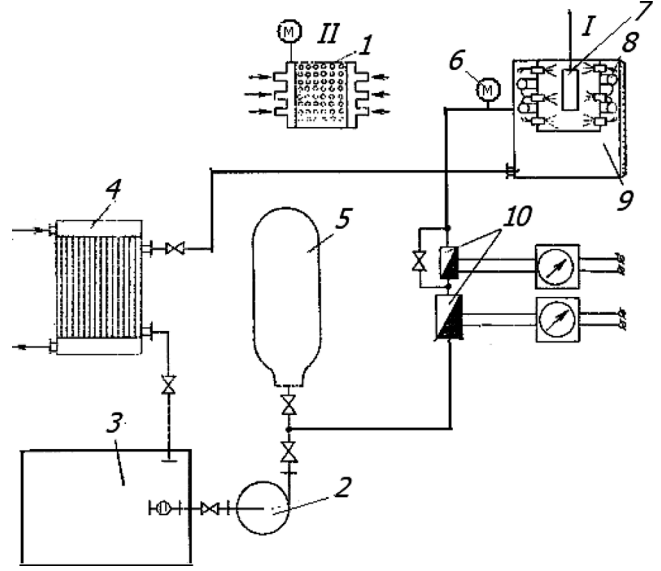
Fig. 6—Installation for quenching steel parts and cylindrical specimens in water jets: I, sprayer with round holes; II, a different kind of sprayer; 1, holes in the sprayer; 2, pump; 3, water tank; 4, chiller; 5, receiver; 6, manometer; 7, cylindrical specimens with the splines; 8, spray system; 9, water tank and spray system; 10, equipment for measuring the amount of water used.

The first step is to calculate all input parameters:

$$D = 0.002m;$$

$$H = 0.01m;$$

$$f = \frac{(\pi/4)D^2}{1 \cdot 10^{-4}} = 0.0314;$$

$$\frac{H}{D} = \frac{0.01m}{0.002m} = 5;$$

$$\text{Pr} = 7.03;$$

$$\text{Pr}^{0.42} = 2.268;$$

$$\text{Re} = \frac{8\,m/s \times 0.002\,m}{1.006 \times 10^{-6}m^2/s} = 15905; \text{ and}$$

$$\text{Re}^{\frac{2}{3}} = 632.$$

The calculated parameters and numbers are within the limits of reliability of dimensionless Eq 15.

Now calculate dimensionless numbers K_1 and K_2:

$$K_1 = \left[1 + \left(\frac{5}{0.6}\sqrt{0.0314}\right)^6\right]^{-0.05} = 0.885; \text{ and}$$

$$K_2 = \frac{\sqrt{0.0314}(1 - 2.2\sqrt{0.0314})}{1 + 0.2(5 - 6)\sqrt{0.0314}} = 0.11.$$

It follows that:

$$\overline{Nu} = 0.835 \times 0.11 \times 632 \times 2.268 = 139.5, \text{ and}$$

$$\alpha_{conv} = \frac{139.5 \times 0.597W/mK}{0.002\,m} = 41652\ W/m^2K.$$

Next, calculate the water flow rate in a sprayer and longitudinal stream in the case when the gap between the cylinder and nozzle is 10 mm. The number of nozzles is 500. The diameter of a nozzle (aperture) is 2 mm, which indicates

that the volume of water running every second through nozzles is 0.01255 m^3, or 45.2 m^3 every hour.

During longitudinal flow of water, when the gap is 10 mm, the water flow rate is:

$$V = (\pi R^2 - \pi r^2)8 \times 3600 = 3.14(0.0016 - 0.0009)8 \times 3600$$
$$= 63.3 \text{ m3/hr.}$$

These calculations show that that sprayer cooling is more effective than cooling by a longitudinal stream. At the lower water flow rate during sprayer cooling, somewhat greater values of heat transfer coefficients are obtained. However, sprayer cooling has a shortcoming: thin nozzles are clogged by oxide scale. To eliminate this shortcoming in practice, slotted nozzles are used.

4.4.3 Sprayers with Slots

Parameters of a slot nozzle are presented in Fig. 5. Slotted nozzles have been discussed previously and are discussed in detail in [9]. At first, it should be noted that the diameter used in calculations of Reynolds numbers and Nusselt numbers includes the so-called hydraulic diameter D, which is equal to the double width of a slot (Fig. 5); that is, $D = 2B$. If the width of a slot is 2 mm, then $D = 0.004$ mm. The dimensionless equation of similarity for slot nozzles, according to [9], has the form:

$$\overline{Nu} = \frac{2}{3}f_0^{\frac{3}{4}}\left(\frac{2Re}{f/f_0 + f_0/f}\right)^{\frac{2}{3}} Pr^{0.42}, \quad (16)$$

where:
$f_0 = [60 + 4(H/D - 2)^2]^{-0.5}$;
$D = 2B$ for slot nozzles;
B is the width of a slot nozzle;

$$f = \frac{D}{2L};$$
$$L = \frac{2\pi R}{n};$$

R is the inner radius of a slotted round sprayer; and
n is the number of slots located at the generatrix.

Example 4.6

Calculate the convection heat transfer coefficient for Example 4.5 above (cooling of the steel cylinder of 60-mm diameter in a sprayer with an inner diameter of 80 mm). Assume that the distance between slots is 10 mm or 0.01 m.

First of all, the value f should be calculated (see Fig. 5):

$$f = \frac{2B}{2L} = \frac{0.002}{0.01} = 0.2$$

and

$$f_0 = \left[60 + 4\left(\frac{0.01}{0.004} - 2\right)^2\right]^{-0.5} = 0.128.$$

For convenience, the dimensionless Eq 16 is shown in a somewhat different form:

$$\overline{Nu} = \frac{2}{3}f_0^{\frac{3}{4}}\left(\frac{2}{f/f_0 + f_0/f}\right)^{\frac{2}{3}} Re^{\frac{2}{3}} Pr^{0.42} \quad (17)$$

or

$$\overline{Nu} = K_1 K_2 Re^{\frac{2}{3}} Pr^{0.42}, \quad (17a)$$

where:

$$K_1 = \frac{2}{3}f_0^{\frac{3}{4}}; \text{and}$$

$$K_2 = \left(\frac{2}{f/f_0 + f_0/f}\right)^{\frac{2}{3}}.$$

The remainder of the input data is now calculated as follows:

$$K_1 = \frac{2}{3}(0.128)^{\frac{2}{3}} = 0.143;$$

$$K_2 = \left(\frac{2}{1.153 + 0.64}\right)^{\frac{2}{3}} = 0.94;$$

$$Pr^{0.42} = 2.268;$$

$$Re = \frac{8m/s \times 0.004m}{1.006 \times 10^{-6}m^2/s} = 31809; \text{and}$$

$$Re^{\frac{2}{3}} = 1004.$$

It follows therefore that:

$$\overline{Nu} = 0.143 \times 0.94 \times 1004 \times 2.268 = 306$$

and

$$\bar{\alpha}_{conv} = \frac{306 \times 0.597W/mK}{0.004m} = 45670 W/m^2K.$$

In comparison with a longitudinal water flow, spray cooling gives a higher value for the heat transfer coefficient. Results of all calculations are presented in Table 6.

4.4.4 Optimal Spatial Arrangements of Nozzles

The term "optimal spatial arrangements" means a combination of geometric variables that yields the highest average transfer coefficient for a given blower rating per unit area of transfer surface for uniformly spaced arrays of nozzles with good outlet flow conditions. There are always three independent geometric variables:
1. Nozzle diameter D (or slot width B)
2. Nozzle-to-nozzle spacing L
3. Nozzle-to-plate distance H (see Figs. 4 and 5)

The following optimal parameters for round nozzles in a sprayer have been identified [7,10]:

$$f_{opt} = 0.0152,$$

$$\left(\frac{H}{D}\right)_{opt} = 5.43,$$

and others.

TABLE 6—Comparison of convection heat transfer coefficients when cooling a cylinder of 60-mm diameter with a longitudinal stream of water, round and slotted jets, with a total gap of 10 mm

Type of cooling	α_{conv} (W/m²K)	Increase in α_{conv} with respect to longitudinal water flow
Longitudinal water flow	28,505	—
Round spray	41,652	46 %
Slot spray	45,670	60 %

Optimal parameters for slot nozzles are:

$$f_{opt} = 0.0718;$$

$$\left(\frac{H}{D}\right)_{opt} = 5.037;\ \text{and}$$

$$\frac{(H/D)^{\frac{1}{3}}}{f^{\frac{2}{9}}} \times \frac{2}{3}f_0^{\frac{3}{4}}\left(\frac{2}{f/f_0 + f_0/f}\right)^{\frac{2}{3}} = 0.355.$$

4.5 IMPORTANT PRACTICAL PROBLEM SOLVED BY DIRECT CONVECTION

Using the above equations, it is possible to perform accurate calculations to optimize the steel quenching process. Consider direct convection, where film boiling and nucleate boiling during quenching are prevented due to a very high velocity of water spray. It was established that nucleate boiling can be suppressed if the following condition is fulfilled [11]:

$$\frac{q}{r^*W}\left(\frac{\rho''}{\rho'}\right)^{1.45}\left(\frac{r^*}{c_pT_s}\right)^{0.33} \leq 4\cdot 10^{-6}, \qquad (18)$$

where:
q is the heat flux density;
r^* is the heat of steam formation (J/kg);
T_S is a saturation (boiling) temperature (K);
ρ' is water density (kg/m^3);
ρ'' is steam density (kg/m^3);
c_p is specific heat capacity of liquid; and
W is the speed of the liquid.
The higher the initial heat flux density, the higher the speed of water must be to satisfy Eq 18 and prevent nucleate boiling.

An experimental installation was designed and built to produce direct convection during intensive quenching (see Fig. 6). It consisted of two sprayers, a powerful pump, a tank with water, a chiller, a receiver, manometers to measure pressure, and devices to measure the amount of water used during experiment. A correlation between the pressure in the sprayer and the convective heat transfer coefficient was established, which is shown in Fig. 6. More information about such an approach can be found in [12–15]. To investigate the impact of intensive quenching on the probability of crack formation and hardness distribution, cylindrical splined specimens made of AISI 1050 and 4340 steels and low hardenability steel 47GT (see Figs. 7 and 8) were included. The diameter of these specimens was 60 mm and their height was 120 mm.

It has been shown that very intensive direct convection (when the convective heat transfer coefficient is higher than
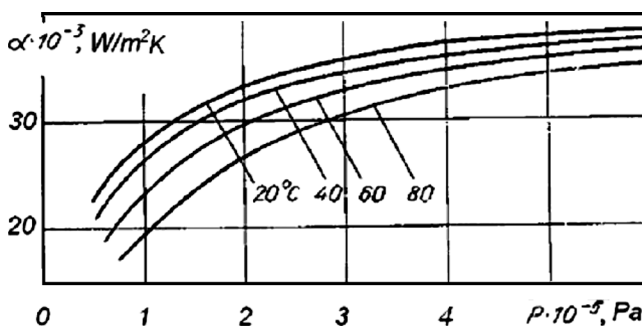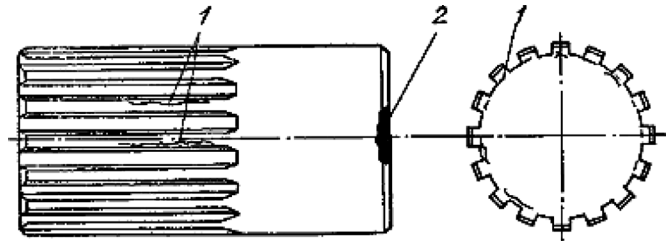
Fig. 8—Cylindrical test specimen with the splines made of different steels, each of 60-mm diameter and 120 mm in height; 1 shows cracks on splines; 2 shows a crack on the edge of specimen when conventional quenching in water.

30,000 W/m^{2}K) prevents crack formation and significantly increases the surface hardness of steels. Some experimental data are provided in Tables 7 and 8.

During the experiments it was noted that the hardness of the cylindrical surface of the test specimens was higher than that of the splined surface of the specimens (see Table 7). This was proposed to be due to the temperature on the cylindrical surface, which drops immediately to the bath temperature, providing very high hardness on the cylindrical surface (63–64 HRC). The temperature on the splined surface drops to saturation temperature T_s, providing a hardness of 59–61 HRC due to self-tempering of the splines. This difference is caused by the different thicknesses of the cylinder and spline. On the cylindrical surface, direct convection was immediately established, while at the same time a self-regulated thermal process was established on the spline surface (see Chapter 2 and [15]).

The dimensionless equations can be used to predict direct convection during steel part quenching and by process optimization. Due to direct convection, it was possible to use the CFD (computational fluid dynamics) modeling to verify the calculations that were discussed above [16–19]. Very useful results for optimizing technological processes have been reported [20–25].

4.6 DISCUSSION

To be sure that dimensionless equations can be used for designing intensive quenching processes, Krukovskyi and colleagues [19] compared simplified calculations with the CFD modeling. For comparison, the cylindrical forging shown in

Fig. 7—Convective heat transfer coefficient versus pressure in the sprayer with water at 20°C, 40°C, 60°C, and 80°C.

TABLE 7—Surface hardness (HRC) of the cylindrical specimens with the splines after convectional and very intensive quenching

Method of cooling	Steel grade	Surface hardness (HRC)	
		Cylindrical surface	Splined surface
Still water at 15°C	AISI 1050	44	56
Pressurized spray cooling at 9 × 10⁵ Pa	AISI 1050	64	61
Still water at 15°C	47GT	57.5	58
Pressurized spray cooling at 9 × 10⁵ Pa	47GT	63	59

Note: Composition of 47GT steel: 0.44–0.51 C; 0.95–1.25 Mn; 0.10–0.25 Si; 0.25 Cr; 0.06–0.12 Ti.

TABLE 8—Impact of cooling rate on crack formation in the cylindrical specimens with the splines

Method of cooling	Steel grade	Numbers of cracks
Still water at 15°C	AISI 1050	2
Pressurized spray cooling at 9×10^5 Pa	AISI 1050	0
Still water at 15°C	47GT	3
Pressurized spray cooling at 9×10^5 Pa	47GT	0

Fig. 9 was used. Fig. 9 shows half of the forging's section for which meshing and calculations were made; the forging is symmetrical.

Let's consider results of CFD simulations in different areas of forgings (points 1–8 in Fig. 9). The water flow of 8 m/s was moving from the upper side of the fixture and then vented through the ring channel along the surface of forging. The distance between the fixture and the forging's surface was 10 mm.

The results of CFD simulations are presented in Figs. 10–12. As one can see from results of simulations, it is impossible to eliminate stagnant areas 1 and 4 with water flowing at 8 m/s. According to the criterion of Eq 18, nucleate boiling should be absent and direct convection should prevail during the process of intensive cooling with a water flow of 8 m/s. However, in stagnant areas, the water flow decreases significantly, and in these areas, nucleate boiling and even film boiling can occur. That is why the configuration of the fixture should be optimized completely to get very smooth cooling around the forging.

CFD modeling doesn't consider the nucleate boiling and film boiling processes, only direct convection. In the future, CFD modeling should take into account film and nucleate boiling, which should be based on critical heat fluxes

Fig. 10—Water flow velocity distribution at the exit of system for quenching of forging. A stagnant area is observed at the surface located near point 1 [19].
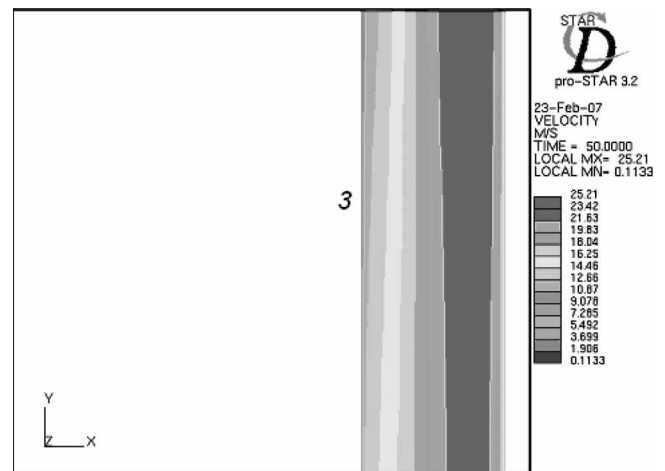
Fig. 11—Water flow velocity distribution at the exit of system for quenching of forging. No stagnant area is observed [19].

Fig. 9—Drawing of the forging (half of its section) and points where temperature field and velocity flow distribution were investigated [19].
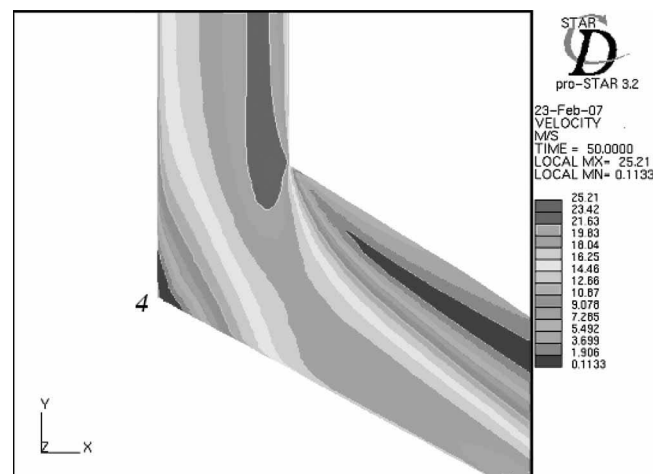
Fig. 12—Water flow velocity distribution at the exit of system for quenching of forging. A stagnant area is observed at the surface located near point 4 [19].
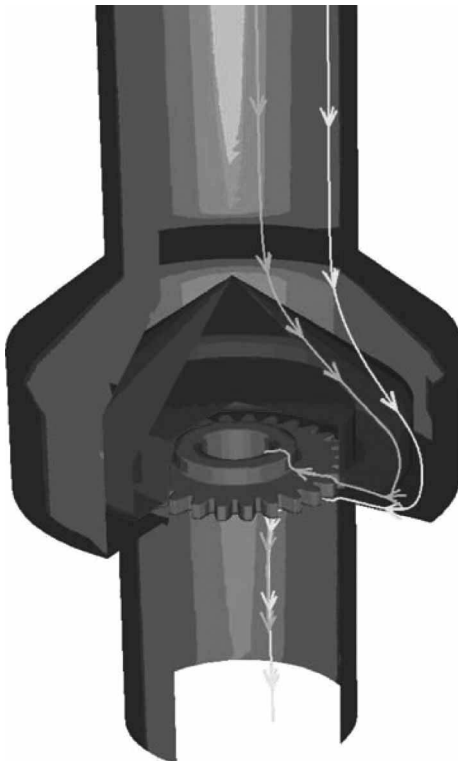
Fig. 13—Cutaway view of the quench fixture showing the gear (red), upstream deflector (blue), and representative water path lines passing over and under the gear (green, yellow) [20].

considerations (see Chapter 3). Currently an international team is working on this [26].

Small stagnant areas were situated at points 1, 4, and 7 (Fig. 9). For these small areas, CFD modeling doesn't give correct results of calculations since it doesn't take into account nucleate and film boiling. Despite that, the cooling time calculation for the core was correct, because the stagnant areas were rather small. To prove this, Krukovskyi and
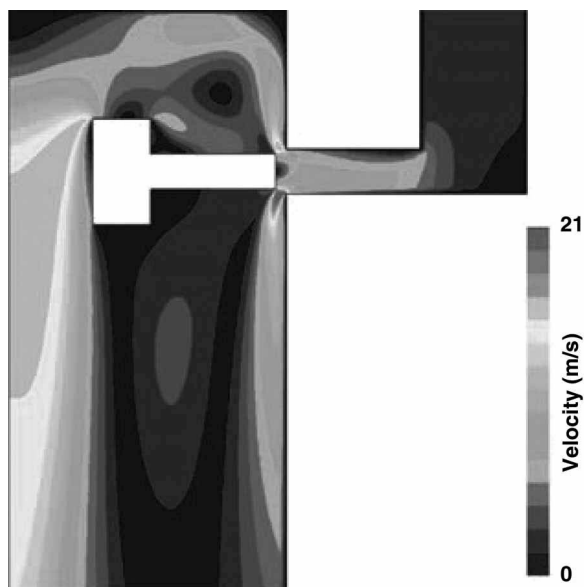
Fig. 14—Total velocity plot of water flowing through quench fixture and around gear blank [20].

colleagues compared the cooling time from the austenitizing temperature T_0 of 870°C to a temperature of 500°C at point 8 [19]. The cooling time calculated on the basis of dimensionless Eq 12 was 37 s, and that calculated using CFD modeling was about 36 s [19]. This means that Eq 12 can be useful at quench system engineering design when water flow in different channels is considered for intensive quenching.

Slot cooling (see Eq 16 and Fig. 5) was used by Banka and colleagues [20] to intensively quench the teeth of carburized gears. Their designed fixture is shown in Fig. 13. The water flow was directed through slots on the teeth of a gear, which provided for an absence of nucleate boiling and created very high compressive residual stresses at the roots of the teeth (see Fig. 14). As a result, fatigue strength of the gears significantly increased [20]. Combining simplified calculations (see Eq 16) with the CFD modeling allows the design of suitable fixtures for quenching different complicated steel parts, including carburized gears [20].

4.7 SUMMARY

1. The dimensionless equations for convection have been analyzed and can be used in practice when designing different kinds of intensive quenching processes.
2. The direct convection during intensive quenching was used to prevent crack formation and increase the hardness on the surface of steel parts.
3. It is emphasized that calculations made on the basis of dimensionless equations coincide well with the results achieved by CFD modeling [19].
4. It is shown that optimized slot cooling is more effective by 60 % compared with the water flow moving with the same speed.
5. Both simplified calculations and CFD modeling are successfully used for designing intensive quenching processes.
6. Special attention should be paid to stagnant areas, which can be sources of local film boiling and can cause distortion and nonuniformity in hardness distribution.
7. Currently an international team is working on developing possibilities for using CFD modeling in the investigation of the film boiling and nucleate boiling processes.

References

[1] Lienhard IV, J. H., and Lienhard V, J. H., *A Heat Transfer Textbook*, 3rd Ed., Phlagiston Press, Cambridge, Massachusetts, 2005.
[2] Isachenko, V. P., Osipova, V. A., and Sukomel, A. S. *Teploperedacha* (Heat transfer), Energomash, Moscow, 1981.
[3] Mayinger, F., Thermo- and Fluid-Dynamic Principles of Heat Transfer During Cooling, *Theory and Technology of Quenching*, Liščić, B., Tensi, H. M., and Luty, W., Eds., Springer-Verlag, Berlin, 1992, pp. 41–72.
[4] Mikheev, M. A., and Mikheeva, I. M., *Osnovy teploperedachi* (Basics of heat transfer), Energy, Moscow, 1977.
[5] Incropera, F. P., and DeWitt, D. P., *Fundamentals of Heat and Mass Transfer,* John Wiley & Sons, New York, 1981.
[6] Žukauskas, A., *High-Performance Single-Phase Heat Exchangers,* Hemisphere, New York, 1989.
[7] Martin, H., Heat and Mass Transfer Between Impinging Gas Jets and Solid Surfaces, *Advances in Heat Transfer,* Hartnett, J. P., and Irvine, T. F., Eds., Vol. 13, Academic Press, New York, 1977, pp. 1–60.
[8] Krötzsch, P., Wärme- und Stoffübergang bei Prallströmung aus Düsen- und Blendenfeldern, *Chem. Ing. Tech.,* Vol. 40, 1968, pp. 339–344.
[9] Martin, H., Impinging Jets, *Hemisphere Handbook of Heat Exchanger Design,* G. F. Hewitt, Coordinating Ed., Hemisphere, New York, 1990, pp. 2-5-6-1.

[10] Martin, H., and Schlünder, E. U., Optimierung von Schlitzdüsentrocknern auf Irund neuer Versuchsergebnisse über den Wärme- und Stoffübergang in solchen Apparaten, *Chem. Ing. Tech.,* Vol. 45, 1973, pp. 290−294.

[11] Sterman, L. S., Heat Transfer Investigation During Boiling Liquids in the Tubes, *Journal of Engineering Physics,* Vol. 24, No. 11, 1954, pp. 2046−2053.

[12] Kadinova, A. S., and Krivizhenko, V. I., Investigation the Cooling Capacity of Different Kinds of Sprayers, *Metal Science and Heat Treatment,* No. 3, 1968, pp. 27−30.

[13] Kobasko, N. I., *Steel Quenching in Liquid Media Under Pressure,* Naukova Dumka, Kyiv, 1980.

[14] Kobasko, N. I., Quenching Apparatus and Method for Hardening Steel Parts, U.S. Patent No. 6,364,974 BI, April 2, 2002.

[15] Kobasko, N. I., Self-regulated Thermal Processes During Quenching of Steels in Liquid Media, *IJMMP,* Vol. 1, No. 1, 2005, pp. 110−125.

[16] Kobasko, N. I., Optimized Quenched Layer for Receiving Optimal Residual Stress Distribution and Superstrengthened Material, *3rd WSEAS International Conference on Applied and Theoretical Mechanics,* Spain, December 14−16, 2007, pp. 168−174.

[17] Krukovskyi, P., Kobasko, N., and Polubinskyi, A., The Process of Semi-Axles Quenching Is Analyzed as Conjugate Heat Transfer Problem, *WSEAS Transactions on Heat and Mass Transfer,* Vol. 1, No. 4, 2006, pp. 563−566.

[18] Krukovskyi, P., Kobasko, N., and Yurchenko, D., Analysis of Heat Transfer Processes during Intensive Quenching of Cylinder-Shaped Forgings on the Basis of CFD Simulation, *Proceedings of the 2nd IASME/WSEAS International Conference on Continuum Mechanics (CM '07),* Portoroz, Slovenia, May 15−17, 2007, pp. 7−11.

[19] Krukovskyi, P., Kobasko, N., and Yurchenko, D., Generalized Equation for Cooling Time Evaluation and Its Verification by CFD Analysis, *Journal of ASTM International,* Vol. 6, No. 5, 2009.

[20] Banka, J. F., Li, Z., Ferguson, B. L., and Aronov, M., CFD and FEA Used to Improve the Quenching Process, *Heat-treating Progress,* September 2008, pp. 50−56.

[21] Ferguson, B. L., Freborg, A., and Li, Z., Residual Stress and Heat Treatment Process Design for Bending Fatigue Strength Improvement of Carburized Aerospace Gears, *5th International Conference on Heat Treatment: Quenching and Control of Distortion,* 2007, pp. 95−104.

[22] MacKenzie, D. S., Kumar, A., and Metwally, H., Optimizing Agitation and Quench Uniformity Using CFD, *Proceedings of the 23rd ASM Heat Treating Society Conference,* 2005, pp. 271−278.

[23] Methodology STAR-CD, Version 3.15, CD Adapco Group, Computational Dynamics Ltd., London, 2001.

[24] MacKenzie, D. S., Li, Z., and Ferguson, B. L., Effect of Quenchant Flow on the Distortion of Carburized Automotive Pinion Gears, *5th International Conference on Heat Treatment: Quenching and Control of Distortion,* 2007, pp. 119−129.

[25] Nallathambi, A. K., Kaymak, Y., Specht, E., and Bertram, A., Optimum Strategies to Reduce Residual Stresses and Distortion During the Metal Quenching Process, *Journal of ASTM International,* Vol. 6, No. 4, 2009.

[26] Kobasko, N. I., Database for Cooling Capacities of Various Quenchants to Be Developed with the Modern Computational and Experimental Techniques, 2006, www.worldses.org/projects/Heat_and_Mass_Transfer.doc.

5

Generalized Equations for Determination of Cooling Time for Bodies of Any Shape During Quenching

N. I. Kobasko[1]

5.1 INTRODUCTION

The generalized equation for cooling time calculation, based on regular thermal condition theory, was achieved and used in thermal engineering in [1] and is presented in this introduction below. It has been widely used in the heat-treating industry in the countries of the former Soviet Union to develop two-step quenching processes [1]. An analytical equation for cooling time calculation is also needed to develop a method for calculating ideal critical diameter, which is based on accurate CCT (continuous cooling transformation) diagram. The ideal critical diameter is used for optimization of the intensive quenching processes. In the last decade, the generalized equation has been used in the United States to develop recipes for intensive quenching–so-called IQ-3 technology–which explores direct intensive turbulent convection [2].

With the development of computers, it is now possible to solve very complicated problems related to the calculation of cooling time for bodies of any shape, which is very important for the steel quenching process. However, numerical calculations are numerical experiments which do not result in generalized data. For each new problem, it is necessary to perform a new set of calculations, which is time consuming and costly. In this chapter, the generalized equation will be compared to analytical solutions to identify advantages in performing this analysis. The procedure for determining the ideal critical diameter from the generalized equation when used in combination with CCT diagrams will also be discussed. Another objective of this chapter is to illustrate what a regular thermal process means and to establish a correlation between cooling time and the generalized Biot number Bi_v and Kondratjev number Kn.

In this chapter, we will show that the generalized equation for cooling time calculation of any shape of bodies can be also obtained by generalization of analytical solutions, which significantly simplifies calculations. The problem to be solved is, for a steel part of any shape that is cooled uniformly on all sides, to determine the cooling time for the core of the steel part from an initial temperature T_0 to given temperature T which approaches the martensite start temperature M_S. Typically, the austenitizing temperature T_0 is within the range of 800−1,200°C.

For medium-carbon and high-carbon steels, the martensite start temperature M_S is between 100°C and 360°C. This means that the dimensionless temperature ratio:

$$\frac{M_S - T_m}{T_0 - T_m} \leq 0.4,$$

where T_m is the quenchant temperature. Usually a regular thermal process is established when this ratio is equal to 0.8. Thus, during the quenching process, as M_S is approached, a regular condition is observed. On the basis of regular thermal conditions theory, it is possible to obtain an equation for the calculation of cooling time for bodies of any shape (see Chapter 6).

An intensive IQ-3 quenching method has been developed (see Chapters 10 and 12) that is based on very intensive direct convection. The film boiling and transient nucleate boiling (or self-regulated thermal process) in this case are completely prevented. During this process, intensive cooling is interrupted when temperature at the core of a steel part is approximately 300−500°C. To prevent film boiling upon immersion of a steel part into the liquid quenchant, the initial heat flux density should be less than the first critical heat flux density, q_{cr1}.

It is generally assumed that, during immersion quenching of steel that has been heated to 800−1,000°C into cold water, three modes of heat transfer will always occur: film boiling, nucleate boiling, and convection (see Chapter 3). This belief is based on Fourier's law, which predicts an extremely high heat flux density at the very beginning of the quenching process. The modified Fourier law [4] is written as:

$$q = -k\nabla T - \tau_r \frac{\partial q}{\partial t},$$

where t is time. This generates the hyperbolic heat conductivity equation [4−6]:

$$\frac{\partial T}{\partial t} + \tau_r \frac{\partial^2 T}{\partial t^2} = a\nabla^2 T.$$

Furthermore, the speed of heat distribution, according to the parabolic equation, tends to infinity [4]. In fact, the speed of heat distribution W_r is a finite value and, according to [4], can be evaluated as follows:

$$W_r = \sqrt{\frac{\lambda}{c\rho\tau_r}},$$

where τ_r is the time of relaxation (for aluminum, $\tau_r = 10^{-11}$ s).

That is why experimental evaluation of τ_r is a very difficult problem. Since the cooling time from 1,000°C to 300−500°C is being evaluated, which is relatively long compared to the time of relaxation, there is no need to consider the

---

[1] IQ Technologies, Inc., Akron, Ohio, and Intensive Technologies Ltd., Kyiv, Ukraine

hyperbolic heat conductivity equation. It is sufficient to consider the parabolic heat conductivity equation and use average thermal properties of materials and a third kind of boundary condition. For such a condition, the generalized equation for cooling time calculation

$$\tau = \left[\frac{kBi_v}{2.095 + 3.867Bi_v} + \ln\frac{T_0 - T_m}{T - T_m}\right]\frac{K}{aKn}$$

is used, which is true for steel parts of any shape. In this equation:

τ is time (s);

k is 1, 2, or 3 for plate, cylindrical, and spherical steel parts, respectively;

Bi_v is the generalized Biot number;

K is the Kondratjev form factor (m²) (see Chapter 6);

Kn is the dimensionless Kondratjev number (see Chapter 6);

a is the thermal diffusivity of a material (m²/s);

T_0 is the initial temperature before cooling; and

T_m is the quenchant temperature.

Detailed information on the theory of regular conditions will be presented in Chapter 6. In this chapter, the generalized equation will be compared with the well-known existing analytical solutions to illustrate the simplified method of calculation and for preparation for the regular conditions theory in Chapter 6.

5.2 CALCULATION OF COOLING TIME FOR BODIES OF SIMPLE SHAPE

The parabolic heat conductivity equation, in the most general form without sources of heat in the solid body, is:

$$\frac{\partial T}{\partial \tau} = a\nabla^2 T. \tag{1}$$

To understand cooling processes associated with steel quenching, first consider the cooling of simple shapes: plate, cylinder, and sphere. The parabolic heat conductivity equations for the symmetrical problem for these shapes are:

$$\frac{\partial T(r,\tau)}{\partial \tau} = a\left(\frac{\partial^2 T(r,\tau)}{\partial r^2} + \frac{j-1}{r}\frac{\partial T(r,\tau)}{\partial r}\right), \tag{2}$$

where:

$\tau > 0$;

$0 < r < R$;

j is 1, 2, or 3 for a plate, cylinder, or sphere, respectively;

boundary conditions are given by:

$$\frac{\partial T(R,\tau)}{\partial r} + \frac{\alpha}{\lambda}[T(R,\tau) - T_e] = 0; \tag{3}$$

initial conditions are:

$$T(r,0) = T_0; \tag{4}$$

and the condition of symmetry is:

$$\frac{\partial T(0,\tau)}{\partial r} = 0. \tag{5}$$

The heat conductivity equation (Eq 1) is solved by a classical method on the basis of the separation of variables, which is performed first by finding a set of particular solutions T_n that satisfy Eq 1 and the boundary conditions of Eq 3. Then, according to the principle of superposition, a series of these equations is made:

$$T = C_1 T_1 + C_2 T_2 + \ldots + C_n T_n = \sum_{n=1}^{\infty} C_n T_n \tag{6}$$

Factors C_n are obtained from the initial conditions of Eq 4.

A particular solution T is sought in the form of the product of two functions: one, $\theta(\tau)$, that depends on time τ only, and another, $\vartheta(x, y, z)$, that depends on coordinates only, that is:

$$T = C\theta(\tau) \cdot \vartheta(x,y,z), \tag{7}$$

where C is any constant.

Substituting the particular solution Eq 7 into Eq 1 yields:

$$\theta'(\tau) \cdot \vartheta(x,y,z) = a\theta(\tau)\nabla^2\vartheta(x,y,z),$$

which can be presented as:

$$\frac{\theta'(\tau)}{\theta(\tau)} = a\frac{\nabla^2\vartheta(x,y,z)}{\vartheta(x,y,z)}. \tag{8}$$

The left side of Eq 8 can either depend only on τ or be a constant number; it does not depend on coordinates. The right side of Eq 8 can either depend only on coordinates or be a constant number; it does not depend on time. Because this equality must occur for any values of time and coordinates, it is possible only in the case that the right and left parts of Eq 8 are equal to a certain constant D; that is:

$$\frac{\theta'(\tau)}{\theta(\tau)} = D = const; \tag{9}$$

and

$$a\frac{\nabla^2\vartheta(x,y,z)}{\vartheta(x,y,z)} = D = const. \tag{10}$$

After integration of Eq 9, Eq 11 is obtained:

$$\theta(\tau) = e^{D\tau} \tag{11}$$

The constant of integration is not indicated here because it can be attributed to constant C. The constant D is chosen based on physical considerations. For the thermal processes tending to temperature balance, when after a long time ($\tau \to \infty$) a certain distribution of temperature must be established, the value of D cannot be positive; it can only be negative. If D were positive, then after a long time the temperature would be greater than any predefined value, that is, it would tend to infinity, which contradicts the physical essence of the process.

Consider a case, when $D \leq 0$. As value D is not set yet, it is possible to write:

$$D = -ak^2, \tag{12}$$

where:

a is the thermal diffusivity of the material; and

k is a constant determined by the boundary conditions.

Substituting these values for D into Eqs 9–11, we arrive at:

$$\theta(\tau) = e^{-ak^2\tau} \tag{13}$$

and

$$\nabla^2\vartheta(x,y,z) + k^2\vartheta(x,y,z) = 0. \tag{14}$$

Eq 14 is often called a Pokel equation, which is well studied in mathematical physics. Thus, applying a classical Fourier

method of variables separation, the equation of heat conductivity is reduced to an equation of the Pokel type, where the solution is determined by the shape of the body, initial distribution of temperature, and conditions of heat transfer with the quenchant.

Assume that for given conditions, the solution of Eq 14 is known–that is, function $\vartheta(x, y, z)$ has been found. Then a particular solution of the equation of heat conductivity (Eq 1) is:

$$T = Ce^{-ak^2\tau} \cdot \vartheta(x, y, z), \tag{15}$$

This solution (Eq 15) satisfies the differential equation of heat conductivity (Eq 1) for any values of C and k; that is, it is a particular solution. Assigning various values to constants C and k, a set of particular solutions is obtained. By the principle of superposition, the general solution is equal to the sum of the particular solutions, according to Eq 6. Constants k are determined by the boundary conditions (Eq 3), and constant C by the initial conditions (Eq 4).

It has been shown [2] that the general solution for bodies of any shape with the third kind of boundary condition can be written as:

$$\frac{T - T_m}{T_0 - T_m} = \sum_{n=1}^{\infty} A_n U_n \exp(-m_n \tau), \tag{16}$$

where:
A_n are temperature amplitudes;
U_n are eigenfunctions dependent on coordinates; and

$$m_1 < m_2 < m_3 \ldots m_n < m_{n+1} \ldots \tag{17}$$

In view of this series of inequalities (Eq 17), over a short time, the cooling process for a body of any shape will be described by an exponent [2]:

$$\theta = A_1 U_1 e^{-m_1 \tau}.$$

It has been established by Kondratjev [3] that:

$$m_1 = \frac{aKn}{K},$$

or

$$m = \frac{aKn}{K},$$

where:
a is the thermal diffusivity of the material;
K is the Kondratjev form factor; and
Kn is the Kondratjev number.

For many forms, the Kondratjev form factor can be found from analytical solution [3]. For example, for a cylinder, $K = R^2/5.783$, and for a sphere, $K = R^2/9.87$ (R is the radius of the cylinder or sphere; others are shown in Chapter 6).

According to the theory of regular conditions, m can be found for any configuration of a steel part. In contrast to m, the temperature amplitudes A_n and eigenfunctions U_n are available only for simple steel parts. There are no data establishing correlation between A_n and the generalized Biot number Bi_v.

To illustrate the meaning of a regular thermal process, the generalized equation will be compared to an analytical solution and a correlation between A_n and the generalized

Biot number Bi_v will be established for the cooling of simple steel parts.

5.2.1 Cooling a One-Dimensional Slab (Plate)

Assume a one-dimensional slab (unbounded plate) with thickness 2R and initial distribution of temperature $T(x, 0) = f(x)$. At the initial moment of time when the plate is immersed into a quenchant with constant temperature $T_c < T(x, 0)$, the heat transfer between the surfaces of the plate and quenchant can be described by Newton's Law of Cooling. The objective is to determine temperature distribution over the thickness of the plate, and also the heat flux density.

Since for a plate j = 1, Eq 2 and the boundary conditions (Eq 3) have the form:

$$\frac{\partial T(x, \tau)}{\partial \tau} = a \frac{\partial^2 T(x, \tau)}{\partial x^2}, \tag{18}$$

$$\lambda \frac{\partial T(R, \tau)}{\partial x} + \alpha[T(R, \tau) - T_c] = 0, \tag{19}$$

$$-\lambda \frac{\partial T(-R, \tau)}{\partial x} + \alpha[T(-R, \tau) - T_c] = 0, \tag{19a}$$

$$T(x, 0) = f(x),$$

$$\frac{\partial T(0, \tau)}{\partial x} = 0. \tag{20}$$

Using the classical approach, with regard to Eq 20, it is possible to present a particular solution of Eq 18 as:

$$\vartheta(x, \tau) = D \cos kx e^{-k^2 a\tau}. \tag{21}$$

Taking into account solution (Eq 21) and boundary condition (Eq 19), it can be rewritten:

$$\frac{\partial \vartheta(R, \tau)}{\partial x} + H\vartheta(R, \tau) = 0. \tag{22}$$

Boundary condition 19a is not used since there is a condition of symmetry (Eq 20). Substituting Eq 21 in Eq 22, we get:

$$-kD \sin kR \cdot e^{-k^2 a\tau} + HD \cos kR \cdot e^{-k^2 a\tau} = 0,$$

or

$$ctgkR = \frac{k}{H} = \frac{kR}{HR} = \frac{kR}{Bi}. \tag{23}$$

The value of $HR = \frac{\alpha}{\lambda}R$ is a Biot number (criterion). If we denote kR by μ, analysis of Eq 23 shows that μ has an uncountable set of values (see Fig. 1); the first six roots μ_n are presented in Table 1. The general solution is equal to the sum of all particular solutions:

$$\vartheta(x, \tau) = \sum_{n=1}^{\infty} D_n \cos \mu_n \frac{x}{R} \exp(-\mu^2 \frac{a\tau}{R^2}). \tag{24}$$

Constants D_n are determined by the initial conditions of Eq 4. The detailed proof of this operation is given in [1].

Cooling of a slab under boundary conditions of the third kind yields the equation:

$$\theta = \frac{T(x, \tau) - T_m}{T_0 - T_m} = \sum_{n=1}^{\infty} A_n \cos \mu_n \frac{x}{R} \exp(-\mu_n^2 F_0), \tag{25}$$
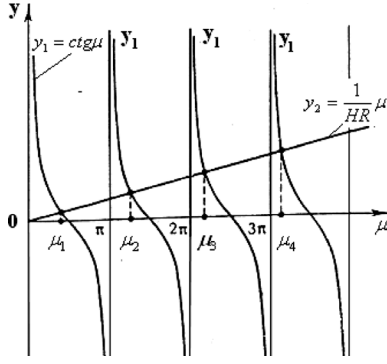
Fig. 1—Graphic method of the determination of roots of the characteristic equation $ctg\mu = \frac{\mu}{Bi}$.

where:

$$A_n = \frac{2 \sin \mu_n}{\mu_n + \sin \mu_n \cdot \cos \mu_n} \qquad (26)$$

and $F_0 = \frac{a\tau}{R^2}$ is a Fourier criterion (number).

Eq 26 can be transformed to the form [1]:

$$A_n = \frac{2 \sin \mu_n}{\mu_n + \sin \mu_n \cdot \cos \mu_n} = (-1)^{n+1} \cdot \frac{2Bi \sqrt{Bi^2 + \mu_n^2}}{\mu_n (Bi^2 + Bi + \mu_n^2)}.$$

The dependence of constants A_n as a function of number Bi is shown in Table 2.

Eq 25 shows that the dimensionless temperature ratio $\theta = \frac{T(x,\tau) - T_m}{T_0 - T_m}$ is a function of number F_0, dimensionless coordinate $\frac{x}{R}$, and criterion Bi; that is:

$$\theta = \psi \left(\frac{x}{R}, Bi, F_0 \right). \qquad (27)$$

Table 1 shows that the roots of the characteristic equation 23 sharply increase, $\mu_1 < \mu_2 < \mu_3 < \ldots < \mu_n < \ldots$. This means that a short time of cooling of a plate can be represented by just the first term of an infinite series (Eq 25):

$$\theta = A_1 \cos \mu_1 \frac{x}{R} \exp(-\mu_1^2 F_{0_1}). \qquad (28)$$

Since the point of interest is a point most remote from a surface, that is, $x = 0$, then $\cos \mu_1 \frac{x}{R} = 1$. Therefore, Eq 28 can be rewritten as:

$$\frac{T(o,\tau) - T_m}{T_0 - T_m} = \frac{A_1}{\exp(m\tau)}; \qquad (29)$$

where $m = \frac{\mu^2 a}{R^2}$. This, in turn, can be rewritten as:

$$\exp(m\tau) = A_1 \frac{T_0 - T_m}{T - T_m}. \qquad (30)$$

Taking the logarithm of the right and left sides of Eq 30, we obtain:

$$m\tau = \ln A_1 + \ln \frac{T_0 - T_m}{T - T_m}. \qquad (31)$$

According to the theory of regular thermal conditions [3,4], the cooling factor m can be represented as:

$$m = \frac{aKn}{K}, \qquad (32)$$

where:
a is the thermal diffusivity of the material;
Kn is the Kondratjev number; and
K is the Kondratjev form factor.

TABLE 1—Roots μ_1 through μ_6 of characteristic equation $ctg\mu = \frac{1}{Bi}\mu$ for an unbounded plate depending on Biot number Bi

Bi	μ_1	μ_2	μ_3	μ_4	μ_5	μ_6
0.01	0.0998	3.1448	6.2848	9.4258	12.5672	15.7086
0.1	0.3111	3.1731	6.2991	9.4354	12.5743	15.7143
1.0	0.8603	3.4256	6.4373	9.5293	12.6453	15.7713
1.5	0.9882	3.5422	6.5097	9.5801	12.6841	15.8026
2.0	1.0769	3.6436	6.5783	9.6296	12.7223	15.8336
4.0	1.2646	3.9352	6.8140	9.8119	12.7966	15.8945
8.0	1.3978	4.2264	7.1263	10.0949	13.1141	16.1675
10	1.4289	4.3058	7.2281	10.2003	13.2142	16.2594
20	1.4961	4.4915	7.4954	10.5117	13.5420	16.5864
30	1.5202	4.5615	7.6057	10.6543	13.7085	16.7691
40	1.5325	4.5979	7.6647	10.7334	13.8048	16.8794
50	1.5400	4.6202	7.7012	10.7832	13.8666	16.9519
100	1.5552	4.6658	7.7764	10.8871	13.9981	17.1093
∞	1.5708	4.7124	7.8540	10.9956	14.1372	17.2788

TABLE 2—Constants A_1 versus Biot number Bi and generalized Biot number Bi_v for an unbounded plate

Bi	Bi_v	A_1	ln A_1
0	0.0000	1.0000	0.0000
0.01	0.0040	1.0020	0.0020
0.1	0.0405	1.0159	0.0158
0.2	0.0811	1.0312	0.0307
0.3	0.1216	1.0450	0.0440
0.4	0.1621	1.0581	0.0565
0.5	0.2026	1.0701	0.0678
0.6	0.2432	1.0813	0.0782
0.7	0.2837	1.0918	0.0878
0.8	0.3242	1.1016	0.0968
0.9	0.3648	1.1107	0.1050
1.0	0.4053	1.1192	0.1126
1.5	0.6080	1.1537	0.1430
2.0	0.8110	1.1784	0.1642
3.0	1.2159	1.2102	0.1908
4.0	1.6212	1.2287	0.2060
5.0	2.0265	1.2403	0.2154
6.0	2.4318	1.2478	0.2214
7.0	2.8371	1.2532	0.2257
8.0	3.2424	1.2569	0.2286
9.0	3.6477	1.2598	0.2310
10	4.0530	1.2612	0.2321
15	6.0800	1.2677	0.2372
20	8.1060	1.2699	0.2389
30	12.159	1.2717	0.2403
40	16.212	1.2723	0.2408
60	24.318	1.2728	0.2412
80	32.424	1.2730	0.2414
100	40.530	1.2731	0.2415
∞	∞	1.2732	0.2415

For an unbounded plate, $K = \dfrac{4R^2}{\pi^2}$. Therefore, cooling time can be represented by the equation:

$$\tau = \left[\ln A_1 + \ln \frac{T_0 - T_m}{T - T_m}\right] \frac{K}{aKn} \qquad (33)$$

However, there is one problem in Eq 33. The value A_1 depends on the number $Bi = \frac{\alpha}{\lambda}R$; however, the value

of Kn is a function of generalized number Bi_v, which is equal to:

$$Bi_v = \frac{\alpha}{\lambda} K \frac{S}{V}, \qquad (34)$$

where:
S is the surface area of a part; and
V is the volume of the part (see Chapter 6).

To eliminate this problem, use the following substitutions [4]:
$Bi_v = 0.405Bi$ for a plate;
$Bi_v = 0.346Bi$ for a cylinder; and
$Bi_v = 0.304Bi$ for a sphere.

Table 2 presents transformation of number Bi into number Bi_v, along with values A_1 and $\ln A_1$ for the mentioned numbers Bi and Bi_v.

Example 5.1

A one-dimensional steel slab is heated to the austenitizing temperature of 860°C. The objective is to calculate the cooling time from 860°C to 360°C at the core of the slab when cooling in a medium with a Biot number Bi of 50. The slab thickness is 20 mm or 0.02 m. For the cooling time calculation, Eq 25 will be used.

Using Table 3 below and Eq 26, the initial values of A_n for a slab at $Bi = 50$ are: $A_1 = 1.2727$; $A_{12} = -0.4227$; $A_3 = 0.2517$; $A_4 = -0.1779$; $A_5 = 0.1365$; and $A_6 = -0.1098$.

The roots of the characteristic equation

$$ctg\mu = \frac{1}{Bi}\mu$$

for the slab are as follows: $\mu_1 = 1.5400$; $\mu_2 = 4.6202$; $\mu_3 = 7.7012$; $\mu_4 = 10.7832$; $\mu_5 = 13.8666$; and $\mu_6 = 16.9519$. The thermal diffusivity of steel within 360−860°C is 5.4×10^{-6} m²/s. The Kondratjev number for the slab is calculated as:

$$K = \frac{L^2}{\pi^2} = 40.527 \times 10^{-6} m^2,$$

where L is the thickness of the slab (0.02 m); $\pi = 3.1415926$. According to the generalized equation presented in the introduction, the cooling time from 860°C to 360°C is equal to 8.59 s where dimensionless temperature ratio $\theta = 0.405$ and $Fo = \frac{4a\tau}{L^2} = 0.464$. Comparison of these results with the analytical solution (Eq 25) gives:

$$\theta = \sum_{n=1}^{6} A_n \exp(-\mu_n^2 Fo) = 0.405 - 6.3 \times 10^{-81} + e^{-512} - e^{-999}$$

$$+ e^{-1652} - e^{-2468}...,$$

where:
e is the base of the natural logarithm (approximately 2.718281828); and
$\lim_{r \to 0} \cos\left(\mu_n \frac{r}{R}\right) = 1$.

The analytical calculation yields the same result as the generalized equation because the second term in the series is very low (6.3×10^{-81}). This means that the generalized equation for cooling of steel parts similar to a slab is true and that the regular thermal condition is already established.

5.2.2 Cooling of a One-Dimensional Cylinder

This calculation example will be for an unbounded cylinder of radius R whose radial temperature distribution is described by a function $f(r)$. At the initial moment of time, the cylinder is

TABLE 3—Roots of characteristic equation $\frac{J_0(\mu)}{J_1(\mu)} = \frac{1}{Bi}\mu$ for a one-dimensional cylinder						
Bi	μ_1	μ_2	μ_3	μ_4	μ_5	μ_6
0.01	0.1412	3.8343	7.0170	10.1745	13.3244	16.4712
0.1	0.4417	3.8577	7.0298	10.1833	13.3312	16.4767
1.0	1.2558	4.0795	7.1558	10.2710	13.3984	16.5312
1.5	1.4569	4.1902	7.2233	10.3188	13.4353	16.5612
2.0	1.5994	4.2910	7.2884	10.3658	13.4719	16.5910
4.0	1.9081	4.6018	7.5201	10.5423	13.6125	16.7073
8.0	2.1286	4.9384	7.8464	10.8271	13.8566	16.9179
10	2.1795	5.0332	7.9569	10.9363	13.9580	17.0099
20	2.2880	5.2568	8.2534	11.2677	14.2983	17.3442
30	2.3261	5.3410	8.3771	11.4221	14.4748	17.5348
40	2.3455	5.3846	8.4432	11.5081	14.5774	17.6508
50	2.3572	5.4112	8.4840	11.5621	14.6433	17.7272
60	2.3651	5.4291	8.5116	11.5990	14.6889	17.7807
80	2.3750	5.4516	8.5466	11.6461	14.7475	17.8502
100	2.3809	5.4652	8.5678	11.6747	14.7834	17.8931
∞	2.4048	5.5201	8.6537	11.7915	14.9309	18.0711

immersed into a quenchant with constant temperature $T_m < T_0$. The objective is to determine the heat flux density and temperature distribution in the cylinder for any time. The differential equation of heat conductivity for an unbounded cylinder in this case is:

$$\frac{\partial T(r,\tau)}{\partial \tau} = a\left(\frac{\partial^2 T(r,\tau)}{\partial r^2} + \frac{1}{r}\frac{\partial T(r,\tau)}{\partial r}\right), \qquad (35)$$

where:
$\tau > 0$; and
$0 < r < R$,
with the following boundary conditions:

$$\frac{\partial T(R,\tau)}{\partial r} + H[T(R,\tau) - T_m] = 0; \qquad (36)$$

$$\vartheta(r,0) = f(r) - T_m = \vartheta_0; \qquad (37)$$

and

$$\frac{\partial \vartheta(0,\tau)}{\partial r} = 0. \qquad (38)$$

As shown above, a particular solution of the equation of heat conductivity by the method of variables separation is:

$$T = Ce^{-ak^2\tau} \cdot \vartheta(x,y,z). \qquad (39)$$

Substituting the particular solution (Eq 39) into differential equation 35, it can be concluded that the function $\vartheta(r)$ must be the solution of a Bessel equation:

$$\vartheta''(r) + \frac{1}{r}\vartheta'(r) + k^2\vartheta(r) = 0. \qquad (40)$$

The general integral of Eq 40 is:

$$\vartheta(r) = CJ_0(kr) + DY_0(kr), \qquad (41)$$

where $J_0(kr)$ and $Y_0(kr)$ are Bessel functions of the first and second kind of the zero order. Since the temperature on the axis of the cylinder ($r = 0$) must be finite, the solution (Eq 41) cannot contain a Bessel function of the second kind which tends to infinity at $r \to 0$ (see Fig. 2). Since the temperature at the center of the cylinder is finite, the physical conditions of the problem require that the constant D must be equal to zero
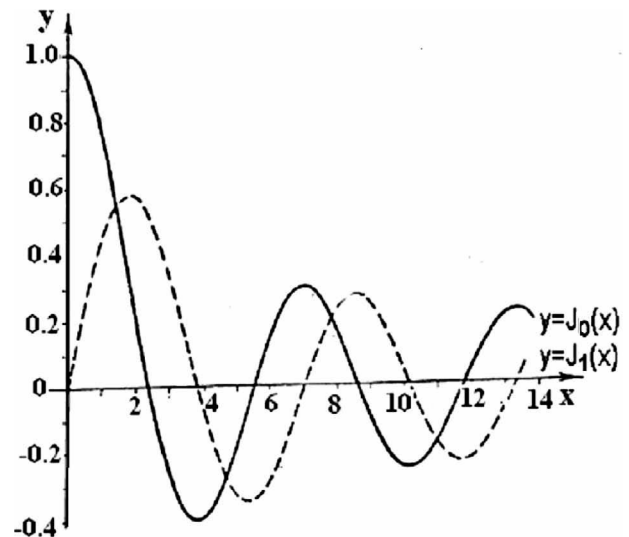
Fig. 2—Charts of Bessel function of the first kind: $J_0(x)$ and $J_1(x)$.

($D = 0$). Then a particular solution of the equation of heat conductivity (Eq 35) has the following form:

$$T = CJ_0(kr)e^{-ak^2\tau}. \qquad (42)$$

Making the particular solution (Eq 42) to satisfy boundary condition 36, we get:

$$\frac{J_0(kR)}{J_1(kR)} = \frac{kR}{HR} = \frac{kR}{Bi}. \qquad (43)$$

In the transcendental equation 43, a new function $J_1(kR)$ was obtained, which should be understood as follows. A Bessel function can be represented as the series:

$$J_0(x) = 1 - \frac{x^2}{2^2} + \frac{x^4}{2^2 \cdot 4^2} - \frac{x^6}{2^2 \cdot 4^2 \cdot 6^2} + \frac{x^8}{2^2 \cdot 4^2 \cdot 6^2 \cdot 8^2} - \cdots$$

This function is called a Bessel function of the first kind of the zero order. Therefore, analogously, if $x = kr$, then the Bessel function is:

$$J_0(kr) = 1 - \frac{(kr)^2}{2^2} + \frac{(kr)^4}{2^2 \cdot 4^2} - \frac{(kr)^6}{2^2 \cdot 4^2 \cdot 6^2} + \frac{(kr)^8}{2^2 \cdot 4^2 \cdot 6^2 \cdot 8^2} - \cdots$$

Differentiating Bessel function $J_0(kr)$ with respect to r gives:

$$J_0'(kr) = -k\left[\frac{kr}{2} - \frac{(kr)^3}{2^2 \cdot 4^2} + \frac{(kr)^5}{2^2 \cdot 4^2 \cdot 6^2} - \cdots\right] = -kJ_1(kr),$$

where:

$$J_1(kr) = \frac{kr}{2} - \frac{(kr)^3}{2^2 \cdot 4^2} + \frac{(kr)^5}{2^2 \cdot 4^2 \cdot 6^2} - \cdots.$$

From the analysis of this series, it follows that, at $r = 0$, $J_0(kr) = 1$ and $J_1(kr) = 0$, which is often used for the calculations.

Plots of the Bessel function versus variable r are presented in Figs. 2 and 3.

If we denote kR by $\mu(\mu = kR)$, then roots μ_n are determined by the transcendental equation:

$$\frac{J_0}{J_1} = \frac{1}{Bi}\mu. \qquad (44)$$

The first six roots of the characteristic equation 44 are presented in Table 3. Constants C_n are determined by boundary condition Eq 37 and described in detail in [1].
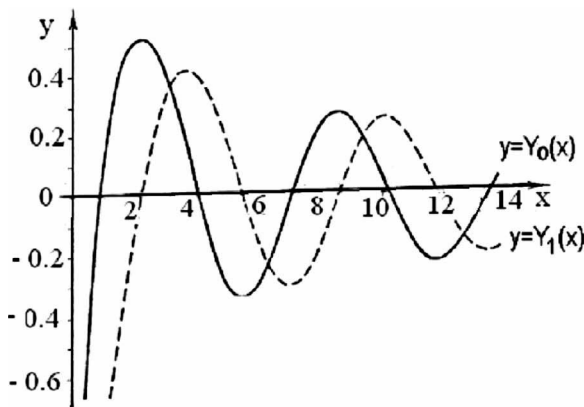
Fig. 3—Charts of Bessel function of the second kind: $Y_0(x)$ and $Y_1(x)$.

Finally, the general solution of the differential equation 35 at the boundary conditions given by Eqs 36–38 is equal to the sum of all particular solutions [1]:

$$\theta = \frac{T(r,\tau) - T_m}{T_0 - T_m} = \sum_{n=1}^{\infty} A_n J_0\left(\mu\frac{r}{R}\right)\exp(-\mu_n^2 F_0), \qquad (45)$$

where A_n are constant factors (so-called initial temperature amplitudes) that are dependent on the Biot number (criterion) (Bi) and are given by:

$$A_n = \frac{2J_1(\mu_n)}{\mu_n[J_0^2(\mu_n) + J_1^2(\mu_n)]}.$$

Since the points most remote from a surface (i.e., $r = 0$) are of interest, then: $\lim\limits_{r \to 0} J_0\left(\mu_n\frac{r}{R}\right) = 1$ (see the expansion of a Bessel function in series).

Due to sharp increase of n roots μ_n (see Table 3) in quite short time, the process of cooling a core of the cylinder will be described by the formula:

$$\theta = A_1 \exp\left(-\mu_1^2\frac{a\tau}{R^2}\right). \qquad (46)$$

Taking the logarithm of the right and left sides of Eq 46 and making the transformation of $A(Bi)$ into $A(Bi_v)$, and also using the theory of regular thermal conditions, a relatively simple equation for the determination of cooling time of cylinder-shaped bodies is:

$$\tau = \left[\ln A_1 + \ln\frac{T_0 - T_m}{T - T_m}\right]\frac{K}{aKn}, \qquad (47)$$

which is similar to Eq 33. In this case:

$$K = \frac{R^2}{\mu_1^2} = \frac{R^2}{5.783}.$$

Dependence of A_1 on number Bi and the generalized number Bi_v is presented in Table 4.

Example 5.2

A one-dimensional cylinder is heated to the austenitizing temperature of 860°C. The objective is to calculate the cooling time from 860°C to 360°C for the core of the cylinder. The cylinder is cooled under conditions of $Bi = 50$. The diameter of the cylinder is 20 mm or 0.02 m. For the cooling time calculation, Eq 45 will be used. The temperature amplitudes for a cylinder at $Bi = 50$ are: $A_1 = 1.5995$; $A_2 = -1.0587$; $A_3 = 0.8396$; $A_4 = -0.7112$; $A_5 = 0.6227$; and $A_6 = -0.5544$.

The roots of the characteristic equation

$$\frac{J_0(\mu)}{J_1(\mu)} = \frac{1}{Bi}\mu$$

for a cylinder are: $\mu_1 = 2.3572$; $\mu_2 = 5.4112$; $\mu_3 = 8.4840$; $\mu_4 = 11.5621$; $\mu_5 = 14.6433$; and $\mu_6 = 17.7272$. The thermal diffusivity of steel within the temperature range of 360–860°C is 5.4×10^{-6} m²/s. The Kondratjev number for the cylinder is calculated as:

$$K = \frac{R^2}{5.783} = 17.292 \times 10^{-6} m^2,$$

where R is radius of the cylinder (0.01 m). According to the generalized equation presented in the introduction, the cooling time from 860°C to 360°C is 4.585 s, where the dimensionless temperature ratio $\theta = 0.405$ and $Fo = \frac{a\tau}{R^2} = 0.2375$.

TABLE 4—Constant A_1 versus Bi and Bi_v for an unbounded cylinder

Bi	Bi_v	A_1	$\ln A_1$
0	0.0000	1.0000	0.0000
0.01	0.0035	1.0031	0.0031
0.1	0.0346	1.0245	0.0242
0.2	0.0692	1.0482	0.0471
0.3	0.1037	1.0711	0.0687
0.4	0.1383	1.0931	0.0890
0.5	0.1729	1.1142	0.1081
0.6	0.2075	1.1345	0.1262
0.7	0.2421	1.1539	0.1431
0.8	0.2766	1.1724	0.1591
0.9	0.3112	1.1902	0.1741
1.0	0.3458	1.2071	0.1882
1.5	0.5187	1.2807	0.2474
2.0	0.6916	1.3377	0.2910
3.0	1.0374	1.4192	0.3501
4.0	1.3832	1.4698	0.3851
5.0	1.7290	1.5029	0.4074
6.0	2.0748	1.5253	0.4222
7.0	2.4206	1.5409	0.4324
8.0	2.8640	1.5523	0.4397
9.0	3.1122	1.5611	0.4454
10	3.4580	1.5677	0.4496
15	5.1870	1.5853	0.4608
20	6.9160	1.5918	0.4649
30	10.374	1.5964	0.4678
40	13.832	1.5988	0.4693
60	20.748	1.6009	0.4706
80	27.664	1.6012	0.4708
100	34.580	1.6014	0.4709
∞	∞	1.6021	0.4713

Comparing these results with the analytical solution of Eq 45:

$$\theta = \sum_{n=1}^{6} A_n \exp(-\mu_n^2 Fo) = 0.4044 - 1.01 \times 10^{-3} + 3.16 \times 10^{-8}$$
$$- 1.156 \times 10^{-14} + ...,$$

where $\lim_{r \to 0} J_0\left(\mu_n \frac{r}{R}\right) = 1$.

In this case, the analytical calculation yields almost the same result as the generalized equation, because the second term in

the series is sufficiently low (0.00101). This means that the generalized equation for cooling time calculation coincides with the results of analytical calculations with an accuracy of 0.4 %.

5.2.3 Cooling a Sphere
Consider a spherical body (ball) of radius R with a known initial distribution of temperature $f(r)$. In this specific case, the temperature can be identical and equal to T_0. At the initial moment of time, the ball is immersed into a quenchant at constant temperature of T_m ($T_m < T_0$). Find the temperature distribution inside the ball for any time.

The differential equation of heat conductivity for the symmetric problem has the form:

$$\frac{\partial T(r,\tau)}{\partial \tau} = a\left(\frac{\partial^2 T(r,\tau)}{\partial r^2} + \frac{2}{R}\frac{\partial T(r,\tau)}{\partial r}\right) \qquad (48)$$

at the following boundary conditions:

$$\lambda \frac{\partial T(r,\tau)}{\partial \tau} + H(T(R,\tau) - T_m) = 0 \qquad (49)$$

$$T(r,0) = f(r) + T_0 \qquad (50)$$

$$\frac{\partial T(0,\tau)}{\partial r} = 0 \qquad (51)$$

The general solution of the above-stated problem is [1]:

$$\theta = \sum_{n=1}^{\infty} A_n \frac{R \sin \mu_n \frac{r}{R}}{r \mu_n} \exp(-\mu_n^2 F_0), \qquad (52)$$

where:

$$A_n = \frac{2(\sin \mu_n - \mu_n \cos \mu_n)}{\mu_n - \sin \mu_n \cos \mu_n}.$$

At the point which is the most remote from the surface (the origin):

$$\frac{R \sin \mu_n \frac{r}{R}}{r \mu_n} = 1, \text{ as } \lim_{r \to 0} \frac{\sin(\mu_n \frac{r}{R})}{(\mu_n \frac{r}{R})} = 1.$$

Roots μ_n of the characteristic equation $tg\mu = -\frac{1}{Bi-1}\mu$ are presented in Table 5. Constants A_1 versus numbers Bi and Bi_v are presented in Table 6.

Using the theory of regular thermal conditions, as for an unbounded plate or cylinder, a simple equation for the calculation of cooling time for the core of the sphere can be obtained:

$$\tau = \left[\ln A_1 + \ln \frac{T_0 - T_m}{T - T_m}\right] \frac{K}{aKn}, \qquad (53)$$

where the Kondratjev form factor K for a sphere is $K = \frac{R^2}{\pi^2}$.

Example 5.3
A one-dimensional sphere is heated to the austenitizing temperature of 860°C. Calculate the cooling time from 860°C to 360°C for the core of the sphere. The sphere is cooled under conditions of $Bi = 50$. The diameter of the sphere is 20 mm or 0.02 m. To determine the cooling time, use Eq 45. The temperature amplitudes for a sphere at $Bi = 50$ are: $A_1 = 1.9964$; $A_2 = -1.9856$; $A_3 = 1.9680$; $A_4 = -1.9441$; $A_5 = 1.9145$; and $A_6 = -1.8802$.

The roots of the characteristic equation

$$tg\mu = -\frac{1}{Bi-1}\mu$$

for a sphere are: $\mu_1 = 3.0801$; $\mu_2 = 6.1606$; $\mu_3 = 9.2420$; $\mu_4 = 12.3247$; $\mu_5 = 15.4090$; and $\mu_6 = 18.4953$. The thermal

TABLE 5—Roots of the characteristic equation $tg\mu = -\frac{1}{Bi-1}\mu$ for spherical-shaped bodies						
Bi	μ_1	μ_2	μ_3	μ_4	μ_5	μ_6
0.01	0.1730	4.4956	7.7265	10.905	14.0669	17.2813
0.1	0.5423	4.5157	7.7382	10.9133	14.0733	17.2266
1.0	1.5708	4.7124	7.8540	10.9956	14.1372	17.2788
1.5	1.8366	4.8158	7.9171	11.0409	14.1724	17.3076
2.0	2.0288	4.9132	7.9787	11.0856	14.2075	17.3364
4.0	2.4557	5.2329	8.2045	11.2560	14.3434	17.449
8.0	2.7654	5.6078	8.5406	11.5408	14.5847	17.6567
10	2.8363	5.7172	8.6587	11.6532	14.6870	17.7481
20	2.9930	5.9921	9.0019	12.025	15.0625	18.1136
30	3.0406	6.0831	9.1294	12.1807	15.238	18.3058
50	3.0801	6.1606	9.2420	12.3247	15.409	18.4953
100	3.1105	6.2211	9.3317	12.4426	15.5537	18.665
∞	3.1416	6.2832	9.4248	12.5664	15.7080	18.8496

diffusivity of steel within the temperature range of 360–860°C is 5.4×10^{-6} m²/s. The Kondratjev number for a sphere with radius $R = 0.01$ m is calculated as:

$$K = \frac{R^2}{\pi^2} = 10.1317 \times 10^{-6} m^2.$$

According to the generalized equation presented in the introduction, the cooling time from 860°C to 360°C for a sphere is 3.139 s, where the dimensionless temperature ratio $\theta = 0.405$ and $Fo = \frac{a\tau}{R^2} = 0.169$.

Comparing these results with the analytical solution (Eq 52):

$$\theta = \sum_{n=1}^{6} A_n \exp(-\mu_n^2 Fo) = 0.4017 - 0.00325 + 1.58 \times 10^{-37}$$
$$- 2.09 \times 10^{-66}...,$$

where $\lim_{r \to 0} \frac{\sin(\mu_n \frac{r}{R})}{(\mu_n \frac{r}{R})} = 1$.

The analytical calculation shows almost the same result as the generalized equation because the second term in the series is only 0.00325. This means that the generalized equation for cooling time calculation coincides with the results of the analytical calculation with an accuracy of 1.6 %.

5.2.4 Cooling a Three-Dimensional Slab (Parallelepiped)

In this example, a plate of dimensions $2R_1 \times 2R_2 \times 2R_3$ is heated until the temperature everywhere is equal to T_0. At the initial moment of time, the plate is immersed into a quenchant at a constant temperature T_m ($T_m < T_0$). Find the temperature distribution at any time. Place the origin of coordinates at the center of a parallelepiped (see Fig. 4).

The problem is mathematically stated as:

$$\frac{\partial T(x,y,z,\tau)}{\partial \tau} = a\left[\frac{\partial^2 T(x,y,z,\tau)}{\partial x^2} + \frac{\partial^2 T(x,y,z,\tau)}{\partial y^2} + \frac{\partial^2 T(x,y,z,\tau)}{\partial z^2}\right],$$
$$(54)$$

where:
$\tau > 0$;
$-R_1 < x < +R_1$;
$-R_2 < y < +R_2$; and
$-R_3 < z < +R_3$.

In addition,

$$\left. \begin{array}{l} \pm\dfrac{\partial T}{\partial x} + \dfrac{\alpha}{\lambda}(T - T_m) = 0 \\[2mm] \pm\dfrac{\partial T}{\partial y} + \dfrac{\alpha}{\lambda}(T - T_m) = 0 \\[2mm] \pm\dfrac{\partial T}{\partial z} + \dfrac{\alpha}{\lambda}(T - T_m) = 0 \end{array} \right\} \qquad (55)$$

and

$$T(x,y,z,0) = T_0. \qquad (56)$$

The temperature distribution is symmetric with respect to the center of the bounded plate. It has been shown [1] that the solution of this problem can be represented as a product of solutions for three unbounded plates with crossing forms in the given parallelepiped:

$$\frac{T(x,y,z,\tau) - T_m}{T_0 - T_m} = \frac{T(x,\tau) - T_m}{T_0 - T_m} \cdot \frac{T(y,\tau) - T_m}{T_0 - T_m} \cdot \frac{T(z,\tau) - T_m}{T_0 - T_m}$$
$$(57)$$

The solution to this problem is:

$$\theta = \sum_{n=1}^{\infty}\sum_{m=1}^{\infty}\sum_{k}^{\infty} A_{n,1}A_{m,2}A_{k,3} \; \cos\mu_{n,1}\frac{x}{R_1} \cdot \cos\mu_{m,2} \cdot \frac{y}{R_2}\cos\mu_{k,3}$$
$$\times \exp\left[-\left(\frac{\mu_{n,1}^2}{R_1^2} + \frac{\mu_{m,2}^2}{R_2^2} + \frac{\mu_{k,3}^2}{R_3^2}\right)a\tau\right], \qquad (58)$$

where:
$$A = (-1)^{(n,m,k)+1}\frac{2Bi\sqrt{Bi^2 + \mu^2}}{\mu(Bi^2 + Bi + \mu^2)};$$

TABLE 6—Constant A_1 versus Bi and Bi_v for a sphere

Bi	Bi_v	A_1	ln A_1
0	0.0000	1.0000	0.0000
0.01	0.0030	1.0035	0.0035
0.1	0.0304	1.0297	0.0293
0.2	0.0608	1.0592	0.0575
0.3	0.0912	1.0880	0.0843
0.4	0.1216	1.1164	0.1101
0.5	0.1520	1.1440	0.1345
0.6	0.1824	1.1718	0.1581
0.7	0.2128	1.1978	0.1805
0.8	0.2432	1.2237	0.2019
0.9	0.2736	1.2488	0.2222
1.0	0.3040	1.2732	0.2415
1.5	0.4560	1.3848	0.3256
2.0	0.6080	1.4793	0.3916
2.5	0.7600	1.5579	0.4433
3.0	0.9120	1.6223	0.4838
4.0	1.2160	1.7201	0.5424
5.0	1.5200	1.7870	0.5805
6.0	1.8240	1.8338	0.6064
7.0	2.1280	1.8673	0.6245
8.0	2.4320	1.8920	0.6376
9.0	2.7360	1.9106	0.6474
10	3.0400	1.9249	0.6549
11	3.3440	1.9364	0.6608
14	4.8640	1.9663	0.6762
16	6.3840	1.9801	0.6831
20	9.4240	1.9905	0.6884
30	12.464	1.9948	0.6905
40	15.504	1.9964	0.6913
50	18.544	1.9974	0.6918
80	24.624	1.9985	0.6924
100	30.704	1.9993	0.6928
∞	∞	2.0000	0.6931

$$ctg\,\mu = \frac{1}{Bi}\mu; \text{ and}$$

$$Bi_i = \frac{\alpha}{\lambda}R_i (i = 1, 2, 3).$$

Consider three cases of cooling of the plate:
1. R_1 and $R_3 \to \infty$: an unbounded plate
2. $R_1 = R_2$, and $R_3 \to \infty$: a long square bar, related to the class of cylindrical bodies
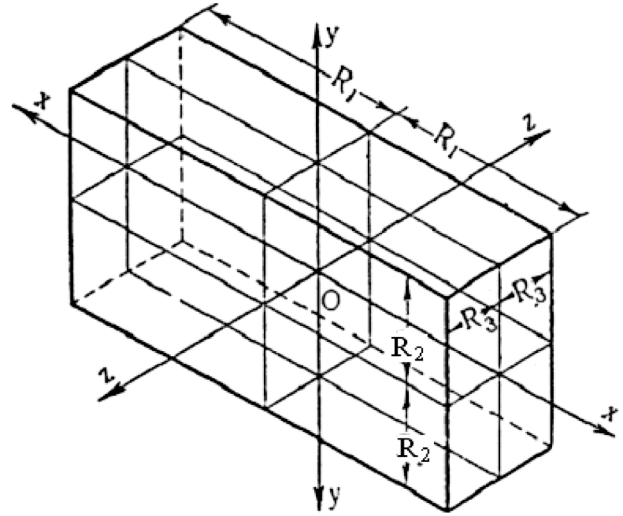
Fig. 4—Parallelepiped (a three-dimensional slab).

3. $R_1 = R_2 = R_3$: a cube, related to spherical bodies

The temperature distribution in an unbounded plate was discussed above (see Eq 25). In this section, the analysis of the solution in Eq 58 with respect to a square bar and cube (cases 2 and 3) will be addressed.

At the origin, all the cosines are equal to 1, and roots $\mu_1 < \mu_2 < \mu_3 < \ldots < \mu_n$ in a short time are:

$$\theta = A_{n,1}A_{m,2}A_{k,3}\exp(-m\tau), \tag{59}$$

where m is a cooling factor, according to the theory of regular thermal conditions.

The conclusion for an unbounded bar (case 2) is:

$$\theta = A_1^2 \exp(-m\tau), \tag{60}$$

and for a cube (case 3):

$$\theta = A_1^3 \exp(-m\tau), \tag{61}$$

where A_1 is the thermal amplitude for an unbounded plate (a constant, see Table 2).

This equivalency of more complex bodies with an unbounded plate is obtained by taking the logarithm of Eqs 59–61 to obtain a simple equation for the determination of cooling time for bodies of various configurations:

$$\tau = \left[k \ln A_1 + \ln \frac{T_0 - T_m}{T - T_m}\right]\frac{K}{aKn}, \tag{62}$$

where:
$k = 1, 2, $ or 3 for an unbounded plate, a square infinite bar, or a cube, respectively; and
K is the Kondratjev form coefficient for a bounded plate [2] with sides $L_1 (= 2R_1)$, $L_2 (= 2R_2)$, and $L_3 (= 2R_3)$, which can be determined from:

$$K = \frac{1}{\pi^2\left[\left(\frac{1}{2R_1}\right)^2 + \left(\frac{1}{2R_2}\right)^2 + \left(\frac{1}{2R_3}\right)^2\right]} = \frac{1}{\pi^2\left[\frac{1}{L_1^2} + \frac{1}{L_2^2} + \frac{1}{L_3^2}\right]}. \tag{63}$$

In Eq 62, in the square brackets, one of the most unexplored terms is the value of $\ln A_1$ and its dependency on Bi and Bi_v. As for the Kondratjev number Kn, there is a

TABLE 7—Constant A_1 versus Bi and Bi_v for an infinite square parallelepiped

Bi	Bi_v	A_1	$\ln A_1$
0	0.0000	1.0000	0.0000
0.01	0.0040	1.0040	0.0040
0.1	0.0405	1.0320	0.0315
0.2	0.0810	1.0630	0.0615
0.3	0.1216	1.0920	0.0880
0.4	0.1621	1.1196	0.1129
0.5	0.2026	1.1451	0.1355
0.6	0.2432	1.1692	0.1563
0.8	0.3242	1.2135	0.1935
1.0	0.4053	1.2526	0.2252
2.0	0.8106	1.3886	0.3283
3.0	1.2159	1.4646	0.3816
4.0	1.6212	1.5097	0.4119
5.0	2.0265	1.5383	0.4307
6.0	2.4318	1.5570	0.4428
7.0	2.8371	1.5705	0.4514
8.0	3.2424	1.5798	0.4573
9.0	3.6477	1.5871	0.4619
10	4.0530	1.5906	0.4641
20	8.1060	1.6126	0.4779
30	12.1590	1.6172	0.4807
40	16.2120	1.6187	0.4816
60	24.3180	1.6200	0.4824
80	32.4240	1.6205	0.4827
100	40.5300	1.6208	0.4829
∞	∞	1.6210	0.4830

TABLE 8—Constant A_1 versus Bi and Bi_v for a cube

Bi	Bi_v	A_1	$\ln A_1$
0	0.0000	1.0000	0.0000
0.01	0.0040	1.0060	0.0060
0.1	0.0405	1.0485	0.0473
0.2	0.0811	1.0966	0.0922
0.3	0.1216	1.1412	0.1321
0.4	0.1621	1.1846	0.1694
0.5	0.2027	1.2254	0.2033
0.6	0.2432	1.2643	0.2345
0.7	0.2837	1.3015	0.2635
0.8	0.3242	1.3368	0.2903
0.9	0.3648	1.3702	0.3150
1.0	0.4053	1.4019	0.3378
1.5	0.6080	1.5356	0.4289
2.0	0.8106	1.6364	0.4925
3.0	1.2159	1.7724	0.5724
4.0	1.6212	1.8550	0.6179
5.0	2.0265	1.9081	0.6461
6.0	2.4318	1.9428	0.6641
7.0	2.8371	1.9682	0.6771
8.0	3.2424	1.9856	0.6859
9.0	3.6477	1.9994	0.6929
10	4.0530	2.0060	0.6962
20	8.1060	2.0479	0.7168
30	12.159	2.0566	0.7210
40	16.212	2.0595	0.7225
60	24.318	2.0620	0.7236
80	32.424	2.0629	0.7241
100	40.530	2.0634	0.7243
∞	∞	2.0639	0.7246

universal relationship between numbers Kn and Bi_v for bodies of any shape [1,2]:

$$Kn = \frac{Bi_V}{\left(Bi_V^2 + 1.437 Bi_V + 1\right)^{0.5}} \qquad (64)$$

The Kondratjev form coefficient K can be calculated for a body of any shape as well, which will be discussed in Chapter 6. Therefore, Eq 62 can also become universal if regularities of behavior of $\ln A_1$ are dependent on Bi_v numbers for any body. At this point, a strategic approach to determine the parameter $\ln A_1$ for bodies of any shape will be developed.

Kondratjev [3] has shown that the problem of heating (or cooling) of a body of a complex shape can be reduced to a problem of heating (or cooling) of a body of a simple shape (a plate, cylinder, or ball) by introduction of the criterion of the approximate similarity. Using this approach, it is possible to classify bodies of any shape into three groups of plate-shaped, cylindrical, and spherical bodies. Plate-shaped bodies can be plates of any kind where the width and length are much greater than the thickness. Cylindrical bodies can be any parallelepipeds where $R_3 \gg R_1$ and R_2, and $R_1 \approx R_2$. Spherical bodies can be a cube or finite cylinder with height approximately equal to its diameter, that is, $Z \approx D$.

5.2.5 Finite Cylinder

For the analysis of $\ln A_1$ for a finite cylinder (Fig. 5), consider the analytical solution describing the distribution of temperature fields in the finite cylinder:

$$\theta = \sum_{n=1}^{\infty}\sum_{m=1}^{\infty} A_{n,1} A_{m,2} J_0\left(\mu_{n,1}\frac{r}{R}\right)\cos\mu_{m,2}\frac{Z}{\ell} \times \exp\left[-\left(\frac{\mu_{n,1}^2}{R^2}+\frac{\mu_{m,2}^2}{\ell^2}\right)a\tau\right],$$

$$(65)$$
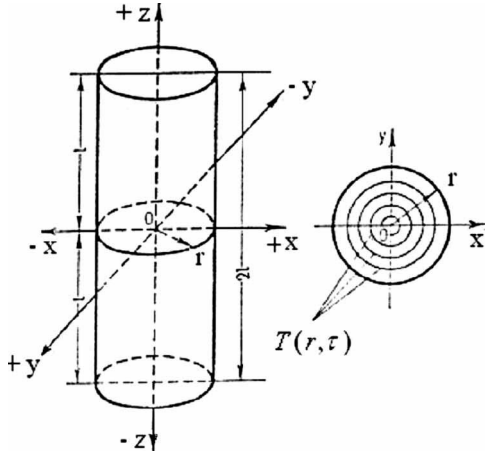
Fig. 5—Schematic of a finite cylinder.

where $A_{n,1}$ and $A_{m,1}$ are constant factors determined by the equations:

$$A_{n,1} = \frac{2Bi_1}{J_0(\mu_{n,1})[\mu_{n,1}^2 + Bi_1^2]}$$

and

$$A_{m,2} = (-1)^{m+1} \frac{2Bi_2\sqrt{Bi_2^2 + \mu_{m,2}^2}}{\mu_{m,2}(Bi_2^2 + Bi_2 + \mu_{m,2}^2)}.$$

At the center of a finite cylinder, the Bessel functions $J_0\left(\mu_{n,1}\frac{r}{R}\right)$ and $\cos\mu_{m,2}\frac{Z}{\ell}$ are equal to 1. The series of Eq 65 quickly converges, because the roots of the characteristic equations sharply increase. Therefore, Eq 65 at the stage of regular thermal conditions is transformed into a simple equation:

$$\theta = A_{1,1} \cdot A_{1,2} \exp(-m\tau). \qquad (66)$$

Taking the logarithm of Eq 66, we get:

$$\tau = \left[\ln A + \ln\frac{T_0 - T_m}{T - T_m}\right]\frac{K}{aKn}, \qquad (67)$$

where:

$$K = \frac{1}{\dfrac{5,783}{R^2} + \dfrac{9.87}{Z^2}}; \text{ and }$$

$A = A_{1,1} \cdot A_{1,2}$.

Values of A_1 versus numbers Bi and Bi_v are presented in Table 9.

Since there are sufficient computational data for the analysis of constants $\ln A$, which are dependent only on numbers Bi and Bi_v, their generalization is obtained by dividing complex bodies into three groups: plate-shaped, cylindrical, and spherical bodies. A plot of the relationship $\Omega(Bi_v) = \ln A(Bi_v)$ is obtained for these three groups using Tables 2, 4, and 6–9. The graphic representation of these relationships is presented in Fig. 6. A universal correlation between the Kondratjev number Kn and the generalized Biot number Bi_v is satisfied by Eq 64, and some numerical data are presented in Table 10.

Fig. 6 shows that the curves related to each group of bodies coincide very well among themselves. For a cube, ball, and finite cylinder, the average value differs from the bottom and top values by just 30 %, which suggests that there is an opportunity to generalize all of the calculation

TABLE 9—Constant A_1 versus Bi and Bi_v for a bounded cylinder (D = Z)

Bi	Bi_v	A_1	ln A_1
0	0.0000	1.0000	0.0000
0.01	0.0036	1.0211	0.0210
0.1	0.364	1.0408	0.0400
0.2	0.0727	1.0809	0.0780
0.3	0.1091	1.1193	0.1127
0.4	0.1454	1.1566	0.1455
0.5	0.1818	1.1923	0.1759
0.6	0.2182	1.2267	0.2044
0.7	0.2545	1.2598	0.2310
0.8	0.2909	1.2915	0.2558
0.9	0.3272	1.3219	0.2791
1.0	0.3636	1.3510	0.3008
1.5	0.5454	1.4775	0.3904
2.0	0.7272	1.5763	0.4551
3.0	1.0908	1.7175	0.5409
4.0	1.4544	1.8059	0.5911
5.0	1.8180	1.8640	0.6227
6.0	2.1816	1.9032	0.6435
7.0	2.5452	1.9310	0.6581
8.0	2.9088	1.9547	0.6703
9.0	3.2724	1.9667	0.6763
10	3.6360	1.9772	0.6817
15	5.4540	2.0097	0.6980
20	7.2720	2.0214	0.7038
30	10.908	2.0301	0.7081
40	14.544	2.0341	0.7100
60	21.816	2.0376	0.7118
80	29.088	2.0383	0.7121
100	36.360	2.0387	0.7123
∞	∞	2.0398	0.7128

data. In [4], a generalized dependence for the value of Ω was found, which is:

$$\Omega = \frac{kBi_V}{2.095 + 3.867Bi_v}. \qquad (68)$$

Considering this dependence, a generalized equation for the calculation of cooling time for bodies of any configuration can be obtained:

$$\tau = \left[\frac{kBi_v}{2.095 + 3.867Bi_v} + \ln\frac{T_0 - T_m}{T - T_m}\right]\frac{K}{aKn}. \qquad (69)$$
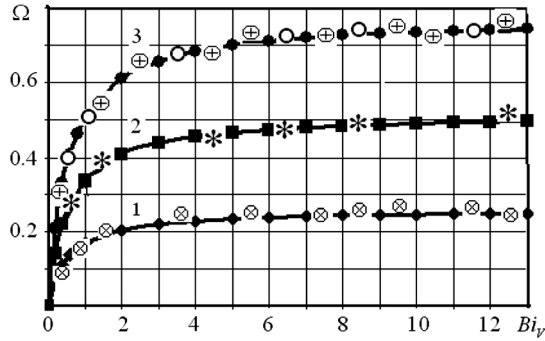
Fig. 6—Ω versus generalized Biot number for: 1, plate-shaped forms; 2, cylindrical forms; 3, spherical forms.

This equation in dimensionless form is:

$$Fo \cdot Kn = \frac{kBi_v}{2.095 + 3.867Bi_v} + \ln\theta_0. \qquad (70)$$

5.3 RESULTS OF CFD MODELING AND COMPARISON WITH THE GENERALIZED EQUATION

It should be emphasized that CFD modeling is required, since steel parts are quenched in a water flow where

Fig. 7—Temperature versus time at the surface (points 1–7) and at the core (point 8) of the cylindrical forging when quenched in water flow in the fixture: a, forging; b, temperature distributions.

empirical Nu = f(Re, Pr) equations are used in making the calculations. It is very important to validate experimental data with simulation results.

The configuration of steel parts and quenching equipment in this study is presented in Fig. 7(a) and Table 11. For CFD modeling of the entire system (forging, water flow plus fixture), the mesh contained 16,000 cells. The time spacing was 0.001 s. The cooling process was calculated for 50 s. The water flow rate at the entrance was 10 m/s. To simulate the heat transfer process, the numerical methods of control volume were used [7]. The study of heat transfer processes during quenching has been performed on the basis of numerical solving of the full system of Navier-Stokes equations.

The quenching process of a cylindrical forging, shown in Fig. 7 (b), was also examined. Table 11 provides an illustration of one-half of the symmetrical forging on which the calculations were performed. CFD simulations on different areas of the forging (points 1–8) were performed.

The surface temperature (at points 1–7) and core temperature (point 8) of the forging versus time is shown in Fig. 7. The cooling times from the austenitizing temperature $T_0 = 870°C$ to a temperature of 500°C at point 8 were compared. The cooling time calculated by the generalized equation was 37 s:
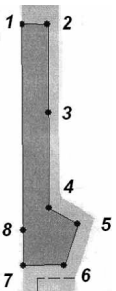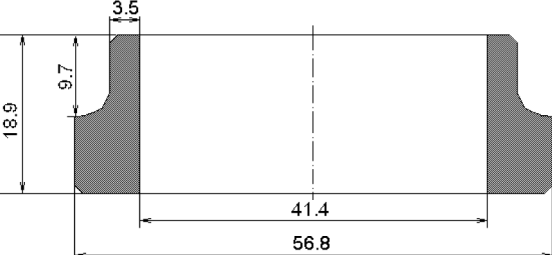
$$t = \left(0.48 + \ln\left(\frac{870 - 20}{500 - 20}\right)\right) \frac{171 \times 10^{-6} m^2}{5.36 \times 10^{-6} m^2/s \times 0.9} \approx 37s.$$

A cooling time in the same range, 38 s, was obtained by CFD simulation, which agrees very well.

Example 5.4

CFD modeling was used to calculate the cooling time for the forging shown in Fig. 8, and it coincided very well with the results achieved from the generalized equation. This example illustrates the calculation procedure if the size of the forging is reduced two, three, four, or more times.

Let's look at a forging reduced by a factor of two from that presented in Fig. 8. It measures 108 mm long and 22.25 mm in diameter. According to regular thermal condition theory, the Kondratjev form factor for a small forging K_{small} can be calculated as $K_{small} = n^2K$. Since the Kondratjev form factor for the previous forging (Example 5.3) is 171×10^{-6} m²

TABLE 10—Universal correlation between generalized Biot number Bi_v and Kondratjev number Kn

Bi_v	ψ	Kn
0.00	1.000	0.000
0.10	0.930	0.090
0.20	0.880	0.170
0.30	0.811	0.243
0.40	0.759	0.304
0.50	0.713	0.356.
0.60	0.671	0.402
0.80	0.599	0.479
1.00	0.540	0.539
2.00	0.356	0.713
3.00	0.264	0.793
4.00	0.210	0.840
5.00	0.174	0.868
6.00	0.148	0.888
7.00	0.129	0.903
8.00	0.114	0.914
9.00	0.103	0.924
10.0	0.093	0.931
20.0	0.048	0.965
30.0	0.033	0.976
∞	0.000	1.000

TABLE 11—Kondratjev form factors for different kinds of steel parts

Drawings of steel parts	K (m²)
	171×10^{-6}
	3.94×10^{-6}

(see Table 11), the Kondratjev number for small forging will be:

$$K_{small} = (0.5)^2 171 \times 10^{-6} = 42.75 \times 10^{-6} m^2.$$

If the forging is cooled from 860°C in a water flow that provides the condition of $Kn = 0.8$, the cooling time from 860°C to the martensite start temperature of 360°C can be calculated by the generalized equation:

$$\tau = \left[0.48 + \ln \frac{860^o C - 20^o C}{360^o C - 20^o C}\right] \frac{42.75 \times 10^{-6} m^2}{5.4 \times 10^{-6} m^2/s \times 0.8} = 13.7 s.$$

Here, $a = 5.4 \times 10^{-6}$ m²/s is the thermal diffusivity of steel.

Example 5.5

A bearing ring made of AISI 52100 steel is quenched intensively in a water flow condition where the generalized Biot number Bi_v is equal to 6. The core of the bearing ring is cooled from 850°C to 240°C, and then intensive quenching is interrupted and further cooling is continued in air. There is a need to calculate the duration of cooling time in water flow. The first step is to calculate the Kondratjev number Kn

Fig. 8—Cylindrical forging made of alloy steel which is quenched intensively in water flow where $Kn = 0.8$.

using the universal correlation between the generalized Biot number Bi_v and Kondratjev number Kn (Eq 4) [3,4]:

$$Kn = \frac{6}{\sqrt{36 + 1.437 \times 6 + 1}} = 0.888.$$

Next, evaluate Ω from Fig. 6 or Eq 68. Since the bearing ring can be considered a cylindrical form that tends toward the plate-shaped form, we will use $\Omega = 0.35$, which is between the cylinder and plate values (see Fig. 6). According to Eq 68 for $k = 1.5$, $\Omega = 0.37$. The Kondratjev form factor for the bearing ring is shown in Table 11. The average value for thermal diffusivity of bearing steel is 5.36×10^{-6} m²/s. Using these data as inputs, the cooling time is determined from the generalized equation:

$$\tau = \left[0.36 + \ln \frac{850^o C - 20^o C}{240^o C - 20^o C}\right] \frac{3.94 \times 10^{-6} m^2}{5.36 \times 10^{-6} m^2/s \times 0.888} = 1.4 s.$$

Example 5.6

A stamp (see Fig. 9) made of AISI D2 steel (1.5 % carbon, 0.30 % silicon, 12 % chromium, 0.80 % molybdenum, and 0.90 % vanadium) is heated in a vacuum furnace to 1,020°C and, after austenitizing, is cooled by gas flow to 120°C in such a way that the average heat transfer coefficient is equal to 140 W/m²K. After cooling is completed, the stamp is double tempered. For example, to provide hardness HRC 59–60, the stamp should be double tempered at 250°C with intermediate cooling to room temperature. For a small Biot number ($Bi < 0.2$), the generalized equation is reduced to a very simple form:

$$\tau = \frac{c\rho V}{\alpha S} \ln \frac{T_0 - T_m}{T - T_m},$$

where:

$$c\rho = \frac{\lambda}{a};$$

$V = L^3 - l^3$; and
$S = 24 l^2.$

Fig. 9—A stamp made of AISI D2 steel that is quenched in air with $\bar{\alpha} = 120 \frac{W}{m^2 K}$.

Given $l = 1.5$ inches or 0.0381 m, we can calculate:
$L = 2l = 3$ inches or 0.0762 m;
$V/S = 0.292l$ or 0.011 m;

$$c\rho = \frac{\lambda}{a} = \frac{26 W/mK}{5.9 \times 10^{-6} m^2/s} = 4.4 \times 10^6 \frac{Ws}{m^3 K};$$

$$\frac{c\rho V}{\alpha S} = 346s;$$

$$\ln \frac{T_0 - T_m}{T - T_m} = \ln \frac{1020^0 C - 20^0 C}{120^0 C - 20^0 C} = 2.3026; \text{ and}$$

$\tau = 2.3026 \times 346s = 797s$ or 13.3 min.

Similar calculations can be done for tempering.

5.4 ANALYSIS OF THE GENERALIZED EQUATION FOR COOLING BODIES OF ANY SHAPE

The generalized dependence in Eqs 69 and 70 has been obtained at constant thermal and physical properties of the material and when there are no heat sources. Actually, the equation of transient heat conductivity has the form [8–14]:

$$c\rho \frac{\partial T}{\partial \tau} = div[\lambda(T)gradT] + Q(T) \qquad (71)$$

where $Q(T)$ is a heat source connected with phase transformations inside of a part to be quenched. If isothermal kinetics of austenite decomposition occur according to:

$$P(\tau) = 1 - \exp[-K_1(T) \cdot \tau^{n(T)},$$

where K_1 and n for each temperature are determined from a TTT (time-temperature-transformation) diagram, then P is a volume fraction of the structural component of steel. In this case, Eq 62 can be represented as:

$$c\rho \frac{\partial T}{\partial \tau} = div[\lambda(T)gradT] + \rho L_c \frac{\partial P}{\partial T} \cdot \frac{\partial T}{\partial \tau}, \qquad (72)$$

where L_c is a specific thermal effect of phase transformations.

Using an average value of heat conductivity $\bar{\lambda}$:

$$C_{eff} \frac{\partial T}{\partial \tau} = \bar{\lambda} div(gradT). \qquad (73)$$

Here,

$$C_{eff} = \rho \left(c \pm L_c \frac{\partial P}{\partial T} \right) \qquad (74)$$

is a so-called *effective specific heat capacity*, which is presented in many handbooks. According to [11], in many cases averaging thermal and physical properties of material yields more exact results of calculations than the exact solution of the equations performed on a computer because not all input data are available. For calculations performed on a computer, some data are given precisely, while others are averaged because of their partial absence, which results in errors exceeding values that are obtained when averaging all thermal and physical characteristics. This means that, in the latter case, averaging of some characteristics results in an error with a sign of plus, and others in a sign of minus, which results in a compensation in the error and therefore, a more exact solution. Experience has shown that the generalized equation is sufficiently accurate, and calculation results agree very well with experiments.

Table 10 presents values of the basic criteria that are used for calculations, namely, for:

$$Kn = \psi Bi_v, \qquad (75)$$

where ψ is a criterion of nonuniformity of the temperature field whose physical sense lies in the characterization of the temperature difference between the surface and temperature average in the volume. That is:

$$\psi = \frac{\bar{T}_{sf} - T_m}{T_v - T_m}, \qquad (76)$$

where:
$\bar{T}_{sf}$ is the average surface temperature; and
T_v is the average volume temperature of the body.
More useful information connected with this subject can be found in [9–14].

5.5 DISCUSSION

It is important to emphasize that the generalized equation can be used to calculate the ideal critical diameter and critical size of any form of steel part. For the purpose of the discussion below, the steel will be AISI 1045 and a CCT diagram for AISI 1045 steel will be used (see Fig. 10).

The generalized equation for the calculation of cooling time for bodies of arbitrary forms, obtained in the analytical form in [1], may be transformed as follows:

$$D = \left(\frac{\bar{a} b \bar{K} n \tau_m}{\Omega + \ln \theta} \right)^{0.5}, \qquad (77)$$

where:
D is the characteristic size (e.g., diameter of a cylinder or sphere, thickness of plate, and so on) (m);
$\bar{a}$ is average thermal diffusivity (m²/s);
$\bar{K}n$ is the Kondratjev number (dimensionless);
τ_m is the limit time of the core cooling from the austenitizing temperature to the martensite start temperature, providing the creation of 99 % or 50 % martensite (see Fig. 10,
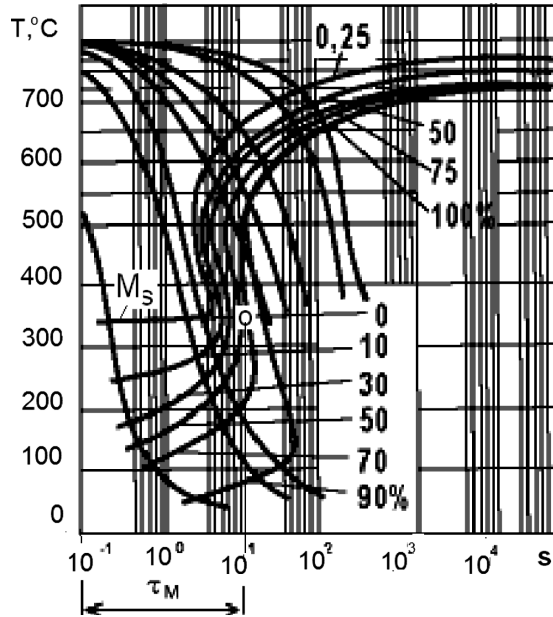
Fig. 10—CCT diagram for AISI 1045 steel.

point O, at the interconnection of the martensite start temperature with the curve showing 50 % martensite);
$\Omega = 0.48$ for a bar (or cylinder);

$$\theta = \frac{T_0 - T_m}{T_M - T_m};$$

T_0 is the austenitizing temperature;
T_m is the temperature of the quenchant; and
T_M is the martensite start temperature at limit time of cooling τ_m.

The optimal residual stress distribution in the quenched steel part occurs in the case of an optimal depth of the hard layer [15–19]. In this case, high compressive stresses at the surface and lower tensile stresses in the core are observed when:

$$\frac{DI}{D_{opt}} = const. \tag{78}$$

The ideal critical diameter is calculated from Eq 77 [19]:

$$DI = \left(\frac{\bar{a}b\tau_M}{\Omega + \ln\theta}\right)^{0.5}, \tag{79}$$

where:
a is the average thermal diffusivity (m²/s);
τ_m is the limit time of the core cooling from the austenitizing temperature to the martensite start temperature, providing the formation of 99 % or 50 % martensite;
b is a constant depending on the shape; and
$Kn = 1$ because cooling is produced in ideal condition when $Bi_v > 100$.

To obtain the best results, the steel parts should be quenched under conditions of $Bi_v > 5$ [20–22].

Optimum stress distribution in the section of steel parts means high compressive stresses at the surface and lower tensile stresses at the core. Since the cooling rate within the martensite range is very high during intensive quenching, additional strengthening of the material is observed [21–23]. High compressive stresses at the surface and additional

strengthening of the material significantly increase the service life of steel parts [21–24].

The advantage of Eq 79 is that it allows the calculation of critical diameters for bodies of any geometry at any required percentage of the martensite in the core. However, CCT diagrams, presenting information about the quantity of martensite formed in a quenched steel part, must be available for each alloy of interest.

Parameter b depends on the shape of the body and is obtained by transforming the Kondratjev form coefficient K to a specific value depending on the diameter or thickness of the part (see Chapter 6). For example, the Kondratjev form coefficient for an unbounded plate is $K = \frac{L^2}{9.87}$; for an unbounded cylinder is $K = \frac{D^2}{23.13}$; and for a sphere is $K = \frac{D^2}{39.48}$. Therefore, the values of b for a plate, cylinder, and sphere are 9.87, 23.13, and 39.48, respectively.

5.6 SUMMARY
1. The generalized equation for calculation of cooling time for bodies of any shape has been analyzed and compared with the analytical solutions and CFD modeling. The accuracy of calculations has been shown to be acceptable (0.4 – 1.6%) if the temperature at the core of steel parts is approaching the martensite start temperature. The results are used for the design of processes connected with the heat treatment of steel parts of both simple and complicated configurations.
2. Using the generalized equation, it is possible to calculate the ideal critical diameter and critical size of any shape of steel part that is used in the heat-treating industry to optimize residual stress distribution and achieve additional strengthening of materials.

References
[1] Kobasko, N. I., *Steel Quenching in Liquid Media Under Pressure,* Naukova Dumka, Kyiv, 1980.
[2] Kobasko, N. I., Aronov, M. A., Powell, J. A., Canale, L. C. F., and Totten, G. E., Intensive Quenching Process Classification and Applications, *Heat Treatment of Metals,* Vol. 31, No. 3, 2004, pp. 51–58.
[3] Kondratjev, G. M., *Teplovye Izmereniya* (Thermal measurements), Mashgiz, Moscow, 1957.
[4] Lykov, A. V., *Teoriya Teploprovodnosti* (Theory of heat conductivity), Vysshaya Shkola, Moscow, 1967.
[5] Kobasko, N. I., and Guseynov, Sh. E., Initial Heat Flux Densities and Duration of Non-stationary Nucleate Boiling During Quenching, *Proceedings of the 5th WSEAS International Conference on Heat and Mass Transfer (HMT '08),* Acapulco, Mexico, January 25–27, 2008, pp. 104–109.
[6] Kobasko, N. I., What Is Duration of Non-stationary Nucleate Boiling and Thermal Equilibrium During Quenching of Steel Parts? *Proceedings of the 6th IASME/WSEAS International Conference on Heat Transfer, Thermal Engineering and Environment (HTE '08),* Rhodes, Greece, August 20–22, 2008, pp. 529–533.
[7] Krukovskyi, P., Kobasko, N., and Yurchenko, D., Generalized Equation for Cooling Time Evaluation and Its Verification by CFD Analysis, *Journal of ASTM International,* Vol. 6, No. 5, 2009.
[8] Kobasko, N. I., Morhuniuk, W. S., and Gnuchiy, Yu. B., *Study of Technological Processes of Machine Part Treatment,* Znanie, Kyiv, 1979.
[9] Kobasko, N. I., and Morhuniuk, W. S., *Study of Thermal and Stress-Strain State at Heat Treatment of Machine Parts,* Znanie, Kyiv, 1983.

[10] Adamova, N. A., Thermal and Physical Fundamentals of Heat Treatment Conditions for Large Rolls, author's abstract of Ph.D. dissertation, Sverdlovsk (VNIIMT), 1986.

[11] Kozdoba, L. A., *Computational Thermal Science,* Naukova Dumka, Kyiv, 1992.

[12] Lienhard IV, J. H., and Lienhard V, J. H., *A Heat Transfer Textbook,* 3rd Ed., Phlogiston Press, Cambridge, Massachusetts, 2005.

[13] Kraus, A. D., Aziz, A., and Welty, J. R., *Extended Surface Heat Transfer,* John Wiley & Sons, New York, 2001.

[14] Kobasko, N. I., and Morhuniuk, W. S., Numerical Study of Phase Changes, Current and Residual Stresses at Quenching Parts of Complex Configuration, *Proceedings of the 4th International Congress of Heat Treatment Materials,* Berlin, 1985, Vol. 1, pp. 465–486.

[15] Kobasko, N. I., Basics of Intensive Quenching–Part I, *Advanced Materials & Processes/Heat Treating Progress,* Vol. 148, No. 3, 1995, pp. 42W–42Y.

[16] Kobasko, N. I., Basics of Intensive Quenching–Part II, *Advanced Materials & Processes/Heat Treating Progress,* Vol. 150, No. 2, 1996, pp. 40CC–40EE.

[17] Kobasko, N. I., Basics of Intensive Quenching–Part III, *Advanced Materials & Processes/Heat Treating Progress,* Vol. 153, No. 2, 1998, pp. 36FF–36HH.

[18] Kobasko, N. I., Quench Process Optimization, *Proceedings of the 6th International Conference "Equipment and Technologies for Heat Treatment of Metals and Alloys", OTTOM-6,* Kharkov, Ukraine, May 16–20, 2005, pp. 88–96.

[19] Kobasko, N. I., Quench Process Optimization for Receiving Super Strong Materials, *WSEAS Transactions on Systems,* Vol. 4, No. 9, 2005, p. 1394–1401.

[20] Kobasko, N. I., Effect of Structural and Thermal Stresses on Crack Formation During Steel Quenching, *Proceedings of the All-Union Conference on Increase in Productivity and Profitability of Heating Furnaces,* Dnipropetrovsk, 1967, pp. 26–27.

[21] Kobasko, N. I., Steel Superstrengthening Phenomenon, *Journal of ASTM International,* Vol. 2, No. 1, 2005.

[22] Kobasko, N. I., The Steel Superstrengthening Phenomenon, Part 2, *International Journal of Microstructure and Materials Properties,* Vol. 3, Nos. 4/5, 2008, pp. 526–547.

[23] Kobasko, N. I., and Prokhorenko, N. I., Effect of Cooling Rate During Quenching upon Crack Formation in Steel 45, *Metal Science and Heat Treatment,* Vol. 53, No. 2, 1964.

[24] Canale, L. C. F., Kobasko, N. I., and Totten, G. E., Intensive Quenching, Part 2: Formation of Optimal Surface Compressive Stresses, *International Heat Treatment and Surface Engineering,* Vol. 1, No. 2, 2007, pp. 60–63.

6

Regular Thermal Process and Kondratjev Form Factors

N. I. Kobasko[1]

6.1 INTRODUCTION

In the previous chapter, regularities of heating and cooling bodies of various geometrical configurations were discussed and a generalized equation for the determination of cooling time for bodies of any shape was presented. A key parameter in this equation is the Kondratjev form factor (coefficient K). This coefficient is also one of the key parameters in the equation for the determination of the duration of nonstationary nucleate boiling. Therefore, it is important to be able to determine Kondratjev form coefficients for use in these calculations. In this chapter, the focus will be on the thermal process and determination of Kondratjev form coefficients. The availability of Kondratjev form coefficients and knowledge of the basic regularities of the thermal process will provide for sufficiently accurate and rapid calculations suitable for use with manufacturing process design.

6.2 REGULAR THERMAL PROCESS

Assume that there is a body, of any shape, with a surface area S and volume V, which is cooled in a quenchant at constant temperature T_m from initial temperature T_0 by a Newtonian cooling process with the third kind of boundary conditions (see Fig. 1) and that it is necessary to study the thermal characteristics of its cooling at the stage of the regular thermal process.

As is known, the differential equation of heat conductivity for such a problem is:

$$\frac{\partial T}{\partial \tau} = a\left(\frac{\partial^2 T}{\partial x^2} + \frac{\partial^2 T}{\partial y^2} + \frac{\partial^2 T}{\partial z^2}\right); \qquad (1)$$

$$\frac{\partial T}{\partial n} + \frac{\alpha}{\lambda}(T - T_m)|_S = 0; \qquad (2)$$

$$T(x,y,z,0) = f(x,y,z). \qquad (3)$$

It has been proved [1,2] that the general solution of this problem for bodies of any shape can be presented as:

$$\frac{T - T_m}{T_0 - T_m} = \sum_{n=1}^{\infty} A_n U_n \exp(-m_n \tau), \qquad (4)$$

where:
A_n are temperature amplitudes; and
U_n are eigenfunctions dependent on coordinates; and

$$m_1 > m_2 < m_3 \cdot m_n < m_{n+1}.... \qquad (5)$$

Given this series of inequalities (Eq 5), in a short time the process of cooling of a body of any shape will be described by a simple exponent [2−4]:

$$\theta = A_1 U_1 e^{-m_1 \tau}. \qquad (6)$$

This equation shows that change in temperature both in space and in time does not depend on the initial temperature distribution. Taking the logarithm of Eq 6 and omitting the indexes, we obtain:

$$\ln \theta = \ln(AU) - m\tau,$$

or

$$\ln \theta = -m\tau + C(x,y,z). \qquad (7)$$

From Eq 7, it follows that the natural logarithm of dimensionless temperature for all points of a body changes linearly with respect to time.

Thus, the process of cooling bodies of any shape can be divided into three stages.

1. The *first stage* of the cooling process (irregular) is characterized by the large effect of the initial temperature distribution, and the correlation between θ and τ can be derived from differential equation 4.
2. The *second stage* of cooling is called a regular process, and the correlation between θ and τ is described by Eq 6 [1,2].
3. The *third stage* of cooling corresponds to the stationary process when the temperature is equal, for all points of a body, to the quenchant temperature T_m (thermal equilibrium).

As for the second stage of cooling, differentiating both parts of the Eq 7 with respect to time yields:

$$\frac{1}{\theta}\frac{\partial \theta}{\partial \tau} = -m = const. \qquad (8)$$

On the left side of Eq 8, there is an expression for the relative speed of change in temperature, which is equal to constant value m. The value of m is measured in Hertz (1/s) and is called a *cooling* (or *heating*) *factor*. During a regular thermal process, the value m depends on neither coordinates nor time and is constant for all points of the body. A cooling factor characterizes the relative speed of change in temperature within a body and depends only on the physical properties of the body, the process of cooling on its surface, and the size and shape of the body.

Thus, the regular process of heating and cooling of different bodies is characterized by a simple exponent, and the cooling factor m for all points of a body remains constant depending on neither coordinates nor time [1,4,5].

Experimentally determining temperature variation with respect to time and presenting this dependence in half-logarithmic coordinates yields a straight line, which shows that:

---

[1] *IQ Technologies, Inc., Akron, Ohio, and Intensive Technologies Ltd., Kyiv, Ukraine*
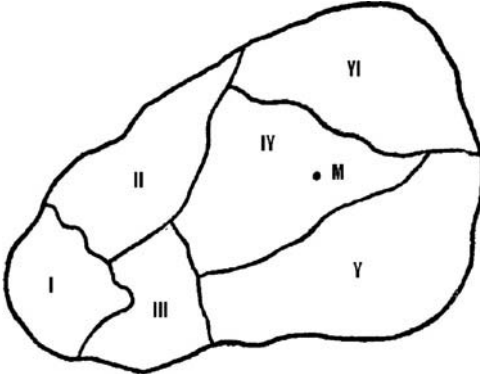
Fig. 1—Body of any shape cooled in a quenchant of constant temperature T_m by Newtonian cooling. The numbered regions are areas that possess different thermal properties; point M indicates a location where the temperature during quenching is at a maximum value.

$$\frac{\ln \theta_1 - \ln \theta_2}{\tau_2 - \tau_1} = \frac{\ln \vartheta_1 - \ln \vartheta_2}{\tau_2 - \tau_1} = m = const,$$

where $\vartheta = T - T_m$.

Now this problem will be considered from a different point of view. The cooling factor m depends on the physical properties of the body, its size and shape, and also conditions of heat transfer at the surface of the body. A similar conclusion can be obtained through the analysis of the thermal balance [4]. It is known that the change in internal energy of a body of any shape is equal to a heat flux:

$$dQ = -c\rho V \frac{\partial \overline{\vartheta}_V}{\partial \tau} d\tau, \tag{9}$$

where:
c is the specific thermal capacity in J/(kgK);
V is the volume of the body (m^3);
ρ is the density of the substance (kg/m^3);
$\overline{\vartheta}_V = \overline{T}_V - T_m$;
$\overline{T}_V$ is volume-average temperature (°C); and
τ is time (s).

For the same time, all heat should be transferred from a surface S to the quenchant due to heat transfer:

$$dQ = \overline{\alpha}\overline{\vartheta}_{sf} S d\tau, \tag{10}$$

where:
$\overline{\vartheta}_{sf} = \overline{T}_{sf} - T_m$; and
$\overline{T}_{sf}$ is the average temperature of the surface of a body at that time:

$$\overline{\vartheta}_{sf} = \frac{1}{S} \int_S \vartheta_{sf} dS.$$

Equating Eqs 9 and 10, we obtain:

$$-\frac{\partial \overline{\vartheta}_V}{\partial \tau} = \frac{\overline{\alpha}S}{c\rho V}\overline{\vartheta}_{Sf},$$

and dividing this expression by $\overline{\vartheta}_V$ yields:

$$-\frac{1}{\overline{\vartheta}_V}\frac{\partial \overline{\vartheta}_V}{\partial \tau} = \frac{\overline{\vartheta}_{sf}\overline{\alpha}S}{\overline{\vartheta}_V(c\rho V)}. \tag{11}$$

Now compare Eq 11 with the Eq 8, which can be shown as:

$$\frac{T_0 - T_m}{T - T_m} \cdot \frac{\partial \left(\frac{T - T_m}{T_0 - T_m}\right)}{\partial \tau} = \frac{1}{\vartheta}\frac{\partial \vartheta}{\partial \tau} = -m$$

or

$$m = -\frac{1}{\vartheta}\frac{\partial \vartheta}{\partial \tau}, \tag{12}$$

where $\vartheta = T - T_m$.

Comparison of Eqs 11 and 12 shows:

$$m = \psi \frac{\overline{\alpha}S}{c\rho V} = \psi \frac{\overline{\alpha}S}{C}, \tag{13}$$

where:

$$\psi = \frac{\overline{T}_{sf} - T_m}{\overline{T}_V - T_m}; \text{ and}$$

$C = c\rho V$ is the full heat capacity of a body.

Eq 13 shows that the cooling factor m of a homogeneous and isotropic body of any shape at finite value of a heat transfer coefficient α is proportional to the heat transfer coefficient and the surface area of the body and is inversely proportional to its thermal capacity. This statement is the *first Kondratjev theorem*. For the exploration of the effect of criterion ψ upon the simple Biot number Bi, which takes into account conditions of the process cooling (heating) at the surface of the body, let's consider two limiting cases:

1. $Bi \to 0$ (practically, $Bi < 0.1$). In this case, $\overline{\vartheta}_{sf} \approx \overline{\vartheta}_V$, and therefore $\psi = 1$.
2. $Bi \to \infty$ (practically, $Bi > 100$). In this case, the problem becomes internal, and the process of cooling a body of any shape is determined only by the size of the body and the thermal and physical properties of the system. In this condition, the temperature at the surface becomes equal to the medium's temperature T_m, and therefore $\psi = \frac{\overline{\vartheta}_{sf}}{\overline{\vartheta}_V} = 0$.

These limiting cases demonstrate that with the change of Bi from 0 to ∞, ψ changes from 1 to 0.

According to the *second Kondratjev theorem*, as $Bi \to \infty$ (or $a \to \infty$), cooling factor m becomes directly proportional to the body's material thermal diffusivity a in m^2/s [1], that is,

$$a = K \cdot m_\infty, \tag{14}$$

where:
K is a Kondratjev form factor (coefficient); and
m_∞ is the cooling factor at $Bi \to \infty$.

The determination of the Kondratjev form factor K is based on the second Kondratjev theorem, Eq 14.

The ratio of the cooling factor m, for a finite heat transfer coefficient, to cooling factor m_∞, at $Bi \to \infty$, is called the Kondratjev number Kn, that is,

$$Kn = \frac{m}{m_\infty}. \tag{15}$$

Lykov [4] has noted that Kn is a key value determining the character of heat transfer of the body of any shape at the stage of a regular process. The number Kn was named in honor of Kondratjev, who developed the theory of regular thermal conditions.

There is the universal relationship between Kn and the generalized Biot number Bi_V:

$$\left(Bi_V = \frac{\alpha}{\lambda} K \frac{S}{V}\right),$$

which can be presented as [1,4]:

$$Kn = f(Bi_V)$$

or:

$$Kn = \psi Bi_V = \frac{Bi_V}{\sqrt{Bi_V^2 + 1.437 Bi_V + 1}}. \qquad (16)$$

This relationship is valid for bodies of any shape and therefore is very important when designing manufacturing processes connected with the cooling or heating of steel parts. The curves $Kn = f(Bi_V)$ for geometrically different bodies– plate, cylinder, ball, parallelepiped, and so forth–were found to be so closely located to each other that practically all of them can be replaced with one averaged curve (see Fig. 2) [4]. Eq 16 was obtained by approximation of this curve.

For a cylinder, plate, or sphere, the regular thermal condition depends on the Fourier number F_0, Bi, a temperature ratio $\frac{T - T_m}{T_0 - T_m}$, and an admissible calculation error ε, and can be evaluated from Figs. 3 and 4. These figures show that at small values of the Biot number (Bi), the core of these bodies quickly passes to the stage of regular thermal conditions. With an increase
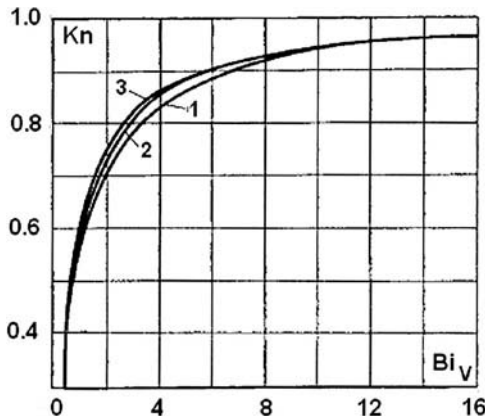
Fig. 2—Universal approximate relationship $Kn = f(Bi_v)$ [4]: 1, plate; 2, ball; 3, cylinder.
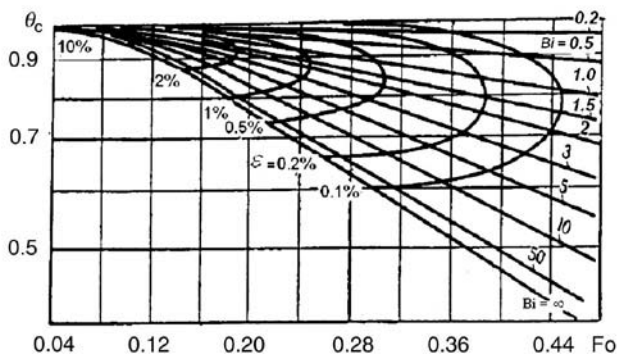
Fig. 3—The beginning of regular thermal process versus F_0, Bi, and an admissible calculation error ε (%) for the core of a plate.
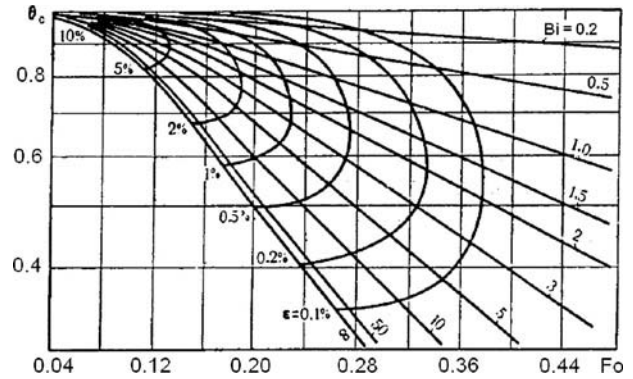
Fig. 4—The beginning of regular thermal process versus F_0, Bi, and an admissible calculation error ε (%) at the axis of a cylinder.

of the Biot number, the relative time of regularization lengthens, reaching its maximum when Bi is about 2. At identical ε and Bi, the time of the beginning of the stage of regular process occurs earlier at the core of a cylinder than at the core of a plate.

In these calculations, $Bi = \frac{\alpha}{\lambda} R; Fo = \frac{a\tau}{R^2}$; a is the heat transfer coefficient; λ is the heat conductivity of the material; a is the thermal diffusivity of the material; τ is time; and R is radius.

Now consider the applicability of the theory of regular thermal conditions to steel quenching processes. In most cases in practice, it is necessary to determine cooling time for steel parts from the temperature of austenization to the martensite start temperature M_S (see Chapter 1). Usually the austenization temperature is within the range of 800– 1,000°C and the martensite start temperature for medium-carbon steels occurs at approximately 350°C. If steel quenching is conducted in quenchants at a temperature of 20°C, the relative temperature at which martensite starts is:

$$\theta = \frac{350^o C - 20^o C}{900^o C - 20^o C} = 0.375.$$

This indicates that for intensive quenching of cylinder-shaped parts, the error that arises due to the approximate calculations is equal to just 0.2 % (see Fig. 4). More significant errors can arise due to averaging the thermal and physical properties of materials and heat transfer coefficients. However, these errors can be reduced to a minimum with the correct choice of average values.

The theory of regular thermal conditions was widely used for the determination of thermal and physical properties of materials. For calculations of cooling time, it was not used in practice, however, because of a lack of study of the time τ_{ir} of the irregular thermal process, which is a part of the cooling process. Total time is the sum of the time of irregular thermal process τ_{ir} and the time of regular thermal process τ_r, that is: $\tau = \tau_{ir} + \tau_r$. Furthermore, there were no generalized equations obtained to calculate cooling (heating) time depending on the Biot number, thermal properties of material, and form and size of a body. The generalized equation for calculation of cooling time for bodies of any shape, provided in Chapter 5 (Eq 60), eliminates this shortcoming.

6.2.1 Application of the Theory of Regular Thermal Conditions to Bodies of Complex Shape

In 1961−1962, a hot discussion occurred between Professor Tret'yachenko [6,7] and the creators of the theory of regular
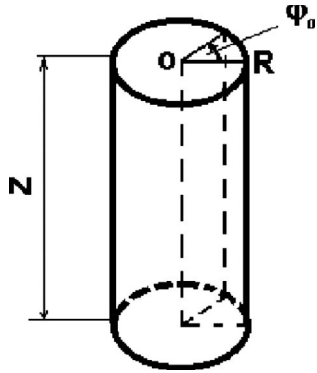
Fig. 5—Wedge-shaped bodies include this sector cut from a finite cylinder with an opening angle of φ_o.

thermal conditions [8,9]. Very distinguished heat treaters, belonging to the school of well-known thermal scientist Kondratjev, took part in that discussion. Tret'yachenko claimed that the theory of regular thermal conditions did not work for bodies with complex geometric configurations, such as turbine blades or wedge-shaped bodies, and a number of experimental facts were presented exposing the incorrectness of the theory.

Included in this discussion was the cooling process for wedge-shaped bodies (see Figs. 5 and 6) as described by the infinite series:

$$\theta = \sum_{n=1}^{\infty} A_n J_n \left(\mu_n \frac{r}{R} \right) \exp(-m_n \tau), \qquad (17)$$

where the terms $J_n \left(\mu_n \frac{r}{R} \right)$ are Bessel functions of the first kind, order n, depending on the opening angle ϕ. It turns out that at the edge of a wedge, along the Z-axis, Bessel functions of order n are equal to zero, and they possess very small values near the Z-axis. During the entire cooling period for wedges at these points, the regular thermal process never occurs and the cooling process is described by the third or even fifth terms of the series, where the Bessel function increases considerably.

In [5] and [10], it was proved that, at the points farthest from the wedge's surface (see Fig. 6), Bessel functions of order n possess maximum values (see Fig. 7). Therefore, at these points, the regular thermal process (regular conditions) occurs, and the cooling process is described by an exponent (Eq 6) that is of greatest interest relative to the work being discussed here. Therefore, the generalized Eq 60 is valid for bodies of a complex shape, including the wedge in Fig. 5.

To verify the reliability of Eq 60, experimental cooling studies were conducted with wedges having different opening angles ϕ [5,10]. For this work, the wedges were made of epoxy resin and cooled in ice water at a constant temperature. In addition to wedges, cooling of epoxy gear wheels (see Fig. 8) was also studied.
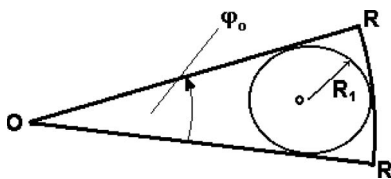
Fig. 6—The location of points the most remote from a surface of a wedge that are within the inscribed circle of radius R_1 ($R_1 < R$).
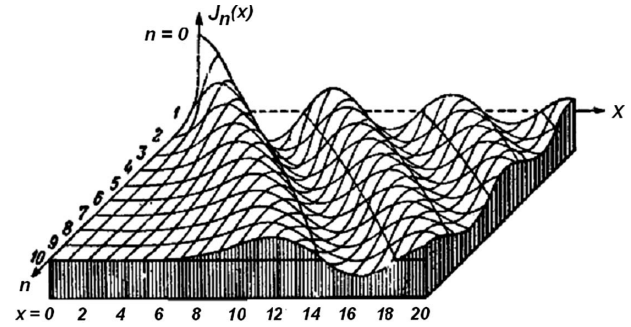
Fig. 7—Bessel functions of the first kind, order n.

The wedge and gear samples shown in Fig. 8 were made of epoxy resin and cooled in a temperature-controlled tank by water flow at 0.5–1.5 m/s (see Fig. 9). Because of low heat conductivity and thermal diffusivity of the epoxy resin, the requirement $Bi \to \infty$ in this condition was met, which allowed the determination of Kondratjev form factors (coefficients K) for the wedges and gears (bodies with a complex geometric configuration).

6.3 KONDRATJEV FORM FACTORS AND A TECHNIQUE OF THEIR DETERMINATION
6.3.1 Analytical Methods
As discussed previously, Kondratjev form factors (coefficients) K are necessary for calculation of the duration of the
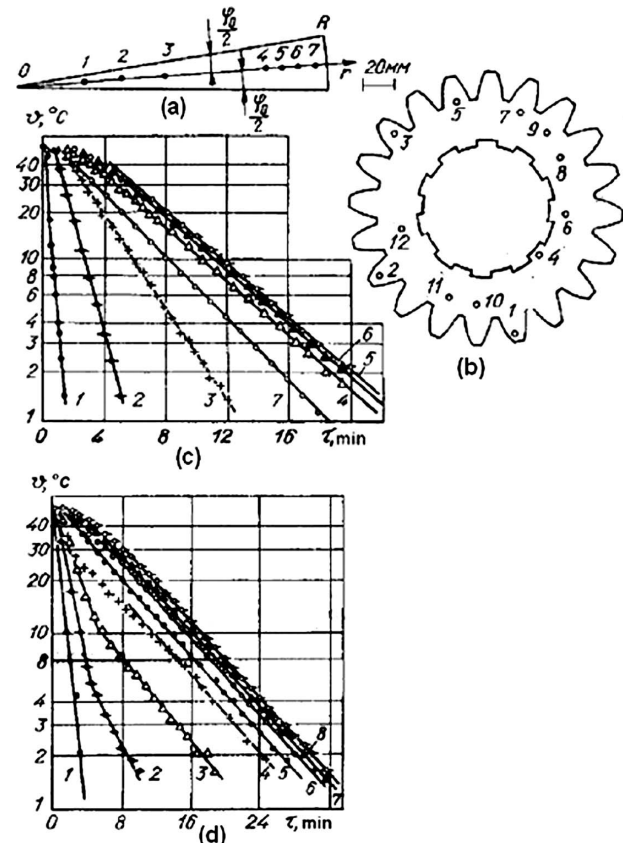
Fig. 8—Wedges and gear wheels used in the study of the regular thermal process: (a) wedge; (b) gear; (c) temperature versus time in semilogarithmic coordinates for wedges; (d) the same for gears ($\vartheta = T - T_m$; T_m is the temperature of the cooling medium).
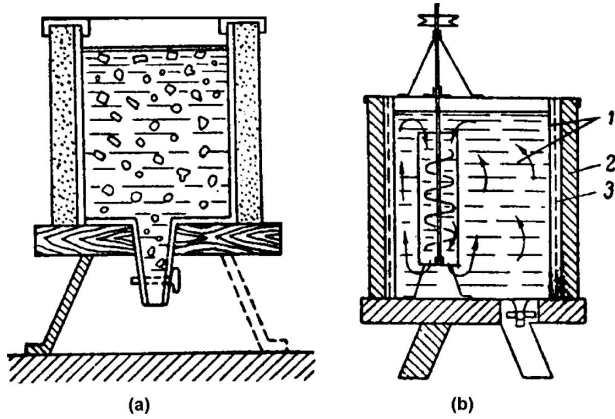
Fig. 9—Temperature-controlled tanks with ice (a) and agitated quenchant (b) for the study of regular thermal processes.

self-regulated thermal process and for calculation of cooling time of bodies with either simple or complex configurations.

For bodies with a simple shape, there are many analytical equations suitable for the determination of Kondratjev form factors. If there is an analytical solution of the equation of nonstationary heat conductivity for a specific part, the appropriate Kondratjev form coefficient can be obtained from this solution by analyzing an exponent of the exponential power under the condition $Bi \rightarrow \infty$. Therefore, since there are many analytical solutions for these conditions, it is possible to present many analytical dependences for the Kondratjev form coefficient (see Table 1).

In addition to a Kondratjev form coefficient K, Table 1 presents values for S/V and KS/V, which are used for these calculations.

For bodies of complex configuration for which there are no analytical solutions, Kondratjev form coefficients are

determined experimentally or by numerical calculation. A detailed technique for the determination of K coefficients based on natural and numerical experiments will now be discussed. Table 2 provides results from computer numerical calculations of Kondratjev factors for different sizes of punches.

6.3.2 Experimental Technique of the Determination of Kondratjev Form Factors

If there is a body of complex configuration, for example, a wedge-shaped part, the junction of the thermocouple must be placed at a point that is farthest from the surface, that is, at the center (core) of the inscribed circle (see Fig. 6). Samples of a complex body can be cast of wax or epoxy resin of which the thermal diffusivity and heat conductivity are well known.

If the thermal diffusivity of the material is unknown, a finite cylinder is made of the material to be tested and the thermal diffusivity a is determined by experiment. The technique is quite simple and consists of the following:
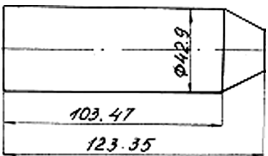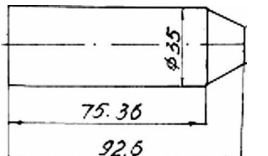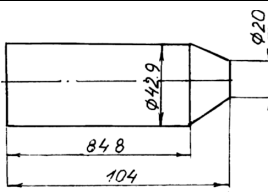
1. A finite cylinder is cooled in a temperature-controlled tank with ice water (see Fig. 9). The change in temperature at the core of the cylinder versus time is recorded under condition $Bi \rightarrow \infty$.
2. A chart of temperature $\vartheta = T - T_m$ versus time is constructed using semilogarithmic coordinates.
3. The cooling factor m is determined using two points located on a straight line (see Fig. 8), by the ratio $m = \dfrac{\ln \vartheta_1 - \ln \vartheta_2}{\tau_2 - \tau_1}$.
4. On the basis of the second Kondratjev theorem, the thermal diffusivity of material a (m²/s) is determined by the equation $a = Km_\infty$ or:

$$a = \frac{m_\infty}{\dfrac{5.784}{R^2} + \dfrac{\pi^2}{Z^2}}. \qquad (18)$$

TABLE 1—Kondratjev form factors K for bodies of a simple configuration (results of analytical calculations), S/V values, and their product, KS/V

Shape of the part	K (m²)	S/V (m⁻¹)	KS/V (m)
Unbounded plate (slab) of thickness L	$\dfrac{L^2}{\pi^2}$	$\dfrac{2}{L}$	$\dfrac{2L}{\pi^2}$
Infinite cylinder of radius R	$\dfrac{R^2}{5.784}$	$\dfrac{2}{R}$	$0.346\,R$
Square infinite prism with equal sides of L	$\dfrac{L^2}{2\pi^2}$	$\dfrac{4}{L}$	$\dfrac{2L}{\pi^2}$
Cylinder of radius R and height Z	$\dfrac{1}{\dfrac{5.784}{R^2} + \dfrac{\pi^2}{Z^2}}$	$\left(\dfrac{2}{R} + \dfrac{2}{Z}\right)$	$\dfrac{2RZ(R+Z)}{5.784Z^2 + \pi^2 R^2}$
Finite cylinder, $R = Z$	$\dfrac{R^2}{8.252}$	$\dfrac{3}{R}$	$0.356\,R$
Finite cylinder, $2R = Z$	$\dfrac{R^2}{8.252}$	$\dfrac{3}{R}$	$0.364\,R$
Cube with sides of length L	$\dfrac{L^2}{3\pi^2}$	$\dfrac{6}{L}$	$0.203\,L$
Finite square plate with sides of length L_1, L_2, L_3	$\dfrac{1}{\pi^2\left(\dfrac{1}{L_1^2} + \dfrac{1}{L_2^2} + \dfrac{1}{L_3^2}\right)}$	$\dfrac{2(L_1L_2 + L_1L_3 + L_2L_3)}{L_1L_2L_3}$	$\dfrac{2(L_1L_2 + L_1L_3 + L_2L_3)L_1L_2L_3}{\pi^2(L_1^2L_2^2 + L_1^2L_3^2 + L_2^2L_3^2)}$
Ball of radius R	$\dfrac{R^2}{\pi^2}$	$\dfrac{3}{R}$	$0.304R$

TABLE 2—Surface (S), volume (V), and Kondratjev form factors K for different punches

Shape and size of parts	S (m²)	V (m³)	K (m²)	$\frac{S}{V}K$ (m)
	11.02×10^{-3}	1.66×10^{-4}	7.92×10^{-5}	5×10^{-3}
	6.87×10^{-3}	8.19×10^{-5}	5.29×10^{-5}	4.44×10^{-3}
	9.76×10^{-3}	1.39×10^{-4}	7.91×10^{-5}	5.56×10^{-3}

5. A model of the steel part is made from the same material. If the steel part is too large, the sizes of a corresponding sample or model are reduced by n times.

6. A junction of the thermocouple is placed at the core of the model, and using the procedures described above, the Kondratjev form factor K is determined by the equation:

$$K = \frac{a}{m_\infty}, \qquad (19)$$

where the thermal diffusivity of material was determined by Eq 18.

Kondratjev form factors obtained based on this experimental approach are shown in Table 3.

By using this technique, Kondratjev form coefficients were determined for wedges, gears, shafts, and wheels of complex configuration (see Table 2). If the sizes of the sample are reduced by n times relative to the dimensions of an actual part, the Kondratjev form factor (coefficient) K is determined from [11]:

$$K = n^2 K_{sample}. \qquad (20)$$
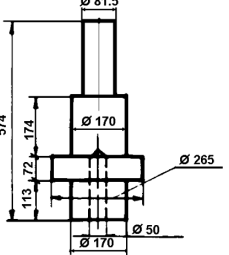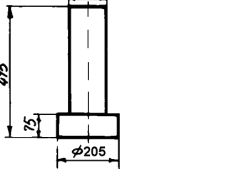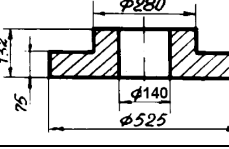
The weakest point in this technique is the necessity of providing condition $Bi \to \infty$. Lykov [4] has noted that the theory of regular thermal conditions has served as a basis for the determination of thermal properties of various materials. However, there are difficulties determining K factors and thermal diffusivity, due to the creation of conditions where $Bi \to \infty$.

Consider, for example, the conditions of cooling a cylinder of 30-mm diameter and 120-mm height made of paraffin, where the heat conductivity is equal to $\lambda = 0.268$ W/mK [12]. For this study, it can be assumed that the $Bi \to \infty$ when experimentally $Bi = 50$. Then, to satisfy the condition $Bi \to \infty$ for the 30-mm diameter cylinder, it is necessary to provide a quench tank where the heat transfer coefficient α is:

$$\alpha = \frac{50\lambda}{0.015m} = \frac{50 \cdot 0.268 \frac{W}{m \cdot K}}{0.015m} = 839 \frac{W}{m^2K}.$$

If the quench tank contains thawing ice and flowing water mixed by a propeller, the heat transfer coefficient in the tank reaches 2,000 W/m²K, which surely creates the condition $Bi \to \infty$.

TABLE 3—Experimental Kondratjev form factors K

Part	Sketch	K, m²
Shaft		1.15×10^{-3}
Center		4.38×10^{-4}
Stock		6.65×10^{-4}
Plug		6.08×10^{-4}

6.3.3 Calculation of Kondratjev Form Factors K by Finite Element Method (FEM) Calculations

There are many software programs for the computation of temperature fields and the stress-strain state of parts to be quenched based on the use of finite element methods (FEM) [14,17−19]. Any of these can be used to determine the Kondratjev form coefficients K using the proposed method of calculation. In the Ukraine, Tandem software is widely used for this purpose [15,16]. Results of FEM calculations obtained using Tandem software are provided in Tables 4 and 5.

The technique for the experimental determination of Kondratjev form coefficient K described above can also be used for numerical calculations. Calculations are based on

the condition of cooling $Bi > 100$, and it is assumed that the thermal properties of a material are constant independent of temperature. The procedure is as follows:

1. The natural logarithm of temperature difference $T - T_m$ versus time at the core of the sample is calculated.
2. The range of temperatures where $\ln(T - T_m)$ is a linear function of time is found.
3. Within this range, the value of m_∞ is calculated, using:

$$m_\infty = \frac{\ln(T_1 - T_m) - \ln(T_2 - T_m)}{\tau_2 - \tau_1}.$$

4. Finally, Kondratjev form factor K is calculated as $K = \frac{a}{m_\infty}$.

Thus, for the determination of K, it is necessary to consider the points most remote from the surface or points at which the temperature corresponds to the average value, that is:

$$\overline{T}(\tau) = \frac{1}{V} \int_0^x \int_0^y \int_0^z T(x,y,z,\tau) dxdydz.$$

(Here it is assumed that the temperature of the quenchant is 0°C.)

For calculations for every five to ten time steps, a cooling factor $m = \frac{\ln \vartheta_1 - \ln \vartheta_2}{\tau_2 - \tau_1}$ is determined, under the condition $Bi \to \infty$ at constant thermal and physical characteristics of the material.

When the regular thermal process is achieved for that specific part, the K factor remains constant. Therefore, within the specified period, Kondratjev form coefficient K is determined by the equation:

$$K = \frac{a}{m},$$

where:
a is a preset value of thermal diffusivity of the material; and
m is the calculated cooling factor under condition $Bi \to \infty$.

The average value K is calculated for all the time periods where m is constant. Results of calculations of Kondratjev form factors (coefficients) K are presented in Tables 4 and 5.

If parts to be quenched have an identical shape but differ in size, recalculation is performed using Eq 20. Tabular values in this case are used as pattern values. Tabular values in Tables 1−5 are used at the simplified calculations for steel quenching design [20,21].

6.4 EVALUATION OF HEAT TRANSFER COEFFICIENTS BASED ON REGULAR THERMAL CONDITIONS AND TESTING STANDARDIZED PROBES

The standardized probes for evaluation of cooling capacity of quenchants are discussed in [22]. Test methods based on ASTM Standards D6200-01, D6482-99, and D6649-00 for determining the cooling characteristics of quenchants by cooling of probes made from Inconel 600 material are widely used in practice [23−25]. The chemical composition of Inconel 600 is: 72 % nickel; 14−17 % chromium; 6−10 % iron; 0.15 % carbon; 0.5 % copper; and 0.5 % silicon. The diameter of the probe is 12.5 mm and its length is 60 mm. Probe details and its general assembly are shown in Fig. 10.

The probe is placed in the preheated furnace and then brought to the required temperature of 850°C. Cooling curves and cooling rate curves are obtained for comparison.

TABLE 4—Kondratjev form factors K for bearing rings and gears
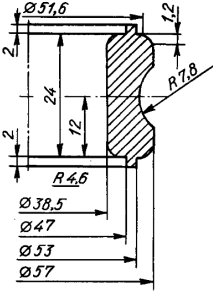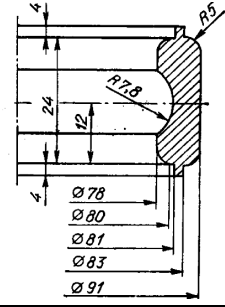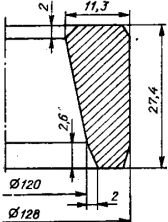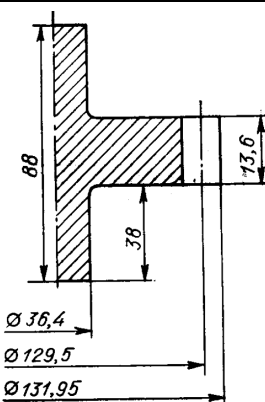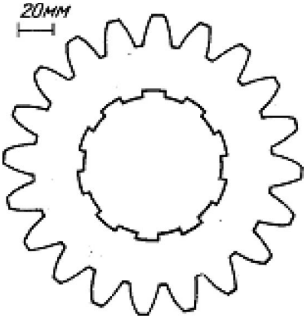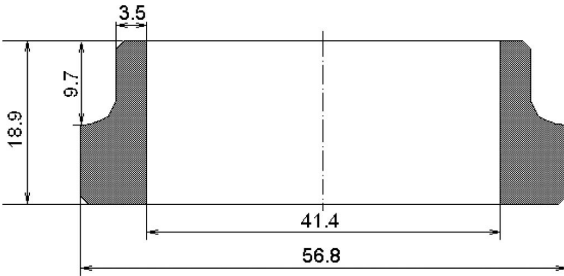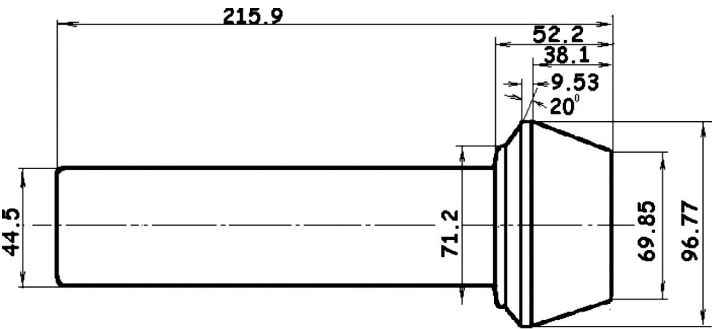
Shape	Sketch	K (m²)
Inner bearing ring 308		5.8×10^{-6}
Outer bearing ring 308		5.4×10^{-6}
Outer bearing ring 7215		8.89×10^{-6}
Gear		5.29×10^{-5}

TABLE 5—Kondratjev form factors *K* obtained from FEM calculations	
Steel part	K (m²)
	73×10^{-6}
	3.94×10^{-6}
	171×10^{-6}

The effect of agitation, the presence of additives, and quenchant contamination based on cooling characteristics can be investigated. The cooling rate is calculated by numerical differentiation of the probe thermocouple output temperature. On the basis of regular thermal condition theory, the use of standardized methods can be considerably extended. This is shown below.
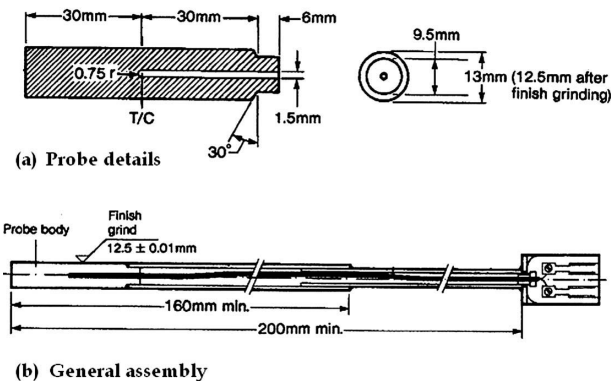
Fig. 10—The standardized Inconel 600 cylindrical probe used for testing different kinds of quenchants: (a) probe details; (b) general assembly [23–25].

One of the earliest probes used for the cooling curve analysis is shown in Fig. 11 [22]. This probe was constructed from a 100 × 300 mm (4 × 12 in.) SAE 5145 alloy by cutting it in half, yielding two 100 × 150 mm sections. Fig. 12 illustrates a smaller probe of 13 × 50 mm described by French [26].

Tagaya and Tamura [27] developed a Japanese Industrial Standard (JIS) for cooling curve acquisition that utilizes a cylindrical silver probe with a thermocouple assembly specifically constructed to determine the surface temperature change with time during quenching (see Fig. 13) [28]. Figs. 14 and 15 provide more information about cooling curve analysis.

Upon initial immersion of the heated probe into cold liquid, there are no bubbles on the metallic surface. At this time, cold liquid is heated to the boiling point of the liquid, and the surface temperature of the probe drops rapidly to the saturation temperature. In this extremely short period of time, heat transfer behaves as a convection process. When
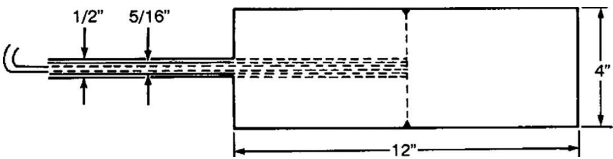
Fig. 11—The SAE 5145 steel probe used by Grossmann [22].
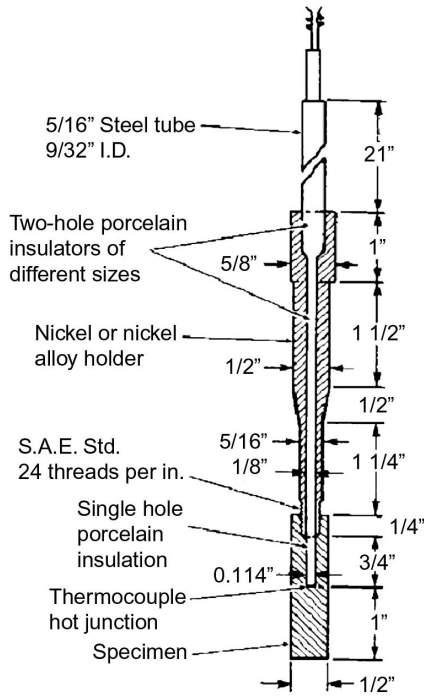
Fig. 12—The probe used by French [26].
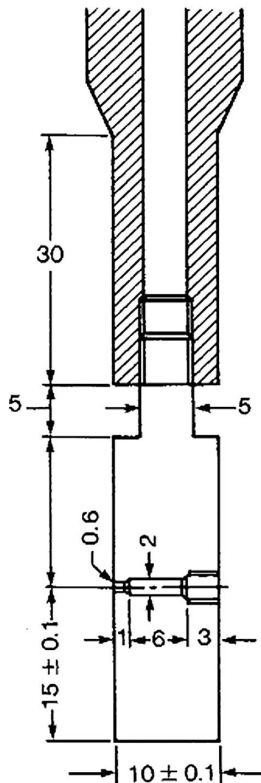
Fig. 13—JIS silver probe [27,28].
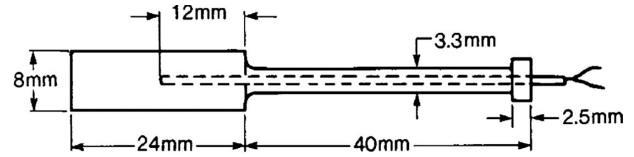
Fig. 14—Cylindrical silver probe [29].

film boiling is established when the initial heat flux density q_{in} is higher than the first critical heat flux density q_{cr1}, that is, when $q_{in} > q_{cr1}$. Nucleate boiling occurs immediately after shock boiling when $q_{in} < q_{cr1}$.

The different boiling processes are shown in Fig. 16. Here T_m is the temperature of the medium, T_s is saturation temperature, and T_{sf} is the surface temperature of the probe. In this last case, only nucleate boiling and convection prevail during cooling (see Fig. 17).

Typical cooling curves obtained during quenching of a steel ball 38 mm in diameter in cold water when full film boiling is absent are shown in Fig. 18. In this figure, line 1 is the core temperature and line 2 is the surface temperature.

Typical stages of cooling, with semilogarithmic coordinates (logarithm of temperature difference against time), are shown in Fig. 19. Here, line 1 illustrates cooling where full film boiling is eliminated, and line 2 illustrates cooling where full film boiling exists.

Shown in Fig. 20 are heat flux densities versus time, which were obtained both when full film boiling exists (a) and when it is absent (b) [10].

Using regular thermal condition theory, it is possible to determine heat transfer coefficients obtained by testing standardized probes. For the cooling rate curve shown in Fig. 21, the regular process starts at point 1. The cooling rate within the area 1–2 can be calculated by differentiation of Eq 6, which results in:

$$v = m(T - T_m). \qquad (21)$$

Proceeding from Eq 21, m and the Kondratjev number Kn can be evaluated because there is a correlation between m and Kn:

$$Kn = \frac{m}{m_\infty},$$

where:
$$m_\infty = \frac{a}{K};$$

a is the thermal diffusivity of the material; and

K is the Kondratjev form factor.

For an "infinitely" long cylinder whose length is more than four times its diameter, the Kondratjev form factor $K = R^2/5.783$.

For Fig. 21, the cooling rate at point 1 is equal to 44°C/s when the surface temperature is equal to 650°C. Assuming the quenchant (medium) temperature T_m is 50°C, then:

$$44°C/s = m \ (650°C - 50°C)$$

or

$$m = 0.073 \ s^{-1}.$$

If a standardized Inconel 600 probe with a diameter of 12.5 mm (see Fig. 10) was used, then it is possible to evaluate $m_\infty = \dfrac{5.784a}{R^2}$, which is true when $Bi \to \infty$. According to Table 6, the average value of thermal diffusivity a is equal to
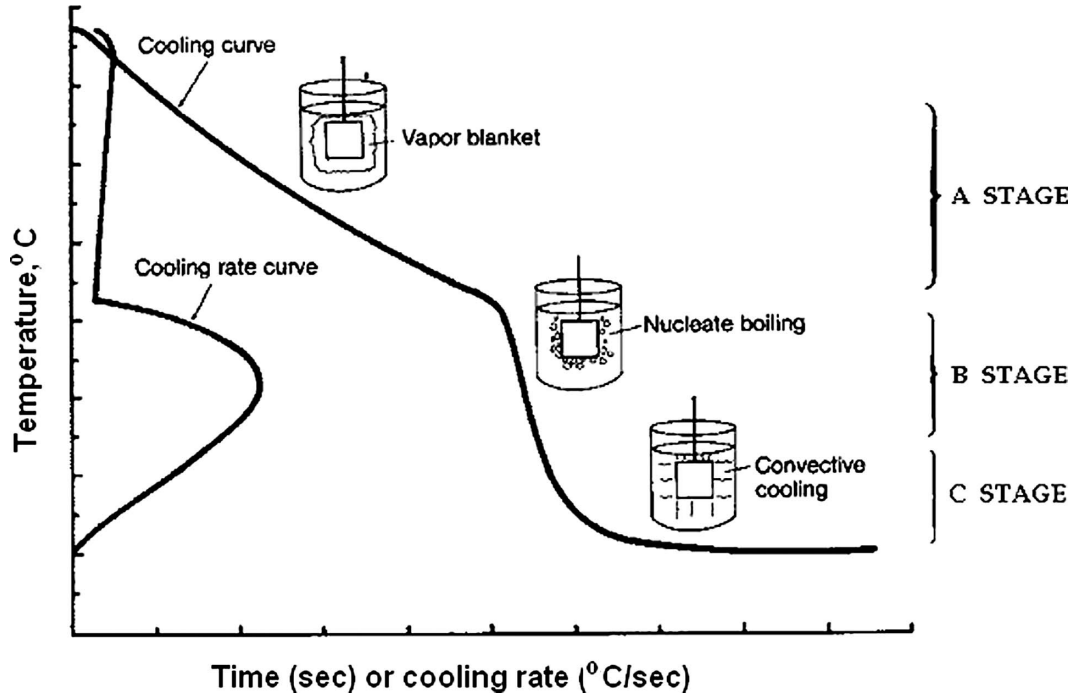
Fig. 15—Illustration of a typical cooling time–temperature curve and cooling rate curve [22].

4.6×10^{-6} m²/s when the temperature is 650°C. For the Inconel 600 probe, $R^2 = 1.5625 \times 10^{-6}$ m², which means that $m_\infty = 0.17$ s^{-1}. Using this value, we can calculate:

$$Kn = \frac{m}{m_\infty} = 0.073\,\text{s}^{-1}/0.17\,\text{s}^{-1} = 0.43.$$

From Eq 16, it follows that $Bi_V = 0.66$ when $Kn = 0.43$. The average heat transfer coefficient may then be calculated as follows:

$$Bi_V = \frac{\alpha}{\lambda}K\frac{S}{V} = 0.66$$
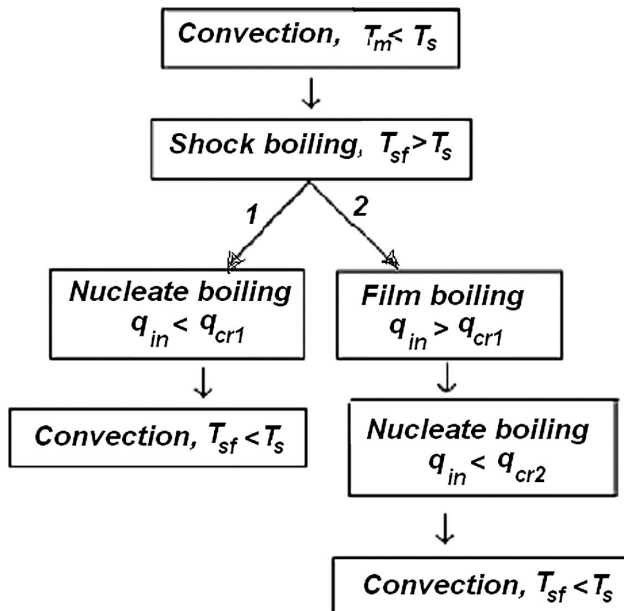
Fig. 16—Two possible boiling processes that may occur during quenching, depending on critical heat flux densities.

or

$$\alpha = \frac{0.66\lambda V}{KS} = 5775 \text{ W}/m^2\text{K}.$$

We also have $\lambda = 18.9$ W/mK; $K = 6.75 \times 10^{-6}$ m²; and $V/S = 0.00313$ m (see Tables 1 and 7).

Therefore, standardized methods, which as a rule utilize cylindrical probes with the thermocouple located at the geometric centers, provide only average data connected with the information on cooling capacity of quenchants. More accurate data can be received by solving the inverse problem [30–32]. For example, very accurate data can be achieved when utilizing the Liscic-Nanmac probe [33] (the inverse problem and Liscic-Nanmac probe are discussed in detail in Chapter 13). This probe may be used to [34–39]:

- Measure the duration of nonstationary nucleate boiling (the self-regulated thermal process)
- Measure heat flux densities and heat transfer coefficients during self-regulated thermal processes
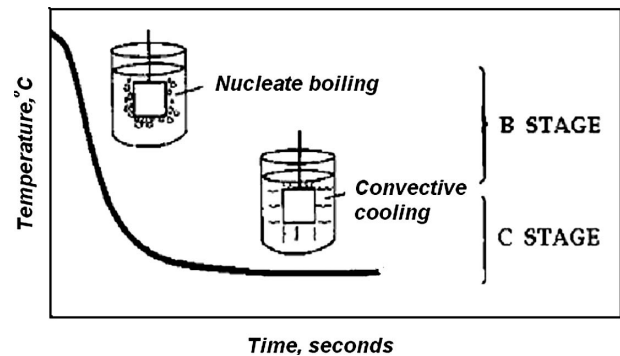
Fig. 17—The two stages of cooling versus time, where nucleate boiling and convection are the primary modes of heat transfer and full film boiling is absent.
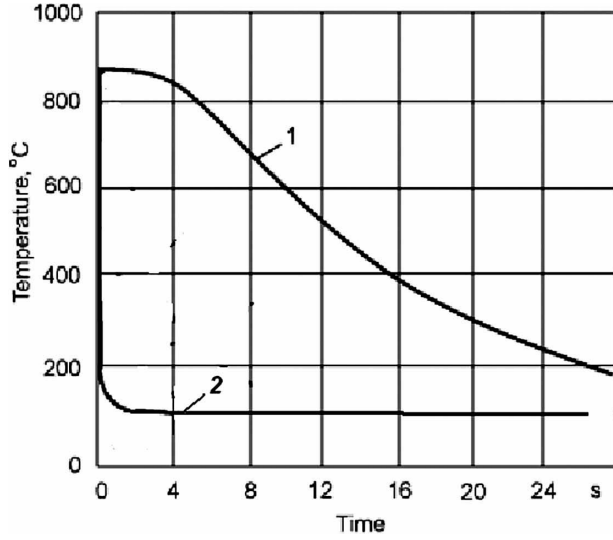
Fig. 18—Typical cooling curves obtained during quenching of a steel ball 38 mm in diameter in cold water when film boiling is absent: 1, core temperature; 2, surface temperature.
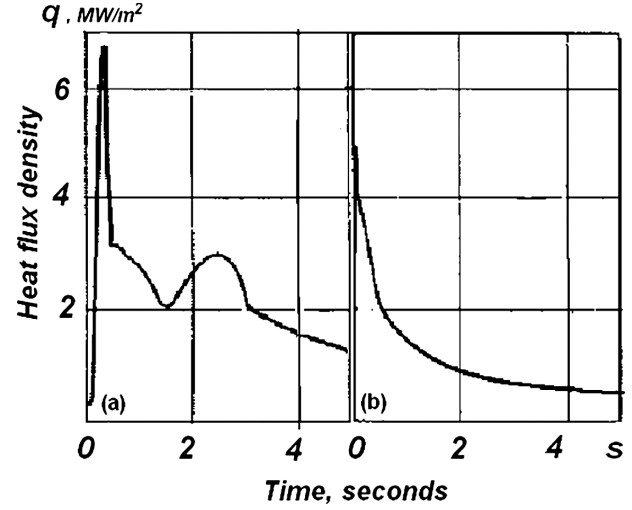
Fig. 20—Heat flux density versus time: (a) when full film boiling exists; (b) when full film boiling is absent [10].
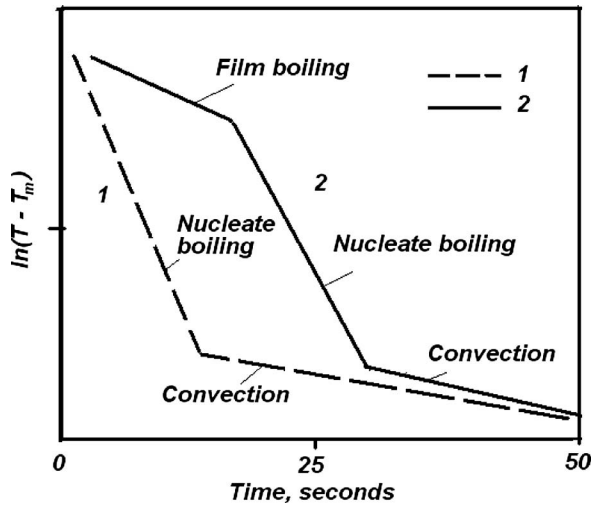
Fig. 19—Typical stages of cooling, shown as the logarithm of temperature difference against time: 1, when full film boiling is eliminated; 2, when full film boiling exists.

Fig. 21—Cooling rate versus surface temperature, showing the regular condition area (1–2) where average heat transfer coefficients can be evaluated.

- Investigate initial heat flux density during immersion of the probe into a quenchant and compare results of measurements with the results of solving parabolic and hyperbolic heat transfer equations to improve existing standards[2]

6.5 DISCUSSION

It was shown in Chapter 5 that the cooling time for any shape of steel part can be calculated using generalized equation 69:

$$m\tau = \left[\frac{kBi_v}{2.095 + 3.867Bi_v} + \ln\frac{T_0 - T_m}{T - T_m} \right] \quad (22)$$

where:

$m = \frac{aKn}{K}$; and

$k = 1$, 2, or 3 for a plate, cylinder, or ball, respectively.

In practice, it is important to compare the results of calculations of the value $m\tau$ with experimental data obtained for the condition $Bi \to \infty$. Table 8 below presents such a comparison. The results of calculations were achieved for

$$\theta = \frac{T - T_m}{T_0 - T_m} = 0.01.$$

This means that:

$$\ln\frac{T_0 - T_m}{T - T_m} = 4.605.$$

---

[2] Currently, the significance of creating a database for cooling capacities of various quenchants to be used in practice by engineers, scientists, and designers is being considered as described in [40].

TABLE 6—Thermal diffusivity *a* of Inconel 600 material versus temperature									
T (°C)	100	200	300	400	500	600	700	800	900
$a \cdot 10^6, \frac{m^2}{s}$	3.7	4.1	4.3	4.8	5.1	5.4	5.6	5.8	6.0
$\bar{a} \cdot 10^6, \frac{m^2}{s}$	3.7	3.9	4.0	4.25	4.4	4.55	4.65	4.75	4.85

Note: $\bar{a}$ is the mean value for the range between 100°C and the stated temperature.

TABLE 7—Thermal conductivity of Inconel 600 versus temperature

T (°C)	100	200	300	400	500	600	700
$\lambda, \frac{W}{mK}$	14.2	16	17.8	19.7	21.7	23.7	25.9
$\bar{\lambda}, \frac{W}{mK}$	14.2	15.1	16.4	16.73	17.23	17.7	20.05

Note: $\bar{\lambda}$ is the mean value for the range between 100°C and the stated temperature.

Furthermore, the ratio

$$\frac{kBi_v}{2.095 + 3.687Bi_v},$$

when $Bi \to \infty$, for the plate-shaped form, cylindrical form, and spherical form has the values 0.258, 0.517, and 0.775, respectively. Taking into account these results, $m\tau$ equates to 4.863, 5.122, and 5.38, respectively, for the three forms. From Table 8, it is evident that the calculation and experimental results correlate very well with each other.

Knowing the value Bi_V, it is possible to calculate the cooling time for any condition when the Kondratjev number Kn can be obtained from Table 9 or 10. Table 9 is used for

TABLE 8—Dimensionless values of relative temperature θ_{reg} and $m\tau$ for points most remote from the surface for bodies of various shapes ($\theta = 0.01$)

Specimen shape	θ_{reg} (experiment)	$m\tau$	
		Experiment	Calculations
Plate	0.98	4.85	4.863
Rectangular prism	0.76	5.00	5.082
Cylinder	0.76	5.09	5.122
Cube	0.61	5.30	5.380
Wedge, $\varphi_o = 10°$	0.88	4.97	4.960
Wedge, $\varphi_o = 15°$	0.75	5.00	5.070
Wedge, $\varphi_o = 30°$	0.74	5.04	5.110
Wedge, $\varphi_o = 45°$	0.76	5.10	5.200
Gear	0.77	5.00	—

conventional cooling technologies, and Table 10 for intensive cooling technologies when $Kn > 0.8$ [37].

It should be noted that Bi_V and Kn during heating and cooling of steel parts can only be positive values. If Bi_V were negative, then Eq 6 would be

$$\theta = A_1 U_1 e^{m_1 \tau},$$

which is not possible. During heating, Eq 6 is written as:

$$\theta = 1 - A_1 U_1 e^{-m_1 \tau}$$

and during quenching, it is written as:

$$\theta = A_1 U_1 e^{-m_1 \tau}.$$

Since the generalized equation 22 is used for both heating and cooling processes, and since Bi_V and Kn are always positive, the difference is only in the term

$$\ln \frac{T_0 - T_m}{T - T_m},$$

which is used for quenching, whereas

$$\ln \frac{T_0 - T_m}{T_0 - T}$$

is used for heating process calculations.

6.5.1 Example of Cooling Time Calculation

Assume that a cylinder 20 mm in diameter and 40 mm in height is cooled at the core from 900°C to 9°C in cold water at 0°C. For this cooling condition, Kn = 0.6, determined by experiment [10]. The Kondratjev form factor K, according to Table 1, is:

$$K = \frac{1}{\frac{5.783}{R^2} + \frac{9.87}{Z^2}} = 15.63 \times 10^{-6} m^2.$$

As was shown previously for a cylinder-shaped form, $m\tau = 5.122$ when

$$\theta = \frac{T - T_m}{T_0 - T_m} = 0.01$$

and $a = 5.55 \times 10^{-6}$ m²/s (see Tables 11 and 12). Then cooling time, according to Eq 22, is:

$$\tau = \frac{5.122 x 15.63 x 10^{-6} m^2}{5.55 x 10^{-6} \frac{m^2}{s} x 0.6} = 24.04 \, sec.$$

The correlations between the generalized Biot number Bi_V and the simple number Bi for bodies that are plate-shaped, cylindrical, and spherical are: $Bi_V = 0.405Bi$, $Bi_V = 0.346Bi$ and $Bi_V = 0.304Bi$, respectively [20,21]. These simplified calculations can be used by engineers and heat treaters when designing optimizing cooling processes [32,33].

TABLE 9—Relationships between generalized small and average Biot number (Bi$_v$ < 4), criterion of temperature field nonsmoothness (Ψ), and Kondratjev number (Kn)

Bi$_v$	Ψ	Kn	Bi$_v$	Ψ	Kn	Bi$_v$	Ψ	Kn
0.00	1.00000	0.00000	0.68	0.64000	0.43536	1.95	0.36263	0.70712
0.01	0.99284	0.00993	0.70	0.63297	0.44308	2.00	0.35637	0.71274
0.02	0.98574	0.01971	0.72	0.62585	0.45061	2.05	0.35032	0.71816
0.04	0.97171	0.03887	0.74	0.61887	0.45796	2.10	0.34447	0.72338
0.06	0.95791	0.05747	0.76	0.61200	0.46513	2.15	0.33880	0.72841
0.08	0.94434	0.07555	0.78	0.60531	0.47214	2.20	0.33331	0.73328
0.10	0.93101	0.09310	0.80	0.59873	0.47898	2.25	0.32799	0.73797
0.12	0.91792	0.11015	0.82	0.59227	0.48566	2.30	0.32283	0.74251
0.14	0.90507	0.12671	0.84	0.58594	0.49319	2.35	0.31783	0.74690
0.16	0.89246	0.14279	0.86	0.57973	0.49857	2.40	0.31298	0.75115
0.18	0.88009	0.15842	0.88	0.57364	0.50480	2.45	0.30827	0.75525
0.20	0.86796	0.17359	0.90	0.56766	0.51089	2.50	0.30369	0.75923
0.22	0.85607	0.18833	0.92	0.56179	0.51851	2.55	0.29925	0.76309
0.24	0.84441	0.20266	0.94	0.55604	0.52268	2.60	0.29493	0.76682
0.26	0.83298	0.21657	0.96	0.55039	0.52837	2.65	0.29074	0.77045
0.28	0.82178	0.23010	0.98	0.54484	0.53395	2.70	0.28665	0.77396
0.30	0.81081	0.24324	1.00	0.53940	0.53940	2.75	0.28268	0.77737
0.32	0.80007	0.25602	1.05	0.52622	0.55253	2.80	0.27882	0.78069
0.34	0.78954	0.26844	1.10	0.51362	0.56498	2.85	0.27505	0.78390
0.36	0.77923	0.28052	1.15	0.50157	0.57680	2.90	0.27139	0.78703
0.38	0.76913	0.29227	1.20	0.49003	0.58804	2.95	0.26782	0.79007
0.40	0.75923	0.30369	1.25	0.47898	0.59873	3.00	0.26434	0.79302
0.42	0.74954	0.31481	1.30	0.46839	0.60891	3.05	0.26095	0.79590
0.44	0.74005	0.32562	1.35	0.45823	0.61861	3.10	0.25764	0.79870
0.46	0.73076	0.33615	1.40	0.44848	0.62787	3.15	0.25442	0.80142
0.48	0.72166	0.34640	1.45	0.43911	0.63672	3.20	0.25127	0.80407
0.50	0.71274	0.35637	1.50	0.43011	0.64517	3.25	0.24820	0.80665
0.52	0.70401	0.36608	1.55	0.42146	0.65326	3.30	0.24520	0.80917
0.54	0.69545	0.37555	1.60	0.41312	0.66100	3.35	0.24228	0.81162
0.56	0.68708	0.38476	1.65	0.40510	0.66842	3.40	0.23942	0.81402
0.58	0.67887	0.39374	1.70	0.39737	0.67553	3.45	0.23662	0.81635
0.60	0.67082	0.40249	1.75	0.38992	0.68236	3.50	0.23389	0.81863
0.62	0.66294	0.41103	1.80	0.38273	0.68892	3.55	0.23122	0.82085
0.64	0.65522	0.41934	1.85	0.37580	0.69523	3.60	0.22862	0.82302
0.66	0.64766	0.42745	1.90	0.36910	0.70129	3.65	0.22606	0.82513

TABLE 10—Relationships between generalized large Biot number ($Bi_v > 4$), criterion of temperature field nonsmoothness (Ψ), and Kondratjev number (Kn)

Bi_v	Ψ	Kn	Bi_v	Ψ	Kn	Bi_v	Ψ	Kn
3.70	0.22357	0.82720	5.45	0.16109	0.87796	12.5	0.07555	0.94434
3.75	0.22113	0.82922	5.50	0.15981	0.87898	13.0	0.07280	0.94641
3.80	0.21874	0.83120	5.55	0.15855	0.87998	13.5	0.07025	0.94833
3.85	0.21640	0.83313	5.60	0.15732	0.88096	14.0	0.06787	0.95012
3.90	0.21411	0.83501	5.65	0.15609	0.88193	14.5	0.06564	0.95179
3.95	0.21186	0.83686	5.70	0.15489	0.88289	15.0	0.06356	0.95336
4.00	0.20967	0.83866	5.75	0.15371	0.88383	15.5	0.06160	0.95482
4.05	0.20751	0.84043	5.80	0.15254	0.88475	16.0	0.05976	0.95620
4.10	0.20540	0.84216	5.85	0.15140	0.88566	16.5	0.05803	0.95749
4.15	0.20334	0.84385	5.90	0.15026	0.88656	17.0	0.05639	0.95871
4.20	0.20131	0.84551	5.95	0.14915	0.88744	17.5	0.05485	0.95986
4.25	0.19932	0.84713	6.00	0.14805	0.88831	18.0	0.05339	0.96095
4.30	0.19738	0.84872	6.10	0.14590	0.89001	18.5	0.05200	0.96198
4.35	0.19547	0.85027	6.20	0.14382	0.89165	19.0	0.05068	0.96296
4.40	0.19359	0.85180	6.30	0.14179	0.89325	19.5	0.04943	0.96389
4.45	0.19175	0.85329	6.40	0.13981	0.89480	20.0	0.04824	0.96478
4.50	0.18995	0.85476	6.50	0.13789	0.89631	21.0	0.04602	0.96642
4.55	0.18817	0.85619	6.60	0.13603	0.89778	22.0	0.04400	0.96792
4.60	0.18644	0.85760	6.70	0.13421	0.89920	23.0	0.04214	0.96929
4.65	0.18473	0.85898	6.80	0.13244	0.90059	24.0	0.04044	0.97055
4.70	0.18305	0.86034	6.90	0.13072	0.90194	25.0	0.03887	0.97171
4.75	0.18140	0.86167	7.00	0.12904	0.90325	26.0	0.03741	0.97278
4.80	0.17979	0.86297	7.20	0.12580	0.90578	27.0	0.03607	0.97377
4.85	0.17820	0.86426	7.40	0.12273	0.90817	28.0	0.03481	0.97470
4.90	0.17664	0.86551	7.60	0.11980	0.91045	29.0	0.03364	0.97556
4.95	0.17510	0.86675	7.80	0.11700	0.91262	30.0	0.03255	0.97636
5.00	0.17359	0.86796	8.00	0.11434	0.91468	35.0	0.02799	0.97970
5.05	0.17211	0.86915	8.50	0.10817	0.91945	40.0	0.02456	0.98221
5.10	0.17065	0.87032	9.00	0.10263	0.92371	45.0	0.02187	0.98417
5.15	0.16922	0.87147	9.50	0.09764	0.92754	50.0	0.01971	0.98574
5.20	0.16781	0.87260	10.0	0.09310	0.93101	60.0	0.01647	0.98810
5.25	0.16642	0.87371	10.5	0.08897	0.93416	70.0	0.01414	0.98979
5.30	0.16506	0.87480	11.0	0.08519	0.93704	80.0	0.01239	0.99106
5.35	0.16371	0.87587	11.5	0.08171	0.93967	100	0.00993	0.99284
5.40	0.16239	0.87692	12.0	0.07851	0.94210	∞	0.00000	1.00000

TABLE 11—Thermal conductivity of supercooled austenite versus temperature									
T (°C)	100	200	300	400	500	600	700	800	900
$\bar{\lambda}, \frac{W}{mK}$	17.5	17.75	18.55	19.25	20.25	21.15	21.90	22.65	23.4
Note: $\bar{\lambda}$ is the mean value for the range between 100°C and the stated temperature.									

TABLE 12—Thermal diffusivity a of supercooled austenite versus temperature									
T (°C)	100	200	300	400	500	600	700	800	900
$\bar{a} \cdot 10^6, \frac{m^2}{S}$	4.55	4.59	4.625	4.75	4.95	5.10	5.19	5.37	5.55
Note: $\bar{a}$ is the mean value for the range between 100°C and the stated temperature.									

6.6 A PROBLEM TO BE SOLVED IN THE NEAREST FUTURE

As is well known, the heat conductivity differential parabolic equation is solved by use of the standard method of variable separation. The partial solution in this case can be presented as [4]:

$$T = C\theta(\tau)\vartheta(x,y,z), \qquad (23)$$

where C is a constant. Then the heat conductivity differential equation can be rewritten as:

$$\frac{\theta'(\tau)}{\theta(\tau)} = \frac{a\nabla^2\vartheta(x,y.z)}{\vartheta(x,y,z)}. \qquad (24)$$

This technique works because the product of functions of independent variables (the left and right parts of Eq 24) are constant, that is:

$$\frac{\theta'(\tau)}{\theta(\tau)} = D = const \qquad (25)$$

$$\frac{a\nabla^2\vartheta(x,y.z)}{\vartheta(x,y,z)} = D = const \qquad (26)$$

A partial solution for Eq 25 is:

$$\theta(\tau) = e^{D\tau}. \qquad (27)$$

The constant D is selected from the main postulate of thermodynamics, which says that in a closed system, sooner or later thermal equilibrium is always established. To satisfy this law, the constant D must be as follows:

$$D = -ak^2, \qquad (28)$$

where:
a is the thermal diffusivity of a material; and
k is evaluated from the boundary condition.

However, ak^2 is always a positive value and cannot be negative; that is:

$$ak^2 > 0. \qquad (29)$$

This means that Tables 9 and 10 must provide only positive generalized Biot numbers. Bi_V cannot be, for example, −0.7185, because that would contradict the main postulate of thermodynamics.

For example, the cooling process in the regular stage can be evaluated using the plain exponent

$$\frac{T - T_m}{T_0 - T_m} = Ae^{-Fo_V\psi Bi_V}, \qquad (30)$$

where:
$Fo_V = \frac{a\tau}{K}$ is the generalized Fourier number;
ψ is the criterion of nonsmoothness temperature distribution; and
Bi_V is the generalized Biot number.

All of these numbers must be only positive values. If one of them is negative, then Eq 30 will give no real solution:

$$\frac{T - T_m}{T_0 - T_m} = Ae^{Fo_V\psi Bi_V}, \qquad (31)$$

which is nonsense from the point of view of mathematical physics because, in this case, during quenching the temperature would exponentially increase.

The question is, is a generalized Fourier number being introduced for complicated steel parts? Conventional Fourier numbers for slab, cylinder, and ball are written as

$$Fo = \frac{a\tau}{R^2},$$

where R is half the thickness of each body. Since it is not possible to locate a similar thickness for a gear, for example, should the half-thickness of a gear tooth or the half-thickness of the main body of the gear be used? This was not known until now. Therefore, the generalized Fourier number is introduced to solve this problem:

$$Fo_V = \frac{a\tau}{K}, \qquad (32)$$

where:
$K = \frac{4R^2}{\pi^2}$ for a slab;
$K = \frac{R^2}{5.784}$ for a cylinder; and
$K = \frac{R^2}{\pi^2}$ for a ball.

For a gear, the generalized Biot number is Fo_V (Eq 32), where K can be taken from Table 5. Thus, the problem connected with the cooling process during quenching is solved for any configuration of steel parts in the regular condition stage.

However, the problem is not solved completely because there still exists a contradiction between the main postulate of thermodynamics and the exponential law of cooling. From Eq 30, it follows that the thermal equilibrium is established when time of cooling tends to infinity, that is, $\tau \to \infty$, but the main postulate of thermodynamics says that the thermal equilibrium is

established in a finite period of time. There is an uncertainty here. To solve this problem, the laws of statistical physics should be considered. There is no sense considering the exponential law of cooling if the temperature difference at the end of cooling is comparable with the average temperature oscillation in a closed system. This problem is now under consideration, and hopefully it will be solved in the near future [34].

It should be noted that, at the present time, a database for Kondratjev numbers is under development. For this purpose, Hart [16], Dante (USA) [17], or Hearts (Japan) [18] software can be used. All results of calculations presented in Chapters 6 and 7 were made using Hart software (the name Hart was chosen from the root of the Ukrainian word for quenching: *hartuvannya*).

References

[1] Kondratjev, G. M., *Regulyarnyi Teplovoy Rezhim* (Regular thermal mode), Gostekhizdat, Moscow, 1954.

[2] Kondratjev, G. M., Regular Thermal Processes, *Proceedings of LITMO,* No. 37, 1959, pp. 5–16.

[3] Isachenko, V. P., Osipova, V. A., and Sukomel, A. S., *Teploperedacha* (Heat transfer), Energomash, Moscow, 1981.

[4] Lykov, A. V., *Teoriya Teploprovodnosti* (Theory of heat conductivity), Vysshaya Shkola, Moscow, 1967.

[5] Kobasko, N. I., Thermal Processes at Steel Quenching, author's thesis of Ph.D. dissertation, Institute of Thermal Science of the National Academy of Sciences of Ukraine, Kyiv, 1969.

[6] Tret'yachenko, G. N., and Kravchuk, L. V., On the Regular Heat Conditions of Solids of Complex Shapes, *Journal of Engineering Physics and Thermophysics,* Vol. 5, No. 8, 1961, pp. 132–137.

[7] Tret'yachenko, G. N., The Basic Preconditions for the Regular Thermal Regime Theory, *Journal of Engineering Physics and Thermophysics,* Vol. 5, No. 9, 1962, pp. 105–111.

[8] Dul'nev, G. N., On Regularization of Temperature Fields, *Journal of Engineering Physics and Thermophysics,* Vol. 5, No. 9, 1962, pp. 112–117.

[9] Chaplina, A. I., On the Criterion of Regular Thermal Regime Under Various Conditions, *Journal of Engineering Physics and Thermophysics,* Vol. 5, No. 9, 1962, pp. 118–125.

[10] Kobasko, N. I., *Steel Quenching in Liquid Media Under Pressure,* Naukova Dumka, Kyiv, 1980.

[11] *Journal of Engineering Physics and Thermophysics,* Vol. 5, 1962, available at www.itmo.by/jepter/CONTE/051962e/conte05.html.

[12] Kondratjev, G. M., *Teplovye Izmereniya* (Thermal measurements), Mashgiz, Moscow, 1957.

[13] Mikheev, M. A., and Mikheeva, I. M., *Osnovy teploperedachi* (Basics of heat transfer), Energy, Moscow, 1977.

[14] Zienkiewiez, O. C., *Finite Element Method in Engineering Science,* Mir, Moscow, 1975.

[15] Kobasko, N. I., Morhuniuk, W. S., and Gnuchiy, Yu. B., *Investigation of Technological Processes of Machine Part Treatment,* Znanie, Kyiv, 1979.

[16] Kobasko, N. I., Morhuniuk, W. S., and Dobrivecher, V. V., Software "Tandem-Hart Analysis" (commercially available from Intensive Technologies Ltd. Kyiv, Ukraine, managers@itl.kiev.ua, www.itl.kiev.ua).

[17] Ferguson, B. L., Freborg, A., and Petrus, G. J., Software Simulates Quenching, *Heat Treating Progress,* 2000, pp. H31–H36.

[18] Inoue, T., and Arimoto, K., Development and Implementation of CAE System "HEARTS" for Heat Treatment Simulation Based on Metallo-thermo-mechanics, *Journal of Materials Engineering and Performance,* Vol. 6, No. 1, 1997, pp. 51–60.

[19] Inoue, T., Metallo-thermo-mechanics: Application to Quenching, *Handbook of Residual Stress and Deformation of Steel,* Totten, G., Howes, M., and Inoue, T., Eds., ASM International, Materials Park, OH, 1992, p. 499.

[20] Kobasko Nikolai, Simplified Method of Calculations for Engineers Dealing with Quenching Design Processes, *Proceedings of the 7th International Conference on Equipment and Technologies*

[21] for Heat Treatment of Metals and Alloys, OTTOM-7,* Kharkov, Ukraine, April 24–28, 2006, pp. 12–21.

[21] Aronov, M. A., Kobasko, N. I., Powell, J. A., and Hernandez-Morales, J. B., Correlation between Grossmann H-Factor and Generalized Biot Number Bi_V, *Proceedings of the 5th WSEAS International Conference on Heat and Mass Transfer (HMT '08),* Acapulco, Mexico, January 25–27, 2008, pp. 122–126.

[22] Totten, G. E., Bates, C. E., and Clinton, M. A., Cooling Curve Analysis, *Handbook of Quenchants and Quenching Technology,* ASM International, Materials Park, OH, 1993, pp. 69–128.

[23] ASTM Standard D6200-97: Standard Test Method for Determination of Cooling Characteristics of Quench Oils by Cooling Curve Analysis, *Annual Book of ASTM Standards,* ASTM International, West Conshohocken, PA, 2001.

[24] ASTM Standard D6482-99: Standard Test Method for Determination of Cooling Characteristics of Aqueous Polymer Quenchants with Agitation (Tensi Method), *Annual Book of ASTM Standards,* ASTM International, West Conshohocken, PA, 2000.

[25] ASTM Standard D6549-00: Standard Test Method for Determination of Cooling Characteristics of Quenchants by Cooling Curve Analysis with Agitation (Drayton Unit), *Annual Book of ASTM Standards,* ASTM International, West Conshohocken, PA, 2000.

[26] French, H. J., A Study of the Quenching of Steels, *Transactions ASST,* May, 1930, pp. 646–727.

[27] Tagaya, M., and Tamura, I., Use of the Silver Sample to Investigate Quenching Process, *Hart. Tech. Mitt.,* Vol. 18, 1963, pp. 63–67.

[28] Heat Treating Oil, Japanese Industrial Standard K 2242, 1980.

[29] Laboratory Test for Assessing the Cooling Curve Characteristics of Industrial Quenching Media, Wolfson Heat Treatment Centre Engineering Group Specification, Wolfson Heat Treating Centre, Aston University, Aston Triangle, Birmingham, England, 1982.

[30] Beck, J. V., and Osman, A. M., Analysis of Quenching and Heat Treating Processes Using Inverse Heat Transfer Method, *Proceedings of Quenching and Distortion Control Conference,* ASM International, September 22–25, 1992, Chicago, pp. 147–154.

[31] Krukovskyi, P. G., *Inverse Heat and Mass Transfer Problems (General Engineering Approach),* Engineering Thermal-Science Institute, Kyiv, 1998.

[32] Tikhonov, A. N., and Glasko, V. B., Application of Regularization Method in Non-Linear Problems, *Jour. of Comp. Math. and Math. Physics,* Vol. 5, No. 3, 1965.

[33] Liščič, B., Tensi, H. M., and Luty, W., *Theory and Technology of Quenching,* Springer-Verlag, Berlin, 1992, pp. 219–247.

[34] Kobasko, N. I., and Guseynov, Sh. E., Initial Heat Flux Densities and Duration of Non-stationary Nucleate Boiling During Quenching, *Proceedings of the 5th WSEAS International Conference on Heat and Mass Transfer (HMT '08),* Acapulco, Mexico, January 25–27, 2008, pp. 104–109.

[35] Kobasko, N. I., What Is Duration of Non-stationary Nucleate Boiling and Thermal Equilibrium During Quenching of Steel Parts? *Proceedings of the 6th IASME/WSEAS International Conference on Heat Transfer, Thermal Engineering and Environment (HTE '08),* Rhodes, Greece, August 20–22, 2008, pp. 529–533.

[36] Krukovskyi, P., Kobasko, N., and Yurchenko, D., Generalized Equation for Cooling Time Evaluation and Its Verification by CFD Analysis, *Journal of ASTM International,* Vol. 6, No. 5, 2009.

[37] Kobasko, N. I., Quenching Apparatus and Method for Hardening Steel Parts, U.S. Patent No. 6,364,974 BI, April 2, 2002.

[38] Dobryvechir, V. V., Kobasko, N. I., Zotov, E. N., Morhuniuk, W. S., and Sergeyev, Yu. S., *Software IQLab* (commercially available from Intensive Technologies Ltd., Kyiv, Ukraine, iqlab@itl.kiev.ua, www.itl.kiev.ua).

[39] Kobasko, N. I., Energy Efficient and Eco-friendly Intensively Quenched Limited Hardenability Low Alloy Steels, *Journal of ASTM International,* Vol. 6, No. 1, 2009.

[40] Kobasko, N. I., Database for Cooling Capacities of Various Quenchants to Be Developed with the Modern Computational and Experimental Techniques, 2006, www.worldses.org/projects/Heat_and_Mass_Transfer.doc.

7

Stress State of Steel Parts During Intensive Quenching

N. I. Kobasko[1]

7.1 INTRODUCTION

It is important to study the effect of cooling during quenching on the magnitude and distribution of residual stresses that remain in parts after their complete cooling, because the service life of machine parts depends on mechanical properties of the material as well as residual stresses. Tensile stresses at the surface of a hardened part reduce its service life, while compressive stresses increase the service life. Furthermore, tensile stresses produce a greater propensity for quench crack formation.

It is known that high surface compressive stresses arise during superficial quenching or quenching of carburized parts. To prevent quench cracks in through-hardening, heat treaters often use oil cooling and alloy steels to increase hardenability. When quenching in oil, stresses are low (due to relatively small temperature gradients), and alloying provides sufficient hardenability of parts. However, more benefits can be obtained when using plain carbon steels combined with intensive quenching with water, although there is a problem of quench-crack prevention due to intensive cooling.

7.2 INTENSIVE QUENCHING PROCESS VARIATIONS

This chapter describes the study of the effect of heat transfer intensity on the magnitude of the residual stresses arising from quenching of cylindrical specimens and steel parts made of various steel grades. It should be noted that regularities of stress distribution during quenching were used to develop the IQ-1, IQ-2, and IQ-3 processes, which may be characterized by high Grossmann factor H > 5 [1].

The *IQ-1 process* is a two-step process. In the first step, a steel part is cooled slowly in oil, an aqueous polymer solution, molten salt, air, or some other media. Upon cooling to the martensite start temperature M_S, the part is intensively cooled within the martensite range until the cooling process is completed [2,3]. During this first step, the austenite–martensite transformation is delayed almost completely, and intensive cooling is performed only within the martensite range. The temperature gradient is not large, and the temperatures at all points in the cross-section transform uniformly and simultaneously to the martensite start temperature. Generally, oils are used at the optimal temperature and polymers are used at the optimal concentration, temperature, and agitation rate.

The *IQ-2 process* is also two-step quenching. In the first step, a part is intensively cooled after austenitizing until

nucleate boiling ceases. Then the part is air cooled to allow equalization of the temperature through the cross-sections. After this process, the part is intensively cooled a second time until the cooling process is completed. There is no nucleate boiling in the second step. The IQ-2 process is based on the self-regulated thermal process [2] (see Chapter 10).

The *IQ-3 process* is the most intensive process because film boiling and nucleate boiling are both completely prevented. Direct convection heat transfer is facilitated by intensive jets or water flows until maximum surface compressive stresses are achieved. The IQ-3 process can be applied to any part in which the optimal depth of the hardened layer can be achieved by interrupting intensive quenching at the appropriate time [4].

The optimal depth of hardness can be also achieved by the proper selection of the chemical composition of steel to provide shell hardening. The basis for the IQ-3 process is the formation of an optimal quenched layer, which is achieved when the Biot number Bi_V is greater than 5 [5]. There is a correlation between the generalized Biot number Bi_V and the conventional Biot number Bi; for bodies that are plate-shaped, cylindrical, or spherical, the correlations are $Bi_V = 0.405Bi$; $Bi_V = 0.346Bi$; and $Bi_V = 0.304Bi$, respectively [1].

In mathematical modeling of thermal and stress-strain states during quenching, a group of equations consisting of the nonlinear equation of transient heat conduction and the corresponding equations of the plasticity theory have been solved. The mathematical model of the processes to be studied is presented below.

7.3 MATHEMATICAL MODELS FOR THE CALCULATION OF THERMAL AND STRESS-STRAIN STATES

The coupled equation of transient heat conduction is [5–9]:

$$c\rho \frac{\partial T}{\partial \tau} - div(\lambda grad T) - \sigma_{ij}\dot{\varepsilon}_{ij}^p + \sum \rho_I l_I \dot{\xi}_I = 0, \qquad (1)$$

with corresponding boundary conditions for film boiling:

$$\left[\frac{\partial T}{\partial r} + \frac{\alpha_f}{\lambda}(T - T_S)\right]_{r=R} = 0 \qquad (2)$$

and initial conditions:

$$T(r, 0) = T_0. \qquad (3)$$

The transition from film boiling to nucleate boiling occurs when the following is fulfilled:

$$q_{cr2} = \alpha_f(T_{sf} - T_S), \qquad (4)$$

---

[1] *IQ Technologies, Inc., Akron, Ohio, and Intensive Technologies Ltd., Kyiv, Ukraine*

where:

$$q_{cr2} = 0.2q_{cr1}. \tag{5}$$

During nucleate boiling, the boundary conditions are:

$$\left[\frac{\partial T}{\partial r} + \frac{\beta^m}{\lambda}(T - T_S)^m\right]_{r=R} = 0 \tag{6}$$

and

$$T(r, \tau_f) = \varphi(r). \tag{7}$$

Finally, in the convection stage, the boundary conditions are similar to those for film boiling:

$$\left[\frac{\partial T}{\partial r} + \frac{\alpha_{conv}}{\lambda}(T - T_m)\right]_S = 0 \tag{8}$$

and

$$T(r, \tau_{nb}) = \psi(r). \tag{9}$$

The condition of transfer from nucleate boiling to one-phase convection is given by $q_{nb} = q_{conv}$. These equations determine boundary conditions of the third kind and describe conditions of heat transfer processes. However, in practice, boundary conditions of the first kind that are obtained from experimental data are often used. In this case, the primary differential equation of heat conductivity must be added with the above conditions:

$$T(r_i, \tau)|_{r_i=R_i} = \varphi(R_i, \tau) \tag{10}$$

where i is the coordinate index and $\varphi(R_i, \tau)$ is a value of temperature at different points of the cooling surface.

Plasticity theory equations are presented in detail in [5,8,9] and have the following form:

$$\dot{\varepsilon}_{ij} = \dot{\varepsilon}^p_{ij} + \dot{\varepsilon}^e_{ij} + \dot{\varepsilon}^T_{ij} + \dot{\varepsilon}^m_{ij} + \dot{\varepsilon}^{tp}_{ij} \tag{11}$$

with relevant initial and boundary conditions, where:
T is temperature;
σ_{ij} is stress
$\dot{\varepsilon}_{ij}$ is total strain rate;
$\dot{\varepsilon}^e_{ij}$ is elastic strain rate;
$\dot{\varepsilon}^p_{ij}$ is plastic strain rate;
$\dot{\varepsilon}^T_{ij}$ is thermal strain rate;
$\dot{\varepsilon}^m_{ij}$ is strain rate for structural dilation due to phase transformations;
$\dot{\varepsilon}^{tp}_{ij}$ is strain rate for structural dilation due to transformation plasticity;
λ is thermal conductivity; and
c is specific heat.

To solve these equations, the finite element method (FEM) described in [10,11] was used. For the investigations of medium-carbon and high-carbon steel grades, AISI 1045 and AISI 52100 steels have been selected. CCT (continuous cooling transformation) diagrams and mechanical properties of the specified steel grades with respect to temperature are presented in [12,13].

Steel phase transformation occurring during the quenching process has been modeled using methods correlating the time–temperature quenching cooling curve with the temperature-dependent thermal, physical, and mechanical properties exhibited by materials with respect to the transformation product formed, as indicated by the corresponding CCT diagrams for the steel of interest. The accuracy of the technique was determined [5,9], and the calculation error did not exceed 3 % with respect

to temperature or 12 % with respect to stress, which provides a basis for the use of the suggested technique in the study of changes occurring in the thermal and stress-strain states in quenched parts with respect to the cooling processes and character of steel phase transformations. Detailed information on residual stress distribution during intensive quenching of steel parts is available from [14–16].

7.4 STRESS STATE OF CYLINDRICAL BODIES AFTER MARTENSITIC THROUGH-HARDENING

Computation of the transient and residual stresses for a cylindrical test specimen of 6-mm diameter made of AISI 1045 steel was conducted for various heat transfer coefficients, where the generalized Biot number Bi_V changed from 0.07 to 35. Note that the correlation between the Biot number Bi and the generalized Biot number Bi_V is presented in [1]. The austenitizing temperature was 1,300K. The results obtained showed that intensive cooling produced surface residual stresses initially decrease, then increase to a maximum value ($Bi_V = 1.4$), and then become compressive at $Bi_V = 4.5$, as shown in Fig. 1.

These observations are explained as follows. At small values of Bi_V, an insignificant temperature gradient is observed. During transformation of austenite into martensite, there are small compressive stresses near the surface due to the greater specific volume of martensite in the initial stage. However, when martensite is formed in the core of a specimen, there are large expansion forces, resulting in tensile stresses at the surface. Under intensive cooling conditions ($Bi_V > 6$), martensite transformations start at a thin superficial layer of a specimen while the temperature at other points is still high. The larger the Bi_V, the larger the temperature gradient at the superficial layer will be, and the greater the distance from the center a layer of martensite will form. When cooling the inner layers, two different processes offset each other: contraction because of decreasing temperature, and expansion because of the formation of martensite, which possesses the greater specific volume in comparison to austenite.

Under conditions of $Bi_V > 6$, the contraction process prevails in the inner points of a specimen. Therefore, the superficial layer of a part is compressed upon quenching
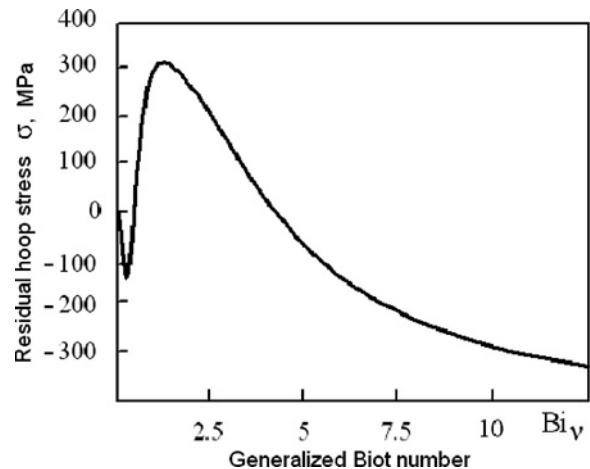
Fig. 1—Residual hoop stresses at the surface of a cylindrical specimen versus the generalized Biot number Bi_V, which is directly related to the cooling rate. Note that the stress changes from tensile to compressive at a Bi_V of about 4.3 [17].

because the contracted inner layers of the part try to move the originally formed layer of martensite closer to the center. When the temperature gradient is small, the outer layer of newly formed martensite, compared to the cold state, is closer to the center. Therefore, there will be tensile residual stresses at the surface due to the increase in specific volume of a material during martensite transformations in inner layers. This suggests that there is a value of Bi_V where the forces contracting the material compensate each other. With a Bi_V of approximately 4.3, there will be zero residual stresses at the surface of the quenched part.

Fig. 1 shows the residual hoop stresses at the surface of the cylindrical test specimen versus the generalized number Bi_V. The correlation between the generalized Bi_V number and the Bi number for cylindrical bodies is $Bi_V = 0.346Bi$.

The character of dependence shown in Fig. 1 depends on the chemical composition of the steel and the shape of the part. However, there is a commonality for parts of different shapes and made of different steel grades. It is necessary to assume that martensite is formed through the entire section of a part to be quenched. The following explanations can be provided for the results obtained using a simple mechanical model (see Fig. 2) [17,18].

The reason why intensive quenching results in high compressive stresses can be explained using the model shown in Fig. 2, which consists of segments (1) joined together by springs (2) to form an elastic ring. The segments are placed on a plane surface and connected with rigid threads (3), which pass through a hole (4) in the center of the ring and are attached to the opposite side of the plane surface.

Now consider the processes that occur when quenching a cylindrical steel test specimen and how they would affect the behavior of the model. Assume that the specimen is being quenched under conditions of intensive cooling. In this case, the surface layer is cooled to a certain depth while the core remains at nearly the austenitizing temperature and is considerably expanded in volume. Let the cooled surface layer correspond to the segmented ring in Fig. 2.

Because metals contract when cooled, the ring segments (1) also will contract. The springs (2) must then extend by an amount that corresponds to the increase in tangential tensile stresses. However, when the surface layer is further cooled, austenite transforms to martensite, which possesses a high specific volume. That is why the cooled layer enlarges or swells.
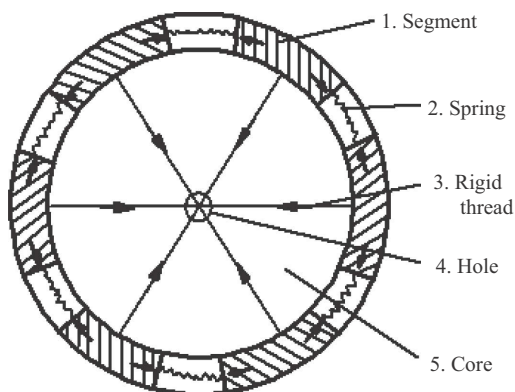
Now imagine that the segments expand. In this case, resulting compression of the springs corresponds to the appearance of tangential compressive stresses on the surface of the part. With additional time, the temperature of the specimen core will drop, and its diameter will decrease. In the model, the core (5) is represented by the smaller blank circle which is held in tension by the rigid threads. When the threads are taut, the springs will also compress. The level of tangential compressive stresses will increase until the austenite in the core of the part transforms to martensite. The core now starts to swell because the specific volume of martensite is greater than that of austenite, which causes the compressive stresses to decrease. In the model, this would be reflected by an enlargement of the inner circle and a resulting decrease in the compressive power of the springs.

The result obtained is of practical interest since it allows quenching alloy and high-alloy steels intensively by water. However, it is necessary to consider that the parts of a complex configuration will require conducting additional calculations for the determination of the value of residual stresses and character of their distribution through the section of the hardened part.

7.5 DISTRIBUTION OF CURRENT STRESSES THROUGH THE SECTION OF CYLINDRICAL PARTS

Numerical computations of residual stresses were performed on cylindrical bodies with diameters of 6, 40, 50, 60, 70, 80, 150, 200, and 300 mm. These computations were performed for AISI 1045 steel and for the cases when the CCT diagram is shifted to the right by 20, 100, or 1,000 s. These calculations simulated the quenching process for steel grades where the formation of martensite is observed through the entire section of a part. The results of this work are discussed below [5,7].

The initial time when thermal tensile stresses appear at the surface of a cylindrical specimen is shown in Fig. 3. When martensite is formed at the surface of a part, current tensile stresses transform into compressive stresses (see Fig. 4). There exists a certain moment of time when the compressive stresses reach their maximum (see Fig. 5), after which they start to decrease as the core swells. These facts agree well with the mechanical model presented in Fig. 2.

Fig. 2—This mechanical model can be used to explain the formation of hoop stresses at the surface of a cylindrical specimen during intensive quenching [17].
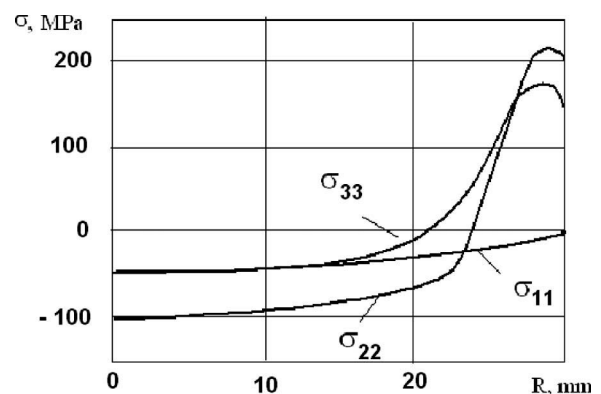
Fig. 3—Stress distribution within the section of a through-hardened cylindrical test specimen of 60-mm diameter at 1 s ($\alpha = 25,000$ W/m^{2}K) [5].
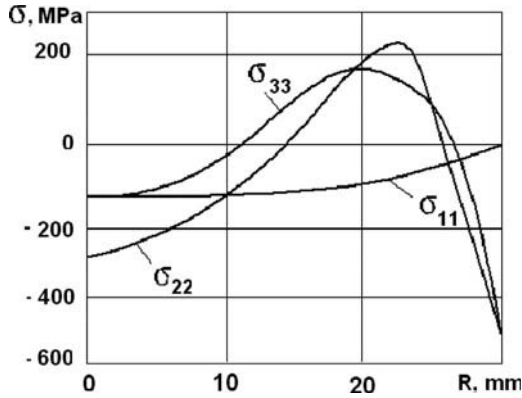
Fig. 4—Stress distribution within the section of a through-hardened cylindrical test specimen of 60-mm diameter at 10 s ($\alpha = 25,000$ W/m^{2}K) [5].

7.5.1 Similarity in the Distribution of Current Stresses Through the Cross-Sections of Parts

The study described above showed that, if a certain condition is met, the distribution of current and residual stresses is similar to those formed in cylinders of different sizes that possess the correlation:

$$\theta = F(\overline{Bi}, \overline{F}_0, r/R), \qquad (12)$$

where:

$$\theta = \frac{T - T_m}{T_0 - T_m};$$

$$Bi = \frac{\overline{\alpha}}{\lambda} R = idem; \text{ and}$$

$$F_0 = \frac{\overline{a}\tau}{R^2} = idem,$$

with *idem* indicating "the same value" or constant.

In this case, the average values of heat conductivity and thermal diffusivity of steel are taken over the interval of temperatures from T_m to T_0, which still produced a good correlation of the distribution of current stresses in cylinders of different sizes. Note that the computer simulation used thermal properties dependent on temperature. However, during discussion, the results of the calculations' average values are
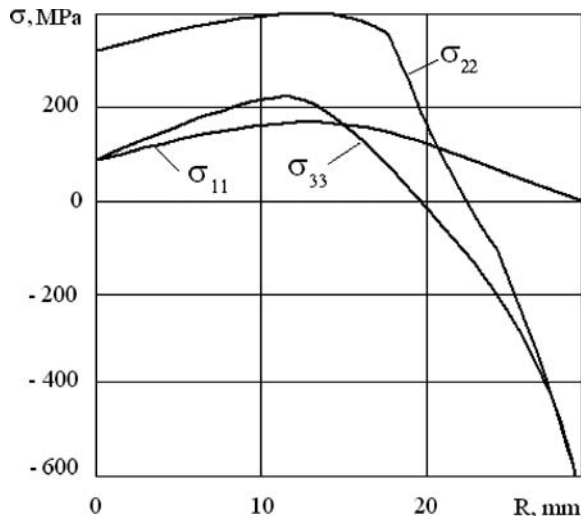
Fig. 5—Stress distribution within the section of a through-hardened cylindrical test specimen of 60-mm diameter at 40 s ($\alpha = 25,000$ W/m^{2}K) [5].

considered, because heat-treating engineers are more familiar with the average values, like the Grossmann H-Factor. Furthermore, all existing standards can provide only average values. Using the average values allows for useful generalizations [19].

Fig. 4 provides a comparison of the computational results for one cylinder of 6-mm diameter and another of 60-mm diameter. In both cases, martensite was formed through the entire section of the cylinder that was obtained by shift of the CCT diagram to the right by 100 s. For a comparison of current stresses, the time chosen was the moment when compressive stresses at the surface of the cylinder to be quenched obtained their maximum values. For the 6-mm-diameter cylinder, this time was 0.4 s; for the 60-mm-diameter cylinder, the maximum compressive stresses at the surface were obtained after 40 s, provided that $\frac{\alpha}{\lambda}R = idem$. This condition was obtained by the computation of current and residual stresses for the 6-mm cylinder at $\alpha = 300,000$W/m^{2}s and for the 60-mm cylinder at $\alpha = 30,000$ W/m^{2}s. For both cases, the Biot number was $Bi = 45$. This means that, in each case, the maximum compressive stresses were obtained at $F_0 = 0.24$, that is, at $\tau = 0.4$ s for the cylinder of 6-mm diameter and at $\tau = 40$ s for the cylinder of 60-mm diameter [17].

The same values of hoop and radial stresses are observed at points with the same ratio r/R (see Fig. 4). Therefore, hoop stresses for both cases are equal to zero at $r/R = 0.65$, which occurs at $r = 1.95$ mm for the smaller cylinder and at $r = 19.5$ mm for the larger one [17].

The results of the calculations, presented in Fig. 6, coincide very well with the results of experiments in [20].

7.5.2 Optimal Hard Layer

From this study, a conclusion regarding the optimal depth of the hardened layer can be drawn. According to the theory of similarity, the maximum surface compressive stresses will
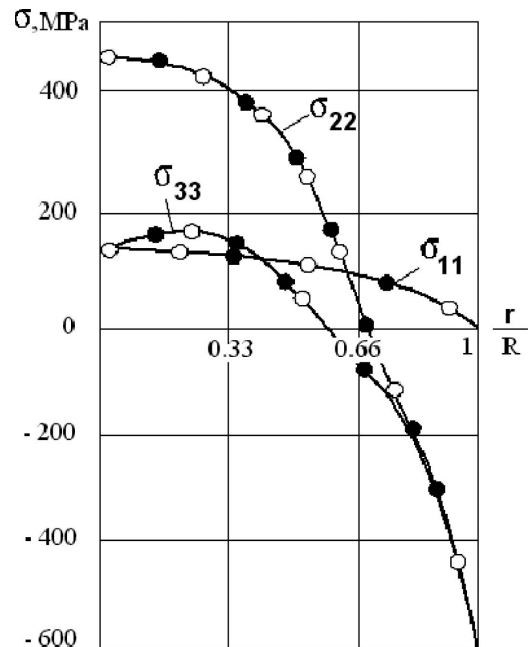
Fig. 6—Stress distribution through the section of two cylindrical specimens, one of diameter 6 mm (black data points) and the other of 60 mm (white data points), at the time of the achievement of maximum compressive stresses at the surface ($Bi = 7$; $F_0 = 0.7$) [17].

correspond to the optimal depth of the hardened layer. If that is true, the following condition must be met:

$$\frac{\Delta r}{R} = idem \tag{13}$$

or

$$\frac{\Delta r}{R} = const,$$

where Δr is the optimal depth of the hardened layer.

Steels of controlled hardenability are normally used for the creation of high surface compressive residual stresses of steel parts [10–12]. However, according to ratio 13, as the section size varies, it is also necessary to vary the steel grade to provide the optimal depth of the hardened layer, which is not always possible to do in practice.

Fig. 7 illustrates the character of phase distribution through the section of a cylinder at the initial moment of time and at the time of achieving maximum surface compressive stresses (medium strip). It is possible to achieve a similar phase distribution through the section of the cylinder in two different ways [9]:

1. Selection of the appropriate steel composition to provide the optimal depth of the hardened layer
2. Interruption of intensive cooling at the time when the maximum surface compressive stresses are formed by cooling in air at the martensite start temperature

The first method permits the replacement of alloy steels with low-alloy or carbon steels. The disadvantage of this method is that when the size of a part changes, it is necessary to select a different steel grade to provide the desired optimal depth of the hardened layer.

The second method can be applied for parts of different sizes. However, for parts with a complex configuration, it is not always possible to provide a uniform martensite layer over the entire surface. In some cases, to obtain a uniform martensite layer, water-air jets are used to provide different cooling intensities at different surface points using different flow rates and water-air fluid compositions.

7.5.3 Comparison of Stresses Achieved by Different Processes with Equivalent Optimal Layers

It is important to analyze the current stresses at the optimal layer of martensite obtained by the two methods described above: interruption of intensive cooling at the time of achievement of maximum surface compressive stresses, and selection
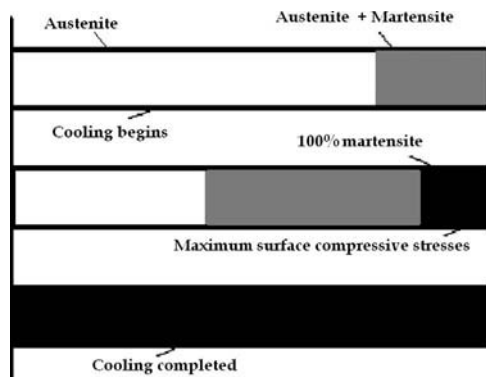
Fig. 7—Optimal depth of the martensite zone corresponding to the maximum surface compressive stresses [7,17,19].
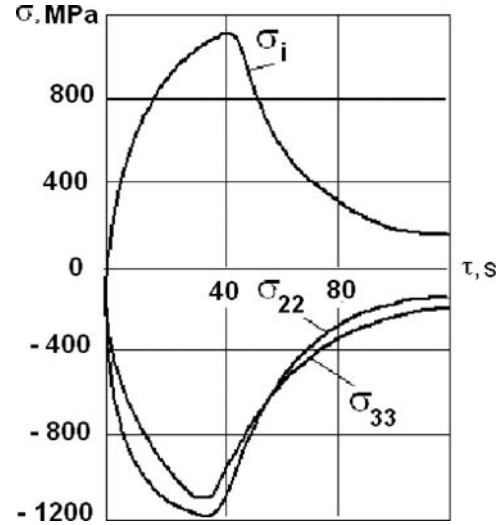
Fig. 8—Stresses at the surface of a cylindrical specimen (dia 60 mm) versus time after through-hardening [7].

of steel compositions. Fig. 8 presents the values of compressive stresses at the time of achievement of the optimal depth of martensite, which yields a maximum of about 1,200 MPa. Approximately the same depth of the hardened layer is achieved using extremely intensive cooling of a 300-mm-diameter cylinder made of AISI 1045 steel (Fig. 9). In both cases, at the optimal depth of martensite, the same values of surface compressive stresses are obtained: 1,200 MPa. The maximum compressive stresses can be increased considerably by increasing the cooling intensity and carbon content of the steel.

7.6 ANALYSIS OF STRESS STATE OF STEEL DURING QUENCHING

In addition to the creation of high surface compressive stresses, it is important to characterize the stress distribution through the cross-section. Fig. 10 shows that in the inner layers, there are tensile stresses that further become compressive in the superficial layers (see also Fig. 11). Axial σ_{22} and hoop stresses σ_{33} are typical. Radial stresses at the surface are
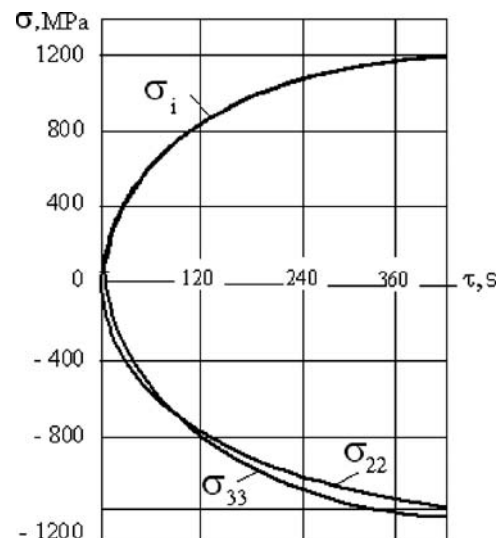
Fig. 9—Stresses at the surface versus time for a cylindrical specimen (dia 300 mm) made of steel 45 (AISI 1045) after shell hardening [7].
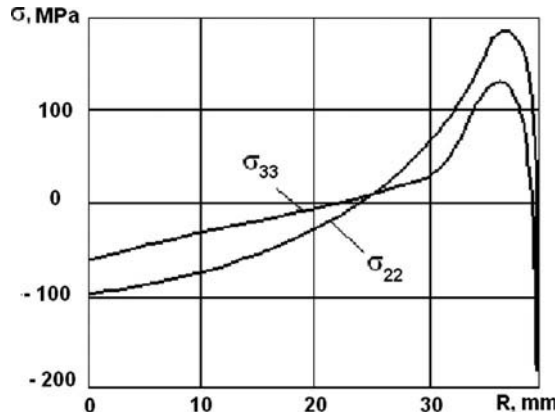
Fig. 10—Stress distribution through the cross-section of a cylindrical specimen (dia 80 mm) made of steel 45 (AISI 1045) after shell hardening for 2 s and a cooling condition $\overline{Bi} = 50$ [15,16].

equal to zero, and at the axis of the cylinder they are equal to the hoop stresses.

This study shows that with very high Biot numbers Bi (which would be typical for large power-machine parts), quench cracks may be formed internally. To avoid quench cracks, for example, when quenching large rotors of turbines, apertures are made at the axis of a rotor, through which the quenchant is pumped. In this case, the inner layers' compressive stresses prevent quench crack formation. The shortcoming of such a method is that it is necessary to bear the significant expense of drilling apertures in large parts.

Therefore, a steel quenching process for large parts that will prevent quench crack formation in continuous parts without axial apertures is of interest. The IQ-3 quenching process, which will be further discussed in Chapters 10 and 12, where the time of achievement of maximum compressive stresses is calculated based on a generalized universal dependence [17,19], was developed to prevent quench crack formation for these applications.

7.7 STRESS STATE OF A COMPLEX PART
7.7.1 Computations for Bearing Rings
Having considered in detail the as-quenched stress state of cylinders, the stress state of parts of more complex configurations
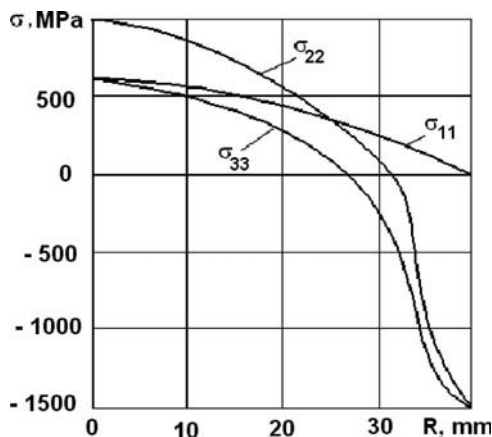
Fig. 11—Stress distribution through the cross-section of a cylindrical specimen (dia 80 mm) made of steel 45 (AISI 1045) after shell hardening when cooling is completed with a cooling condition of $\overline{Bi} = 50$ [15,16].

will now be addressed. There are reliable experimental data that can be used for computations for such parts as railway bearing rings and carburized plugs [21–25]. Some of these rings were made of low-hardenability, high-carbon steels that provide a nearly optimum hard layer. These rings have undergone cyclic tests, and the results were compared with those produced by typical quench processing [15,16]. For this reason, the complex ring shown in Fig. 12 [23] will be used.

The CCT diagram for AISI 52100 steel, shown in Fig. 13, was used for calculations [12,16]. For simulation of steels of low hardenability, the diagram was shifted to the left in the area of pearlite and other intermediate transformations (4 and 3, respectively, in Fig. 13). In this way, it was possible to obtain approximately the same depth of martensite as obtained by experiment for a ring made of low-hardenability steel.

The purpose of this work is to analyze the stress state of parts of more complex configuration in different cases, including:
1. A ring made of AISI 52100 steel and through-hardened in oil (Fig. 13)
2. A ring made of low-hardenability steel with the same content of carbon as in AISI 52100 (Fig. 14) and intensively quenched

In both quenching simulations, the mechanical properties (in austenite and martensite states) were considered to be identical. Their temperature dependencies are presented in Figs. 15 and 16 [14–16]. The coefficient of linear expansion α_T, as a function of temperature, exhibits the following feature: When the martensite transformation starts, the coefficient of linear transformation α_T becomes negative. The physical meaning of this is that, when the temperature of the material decreases, the material does not contract, but rather expands because of the greater specific volume of
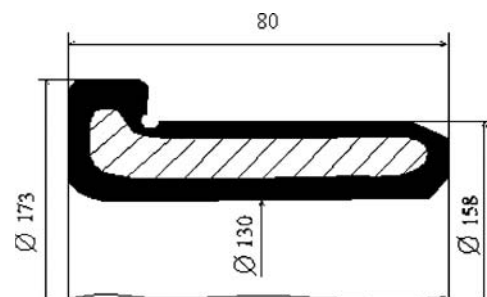

Fig. 12—Outline of a railway-bearing ring.
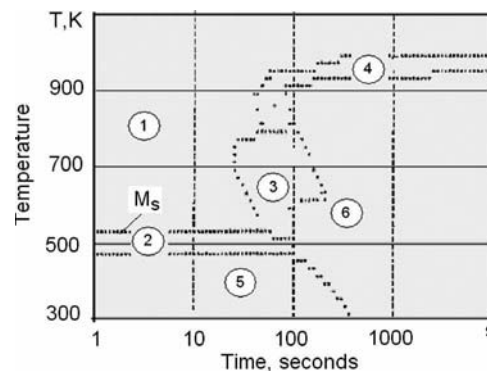
Fig. 13—CCT diagram for AISI 52100 steel: 1, austenite; 2, martensite ($\leq$ 50 %); 3, bainite; 4, pearlite; 5, martensite ($\geq$ 50 %); 6, mixed structure [15,16].
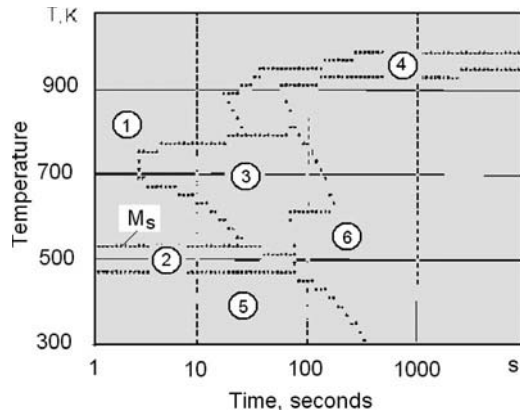
Fig. 14—CCT diagram for low-hardenability bearing steel with low content of Mn and Cr: 1, austenite; 2, martensite ($\leq$ 50%); 3, bainite; 4, pearlite; 5, martensite ($\geq$ 50%); 6, mixed structure [15,16].
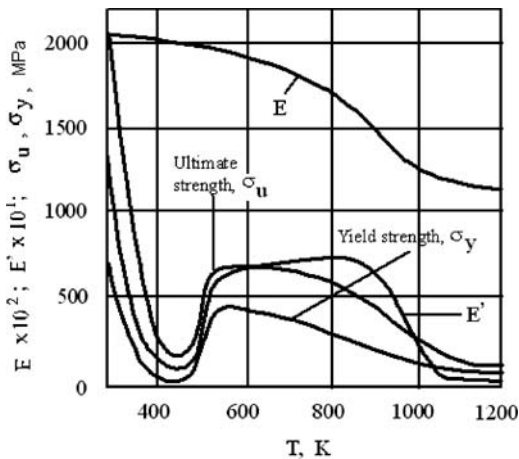
**Fig. 15**—Strength properties, elastic modulus E, and hardening modulus E′ of steel ShKh15 (AISI 52100) [14–16].
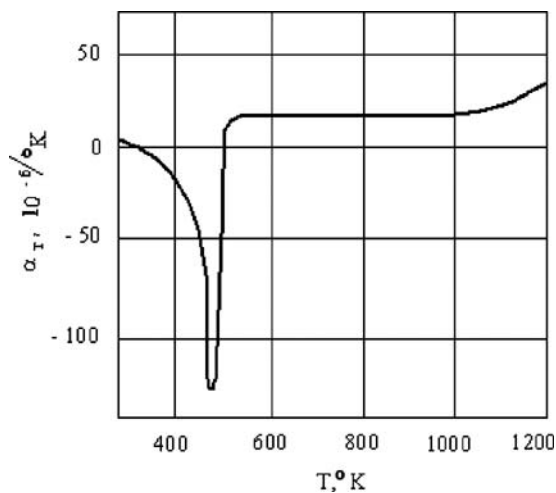
Fig. 16—Coefficient of linear expansion α_T of steel ShKh15 (AISI 52100) vs. temperature [14–16].

martensite. The greater the carbon content in the steel, the more negative α_T is, as shown in Fig. 16.

Within the martensite range, superplasticity is also observed, which is evident from the sharp decrease of yield strength σ_y and ultimate strength σ_u (see Fig. 15).

Using these mechanical properties and CCT diagrams and FEM analysis, the as-quenched stress state of the ring was calculated. Oil quenching of AISI 52100 steel produced through-hardening (Fig. 17(a)), formation of small tensile stresses at the surface, and small compressive stresses in the core (see Fig. 18a). If the ring is made of a low-hardenability steel and is quenched by intensive water jets or water flow, then a uniform martensite layer at the surface of the ring with a high hardness is formed (see Figs. 17(b) and 18(b)). Results of fatigue testing are presented in Fig. 19. Thus, when compared to quenching in oil, higher surface residual compressive stresses are observed, reaching values of 1,000 MPa, while there are tensile stresses in the core where the material is soft [14–16].

It should be noted that such a distribution is reasonable if the ring has identical sections along the height. If a ring contains variable section sizes and has grooves at the end, however, it is not always possible to create compressive stresses in the grooves. Usually tensile stresses appear in the grooves, which results in splitting of the flanges. In this case, it is not useful to use low-hardenability steels, since the thin part is through-hardened and therefore there may be cracks or splitting of flanges in thin parts. These calculations provide a qualitative representation of the residual stress distribution through the cross-section of rings, but nevertheless they are of practical interest.

7.7.2 Computations for Splined Half-Axles

Structural transformations occurring during quenching were considered based on both the thermophysical and mechanical
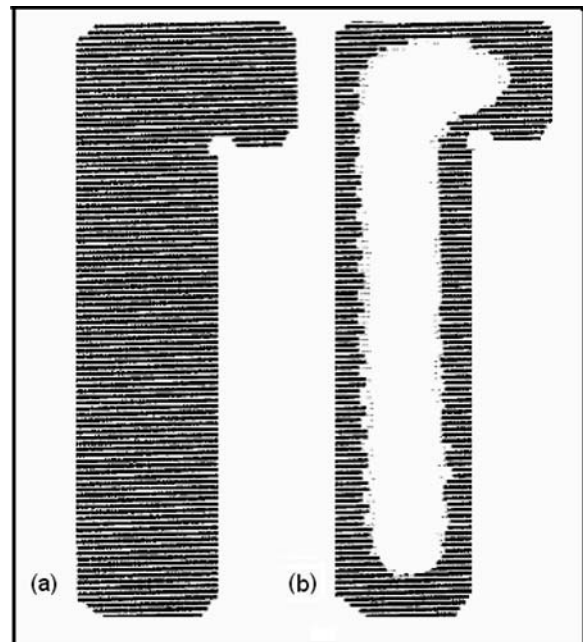
Fig. 17—Character of the phase distribution through the cross-section of a bearing ring: (a) through-hardened bearing ring; (b) shell-hardened bearing ring. The dark color is martensite, and the light color represents intermediate phases [14–16].
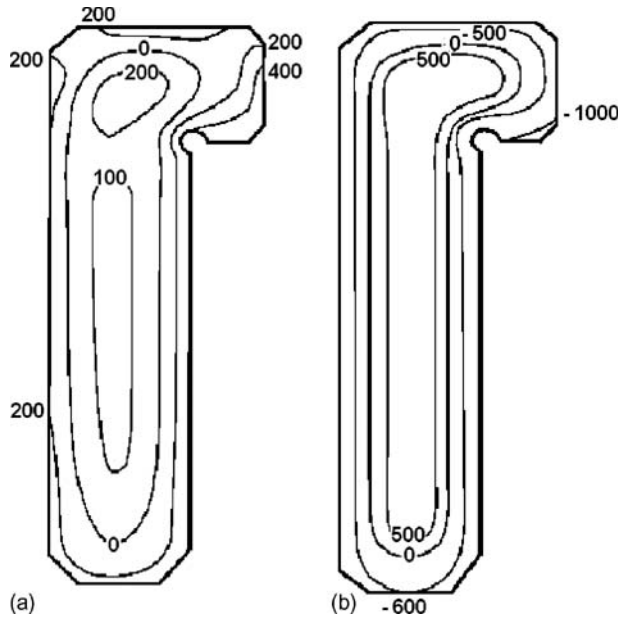
Fig. 18—Distribution of hoop stresses σ_{33} through the cross-section of a bearing ring after it is through-hardened in oil (a) and after it is intensively quenched using water jets with the formation of martensitic shell layer at the surface (b) [15,16].
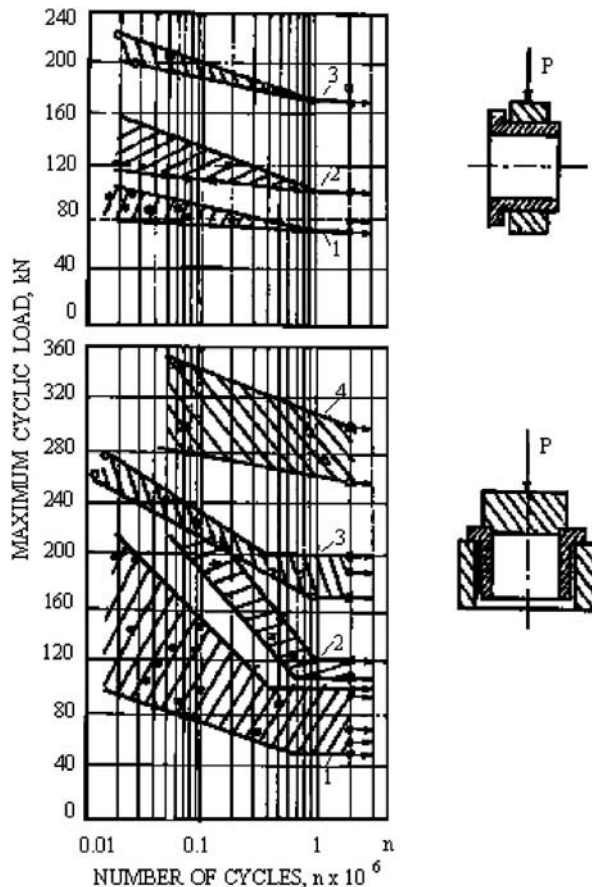
Fig. 19—Fatigue testing results for inner rings of railway car bearings made of various steels (the numbers of the curves correspond to numbers of steel and heat treatment variants in Table 1) [15,16].

properties as a function of material temperature and the cooling temperature and time represented by the CCT diagram of the steel (Fig. 20) [26]. At each time and space step, the results were compared with CCT diagrams, and new thermal and mechanical properties of a material for the next step were chosen depending on the structural components [5,7,22]. Hart software was used for the calculations [5,7,16].

Computations were performed on the part shown in Fig. 21, which was made of AISI 1045 steel (see Fig. 20). The current and residual stresses were calculated both for AISI 1045 steel and for the case when the CCT diagram was shifted to the right by 1,000 s. This permitted the simulation of alloyed steel quenching with martensite formation observed over the entire section of the part after quenching. The calculation was performed for oil quenching, quenching in still water, and intensive water flow. The heating temperature was 1,130K.

The analysis results in Fig. 22 show that when quenching in oil, considerable tensile residual stresses (250 MPa) arise at the bottom of the spline (alloyed steel). However, when quenching the same steel in intensive water flow, residual stresses at the surface remain compressive. When quenching alloyed steel, maximum compressive stresses were observed, which subsequently decreased. The greater the rate of cooling, the higher the compressive stresses at the surface of the quenched part. Thus, during oil quenching, maximum compressive stresses were 225 MPa, while for quenching in an intensive water flow, they were 1,100 MPa.

The depth of the hardened layer (martensite range) corresponding to the maximum compressive stresses in the spline bottom is shown in Fig. 23 where M is the austenite region, M + B is the region containing 0−50 % martensite, and P is the martensite region. The optimal depth of the martensite layer corresponds to maximum compressive stresses. Further martensite penetration into the part causes a decrease of compressive stresses, which may be attributed to the larger specific volume of martensite as the part core swells and residual tensile stresses (up to 350 MPa) form at the surface (see Fig. 23). Due to the high compressive residual stresses at the surface of steel parts and the steel superstrengthening phenomenon [27,28], the parts' service life significantly increases (see Table 2).

It should be noted that Hart software is two-dimensional code for temperature fields and stress distribution calculations [5,15,16]. At present, the most powerful software is the three-dimensional Dante, which is widely used in the United States [30−36]. The Dante predictive heat treatment software tool provides significant insight into the process sensitivity, particularly on the effect of variations in boundary conditions [30−36]. It is widely used for designing and optimizing intensive quenching processes [37−39], including those that were developed early and those that will be developed in the future. Combining Dante software with the appropriate databases for boundary condition and CCT-TTT diagrams, the next significant step in intensive quenching development is possible.

7.8 DISCUSSION

As a result of numerous calculations, two basic conclusions have been made. The first is that through-hardening with intensive cooling produces very high surface compressive stresses, which are compensated by small internal tensile stresses [5,7,16]. This is important because alloy and high-alloy steels can be quenched intensively in water without

TABLE 1—Structure and hardness of inner rings of railway bearings made of various steels [23]				
	Values for rings made of the following steels:			
Parameters	ShKh15SG	18KhGT	ShKh4	ShKh4
Number of steel and heat treatment variant	1	2	3	4
Surface hardness (HRC)	60–61	59–61	62–64	62–64
Depth of hard layer (mm): (a) HRC > 58 (b) HRC > 55	Through-hardening	(a) 0.7–0.9 (b) 1.8–2.1	(a) 1.5–2 (b) 2.4–2.7	(a) 1.5–4 (b) 3–4.5
Core hardness (HRC)	60–61	32–35	36–40	40–45
Microstructure in the core	Martensite, carbides	Low-carbon martensite	Sorbite, troostite	Troostite
Percentage of retained austenite at the surface (%)	14–16	8–10	6–8	6–8
Grade of austenitic grain size	9–10	9	10–11	10–11
Note: Chemical composition of Russian steels are provided in the appendix of the book				

quench crack formation. Therefore, in some cases, the use of expensive and flammable oils and aqueous high-concentration polymer solutions can be avoided.

Although the existence of internal tensile stresses can result in quench crack formation in the core, the propensity for quench cracking is reduced because:
1. The internal tensile stresses are relatively small.
2. Intensive cooling can be interrupted when the core is sufficiently viscous that tensile stresses cannot lead to internal crack formation.
3. After intensive quenching, it is possible to immediately temper (snap-temper) to prevent quench crack formation. Additional information is available in [15–18].

The second conclusion is that, during through-hardening of steel, initially there are enormous surface compressive stresses, but these gradually disappear or transform into tensile stresses. Quenching technology has been developed that permits selection of the conditions that produce maximal surface compressive residual stresses [4,15–17].

To demonstrate the potential increase in service life due to the creation of surface compressive stresses, inner rings

of bearings were made of different steels and two cases were considered [16,23]:
1. Through-hardening of bearing rings
2. Quenching of bearing rings to a certain depth using a low-hardenability bearing steel

The results obtained were summarized in Table 1. Fatigue tests have shown that the service life of rings is longer when the depth of the hardened layer is closest to the optimum (see Figs. 17–19). The service life of steel parts is affected not only by the magnitude of the compressive residual stresses but
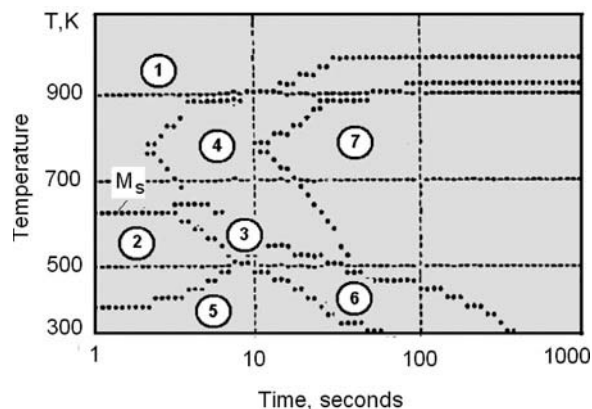
Fig. 20—CCT diagram of AISI 1045 steel: 1, austenite; 2, martensite (≤ 50 %); 3, bainite; 4, pearlite; 5, martensite (≥ 50 %); 6 and 7, mixed structures [26].
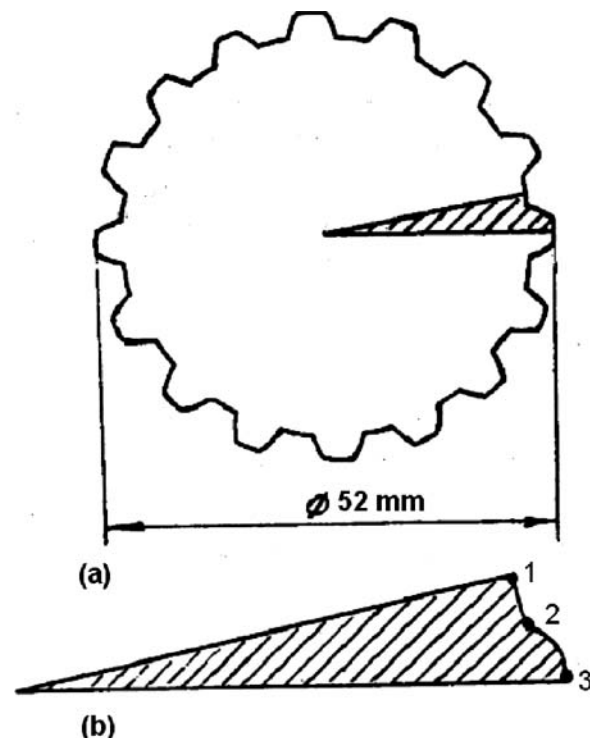
Fig. 21—Sketch of cross-section of splined half-axle (a) and meshing for finite-element method (b): 1, spline bottom; 2, spline side surface; 3, spline tooth.
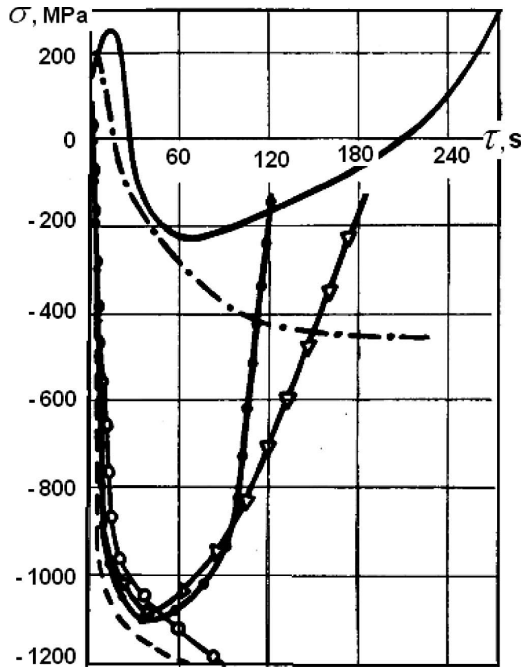
Fig. 22—Current hoop stresses vs. time in the process of splined half-axle surface cooling in various quenching media in the spline bottom [26]: ▬▬ oil cooling (alloyed steel, through hardening); ▪—▪ the same (carbon steel); ♦—♦ cooling in still water (alloyed steel); ▬▬ the same (carbon steel); —▽— cooling in intensive water flow of 8 m/s (alloyed steel); ▬○▬ the same (carbon steel).
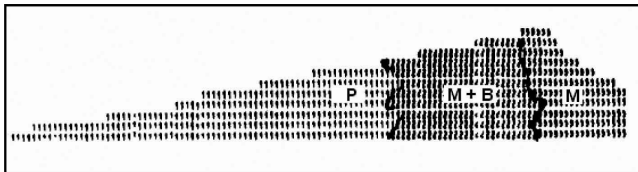
Fig. 23—Phase distribution across the half-axle section at the time of reaching maximum compressive hoop stresses in the spline bottom [26]: P, pearlite; M, martensite; B, bainite.

also by the mechanical properties of a material that is being improved by intensive quenching, especially in the optimal superficial layer. This aspect of the study will be considered in more detail in Chapter 9, which presents the effect of increasing the cooling rate within the martensite range on the mechanical properties of various steel grades.

Computer simulation was also used to investigate two-step quenching and distortion based on the mathematical models discussed above [5,7,8,16]. Using the bearing ring illustrated in Fig. 24, quenching was conducted in oil at the optimum temperature. Cooling in oil during the first stage was interrupted to minimize distortion. Intensive cooling and washing were conducted simultaneously during the second

step of the process. Minimal distortion after the second stage was observed by cooling in air or after a very intensive shower [14]. It appears that the conicity of the rings is less when cooling very fast within the martensite range, as compared with a moderate intensity (see Table 3 and Fig. 25).

Computer simulations established that there is minimal distortion of the bearing rings during their quenching in oil (see Fig. 24). Fig. 25 shows displacements of the generatrix of the inner surface of the bearing ring during hardening in oil after 30 s, 39 s, and complete cooling [8,15,25]. Minimal distortion was observed after cooling in oil for 30 s (Fig. 25, curve 3). The computer simulation shows that minimal distortion can be fixed when interruption is made at 30 s during cooling in oil and then very slow or very fast cooling is applied (see Table 3).

Distortion decrease after very intensive cooling can be explained by Fig. 26, which shows the phase transformation during moderate cooling (a) and during extremely intensive cooling (b) with $Bi_V > 6$. When moderate cooling takes place (Fig. 26(a)), the phase transformation starts in the thin section of the part and, due to the change of specific volume of martensite, results in an increase in distortion. In the case of intensive cooling (Fig. 26(b)), a thin shell of martensite forms uniformly over the entire surface and fixes the shape of the part, so the distortion is lower [8,15,25].

Along with the distortion evaluation, Hart software allows prediction of the place and time of crack formation in the bearing rings, shown in Fig. 24, during moderate cooling in water [40]. For this purpose, a generalized criterion was selected as a failure criterion during hardening:

$$\chi\sigma_i + (1 - \chi)\sigma_1 \leq \sigma_t, \qquad (14)$$

where:

$\chi = \dfrac{\sigma_t}{\sigma_c}$;

σ_t is ultimate tensile strength;
σ_c is ultimate compressive strength;
σ_1 is greatest principal stress; and
σ_i is stress intensity.

Using Eq 14, Morhuniuk and colleagues [9,14,40] estimated the place and time where cracks had appeared after quenching in still water at 20°C in the bearing rings (see Figs. 24 and 26).

These important investigations are being continued by Japanese scientists and engineers, who have made significant contributions to computer simulations of the quenching processes and comparison of the results of calculations with the results of accurate experiments [41–47]. In particular, Sugianto and colleagues [47] visually detected the cracks in an eccentric-holed disk quenched in still water. Metallography and fractography were carried out by optical and scanning electron microscopes, indicating the structure of band martensite and intergranular cleavage fractures.

A computer simulation was also used to predict the formation of transient and residual stresses in an eccentric-holed

TABLE 2—Fatigue tests of KrAZ truck half-axles [22,29]			
Quenching method	Steel grade	Numbers of cycles to fracture	Notes
Oil	AISI/SAE 4340	3.8–4.6 × 10⁵	Half-axles were destroyed
Intensive water spray cooling	AISI/SAE 1040 or AISI/SAE 1045	3.0–3.5 × 10⁶	No fracture observed
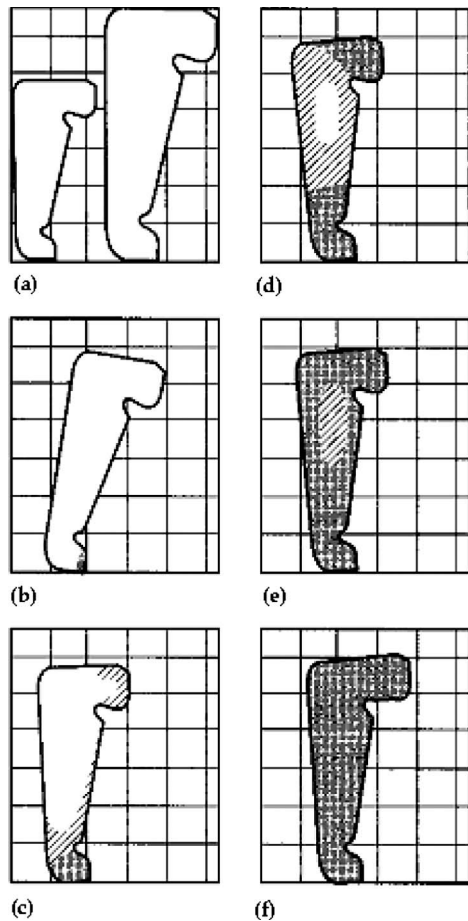
Fig. 24—Structural composition and shape of the bearing ring profile during hardening: (a) is initial (cold and heated state); (b) through (f) are the states during cooling. The unshaded area is austenite, single hatching indicates the area up to 50 % martensite, and cross-hatching indicates 100 % martensite.

Fig. 25—Displacements of the generatrix of the inner surface of the bearing ring during hardening (lines denote computed data, and circles experimental data): 1, after machining (see Fig. 24(a), left side); 2, after heating to austenite temperature (Fig. 24(a), right side); 3, after cooling in oil for 30 s; 4, after cooling in oil for 39 s; 5, after complete cooling in oil [8,15,25].

disk quenched in different conditions to predict crack formation. Results of calculations were compared with the results of experiments [44,46,47].

Taking into account all experimental and computer simulation data, intensive technologies were further developed and optimized in the United States for many steel parts and tools [28,48–54]. Especially good results were achieved for AISI S5 punches. Their service life after intensive quenching increased two times [48]. The distortion of S5 cylinders after oil and intensive quenching has been studied using dimensions of 1.5 inches (38.1 mm) in diameter and 2.2 inches (55.9 mm) long [48].

TABLE 3—Conicity of the bearing ring depending on the cooling conditions within the martensite range at the second stage of cooling [5,15]

Method of cooling	Conicity
In air	0.044
In oil	0.045
In circulating water	0.051
Under very intensive shower	0.005

The results showed that the difference in quenching rates between the oil and the intensive quenching process affects the distortion patterns of the cylinders. The distortion map of the oil-quenched cylinder is shown in Fig. 27. The arrows indicate the direction and magnitude of movement. The cylinder is bulged around the center perimeter, with the center diameter about 0.0032 inches (0.0813 mm) larger than the top and bottom diameters. The distortion map of an intensively quenched cylinder is shown in Fig. 28. The cylinder has an "hourglass" shape, with the center diameter about 0.0032 inches (0.0813 mm) smaller than the sides.

Heat treatment simulation of 10 and 22-mm water-quenched cylindrical specimens was performed, and the results were compared with experiments, in an attempt to explain the mechanism of producing distortions and residual stresses. The mechanism of quench distortion and stress generations in through-hardened and incompletely hardened test specimens was explained by changes of the thermo-phase transformation, elastic, plastic, transformation plastic, and total strains [5,7,41,48,49].

The process of quenching of carburized rings was also examined [41]. The origin of distortion–namely, a decrease of the inner and outer diameters and an increase of the height in the carburized and quenched ring–was explained by examining each simulated strain distribution. It was shown that the transformation plastic strain strongly affects quench distortion [41]. Simulated elastic strain changes explained why high compressive residual stresses are produced in the cases of the carburized ring [33,41,48].

It should be noted that, at present time, it is possible to predict the distortion and magnitude of residual stresses by using commercially available software to simulate the quenching processes [34]. The results have shown that the
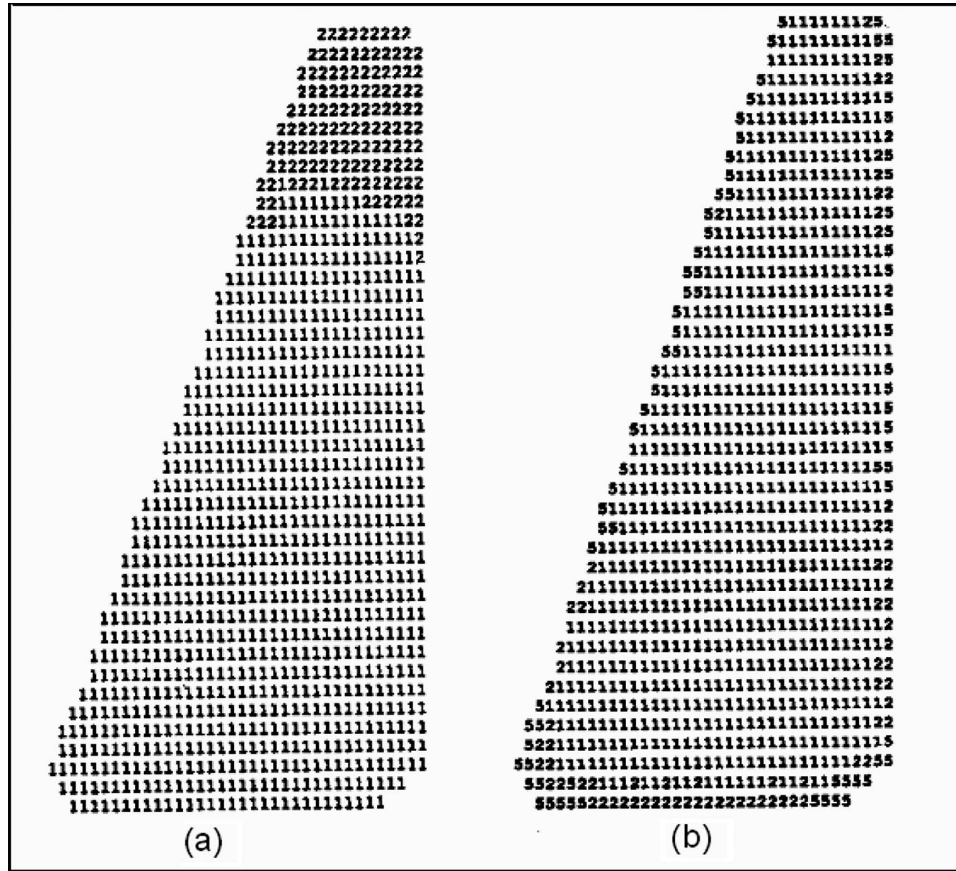
Fig. 26—Phase distribution at slow (a) and intensive (b) cooling at the very beginning: 1, austenite; 2 and 5, martensite.
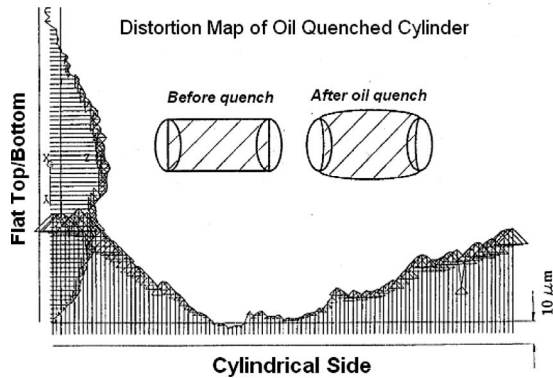
Fig. 27—Distortion map of an oil-quenched cylinder [48].
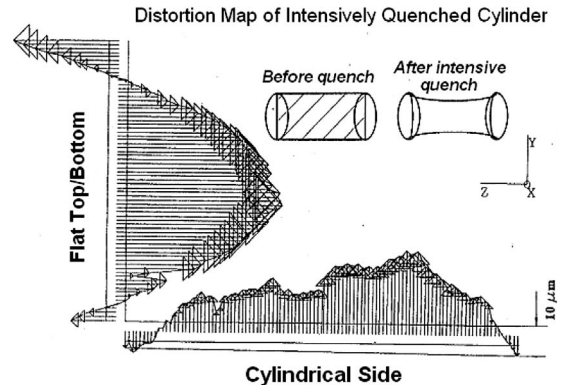
Fig. 28—Distortion map of an intensively quenched cylinder [48].

cooling capacity of quenchants affects distortion and residual stresses. However there is no appropriate database for the cooling capacities of different kinds of quenchants or critical heat flux densities, which are needed for computer simulation. This is a problem that must be addressed in the future.

7.9 SUMMARY

1. It has been established that, when a steel part is subjected to through-hardening with an increasing cooling rate, residual hoop stresses at first grow as tensile stresses, and then, with large Biot numbers, they transform to compressive stresses despite the increase in the specific volume of martensite in the core of the part.

2. It has been shown that transient compressive hoop stresses at the surface of parts during through-hardening achieve a maximum and then decrease or disappear completely. This will help to develop and optimize new quenching processes for producing maximum surface compressive stresses that will increase service life.

3. Maximum surface compressive stresses correspond to the optimal depth of the hardened layer.

4. The similarity in distribution of residual stresses through the section of parts to be quenched has been demonstrated.

5. It has been established that with an increase in the section size, the optimal depth of the hardened layer increases in such a way that the ratio $\Delta r/D$ is constant,

where Δr is thickness of the optimal layer and D is the characteristic size of the part.

6. The basic regularities of stress distribution for bodies of simple shape are attainable for bodies of more complex configuration, as well.

7. It has been shown that high compressive stresses at the quenched surface result in an increase in cyclic fatigue strength.

8. The opportunity of using the regularities for the development of intensive quenching technologies is emphasized.

9. The specific methods of using the optimal hard layer for increase in service life of bearing rings and semi-axles have been discussed.

10. The results of investigations are applied in practice.

References

[1] Aronov, M. A., Kobasko, N. I., Powell, J. A., and Hernandez-Morales, J. B., Correlation between Grossmann H-Factor and Generalized Biot Number Bi$_V$, *Proceedings of the 5th WSEAS International Conference on Heat and Mass Transfer (HMT '08),* Acapulco, Mexico, January 25–27, 2008, pp. 122–126.

[2] Kobasko, N. I., Self-regulated Thermal Processes During Quenching of Steels in Liquid Media, *International Journal of Microstructure and Materials Properties,* Vol. 1, No. 1, 2005, pp. 110–125.

[3] Kobasko, N., Aronov, M., Powell, J., and Totten, G., One More Discussion: "What Is Intensive Quenching Process?", *Journal of ASTM International,* Vol. 6, No. 1, 2009.

[4] Kobasko, N. I., Quenching Apparatus and Method for Hardening Steel Parts, U.S. Patent No. 6,364,974 BI, April 2, 2002.

[5] Kobasko, N. I., and Morgany, V. S., Numerical Study of Phase Changes, Current and Residual Stresses at Quenching Parts of Complex Configuration, *Proceedings of the 4th International Congress of Heat Treatment Materials,* Berlin, 1985, Vol. 1, pp. 465–486.

[6] Kobasko, N. I., and Morgany, V. S., *Investigation of Thermal and Stress-State in the Process of Heat Treatment,* Znanie, Kyiv, 1981.

[7] Kobasko, N. I., and Morhuniuk, W. S., *Issledovanie teplovogo i napriazhenno-deformirovannogo sostoyaniya pri termicheskoy obrabotke izdeliy mashinostroeniya* (Study of thermal and stress-strain state at heat treatment of machine parts), Znanie, Kyiv, 1983.

[8] Inoue, T., and Arimoto, K., Development and Implementation of CAE System "Hearts" for Heat Treatment Simulation Based on Metallo-thermo-mechanics, *Journal of Materials Engineering and Performance,* Vol. 6, No. 1, 1997, pp. 51–60.

[9] Morhuniuk, W. S., Steel Articles During Hardening, *Strength of Materials,* Vol. 14, 1982, pp. 807–814, translated from *Problemy Prochnosti,* No. 6, 1982, pp. 80–85.

[10] Zienkiewiez, O. C., *The Finite Element Method in Engineering Science,* Mir, Moscow, 1975.

[11] Mastorakis, N. E., and Martin, O., Eds., *Finite Elements,* WSEAS Press, Athens, 2007.

[12] Vander Voort, G. F., *Atlas of Time–Temperature Diagrams for Irons and Steels,* ASM International, Materials Park, OH, 1991.

[13] Totten, G., Howes, M., and Inoue, T., Eds., *Handbook of Residual Stress and Deformation of Steel,* ASM International, Materials Park, OH, 2002.

[14] Kobasko, N. I., Morhuniuk, W. S., and Dobrivecher, V. V., Control of Residual Stress Formation and Steel Deformation During Rapid Heating and Cooling, *Handbook of Residual Stress and Deformation of Steel,* Totten, G., Howes, M., and Inoue, T., Eds., ASM International, Materials Park, OH, 2002, pp. 312–330.

[15] Kobasko, N. I., Morhuniuk, W. S., and Ushakov, B. K., Designing of Steel Intensive Quench Processes, *Handbook of Metallurgical Process Design,* Totten, G., Funatani, K., and Xie, L., Eds., Marcel Dekker, New York, 2004, pp. 733–764.

[16] Kobasko, N. I., Morhuniuk, W. S., and Ushakov, B. K., Design of Steel-Intensive Quench Processes, *Steel Heat Treatment: Equipment and Process Design,* Totten, G. E., Ed., CRC Press, New York, 2007, pp. 193–237.

[17] Kobasko, N. I., Basics of Intensive Quenching, *Advanced Materials & Processes/Heat Treating Progress,* Part I, Vol. 148, No. 3, 1995, pp. 42W–42Y; Part II, Vol. 150, No. 2, 1996, pp. 40CC–40EE; Part III, Vol. 153, No. 2, 1998, pp. 36FF–36HH.

[18] Totten, G. E., Kobasko, N. I., and Canale, L. C. F., Mechanism of Surface Compressive Stress Formation by Intensive Quenching, *Mecanica Computacional* (Buenos Aires), Vol. 24, 2005, available at http://www.fain.uade.edu.ar/mecom2005/SESION5/Gtotten_Conferencia.pdf.

[19] Kobasko, N. I., Generalization of Results of Computations and Natural Experiments at Steel Parts Quenching, *Proceedings of the First International Conference on Thermal Process Modeling and Computer Simulation,* Shanghai Jiaotong University, March 28–30, 2000, Shanghai, Vol. 5, No. 1, 2000, pp. 128–134.

[20] Hernandez-Morales, B., et al., Residual Stress Measurement in Forced Convective Quenched Steel Bars by Means of Neutron Diffraction, *Proceedings of the 2nd International Conference on Quenching and the Control of Distortion,* ASM International, Cleveland, OH, 1996, pp. 203–214.

[21] Morhuniuk, W. S., Kobasko, N. I., and Kulakov, A. N., Predicting the Deformation of Bearing Races During Hardening, *Metal Science and Heat Treatment,* Vol. 24, No. 9, 1982, pp. 22–24.

[22] Kobasko, N. I., Intensive Steel Quenching Methods, *Theory and Technology of Quenching,* Liščić, B., Tensi, H. M., and Luty, W., Eds., Springer-Verlag, Berlin, 1992, pp. 367–389.

[23] Ouchakov, B. K., and Shepeljakovsky, K. Z., New Steels and Methods for Induction Hardening of Bearing Rings and Rollers, *Bearing Steels: Into the 21st Century,* Hoo, J. J. C., and Green, W. B., Jr., Eds., ASTM, West Conshohocken, PA, 1998, pp. 307–320.

[24] Kobasko, N. I., Morhuniuk, W. S., and Lushchik, L. V., Study of Thermal Stresses Formed in Steel Products Due to High-Rate Quenching, *Sov. Mater. Sci. Rev.,* No. 1, 1987, pp. 27–32.

[25] Kobasko, N. I., Current and Residual Stresses During Quenching of Steel Parts, *Finite Elements,* Mastorakis, N. E., and Martin, O., Eds., WSEAS Press, Athens, 2007, pp. 86–99.

[26] Kobasko, N. I., Morgany, V. S., and Morganyuk, A. P., Hardening of Complex Configuration Bodies by Intensive Cooling, *Proceedings of the 7th International Congress on Heat Treatment of Materials,* December 11–14, 1990, Moscow, Vol. 2, 1990, pp. 232–239.

[27] Kobasko, N. I., Basics of Intensive Quenching–Part IV, *Advanced Materials & Processes/Heat Treating Progress,* Dec. 12, 1999, pp. H31–H33.

[28] Kobasko, N. I., The Steel Superstrengthening Phenomenon, Part 2, *International Journal of Microstructure and Materials Properties,* Vol. 3, Nos. 4/5, 2008, pp. 526–547.

[29] Kobasko, N. I., *Steel Quenching in Liquid Media Under Pressure,* Naukova Dumka, Kyiv, 1980.

[30] Dowling, W., Pattok, T., Ferguson, B. L., Shick, D., Gu, Y., and Howes, M., Development of a Carburizing and Quenching Simulation Tool, *The 2nd International Conference on Quenching and Control of Distortion,* ASM International, Cleveland, OH, 1996.

[31] Ferguson, B. L., Freborg, A. M., Petrus, G. J., and Collabresi, M. L., Predicting the Heat Treat Response of a Carburized Helical Gear, *Gear Technology,* 2002, pp. 20–25.

[32] Freborg, A. M., Ferguson, B. L. Aronov, M. A., Kobasko, N. I., and Powell, J. A., Intensive Quenching Theory and Application for Imparting High Residual Surface Compressive Stresses in Pressure Vessel Components, *SAE Journal of Pressure Vessels Technology,* Vol. 125, 2003, pp. 188–194.

[33] Freborg, A. M., Li, Z., Ferguson, B. L., and Schwann, D., Improving the Bend Fatigue Strength of Carburized Gears, *MS&T '04,* ASM International, Materials Park, OH, 2004, Vol. 4, pp. 227–234.

[34] Ferguson, B. L., Li, Z., and Freborg, A. M., Modeling Heat Treatment of Steel Parts, *Computational Materials Science,* Vol. 34, No. 3, 2005, pp. 274–281.

[35] Ferguson, B. L., Freborg, A. M., and Li, Z., Improving Gear Performance by Intensive Quenching, *Proceedings of the 24th ASM Heat Treating Conference,* 2007, pp. 156–162.

[36] Ferguson, B. L., and Freborg, A. M., A Design Tool for Tuning and Optimizing Carburizing and Heat Treat Process, *SAE International Off-Highway Congress,* Las Vegas, Nevada, March 19–21, 2002, SAE Technical Paper Series 2002-01-1475.

[37] Kobasko, N. I., Method of Overcoming Self-deformation and Cracking During Quenching of Metal Parts, *Metal Science and Heat Treatment,* No. 4, 1975, pp. 12−16.

[38] Aronov, M. A., Kobasko, N. I., and Powell, J. A., Basic Principles, Properties and Metallurgy of Intensive Quenching, *SAE International Off-Highway Congress,* Las Vegas, Nevada, March 19−21, 2002, SAE Technical Paper Series 2002-01-1338.

[39] Aronov, M. A., Kobasko, N. I., and Powell, J. A., Application of Intensive Quenching Technology for Steel Parts, *SAE International Off-Highway Congress,* Las Vegas, Nevada, March 19−21, 2002, SAE Technical Paper Series 2002-01-1340.

[40] Morhuniuk, W. S., Kobasko, N. I., and Kharchenko, V. K., On the Possibility of Predicting Quench Cracks, *Problemy Prochnosti,* No. 9, 1982, pp. 63−68.

[41] Arimoto, K., Horino, T., Ikuta, F., Jin, C., Tamura, S., and Narazaki, M., Explanation of the Origin of Distortion and Residual Stress in Water Quenched Cylinders Using Computer Simulation, *Journal of ASTM International,* Vol. 3, No. 5, 2006, pp. 1−22.

[42] Arimoto, K., Yamanaka, S., and Funatani, K., Explanation of the Origin of Distortion and Residual Stress in Carburized Ring Using Computer Simulation, *Journal of ASTM International,* Vol. 5, No. 10, 2006, pp. 1−9.

[43] Arimoto, K., Li, G., Arvind, A., and Wu, W. T., The Modeling of Heat Treating Process. *Proceedings of the 18th Heat Treating Conference,* Rosemont, Illinois. Wallis R. A., and Walton, H. W., Eds., ASM International, Materials Park, OH, 1998, pp. 23−30.

[44] Arimoto, K., Lambert, D., Lee, K., Wu, W. T., and Narazaki, M., Prediction of Quench Cracking by Computer Simulation. *Proceedings of the 19th Heat Treating Conference,* Cincinnati, S. J. Midea and G. D. Paffmann, Eds., ASM International, Materials Park, OH, 1999, pp. 435−440.

[45] Totten, G. E., Narazaki, M., and Blackwood, R. R., "Failures Related to Heat Treating Operations," in ASM Handbook, Vol. 11, Failure Analysis and Prevention, 2002, ASM International, Materials Park, OH, pp. 192-223.

[46] Arimoto, K., Ikuta, F., Horino, T., Tamura, S., Narazaki, M., and Mikita, Y., Preliminary Study to Identify Criterion for Quench Crack Prevention by Computer Simulation, *Proceedings of the 14th Congress of International Federation for Heat Treatment and Surface Engineering,* October 26−28, 2004, Shanghai, 2004, pp. 486−493.

[47] Sugianto, A., Narazaki, M., Kagawara, M., and Shirayori, A., Failure Analysis and Prevention of Quench Crack of Eccentric Holed Disk by Experimental Study and Computer Simulation, *Engineering Failure Analysis,* Vol. 16, No. 1, 2009, pp. 70−84.

[48] Aronov, M. A., Kobasko, N. I., Powell, J. A., Schwam, D., Wallace, J. F., Vanas, J. H., and Olson, W. R., Experimental Study of Intensive Quenching of Punches, *Proceedings of the 19th Heat Treating Conference* [CD-ROM], Cincinnati, Midea, S. J., and Paffmann, G. D., Eds., ASM International, Materials Park, OH, 1999.

[49] Totten, G. E., Canale, L. C. F., Kobasko, N. I., Powell, J. A., and Aronov, M. A., Têmpera Intensiva: Levantamento Histórico de um Processo Usualmente Desconhecido, SAE Technical Paper Series 2002-01-3398, 2002.

[50] Kobasko, N. I., Totten, G. E., Canale, L. C. F., Powell, J. A., and Aronov, M. A., Fundamentos Metalúrgicose Levantamento dos Processos de Têmpera Intensiva, SAE Technical Paper Series 2002-01-3399, 2002.

[51] Kobasko, N. I., Aronov, M. A., Canale, L. C. F., and Totten, G. E., Metallurgy of Intensive Quenching Process and Implications with Respect to Steel Properties, *58th Congresso Annual Da ABM,* July 21−24, 2003, Rio De Janeiro, Brazil, pp. 3362−3380.

[52] Kobasko, N. I., Quench Process Optimization for Receiving Super Strong Materials, *WSEAS Transactions on Systems,* Vol. 4, No. 9, 2005, pp. 1394−1401.

[53] Kobasko, N. I., Energy Efficient and Eco-friendly Intensively Quenched Limited Hardenability Low Alloy Steels, *Journal of ASTM International,* Vol. 6, No. 1, 2009.

[54] Kobasko, N. I., Totten, G. E., and Canale, L. C. F., Intensive Quenching: Improved Hardness and Residual Stress, *Heat Treating of Metals,* Vol. 32, No. 5, 2007, pp. 84−89.

8

Steel Quenching in Liquid Media Under Pressure

N. I. Kobasko[1]

8.1 INTRODUCTION

It has been shown in earlier chapters that during nonstationary nucleate boiling, a self-regulated thermal process occurs, where the surface temperature of a part to be quenched is kept above the saturation temperature. This provides an opportunity to greatly affect the martensite transformation process by either retarding or accelerating it. There are two methods available. The first is to use additional pressure to increase the boiling point of the boundary liquid layer. The second is to use high-concentration aqueous solutions of salts or alkalis where the saturation temperature is increased. The use of both approaches is effective when quenching high-carbon steels where the martensite start temperature M_S is less than 200°C (that is, $M_S \leq 200°C$).

Experimental studies have been conducted to examine the effect of pressurization on the temperature distribution in hardened parts, the probability of quench crack formation, and distortion. By retarding the transformation of the supercooled austenite into martensite, there is an opportunity to apply low-temperature thermomechanical treatment (LTMT) to increase the mechanical and plastic properties of quenched steels. Increasing the pressure increases the critical heat flux densities q_{cr1} and q_{cr1} and decreases the probability of full film and transitive boiling, which in most cases causes nonuniform surface hardness and increased distortions.

Although these factors may justify the development of new technologies, perhaps the most important is the potential to control (regulate) the temperature field of a part to be quenched when $Bi \to \infty$. Generally when $Bi \to \infty$, the surface temperature of a part during quenching becomes equal to the temperature of the quenchant, and therefore it is impossible to change the temperature field of the part. During the boiling process, the surface temperature decreases sharply to the boiling temperature of the boundary liquid layer, and during the self-regulated process it is maintained at approximately at the same level. However, by applying pressure or additives to the quenching solution, it is possible to vary the saturation temperature, which will result in a change of the surface temperature during the self-regulated thermal process. With high-carbon steels, although the martensite start temperature M_S is below 200°C, it is still possible to increase the boiling temperature of a boundary liquid layer up to M_S, which will retard the transformation of austenite into martensite when the maximal temperature gradients are normally observed in the part.

This concept may be used to control the temperature field of a part to be quenched when $Bi \to \infty$, which expands the potential of LTMT and is a basis for the development of new intensive quenching technologies. Experimental data illustrating the use of this concept are presented below.

8.2 QUENCHING PROCESSES UNDER CONTROLLED PRESSURE

Steel quenching processes performed using water and aqueous solutions under controlled pressure were studied using the testing system shown in Fig. 1. The system consisted of an induction heating device (5), a tightly closed quenching chamber (2), a vacuum pump for evacuation and for creation of an underpressure in the chamber, a cylindrical pressure vessel (7) with the compressed air, and measuring devices (8–10) for monitoring temperature fields in test specimens and pressure in the chamber [1,2].

Inside the chamber was an inductor (4), induction installation (5), coil pipe (1) for cooling (quenchant), electric heaters, and a test specimen (8) suspended on a mobile rod, which moves up and down by turning a solenoid (6) on or off. Observation windows on lateral walls permitted visual monitoring of the formation of vapor films throughout the process. Compressed air was introduced into the chamber from a tank (7), which was used for cooling specimens under pressure. A vacuum pump was connected here for the creation of underpressure above the bath and for vacuum-cooling test specimens. The temperature of the quenchant was measured at different points in the tank by using chromel-copper thermocouples delivered through the bottom of the chamber to potentiometer EPP-098. The temperature of the specimen was determined by using chromel-alumel thermocouples inserted into the chamber through the seal in the top cover. Temperature fields were recorded using two potentiometers (EPP-09 and PS-11) and an oscillograph (N105) [1].

Tests were performed using a cylindrical specimen of 20-mm diameter made of austenitic Kh18N9T or Kh18N10T (AISI 304) steel. Stainless steel specimen material was used because when steel is austenitized, its thermal and physical properties differ very little from the thermal and physical properties of Kh18N9T (AISI 304) steel.

Differential chromel-alumel thermocouples were made of 0.2-mm-diameter wire. The junctions of the thermocouples were welded inside the test specimen, and at the surface, the thermocouple extensions were recessed in grooves and covered by foil. To prevent the possibility of quenchant penetration into apertures at the end-face of a test specimen, a tube was welded to isolate the inner thermocouples from the liquid. The test specimen assembly was fixed on a mobile

---

[1] *IQ Technologies, Inc., Akron, Ohio, and Intensive Technologies Ltd., Kyiv, Ukraine*
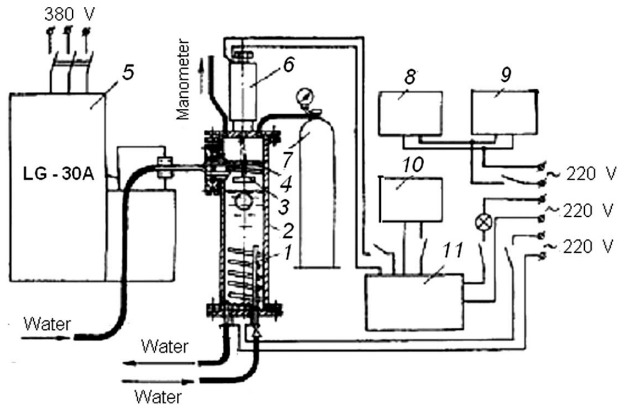
Fig. 1—Schematic illustration of the installation used for quenching steel test specimens in liquid media using controlled pressure: 1, coil pipe; 2, chamber casing; 3, test specimen; 4, inductor; 5, induction installation; 6, solenoid; 7, tank with compressed air; 8 and 9, potentiometers EPP-09 and PS-11; 10, oscillograph N105; 11, rectifier V-26.

rod, which, when the solenoid was turned on, pulled the specimen into the inductor to be heated.

This test apparatus was used for the study of cooling properties of quenchants under controlled pressure. For the study of the effect of pressure on distortion and to assess the probability of quench crack formation, a special experimental stand was made, consisting of a tightly closed tank inside of which was an electric furnace used for heating of test parts (see Fig. 2). At the bottom part of the electric furnace,
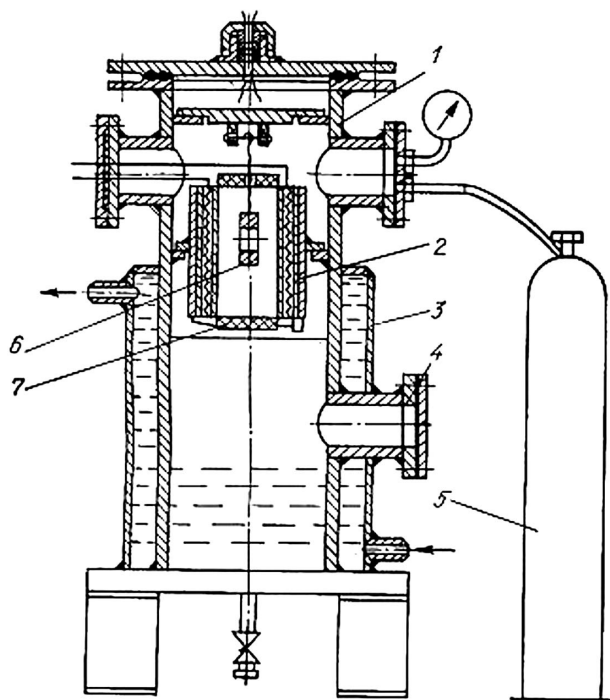
Fig. 2—Testing installation for steel quenching in water and aqueous solutions under controlled pressure: 1, installation case; 2, electric furnace; 3, chamber casing; 4, hatch for unloading parts; 5, tank with compressed gas; 6, test specimen; 7, door of the electric furnace, under which there is a sliding reflecting screen.

there was a door that was opened by an electric relay. When heating to the austenitization temperature, a steel part was suspended from a special device, which, when turned on, dropped the part into the quenchant.

The quenching experiments were conducted as follows. At the beginning of the experiment, the vacuum pump removed air from the chamber, and the chamber was then filled with an inert gas. When the electric furnace reached the required austenitization temperature and after soaking for the required time at temperature, the electric furnace door was opened using an electric relay, the dropping device was turned on, and the part was dropped (by gravity) into the quench tank located at the bottom of the chamber. The chamber was pressurized using an inert gas, which was delivered into the chamber from a tank. The part was unloaded from the chamber through the hatch (4 in Fig. 2). A constant quenchant temperature was maintained by the water-jacketed chamber. For this purpose, casing (3) was attached to the outer wall of the chamber, to which water was supplied.

Water and aqueous solutions of salts and alkalis of various concentrations were used as quenchants for steel quenching under pressure. The choice of solutions of salts and alkalis was made with a double purpose. First, as has been shown, there is an optimal concentration of salts and alkalis in water, at which the first critical heat flux density q_{cr1} reaches a maximum, that provides more intensive and uniform cooling of a part's surface due to minimization of the probability of the formation of vapor films. The use of aqueous solutions of salts and alkalis (electrolytes) of optimal concentration together with high pressure significantly raises the critical heat flux density. Second, the use of aqueous solutions of salts and alkalis of high concentration increases the saturation temperature.

The test stand shown in Fig. 2 has been used to study the effect of pressure on the steel quenching process. In particular, it can be used for the study of the effect of pressure on the process of quench crack formation, deformation and distortion, hardening capacity, and hardenability of steel parts, as well as on the effect of pressure on residual stresses that arise during quenching. Initially, the quenchants were not agitated (still) during the steel quenching, and only natural circulation of the quenchant was observed.

The effect of pressure upon temperature distribution was studied using a cylindrical specimen of 20-mm diameter. Experiments were conducted at atmospheric pressure and at pressures of 0.3, 0.6, and 0.9 MPa. Temperatures at various points of the specimen are shown in Fig. 3. During cooling in water under atmospheric pressure, nonuniform cooling of the part's surface was observed due to the formation of localized vapor films. When the pressure on the quenchant was increased, the film boiling process disappeared, and the temperature of the surface of the part decreased quickly to the saturation temperature of the quenchant, after which nucleate boiling proceeded to the saturation temperature of the quenchant.

Fig. 3 shows that, during nucleate boiling at atmospheric pressure for 10 s, the temperature at the surface of a specimen changed from 120°C to 100°C, while at the center of the specimen, the temperature changed from 730°C to 250°C. At high pressure, in particular, 7×10^5 Pa (0.7 MPa), the temperature at the surface sharply decreased to 190°C and, after 10 s, to approximately 170°C. In this same time, the temperature at the distance of $r/R = 0.31$ was reduced
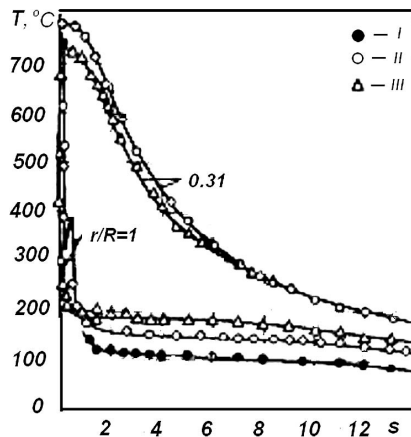
Fig. 3—Effect of pressure on the temperature field of a cylindrical specimen of 20-mm diameter made of steel Kh18N9T (AISI 304): I, 0.1 MPa; II, 0.4 MPa; III, 0.7 MPa (R is the radius of the cylinder; r is the coordinate or distance from the core).

from 730°C to 220°C. When the pressure was increased further, the temperature of the surface also increased. During nucleate boiling, this temperature did not change significantly, and with increasing pressure, the duration of nucleate boiling decreased somewhat, transitioning earlier into single-phase convection.

These results are important from a practical point of view since the transformation of the supercooled austenite into martensite–in particular, for high-carbon steels–starts at 200°C and below. For low-carbon and medium-carbon steels, the martensite start temperature M_S is characteristic, below which, with an increase in cooling rate, intensive transformation of a greater part of austenite into martensite starts. For medium-carbon steels, the M_S temperature is approximately 150−200°C. Therefore, for these steels, the application of a low pressure over the liquid quenchant during quenching will delay the transformation of a greater part of austenite into martensite, and for high-carbon steels, transformation is completely avoided. Such a delay is feasible only during nucleate boiling where there is a minor alteration of the surface temperature and essential change of temperature of inner points of the specimen.

It should be noted that one can delay the phase transformations through pressure by reducing martensite start temperature M_S instead of increasing the surface temperature of a body up to M_S. In practice, low pressures do not exhibit an effect upon M_S temperature. Only at very high pressure (about 3×10^8 Pa or 300 MPa) will a shift of M_S to a lower temperature occur.

Fig. 3 also shows that when quenching in water, high thermal gradients may occur during nucleate boiling, which would lead to high thermal stresses. In addition, because of the high specific volume of martensite formed as a result of the quenching process, significant transformational stresses would be formed as well. It is necessary to consider that untempered martensite is a fragile microstructure, and the transformation of austenite into martensite in the presence of high thermal gradients is associated with the danger of quench crack formation. The delay of transformation of austenite into martensite during nucleate boiling minimizes the possibility of crack formation. Shteinberg [3] has noted that quench cracks arise only when there is more than 50 % martensite in the supercooled austenite. Quench cracks do not

form in this case because of the high plasticity of supercooled austenite. Therefore, control of pressure during steel quenching is a powerful tool to control distortion and quench-cracking of parts.

The use of variable pressure is of interest because, in practice, it is difficult to control pressure at a constant level. When loading and unloading parts from the quench chamber, the pressure decreases to atmospheric pressure. To study the effect of variable pressure on temperature at the surface of a part during quenching, an experiment was performed in the system shown in Fig. 1. The chamber pressure from the time of immersion of the heated specimen into a quenchant increased from atmospheric to 9×10^5 Pa (0.9 MPa). Fig. 4 shows the linear variation of surface temperature of a cylindrical 20-mm-diameter specimen versus pressure.

Inner points of the specimen during nucleate boiling were intensively cooled, and with increasing pressure, the surface temperature at first increased slightly and then decreased to the quenchant temperature. The slight increase of surface temperature came about because, at the completion of the nucleate boiling process, the chamber pressure increased insignificantly, and only during convection did it reach 0.9 MPa. This shows that it is possible to control the surface temperature using pressure only during nucleate boiling. During convection, it is practically impossible to control the surface temperature.

This observation has also been shown by numerical calculations described in [1]. Fig. 4(b) provides experimental data illustrating the effect of variable pressure during a variation of temperature at the surface and within the specimen [1]. Therefore, by both experimental and numerical data, the character of variation of temperature at the surface and within a steel test specimen is identical.

However, numerical calculations show that cooling within a test specimen is somewhat faster than indicated by experimental data. This is explained as follows. Upon immersion of a test specimen in a quench tank at atmospheric pressure, localized vapor films are formed, and once formed, they do not disappear even with a further increase in
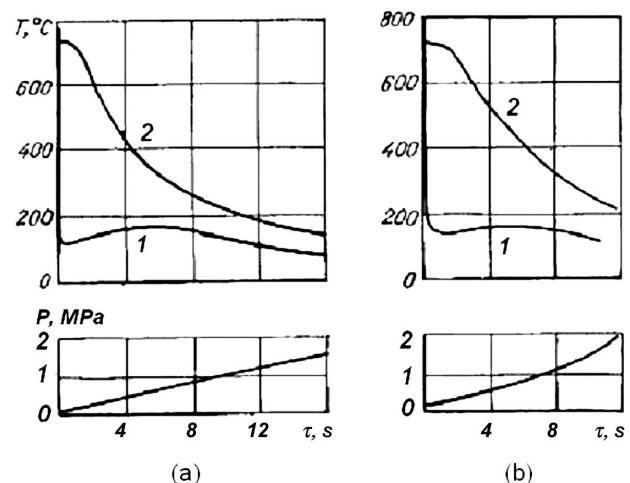
Fig. 4—Effect of variable pressure during a change in temperature at the surface and core of a 20-mm-diameter cylindrical Kh18N9T (AISI 304) steel test specimen during cooling in water at 20°C: (a) numerical calculation; (b) experimental data; 1, at the surface; 2, at a point a distance of 6.2 mm from the center.
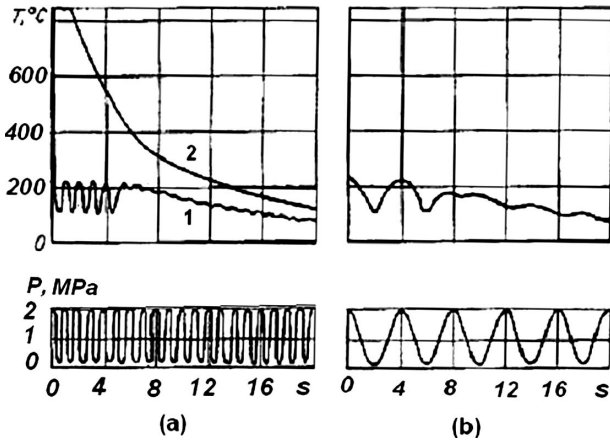
Fig. 5—Effect of a harmonic variation of pressure on surface temperature of a cylindrical 20-mm-diameter Kh18N9T (AISI 304) test specimen, cooled in water at 20°C: (a) at a frequency of 1 Hz; (b) at a frequency of 0.25 Hz; 1, surface temperature; 2, core temperature.

pressure. This may occur outside of a junction of the thermocouple welded in the specimen and appreciably slow down the cooling rate at points within the specimen.

It is of practical interest to study the effect of variable pressure on the surface temperature during nucleate boiling. Fig. 5 presents the effects of variable pressure on the temperature at the surface of a test specimen during cooling from 850°C in water at 20°C. When the pressure changes harmonically in this way, the surface temperature changes harmonically also. This is typical for a nucleate boiling process. Calculations have shown that during convection there is an insignificant change in the surface temperature due to the change in physical characteristics of the quenchant.

Fig. 6 illustrates the effect of pressure on the temperature field for a cylindrical specimen obtained using a finite-difference numerical computation. These data show that
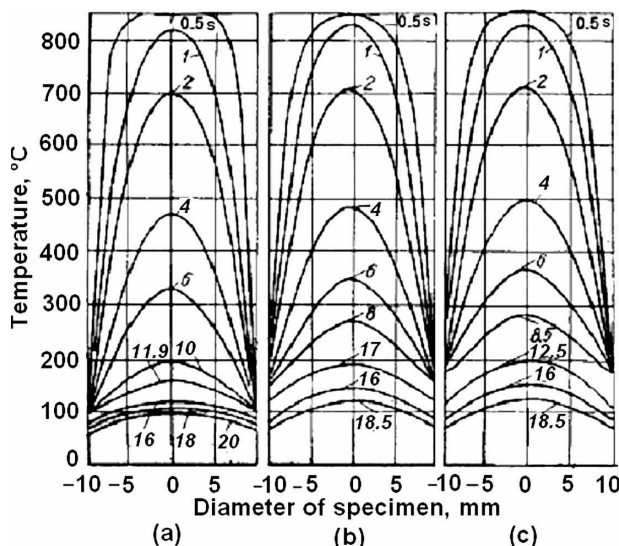
Fig. 6—Temperature field of a 20-mm-diameter cylindrical Kh18N9T steel test specimen cooled from 850°C in water at 20°C: (a) at atmospheric pressure; (b) at a pressure of 7×10^5 Pa (0.7 MPa); (c) at a pressure of 10×10^5 Pa (1 MPa).

during the existence of high thermal gradients inside a cooled specimen, the surface temperature is 10−30°C greater (depending on the size of a specimen) than the saturation temperature of the quenchant. At the conclusion of the nucleate boiling process, the temperature gradient is equalized and the temperature of the specimen gradually decreases to the temperature of the quenchant.

It is known that high intensity of heat transfer during nucleate boiling is due to the formation, growth and dispatch of vapor bubbles which causes the heat transfer. For the formation and growth of vapor bubbles, it is necessary that the boundary liquid layers be superheated to a temperature above the saturation temperature.

Not all vapor bubbles in a superheated liquid are able to undergo further growth, but only those whose diameter exceeds the critical size D_{min}, which is determined by:

$$D_{min} = \frac{4\sigma T_S}{\rho'' r^* (T - T_S)}, \qquad (1)$$

where:
σ is surface tension;
r^* is the latent heat of vapor formation;
T_S is the boiling (saturation) temperature;
T is temperature of a wall; and
ρ'' is the density of vapor.
Therefore, as shown in Fig. 6, during nucleate boiling, the temperature field of parts to be quenched can be controlled by pressure.

Table 1 shows the effect of pressure on the temperature of a boundary liquid layer. With increasing pressure, the surface temperature is always higher than the boiling temperature of a boundary liquid layer by 10−30°C and changes insignificantly during nucleate boiling, as shown in Fig. 6.

Thus, by changing pressure, one can effectively control the surface temperature of a part to be quenched under any given condition, which can be used for controlling the process of transformation of supercooled austenite into martensite. Using CCT (continuous cooling transformation) diagrams and knowing the martensite start (M_S) temperatures, one can design optimal steel quenching conditions using Table 1.

8.2.1 Formation of a Boundary Liquid Boiling Layer and Critical Heat Flux Density

Previously, the effect of pressure on the temperature field during quenching was discussed. Upon immersion of austenitized steel into a quenchant, nucleate boiling occurs immediately, but the surface temperature can be controlled by pressure. However, during quenching, the formation of localized and stable vapor films, which interrupt the overall surface cooling process, was observed. This nonuniform film boiling process is undesirable in industrial quenching processes since it results in nonuniform surface hardness, deformations, distortions, and so on. Therefore, it is of practical interest to consider the effect of pressure on the formation of a boundary liquid boiling layer and the occurrence of film boiling.

When a heated specimen is immersed into an underheated liquid, the boundary liquid boiling layer is formed first, after which nucleate or film boiling appears. Typically, the formation of a boundary liquid boiling layer in nonstationary conditions of heat transfer is usually not considered; however, this is the initial phase from which all other boiling processes start to develop. This is evident when considering

TABLE 1—Water saturation temperature versus pressure							
P (MPa)	T_S (°C)	P (MPa)	T_S (°C)	P (MPa)	T_S (°C)	P (MPa)	T_S (°C)
0.1	99.64	1.1	184.05	2.1	214.84	3.2	237.44
0.2	120.23	1.2	187.95	2.2	217.24	3.4	240.88
0.3	133.54	1.3	191.60	2.3	219.55	3.6	244.16
0.4	143.62	1.4	195.04	2.4	221.77	3.7	247.31
0.5	151.84	1.5	198.28	2.5	223.93	3.8	250.33
0.6	158.84	1.6	201.36	2.6	226.03	3.9	253.24
0.7	164.96	1.7	204.30	2.7	228.06	4.0	256.05
0.8	170.42	1.8	207.10	2.8	230.04	4.1	258.75
0.9	175.35	1.9	209.78	2.9	231.96	4.2	261.37
1.0	179.88	2.0	212.37	3.0	233.83	4.3	263.91

the time dependence of heat flux density by solving reverse problems of nonstationary thermal conductivity [4,5]. For this work, cylindrical specimens of 20 and 30-mm diameter were cooled in water at various temperatures under atmospheric and higher pressure conditions.

Calculations showed that the heat flux density during water quenching of a 30-mm-diameter specimen at first grows from zero to 6.8 MW/m^2 and then drops sharply, as shown in Fig. 7. When cooling from 840°C, two maxima of heat flux density are observed, which are attributable to the first and second crises of boiling [5]. In the first part of the curve (see Fig. 7), for rather a short time (0.2 s), the boundary liquid boiling layer is formed and the first critical heat flux density q_{cr1} is reached. Then the process of film boiling occurs, and the second maximum of heat flux density is caused by the second crisis of boiling. As the initial temperature decreases, which is equivalent to a decrease in the heat flux density, the second maximum must disappear, because at small heat flux densities the crisis of boiling may not occur. In this case, a boundary liquid boiling layer is formed and the liquid boils, during which the heat flux density reaches a maximum that depends on the temperature gradient of the body

and thermal conductivity of the material. Then, the heat flux density decreases approximately exponentially. This change in the heat flux density is observed during cooling a cylindrical specimen of 30-mm diameter from 447°C in water at 20°C (Fig. 7(b)).

For the test specimens studied, a boundary liquid boiling layer is formed for a short time. For example, during cooling of a 30-mm-diameter cylindrical specimen from 850°C in water at 20°C, the time of the first period, during which the first maximum of heat flux density is reached, is approximately 0.2 s, while the time of nucleate boiling for this specimen is 22 s. The time of the first period is thus about 1 % of the total time of nucleate boiling.

In some cases, there may be no experimental data for boundary conditions for the first period; the time may be neglected since nucleate boiling is established immediately upon immersion into the quenchant. Such an approach provides only an approximate solution; however, when there is no film boiling, satisfactory agreement between computed data and experimental results is obtained.

Fig. 7(a) shows that when there is film boiling, the heat flux density during cooling reaches a critical value that agrees well with experimental results obtained under stationary conditions. Table 2 below presents results of the determination of the first critical heat flux density q_{cr1} versus water temperature based on experimental data.

When the pressure increases, q_{cr1} increases. Tolubinskiy and Fedorchenko [6,7] studied the effect of pressure and deep underheating on the first critical heat flux density. Some of their results are presented in Fig. 8. These data show that steel quenching under pressure possesses a number of advantages. By increasing pressure, not only is the process of transformation of austenite into martensite during the period of high thermal stresses delayed, but the value
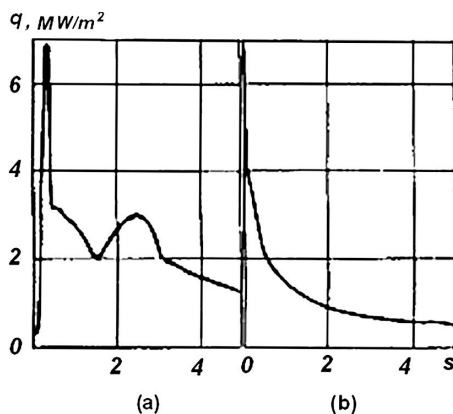
Fig. 7—Heat flux density versus time during the cooling of a cylindrical specimen of 30-mm diameter in water at 20°C: (a) cooling from 840°C; (b) cooling from 447°C.

TABLE 2—The first critical heat flux density q_{cr1} versus water temperature						
T (°C)	0	18	38	75	89	100
q_{cr1} (MW/m^2)	6.5–7	5.8	4.8	2.4	1.91	1.45–1.6
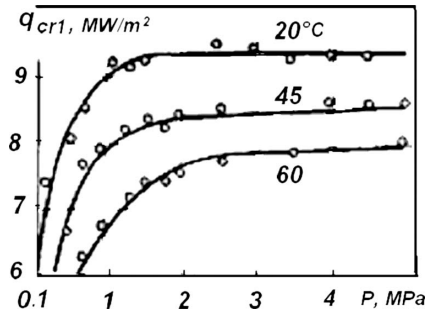
Fig. 8—First critical heat flux density q_{cr1} versus pressure and temperature of water.

of q_{cr1} is significantly increased, which will result in the avoidance of the formation of vapor films.

When the pressure increases, underheating of the liquid also increases because the saturation temperature increases (see Table 1). The greater the underheating of a liquid with respect to the saturation temperature, the more heat is necessary for the formation of a boundary liquid boiling layer, the lower the temperature at the surface of a part during quenching, and the lower the probability of the formation of vapor films.

To examine this process in detail, consider the time dependence of the heat flux density during cooling of a 30-mm-diameter cylindrical specimen in an alkaline solution of sodium hydroxide (NaOH), where the critical heat flux density q_{cr1} is higher than the initial maximum heat flux density (see Fig. 9). The maximum heat flux density does not exceed 11 MW/m², while q_{cr1} during quenching under pressure or in aqueous solutions of alkalis is much higher than this value.

During steel quenching under pressure in an aqueous electrolyte solution, in some cases there is no film boiling at all. The only phenomenon observed is the formation of a boundary liquid boiling layer, which may be neglected with minimal error. The primary cooling processes are nucleate boiling and single-phase convection. The absence of film
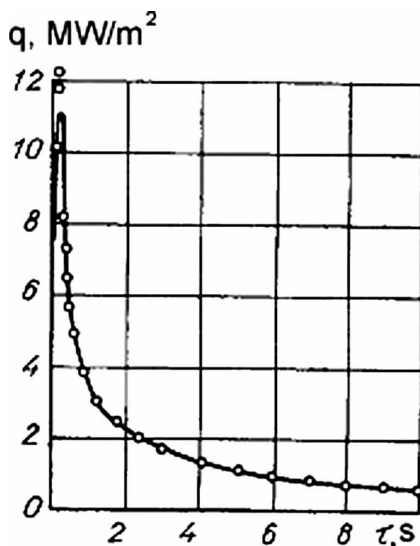
boiling during steel quenching is notable, because it was formerly believed that during steel quenching from high temperatures, full film boiling would always be observed.

8.3 EFFECT OF PRESSURE ON QUENCH CRACK FORMATION

When there is no film boiling during steel quenching, high temperature gradients are observed, because during nucleate boiling the most intensive heat transfer at which $Bi \rightarrow \infty$ is obtained. Therefore, it is necessary to determine if it is possible to avoid quench crack formation during intensive heat transfer due to the increase in pressure upon the quenchant. It is also important to determine the effect of pressure on quench distortion. Therefore, a study was conducted using the experimental test rig shown in Fig. 2 to determine the effect of pressure on distortions and quench crack formation. The experiments were conducted using bearing rings and split keys made of ShKh15 (AISI 52100) steel. Parts made of this steel are among the most sensitive to quench crack formation, especially during quenching in water, and for this reason they were selected for this study.

The bearings were heated to 860−870°C, and then they were quenched in water until the cooling process was complete. Constant pressure was maintained on the surface of the quenchant. As the pressure increased, the probability of quench crack formation decreased, as shown in Fig. 10. During water quenching at atmospheric pressure, all of the test specimens possessed quench cracks observable to the naked eye. As the pressure increased, the number of test specimens with cracks sharply decreased. At a pressure of 10×10^5 Pa, cracking was observed only on a few specimens. It was not possible to avoid the quench crack formation completely, because during water quenching the convection heat transfer coefficient is quite large and therefore thermal stresses during single-phase convection are still sufficient to cause some cracking.

To reduce the convection heat transfer coefficient in water, various salts and alkalis can be added. At a 20 % concentration of salts and alkalis in water and a pressure of 3×10^5 Pa, crack formation was completely avoided. For this experiment, aqueous solutions of calcium chloride ($CaCl_2$) and sodium hydroxide (NaOH) were used.

Quench cracks were not formed during quenching in high-concentration, aqueous solutions at atmospheric pressure if the concentration of the solutions provided a boiling temperature of the boundary liquid layers of about 130−140°C.

Fig. 9—Heat flux density versus time during cooling of a cylindrical specimen of 30-mm diameter from 830°C in 5 % aqueous solution of NaOH at 20°C.
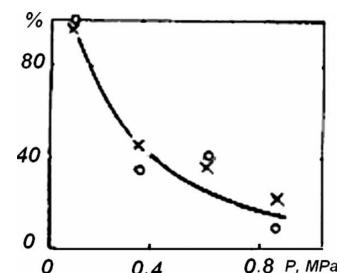
Fig. 10—Effect of pressure on the quenchant on quench crack formation for bearing rings made of ShKh15 (AISI 52100) steel: X, 208/01 bearing ring; O, 308/01 bearing ring. Temperature of the water quenchant was 30–40°C.

8.3.1 Quenching in Aqueous Solutions of Salts and Alkalis of High Concentration

High concentrations of salts and alkalis, for example, calcium chloride and sodium hydroxide, in water raise the boiling temperature of the solution, and therefore, the application of high-concentration solutions is equivalent to an increase of pressure. Furthermore, the increase of salt and alkali concentrations results in the reduction of the convection heat transfer coefficient. Therefore, the cooling rate is reduced during the transformation of austenite into martensite, which reduces quench crack formation. Fig. 11 shows the temperature at the surface of a part during quenching in water at 20°C, and in a high-concentration solution of calcium chloride and oil.

When quenching in a salt solution, the surface temperature increases. However, during quenching in water and high-concentration salt solutions, film boiling is observed due to the delay of the cooling process. By increasing the concentration of salts and alkalis in water, the critical heat flux density q_{cr1} decreases. Therefore, when quenching in high-concentration solutions of salts and alkalis, the possibility of quench crack formation is eliminated and distortion, as shown in Fig. 12, is minimized.

The reduction of ovality of rings during quenching in aqueous solutions is related to the delay of transformation of austenite into martensite, which reduces transformational stresses due to the different specific volumes of microstructures formed. This process leads to a nonuniform phase transformation, which is why nonuniform cooling results in increased deformations and distortion.

When quenching into solutions with an increased boiling temperature in the range of 130−140°C, quench cracking was not observed with specimens made of ShKh15 (AISI 52100) steel, as shown in Table 3. Fig. 13 illustrates the cooling process for the inner points of a split key performed in various quenchants. The cooling rate of specimens in water and aqueous solutions, within the range of temperatures of 200−300°C, differs very little. This suggests that the slight increase of the surface temperature during nucleate boiling led to a delay of the transformation of austenite into martensite, during which time high thermal stresses exist, and therefore no quench cracks were formed.
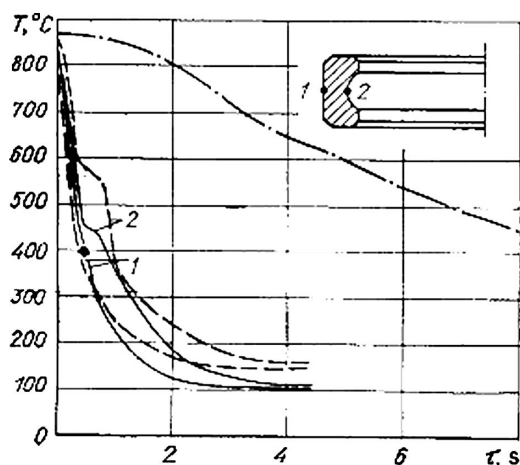
Fig. 11—Surface temperature versus time for bearing ring 308/01 cooled in water at 20°C (solid curves); an aqueous solution of CaCl$_2$ ($\rho = 1,280$ kg/m^3) at 30°C (dashed curves); and oil (dash-and-dot curve).
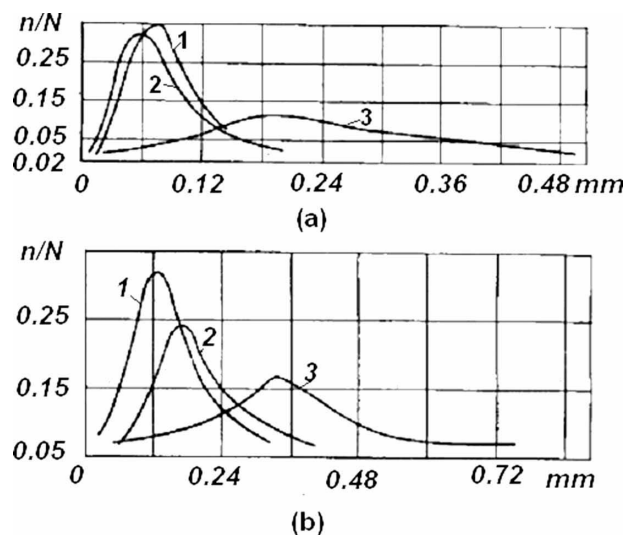
Fig. 12—Ovality of bearing rings 208/01 (a) and 308/01 (b) during quenching from 860°C in various quenchants at 30–40°C in: 1, oil; 2, an aqueous solution of CaCl$_2$ ($\rho = 1,280$ kg/m^3); 3, water.

The test specimens, whose shapes are shown in Fig. 14, were bearing rings, split keys made of ShKh15 (AISI 52100) steel used in automobile industry, and splined specimens of half-axles of KRAZ (Kremenchuk Automobile Zavod) automobiles. The test specimens were made of AISI 1045, 47GT, and 40KhN2MA (AISI 4340) steel. In addition, cylindrical specimens of 6-mm diameter of 45, 40Kh, U7A, and 60SA steels were prepared for a break test and for the study of the quenching process. The chemical composition of various steel grades is presented in Table 4. The critical points of phase transformations for the mentioned steel grades are presented in Table 5.

These data show that even a slight increase in the temperature at the surface of parts to be quenched during nucleate boiling by increasing pressure or by the use of various additives to increase the boiling temperature of the solutions results in a sharp reduction or full elimination of quench crack formation.

The application of high-concentration aqueous solutions in practice is not always expedient because equipment may become contaminated, corrosion of the metal surface occurs, and additional costs for the purchase of chemicals are required, along with increased environmental concerns. Therefore, most quenching is performed in water under pressure or, in some cases, under pressure in aqueous salt solutions at their optimal concentration. In case of quench crack formation during quenching in water under pressure, the cooling process is interrupted at the end of the nucleate boiling process. Subsequent cooling is performed much more slowly, either in air or in a slower quenching media. For this purpose it is important to be able to calculate the duration of nucleate boiling, that is, the duration of time during which there is a delay of transformation of a great bulk of the supercooled austenite into martensite.

8.4 THERMOMECHANICAL TREATMENT OF STEELS WITH THE USE OF PRESSURE

Steel quenching in water and electrolytes of optimal concentration and increased boiling temperature is similar to isothermal quenching, except that with isothermal quenching

TABLE 3—Effect of saturation temperature of salt solutions upon quench crack formation in split keys made of ShKh15 (AISI 52100) steel

Quenchant	Temperature of quenchant (°C)	Density of quenchant (kg/m³)	Saturation temperature (°C)	Number of parts with cracks	Surface hardness (HRC)
Water solution of NaOH	22	1,000	100	50	64
	24	1,250	107	60	65
	24	1,330	116	10	64.5
Aqueous solution of CaCl₂	45	1,480	130	0	64.5
Oil	26	890	—	0	62

the cooling process is slowed and it is necessary to use high-alloy steels to obtain hardenability. Isothermal quenching can be performed for parts of small sizes. Unlike isothermal quenching, quenching under pressure can be performed only during nucleate boiling; at the conclusion of nucleate boiling, the surface temperature approaches the quenchant temperature, so it is important to calculate the duration of nucleate boiling.

Isothermal quenching is performed in molten salts, hot oils, molten metals, or other media where the temperature is maintained above or near the martensite start temperature M_S. Therefore, during isothermal quenching, transformation of austenite into martensite is prevented because the bath temperature T_m is higher than the martensite start temperature, that is, $T_m \geq M_S$. The microstructure of the steel after isothermal quenching is finely divided sorbite or bainite.

To expand the potential of isothermal steel quenching in molten salts, a small amount of water is added to increase the quenching severity [8,9]. However, relative to quenching in water and electrolytes, the cooling capacity of such molten salts with water additions is rather low. Quenching in water and in aqueous solutions under pressure eliminates these shortcomings [1].

As indicated previously, it is possible to use high-concentration aqueous solutions of salts and alkalis. Fig. 15 illustrates the boiling temperature versus the concentration of sodium hydroxide (NaOH) and potassium hydroxide (KOH) in water. High solubility of alkalis can be obtained using warm water. For isothermal quenching, it is not necessary to warm the aqueous solution up to temperature M_S; it is sufficient if the boiling temperature of the solution is at M_S.

This process was demonstrated as follows. A part was heated to the austenitization temperature and immersed into the quenching solution, for example, a 50 % sodium hydroxide solution at 30–40°C. The boiling temperature of the boundary liquid layer of such a solution, according to the data shown in Fig. 15, is approximately 150°C. At the conclusion of nucleate boiling, the duration of which was calculated as shown in Chapter 5, the part was cooled in air or was placed into an electric furnace at 150–200°C. If higher isothermal temperatures are required, solutions of higher concentrations are used. In this case, to increase of solubility of salts and alkalis, it was necessary to increase the bath temperature (see Fig. 15).

Methods of low-temperature thermomechanical treatment (LTMT) have been developed for isothermal quenching processes. Typically, after austenitization, a part is cooled to a temperature at which the supercooled austenite contains

Fig. 13—Temperature at the center of a split key versus time during quenching from 850°C in various quenchants: I, an aqueous solution of NaOH at 40°C ($\rho = 1,250$ kg/m³); II, an aqueous solution of NaOH at 24°C ($\rho = 1,330$ kg/m³); III, an aqueous solution of CaCl₂ at 27°C ($\rho = 1,480$ kg/m³); IV, a solution of 40 % glycerin, 20 % NaCl, and 40% water. The solid line denotes water at 22°C; the dashed line denotes oil at 24°C.
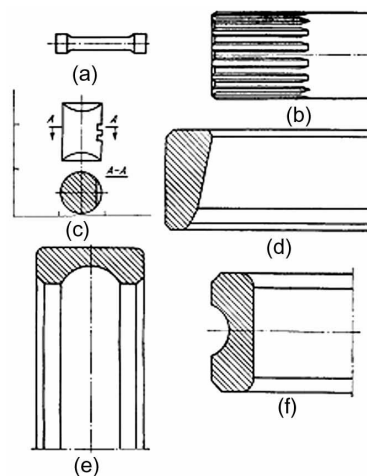
Fig. 14—Shapes of the specimens studied: (a) specimen for break test; (b) slot specimen of a half-axle of KRAZ automobile; (c) split key; (d), (e), and (f) bearing rings.

TABLE 4—Chemical composition of steels								
Steel grades	**Percentage of composition (% weight)**							
	C	**Si**	**Mn**	**S (max)**	**P (max)**	**Cr**	**Ni**	**Others**
45 AISI 1045	0.42–0.50	0.17–0.37	0.5–0.8	0.04	0.04	0.25	0.25	—
40Kh AISI 5140	0.36–0.44	0.17–0.37	0.5–0.8	0.035	0.035	0.80–1.10	0.25	—
ShKh15 AISI 52100	0.95–1.10	0.15–0.35	0.20–0.40	—	—	1.30–1.65	0.25	—
40KhN2MA AISI 4340	0.37–0.44	0.17–0.37	0.50–0.80	—	—	0.60–0.90	1.25–1.65	0.15–0.25
60S2 AISI 9260	0.57–0.62	1.05–1.20	0.60–0.90	0.04	0.04	0.30	0.40	0.25
U7A AISI 1070	0.65–0.74	0.15–0.30	0.15–0.30	—	—	0.15	—	—
U8 AISI 1080	0.75–0.84	0.15–0.30	0.15–0.30	—	—	0.15	—	—
U12 AISI W1	1.15–1.24	0.15–0.35	0.15–0.35	—	—	0.20	—	—

no more than 25 % martensite, and the part is maintained at this temperature. The temperature is equalized throughout the part, at which time the parts are cooled under pressure in an aqueous electrolyte solution at an optimal concentration. The required isothermal temperature is dependent on the pressure. At the conclusion of the process, the part is subjected to plastic deformation, and then it is intensively quenched to achieve complete transformation of the austenite into martensite.

Another method of LTMT [10] involves cooling the part to a temperature where it is held isothermally so that, in the supercooled austenite, no more than 50 % martensite is formed. Then the part is subjected to the further treatment as described above [10–13]. The distinctive feature of this method is that the part is held isothermally in a cold quenchant, where temperature is controlled by pressure. This method extends the potential of LTMT since intensive quenching is performed, which allows the use of carbon steels and parts with a large section size. Isothermal transformation temperatures where no more than 25 % martensite is formed in austenite are given in Table 6. For many steel grades, the application of pressure for the implementation of isothermal transformation during intensive quenching is required.

If equipment has not been modified for pressurization, it is sometimes possible to use high concentrations of aqueous salt solutions. However, is it impossible to perform this process without pressurization when conducting the quenching process at first in water at atmospheric pressure and then subjecting the parts to plastic deformation as described above, because when cooling in water, at the surface temperature where there are no local vapor films, the temperature quickly cools to the saturation temperature of water (100–130°C). Therefore, in the surface layers of the part for the majority of steel grades, more than 50 % martensite is formed. Subjecting such a part to further treatment, such as

TABLE 5—Temperatures of phase transformations of steel grades studied				
Steel grade	**A_{c1}**	**A_{c3}**	**M_S (°C)**	**Temperature of heating (°C)**
45 AISI 1045	740	805	345	850
40Kh AISI 5140	730	760	330	840
40KhN2MA AISI 4340	680	775	390	830
60S2 AISI 9260	775	830	300	860
U7A AISI 1070	720	760	280	810
U8 AISI 1080	730	740	245	800
U12 AISI W1	720	—	200	780–800
ShKh15 AISI 52100	750–795	—	245	860
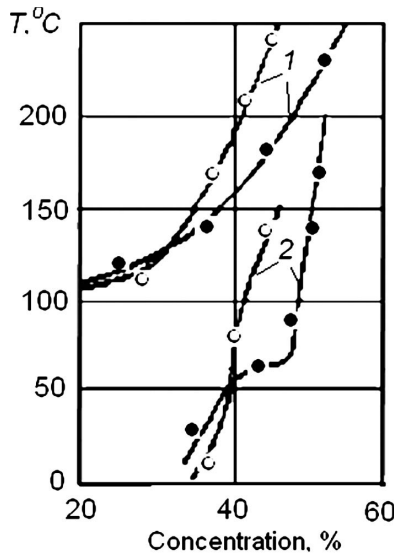
Fig. 15—Boiling temperature of solutions (1) and their maximal solubility in water (2) versus concentration in water: black data points, NaOH; white data points, KOH.

plastic deformation, isn't reasonable since the martensite has not been tempered and is a fragile microstructure that, under the effect of mechanical loadings, can break. In addition, during water quenching, film boiling is observed, which slows the cooling process and leads to potential transformation of austenite in the intermediate area.

The use of pressure is also effective for high-temperature thermomechanical treatment (HTMT) for parts exposed to stamping or rolling in dies where some portion may undergo partial cooling. For example, during rolling of ShKh15 (AISI 52100) steel bearing rings in dies of an automated line, the rings are partially cooled, and afterward it is impossible to implement HTMT using the usual conditions. During quenching in oil, troostite spots are formed in the cooled area of a ring; when quenching in water, there is a high probability of quench crack formation and there are large tensile residual stresses that exhibit an adverse effect on the service life of the bearings. This is one reason why HTMT is not now used in the bearing industry [10–14].

However, this problem can be solved if the rings after rolling are quickly cooled to a temperature where the supercooled austenite contains no more than 50 % martensite and then maintained at the same temperature until the temperature is equalized throughout the cross-section of the ring, at which time the rings are cooled in a jet of wet air or in another slow-cooling quenchant. Using this technology, parts are quickly cooled to an intermediate temperature so that troostite spots are not formed, and the same temperature is maintained for a sufficient time until a great bulk of austenite is transformed into martensite, which eliminates the possibility of quench crack formation. This quenching process may be conducted with the use of electrolytes at an optimal concentration and pressure according to conditions described above.

8.5 QUENCH PROCESS UNDER PRESSURE FOR TOOLS

The method of quenching in water and aqueous solutions under controlled pressure, or in high-concentration aqueous solutions of salts and alkalis that increase the boiling temperature, may be effectively used in the tool industry to take advantage of intensive quenching technologies for tools and

TABLE 6—Isothermal temperatures for various steel grades where no more than 25 % martensite in the supercooled austenite is formed

Steel grade	Austenitization temperature (°C)	Content of carbon in steel (%)	Temperature	
			M_S	Formation of 25% martensite
30G2M	—	0.30	350	320
40KhM	—	0.38	350	280
40 (AISI 1040)	850	0.43	340	250
50 (AISI 1050)	825	0.53	310	290
45(AISI 1045)	880	0.44	350	310
R18 (AISI T1)	1,300	0.72	190	150
R18K5	—	0.72	185	130
ShKh15 (52100)	860	1.04	245	190
ShKh15SG	850	0.99	200	120
9Kh (AISI L2)	980	0.97	150	90
Carburized 20KhN2M (4320)	850	1.18	140	120
U8 (AISI 1080)	850	0.81	235	150
U10 (AISI W1)	780	1.1	200	130

other parts made of high-carbon steels. Intensive quenching is important since it not only yields advantages related to increasing labor productivity and hardenability of steel but also provides improvement in the mechanical properties and thus the service life of tools. However, during intensive quenching, thermal and transformational stresses are high, and therefore the probabilities of material failure increases. For example, in practice, quenching processes are usually conducted in oil, which may prove insufficient for tools because of low cooling rates. During intensive quenching in water, for example, high transformational and thermal stresses may lead to quench crack formation. Quenching tool steels in water and aqueous solutions under pressure eliminates this problem.

Fig. 16 presents the basic scheme of an automated process for steel heat treatment under controlled pressure. The quenching process is conducted as follows. When the piston is at starting position I, the part (5), which is austenitized, is delivered to the tray (1). At this time, the driving mechanism is turned on, and the piston occupies work position II, hermetically closing the top of the quench tank. Simultaneously, through an aperture (2), compressed air is introduced, creating the necessary pressure between the quenchant and the piston (cover). Pressure is delivered so that the quenchant saturation temperature approximates the M_S temperature. When quenching in water under pressure, during nucleate boiling there is a delay in the transformation of austenite into martensite; therefore, the effect of high thermal stresses consists of the supercooled austenite. Quench cracks under these conditions are not formed.

After nucleate boiling is completed, the surface temperature decreases to quenchant temperature. The formation of the ferromagnetic martensitic phase is fixed by the solenoid (6). The signal from the solenoid is amplified (A) and triggers the relay (R) to actuate the driving mechanism (G), which moves the piston (3) to top starting position I. The

Fig. 16—Basic scheme of the automated process of steel quenching in water and aqueous solutions under pressure: 1, tray; 2, aperture for pumping in compressed air; 3, mobile piston (cover); 4, case of the quench tank; 5, the part to be quenched; 6, solenoid for fixing the initial time of transformation of austenite into martensite; A, the amplifier of a signal of the martensite start; R, relay of current; G, driving mechanism; I, starting position; II, work position.

part (5) is ejected from the tray (1) and delivered for tempering. It is replaced by the next part, and the cycle is repeated again [1]. This cooling process may be used for continuous automated industrial lines.

This described quenching method [1] expands the potential of low-temperature thermomechanical treatments. At the end of the nucleate boiling process, the steel part consists wholly or partially of supercooled austenite. The temperature in the core of the part at the end of nucleate boiling, depending on its size and system pressure, reaches values related to the relative stability of supercooled austenite. Therefore, after nucleate boiling, the part consists completely of supercooled austenite and can be subjected to the plastic deformation, that is, LTMT. In this case, the mechanical and plastic properties of the steel are improved.

The method of steel quenching in water and aqueous solutions under controlled pressure can be effectively applied for those steel grades that have a martensite start temperature M_S equal to or less than 200°C. For medium-carbon steels, intensive quenching within the martensite range is recommended [14–16].

8.6 PROSPECTS OF STEEL QUENCHING IN LIQUID MEDIA UNDER CONTROLLED PRESSURE

Steel quenching in water and aqueous solutions under controlled pressure possesses a number of advantages relative to other cooling processes. One advantage is that water is the least expensive quenchant. Another advantage is that, when quenching in water under pressure, high heat transfer coefficients are achieved, which improves the ability to harden steel considerably. Water is the most common quenching medium, and it is also used for superficial quenching of parts during induction heat treatment.

Pressure-controlled delay of transformation of austenite into martensite during nucleate boiling with the further intensive quenching during convection provides further improvement in mechanical properties, thus expanding the potential of LTMT. For the implementation of steel quenching in water and aqueous solutions under controlled pressure, it is necessary to construct custom quenching installations and devices. Such installations and devices can be connected in a single industrial line, with the continuous production process beginning from processing preforms with a lathe and finishing with the release of heat-treated parts.

Since it is necessary to intensify heat transfer within the martensite range to provide the condition of $Bi \rightarrow \infty$, the mathematical description of quenching processes under these conditions becomes considerably simpler. Reliable control over the temperature field of parts to be quenched under conditions close to $Bi \rightarrow \infty$ using water and applying computer-aided control systems will expand opportunities for the use of controlled pressure quenching processes to obtain high-strength and heavy-duty materials. Intensification of the heat transfer process during martensitic transformation improves steel strength, which significantly increases service life even of carbon steels. Therefore, a great bulk of machine parts, work tools, and equipment of various kinds may be made of inexpensive carbon steels, while more expensive alloys may be saved for other purposes.

The immediate tasks in the improvement of steel quenching technology are the description of all processes by mathematical models and the development of computer automated production lines [17–19].

Another interesting development is the increasing use of vacuum furnaces for heat treatment of tools utilizing water and aqueous solution quenching under pressure. In this case, heating of tools is performed in vacuum, and quenching is performed in an adjacent chamber under pressure.

In practice, heat treatment of tools is often performed with isothermal quenching in molten salts. The quenching method described above permits the replacement of molten salts with aqueous solutions of salts and alkalis at high concentration, which possess a high boiling temperature of a boundary liquid layer–that is, $M_S \approx T_S$–considerably reducing costs and simplifying heat treatment.

To illustrate, consider the process of quenching a part in clamped condition (fixture or press quenching) using quenchants under pressure [1,20–24]. Parts made of alloyed steels are usually cooled in oil in the clamped condition to minimize distortion. There are many special installations, one of which is shown in Fig. 17 [25], that can be adapted for quenching parts in water under pressure. Such processes are efficient when using high-carbon steels with an M_S of approximately 200°C or lower. In this case, the martensite transformation may be delayed to obtain optimal mechanical properties.

During phase transformations, superplasticity is observed where resistance to deformation is reduced by two or three orders of magnitude [20]. This provides new opportunities for punching by minimizing deformability and distortion of hardened parts and reduces defects due to turning [21–24].

Quenching of stamps under pressure permits the use of water instead of oils, since pressurization increases the saturation temperature of water, which delays the martensite transformation during the self-regulated thermal process. When the temperature of the core reduces to M_S, the steel becomes superplastic, and during this period the shape of the part is corrected using only small forces–that is, the part receives the required shape set by stamp. Abnormal reduction in yield strength near the M_S temperature and the probable reasons of such behavior are discussed in [20].

Using pressure, it is possible to influence the temperature field of a part to be quenched, delaying the transformation of austenite into martensite and controlling the superplasticity process, thus easily correcting existing defects in a part to be quenched, which will minimize distortion.

As an example, assume that a part is cooled from the austenitization temperature of 820°C and the martensite start temperature M_S is observed at 180–220°C. The part has
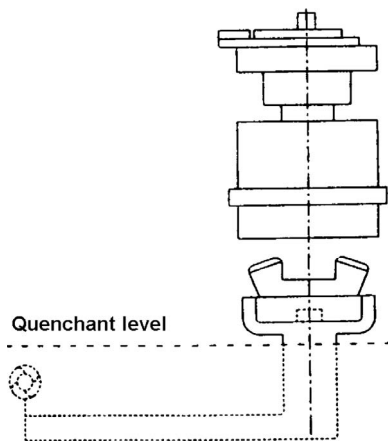
Fig. 17—System for quenching gears under pressure.

the shape of a ring with an internal diameter of 200 mm and an outer diameter of 250 mm. The height of the ring is 30 mm. Calculate the pressure and duration of the nucleate boiling process during which martensite transformation can be delayed.

During the nucleate boiling process, when martensite transformation is delayed, it is necessary to apply a force to the ring to avoid distortion and to correct existing defects. To delay the transformation of austenite into martensite below M_S (180°C), it is necessary to perform quenching under pressure of 10 atmospheres (1 MPa) [1]. In this case, the temperature at the surface of the ring during nonstationary nucleate boiling (the self-regulated thermal process) will be supported for enough time at 180°C. The duration of the self-regulated thermal process is determined by Eq 2 (see Chapter 2 and [1,26]):

$$\tau = \left[0.48 + 3.21 \ \ln \frac{\vartheta_I}{\vartheta_{II}}\right] \frac{K}{a}, \qquad (2)$$

where:

$$\vartheta_I = \frac{1}{7.36} \left[\frac{2\lambda \left(\vartheta_0 - \vartheta_I\right)}{R}\right]^{0.3}; \qquad (3)$$

$$\vartheta_{II} = \frac{1}{7.36} \left[\alpha_{conv}(\vartheta_{II} + \vartheta_{uh})\right]^{0.3}; \qquad (4)$$

$\lambda = 22$ W/mK is the heat conductivity of steel;
$\vartheta_0 = 820°C - 180°C = 640°C$;
$L = 0.025$ m is the thickness of the ring;
$Z = 0.03$ m is the height of the ring;
$\alpha_{conv} = 1,000$ W/m²K is the heat transfer coefficient during convection;
$\vartheta_{uh} = 180°C - 20°C = 160°C$;
$\vartheta_I = 9.2°C$ is the temperature at the beginning of the self-regulated thermal process calculated by Eq 3;
$\vartheta_{II} = 5°C$ is the temperature at the end of the self-regulated thermal process calculated by Eq 4:

$$\ln \frac{\vartheta_I}{\vartheta_{II}} = 0.61;$$

$a = 5.36 \times 10^{-6}$ m²/s is the thermal diffusivity of steel; and
$K = \dfrac{1}{\frac{9.87}{(0.03)^2} + \frac{9.87}{(0.025)^2}} = 37.4 \cdot 10^{-6}m^2$ is the Kondratjev form factor.

Substituting all input data to the first equation (Eq 2), we obtain:

$$\tau = [2.44] \frac{37.4 \cdot 10^{-6}m^2}{5.36 \cdot 10^{-6}m^2/_s} = 17 \ \sec.$$

Thus, in this example, the self-regulated thermal process lasts for 17 s, and transformation austenite into martensite can be delayed for 17 s, too. During this period, when material is still plastic, a press quenching can be applied to eliminate distortion or to fix it by press forces. After 17 s, it would be dangerous to apply forces, since a brittle layer of martensite appears at the surface of the ring and applied forces could damage the ring, generating cracks.

The generalized equation 69 from Chapter 5 can be used also for designing pressurized quenching processes. For

example, it is possible to estimate the temperature at the core of the ring at 17 s using Eq 69. Substituting, we obtain:

$$\tau = \left[0.48 + \ln\frac{820\degree C - 20\degree C}{250\degree C - 20\degree C}\right]\frac{37.4 \cdot 10^{-6}m^2}{5.36 m^2/s \cdot 0.7} = 16.9 \text{ sec,}$$

where $Kn \approx 0.7$ is the Kondratjev number. This means that at the end of nucleate boiling, the surface temperature will be 180°C and the core temperature of the ring will be 250°C. No martensite transformation will take place during this period, and the material will still be plastic during this period of time, so press quenching can be applied to prevent distortion.

These examples show that Eq 2 can be successfully used for engineering calculations. More accurate calculations may be performed by computer simulation using a reliable database of experimental data. Detailed information describing quenching of steel parts under pressure can be found in [1,2,26–32].

8.7 DISCUSSION
Quenching of steel parts and tools under pressure has several benefits. The most important are:
- It allows the potential utilization of low-temperature thermomechanical treatment, which brings further improvement in the mechanical properties of steel.
- It reduces distortion of quenched steel parts and tools.
- It eliminates film boiling when quenching steel products in water flow under pressure.
- It can be combined with press quenching to significantly reduce distortion.
- It can be used with vacuum furnaces.

Currently, quenching in pressurized water flow is used in the production of semi-axles for trucks [1], rebars [27], and rods and wires [32]. The mass production of rebars in India is shown schematically in Fig. 18 [27].

A more detailed drawing of the cooling chamber for quenching rods and wires, including rebars, is shown in Fig. 19 [1,32]. Water pressure at the entrance of the cooling chamber is 0.3–0.35 MPa, and the water flow minimum in the chamber is 8 m/s. This process can be significantly improved if an optimized quenched layer is utilized after intensive quenching of rebars and rods [1,33].
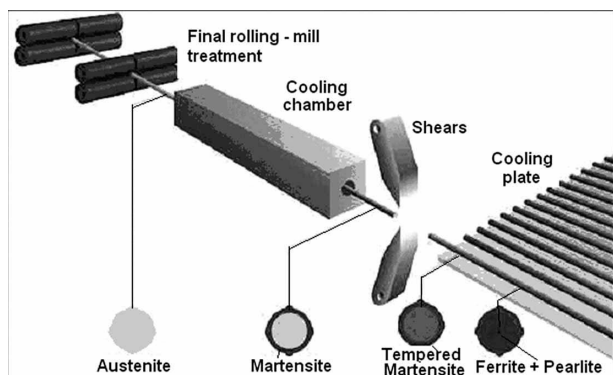
Fig. 18—Illustration of the line for rebar production in India, which includes high-temperature thermomechanical treatment combined with intensive quenching [27].
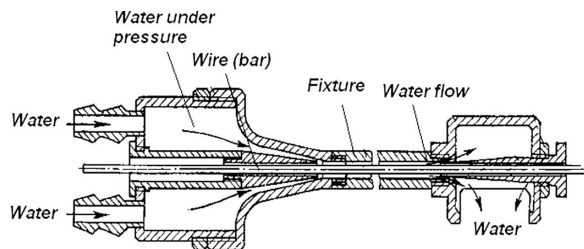
Fig. 19—Cooling chamber used for intensive quenching of rods and wires [32].

8.8 SUMMARY
1. Steel quenching in water and water-salt solutions under extra pressure eliminates film boiling and delays transformation of austenite into martensite during nucleate boiling. This expands the potential for application of low-temperature thermomechanical treatment when quenching alloy and high-alloy steel grades tools in water.
2. Vacuum furnace production of heavy-duty tools may be performed by using an adjacent pressurized quench chamber.
3. Molten salts used for isothermal quenching may be replaced with high-concentration water-salt solutions, which reduce the cost of the process of heat treatment.

References
[1] Kobasko, N. I., *Steel Quenching in Liquid Media Under Pressure,* Naukova Dumka, Kyiv, 1980.
[2] Kobasko, N. I., Steel Quenching in Liquid Media Under Pressure, *Proceedings of the 4th WSEAS International Conference on Heat and Mass Transfer,* Gold Coast, Queensland, Australia, January 17–19, 2007, pp. 98–103.
[3] Shteinberg, M. M., *Heat Treatment of Steel,* Metallurgizdat, Moscow, 1945.
[4] Kobasko, N. I., Kozdoba, L. A., and Moshnyanskiy, A. F., Solving Reverse Non-Linear Problems of Non-Stationary Thermal Conductivity on Electrical Models, *Teplofizika i teplomekhanika,* No. 31, 1976, pp, 25–29.
[5] Kobasko, N. I., and Kasyanova, M. D., Study of Some Peculiarities of Non-Stationary Heat Transfer at Quenching, *Teplofizika i teplotekhnika,* No. 33, 1977, pp. 57–71.
[6] Tolubinskiy, V. I., and Fedorchenko, B. Ya., Effect of Pressure and Position of the Surface upon Crisis of Heat Transfer in Case of Boiling in Great Pool of Liquid at Underheating, *Izvestiya Vuzov,* Section *Energiya,* No. 7, 1967, pp. 35–40.
[7] Tolubinskiy, V. I., and Fedorchenko, B. Ya., Effect of Pressure and Underheating upon Crisis of Heat Transfer in Case of Boiling in Great Pool of Liquid, *Teploobmen i Hidrodinamika v dvukfaznykh sredakh* (Heat transfer and hydrodynamics in two-phase media), Naukova Dumka, Kyiv, 1967, pp. 24–30.
[8] Biryukova, V. N., Cooling Capacity of Melts of Salts and Alkalis Containing Water, *Metal Science and Heat Treatment,* No. 11, 1967, pp. 58–62.
[9] Biryukova, V. N., Device for Supplying Water to Melts of Salts and Alkalis (Ustroystvo dlya vvedeniya vody v rasplavy soley i shchelochey), Inventor's Certificate No. 202,983 (USSR), *Bulletin of Inventions,* No. 20, 1967.
[10] Astafiev, A. A., Zeymetdinov, Kh. Kh., Prozorov, L. V., et al., Method of Thermomechanical Treatment of Steels and Alloys (Sposob termomekhanicheskoy obrabotki stali i splavov), Inventor's Certificate No. 517,650 (USSR), *Bulletin of Inventions,* No. 22, 1976.
[11] Ivanova, V. S., and Gordienko, L. K., *Novye puti povysheniya prochnosti metallov* (New ways of increasing metal durability), Nauka, Moscow, 1964.
[12] Bernshtein, M. L., *Termomekhanicheskaya obrabotka metallov i splavov* (Thermomechanical treatment of metals and alloys), Vol. 1, Moscow, Metallurgiya, 1968.

[13] Bernshtein, M. L., *Termomekhanicheskaya obrabotka metallov i splavov* (Thermomechanical treatment of metals and alloys), Vol. 2, Moscow, Metallurgiya, 1968.

[14] Kobasko, N. I., Hardening Method of Alloy Steels, Ukraine Patent No. 27,059, filed February 17, 1995.

[15] Kobasko, N. I., Quenching Apparatus and Method for Hardening Steel Parts, U.S. Patent No. 6,364,974 BI, April 2, 2002.

[16] Kobasko, N. I., Intensive Steel Quenching Methods, *Theory and Technology of Quenching*, Liščić, B., Tensi, H. M., and Luty, W., Eds., Springer-Verlag, Berlin, 1992, pp. 367–389.

[17] Inoue, T., and Arimoto, K., Development and Implementation of CAE System "Hearts" for Heat Treatment Simulation Based on Metallo-thermo-mechanics, *Journal of Materials Engineering and Performance*, Vol. 6, No. 1, 1997, pp. 51–60.

[18] Ferguson, B. L., Freborg, A., and Petrus, G. J., Software Simulates Quenching, *Heat Treating Progress*, 2000, pp. H31–H36.

[19] Kobasko, N. I., Morhuniuk, W. S., and Dobrivecher, V. V., Control of Residual Stress Formation and Steel Deformation During Rapid Heating and Cooling, *Handbook of Residual Stress and Deformation of Steel*, Totten, G., Howes, M., and Inoue, T., Eds., ASM International, Materials Park, OH, 2002, pp. 312–330.

[20] Shteinberg, M. M., Zhuravlev, L. G., Povolotskyi, V. D., and Peysokov, Yu. V., On Temperature Dependence of Yield Strength of Austenitic Steels Undergone Through Martensite Transformation During Deformation, *FMM*, Vol. 43, No. 4, 1977, pp. 786–792.

[21] Sharshorov, V. M., Tikhonov, A. S., Bulat, S. I., et al., *Superplasticity of Metallic Materials*, Nauka, Moscow, 1973.

[22] Vorobiev, V. G., On Changes of Mechanical Properties Versus Time During Inner Transformations, *Metallovedenie i obrabotka metallov*, No. 3, 1958, pp. 35–38.

[23] Firger, I. V., Small-Distortion Quenching of Machine Parts, *Issues of Quench Cooling*, Energiya, Moscow, 1969, pp. 89–93.

[24] Spector, A. G., and Marennikova, I. A., Effect of Value of Clamping Force upon Preserving the Shape of Rings During Quenching in Stamps, *Issues of Quench Cooling*, Energiya, Moscow, 1969, pp. 66–72.

[25] Totten, G. E., and Howes, M. A. H., *Steel Heat Treatment Handbook*, Marcel Dekker, New York, 1997.

[26] Kobasko, N. I., Self-regulated Thermal Processes During Quenching of Steels in Liquid Media, *International Journal of Microstructure and Materials Properties*, Vol. 1, No. 1, 2005, pp. 110–125.

[27] Thermomechanical Treatment for Reinforcement Bars Opening Up New Vistas, *Evo Tech PVT LTD*, www.evotech.in.

[28] Kobasko, N. I., The Steel Superstrengthening Phenomenon, Part 2, *International Journal of Microstructure and Materials Properties*, Vol. 3, Nos. 4/5, 2008, pp. 526–547.

[29] Kobasko, N. I., Energy Efficient and Eco-friendly Intensively Quenched Limited Hardenability Low Alloy Steels, *Journal of ASTM International*, Vol. 6, No. 1, 2009.

[30] Kobasko, N., Aronov, M., Powell, J., and Totten, G., One More Discussion: "What Is Intensive Quenching Process?", *Journal of ASTM International*, Vol. 6, No. 1, 2009.

[31] Krukovskyi, P., Kobasko, N., and Yurchenko, D., Generalized Equation for Cooling Time Evaluation and Its Verification by CFD Analysis, *Journal of ASTM International*, Vol. 6, No. 5, 2009.

[32] Gridnev, V. N., Meshkov, Yu. A., Oshkaredov, S. P., and Chernenko, N. F., Technological Basics of Electrical Heat Treatment of Steel, Naukova Dumka, Kyiv, 1977.

[33] Kobasko, N. I., and Morhuniuk, W. S., *Issledovanie teplovogo i napriazhenno-deformirovannogo sostoyaniya pri termicheskoy obrabotke izdeliy mashinostroeniya* (Study of thermal and stress-strain state at heat treatment of machine parts), Znanie, Kyiv, 1983.

9

The Steel Superstrengthening Phenomenon

N. I. Kobasko[1]

9.1 INTRODUCTION

The conventional method for improvement of mechanical properties of materials requires the use of alloying elements, which significantly increases their cost. Alloy steels usually are quenched in oils or polymers of high concentration to eliminate crack formation. However, slow cooling in oils decreases the mechanical properties of the materials. This means that more alloy elements need to be added to the material to satisfy the requirements of industry. This chapter discusses new ways of improving the mechanical properties of materials by intensive quenching, especially increasing the cooling rate within the martensite range. It will be shown that intensive cooling within the martensite range is equal to low-temperature thermomechanical treatment and increases the strength and plastic properties of materials [1–4].

9.2 ALTERNATIVE WAYS OF ACHIEVING HIGH-STRENGTHENED MATERIALS

Superstrengthening of metals was first reported in 1967 [3] and has been cited often since that time [5–10]. "Superstrengthening" involves intensive cooling within the martensite range to produce additional strengthening with a simultaneous improvement of plastic properties. There is also an alternative explanation of the superstrengthening effect that involves intensive cooling within a range higher than the martensite start temperature M_S, which results in additional strengthening of metals due to a "freezing of vacancies" formed during the heating process [6,7].

High strength can be achieved in two ways:

1. By obtaining a defectless structure (ideal monocrystals), or
2. By the creation of extremely high dislocation density in the material.

Both processes result in a substantial increase in steel strength [11,12]. However, the second process, which is designated as *thermomechanical heat treatment*, typically requires a large capital investment. During heat treatment, especially thermomechanical treatment, a very high density of dislocations is formed in the metal, resulting in its strengthening.

The effect of mechanical rolling on the physical and mechanical properties of metals has been studied [13], from which the idea to use rapid cooling within the martensite range to create high-strength materials arose. Initially this seemed to be unfeasible because it was generally believed that the high cooling rates associated with intensive cooling within the martensite range would result in significant increases in thermal and structural stresses, high distortions, and an increased propensity for crack formation [14]. At the time, the ideal cooling process was thought to be rapid cooling within the pearlite range (550–650°C) and slow cooling within the martensite range (below 300°C).

It was subsequently shown that, although cooling rate increases within the martensite range do initially increase the probability of quench crack formation, after a maximum cooling rate is exceeded, the probability of cracking decreases to zero (see Fig. 1) [1]. Distortions behave similarly: increased cooling rates within the martensite range initially increase distortions, but after a maximum cooling rate is exceeded, distortion decreases.

It was subsequently established that within the martensite range there is a critical cooling rate above which not only does the probability of quench crack formation decrease but superstrengthening of metals is also observed [1–3,15]. However, further experimental validation results were variable; in some cases, this effect was clearly observed, and in others when the chemical composition of steel was changed, the effect was not observed.

The reason for these effects is related to the self-regulated thermal process [16,17], where intensive quenching eliminates film boiling and cooling occurs by nucleate boiling. Under these conditions, the surface temperature of the steel sharply decreases to the boiling temperature of the liquid and is maintained at this level (see Fig. 2). The duration of the self-regulated thermal process is determined by this equation (see Chapter 2):

$$\tau_{nb} = \left[\Omega + b \ln \frac{\vartheta_I}{\vartheta_{II}}\right] \frac{K}{a}, \qquad (1)$$

where:
τ_{nb} is time (s);
$\Omega = 0.48$ (for cylinders);
$b = 3.21$;
ϑ_I is the overheat at the beginning of the self-regulated thermal process;
ϑ_{II} is the overheat at the end of the self-regulated thermal process;
K is the Kondratjev form factor (m²); and
a is the thermal diffusivity of steel (m²/s).

If the self-regulated thermal process is observed within the martensite range, it results in the delay of transformation of austenite into martensite. The duration of this delay is determined by Eq 1. The cooling rate of the superficial layers in this case approaches zero. Under these conditions, no superstrengthening of the material is observed because cooling rate approaches zero. To avoid this, it was suggested to increase the boundary liquid layer boiling temperature to the martensite start temperature M_S [4] and then to utilize intensive cooling during the second stage.

Fig. 2 shows that the surface temperature sharply decreases to the boiling temperature of the boundary liquid

---

[1] *IQ Technologies, Inc., Akron, Ohio, and Intensive Technologies Ltd., Kyiv, Ukraine*
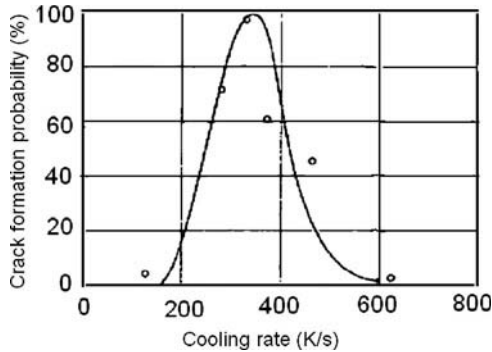
Fig. 1—Effect of cooling rate within the martensite range on cracking in cylindrical samples of 6-mm diameter made of 40Kh steel (0.42 % C, 0.60 % Mn, 0.28 % Si, 0.95 % Cr, 0.25 % Ni).

layer and that the time τ_{nb} remains constant until nonstationary nucleate boiling is completed [17,18]. If the boundary liquid layer boiling temperature is increased to the martensite start temperature M_S, the transformation of austenite into martensite will be delayed for the time of τ_{nb}. By exploiting this effect, it is possible to provide intensive cooling during the second cooling stage, after the nucleate boiling process of the first stage (see Fig. 2). This may be accomplished by using aqueous solutions of calcium chloride ($CaCl_2$) and magnesium chloride ($MgCl_2$). During quenching in aqueous solutions of these salts–with additional additives to prevent corrosion of the metal surface–the boiling temperature of the boundary liquid layer reaches 180°C or more. Therefore, the transformation of austenite into martensite is delayed during the first stage. Dependence of the boiling temperature of the boundary liquid layer upon the concentration of calcium chloride in water is shown in Fig. 3.
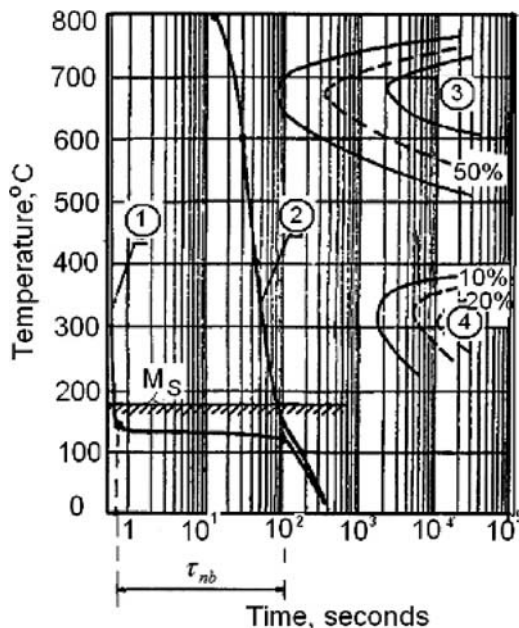
Fig. 2—Temperature versus time at the surface (1) and the core (2) of a cylindrical sample of 60-mm diameter during quenching in an aqueous solution of $CaCl_2$ and comparison with the CCT diagram. These are compared to curves for pearlite (3) and bainite (4), where the percentages indicate the amount of the microstructure formed in each area.
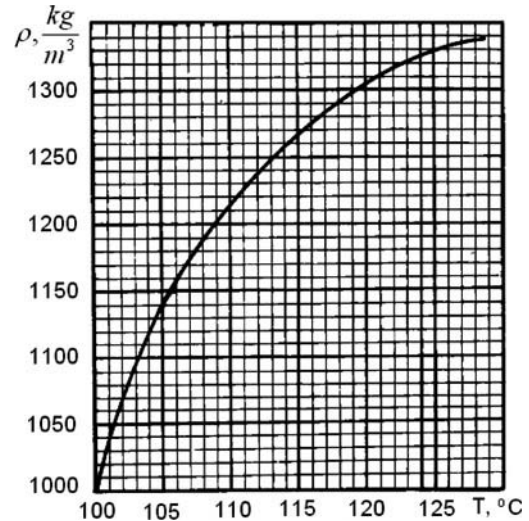
Fig. 3—Saturation temperature vs. concentration for an aqueous solution of $CaCl_2$.

This heat treatment process is easily implemented when quenching high-carbon steels. When quenching medium-carbon steels, it is expedient to conduct intensive cooling at high Biot numbers ($Bi \rightarrow \infty$), so that the surface temperature constantly decreases from the austenitizing temperature to quenchant (medium) temperature. The martensite start temperature of these steels is around 300°C, and decreasing the temperature at the surface of steel to 20°C or below permits high cooling rates in superficial layers of the parts to be quenched. Due to the high cooling rates within the martensite range, superstrengthening of the material is achieved.

9.3 NATURE OF THE SUPERSTRENGTHENING PHENOMENON

To understand the nature of superstrengthening, consider the scheme shown in Fig. 4. Imagine a superficial layer compressed to the limit (1,200–1,500 MPa) in which there are plates of martensite possessing a greater specific volume
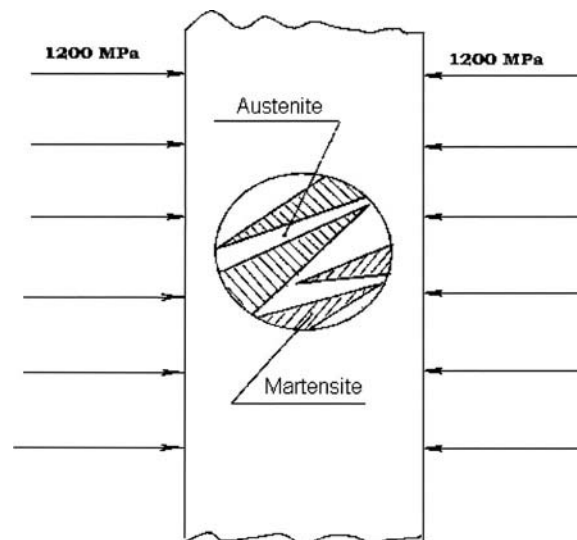
Fig. 4—The transformation scheme of austenite into martensite in the compressed layer, illustrating the effect of additional strengthening (superstrengthening) of the material.

than the initial phase structure of supercooled austenite. The period of appearance of such plates is very short at less than 10^{-6} s. The plates of martensite deform the supercooled austenite that is between them, as shown in Fig. 4. In this figure, the hatched area indicates martensite, and the light area, the supercooled austenite.

The higher the cooling rate is within the martensite range, the greater will be the extent to which the austenite is deformed, and the higher the dislocation density. Conversely, during rapid cooling, there is not enough time for the dislocations to accumulate in the grain boundaries and to form nuclei of future microcracks; they are frozen in the material. Thus, the superficial layer acts like a blacksmith: under conditions of high stress, the plates of martensite arise explosively, deforming the austenite and creating extremely high dislocation densities, which are frozen during rapid cooling. This process is analogous to low-temperature thermomechanical treatment (LTMT).

During plastic deformation—and in particular, during LTMT—the dislocation density is high. During LTMT, the density of dislocations have been found to be as high as 10^{13} cm^{-2} [19], and material strengthening occurs primarily due to the formation of high-density dislocations and the presence of fine carbides, which function as a barrier for dislocations. One question that arises is why subcritical cooling rates do not produce the steel strengthening effect. Appreciable steel strengthening and increased cyclic fatigue strength are only observed to occur from a certain cooling rate within the martensite range.

During quenching, when austenite is transformed into martensite, high-density dislocations are formed under stresses. These dislocations, due to the increased temperature, move in the steel until they encounter a barrier such as grain boundaries or fine-dispersion inclusions (carbides). The dislocations accumulate at grain boundaries, forming potential nuclei for microcrack formation. If the size of a nucleus increases to a critical size, the crack grows further and propagates into the solid body.

Griffith identified the dependence between the critical size of an ellipse-shaped crack and the stresses necessary for its growth in a plate as [20]:

$$\sigma = \sqrt{\frac{2\gamma E}{\pi l}} \tag{2}$$

where: 2γ is the superficial energy connected with the formation of two new surfaces; E is the Young module; and l is the length of a crack.

When the cooling rate within the martensite range is very high, large amounts of austenite transforms into martensite over a short time and the transformation process exhibits an explosive character. Because of this rapid temperature decrease, the dislocations are "frozen" and do not have time to accumulate at the grain boundaries; therefore, nuclei that could lead to potential microcracks are not formed. Because of the explosive character of the transformation, it is likely that the dislocation density formation in the steel is so high that dislocation movement is inhibited, thus forming a special state which can exist for only a short time. As the temperatures increase, this special state ceases to exist, and the usual dislocation propagation mechanism resumes. Dislocations without congestion at grain boundaries can be fixed by rapid cooling to low temperatures, where the process of fixing dislocations is completed by atomic carbon or other elements.

It is proposed that quenching with high cooling rates within the martensite range is equivalent to the LTMT process and, in some cases, is more efficient when it is related to the improvement in fatigue characteristics. From a practical point of view, this is an important factor, because the LTMT process requires the application of special equipment for plastic deformation and implementation of more complicated and expensive technology. To achieve the superstrengthening effect, it is necessary to follow specific process recommendations that will be discussed subsequently.

9.4 EXPERIMENTAL VALIDATION OF SUPERSTRENGTHENING EFFECT

9.4.1 Phenomenon of Nonlinear Wave Mechanics

Numerous papers have been published, by many authors, concerning vibromixing processes. However, there is a special vibromixing of a two-phase system (air–liquid) where thousands of air bubbles are vibrating and tuned with the resonance frequency of the system (see Fig. 5). At that moment when they become tuned with the resonance frequency of the system, the bubbles go to the bottom of the liquid and, by resonance vibration, accelerate the heat transfer coefficients by two to five times (see Table 1) [10].

The main author of the theory of nonlinear wave mechanics of multiphase systems, Prof. R. F. Ganiev, says that it is the scientific basis for new wave technologies development and has no analogues in world practice. He has emphasized that new wave technologies were designed for many industries: engineering, environmental sciences, the chemical industry, materials science (especially when developing nanocomposites), the food processing industry, and many others. They can be also used in metallurgy for getting very fine microstructures and even nanostructures [21].

9.4.2 Experimental Device

The schematic of the experimental apparatus used for experimental validation of the superstrengthening effect is shown in Fig. 5. The apparatus utilizes a Dewar flask built in a metal casing, in which the lateral walls are equipped with windows made of acrylic plastic for observation and control of the process. The casing with a vessel is rigidly fixed on the vibrator. The vibration of a vessel with liquid nitrogen (Fig. 5, 3) was performed using a vibration stand VEDS-100A (2), which includes an electrodynamic vibrator (2) and control station (5). The latter consists of a generator of sine-wave oscillations, a power amplifier, and an acceleration-measuring
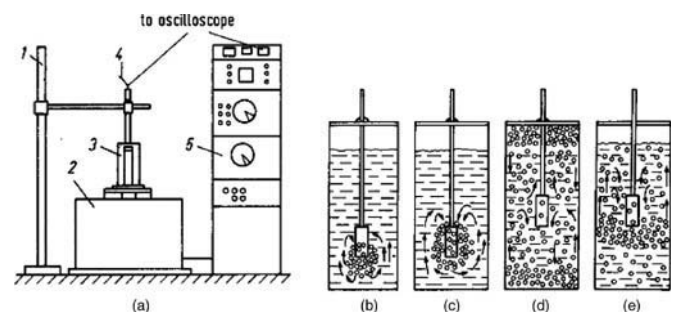
Fig. 5—Experimental apparatus (a): 1, fixture (supporting arm); 2, electrodynamic vibrator; 3, test tank with liquid nitrogen; 4, thermocouple; 5, control station. Schemes of movement of the air bubbles are depicted in conditions of vibromixing in water (b and c) and liquid nitrogen (d and e).

TABLE 1—Heat transfer coefficients depending on the state of a cooling medium [10]					
Cooling medium	Temperature of medium (°C)	Cooling conditions	Frequency of vibrations (Hz)	Acceleration of vibrator (g_{cr}/g_o)	Heat transfer coefficient α (W/m²K)
Liquid nitrogen	−196	No vibrations	—	—	160–230
Liquid nitrogen and vapor	−196	Vibromixing	72	17	331–532
Liquid nitrogen and vapor of helium	−196	Blowing the bath with helium during vibromixing	72	17	234–544
Water	20	No vibrations	—	—	1,600–1,800
Water	20	Vibromixing	20	10	2,800
Water–air	20	Contact of a big number of air bubbles with the sample:			
		−partial	160	15–17	4,490
		−full	167	15–17	6,260
		−vibromixing	60–70	15–17	5,890–8,640

device connected to a piezoelectric acceleration gauge. Test specimens were heated to austenitizing temperature in electric furnace MP-2UM.

During direct cooling from the austenitizing temperature in liquid nitrogen, the film boiling process occurred so intensively that specimens made of plain carbon and medium-alloy steels were not hardened. To provide the necessary cooling rate for the test specimens at high temperature and to delay the transformation of austenite into martensite, two-step quenching in a water-salt solution of high concentration calcium chloride at a bath temperature of 30−40°C was performed. The duration of the first step of cooling was equal to the time of the self-regulated thermal process. The self-regulated thermal process for this solution was dependent

on size of specimens and was above 150°C (see Table 2). When quenching in water-salt solutions of high concentration, the surface temperature of tested specimens during the self-regulated thermal process was a little bit greater than 150°C. Therefore, the greatest amount of austenite transformation into martensite occurred during the second step of cooling, in vibrating liquid nitrogen (see Fig. 5(d and e)).

Film boiling was prevented at the first step of cooling in the water-salt solution of high concentration, and quenching during that period was by the self-regulated thermal process. The duration of self-regulated thermal process was calculated by Eq 1 and, for samples of 5, 6, and 10-mm diameter, is presented in Table 2.

As seen in Table 2, the transformation of austenite into martensite during quenching in a concentrated aqueous salt solution was delayed 1.2–4.9 s, depending on the specimen size and the agitation intensity of the water-salt solution. This time was sufficient to perform two-step quenching. The transformation of austenite into martensite was delayed during the first step of the quenching process, and very intensive cooling was performed during the second step in agitated liquid nitrogen at the resonance frequency to provide maximum heat transfer (see Fig. 5(d and e)) [4,5,17]. By adjusting variation frequency and amplitude, it was possible to adjust the cooling rate within the martensite range. Calculations show that the cooling rate of specimens within the martensite range was adjusted from 6°C/s to 30°C/s (see examples 9.1 and 9.2).

Fig. 6 presents the decrease in temperature of a cylindrical test specimen of 12-mm diameter that was cooled from 100°C in a vessel with liquid nitrogen agitated (by vibromixing) at a frequency of 70 Hz and acceleration of $g = 17g_o$. This experiment shows that the vibromixing process intensifies heat transfer, causing the test specimen to be cooled faster [10].

9.4.3 Results of Two-Step Quenching Experiments

Different steel grades were selected for this test: 45 (AISI 1045), 60S2 (AISI 9260), and U7 (AISI 1070), which have

TABLE 2—Duration of the self-regulated thermal process when quenching cylindrical test specimens in aqueous solutions of salts with convection heat transfer coefficients of 300 or 400 W/m²K and a temperature of boiling of the boundary liquid layer of 150°C

Convection heat transfer coefficient (W/m²K)	Specimen diameter (mm)	Duration of self-regulated thermal process (s)
300	5	1.3
	6	1.9
	10	4.9
400	5	1.2
	6	1.78
	10	4.6

Note: Austenitizing temperature was 800°C; temperature of aqueous solution was 50°C.

Fig. 6—Effect of the frequency of vibration on the cooling process of a cylindrical test specimen made of Kh18N9T (AISI 304) steel, diameter 12 mm, in liquid nitrogen: 1, unagitated; 2, with vibro-mixing [10].

different martensite start temperatures of 350°C, 300°C, and 230°C, respectively. The temperatures at which 50 % martensite is formed in supercooled austenite are 210°C, 190°C, and 140°C, respectively. Therefore, the effect of strengthening must be observed in high-carbon steels in which transformation of the greatest amount of austenite into martensite occurs at a temperature below 150°C. To expand the utility of this technique, it is possible to use pressure or intensively cooling solutions possessing a higher saturation temperature. The cooling time (duration of nucleate boiling) is calculated using Eq 1.

If the cooling of the test specimen had continued to room temperature at the first step, any further cooling at the second step, with or without agitation, in liquid nitrogen would have had no effect on the mechanical properties and additional strengthening. This was validated using cylindrical test specimens of 5 and 6 mm diameters that were first cooled in a high-concentration salt solution for different times: 1, 2, or 3 s, and also until completion of cooling.

After the test specimens were quenched in different conditions, they were tempered and polished, and then their mechanical properties were determined. Specimens made of AISI 1045 and U7A (AISI 1070) steel were tempered at 360–370°C for 2 hours; the 60S2 (AISI 9260) steel specimens were tempered at 460°C, with the same duration of the cooling process. The test results are presented in Table 3.

These data show that whether quenching AISI 1045 steel in water, aqueous solutions of different salt concentrations, or oil, there are no appreciable distinctions in the mechanical properties of the steel because martensite transformations had already occurred before the test specimens were placed into the tank with the agitated nitrogen.

When quenching test specimens made of U7 (AISI 1070) steel, the martensite transformation was completed at a lower temperature, and therefore some portion of the martensitic transformation occurred in a chloride solution and the other portion in the liquid nitrogen agitated at the resonant frequency. Therefore, an increase in strength of U7 (AISI 1070) steel is observed, while maintaining its rather high plastic properties. When increasing the duration of cooling in a high-concentration chloride solution considerably with respect to the calculated value, the strength begins to decrease. This indicates that the temperature at the surface during cooling in a water-salt solution for this time significantly decreased below 150°C, showing that the transformation

primarily occurred in the first step in the water-salt solution and that the increased cooling rate in liquid nitrogen exhibited a much lesser effect.

During longer cooling durations in a solution of calcium chloride as well as during conventional quenching, the effect of steel strengthening wasn't observed. This fact shows that martensite transformations occurred in the water-salt solution due to the longer time of cooling that prevails during the self-regulated thermal process. Strengthening also occurred during quenching of specimens made of 60S2A (AISI 9260) steel (see Tables 2 and 3) subjected to the same or a similar procedure of two-step cooling.

It should be also noted that after two-stage quenching in nonagitated liquid nitrogen using any of the cooling conditions described above, the effect of strengthening was not observed. The ultimate strength (R_m) and plastic properties of the material changed very little, although the process of cooling was performed at different rates within the martensite range. This suggests that only when beginning with a certain cooling rate within the martensite range is the material strengthened. Moreover, during two-stage quenching in nonagitated nitrogen, some test specimens made of U7A (AISI 1070) steel exhibited cracking. At higher rates of intensive cooling in the liquid nitrogen and agitation at the resonant frequency, quench cracks were not observed.

The maximum material strengthening effect can appear only if the martensitic transformation process is completely stopped during the first stage of cooling and when the second stage of cooling is performed in a cryogenic liquid with cooling rates considerably exceeding the critical value.

The extent to which it is possible to improve the mechanical properties by intensification of heat transfer within the martensitic transformation range is shown in Table 3, which provides comparative mechanical properties of U7A (AISI 1070) and 60S2A (AISI 9260) steels quenched by different processes. These data show that the intensification of heat transfer produces material strengths similar to those that are achievable by thermomechanical treatment.

In addition to laboratory studies, industrial tests were performed with punches made of R6M5 (AISI M2) steel used for nut-pressing machines (see Fig. 7). Quenching of the punches was performed in aqueous solutions of salts. The industrial tests showed that the service life of the punches increased, on average, by 2.5 times (see Table 4). Thus, the intensification of cooling within the martensite range results in an increase in strength and service life for steel parts.

9.4.4 Formation of "Packet" Martensite

Electron photomicrographs of R6M5 (AISI M2) steel after conventional and intensive quenching are shown in Fig. 8 (a) and (b), respectively. Microstructures of the conventionally quenched steel after 5,000 fatigue cycles and the intensively quenched steel after 16,500 cycles are shown in Fig. 8 (c) and (d), respectively.

It is important to note that the martensite that forms by conventional quenching (Fig. 8(a)) exhibits a "plate" or "needle" morphology, whereas the martensite formed by intensive quenching (Fig. 8(b)) exhibits primarily a "packet" type morphology. Differences in the microstructures of the fatigue-cycled steels are thought to be due to more stable grain boundaries in the intensively quenched material [1,2]. Therefore, the improved tool durability is attributable to the packet martensite formed by intensive quenching. Along

TABLE 3—Comparative data on mechanical properties of specimens made of U7A (AISI 1070) and 60S2A (AISI 9260) steels, treated in different ways

Steel	Quenching	Temperature (°C)		Strength (MPa)		A (%)	Z (%)
		Heating	Tempering	R_m	$R_{p0.2}$		
U7A (AISI 1070)	In oil MS-20 at 150°C	800	360	1,350	1,270	4.8	29
	In 10 % $CaCl_2$ solution	800	360	1,440	1,400	7	26
	In 10 % $CaCl_2$ solution for 1 s with transfer to still liquid nitrogen	800	360	1,450	1,400	6.4	29
	In 50 % $CaCl_2$ solution for 1 s with transfer to liquid nitrogen (vibromixing)	820	360	1,610	1,570	7.9	31
60S2A (AISI 9260)	In oil MS-20 at 150°C	860–880	460–480	1,580	1,410	7	38
	In 10 % $CaCl_2$ solution	870	460–480	1,420	1,260	8.2	36
	In 10 % $CaCl_2$ solution for 1 s with transfer to still liquid nitrogen	870	460–480	1,460	1,380	6.7	19
	In 50 % $CaCl_2$ solution for 1 s with transfer to liquid nitrogen (vibromixing)	880	460–480	1,920	1,740	4	26

Note: Composition of U7A steel (%): 0.65–0.74 C; 0.15–0.35 Si; 0.15–0.30 Mn; <0.15 Cr; <0.20 Ni; <0.20 Cu. Composition of 60S2A steel (%): 0.58–0.63 C; 1.6–2.0 Si; 0.6–0.9 Mn; <0.3 Cr; <0.25 Ni; <0.20 Cu.

with the mechanical improvement of the material, the intensive quenching creates compressive residual stresses at the surface. Both the mechanical improvement of the material and the compressive residual stresses increase the service life of tools [22–24].

To further explain the advantages of intensive steel quenching methods, the concept of the previously developed *rapid interrupted cooling process* will be applied [25–28]. Rapid interrupted cooling occurs when the superficial and central layers of a part to be hardened are cooled within the temperature range of 500–850°C at a certain rate so that there is no pearlitic transformation. Rapid interrupted cooling is usually fulfilled by air water spray to provide a cooling rate less than intensive quenching in order to receive only bainitic and not martensitic structure. The difference between intensive quenching processes and the rapid interrupted cooling

process is illustrated by Fig. 9. Upon reaching a temperature of 500–600°C, a part is cooled in air at a rate of less than 0.4°C/s or is held isothermally at the bainitic transformation temperature (see Fig. 9(c)).

It has been established that for heat treatment of pipes made of 32G2 (AISI 1330) steel using rapid interrupted cooling, the minimum cooling rate must be 40–50°C/s, and the temperature at the end of interrupted cooling must be 440–460°C [27]. Examination of the power capacity of fracture and character of the break showed that the optimal process of rapid interrupted cooling provides an ultimate strength and yield strength comparable with high-tempered martensite [27]. By optimizing the rapid interrupted cooling process, it is possible to obtain the same dislocation structure, morphology, and phase distribution as in steels subjected to

Fig. 7—Punch made of the molybdenum high-speed steel R6M5 (AISI M2). Intensive quenching in aqueous chloride solutions increased the tool life by 2.5 times. The punch is 126 mm long, and its maximum diameter is 15.3 mm. Its microstructure is shown in Fig. 8.

TABLE 4—Results of testing punches on automatic line "National-164" with performance of 175 strikes per minute

Number of strikes until the destruction of punches		
Normal quenching	Intensive quenching	Increase in service life (multiple)
6,460	15,600	2.4
6,670	16,500	2.9
3,200	5,300	1.65
4,000	12,075	3.0
6,620	8,110	1.2
2,890	10,500	3.6
2,340	7,300	3.1
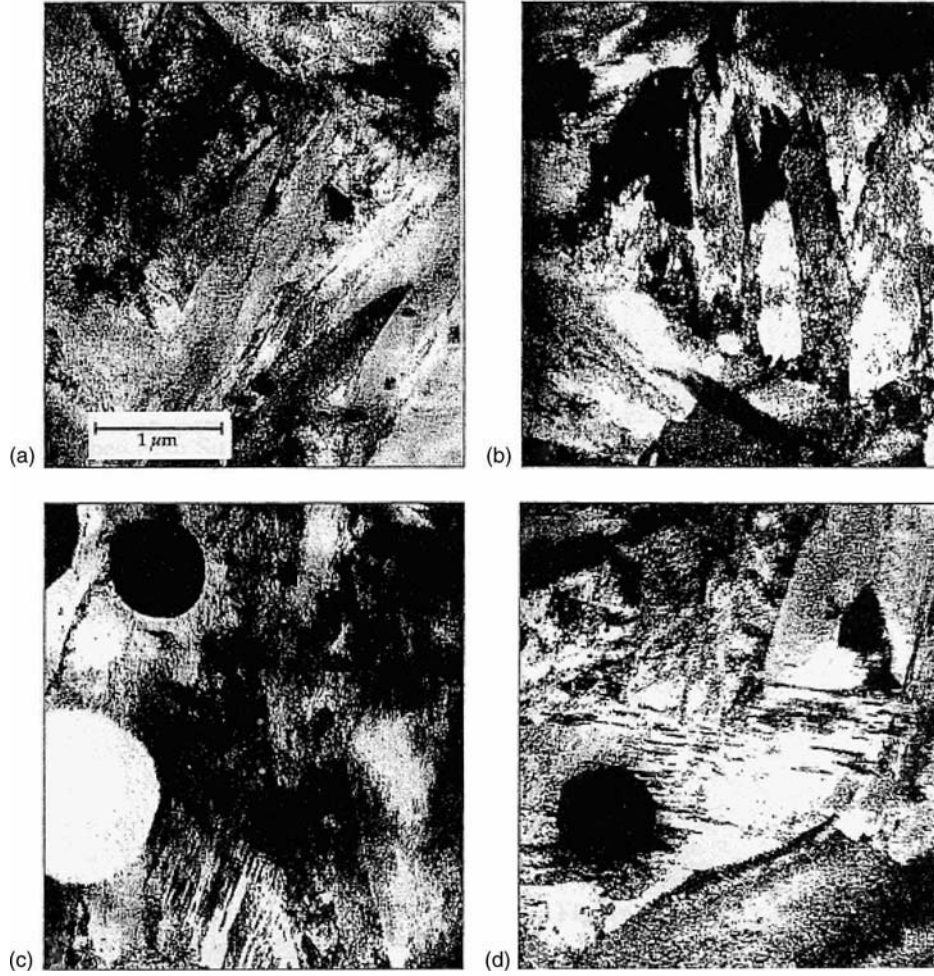
Fig. 8—Electron photomicrographs of R6M5 (AISI M2) steel punches after conventional and very intensive quenching: (a) normal martensitic structure after conventional quenching; (b) packet-morphology martensite after very intensive quenching; (c) conventionally quenched steel after 5,000 cycles of fatigue testing; (d) intensively quenched steel after 16,500 cycles of fatigue testing. The intensively quenched material may have stable grain boundaries, magnified 20,000 times.

obtaining high tempered martensite (see Fig. 9(c)). It has been established that in both cases, the fine structure of steel is characterized by the presence of a dislocation fragmentation of the matrix with a uniformly distributed disperse carbide phase [27].

It has been reported that rapid cooling of supercooled austenite, disregarding the martensite transformation, may result in an increase of strength by freezing vacancies that are formed at high temperatures [6]. It was also reported that it is possible to thermally strengthen corrosion-resistant austenitic steel [6]. However, it is first necessary to determine the extent of such thermal hardening and cooling rates to be achieved.

Using these results, the expediency of using these quenching methods can be demonstrated [29,30]. It has been shown that superficial layers are cooled at the greatest possible rate, because the Kondratjev number Kn is between 0.8 and 1, that is, $Bi_v \rightarrow \infty$. Note that Kn changes from 0 to 1 when the generalized Biot number Bi_v changes from 0 to ∞ and is written as (see Chapter 6):

$$Kn = \psi Bi_V = \frac{Bi_V}{\sqrt{Bi_V^2 + 1.437 Bi_V + 1}}. \tag{3}$$

According to Eq 3, when Kn changes from 0.8 to 1, Bi_v changes from 3.2 to ∞ [31]. When $Bi_v = 3.2$ and $Kn = 0.8$,

$$\Psi = \frac{\overline{T}_{sf} - T_C}{\overline{T}_V - T_m} = 0.25, \tag{4}$$

where:

$\overline{T}_{sf}$ is the average temperature around the surface of a steel part;

$\overline{T}_V$ is the average temperature through a section of the steel part; and

T_m is the quenchant temperature.

Within the superficial layers of alloyed and high-alloy steels, supercritical cooling rates are achieved within the martensite transformation range, causing additional material strengthening and, at the same time, improvement of plastic properties. Furthermore, within the superficial layer, compressive stresses are formed that can be fixed by interrupting the intensive cooling process at the moment of reaching maximum compressive stresses. In [30], it is shown that the maximum compressive stresses are observed when the core achieves a temperature of 450−500°C. Therefore, when new quenching methods are used, in superficial layers there is
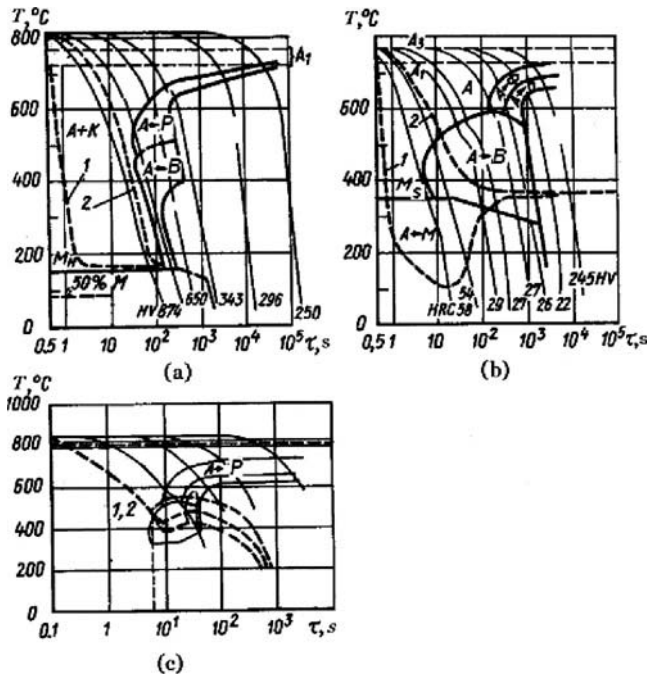
Fig. 9—Explanation of the methods of quenching using CCT diagrams: (a), IQ-2 process; (b), IQ-3 process; (c), rapid interrupted cooling; 1, temperature vs. time at the surface; 2, temperature vs. time at the core.

additional strengthening of material, high compressive stresses are formed, and the central layers are cooled under conditions of rapid interrupted cooling. Therefore, the mechanical properties of the material in the core must achieve the mechanical properties obtained after normal martensite quenching and tempering. It has also been noted that, with the intensification of cooling of alloyed steels, the threshold of cold fragility is decreased and the parameters describing viscosity of material fracture are improved [30,32,33].

Fig. 9 presents a comparison of three quenching methods: IQ-2 (a), IQ-3 (b), and rapid interrupted cooling. It shows that the first two methods (IQ-2 and IQ-3) provide very intensive cooling of superficial layers where superstrengthening of material is observed and the core is cooled under conditions of rapid interrupted cooling [9].

For the study of mechanical properties in the core, cylindrical test specimens of diameters of 50, 60, and 70 mm were made of different steels, heated to austenitizing temperature under identical conditions, and then cooled in mineral oil and aqueous solutions of chlorides. To test tensile strength and impact strength, samples were cut from the core of the cylindrical specimens.

Analysis of the experimental data has shown that the steels tested may be divided into three groups. The first group consists of steels 40Kh, 35KhM, 38KhMYuA, 25Kh1MF, and others, for which, after quenching in chloride solutions, the impact strength increases by two to three times and yield strength, in some cases, increases by 30 %. So, for 35KhM steel at the same values of $\sigma_{p0,2} \cong 820$ MPa, the impact strength a_k during quenching in oil is 44–53 J/cm^2, while during quenching in chloride, it is 140–150 J/cm^2. Similar results were obtained also for other steels (see Table 5) [34].

After quenching in oil and tempering, the structure of 40Kh steel consists of grains sorbite-like pearlite and ferrite

as lines with traces of more large grains; after quenching in water-salt solutions and tempering, it consists of sorbite. Steels 35KhM and 25Kh1MF after quenching in water-salt solutions and tempering have the structure of bainite of more dense structure than during quenching in oil and tempering [34].

These applications of intensive quenching methods for alloyed and high-alloy steels are progressive; as hardenability of steel parts increases, strength and plastic properties are improved [4,33,35,36]. Thus, alloyed and high-alloy constructional steels can be intensively cooled during quenching without quench crack formation due to the formation of high compressive stresses at the surface. The mechanical properties (R_m and $R_{p0.2}$) of the alloyed steels after intensive cooling, in some cases, are higher by 20–30 % than after quenching in oil, while at the same time the impact strength increases by two or three times. This improvement is due to the increase in hardenability of steel parts.

9.5 PRACTICAL APPLICATIONS

It has been shown that intensive cooling within the martensite range is accompanied by simultaneous improvement of strength and plastic properties. Experience has shown that only beginning with a certain cooling rate within the martensite range (>20°C/s) are ultimate strength and yield strength substantially improved, and the plastic properties are improved as shown by narrowing and elongation upon breakage. It has also been noted that intensively quenched samples or parts require higher tempering temperatures by 30–50°C than samples quenched in oil, even higher if the steel contains silicon [4].

Can these results be efficiently used in practice? Can high cooling rates within the martensite range be achieved with real parts in industrial conditions? The answers are yes. These steels exhibited martensite start temperatures M_S of 250–350°C and martensite finish temperatures within the range of 30–70°C.

During intensive cooling, the temperature at the surface of a part to be cooled sharply decreases within 0.1 s to the temperature of the quenchant, and therefore the superficial layers are cooled within the martensite range (50–350°C at a rate much greater than 20°C/s. Parts made of steels having a carbon content of up to 0.6 % may be cooled by intensive water streams or intensive jets. In this case, the effect of additional strengthening of material appears since very high cooling rates are achieved within the martensite range: 50–350°C.

As for steels where the martensite finish temperature M_f is below room temperature, it is necessary to use two-stage quenching. At the first stage, parts are intensively cooled from austenitizing temperature to martensite start temperature M_S. At the second stage, the parts are cooled in the liquid media or in a liquefied layer where the temperature is much lower than room temperature. These processes will now be considered in greater detail.

9.5.1 Fluidized Bed Quenching at Low Temperatures

Fluidized beds can be successfully used for the intensification of heat transfer processes within the martensite range if the bed is used at low temperatures. The heat carrier has the form of firm particles, which may be fine particles of copper or aluminum. During intensive injection of these particles,

TABLE 5—Mechanical properties of different steels after intensive quenching									
Steel	Quenchant	Temperature (°C)		Strength (MPa)		A (%)	Z (%)	a_k (J/cm^2)	HB
		T_o	Tempering	R_m	$R_{p0.2}$				
35KhM (ASTM 4135)	Oil	860	540–550	960 955	775 770	14.0 16.0	53 57	54.0 54–55	285 293
	Water-salt solution	860	550	970 970	820 820	17.0 17.0	63 59	150 140	285
38Kh2N2MA (AISI 4340)	Oil	860	540–550	1,000 980	860 810	13.5 12.0	58 57	110 102	—
	Water-salt solution	860	540–550	1,095 1,055	965 945	12.5 12.5	57 60	90 94	—
40Kh (AISI 4140)	Oil	860	560	770 780	575 575	23.0 21.0	64 64	13.8 11.3	217
	Water-salt solution	860	540–560	855 860	700 695	18.5 16.5	67 65	150 168	269
25Kh1MF	Oil	920	660	755	630	18.5	74	70	229
	Water-salt solution	880–920	660	920 870	820 780	15.0 16.0	68 69	170 190	285
38Kh2MYuA	Oil	960	670	825	665	11.0	28	63–75	—
	Water-salt solution	960	670	885	690	19.0	59	155–165	

Notes: Composition of 35KhM steel (%): 0.30–0.37 C; 0.50–0.80 Mn; $\leq$ 0.035 P; $\leq$ 0.035 S; 0.17–0.37 Si; 0.90–1.20 Cr; 0.15–0.25 Mo; $\leq$ 0.30 Cu; $\leq$ 0.30 Ni; $\leq$ 0.03 Ti; $\leq$ 0.05 V; $\leq$ 0.20 W. Composition of 38Kh2N2MA steel (%): 0.33–0.40 C; 0.25–0.50 Mn; $\leq$ 0.025 P; $\leq$ 0.025 S; 0.17–0.37 Si; 1.30–1.70 Cr; 0.30–1.70 Ni; 0.20–0.30 Mo; $\leq$ 0.1 Al; $\leq$ 0.30 Cu; $\leq$ 0.05 Ti. Composition of 40Kh steel (%): 0.34–0.44 C; 0.50–0.80 Mn; $\leq$ 0.04 P; $\leq$ 0.04 S; 0.17–0.37 Si; 0.8–1.1 Cr; $\leq$ 0.3 Ni. Composition of 25Kh1MF steel (%): 0.22–0.29 C; 0.40–0.70 Mn; $\leq$ 0.030 P; $\leq$ 0.025 S; 0.17–0.37 Si; 1.50–1.80 Cr; 0.25–0.35 Mo; $\leq$ 0.20 Cu; $\leq$ 0.30 Ni; $\leq$ 0.05 Ti; $\leq$ 0.20W. Composition of 38Kh2MYuA steel (%): 0.35–0.42 C; 0.30–0.60 Mn; $\leq$ 0.025 P; $\leq$ 0.025 S; 0.20–0.45 Si; 1.35–1.65 Cr; 0.15–0.25 Mo; 0.70–1.1 Al; $\leq$ 0.30 Cu; $\leq$ 0.30 Ni; $\leq$ 0.03 Ti; $\leq$ 0.05 V; $\leq$ 0.20 W.

high heat transfer coefficients of 1,000−2,000 W/m^{2}K are obtained. Compared to the convection heat transfer coefficient of oil, α_{conv}, of 300−350 W/m^{2}K, the heat transfer coefficient is higher in the fluidized bed by almost an order of magnitude. In addition, considering the difference of temperatures between the part to be cooled and the quenchant, the cooling rate within the martensite range must be significant. Possible ways of implementing such a process will now be considered [36,37,38].

Fig. 10 shows an installation for providing the intensification of heat transfer in the process of cold treatment of metals [25,26]. The installation contains a tank (1) filled with the disperse heat-carrier (2). Vertical pipes (4) are attached to the bottom of the tank through the punched lattice (3) and fed from a source of compressed gas (5), and the heated gas is removed from vertical pipes through a branch pipe (6).

The working principles of this installation are as follows: Compressed gas (air) from the compressor is supplied to the quench tank filled with a heat carrier of high thermal capacities (for example, copper or aluminum), through the vertical pipes in the bottom of the quench tank. According to the Rank effect [37], in the vertical pipes the streams of compressed air are divided into cold and hot. Cold air is supplied through a punched lattice (for uniform distribution of the stream) to the quench tank. Due to the increased

pressure of the cold air, the disperse heat carrier boils (pseudofluidizes), mixes the bubbles, and is cooled to the temperature of the cold air, at which time the heated parts to be quenched are placed into the bed and held for the desired time.

The change in the passage cross-section of the pipelines bringing compressed cooled air to the quench tank adjusts the degree of supercooling of the quenchant. During quench cooling by this method, strength and performance of the steel increases by 15 % compared with alternative processes. This method allows intensified cooling of practically any steel due to the preliminary deep (below the martensite finish temperature) cooling of the heat carrier. In this case, there is no need for cryogenic liquids, and the system provides for uniform heat removal from the entire surface, resulting in the preservation of its geometry.

The installation in Fig. 10 can be also used during two-stage quenching. During the first stage, the part is cooled in aqueous solutions with a high boiling temperature of a boundary liquid layer, and during the second stage it is cooled in the fluidized bed at subzero temperatures.

Now let's consider a specific example and appropriate calculations illustrating the application of this technology [37]. Note that the installation shown in Fig. 10 may be supplied with vapors of liquefied gases for the intensification of
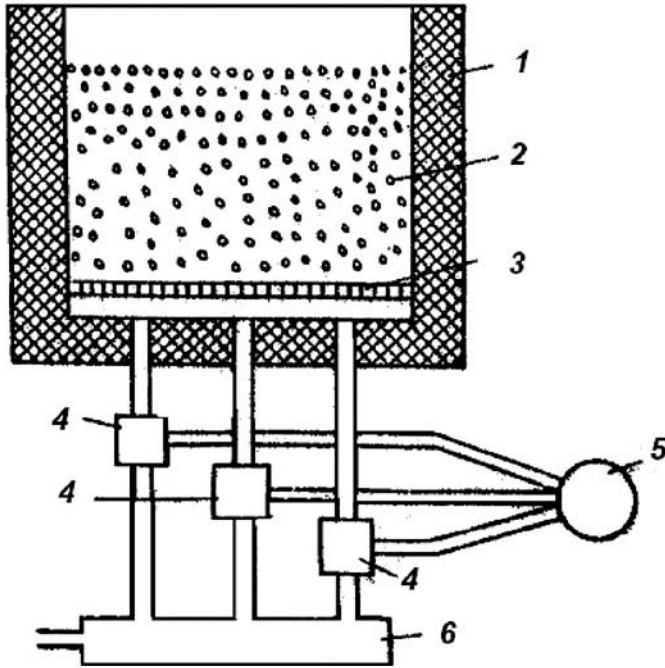
Fig. 10—Apparatus for implementation of cooling at negative Celsius temperature [36,37].

heat transfer and essential decrease in temperature of the fluidized bed.

Example 9.1

A cylindrical part with a diameter of 12 mm and height of 45 mm made of U7 steel is at first cooled from 800°C in a 10 % aqueous solution of sodium carbonate (Na_2CO_3) at 20°C. When the core reaches 300°C, the part is immersed into the fluidized bed with a temperature of -40°C and held there until it is completely cooled. Determine the cooling time of the part during the first stage of cooling in the aqueous solution of sodium carbonate and the cooling rate at the core during the second stage when it is cooled in the fluidized bed.

The following input data are known:
- The average thermal diffusivity of the overcooled austenite is $\bar{a} = \dfrac{\lambda}{\rho\, c_p}(m^2/s)$, and for the range of 300–800°C is equal to 5.4 $\times$ 10^{-6} m²/s.

- The Kondratjev number Kn for the first stage = 0.6.
- R = 0.006 m
- Z = 0.045 m
- The Kondratjev form coefficient $K = \dfrac{1}{\frac{5.783}{R^2} + \frac{9.87}{Z^2}}$ is equal to 6.04 $\times$ 10^{-6} m².
- The heat transfer coefficient of the fluidized bed is equal to 2,000 W/m²K.
- Kn for the second stage = 0.235
- The average thermal diffusivity of the part at low temperatures is equal to 4.4 $\times$ 10^{-6} m²/s.

Using these input data, the cooling time during the first stage is calculated from the following equation (see Chapter 5):

$$\tau = \left[0.48 + \ln\frac{T_0 - T_C}{T - T_C}\right]\frac{K}{a\,Kn}. \tag{5}$$

Substituting, we obtain:

$$\tau = \left[0.48 + \ln\left(\frac{800°C - 20°C}{300°C - 20°C}\right)\right]\frac{6.04 \cdot 10^{-6}m^2}{5.4 \cdot 10^{-6}m^2/s \cdot 0.6} = 2.8\ s.$$

Thus, the cooling time of the part during the first stage is equal to just under 3 s. The cooling rate during the second stage when the temperature of the core is 200°C is calculated from:

$$v = \frac{\bar{a}\,Kn}{K}(T - T_m),$$

from which we determine:

$$v = \frac{4.4 \cdot 10^{-6}m^2/s \cdot 0.235}{6.04 \cdot 10^{-6}m^2}(200°C - (-40°C)) = 41°C/s.$$

This example shows that the cooling rate at the core of the part at the martensite start temperature is equal to 41°C/s, which is sufficiently high for the phenomenon of super-strengthening to be observed.

9.5.2 Use of Cryogenic Quenchants and Special Devices

The cooling rate within the martensite range, when cooling in cryogenic quenchants, is high due to the large temperature difference between the steel part and the cryogenic quenchant. A comparison of heat transfer coefficients that are achievable in cryogenic quenchants are presented in Table 1 [10].

To increase the cooling rate within the martensite range, it is necessary to increase the heat transfer coefficient during cooling in the cryogenic quenchant. For this purpose, simple devices that considerably increase the heat transfer coefficient are used. One of these devices is described in [4,10] and depicted in Fig. 11. The device has the form of a bell vibrating in the cryogenic quenchant and in which a gas such as helium that possesses high heat conductivity is supplied (see Table 6).

During quenching in liquid nitrogen, a gas film is formed around the part, which sharply decreases the cooling process. Therefore, for the intensification of heat transfer processes in liquid nitrogen, it is expedient to add helium, whose heat conductivity and thermal diffusivity are higher by an order of magnitude than nitrogen's (see Table 1).

If intensive circulation of helium cooled to -196°C around a part to be quenched is achieved, the intensity of
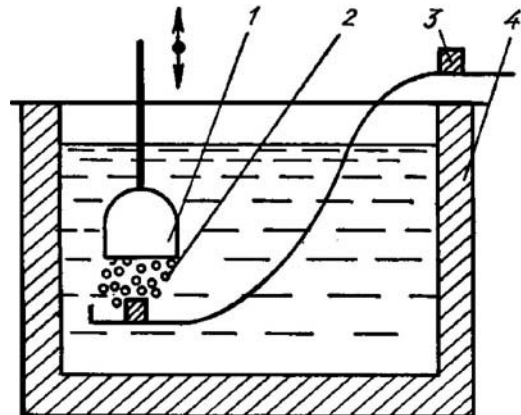
Fig. 11—Installation for steel quenching in a cryogenic biphasic medium: 1, bell; 2, bubbles of helium; 3, part to be quenched; 4, thermostat [4,10].

TABLE 6—Thermophysical properties of the gaseous quenchants at 20°C		
Medium	**λ (W/mK)**	**a (m²/s)**
Air	24.423	1.87×10^{-6}
Nitrogen	23.260	1.91×10^{-6}
Helium	143.049	15.33×10^{-6}

cooling of the parts will sharply increase. To keep bubbles of helium in liquid nitrogen, one may use special devices like that in Fig. 11, consisting of a vibrating vessel in which the cooled helium moves. When vibrating a bell-shaped vessel at the resonant frequency, bubbles of helium in the suspension are kept in the liquid under the bell, making large oscillatory movements. Due to fluctuations of the bubbles and the high heat conductivity of helium, the intensity of heat transfer during martensite transformation is appreciably increased. Since the bubbles of helium are supported in suspension, very little helium is lost during quenching. Only for a short time during the initial period of cooling, when the part drops through the chute into the liquid nitrogen and reaches the helium bubbles, is it necessary to blow cooled helium, because at this initial stage of cooling, intensive evaporation of nitrogen occurs, which can suppress the bubbles of helium and be a part of heat transfer, slowing down the cooling process.

The effect of heat conductivity of a gas on the heat transfer coefficient at film boiling is derived from the analysis of the generalized equation of similarity:

$$\alpha_{fb} = 0.18\lambda \left[\frac{g}{v\,a} \frac{\rho' - \rho''}{\rho''} \right]^{1/3}. \qquad (6)$$

From Eq 6, it follows that α_{fb} is directly proportional to the heat conductivity of the gas that shrouds a part during cooling. Considering that the bubbles of helium are vibrating, the intensity of heat transfer increases due to not only the increase in heat conductivity but also the intensive circulation of the gas. This method of cooling can be combined effectively with steel quenching in aqueous solutions to be conducted during the first stage of cooling.

Example 9.2

A small die made of AISI 52100 steel is first cooled in 30 % bischofite solution (hydrated magnesium chloride [$MgCl_2$], a sea salt concentrate) at 40°C. The diameter of the die is 50 mm and its height Z is 40 mm. The austenitizing temperature is 860°C. The convection heat transfer coefficient of aqueous bischofite solution at a temperature of 40°C is 425 W/m²K. The average thermal diffusivity of the material for the temperature range of 860°C down to 150°C is 5.5×10^{-6} m²/s, and the average thermal conductivity $\overline{\lambda}$ is 23 W/mK. The values for the second cooling stage are: $\lambda = 14$ W/mK and $a = 4 \times 10^{-6}$ m²/s. The heat transfer coefficient in liquid nitrogen during bell vibration (see Fig. 11) is 350 W/m²K.

Calculate the time of the self-regulated thermal process, that is, the time of cooling during the first cooling stage, and the cooling rate during the second stage when the temperature at the core is 150°C.

Applying Eqs 36−38 of Chapter 2, the cooling time for the first stage is:

$$\tau = \left[0.48 + 3.21 \ \ln\frac{\vartheta_I}{\vartheta_{II}} \right] \frac{K}{a},$$

and the temperature at the beginning and end of the self-regulated thermal process and the Kondratjev form factor are given by:

$$\vartheta_I = \frac{1}{7.36}\left[\frac{2 \cdot 23(760 - \vartheta_I)}{0.02} \right]^{0.3};$$

$$\vartheta_{II} = \frac{1}{7.36}\left[425(\vartheta_{II} + 100°C) \right]^{0.3}; \text{ and}$$

$$K = \frac{1}{\frac{5.783}{(0.025)^2} + \frac{9.87}{(0.04)^2}} = 64.84 \cdot 10^{-6} m^2.$$

After simplification, we determine that $\vartheta_I = 10.1°C$, $\vartheta_{II} = 3.36°C$, and $K = 64.84 \times 10^{-6}$ m².

Therefore, the cooling time for the first cooling stage is approximately 47 s. The cooling rate of the part during the second cooling stage is determined from:

$$v = \frac{a\,Kn}{K}[150°C - (-196°C)]$$
$$= \frac{4 \cdot 10^{-6}m^2/s \cdot 0.15 \cdot 346°C}{64.84 \cdot 10^{-6}m^2} = 3.2°C/s,$$

where $Kn = 0.15$ (see Chapter 6).

This cooling rate of 3.2°C/s is not sufficient to obtain superstrengthening of the steel. However, experiments have shown that the service life of dies quenched in this manner is doubled, which indicates that the positive effects were achieved during the first cooling stage and no advantage was obtained from the second cooling stage in liquid nitrogen. One-stage cooling of dies made of AISI 52100 steel in bischofite has confirmed the increase of service life of dies by 1.5 to 2 times [37].

When cooling smaller parts made of alloyed and normal high-carbon steels in liquid nitrogen, superstrengthening may be observed, because the cooling rate depends on the part size. If all parts are cylindrical with a diameter of 6 mm, then the cooling rate during the second cooling stage is:

$$v = \frac{4 \cdot 10^{-6}m^2 \cdot 0.0314 \cdot 346°C}{1.56 \cdot 10^{-6}m^2} \approx 28°C/s,$$

where:

$$K = \frac{R^2}{5.783} = 1.56 \cdot 10^{-6}m^2; \text{ and}$$

$$Kn = 0.0314.$$

This cooling rate is sufficient to obtain additional strengthening of the steel.

9.5.3 Use of Aqueous Salt Solutions Cooled Below Room Temperature

Aqueous solutions of some salts can be cooled below room temperature down to −80°C (see Table 7). These cold water-salt solutions can also be agitated. Table 7 shows the solubility S in grams of waterless substance per 100 grams of pure solvent, and T_p indicates in which cases the solid phase is formed and shows that aqueous solutions of LiCl can be overcooled down to −80°C.

In addition to reducing the temperature of aqueous solutions, it is necessary to increase the convection heat transfer coefficient. This may be done by using a special device described in [4], which is shown in Fig. 12. For the intensification

TABLE 7—Solubility of salts in water (limit of negative temperatures achievable in aqueous CaCl$_2$, ZnCl$_2$, and LiCl solutions)

CaCl$_2$			ZnCl$_2$			LiCl		
T (°C)	S	T$_p$	T (°C)	S	T$_p$	T (°C)	S	T$_p$
0	59.5		0	208		0	69.2	
−15.5	53.3		−10	189		−20	58.4	2 H$_2$O
−26.5	50.8		−30	160	3 H$_2$O	−68	40.3	3 H$_2$O
−35.7	48.7		−40	127		−80	33.9	5 H$_2$O
−55	45.75	6 H$_2$O	−50	113				
			−62	104	4 H$_2$O			
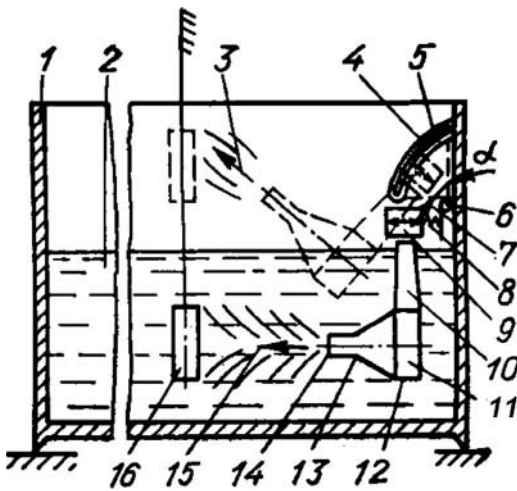
Fig. 12—Installation for steel quenching at negative temperature: 1, tank; 2, quenchant; 3, open spray; 4, arc-shaped groove; 5, clamp; 6, hinge; 7, platform; 8, shock-absorber; 9, activator of vibrations; 10, supporting arm; 11, hollow cone having different sections at points 12, 13, and 14; 15, submerged spray; 16, specimen or tool to be quenched [4,10].

of processes of cooling within the martensite range, it is possible to establish submerged or open sprays (15 and 3, respectively, in Fig. 12).

It is difficult to create sprays using mechanical pumps such as centrifugal and positive displacement pumps because freezing of the pipelines occurs during the pumping process. The most reliable way to create sprays in a liquid is to create vibrations in the liquid using a special device that consists of a hollow cone (Fig. 12, 11) where the ratio of the inlet diameter D to the outlet diameter d–that is, D/d–is less than 2 [4].

When the hollow cone is vibrated, the velocity of movement in its narrow part is much more than in the inlet cross-section, and therefore, during the flow of the liquid, a difference of pressures is created, forming a liquid spray (Fig. 12, 15). Experiments have shown that, depending on the amplitude and frequency of the vibrations of the hollow truncated cone, the velocity of the spray (jet) flow can be adjusted in a wide range [4,10]. Using a simple device like that in Fig. 12, one can create both submerged and open sprays in liquid nitrogen or cold water-salt solutions.

The cooling properties of sprays of cold water-salt solutions are not yet deeply and widely studied. There are, however, a number of works devoted to the study of the cooling capacity of water sprays, where it is shown that when cooling in cold water flow or water sprays, one may prevent the film boiling and nucleate boiling processes [4,18,33]. In this case, convection prevails, since nucleate boiling is rather short or is completely prevented [4,24,33].

These examples show that by using the devices for intensifying convection at low temperatures, it is possible to create high-strengthened materials by using the appropriate heat treatment process.

9.6 DISCUSSION

It is very important to know the temperature range where intensive cooling results in the effect of superstrengthening. Table 8 shows that intensive cooling of test specimens made

TABLE 8—Comparison of the mechanical properties of different steels quenched in oil and quenched with the intensification of heat transfer within the martensite range

Quenching method	V (°C/s)	Steel grade	Strength (MPa)		A (%)	Z (%)
			R$_m$	R$_{p0.2}$		
Oil	3–6	U7A	1,400	1,250	4	—
		60S2A	1,476	1,355	8.5	—
Two-step intensive quenching	30	U7A	1,610	1,570	7.9	31
		60S2A	1,920	1,740	5	22
Note: V is cooling rate within the martensite range.						
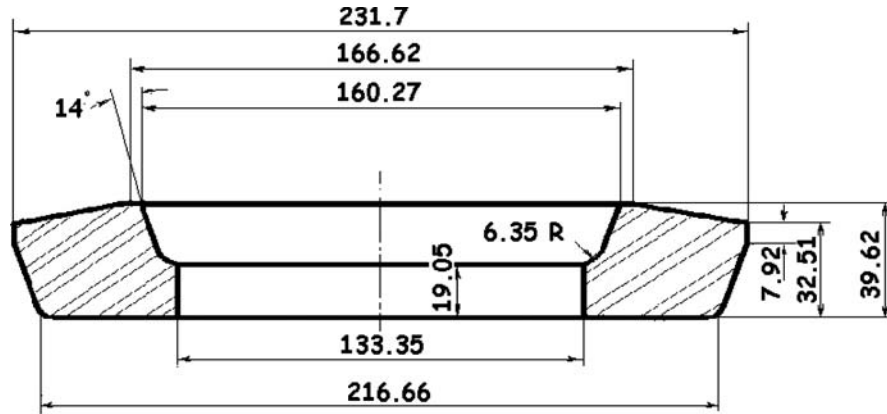
Fig. 13—Sketch of forging.

of various steel grades from the austenitizing temperature to the martensite start temperature M_I does not result in appreciable additional strengthening. Therefore, the strength of small test specimens quenched in oil and aqueous salt solutions differs very little. Only rapid cooling within the martensite range during the second step of cooling yields additional strengthening with improvement of its plastic properties (see Table 8).

This is similar to the effect of high-temperature thermomechanical treatment, because in addition to the appearance of high compressive stresses, the deformation of unstable austenite occurs both at high temperatures and during the supercooling stage above the M_S temperature. To obtain an insight into this process, computations of the stress-strain state and intensity of plastic deformations of austenite were performed for the forging illustrated in Fig. 13, which was cooled in conditions $Bi \to \infty$.

The distribution of temperature fields in the forging– which was cooled with a heat transfer coefficient of 20,000 W/m^{2}K–20 s after the forging was immersed into a quenchant is shown in Fig. 14. Such a quenching intensity can be achieved by water spray or water flow produced in special tanks. As Fig. 14 shows, the forging's core reaches temperatures of 700−750K, where the formation of intermediary phases with high mechanical properties occurs.

Fig. 15 shows that the safety factor reaches the lowest values in the layers located between the surface and the core of the part and equals 1.4−1.5. If the safety factor is less than 1, material fracture occurs [31]. The phase distribution at 20 s is presented in Fig. 16. Such a phase distribution in a forging provides high compressive stresses at the quenched surface and comparatively low tensile stresses at the core.

Hoop stresses at the moment of interruption of intensive quenching are shown in Fig. 17. This shows that intensive


```
             .444444444..444444.......
          .444........5...55......4444444.........
        .444..555555555...5....555555........4444444........
      .44...5555......6..666..66666........555555......44444444...
     .4.555.....66666...66..66666666666........555555....4444444.
   .44..5....666.........77...77777......666666......5555.....4444.
  44...55...666......777777777777777777777....66666....55555....444.
 44..555..66....77777................7777777....66666...555...444.
 44.555..666....7777...................77777......666...555...444
 44..55.666....7777......88.88888888.8......77777....666...555..44..
..444.555...66...7777......88888888888888.......77777...666..555..444.
.444...555...66...77777.....888888888888888888......7777...6666..555...4.
.444..5555..666...77777......888888888888888888.....77777....66...55..44.
.44..555...6666...77777.......88888888888........7777.....66..555...4..
.44...555...666.....77777...............777777....66...555..44.
.44...555....66......7777777.............77777777...66666..555..44.
.444...555....66666......7777777777777777777......666666...555.444.
.444...55555....6.666666......................666666666..5555...44.
.4444....55555...........66666666666666666...........5.5555...4444
.44444......55555555.........................55555555.....444..
..4444444444.........................................44444444.
...4..4.4.4.4.4444.4.44.4.................4.4.4444.4.4..4.444.
```

Legend

3	200−250
4	300−350
5	400−450
6	500−550
7	600−650
8	700−750

Fig. 14—Temperature field (K) in the forging at the time of reaching the maximum compressive stresses at the surface at 20 s.

Legend

6	1.4-1.5
7	1.5-1.6
8	1.6-1.7
9	1.7-1.8
A	1.8-1.9
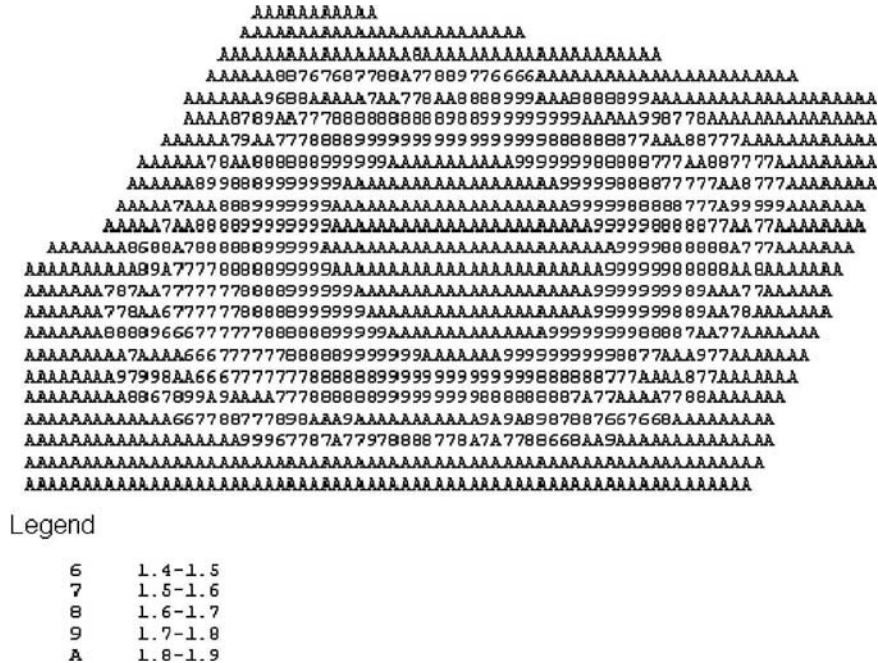
Fig. 15—Safety factor (SF) at the time of reaching the maximum compressive stresses at the surface at 20 s.

quenching of forgings prevents crack formation due to high compressive residual stresses at the surface of steel parts and lower residual tensile stresses at their core. The plastic strains intensities in the forging at 20 s are shown in Fig. 18.

It should be emphasized that the service life of steel parts increases due to the steel superstrengthening phenomenon [1,2] and creation of high compressive residual stresses at the surface [4,31]. For example, the surface cooling rate of a forging within the martensite range was high enough to provide superstrengthening and high compressive residual stresses simultaneously. Both factors are responsible for increasing the service life of components. Su Chun-xia and colleagues [39] also noticed that interrupted intensive quenching provides fine microstructure of manganese-chromium-nickel-molybdenum steel.

Another opportunity to use both factors in practice is intensive quenching of low-hardenability steels, where chemical composition, residual stress distribution, and the super-strengthening effect are optimized [23,40,41].

9.7 SUMMARY

1. During intensive quenching, the effect of additional strengthening (superstrengthening) is observed, which is connected with the intensification of cooling rate within the martensite range.
2. The process of intensive cooling should be interrupted upon achieving the maximum compressive stresses at the surface when the core achieves a temperature of 350−600°C. The core in this case is cooled by the scheme of rapid interrupted cooling.
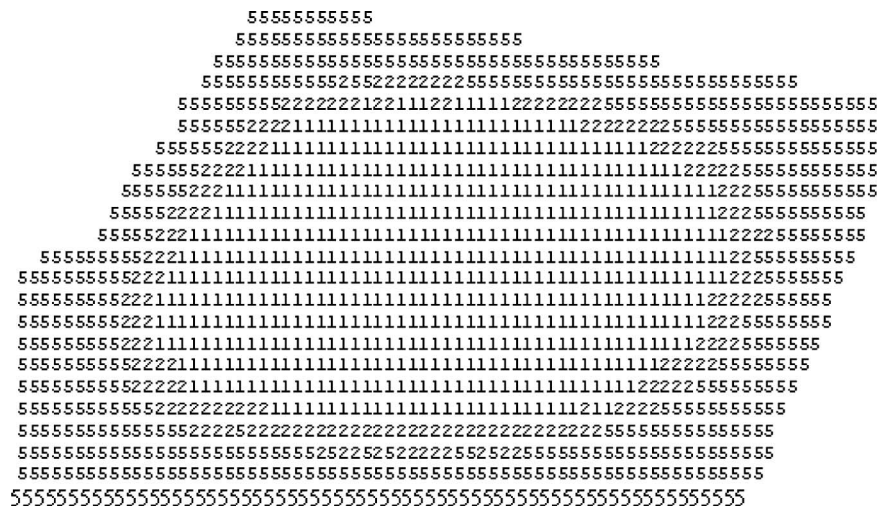
Fig. 16—Phase distribution in the forging at the time of reaching the maximum compressive stresses at the surface at 20 s: 1, austenite; 2 and 5, martensite.

```
                  ...7.888..A
                8AC.H.JK.M.O..H.J.........
              .DF....UX.YYZUX.Y..U..............DDDDD
             .E...Vſ.„.†.„ƒƒ....□□.Z.Y...UUUUUUUMKKK......EEEEE
            .HKPTU..ſ.„„+.„ध़ा.ध़..-‡.^.ध़ध़ध़.........YY...2UT..S.R.Q.II.FE...
            ..VXZſ„.^.□◙◙◙......◙◙◙.◌.-...-....◌.„„.......ſ.......QP.M.E.
            ..MR.X.ſ.^□.◙◙◙◙◙◙◙...◌◌.-..--.....—.◌...<.......ƒ.DYWV..NH.C
            ..N.UXY..†....◌◌..◌◌◌..——.-......-.—◌◌.◙◙◙....‡‡‡....□.TSO.G.
           FJ.....ZſЦ„——..............--...—....◌.◙◙◙_◙◙...%‡‡†...XV.O...B
           ...WXY..^.....-----------...--.—..◌.^.◙◙◙◙◙◙◙_.‡††.......N..
           .M.TX..`...........————....„„„„„„„.-—.-.◌.◌◌.◙◙◙_...†„.Z.....F
          8..K.WYZ.ƒ„.—.......——....---.....„„„„„„.--.._.—..◌◌....◙_.ƒƒ.Z.TOJH.
          ...JOT.YZZſƒ.□.````````..——...-.....„„„„„.-—.—...````````..``^..ZY.VTOKE
          .GL.W.Y.ZZſ†..```..—........-.-.....„„„„„.-—.—.........-..Y.Y.UTK.D
          C....YZ...ſ^<`.........``.-..—..-—...„„„..---..——.........YY..V.OK..
          EIKS.X..ſſ..`-..◙◙◙◙◙...◌`...-..-—.......---.—..```````□....YY..JG.
          F..SWYY.....†.`.◙◙◙◙◙◙◙...`◌...—...---..—...-..◙◙◙◙`—..‡ƒ..ZU.JF.
          FI..U.X.Z..ƒƒ„<..◙◙◙◙◙◙◙..``..---...-...—.◙◙◙`.``.‡†.□ZU...D
          D...TWX.ƒ.„-.„„„.^..—-.....``.—..--------...-.```◙.◙.`-.``ध़ध़.‡.†ƒDYVTOKE
          BE..QRUXYZ.ſ.„.„„†..„„„...‡.^.%...<<<<<<<<.%.^..†...††..‡‡‡..ZXVQM.G
          9CFIM.R.V...Z.ſ..ƒƒƒƒ..□.Z...ZZZZZZZZZZZZZ.□.ƒ.„....ƒ.□.XW....ED
          ..9D.K..NO.QRS.T.U..VV............................VVW.UT....NMK..E.
          477989EBGCIDJ..K.LFMF.....N.NFF..............N.N...LLFLFK.EID.ED.
```

Legend

2	-1440 – -1420	F	-920 – -900	S	-400 – -380	^	120 – 140
3	-1400 – -1380	G	-880 – -860	T	-360 – -340	%	160 – 180
4	-1360 – -1340	H	-840 – -820	U	-320 – -300	<	200 – 220
5	-1320 – -1300	I	-800 – -780	V	-280 – -260	Ц	240 – 260
6	-1280 – -1260	J	-760 – -740	W	-240 – -220	`	280 – 300
7	-1240 – -1220	K	-720 – -700	X	-200 – -180	"	320 – 340
8	-1200 – -1180	L	-680 – -660	Y	-160 – -140	–	360 – 380
9	-1160 – -1140	M	-640 – -620	Z	-120 – -100	—	400 – 420
A	-1120 – -1100	N	-600 – -580	Г	-80 – -60	~	440 – 460
B	-1080 – -1060	O	-560 – -540	ƒ	-40 – -20	◙	480 – 500
C	-1040 – -1020	P	-520 – -500	„	– 20	>	520 – 540
D	-1000 – -980	Q	-480 – -460	†	40 – 60		
E	-960 – -940	R	-440 – -420	‡	80 – 100		

Fig. 17—Hoop stresses S33 in the forging at the time of reaching the maximum compressive stresses at the surface at 20 s.

3. The potentialities of combined heat treatment of forgings include high-temperature thermomechanical treatment and intensive quenching to maximize the effect of material superstrengthening.

4. Intensive quenching of forgings is interrupted when there are maximum compressive stresses at the surface and small tensile stresses at the core. In many cases, this happens when the core temperature drops to 400−500°C.

```
                  SPOIHGGGHHG
                JJIIFEEEEEEEGGGFFECCCBEEB
               HHHFFFEDDCCCCDDDDDEEEDDCDDDDDDDDBBBBBBBB
              FFGFEEDCCCCCABAA9BBA99BBAAAAACCCCCCDDDDDDEEECDDDEFFG
             DEEEDDDCCB88777545433244333337B889999CCCCCCDDDDDDEEGGHIJLNID
             CEDCCBA8766555555544443322111111111144567B99BCCCDDDDEEHFGGGGGGG
             CDEDDC98654455555544443332222222211122233445578 9BBCDDDDDCCCCEFEE
             CDEDCB9754334444444444433333333333333334444455555567ABCCDDDDCCCEEFF
             CDEDCA964122333444444444443339339933944444455555655567ACDDDDDEEOV.
             CDECA963212233344444444444444444444444444444444555555555665567ABCCCCDEHJM
             EEEDC9431223344445555555554444444444444444444444444455555554369ABBCCDFGDG
            OLIHHDDDCA75244556666655555555555555555555554444444444444444444349ABBCDDEDC
           NMKWJHFEDBB96546777787776666666655555555555544444444444332233589ABCCDDB
           JHHIEDCBAA745787888988877777766666655555555554444444444443322113579ABCDCB
           GGHEDCBA98654899999999988877776666655555554444444444444444433222112489ABCDCB
           FFFDBAAAA97668AA99999988888777665555554444444443333333333322346799ACCDCB
           EEECBAAAAA74469BAA9999988887776655555544444333333334444434467ABBCCDCB
           EEFDCCCCCBA98458B99988888777766655544433333333334444454333345 9BBCCDEEDB
           FFFEDCDCCCBBA8655444456665554433222Z2222222ZZ2333444444455CCCDDDEEEED
           FGGFEEEDDDDDDCBA986987543333333322222 22333344445 789ABCCBCDEEEDDEFGF
           IIIGFEEDDDDDDDDCCBBBAA99887777777666 7777788899AABCCCDDDEEEEEFFFHHH
           MLKFEEEFFFFEEEDDDDDDDDDDDDDDDCCCCCCCCCCCCCDDDDDDDDDDDDDDDEEFGGHHIII
           FKJHIFGKHEGFGFGFFFDECEECEBEBEBBEBEBEBEBBEBEBEBECEEEEDFFGHIGIHJLL
```

Legend

1	.000-.001	D	.012-.013	P	.024-.025
2	.001-.002	E	.013-.014	Q	.025-.026
3	.002-.003	F	.014-.015	R	.026-.027
4	.003-.004	G	.015-.016	S	.027-.028
5	.004-.005	H	.016-.017	T	.028-.029
6	.005-.006	I	.017-.018	U	.029-.030
7	.006-.007	J	.018-.019	V	.030-.031
8	.007-.008	K	.019-.020	W	.031-.032
9	.008-.009	L	.020-.021	X	.032-.033
A	.009-.010	M	.021-.022	Y	.033-.034
B	.010-.011	N	.022-.023	Z	.034-.035
C	.011-.012	O	.023-.024		

Fig. 18—Plastic strains intensity in the forging at time = 20 s.

5. The suggested technology based on the superstrengthening effect and creation of high compressive residual stresses yields large economic benefits due to increase service life of steel parts and the use of plain water as a quenchant instead of oils.

References

[1] Kobasko, N. I., Steel Superstrengthening Phenomenon, *Journal of ASTM International,* Vol. 2, No. 1, 2005.

[2] Kobasko, N. I., The Steel Superstrengthening Phenomenon, Part I, *International Journal of Materials and Product Technology,* Vol. 24, Nos. 1–4, 2005, pp. 361–374.

[3] Kobasko, N. I., Effect of Structural and Thermal Stresses on Crack Formation During Steel Quenching, *Proceedings of the All-Union Conference on Increase in Productivity and Profitability of Heating Furnaces,* Dnipropetrovsk, 1967, pp. 26–27.

[4] Kobasko, N. I., *Steel Quenching in Liquid Media Under Pressure,* Naukova Dumka, Kyiv, 1980.

[5] Kobasko, N. I., Intensive Steel Quenching Methods, *Theory and Technology of Quenching,* Liščić, B., Tensi, H. M., and Luty, W., Eds., Springer-Verlag, Berlin, 1992, pp. 367–389.

[6] Gul', Yu. P., Chmeleva, V. S., and Kirichenko, V. V., Contemporary Aspects of the Quench Cooling of Steel, *Metal Science and Heat Treatment,* Vol. 31, No. 9, 1989, pp. 639–644.

[7] Sverdlin, A., Ness, A., and Ganiev, R., New Method of Heat Treatment Using the Wave Technology, *Proceedings of the 22nd Heat Treating Society and 2nd International Surface Engineering Congress,* September 15–17, 2003, Indianapolis, IN, pp. 77–83.

[8] Kobasko, N. I., The Steel Superstrengthening Phenomenon, Part 2, *International Journal of Microstructure and Materials Properties,* Vol. 3, Nos. 4/5, 2008, pp. 526–547.

[9] Kobasko, N. I., Increase the Service Life and Reliability of Components Through the Use of New Quenching Technology, *Metal Science and Heat Treatment,* Vol. 31, No. 9, 1989, pp. 645–653.

[10] Ganiev, R. F., Kobasko, N. I., Kulik, V. V., et al., *Oscillation Phenomena in Multi-phase Media and Their Use in Technology,* Tekhnika, Kyiv, 1980.

[11] Oding, I. A., Ivanova, V. S. Burdukskiy, V. V., and Gelinov, V. N., *Theory of Creep and Durability of Metals,* Metallurgizdat, Moscow, 1959.

[12] Ivanova, V. S., and Gordienko, L. K., *Novye puti povysheniya prochnosti metallov* (New ways of increasing metal durability), Nauka, Moscow, 1964.

[13] Psarev, V. I., and Kobasko, N. I., High-Temperature Annealing of Cold-Rolled Transformer Steel, *Scientific 1959 Yearly Journal of Chernivtsy State University,* 1960, pp. 613–616.

[14] Gudtsov, N. T., Bernshtein, M. L., and Rakhshtadt, A. G., Eds., *Metal Science and Heat Treatment (Handbook),* Metallurgizdat, Moscow, 1957.

[15] Kobasko, N. I., and Prokhorenko, N. I., Effect of the Quenching Rate on the Formation of Cracks in Steel No. 45, *Metal Science and Heat Treatment,* Vol. 6, No. 2, 1964, pp. 104–105.

[16] Kobasko, N. I., Thermal Processes in Quenching of Steel, *Metal Science and Heat Treatment,* Vol. 10, No. 3, 1968, pp. 3–10.

[17] Kobasko, N. I., Self-regulated Thermal Processes During Quenching of Steels in Liquid Media, *International Journal of Microstructure and Materials Properties,* Vol. 1, No. 1, 2005, pp. 110–125.

[18] Kobasko, N. I., Technological Aspects of Quenching, *Metal Science and Heat Treatment,* Vol. 33, No. 4, 1991, pp. 253–263.

[19] Yukio, H., Motozo, N., and Shigeharu, K., One Consideration on the Strengthening Mechanism of Ausformal Steel, *Bull. Fac. Educ. Kanazawa Univ. Nat. Sci.,* 1974, No. 23, pp. 35-43.

[20] Malinkina, E. I. *Crack Formation During Heat Treatment of Steel Parts,* Mashinostroenie, Moscow, 1965.

[21] Kobasko, N. I., Secondary Intensive Cooling of Melted Materials for Getting Their Fine Microstructures, *Proceedings of the 6th IASME/WSEAS International Conference on Heat Transfer,*

[22] Kobasko, N. I., Aronov, M. A., Canale, L. C. F., and Totten, G. E., Metallurgy of Intensive Quenching Process and Implications with Respect to Steel Properties, *58th Congresso Annual Da ABM,* July 21–24, 2003, Rio De Janeiro, Brazil, pp. 3362–3380.

[23] Kobasko, N. I., Quench Process Optimization for Receiving Super Strong Materials, *WSEAS Transactions on Systems,* Vol. 4, No. 9, 2005, pp. 1394–1401.

[24] Kobasko, N. I., Energy Efficient and Eco-friendly Intensively Quenched Limited Hardenability Low Alloy Steels, *Journal of ASTM International,* Vol. 6, No. 1, 2009.

[25] Uzlov, I. G., Peculiarities of Cooling, Structure Formation and Properties of Mass Metal Products During Their Industrial Heat Treatment, *MiTOM,* No. 9, 1989, pp. 14–19.

[26] Babich, V. K., Technological Bases of Heat Treatment of Mass Products, *Metal Science and Heat Treatment,* No. 11, 1987, pp. 30–31.

[27] Chmeleva, V. S., Study and Design of Conditions and Technology of Heat Treating Cased Tubes with the Intensification of Quench Cooling with the Use of Interrupted Rapid Cooling, Ph.D. Dissertation, National Metallurgical Academy of Ukraine, Dnipropetrovsk, 1983.

[28] Deyneko, L. N., Kobasko, N. I., Dobrivecher, V. V., and Litvinenko, E. I., An Overview of Technology and Equipment for Hardening of Large Steel Parts, *Journal of ASTM International,* Vol. 6, No. 2, 2009.

[29] Kobasko, N. I., On the Problem of Intensification of Heat and Mass Transfer Processes, *Promteplotekhnika,* Vol. 18, No. 1, 1996, pp. 57–60.

[30] Kobasko, N. I., Method of Parts Quenching Made of High-Alloy Steels, Inventor's Certificate No. 1,215,361 (USSR), *Bulletin of Inventions,* No. 7, 1988.

[31] Kobasko, N. I., Morhuniuk, W. S., and Dobrivecher, V. V., Control of Residual Stress Formation and Steel Deformation During Rapid Heating and Cooling, *Handbook of Residual Stress and Deformation of Steel,* Totten, G., Howes, M., and Inoue, T., Eds., ASM International, Materials Park, OH, 2002, pp. 312–330.

[32] Borisov, I. A., Increase in Durability of Power Machine Parts by Intensification of their Quench Cooling, *Metal Science and Heat Treatment,* Vol. 31, No. 9, 1989, pp. 23–28.

[33] Aronov, M. A., Intensive Quenching Technology for Heat Treating and Forging Industries, Final Technical Report, DOE Award Number DE-FC36-03ID 14463, 2005.

[34] Mukhina, M. P., Kobasko, N. I., and Gordeeva, L. V., Hardening of Structural Steels in Cooling Media Based on Chlorides, *Metal Science and Heat Treatment,* Vol. 31, No. 9, 1989, pp. 677–682.

[35] Shepeliakovskii, K. Z., Deviatkin, V. P., Ushakov, B. K., and Fedin, V. M., Peculiarities and Conditions of Rational Application of Fast-Moving Water Flows as Quenchant, *Metal Science and Heat Treatment,* Vol. 31, No. 9, 1989, pp. 30–36.

[36] Kobasko, N. I., *Quenchants and Devices for the Implementation of New Steel Quenching Methods,* Znanie, Kyiv, 1991.

[37] Khalatov, A. A., Lisovoy, V. A., and Kobasko, N. I., Method of Steel Quenching, Inventor's Certificate No. 1,375,661 (USSR), *Bulletin of Inventions,* No. 7, 1988.

[38] Bubnov, V. A., Martynenko, O. G., and Kalilets, V. I., A Note on the Theory of the Rank Effect, *Journal of Engineering Physics and Thermodynamics,* Vol. 29, No. 6, 1975, pp. 1519–1522.

[39] Chun-xia, S., Yong, W., and Qi-sheng, Z., Effect of Interrupted Quenching Temperature in Direct Quenching on Microstructure and Properties of Low Carbon Mn-Cr-Ni-Mo Steel, *Heat Treatment of Metals (Jinshu Rechuli),* Vol. 35, No. 1, 2010, pp. 85–88.

[40] Kobasko, N. I., Current and Residual Stresses During Quenching of Steel Parts, *Finite Elements,* N. E. Mastorakis and O. Martin, Eds., WSEAS Press, Athens, 2007, pp. 86–99.

[41] Kobasko, N. I., Quench Process Optimization, *Proceedings of the 6th International Conference "Equipment and Technologies for Heat Treatment of Metals and Alloys," OTTOM-6,* Kharkov, Ukraine, May 16–20, 2005, pp. 88–96.

Thermal Engineering and Environment (HTE '08), Rhodes, Greece, August 20–22, 2008, pp. 539–542.

10

Intensive Steel Quenching Methods

N. I. Kobasko[1]

10.1 INTRODUCTION

In the previous chapters, processes and their mathematical description that form a basis for the development of new intensive steel quenching methods have been considered. The primary concept of the new intensive quenching methods is to perform intensive cooling within the martensite transformation range of the steel of interest.

There are various methods for performing intensive cooling within the martensite range, such as those illustrated in Fig. 1. The process represented in the figure by the straight line on the left ("Fast + fast") shows the process of intensified cooling throughout the entire cooling process, from the austenitization temperature to the final bulk quenchant temperature. However, in this case, the rapid cooling is insufficiently intensive to prevent quench crack formation as might occur during cold water quenching. Therefore parts made of alloyed steels are typically quenched in oils or aqueous solutions of polymers at high concentration to reduce the cooling rate within the martensite range. This quenching process is illustrated by the second set of lines in Fig. 1 ("Slow [or fast or intensive] + slow").

The third line of Fig. 1 ("Slow + intensive") illustrates the quenching process designated as IQ-1, which consists of slow cooling from the austenitization temperature until the start of the martensite transformation, at temperature M_S, below which the steel part is cooled very intensively. In practice, the IQ-1 process is performed by first slowly cooling the alloyed steel in an aqueous polymer quenchant solution at a high concentration or in petroleum oils to the M_S temperature, followed by rapid cooling using intensive water jets, which provide a high cooling rate within the martensite range with the added benefit of washing the part.

IQ-2 intensive steel quenching technology is a three-stage cooling process. The first step involves intensive cooling without film boiling until the superficial layers contain 50 % martensite. At this point, the intensive cooling process is interrupted, and the steel is cooled in air, where the temperature is equalized throughout the cross-sections and self-tempering of the newly formed martensite in superficial layers occurs. Finally, intensive cooling is continued until the martensite transformation is completed.

The straight line at the right of Fig. 1 ("Intensive + intensive") illustrates the IQ-3 process, in which intensive cooling is performed by a method that eliminates both film boiling and nucleate boiling. This is accomplished by using powerful jets or streams of water to lower the surface temperature of the steel almost immediately to the temperature of the quenchant. In this way, maximum thermal gradients between the superficial layers and the core are created. The

process of intensive cooling is performed until maximum surface compressive stresses are formed, which is the optimal condition.

Intensive quenching processes designated as IQ-4 and IQ-5 are not shown in Fig. 1 since they are difficult to illustrate schematically. The IQ-4 intensive quenching process is used for parts with a complicated configuration. Different sections are cooled in such a way that, in each section, the Biot number remains constant and exceeds a certain specified value, which leads to the creation of a uniform martensite shell over the entire surface. As a result, high surface compressive stresses are formed at the superficial layers, which prevents quench crack formation and minimizes distortion.

The IQ-5 intensive quenching process is used for machine cutting parts and is applied for quenching a section while completely insulating other surfaces from contact with the quenchant. This method permits the creation of high surface compressive residual stresses instead of tensile stresses over the working surface of the part.

These intensive quenching processes are considered in detail in this chapter and are accompanied by numerous examples of simplified calculations [1−5].

10.2 IQ-1 INTENSIVE QUENCHING TECHNOLOGY

Historically the first intensive quenching process was IQ-1, in which the intensification of cooling is performed only within the martensite transformation range. Cooling of the steel from the austenitization temperature to the martensite start temperature M_S is performed slowly in hot oils or high concentrations of water-salt solutions, aqueous polymer solutions, and so on. Upon reaching the M_S temperature at the surface, the steel is unloaded from the quench tank and placed under intensive jets of water or jets of nitrogen (cryogenic treatment).

Two problems were encountered with this process: crack formation and distortion. These problems were solved by optimizing the IQ-1 process using appropriate boundary conditions.

The heat transfer coefficient versus temperature at the surface of a test specimen using a modified petroleum oil (MZM-16) is shown in Fig. 2. The average value of the heat transfer coefficients for the temperature range of 300−800°C for oil at 120°C and a 30 % (high) concentration of a water−PAG polymer solution are presented in Table 1. Thermal properties of the supercooled austenite as a function of temperature are shown in Tables 2 and 3.

Using the thermal properties of the supercooled austenite and the corresponding heat transfer coefficients, it is possible to perform computations based on both the approximate

[1] IQ Technologies, Inc., Akron, Ohio, and Intensive Technologies Ltd., Kyiv, Ukraine
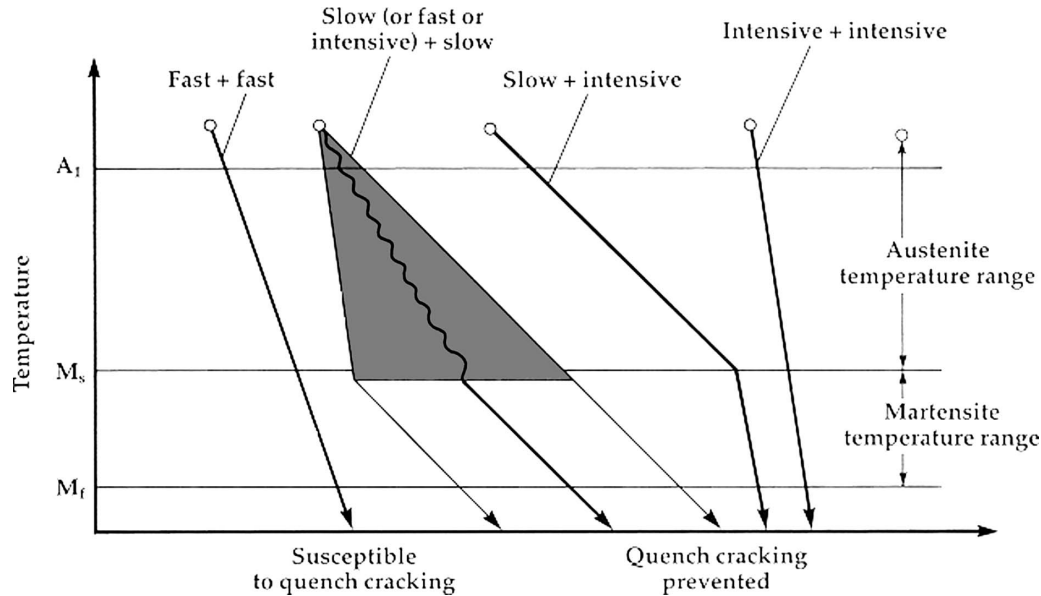
Fig. 1—Different techniques of intensive quenching.

method and by computer simulation. Examples will now be provided illustrating the use of simplified calculations for quenching of plate-shaped, cylindrical, and spherical bodies.

Example 10.1

A round plate with a diameter of 120 mm and a thickness of 6 mm is to be cooled from 860°C in a concentrated aqueous polymer solution. The heat transfer coefficient for the temperature range of 300−800°C is 700 W/m²K. The plate is made of AISI 4140 steel. The CCT (continuous cooling transformation) diagram for AISI 4140 steel is shown in Fig. 3. The martensite start temperature M_S for AISI 4140 is 365°C. Find the time of cooling of the core of the plate from 860°C to 400°C and predict the microstructure using the data from the CCT diagram in Fig. 3 corresponding to this time. For calculations, use the generalized equation (Eq 69) presented in Chapter 5. At the first step, calculate the Kondratjev form factor (coefficient) K and generalized Biot number Bi_V.

The Kondratjev form coefficient K for a plate of a round shape can be calculated by the equation:

$$K = \frac{1}{\frac{5.783}{R^2} + \frac{9.87}{Z^2}},$$

where:
R is the radius of the plate (m); and
Z is the thickness of the plate (m).

Substituting the given sizes of the plate in the above-stated formula, we obtain:

$$K = \frac{1}{\frac{5.783}{(0.06)^2} + \frac{9.87}{(0.006)^2}} = 3.63 \cdot 10^{-6} m^2.$$

The generalized Biot number Bi_V is determined by the equation:

$$Bi_V = \frac{\alpha}{\lambda} K \frac{S}{V},$$

where (substituting the known values):

$$\frac{S}{V} = \frac{2(R + Z)}{RZ} = 2\frac{(0.06 + 0.006)}{0.06 \cdot 0.006} = 366.7 \frac{1}{m}.$$

The average thermal conductivity for the temperature range of 300−800°C is approximately 22 W/mK (see Table 2). Therefore, the generalized Biot number Bi_V is:

$$Bi_V = \frac{700 \frac{W}{m^2 K}}{22 \frac{W}{mK}} \cdot 3.63 \cdot 10^{-6} m^2 \cdot 366.7 \frac{1}{m} = 0.042.$$

Fig. 2—Dependence of the heat transfer coefficient of accelerated petroleum MZM-16 oil on the surface temperature of a test specimen 20 mm in diameter made of AISI 304 steel.

TABLE 1—Average values of heat transfer coefficients for MZM-16 oil at 80–100°C and PAG polymer of 30 % concentration at 30°C within the temperature range of 300–800°C (no agitation)		
Quenchant	Temperature range (°C)	Average heat transfer coefficient (W/m²K)
MZM-16	300–800	1,800–2,000
	120–350	350
30 % PAG polymer	300–800	700

TABLE 2—Thermal conductivity of supercooled austenite versus temperature									
T (°C)	100	200	300	400	500	600	700	800	900
$\lambda, \frac{W}{mK}$	17.5	18	19.6	21	23	24.8	26.3	27.8	29.3
$\bar{\lambda}, \frac{W}{mK}$	17.5	17.75	18.55	19.25	20.25	21.15	21.90	22.65	23.4
Note: $\bar{\lambda}$ is the mean value for the range between 100°C and the stated temperature.									

TABLE 3—Thermal diffusivity a of supercooled austenite versus temperature									
T (°C)	100	200	300	400	500	600	700	800	900
$a \cdot 10^6, \frac{m^2}{s}$	4.55	4.63	4.70	4.95	5.34	5.65	5.83	6.19	6.55
$\bar{a} \cdot 10^6, \frac{m^2}{s}$	4.55	4.59	4.625	4.75	4.95	5.10	5.19	5.37	5.55
Note: $\bar{a}$ is the mean value for the range between 100°C and the stated temperature.									

Using the universal correlation between Kn and Bi_V, we can now find the Kondratjev number Kn:

$$Kn = \frac{Bi_V}{(Bi_V^2 + 1.437 Bi_V + 1)^{0.5}}$$
$$= \frac{0.042}{(0.00176 + 0.0604 + 1)^{0.5}} = 0.043.$$

Now using the generalized dependence, Eq 60, we can calculate the duration of cooling of a round plate from 860°C to 400°C:

$$\tau = \left[\frac{kBi_V}{2.095 + 3.867 Bi_V} + \ln \frac{T_0 - T_S}{T - T_S} \right] \frac{K}{aKn}$$
$$= \left[0.019 + \ln \frac{860^oC - 100^oC}{400^oC - 100^oC} \right] \frac{3.63 \cdot 10^{-6} m^2}{5.36 \cdot 10^{-6} \frac{m^2}{S} \cdot 0.043}$$
$$= 14.93 s \approx 15 s.$$

Thus, the core of a round plate cools from 860°C to 400°C in 15 s.

The CCT diagram for AISI 4140 steel shown in Fig. 3 indicates that, after cooling for 15 s, the core is in the austenite condition. If, for the second cooling stage, the plate is cooled intensively by water jets, martensite quenching will occur throughout the entire section, and at the same time, the plate will be cleaned of any remaining surface deposits

Fig. 3—CCT diagram of AISI 4140 steel with superimposed calculated cooling curves for the surface (S), three-quarter radius (3/4 R), and center (C) of a round bar of 50-mm diameter [6].

from the polymer quenchant. As a result of intensive cooling, the mechanical properties of the material are improved.

Example 10.2
Cylindrical punches (Ø12 mm, and height 120 mm) made of AISI M2 steel are cooled in hot oil at 120°C. The heat transfer coefficient of the oil is 2,000 W/m²K. Determine the time of cooling of the core from 1,200°C to 300°C using the following thermal properties of the steel:

- $\bar{a} = 5.63 \cdot 10^{-6} \frac{m^2}{s}$;
- $\bar{\lambda} = 23 \frac{W}{mK}$.

First, we calculate the Kondratjev form coefficient K for the cylinder, the generalized Biot number Bi_V, and the Kondratjev number Kn as follows:

$$K = \frac{R^2}{5.783} = \frac{(0.006)^2}{5.783} = 6.225 \cdot 10^{-6} m^2;$$
$$Bi_V = \frac{\alpha}{\lambda} K \frac{S}{V} = \frac{2000 \frac{W}{m^2 K}}{23 \frac{W}{mK}} \cdot 6.225 \cdot 10^{-6} m^2 \cdot \frac{2}{0.006} = 0.18;$$
$$Kn = \frac{Bi_V}{(Bi_V^2 + 1.437 Bi_V + 1)^{0.5}} = 0.16.$$

Substituting these results into Eq 60 ($k = 2$, $Bi_V = 0.18$), we find:

$$\tau = \left[\frac{kBi_V}{2.095 + 3.867 Bi_V} + \ln \frac{1200^oC - 120^oC}{300^oC - 120^oC} \right]$$
$$\times \frac{6.225 \cdot 10^{-6} m^2}{5.63 \cdot 10^{-6} \frac{m^2}{S} \cdot 0.16} = 13.3 s.$$

During cooling in hot oil, a small temperature gradient through the cross-section of a punch is observed, which can be calculated by the universal correlation:

$$Kn = \psi Bi_V, \quad (1)$$

where ψ is the criterion of nonuniformity of the temperature field. From this, with $Bi_V = 0.18$, it follows that:

$$\psi = (Bi_V^2 + 1.437 Bi_V + 1)^{-0.5} = 0.88.$$

On the other hand, the ψ criterion is also equal to:

$$\psi = \frac{\bar{T}_{sf} - T_m}{\bar{T}_V - T_m}, \quad (2)$$

where:

$\bar{T}_{sf}$ is the average temperature at the surface;

$\bar{T}_V$ is the average temperature across the volume; and

T_m is the temperature of the medium.

From Eq 2, if $\psi = 1$, then $\bar{T}_{sf} = \bar{T}_V$, and the temperature field is uniform, that is, the temperature of the part through the entire cross-section is the same. If $\psi = 0$, the surface of a part has the same temperature as the medium. Since $\psi = 0.88$ differs only slightly from 1, during quenching of the punch in hot oil, a small gradient of temperature on the cross-section is observed. When the core temperature of the punch falls to 300°C, the part is unloaded from the hot oil, and the cooling is continued in cold water jets, which increases the service life of the punch.

Now consider the quenching process for parts of more complicated configuration, using the results of the numerical calculations made by IQLab and Tandem-Hart software [1–3]. This software was used to simulate the quenching process for the carburized plug shown in Fig. 4(a). The plug was made of steel having the following chemical composition: 0.11–0.16 % carbon; 0.9–0.7 % silicon; 0.9–1.5 % manganese; and 0.5–0.8 % chromium.

Fig. 4(b) illustrates the quenching process for the carburized plug in hot oil at 137°C. The temperature at the surface of the plug was measured experimentally at three points (1, 2, and 3 in Fig. 4(b)). The plug was carburized only on the inner side to the depth of 1.8 mm. The external side of the plug was covered with copper to prevent carburization. After cooling in hot oil at 137°C, the plug was transferred to a special chamber, where the plug was cooled cryoscopically using jets of liquid nitrogen at −172°C. Due to the large temperature difference between the surface of the plug and the liquid nitrogen and the high heat transfer coefficients of jets of liquid nitrogen, a high cooling rate within

(a)

(b)
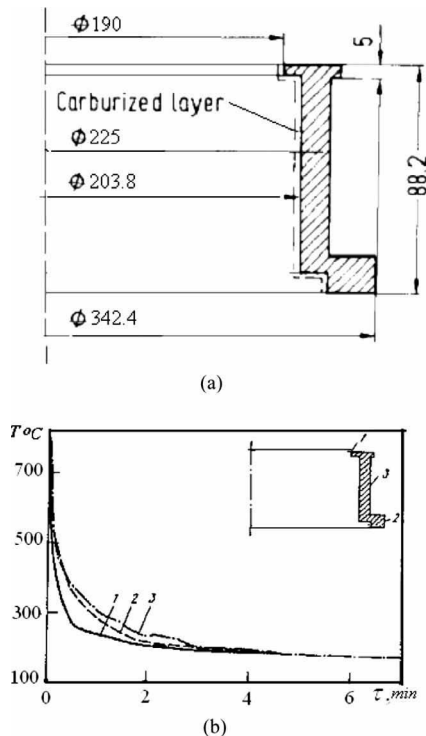
Fig. 4—(a) Sizes of the carburized plug; (b) Surface temperature versus time during quenching of the plug in oil at 137°C [1].
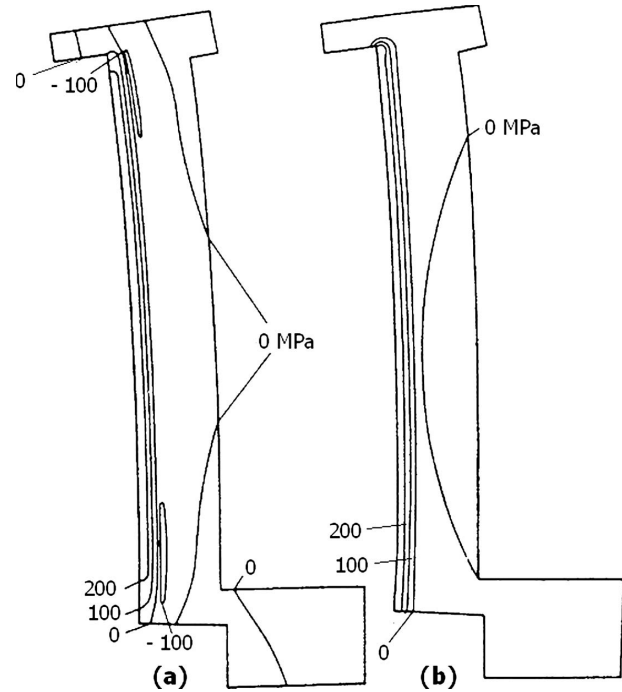
Fig. 5—Distribution of axial (a) and circumferential (b) stresses in the carburized plug at the end of the first cooling stage (deformation enlarged by 25 times in the illustration).

the martensite range was achieved. However, due to the low temperature, the plug was cooled below M_f and the hardness at the carburized surfaces reached HRC 66–67.

It is important to determine the character of distortion of the carburized plugs during each stage of cooling. The Tandem-Hart simulation shows the different character of the distortions during the first and second stages [1–3]. During the first stage of cooling in hot oil, the plug was "barrel-shaped." At the inner surface, small tensile residual stresses appeared (see Fig. 5). During the second stage of cooling of the plug in jets of liquid nitrogen, due to the greater specific volume of martensite, distortion of the plug was in the opposite direction, that is, it became concave toward the center (see Fig. 6). For better visualization, the distortions in Figs. 5 and 6 are magnified by 25 times. It should be noted also that after the full transformation of austenite into martensite during the second stage of cooling of the carburized plug, very high compressive stresses are observed in the carburized layer, with values in the range of 1,000–1,450 MPa (see Fig. 6). The lower values are for transformation of austenite into martensite in the carburized layer (HRC 66–67); the higher values are compressive stresses at the carburized surface.

The IQ-1 process is not widely used in practice, except for carburized plugs. The use of plain water for intensive quenching of steel is more attractive. However, in this case, it is required to develop special devices, setups, and automated industrial lines that facilitate intensification of the quenching process. In practice, the IQ-2 and IQ-3 processes are more commonly used. In the next section, the IQ-2 process, which is suitable for both batch quenching and continuous processes, is considered in greater detail.

10.3 IQ-2 INTENSIVE QUENCHING TECHNOLOGY

To understand the IQ-2 process, let's consider the CCT diagram shown in Fig. 7, where M_S is the martensite start
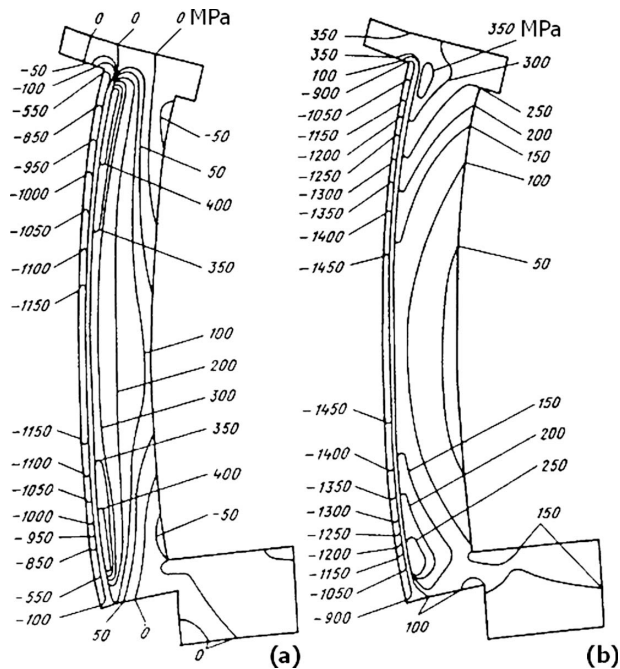
Fig. 6—Distribution of axial (a) and circumferential (b) residual stresses in the carburized plug at the end of the second cooling stage at $\alpha = 1,000$ W/m²K (distortion enlarged by 25 times in the illustration).

temperature of 180°C. Now assume that a cylindrical specimen 20 mm in diameter is made of steel that has the same CCT diagram as that in Fig. 7. Then, according to the experiments presented in Chapter 8, the surface temperature will
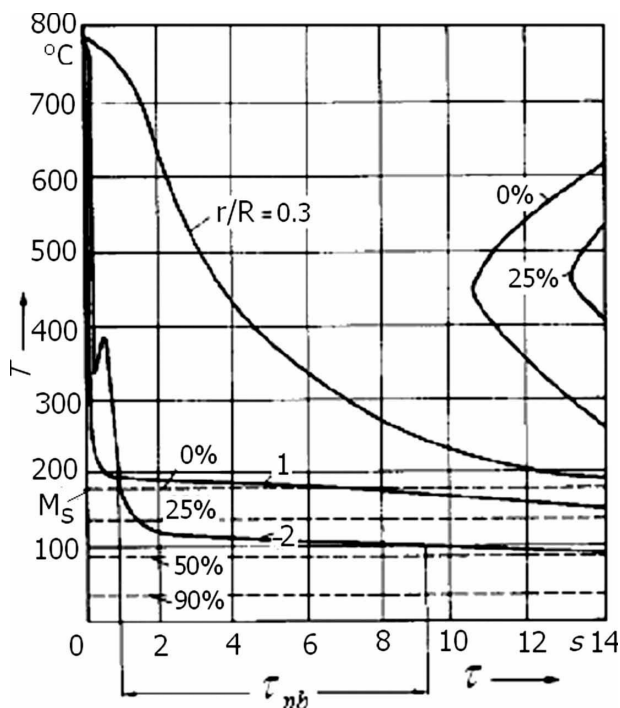
Fig. 7—Pressure adjustment of the cylindrical part's (diameter 20 mm) surface temperature with water cooling at 20°C: 1, quenching under pressure 0.7 MPa; 2, quenching under pressure 0.1 MPa.

be significantly dependent on pressure. When the pressure is 0.7 MPa, the surface temperature during nucleate boiling is maintained at 180°C (see Chapter 2). This is seen in Fig. 7, where curve 1 is for a pressure of 0.7 MPa; curve 2 is for normal atmospheric pressure, that is, 0.1 MPa.

During nucleate boiling, the surface temperature of the test specimen is supported at approximately the level that corresponds to the boiling temperature of a boundary liquid layer. Changing the static quenchant pressure or increasing the concentration of water-salt solutions, one can control the temperature at the surface of the test specimen or steel parts during the nucleate boiling process. At the end of nucleate boiling, intensive cooling is interrupted, and equalization of the temperature through sections of the steel parts is provided in air. Then intensive quenching continues, to create an accelerated cooling rate within the martensite range, which can be combined with the washing of the parts.

The IQ-2 process is a three-step cooling that consists of:
- The nucleate boiling process providing no more than 50 % martensite at the surface of steel parts during the first step (see Fig. 7)
- Cooling in air to provide equalization of temperature through the sections of the parts
- Intensive cooling with convection, combined with the washing of the steel parts

Therefore, it is necessary to interrupt the intensive cooling process at the end of nucleate boiling and to cool in air to maintain the equalizing temperature through the cross-section of the test specimen. Interruption of the process also results in self-tempering of the newly formed martensite in the superficial layers. As a result of self-tempering, there is an improvement of the mechanical properties, especially material ductility, in the superficial layer of the steel parts.

This is the essence of the IQ-2 intensive quenching process. The technology was used for the first time in Ukraine and further developed and applied into practice in the United States [7–12]. This technology is applicable for high-carbon steels, including alloy steels with a martensite start temperature below 200°C, that is, $M_S \leq 200$°C (see Fig. 7).

For medium-carbon steels, the situation is radically different. The problem is with the formation of 50 % martensite above 200°C (see Fig. 8), because it is practically impossible to maintain the boiling temperature at this level. Therefore, when quenching low-carbon and medium-carbon steels, it is necessary to find the conditions when 50 % of martensite through the cross-section of the part to be quenched is reached.

The CCT diagram of Fig. 8 shows that during water quenching at atmospheric pressure, almost 100 % martensite is formed during nucleate boiling. This means that during intensive cooling, because of the large temperature gradient through the cross-section, the martensite shell, which should be formed in the superficial layer, moves from the surface to the core of the part. It is therefore necessary to interrupt the intensive cooling process at the time when compressive stresses are at their maximum.

It has been established [4,7,13] that 50 % martensite is obtained at the time of reaching maximum surface compressive stresses. By interrupting the intensive cooling process at the end of nucleate boiling, it is possible to obtain simultaneously very high hardness in the superficial layers, high surface compressive residual stresses, and a plastic core. Due to
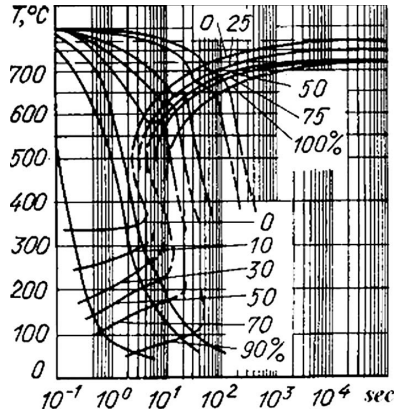
Fig. 8—CCT diagram of AISI 1045 medium-carbon steel.

the high cooling rate within the martensite range, which is reached because the martensite finish temperature M_f is greater than the boiling temperature of the liquid T_S ($M_f > T_S$), improved mechanical properties are observed in the superficial layers.

As an illustration, consider the quenching process for a cylinder of 50-mm diameter made of AISI 1045 steel. The cylinder is heated to 860°C and then is quenched in flowing water with a flow rate of 1.5 m/s, where the transfer coefficient during convection is 5,000 W/m²K. Determine the duration of nonstationary nucleate boiling and analyze the process with respect to the CCT diagram in Fig. 8.

For this purpose, the generalized equation, which has the following form,

$$\tau = \left[\Omega + f \ln \frac{\vartheta_I}{\vartheta_{II}}\right] \frac{K}{a} \qquad (3)$$

will be used. For this example:
$\Omega = 0.48$;
$f = 3.21$;
$K = R^2/5.783 = 108.1 \times 10^{-6}$ m²; and
$a = 5.36 \times 10^{-6}$ m²/s.

Values ϑ_I and ϑ_{II} can be calculated by equations presented in Chapter 2. Eq 37 states:

$$\vartheta_I = \frac{1}{\beta}\left[\frac{2\lambda(\vartheta_0 - \vartheta_I)}{R}\right]^{0.3}, \qquad (4)$$

where, in this instance:
β, according to Tolubinsky's equations [6], is equal to 7.36;
$\lambda = 22$ W/mK;
$R = 0.25$ m; and
$\vartheta_0 = T_0 - T_S = 860°C - 100°C = 760°C$.

Substituting these values into Eq 4 yields:

$$\vartheta_I = 0.136[1760(760 - \vartheta_I)]^{0.3}. \qquad (5)$$

This can be reduced iteratively by substituting into the right side of Eq 5 any value for ϑ_I, preferably close to the true condition. For example, starting with $\vartheta_I = 30°C$, we calculate:

$$\vartheta_I = 0.136[1760(760 - 30)]^{0.3} = 9.25°C.$$

Revising the formula using the value of 9.25°C in Eq 5, the second iteration yields:

$$\vartheta_I = 0.136[1760(760 - 9.25)]^{0.3} = 9.33°C,$$

and carrying this one step further refines the value to:

$$\vartheta_I = 0.136[1760(760 - 9.33)]^{0.3} = 9.33°C.$$

The value of ϑ_{II} is similarly calculated using Eq 2.38:

$$\vartheta_{II} = \frac{1}{7.36}[\alpha_{conv}(\vartheta_{II} + \vartheta_{uh})]^{0.3}, \qquad (6)$$

where, for this example:
$\alpha_{conv} = 5,000$ W/m²K; and
$\vartheta_{uh} = T_S - T_m = 100°C - 20°C = 80°C$.

Substituting these values into Eq 6, a similar ratio is obtained:

$$\vartheta_{II} = 0.136[5000(\vartheta_{II} + 80)]^{0.3}. \qquad (7)$$

Solving iteratively in the same way as for Eq 5, we set any value of ϑ_{II} in the right part of Eq 7, for example, $\vartheta_{II} = 5°C$, for the first step:

$$\vartheta_{II} = 0.136[5000(5 + 80)]^{0.3} = 6.64°C.$$

Repeating this procedure, we get:

$$\vartheta_{II} = 0.136[5000(6.64 + 80)]^{0.3} = 6.67°C;$$

and that value remains the same for the third iteration, so $\vartheta_{II} = 6.67°C$.

Thus, the duration of nonstationary nucleate boiling for a cylindrical sample of 50-mm diameter, cooled in a quench tank, where $\alpha_{conv} = 5,000$ W/m²K is reached, is equal to:

$$\tau = \left[0.48 + 3.21 \ln \frac{9.33°C}{6.67°C}\right] \frac{108.1 \cdot 10^{-6} m^2}{5.36 \cdot 10^{-6} m^2/s} \approx 31.4s.$$

With an increase of the convection heat transfer coefficient α_{conv}, the duration of nonstationary nucleate boiling decreases. And, conversely, with a reduction of α_{conv}, the duration of nonstationary nucleate boiling increases.

Table 4 presents the duration of nonstationary nucleate boiling τ_{nb} for a cylindrical sample of 50-mm diameter, cooled in circulating water, providing various values for the convection heat transfer coefficient. From Table 4, we see that during quenching in still water, where the convection heat transfer coefficient α_{conv} is equal to 1,700 W/m²K, the duration of nucleate boiling τ_{nb} is 52.7 s. The temperature of the core of the cylinder at the end of nucleate boiling is also presented in Table 4.

At the center of the cylinder, for each specific case presented in Table 4, it is possible to estimate the temperature by the following equation:

$$T = T_S + (T_0 - T_S)e^{-\left(\frac{c_1 \bar{a}\tau}{K} - 0.24k\right)}, \qquad (8)$$

where:
T_S is the saturation temperature;
T_0 is the austenitization temperature;

TABLE 4—Duration of nonstationary nucleate boiling τ_{nb} versus convection heat transfer coefficient α_{conv} for water at a temperature of 20°C

α_{conv} (W/m²K)	1,700	2,500	5,000	10,000
τ_{nb} (s)	52.7	43.9	35.5	17.5
Temperature at the core (°C)	354	397	431	828

C_1 is a constant;

$\bar{a}$ is the average thermal diffusivity of the material;

τ is the time at the end of nucleate boiling; and

$k = 1, 2,$ or 3 for plate-shaped, cylindrical, or spherical bodies, respectively.

During quenching in a still quenchant, the duration of transient boiling is about 53 s, and the temperature in the core of the cylinder at the end of this period is about 354°C. Determining the corresponding parameters for AISI 4140 steel with the CCT diagram in Fig. 3, we find that approximately 40 % bainite is formed in the core of the cylinder, which will provide a hardness of HRC 46 after complete cooling of the core. On the surface and in the superficial layers of the cylinder, 100 % martensite is formed, which, according to Fig. 3, provides a hardness greater than HRC 58, because the surface temperature drops very quickly.

It should be noted that this estimation is approximate. The exact solution of this problem can be obtained by computer simulation taking into account all of the subtleties of the transformation of the supercooled austenite into martensite, along with the intermediate phases. However, even with the approximate approach, this method is a powerful tool for use in preliminary thermal process design.

With IQ-2 intensive quenching, a cylindrical specimen after the finish of nucleate boiling is unloaded from a quench tank to cool in air, where self-tempering of a superficial layer occurs. Then cooling is continued until reaching the temperature of the quenching medium. If a cylinder is cooled in water streams of 1.5 m/s where the average heat transfer coefficient is $\alpha_{conv} = 5,000$ W/m²K, the duration of nonstationary nucleate boiling in this case is 35.5 s and the temperature of the core reaches 431°C. According to the CCT diagram in Fig. 8, bainite will be observed in the core, and the when the surface reaches 100°C, 100 % of martensite is formed. After unloading the cylinder to air-cool and self-temper the superficial layer, intensive cooling of the cylinder is continued until the temperature of the medium is achieved.

Thus, by changing the convection heat transfer coefficient (α_{conv}), it is possible to control the duration of nonstationary nucleate boiling and obtain various core temperatures at the finish of the nucleate boiling process.

10.3.1 Importance of the Intensification of Heat Transfer at the Time of Immersion into the Quenchant

When implementing IQ-2 intensive technology, it is important to create intensive jets or streams of water at the initial time of immersion of the steel into the quenchant. This is necessary to prevent the formation of a steam film at the surface of the parts to be quenched. Intensification upon immersion must be performed so that the heat flux density q from the surface of parts is no greater than the first critical heat flux density q_{cr1}, that is, $q \le q_{cr1}$. Further intensification of the heat transfer during implementation of IQ-2 may not be performed since it is related to the reduction in the surface temperature of the steel to the temperature of the medium. (It is possible to actually implement IQ-3 technology, while thinking that IQ-2 technology is being used.)

There are numerous methods to intensify the heat transfer process at the time of immersion of steel into a quenchant by increasing the first critical heat flux density. First of all, neutral aqueous solutions of salts of optimal concentration can be applied, providing the maximum value of q_{cr1}. In practice, for this purpose, chutes are used in which water is intensively circulated or powerful jets for prevention of process of film boiling are arranged. Such installations and their hydrodynamics will be discussed in Chapter 11.

The discussion in this chapter will be limited to illustrating the initial time when there is no film boiling and a very high heat transfer coefficient is formed. To this end, we will now calculate a heat transfer coefficient during nucleate boiling when $\vartheta_I = 9.33$°C. According to the equation of Tolubinsky (see Chapter 2, Eq 10),

$$\alpha_{nb} = \beta^{3.33}\vartheta_I^{2.33},$$

or

$$\alpha_{nb} = (7.36)^{3.33}(9.33)^{2.33} \approx 140,128 W/m^2K.$$

Therefore, the generalized Biot number Bi_V, given by

$$\left(Bi_V = \frac{\alpha}{\lambda}K\frac{S}{V} \right)$$

is equal to 52.6. This calculation shows that during quenching, when there is no film boiling, the surface temperature is practically equal to the boiling temperature of a liquid. The temperature remains at this level for a long time and then eventually decreases somewhat during the nonstationary nucleate boiling [7,8].

Despite very high values of heat transfer coefficients during nucleate boiling, the cooling rate within the martensite range may be zero if $M_S \le T_S$. This means that, during boiling, there is a delay of the transformation of austenite into martensite.

10.3.2 Equations for Calculating the Speed of Industrial Conveyors

Two methods of quenching medium-carbon and high-carbon steels, IQ-1 and IQ-2, have been discussed so far. For both methods, there were no generalized dependences since different equations were used. For the IQ-2 process with two possible ways of cooling, it is possible to combine the generalized equations developed earlier into a single equation:

$$\tau = [\Omega + b\ln\theta]\frac{K}{aKn}, \tag{9}$$

where, for medium-carbon steels:

$b = 1$; and

$$\theta = \frac{T_0 - T_S}{T - T_S},$$

and for high-carbon steels:

$b = 3.21$; and

$$\theta = \ln\left(\frac{\vartheta_I}{\vartheta_{II}}\right).$$

To unload steel from the quench tank at the appropriate time of reaching the maximum surface compressive stresses or the completion of nucleate boiling, it is sufficient to establish a certain conveyor speed while the steel is immersed into a quenchant. This conveyor speed should be calculated by the equation:

$$W = \frac{L}{\tau} = \frac{aLKn}{(\Omega + b\ln\theta)K}. \tag{10}$$

In Eq 10, the speed of the conveyor is given in m/s. To set the speed in m/hr, it is necessary to multiply the answer by 3,600. Including this factor in the numerator, the equation takes the form:

$$W = \frac{0.36 \cdot 10^4 aLKn}{(\Omega + f\ln\theta)K}, \tag{11}$$

in which the result is speed of the conveyor in m/hr.
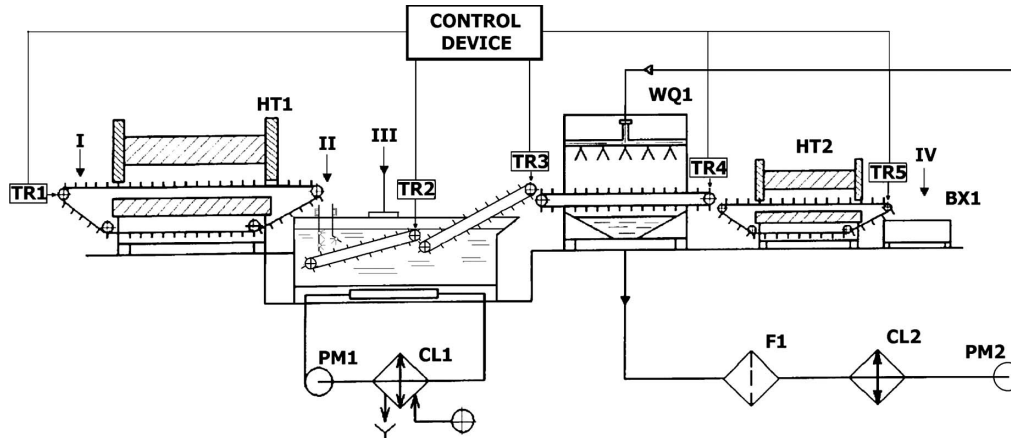
Fig. 9—Industrial installation for the implementation of IQ-2 technology [10]: I, loading point for steel parts to the conveyor for heating in heater HT1; II, chute with intensive cooling devices; III, quenching tank with two conveyors; IV, unloading point of steel parts from heater HT2; TR1–TR5, speed control units for conveyor belts 1, 2, 3, 4, and 5 operated by the control device; HT1 and HT2, heaters 1 and 2; WQ1, washing and quenching device; PM1 and PM2, pumps 1 and 2; CL1 and CL2, coolers 1 and 2; F1, filter; BX1, container for quenched parts.

The basic scheme of an industrial installation for the implementation of IQ-2 intensive quenching is shown in Fig. 9. The continuous industrial line (conveyor) consists of conveyor furnace HT1, which in section I is loaded automatically. Furnace HT1 is connected to a computer control device, which is schematically shown at the top in Fig. 9.

The speed of the conveyor in the furnace is set by computer depending on the shape and size of the parts and chemical composition of the steel. Parts, after being heated to the austenitization temperature and kept at the same temperature for some time, are delivered to a chute (II), where intensive circulation of the quenchant is performed. The quenchant may be an aqueous solution of neutral salts of optimal concentration that provides the maximum value of the first critical heat flux density q_{cr1}. In addition, aqueous salt solutions should prevent surface corrosion of metals. Intensive circulation of the quenchant in the quenching tank and an optimal concentration of the aqueous solution eliminates film boiling or causes it to practically vanish. Fig. 9 shows that the quench tank has two conveyors that move at various speeds and are connected to the control unit through drives TR2 and TR3.

When heated parts come through the chute (II) to the first conveyor, they are cooled very intensively, since there is no film boiling and the surface temperature is kept at the boiling level of a boundary liquid layer; for pure water, for instance, this level is 100°C. Depending on the shapes and sizes of parts to be quenched, the control unit sets a certain speed of the first conveyor in the quench tank. The speed of the first conveyor is calculated by Eq 11 and provides unloading of parts to be quenched from the quenchant when nucleate boiling is completed or–for low-carbon and medium-carbon steels–when reaching the maximum compressive stresses in the superficial layers of the part.

The first conveyor transfers the parts being quenched to the second conveyor, where the temperature throughout their cross-sections is equalized in air and the martensite layer that is formed at the surface is self-tempered.

The speed of the second conveyor is also regulated by the control unit through drive TR3. Equalization of the temperature throughout the parts after air cooling may be checked by using a semiconductor sensor (like a barometer) that senses the maximum temperature on a heated surface of parts during their self-tempering.

The temperature of the quenchant in the tank is kept at the constant level by use of a refrigerator (CL1). To maintain the optimal concentration of the solution, it is necessary to check it from time to time.

The parts after self-tempering move to the following conveyor through the washing and quenching device (WQ1), where they are washed and further cooled intensively. The speed of this conveyor is regulated by the control unit through drive TR4. The temperature of the water in the washing tank is also kept at a constant level by means of refrigerator CL2.

The parts that have been washed out then go to the tempering furnace HT2, where they are finally tempered. The speed of the conveyor of the tempering furnace is regulated by the control unit through drive TR5. The ready parts after heat treatment are collected in storage unit BX1.

The scheme of the line for IQ-2 intensive quenching described here shows that it is sophisticated. Knowledge of the peculiarities of heating and cooling of the parts to be quenched is necessary, and the parameters for optimization of the process using the control unit must be determined.

Specific examples of the implementation of IQ-2 intensive quenching will now be considered and some simplified engineering calculations performed. However, more accurate computations are performed by computer simulations with commercially available software [14,15].

10.3.3 Examples of IQ-2 Implementation
The novelty of intensive quenching technologies lies in the opportunity to intensify the heat transfer within the martensite range and to regulate the temperature at the surface of steel parts to be quenched when the heat transfer coefficient approaches infinity, that is, $Bi \rightarrow \infty$. This was not previously evident, since it was assumed that at $Bi \rightarrow \infty$ the temperature at the surface of steel parts was always equal to the medium (quenchant) temperature T_m.

Example 10.3
A die made of ShKh15 (AISI 52100) steel, with diameter $D = 2R = 50$ mm and height $Z = 25$ mm, is quenched from

860°C in an aqueous solution of calcium chloride ($CaCl_2$) or magnesium chloride ($MgCl_2$) with additives of calcium hydroxide ($Ca(OH)_2$) to prevent corrosion [13]. The density of the solution is 1,320 kg/m³, which provides a boiling temperature for a boundary liquid layer at 125°C and formation of 50 % of martensite at the end of the nucleate boiling process. The quenching bath temperature is 50°C. Unloading is arranged at the completion of the nucleate boiling process by setting the time of cooling for the first step.

In this case, the duration of the first step is calculated using Eq 3:

$$\tau = \left[\Omega + f \ln \frac{\vartheta_I}{\vartheta_{II}}\right]\frac{K}{a},$$

along with:

$$\vartheta_I = \frac{1}{\beta}\left[\frac{2\lambda(\vartheta_0 - \vartheta_I)}{R}\right]^{0.3};$$

$$\vartheta_{II} = \frac{1}{\beta}[\alpha_{conv}(\vartheta_{II} + \vartheta_{Ha\partial})]^{0.3}; \text{ and}$$

$$K = \frac{1}{\dfrac{5.783}{R^2} + \dfrac{9.87}{Z^2}}.$$

Using the given dimensions $R = 0.025$ m and $Z = 0.025$ m and the other inputs:
$\bar{a} = 5 \times 10^{-6}$ m²/s;
$\Omega = 0.72$;
$\lambda = 22$ W/mK; and
$\alpha_{conv} = 420$ W/m²K,
we can determine:

$K = \dfrac{1}{\dfrac{5.783}{R^2} + \dfrac{\pi^2}{Z^2}} = 4 \cdot 10^{-5}m^2$;

$R^2 = (0.025 \text{ m})^2 = 6.25 \times 10^{-4}$ m²;
$Z^2 = 6.25 \times 10^{-4}$ m²;
$B = 3$;
$\vartheta_{uh} = 125°C - 50°C = 75°C$;
$\vartheta_I = 23.6°C$;
$\vartheta_{II} = 7.67°C$;
$\vartheta_I / \vartheta_I = 3.08$; and
$\ln 3.08 = 1.12$.

Substituting the initial data in Eq 3:

$$\tau = \left[0.72 + 3.21 \ln \frac{23.6}{7.67}\right]\frac{4 \times 10^{-5}m^2}{5 \times 10^{-6}m^2/s} = 34.5s.$$

Upon unloading, the die is cooled in air or washed in water and then tempered. The service life of the die increased in comparison with quenching in oil by 1.5 times.

Example 10.4
Fasteners of cylindrical shape are needed for work in the cold climate of Siberia and require appropriate impact strength at −70°C. The fasteners are made of alloyed AISI 4140 steel and are specified to be quenched from 860°C in 6 % agitated (0.5 m/s) water-salt solution of sodium nitrate ($NaNO_3$) at 20°C. The average diameter of the fasteners is 12 mm. The quenching of fasteners is performed using a continuous line equipped with conveyor belts depicted in Fig. 9. There is a need to upload the fasteners from the water-salt solution at the end of the nucleate boiling process. The length of the conveyor immersed into the water-salt solution is 1.2 m.

The heat transfer coefficient during the single-phase convection is 2,900 W/m²K. Other inputs are:
$\bar{a} = 5.3 \times 10^{-6}$ m²/s;
$\lambda = 22$ W/mK;
$\Omega = 0.48$;
$T_0 = 860°C$;
$T_m = 20°C$; and
$T_S = 100°C$.

In this example, we find:

$$K = \frac{R^2}{5.783} = \frac{36 \times 10^{-6}m^2}{5.783} = 6.2 \times 10^{-6}m^2.$$

Values of ϑ_I and $\vartheta_I I$ are determined by the equations presented in Example 10.3:
$\vartheta_I = 36°C$;
$\vartheta_{II} = 14°C$; and
$\ln \vartheta_I / \vartheta_I = 0.95$.

Then, according to Eq 11:

$$W = \frac{0.36 \times 10^4 \times 5.3 \times 10^{-6} \times 1.2}{[0.48 + 3.21 \times 0.95]6.2 \times 10^{-5}} = 648.6 m/h.$$

The speed of the conveyor should be not less than 649 m/h or 11 m/min.

As a result of this process, high durability and high impact strength at −70°C are reached. It is no longer necessary to apply oil as a quenchant.

Example 10.5
A die of 90-mm diameter and 40-mm height used for the cultivation of artificial diamonds is made of R6M5 (AISI M2) steel and is quenched from 1,200°C in an aqueous solution of bischofite ($\rho = 1,300$ kg/m³) in which, by the completion of nucleate boiling, 50 % martensite ($T_S = 120°C$) is formed. Determine the frequency of unloading from the tray in the bath so that the completion of nucleate boiling coincides with unloading from the tray:

$$W = \frac{0.36 \times 10^4 \bar{a}}{[0.24 + 3.21 \ln \theta]K}.$$

Input factors are:
$L = 1$;
$Kn = 1$;
$\vartheta_I = 27°C$;
$\vartheta_{II} = 7.5°C$;
$\ln \vartheta_I / \vartheta_I = 1.28$;
$\bar{a} = 5.6 \times 10^{-6}$ m²/s; and

$K = \dfrac{1}{\dfrac{5.783}{R^2} + \dfrac{\pi^2}{Z^2}} = 1.02 \cdot 10^{-4}m^2. \ m^2.$

By substitution:

$$W = \frac{0.36 \times 10^4 \times 5.6 \times 10^{-6}}{[0.24 + 3.21 \times 1.28]1.02 \times 10^{-4}} = 45 \text{ cycles per hour.}$$

Thus, the duration of one cycle is:

$$\tau = 3,600/45s = 80s.$$

For average-size parts, the completion of nucleate boiling coincides with the time of formation of maximum surface compressive stresses. Therefore, the interruption of intensive cooling at this time will provide the optimal depth of a superficial layer for which the maximum surface compressive stresses is achieved.

Example 10.6

Calculate the conveyor speed during quenching of pins, 20 mm in diameter ($R = 0.01$ m), made of 40Kh (AISI 4140) steel, if it is known that $L = 1.5$ m; $Kn = 0.6$; $f = 1$. The temperature of the core of the pin at the time when maximum compressive stresses at the surface are achieved is 400°C. The austenitization temperature T_0 is 860°C. The quenchant and quenching conditions are the same as those in Example 10.5.

Taking all of these facts into account and substituting the data provided into Eq 11 (and using $K = R^2/5.783$) yields:

$$W = \frac{0.36 \times 10^4 \times 1.5 \times 0.6 \times 5.783}{\left[0.48 + \ln\left(\frac{860-20}{400-20}\right)\right] 1 \times 10^{-4}}$$

$$= 132 m/\text{min} \quad or \quad 2.2 \ m/s.$$

After self-tempering in air, the pins are cooled and washed and go for two hours tempering (see Fig. 9). As a result, it was possible to replace the oil with a water-salt solution. The impact strength of the steel increased by three times at a temperature of −70°C.

The examples above illustrate the application of the present technology for various steel grades. It should be noted that for some high-carbon, high-alloy steels, 50 % martensite in the supercooled austenite is formed at a temperature below 100°C (see Table 5). Therefore, these steel grades may be quenched in aqueous salt solutions of optimal concentration where the most intensive cooling occurs and the boiling temperature is close to 100°C.

10.4 IQ-3 INTENSIVE QUENCHING TECHNOLOGY

The most intensive steel quenching process is IQ-3 [12,13], because film boiling and nucleate boiling are eliminated and the heat transfer coefficients are significantly increased during forced convection. Therefore, IQ-3 is primarily a direct convection process. In IQ-3, steel is intensively cooled until maximum surface compressive stresses are formed with an optimal depth of the hardened layer, at which point the part is cooled in air or maintained at the M_S temperature. The service life of steel parts after IQ-3 processing is increased by 1.5 to 2 times compared to conventional oil quenching. Therefore, in view of the potential importance of IQ-3 [12,13], the criteria on which this technology is based are discussed in this section.

TABLE 5—Martensite start temperature and the temperature at which 50 % martensite for some tool steels is formed

Steel grade	Austenitization temperature (°C)	Carbon content (%)	M_S (°C)	M_{50}
R18 (AISI T1)	1,230	0.81	160	80
	1,290	0.81	140	60
R12 (similar to T1)	1,210	0.87	210	120
	1,270	0.87	155	77
Kh12 (AISI D3)	950	2.07	210	115
	970	2.08	184	110
	1,050	2.08	70	—
	1,180	2.07	−85	—

10.4.1 Criterion for Determining the Absence of Nonstationary Nucleate Boiling

The criterion for determining the absence of nucleate boiling at the surface being quenched is based on the generalized equation for the duration of nonstationary nucleate boiling—and of the self-regulated thermal process—and has the form (Eq 3):

$$\tau = \left[\Omega + f \ln\frac{\vartheta_I}{\vartheta_{II}}\right] \frac{K}{a}.$$

In this equation, Ω determines the duration of the irregular thermal process and is a relatively small value. The duration the nonstationary nucleate boiling is determined by the second term of Eq 3, $f \ln\frac{\vartheta_I}{\vartheta_{II}}$. To avoid nucleate boiling, it is necessary that this term be equal to zero.

To calculate ϑ_I and ϑ_{II}, we use Eqs 4 and 6:

$$\vartheta_I = \frac{1}{\beta} \left[\frac{2\lambda(\vartheta_0 - \vartheta_I)}{R}\right]^{0.3}$$

and

$$\vartheta_{II} = \frac{1}{\beta} [\alpha_{conv}(\vartheta_{II} + \vartheta_{uh})]^{0.3}.$$

By equating ϑ_I and ϑ_{II}, the criterion determining the absence of nonstationary nucleate boiling is derived:

$$\left[\frac{2\lambda(\vartheta_0 - \vartheta_I)}{R}\right]^{0.3} \equiv [\alpha_{conv}(\vartheta_{II} + \vartheta_{uh})]^{0.3}, \qquad (12)$$

or because in Eq 12, $\vartheta_I \equiv \vartheta_{II}$,

$$Bi = \frac{2(\vartheta_0 - \vartheta_I)}{\vartheta_I + \vartheta_{uh}}. \qquad (13)$$

Eq 13 is the basic criterion that determines the absence of nonstationary nucleate boiling during steel quenching.

To understand the criterion dependences of Eq 13, specific examples of steel quenching for plate-shaped, cylindrical, and spherical parts are provided below.

Example 10.7

A round plate of 160-mm diameter and a thickness of 20 mm made of AISI M2 steel is cooled with 20°C water on both sides from 1,180°C. Determine the value of the convection heat transfer coefficient required to suppress both film and nucleate boiling.

From the statement of the problem it follows that:

$$\vartheta_0 = 1,180°C - 100°C = 1,080°C,$$

and

$$\vartheta_{uh} = 100°C - 20°C = 80°C.$$

To determine the value of ϑ_I using Eq 4 when the material and quenchant possess the following thermal and physical properties:
$\lambda = 23$ W/mK; and
$\beta = 7.36$,
we substitute and get:

$$\vartheta_I = \frac{1}{7.36} \left[\frac{2 \cdot 23(1080 - \vartheta_I)}{0.01}\right]^{0.3}.$$

Reducing the equation, we arrive at $\vartheta_I = 13.8°C$.

To calculate Bi for single-phase convection, we use Eq 13:

$$Bi = \frac{2(1080^0C - 13.8^0C)}{13.8^0C + 80^0C} = 22.73.$$

Knowing Bi for convection, it is then possible to calculate the heat transfer coefficient required to suppress nucleate boiling:

$$\alpha_{conv} = 22.73\frac{23W/mK}{0.01m} = 52287\frac{W}{m^2K}.$$

This heat transfer coefficient can be created by water jet cooling. Calculations of jet cooling were considered in detail in Chapter 4.

Example 10.8

Truck semi-axles of 42 mm in diameter that are made of 40G (AISI 1540) steel are cooled in a stream of water at 20°C from 870°C in a special chamber with a folding cover (see Figs. 10–13). The inner diameter of the quench chamber is 80 mm. Determine the speed of a stream of water in the quench chamber where nucleate boiling is suppressed. To solve this problem, it is only necessary to calculate the convection heat transfer coefficient α_{conv}.

From the statement of the problem, it follows that:

$$\vartheta_0 = 870°C - 100°C = 770°C$$

and

$$\vartheta_{uh} = 100°C - 20°C = 80°C.$$

The average heat conductivity for 40G steel is 22 W/mK; $R = 0.021$ m.

From this data, the Bi number is determined to assure the absence of transient nucleate boiling by using Eq 13:

$$Bi = \frac{2(770^0C - \vartheta_I)}{\vartheta_I + 80^0C},$$

where:

$$\vartheta_I = \frac{1}{7.36}\left[\frac{2 \cdot 22(770^0C - \vartheta_I)}{0.021}\right]^{0.3} = 9.86^0C.$$

Therefore:

$$Bi = \frac{2(770^0C - 9.86^0C)}{89.86^0C} = 16.9.$$

To avoid the self-regulated thermal process and assure only single-phase convection, α_{conv} must be greater than the value determined by the following equation:

$$\alpha_{conv} = 16.9\frac{22W/m \cdot K}{0.021m} = 17705\frac{W}{m^2K}.$$

The value of the convection heat transfer coefficient is determined from Eq 14 of Chapter 4:

$$Nu = 0.03Re^{0.8}Pr^{0.43}.$$

The speed of a stream of water is determined from the Reynolds number:

$$Re = \left(\frac{Nu}{0.03\,Pr^{0.43}}\right)^{1.25}.$$

Since Re $= wD/v$, the average speed of water in the quench chamber is calculated from:

$$W = \frac{v}{D}\left(\frac{Nu}{0.03\,Pr^{0.43}}\right)^{1.25}.$$

Computations have shown that the average speed of water is equal 4.9 m/s, which may be implemented in practice. However, it is actually necessary to create a water flow of 5 m/s to assure intensive convection immediately from the very beginning of quenching.

Example 10.9

Different kinds of equipment for conventional and intensive quenching are described in Chapters 11 and 12 and in recently published papers [17–19]. Detail information on the self-regulated thermal process and water spray cooling was provided in Chapters 2 and 4. This example shows that convective heat transfer coefficients are reliable and can be realized by different methods in practice. In Eastern Europe, spray cooling for bearing rollers and balls is sometimes used. To prevent corrosion, a small amount of sodium carbonate (Na_2CO_3) is added to the water.

Balls of 20 mm in diameter made of AISI 52100 steel are cooled by water spray at 20°C in a special installation from a temperature of 860°C. Determine the value of the convection heat transfer coefficient to prevent the self-regulated thermal process.

From the statement of the problem, it follows that:
$\vartheta_0 = 760°C$;
$\vartheta_{uh} = 80°C$;
$\lambda = 22$ W/mK;
$R = 0.01$ m;
$\beta = 7.36$; and

$$\vartheta_I = \frac{1}{7.36}\left[\frac{2 \cdot 22(760 - \vartheta_I)}{0.01}\right]^{0.3} = 12.25^0C.$$

The criterion for the absence of the self-regulated thermal process is calculated as follows:

$$Bi = \frac{2(760^0C - 12.25^0C)}{12.25^0C + 80^0C} = 16.2,$$

and the convection heat transfer coefficient is determined thus:

$$\alpha_{conv} = 16.2\frac{22W/m \cdot K}{0.01m} = 35665\frac{W}{m^2K}.$$

In this condition of cooling, the self-regulated thermal process is prevented from the beginning of intensive quenching.

These examples show that simplified calculations significantly contribute to quench process design. As a part of this design, it is also necessary to calculate water flow requirements and to select appropriate pumps. Using Eq 13 facilitates these calculations, which significantly reduces the time and cost without resorting to more complicated computer simulations. However, in an effort to utilize intensive quenching methods, the desired maximum flow rates of water, up to 20–30 m/s, are not always reasonable, especially in the case of quenching very large parts. Eq 13 permits the determination of the appropriate flow rate of water or speed of jets necessary to provide single-phase convection, avoiding

nonstationary nucleate boiling, upon immersion of a part into a quenchant.

10.4.2 Computation of the Time to Achieve Maximum Surface Compressive Stresses

Computation of the time of achieving maximum surface compressive stresses at the surface and formation of the optimal depth of the hard layer is of practical interest. This problem was discussed in Chapter 7. In the discussion below, an illustration of a simplified calculation based on computer simulation of the stress-strain state of parts after quenching will be provided. The simulation yields the core temperature at the time of the formation of maximal surface compressive stresses, which is dependent on the generalized Biot number and the shape and size of the part.

The results of various calculations are presented in tables that form a database for the simplified calculations. Another database presented is of Kondratjev form coefficients relating to those various configurations. These databases facilitate the calculation of the time required to obtain maximal surface compressive stresses.

Example 10.10

It is known that compressive residual stresses are reached at the surface of cylinders made of AISI 1040 and AISI 1050 steels when intensive quenching at the core is interrupted at 450°C in the condition $Kn = 0.8$ [12,13]. Determine the time required to obtain maximal compressive residual stresses at the surface of a cylinder 20 mm in diameter that is cooled from 840°C by water flow. The quenchant temperature is 20°C.

For this purpose, use the generalized equation from Chapter 5 (Eq 69):

$$\tau = \left[2 \cdot 0.24 + \ln \frac{840^0 C - 20^0 C}{450^0 C - 20^0 C}\right] \frac{K}{\bar{a} \, Kn}.$$

The Kondratjev form coefficient for the cylinder is equal to:

$$K = \frac{R^2}{5.783} = \frac{1 \cdot 10^{-4}}{5.783} = 17.29 \cdot 10^{-6} m^2.$$

In addition,
$\bar{a} = 5.36 \times 10^{-6}$ m^2/s; and
$Kn = 0.8$.

Using the initial data, the generalized equation is used to find the time to obtain maximal surface compressive stresses for a cylinder 20 mm in diameter:

$$\tau = [0.48 + 0.646] \frac{17.29 \cdot 10^{-6} m^2}{5.36 \cdot 10^{-6} m^2/s \cdot 0.8} = 4.54 \, s.$$

The advantage of IQ-3 intensive quenching technology lies in the ability to create cooling conditions that eliminate the self-regulated thermal process (nonstationary nucleate boiling). When maximum surface compressive stresses are formed, the intensive cooling process is interrupted, and then the temperature is maintained at M_S or the immediate tempering temperature. In addition, the formation of maximum surface compressive stresses corresponds to the optimal depth of the hardened layer.

The previous example was related to through-hardening. If steel of low hardenability is used and the martensite layer that is formed is optimal, then it is possible to perform the
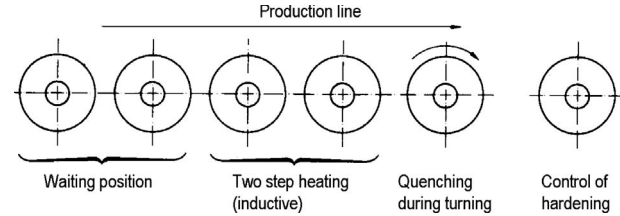
Fig. 10—Schematic of an automatic device for the quenching of long semi-axles in water [4].

cooling process without fear of reducing the value of surface compressive stresses. In this case, it is sufficient to create the conditions of intensive cooling by preventing the nucleate boiling process.

10.4.3 Application of IQ-3 Technology for Quenching Truck Semi-Axles

IQ-3 intensive technology is widely and successfully used for quenching truck semi-axles. The basic scheme of the industrial line is presented in Fig. 10, which consists of several sections [4,20,21].

The first section is for loading and holding. At the appropriate time, the semi-axles are delivered to the heating unit as the first step of a continuous process. The next section for induction heating of the semi-axles has two positions. In the first position, the semi-axles are heated to a temperature below A_{C1}, and in the second position, the semi-axles are finally heated to the austenitization temperature. The semi-axles are then quenched in a special chamber by intensive water streams. The chamber is cylinder-shaped with a folding cover that allows loading semi-axles to the chamber. Semi-axles at both sides are clamped by their centers, at which time they are rotated. Upon closing the cover of the chamber, the intensive longitudinal stream of water is formed, the flow rate of which is calculated by Eq 13.

A detailed schematic of the quench chamber is presented in Fig. 11, which shows the quench chamber itself (2), with a mechanical drive (4) for rotation of semi-axles (1) and a monitoring and control system (5–8). A gauge (5) analyzes the noise effects related to the boiling of the boundary liquid layer. From these results, it is possible to determine if nucleate boiling is occurring. This is very important, since the calculation made by the criterion of absence of nucleate boiling is always verified by this gauge. Another gauge (6) monitors the presence of the martensitic ferromagnetic
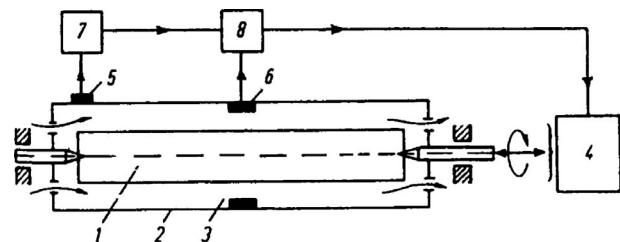
Fig. 11—Detailed scheme of quench chamber with automatic control [21]: 1, semi-axle; 2, quench chamber; 3, pressurized water flow; 4, mechanical drive for semi-axles; 5, sensor for analyzing the process of nucleate and film boiling; 6, sensor for analyzing the portion of transformed structures by the changing ferromagnetic state; 7, electronic device (amplifier and microprocessor); 8, amplifier.

phase. The gauge can be graduated for the optimal depth of the hardened layer where the maximal surface compressive stresses are formed. The other two gauges (7 and 8) are simultaneously signal amplifiers and microprocessors for the control of the quenching process.

Assume that a semi-axle is made of alloyed steel to provide through-hardening of the semi-axle by intensive water flow (see Fig. 11). At the time of reaching the optimal depth of the hardened layer and the maximum surface compressive stresses, microprocessor 8 stops water delivery to the quench chamber, the folding cover of the chamber is opened, and the semi-axle is unloaded into the air and goes for further tempering [5,20].

The technology of punching of semi-axles in the automatic industrial line is shown in Fig. 12 [5,20].

Consider semi-axles 40 mm in diameter and made of 40G (AISI 1540) steel. The manufacturing process for the axles illustrated in Fig. 12 consists of

1. milling of an axle to a length of 1.152 m
2. preliminary center-adjustment with simultaneous removal of facets at both sides of the axle
3. induction heating of the axle
4. punching a flange
5. preliminary set of the heated metal
6. punching a flange for one transition
7. water cooling of the part's section adjoining the fillet of the flange
8. induction heating of the end of the specimen for making a slot thickening
9. making a slot thickening with simultaneous shaping of a final centering aperture on the slot end of the semi-axle
10. induction heating of the rim of the flange and slot thickening for normalization with the subsequent cooling in air
11. water cooling of the flange and slot thickening
12. center-adjustment of the semi-axles at the section of the flange
13. drilling of an aperture for output of the center at the slot end of the semi-axle
14. partial mechanical treatment of the flange [5,20,21]

After the further turning treatment (cutting of slots), quenching of the semi-axles by water stream under superfluous pressure is performed in the automatic installation presented in Fig. 13. The operations of the automatic installation are performed in the following sequence. The carriage with semi-axles on prisms (7) and rollers-lunettes (8) and the rod (14) in the
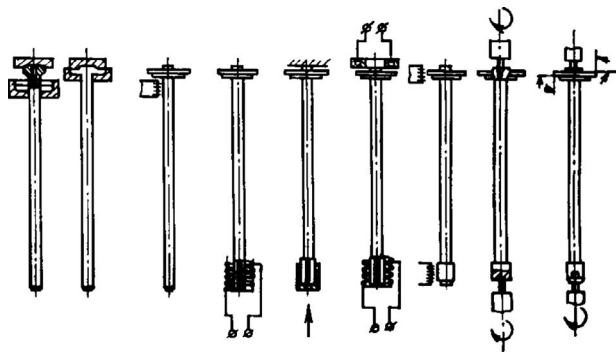
Fig. 12—The technology of punching of semi-axles in the automatic industrial line [5,20].
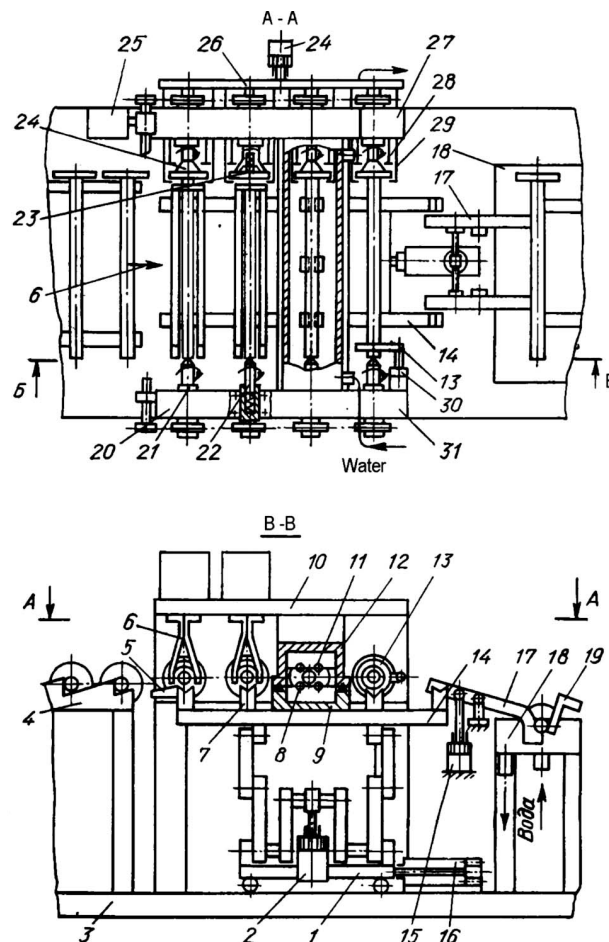
Fig. 13—The automatic installation for quenching semi-axles of GAZ automobiles by water streams under superfluous pressure: 1, carriage; 2, pneumocylinder of vertical movement of the rod by means of the lever system; 3, base; 4, storage; 5, knives for capture of the next semi-axle; 6, longitudinal-loopback inductor; 7, prism; 8, rollers-lunettes; 9, bottom shutter of the quench chamber; 10, plate; 11, rollers-lunettes; 12, motionless shutter of the quench chamber; 13, induction coil for quality control of heat treatment; 14, rod; 15, pneumocylinder for horizontal movement of the carriage; 16 and 17, lever and the pneumocylinder, respectively, for transfer of semi-axles from prisms of the transport device to the bath; 18, bath for final cooling of semi-axles; 19, unloading shoot; 20, block; 21, glass; 22 and 23, spring-expanded centers; 24, cap friction clutch; 25, drive containing the electric motor, a reducer, and transmission; 26, crossbeam; 27, block; 28, motionless thrust blocks; 29, drafts-strippers; 30, pneumocylinder; 31, connecting frame.

bottom position moves from a loading position to unloading one. At the end of a course, the rod moves to the top position, and thus semi-axles are delivered to inductors while the shutters of the quench chamber are closed, covering the core of the semi-axle by rollers-lunettes. Then, the crossbeam (26) and also the friction clutches (24) and drafts-strippers (29) connected with it move. Semi-axles are fixed at the center (22 and 23), come off a prism, and are clamped between the friction clutches (24) and spring-expanded center (22). The induction coil is delivered to the core of the semi-axle, and the rotation of semi-axles is activated. Detailed information on technology and equipment can be found in [4,19].

Semi-axles are heated at two positions. At the first position, the core of the semi-axle and fillet of the flange are

heated to 600−700°C, and at the second position, they are heated to the quenching start temperature. Next, the semi-axles are quenched in a fast-moving stream of water under a small pressure, and then the quality of quenching of the semi-axles is controlled. Rollers-lunettes restrict the distortion of the semi-axles [5,20]. At the end of the quenching process and full drainage of water from the quench chamber, which is performed by compressed air brought into the quench chamber, a rod (14) goes down, while the semi-axles remain in the centers of all four positions of the automatic installation. The carriage (1) moves to a loading position, and the next semi-axle from the store is transferred by means of a knife (5) to prisms of the transportation mechanism, and the rod moves back to the top position. By this time, the heating of the semi-axles at both positions concludes, rotation ceases, and the crossbeam (26) and coil (18) return to the starting position. Strippers (29) remove the semi-axles from the centers of the block (27). Thus, a part is heated to the austenitization temperature and stacked on rollers-lunettes of the bottom shutter (9) of the quench chamber, and other semi-axles are placed on prisms of the transport mechanism.

The semi-axles are transferred from prisms of the transport mechanism to the bath (18) by means of levers (17), while a pneumatic cylinder (15) moves. Other levers take the semi-axles from the bath to a shoot (19), while the pneumatic cylinder comes back to the initial bottom position. The automatic installation is supplied with two generators OPCH-250-2,4. Cooling is performed with the use of a pump having a productivity of 162 m³/hr with the hydrovalve open at the time of quenching. The depth of the zone of pure martensite hardened in the semi-axles reaches 2−7 mm.

Intensification of the heat transfer process within the martensite range, beginning from certain values of the cooling rate, results in appreciable material strengthening [13,18]. The intensified heat transfer processes within the martensite range may be performed in various ways: application of intensive shower cooling, water jets, applying vibration or ultrasonic oscillations to the quenchant, and so forth. Methods used most widely in practice are water flow and spray cooling (see Chapter 4). The advantage of the latter is that, in industrial conditions, it is easier to organize stable and uniform cooling of parts to be quenched and also to implement combined ways of cooling. In addition, the characteristics of heat transfer in ring tubes are now well investigated. Numerous experimental data have been generalized, and equations of similarity for calculation of heat transfer coefficients in channels have been obtained. Also, the crisis of heat transfer during boiling in channels has been sufficiently studied (see Chapter 4) [22−25]. Thus, calculations of optimal steel quenching conditions for quenching by water spray may be performed.

Table 6 presents results of calculations of the convection heat transfer coefficient depending on the average flow rate at various temperatures and sizes of the ring channel with regard to semi-axles of 40-mm diameter. These data show that increasing the flow rate relative to the surface increases the convection heat transfer coefficient. Increasing flow rates also increase the first critical heat flux density (see Table 7). These results are valid for ring channels with the width of the clearance exceeding 1.2 mm. It is apparent from these tables that with increasing flow rate, the first critical heat flux density and convection heat transfer coefficient increase.

By solving the inverse problem of nonstationary heat conductivity (see Chapter 13), it is possible to determine the initial heat flux densities that are observed during steel quenching of, for example, semi-axles. For the most intensive and uniform cooling, it is necessary to avoid the formation of steam films. This may be done by increasing the water flow rate to such values that the first critical heat flux density exceeds the maximum heat flux density observed at the initial time of steel quenching.

Experimental data show that during quenching of cylindrical bodies with a diameter of 30−40 mm, the initial heat flux density can reach 8−10 MW/m². To eliminate the

TABLE 6—Convection heat transfer coefficient in a ring tube $\Delta d = d_2 - d_1$ (W/(m² · °C))

W (m/s)	20°C			40°C		
	0.02	0.01	0.06	0.02	0.04	0.06
0.5	2,863	2,837	2,893	3,470	3,438	3,505
1	4,385	4,940	5,036	6,041	5,986	6,103
2	8,680	8,601	8,769	10,519	10,422	10,626
3	12,006	11,897	12,129	14,549	14,416	14,697
4	15,113	14,975	15,267	18,314	18,147	18,500
5	18,067	17,902	18,251	21,893	21,693	22,116
6	20,904	20,713	21,117	25,331	25,100	25,586
7	23,648	23,432	23,889	28,656	28,394	28,948
8	26,314	26,074	26,582	31,886	31,595	32,211
9	28,914	28,650	29,208	35,037	34,717	35,394
10	31,456	31,169	31,777	38,118	37,770	38,507

TABLE 7—The first critical heat flux density versus water temperature and water flow rate with respect to the surface.

W (m/s)	20°C	30°C	40°C	50°C	60°C
5	7.94	7.18	6.43	5.67	4.91
6	9.32	8.44	7.57	6.70	5.83
7	10.57	9.59	8.62	7.64	6.66
8	11.70	10.63	9.56	8.49	7.42
9	12.76	11.60	10.44	9.29	8.13
10	13.74	12.51	11.27	10.03	8.79
15	17.97	16.39	14.81	13.23	11.65
20	21.40	19.56	17.71	15.85	14.00

possibility of the formation of a steam film, the water flow rate at $T_m = 20°C$ must be within the limits of 5–7 m/s (see Table 7). Under these conditions, the surface temperature of a body quickly decreases to 120–130°C and then, during nucleate boiling, changes insignificantly.

For the implementation of the IQ-3 method for boring pipes and locking connections, a mechanized installation has been designed and constructed that includes induction heating. The basic scheme of the installation is shown in Fig. 14.

The sequence of the work on it is as follows. The boring pipe is put on roller conveyer (1) and then passes through the leading cartridge (2) and moves to the inductor (3). At this time, the rotating tightening cartridge (7) grasps the pipe, and by means of the mobile carriage (14), translational-rotational movement of the boring pipe is performed. At the beginning of translational-rotational movement, the induction installation is turned on, and the superficial layers of the pipe are heated to the austenitization temperature. The temperature of heating is regulated by the preset inductor capacity and speed of the translational movement of the boring pipe. Thus, the optimal depth of the heated layer and maximum surface compressive stresses are formed on the pipe using an intensive shower through a sprayer to fulfill Eq 13. When the carriage moves to the end of the conveyer, a special mechanism pushes the pipe from the tightening cartridge and sliding plugs (5) drop the pipe from the roller conveyer. The carriage returns to the starting position, and the cycle begins again.

In this example, the optimal depth of the hardened layer and supercritical cooling rate at the surface of the boring pipes is achieved by water delivery to the sprayer under pressure, and therefore the water flow rate and heat transfer coefficient are increased considerably. The application of this technology increases the service life of the boring pipes and locking connections.

10.5 IQ-4 INTENSIVE QUENCHING TECHNOLOGY

The IQ-4 intensive quenching technology process is related to heat treatment of parts with a complex configuration, in particular, shafts with different sections along the length [26]. Usually such parts are cooled by water-air jets that are regulated in such a way that smaller values of heat transfer coefficients are created on thin sections, and correspondingly larger coefficients on thicker sections. Typically, for IQ-4 processes, large sections of a shaft are cooled by water sprays at a flow rate of 2.5–14 m^3/m^2hr, and thin sections at a flow rate of 14–25 m^3/m^2hr [26]. The IQ-4 intensive cooling process is interrupted when the core temperature reaches 450–500°C [26]. This method results in a reduction of the cold brittleness temperature and facilitates the formation of high surface compressive residual stresses [26].

Thus, quenching of alloy steel parts with a complex configuration is performed in such a way that thick and thin sections are cooled under identical conditions to provide equal Biot numbers $Bi \geq 20$, which results in the formation of uniform surface compressive residual stresses. Therefore, for the thinner section of the part, the flow rate of a water-air mixture is greater because $Bi = \alpha R/\lambda$, which means that the condition $Bi \geq 20$ is fulfilled at higher values of heat transfer coefficient α.

The selection of parameters for the water flow rate for water-air cooling and values of pressure for jet cooling are based on the experimental data presented in [26].

When applying the IQ-4 process at the surface of thin sections, instead of tensile stresses (as in the case of the conventional cooling process), compressive residual stresses are formed as shown in Table 8. Improvement of mechanical properties, a decrease in cold brittleness temperature, and the formation of compressive surface residual stresses results in an increase of service life of hardened steel parts [4].

Example 10.11
A shaft made of 35KhM (AISI 4135) steel as shown in Fig. 15 is heated to 870°C and then cooled in a water-air cooling installation. At thick sections with diameters 636 and 540 mm, the part is cooled by the water-air mix at the flow rate of

Fig. 14—Basic schematic of the installment for quenching boring pipes and locking connections: 1, roller conveyer; 2, leading cartridge; 3, indicator; 4, pneumocylinder; 5, sliding plugs; 6, sliding pickups; 7, tightening cartridge; 8, electric motor; 9, pneumocylinder; 10, deflective rollers; 11, steel rope; 12, electric motor; 13, drum; 14, pneumocylinder; 15, guides; KB1–KB5, final switches.

TABLE 8—Values of residual axial σ_{22} and hoop σ_{33} stresses, in MPa, at the surface of shafts depending on cooling conditions

Shaft diameter (mm)	Earlier method (oil quenching)		Present method (differential water spray quenching)	
	σ_{22}	σ_{33}	σ_{22}	σ_{33}
200	+310	+350	−50	−80
500	+400	+440	−160	−300
1,000	+100	+170	−400	−600
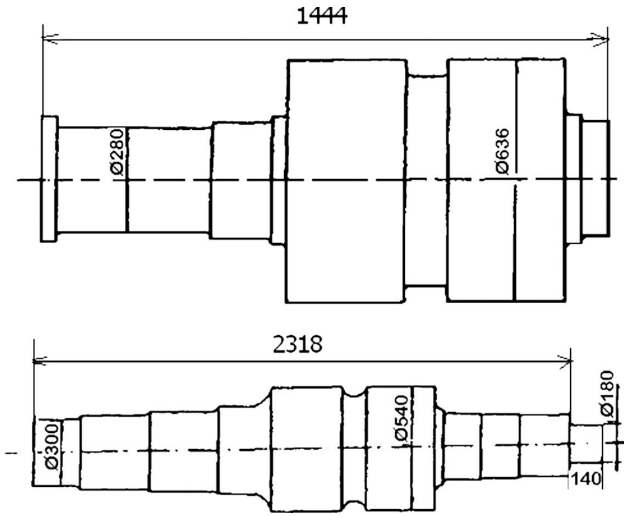
Fig. 15—Sketch of a large part with different sections along the length.

9.5 m³/m²hr, while thin sections with diameters 280 and 300 mm are cooled at a flow rate of 20.6 m³/m²hr. The process of intensive cooling at thin sections is interrupted in 13.6 min, and at thick sections in 45.7 min. The part is further cooled completely in air and then normally tempered. As a result of the application of the IQ-4 process, the hardening capacity is increased and the core strength is increased by 20 %, while at the same time the impact strength is increased by 1.5 to 2 times and the water-air mixture can be recycled.

The selection of quenching conditions is based on the following. At thick sections, with the flow rate of 9.5 m³/m²hr, the following condition occurs [26]:

$$Bi = \frac{1450\frac{W}{m^2K} \cdot 0.315m}{22.5\frac{W}{m \cdot K} \cdot K} = 20.3.$$

At thin sections, with a flow rate of 20.6 m³/m²hr, the corresponding condition is [26]:

$$Bi = \frac{3000\frac{W}{m^2K} \cdot 0.15m}{22.5\frac{W}{m \cdot K} \cdot K} = 20.$$

Therefore, at both the thick and thin sections of the part, sufficient compressive stresses ($Bi > 18$) are created to minimize the possibility of quench crack formation.

The thin section of the part is cooled during a time that is determined from:

$$\tau = \left[2 \cdot 0.24 + \ln\frac{870^0C - 30^0C}{500^0C - 30^0C}\right]\frac{K}{\bar{a}\,Kn}$$

$$= (0.48 + 0.58) \cdot \frac{225 \cdot 100}{5.783 \cdot 5.63} = 13.6\,\text{min} \approx 14\,\text{min},$$

where $K = R^2/5.783$;
$Kn \approx 0.9$; and
$\bar{a} = 5.63 \times 10^{-6}$ m²/s.

Cooling time for the thick sections is determined similarly:

$$K = \frac{1}{\frac{5.783}{R^2} + \frac{9.86}{Z^2}} = 1.31 \cdot 10^{-2} m^2;$$

and

$$\tau = 1.06\frac{1.31 \cdot 10^{-2}}{0.9 \cdot 5.63 \cdot 10^{-6}60} \approx 45.7\,\text{min}\,.$$

The advantage of the IQ-4 process compared to conventional cooling processes is the high compressive residual stresses at the surface. These stresses are formed uniformly over the entire surface of hardened steel part, which minimizes the probability of quench crack formation. When using the conventional quenching process, there are tensile stresses on the surface of thin sections that become compressive stresses at the thick sections, resulting in high concentrations of stresses at the points of transition between thick and thin sections that are related to the increased danger of quench crack formation.

The cooling rate at thin sections is increased by two to four times, which results in:
- The viscous characteristics and mechanical properties of the steel are improved.
- The threshold of cold brittleness is decreased.
- Labor productivity, due to more intensive cooling of thin sections of a shaft, increases.
- Because of the improvement of mechanical properties of material and creation of surface compressive stresses, the service life of the parts is increased.
- There is an opportunity to replace high-alloy steels with lower alloyed materials.
- The control and automation of quenching processes becomes simpler.
- The stability of the manufacturing process is increased.
- Water consumption is decreased.

In summary, the IQ-4 quenching process is used for parts with a complex configuration, and it includes heating to the austenitization temperature, holding the part at this temperature for the required time, and then cooling the different sections separately using sprayed water. Thick sections are cooled at flow rates of 2.5–14 m³/m²hr, and thinner sections at a flow rate of 14–25 m³/m²hr. The spray cooling process is interrupted when the core temperature reaches 450–500°C, and then the parts are finally cooled in air and tempered.

10.6 IQ-5 INTENSIVE QUENCHING TECHNOLOGY

The essence of IQ-5 intensive quenching technology consists of the partial insulation of the surface of a complex part to prevent contact with intensive jets of water while the uninsulated surface is cooled intensively. The insulation is put on the surface so that high compressive stresses are formed on the working surface of parts. More particulars on this technology can be found in [27,28]. To aid in understanding of IQ-5 quench processing, selected examples of the successful implementation of this process will now be provided.

10.6.1 Intensive Hardening of Agricultural Machine Cutting Parts

Durability and strength of agricultural machine cutting parts–in particular, segments for mowers and combines– have an appreciable effect on the labor productivity and quality of harvesting. Cutting parts typically possess a complicated shape, as shown in Fig. 16, for example, and in some cases, the edge has a notch leading to stress concentration during heat treatment. For this reason, cutting parts of agricultural machines are usually quenched in mineral oils.
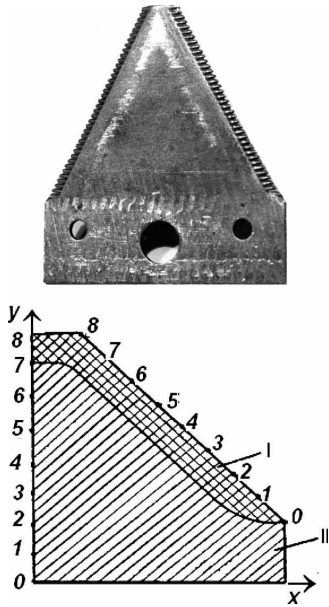
Fig. 16—Photograph (*top*) and computation area (*bottom*) of a segment: I, area heated by induction only; II, area heated due to heat conductivity of the material [16].

Typically, segments made of 70G (AISI 1070) steel are heated by induction to 870–890°C and cooled by oil spray [27,28]. Such oil quenching processes pollute the environment and often result in fires. Therefore, it is desirable to replace the petroleum oils with fire-resistant or nonflammable quenchants, ideally just plain water.

It has been found that it is possible to use intensive quenching for heat treatment of segments made of 70G steel. When cooling segments by intensive spray of water with simultaneous insulation of the core II of segment (see Fig. 16), high compressive residual stresses are formed at the lateral surfaces, which minimizes the possibility of quench crack formation [16,27]. This can be illustrated by numerical calculations.

10.6.2 Calculation Results

Fig. 17 presents the results of calculations of residual stresses at the lateral side (curve I) and at the axis of the segment (curve II) when the segment is cooled intensively by jets ($Bi \to \infty$). The graph shows that all lateral surfaces of the segment exhibit small tensile stresses, while at the axis of the segment the residual stresses are mainly compressive.
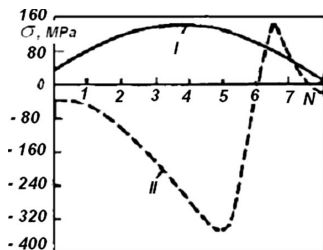
Fig. 17—Residual stress distribution in conditions of intensive uniform cooling [16,29]: I, at the lateral side of the segment; II at the axis.

When heating the base of the segment to 500°C at the time of intensive cooling of the lateral surface, the distribution of residual stresses in the segment is significantly different. Instead of tensile stresses at the lateral surface, there are compressive stresses. From Fig. 18, it is evident that at the lateral surfaces of the segment, there are compressive stresses, while at the axis the stresses are tensile. Also at the lateral surfaces, the distribution of residual stresses is complex. There are points in which the residual stresses become tensile. The distribution of residual stresses in the segment may be optimized by selection of the optimal heating temperature of the base of the segment.

Fig. 19 presents the calculation results of the safety factor under conditions of intensive cooling of the segment either without (Fig. 19(a)) or with (Fig. 19(b)) heating the base of the segment. These calculations show that in any case, heating of the base results in an increase of the safety factor, which minimizes the probability of quench crack formation. All calculations were made using Hart software [29].

10.6.3 Practical Appreciation of the Results

The results above allowed a change of the heat treatment of the 70G steel segments:
- to use a single automatic industrial line for punching and heat treatment of segments, which will increase the labor productivity;
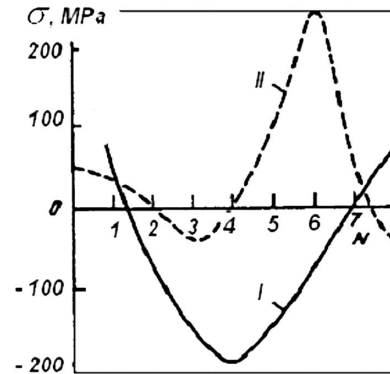
Fig. 18—Distribution of residual stresses in conditions of intensive cooling when the flat core is insulated [16,29]: I, at the lateral side of the segment; II at the axis.

(a)   (b)
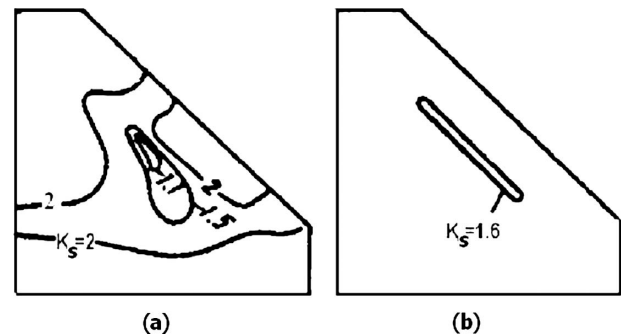
Fig. 19—Distribution of safety factor K_S during intensive uniform cooling (a) without heating the bases of the segment and (b) with heating of the segment.

- to avoid the emission of polluting substances to the environment;
- to replace expensive oils with water; and
- to improve the mechanical properties of the material after quenching due to intensive cooling.

10.7 DISCUSSION

Chapter 7 discussed the optimal quenched layer that provides optimal residual stress distribution: high compressive residual stresses at the surface of steel parts and small tensile residual stresses at their core. The optimal quenched layer can be designed by appropriate interruption of intensive quenching or by optimizing the chemical composition of the steel. In Chapter 9, the steel superstrengthening phenomenon was described as allowing an improvement in yield strength and plastic properties simultaneously. The effect of superstrengthening is observed after intensive quenching within the martensite range. To prevent crack formation during intensive quenching, compressive or neutral residual stresses at the surface of steel parts must be designed. When tensile stresses are appearing at the surface, they result in crack formation because untempered martensite is brittle and sensitive to crack formation. Both residual stress formation and the superstrengthening phenomenon should be considered together to effectively prevent crack formation during intensive quenching.

For example, the IQ-1 process, at the first step of cooling, uses oil as a quenchant. However, this doesn't create compressive residual stresses in steel parts made of alloy steels; only carburized steel parts have compressive residual stresses after quenching in oil. This means that the IQ-1 process can be successfully used only for carburized steel parts. For such parts, in some cases, intensive cryogenic treatment can be applied at the third step of cooling.

The IQ-2 process is widely used for batch quenching [4,5,30,31,32]. At the first step of cooling, compressive stresses appear at the surface of steel parts, which allows further intensive quenching after self-tempering during the second stage of cooling. As a result, compressive residual stresses and superstrengthening increase the service life of steel parts.

The IQ-3 process is used for single-part quenching [8,18,19]. Its first use was for truck semi-axle quenching in water flow in the former Soviet Union [13]. Currently, modified IQ-3 technology is patented in Ukraine and in the United States [12] and is becoming popular for the heat-treating industry [19].

The differential water-air or water spray IQ-4 technology was used for the first time in Ukraine for quenching large rollers and rotors [26]. The use of expensive and flammable petroleum quench oils as quenchants has been replaced by water-air quenching.

IQ-5 intensive quenching technology was developed for the agricultural cutting blades. It can allow the replacement of oil-spray quenching with water-spray quenching. Flammable petroleum quench oil was replaced by plain water, and an ecological problem was solved [16,27,28].

At present, IQ-2 and IQ-3 intensive technologies are in use in the United States [12,19]. The IQ-4 and IQ-5 intensive quenching technologies could be used for agricultural needs if special equipment is designed and manufactured.

Sometimes application of intensive quenching processes in the heat-treating industry is restricted by existing standards. For example, fasteners made of alloy steels, according to an existing standard, can be quenched in oil, but not in water. However, it has now been shown that fasteners can be successfully quenched in water to provide improvement of mechanical properties (see Chapter 12) [33].

To be widely used in the heat-treating industry, up-to-date heat treating processes [34,35] and thermal engineering [36] should be put together to provide heat treaters with modern tools for designing conventional and intensive quenching processes. Some chapters in this book will help heat treaters to make the first step in approaching the idea.

10.8 SUMMARY

1. This chapter presented the intensive steel quenching methods designated IQ-1, IQ-2, IQ-3, IQ-4, and IQ-5, which permit the creation of high surface compressive residual stresses of steel parts and improvement of mechanical properties. Both of these factors result in a significant increase in the service life of steel parts.
2. IQ-1 is a three-step cooling process. At the first step, steel parts may be cooled in hot oils where the critical heat flux density has its maximum value. At the second step, self-tempering is provided, and at the third, cryogenic accelerated cooling may be used to improve the properties of the material.
3. The IQ-2 cooling process also has three steps. At the first step, steel parts are cooled in agitated cold water or water-salt solutions of optimal concentration where the critical heat flux density has its maximum value. The first step of cooling continues until the core temperature of the steel parts reaches 300–600°C to provide compressive residual stresses at the surface; the ideal core temperature depends on the configuration of the part. At the second step, self-tempering is provided. At the third, intensive cooling and washing are conducted simultaneously, and after complete cooling, steel parts go to the final tempering process (as shown in Fig. 9).
4. IQ-3 is a one-step cooling process, also called direct convection [12]. The steel parts are cooled so fast in agitated cold water or water-salt solutions of optimal concentration that film and nucleate boiling are eliminated. The intensive cooling continues until the core temperature of the parts reaches 300–600°C, depending on the configuration of the part, to provide compressive residual stresses at the surface. After interrupting of intensive cooling, steel parts go to the final tempering process.
5. The IQ-4 process is differentiated cooling, which depends on the cross-section of steel parts and is used to create smooth martensitic shell at the part's surface. The intensive cooling continues until the core temperature in each section reaches 450°C to provide compressive residual stresses at the surface. After interruption of intensive cooling in the larger section, the steel part goes to the tempering process.
6. IQ-5 is also a differentiated cooling process. Some areas of steel part are insulated from the intensive cooling to create compressive residual stresses instead of tensile stresses.

References

[1] Kobasko, N. I., Morhuniuk, W. S., and Lushchik, L. V., Study of Thermal Stresses Formed in Steel Products Due to High-Rate Quenching, *Sov. Mater. Sci. Rev.,* No. 1, 1987, pp. 27–32.

[2] Kobasko, N. I., Intensive Steel Quenching Methods, *Theory and Technology of Quenching,* Liščić, B., Tensi, H. M., and Luty, W., Eds., Springer-Verlag, Berlin, 1992, pp. 367–389.

[3] Kobasko, N. I., Morhuniuk, W. S., and Dobrivecher, V. V., Control of Residual Stress Formation and Steel Deformation During Rapid Heating and Cooling, *Handbook of Residual Stress and Deformation of Steel,* Totten, G., Howes, M., and Inoue, T., Eds., ASM International, Materials Park, OH, 2002, pp. 312–330.

[4] Kobasko, N. I., Intensive Steel Quenching Methods, *Quenching Theory and Technology,* 2nd Ed., Liščić, B., Tensi, H. M., Canale, L. C. F., and Totten, G. E., Eds., CRC Press, New York, 2010, pp. 400–459.

[5] Kobasko, N. I., Aronov, M. A., Powell, J. A., Canale, L. C. F., and Totten, G. E., Improved Production of Automotive Parts by Intensive Quench Processing, *La Metallurgia Italiana,* No. 2, 2006, pp. 13–22.

[6] Liščić, B., Tensi, H. M., and Luty, W., *Theory and Technology of Quenching,* Springer-Verlag, Berlin, 1992.

[7] Kobasko, N. I., Method of Steel Quenching, Inventor's Certificate No. 797,243 (USSR), *Bulletin of Inventions,* No. 7, 1988.

[8] Aronov, M. A., Kobasko, N. I., and Powell, J. A., Practical Application of Intensive Quenching Process for Steel Parts, *IFHTSE 2000 Congress,* Melbourne, Australia, October 29–November 2, 2000.

[9] Aronov, M. A., Kobasko, N. I., Powell, J. A., Wallace, J. F., and Schwam, D., Practical Application of the Intensive Technology for Steel Parts, *Industrial Heating,* No. 4, 1999, pp. 59–63.

[10] Kobasko, N. I., Intensive Steel Quenching Methods on the Way of Automation, *Proceedings of the 1st International Automotive Heat Treating Conference,* ASM International, Puerto Vallarta, Mexico, July 13–15, 1998, pp. 430–438.

[11] Totten, G. E., Kobasko, N. I., Aronov, M. A., and Powell, J. A., Overview of Intensive-Quenching Processes, *Industrial Heating,* Vol. 69, No. 4, 2002, pp. 31–33.

[12] Kobasko, N. I., Quenching Apparatus and Method for Hardening Steel Parts, U.S. Patent No. 6,364,974 BI, April 2, 2002.

[13] Kobasko, N. I., *Steel Quenching in Liquid Media Under Pressure,* Naukova Dumka, Kyiv, 1980.

[14] Ferguson, B. L., Freborg, A., and Petrus, G. J., Software Simulates Quenching, *Heat Treating Progress,* 2000, pp. H31–H36.

[15] Inoue, T., and Arimoto, K., Development and Implementation of CAE System "Hearts" for Heat Treatment Simulation Based on Metallo-thermo-mechanics, *Journal of Materials Engineering and Performance,* Vol. 6, No. 1, 1997, pp. 51–60.

[16] Kobasko, N. I., Eco-Friendly Intensive Quenching Technology IQ-5, *Proceedings of the 6th IASME/WSEAS International Conference on Heat Transfer, Thermal Engineering and Environment (HTE '08),* Rhodes, Greece, August 20–22, 2008, pp. 534–538.

[17] Kobasko, N. I., Quench Process Optimization for Receiving Super Strong Materials, *WSEAS Transactions on Systems,* Vol. 4, No. 9, 2005, pp. 1394–1401.

[18] Kobasko, N. I., Current and Residual Stresses During Quenching of Steel Parts, *Finite Elements,* Mastorakis, N. E., and Martin, O., Eds., WSEAS Press, Athens, 2007, pp. 86–99.

[19] Aronov, M. A., Intensive Quenching Technology for Heat Treating and Forging Industries, Final Technical Report, DOE Award Number DE-FC36-03ID 14463, 2005.

[20] Natanzon, E. I., Simultaneous Quenching of Truck Semi-Axles, *Avtomobilnaya Promyshlenist,* No. 10, 1976, pp. 33–35.

[21] Kobasko, N. I., Lisovoy, V. A., and Khalatov, A. A., Method of Controlling Quenching Process, Inventor's Certificate No. 4,145,886 (USSR), *Bulletin of Inventions,* No. 18, 1988.

[22] Mikheev, M. A., and Mikheeva, I. M., *Osnovy teploperedachi* (Basics of heat transfer), Energy, Moscow, 1977.

[23] Incropera, F. P., and DeWitt, D. P., *Fundamentals of Heat and Mass Transfer,* John Wiley & Sons, New York, 1981.

[24] Žukauskas, A., *High-Performance Single-Phase Heat Exchangers,* Hemisphere, New York, 1989.

[25] Martin, H., Heat and Mass Transfer Between Impinging Gas Jets and Solid Surfaces, *Advances in Heat Transfer,* Hartnett, J. P., and Irvine, T. F., Eds., Vol. 13, Academic Press, New York, 1977, pp. 1–60.

[26] Kobasko, N. I., Quenching Method for Steel Parts of Complex Configuration, Inventor's Certificate No. SU1733484A1, C21, D1/78.

[27] Kobasko, N. I., Intensive Method for Thermal Hardening of Cutting Parts for Agricultural Machines, *Promyshlennaya Teplotekhnica,* Vol. 19, No. 1, 1997, pp. 30–33.

[28] Tensi, H. M., Kobasko, N. I., and Morhuniuk, W. S., Specific Features of Using Intensive Methods of Quenching for the Strengthening Part of Complex Configuration, *Proceedings of International Heat Treating Conference: Equipment and Process,* April 1994, Schaumburg, IL, ASM International, Materials Park, OH, 1994, pp. 239–241.

[29] Kobasko, N. I., Morhuniuk, W. S., and Dobrivecher, V. V., Software "Tandem-Hart Analysis" (commercially available from Intensive Technologies Ltd. Kyiv, Ukraine, managers@itl.kiev.ua, www.itl.kiev.ua).

[30] Takeshi, N., Method of Steel Quenching, Application 61-48514 (Japan), 16.08.1984, No. 59-170039.

[31] Aronov, M. A., Kobasko, N. I., and Powell, J. A., Basic Principles and Metallurgy of Intensive Quenching Methods, *IFHTSE 2002 Congress,* Columbus, OH, October 7–10, 2002, pp. 96–103.

[32] Kobasko, N. I., Aronov, M. A., Powell, J. A., Ferguson, B. L., and Freborg, A. M., Correlation Between Optimal Quenched Layer, Stress Distribution and Chemical Composition of Low-Hardenability Steels, *Proceedings of the 6th IASME/WSEAS International Conference on Heat Transfer, Thermal Engineering and Environment (HTE '08),* Rhodes, Greece, August 20–22, 2008, pp. 543–549.

[33] Daming, M., Intensive Quenching Method for Preventing Quench Cracking, *IFHTSE 1990 Congress,* Moscow, December 1990, pp. 62–71.

[34] Totten, G. E., and Howes, M. A. H., *Steel Heat Treatment Handbook,* Marcel Dekker, New York, 1997.

[35] Totten, G. E., Bates, C. E., and Clinton, M. A., *Handbook of Quenchants and Quenching Technology,* ASM International, Materials Park, OH, 1993.

[36] Lienhard IV, J. H., and Lienhard V, J. H., *A Heat Transfer Textbook,* 3rd Ed., Phlogiston Press, Cambridge, Massachusetts, 2005.

11

Design of Industrial Quenching Systems

N. I. Kobasko[1] and G. E. Totten[1]

11.1 INTRODUCTION

Previous chapters described methods for designing industrial quenching processes for steel, including intensive quenching processes. This chapter provides detailed descriptions, with specific examples, of the use of generalized equations and the new steel quenching methods. It will also be shown that the generalized equation is applicable to any quenching process. This approach is the first step in the creation of modern automated quenching processes. The second step is computer simulation of these processes, including rigorous experimental validation. Using this methodology, it is possible to estimate the conveyor speed.

11.2 RELATIONSHIP BETWEEN THE GROSSMANN H VALUE AND GENERALIZED BIOT NUMBER Bi_V

In practice, it is necessary to quantify quenching conditions. The expression used by heat treaters for this purpose is the Grossmann quench severity factor, or H value. H values, as shown in the graph in Fig. 1, are determined from measurements of a series of quenched cylinders like those shown in Fig. 2, quenched in oil or water.

In the chart shown in Fig. 1, the Du/D values on the y-axis represent the ratio of the diameter of the center portion that remains unhardened (Du) to the full diameter (D) for several of the bars of the cylinder series. Measured values of Du/D can be plotted against the D values on transparent paper with the same coordinates as shown in Fig. 1 [1]. This curve can then be matched to one of the curves of the chart. The H-value will then be the quotient of the $H \times D$ value of any point on this curve and the corresponding actual diameter. Some results of such an approach are provided in Table 1 [1,2].

For numerical analysis, the Biot number is typically used, which is a dimensionless number given by:

$$Bi = \frac{\alpha}{\lambda} R,$$

where:
α is the heat transfer coefficient;
λ is the heat conductivity of the material; and
R is the radius of a cylinder or ball or half the thickness of a plate.

In the theory of regular heat conditions [2], the characteristic size (L) is a value that includes three parameters S, V, and K, related as follows:

$$L = \frac{S}{V} K$$

where:
K is the Kondratjev form factor;
V is the volume of the body (m^3); and
S is the surface area (m^2).

In this case, the generalized Biot number Bi_V is defined as [3]:

$$Bi_V = \frac{\alpha}{\lambda} L = \frac{\alpha}{\lambda} K \frac{S}{V}.$$

For bodies that are plate-shaped, cylindrical, or spherical, the corresponding Bi_V values are:
- plate-shaped: $Bi_V = 0.405 Bi$
- cylindrical: $Bi_V = 0.346 Bi$
- spherical: $Bi_V = 0.304 Bi$

This approach permits a correlation between the Kondratjev number Kn, the criterion of temperature field nonsmoothness ψ, and the generalized Biot number Bi_V, given by:

$$Kn = \Psi Bi_V. \tag{1}$$

This relationship is true for bodies of any arbitrary shape, and when the range of the generalized Biot number Bi_V varies from 0 to ∞, the Kondratjev number Kn varies from 0 to 1, and the criterion of temperature field nonsmoothness ψ varies from 1 to 0. The physical sense of the criterion of temperature field nonsmoothness ψ follows from the equation given below:

$$\Psi = \frac{\overline{T}_{sf} - T_m}{\overline{T}_V - T_m},$$

where:
$\overline{T}_{sf}$ is the average temperature on the surface of the body;
T_m is the temperature of the quenchant; and
$\overline{T}_V$ is the volume-average temperature (see Chapter 6).

Comparison of the data provided in Table 2 shows the similarity between Grossmann H values with generalized Biot numbers Bi_V. When quenching cylindrical specimens 38.1 mm in diameter in a high-speed system that provides a convective heat transfer coefficient of 12,000–20,000 W/m^{2}K, a generalized Biot number Bi_V within the range of 3.6 to 6.0 is obtained.

Tables 1 and 2 suggest that since hardenability of steel parts is directly proportional to $\Psi = \dfrac{\overline{T}_{sf} - T_m}{\overline{T}_V - T_m}$ and there is universal correlation $Kn = \Psi Bi_V$, then Grossmann H values and generalized Biot numbers Bi_V are the same values [4].

11.3 CALCULATION OF KONDRATJEV NUMBERS Kn FOR VARIOUS QUENCHANTS

Kondratjev numbers (Kn) may be calculated from cooling rates at the core of cylindrical test specimens at temperatures of 1,300°F (704°C), 650°F (343°C), and 400°F (204°C) since there exists a correlation between the cooling rate v

---

[1] IQ Technologies, Inc., Akron, Ohio, and Portland State University, Portland, Oregon

170
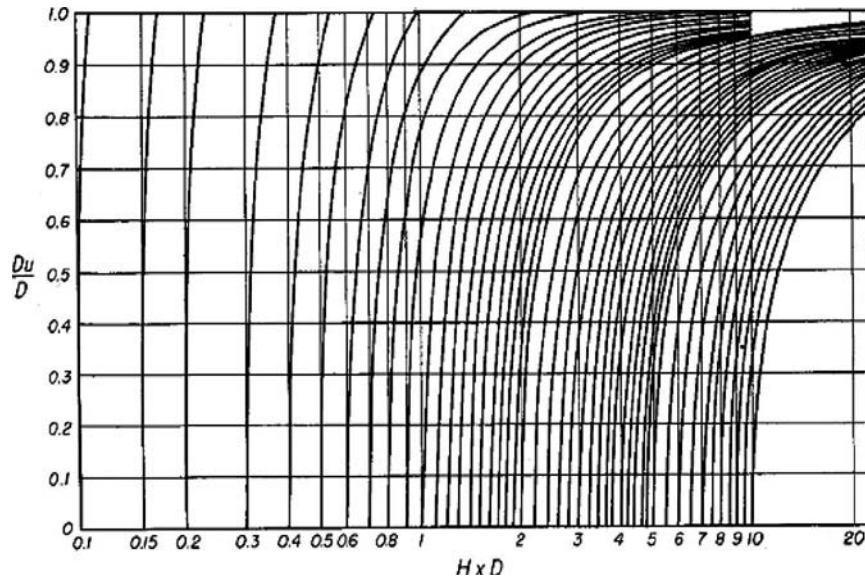
Fig. 1—Chart for estimating Grossmann H values from a cylinder series [1].
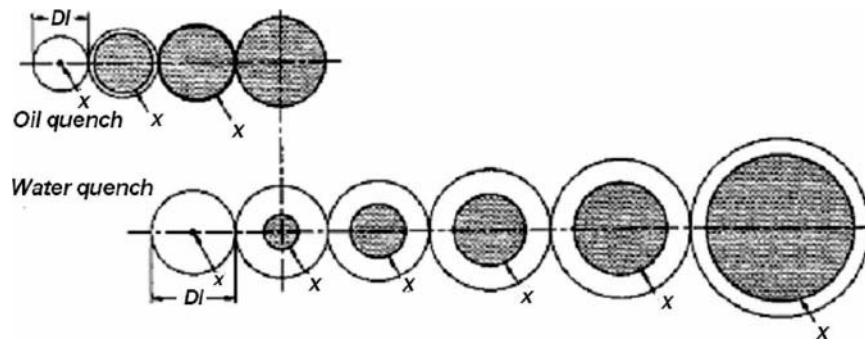
Fig. 2—Hardenability depending on cylinder size.

and Kondratjev number Kn [5]:

$$v = \frac{\bar{a}\,Kn}{K}(T - T_m), \qquad (2)$$

where:
v is the cooling rate (°F/s or °C/s);
$\bar{a}$ is the average thermal diffusivity (m²/s); and
K is the Kondratjev form factor (m²).

For an infinite cylinder, the Kondratjev form factor is:

$$K = \frac{R^2}{5.783}.$$

TABLE 1—Effect of agitation on quench severity as indicated by Grossmann quench severity factors (H values) [1,2]

Agitation	Grossmann H–value		
	Oil	Water	Brine
None	0.25–0.3	0.9–1.0	2.0
Mild	0.30–0.35	1.0–1.1	2.0–2.2
Moderate	0.35–0.4	1.2–1.3	—
Good	0.4–0.5	1.4–1.5	—
Strong	0.5–0.8	1.6–2.0	—
Violent	0.8–1.1	4.0	5.0

TABLE 2—Comparison of cooling capacities of different cooling media on the basis of tests with cylindrical probes of 1.5-in. (38.1-mm) diameter

Cooling medium	Bi_V	
	No agitation	Agitation of 100 fpm (0.508 m/s)
Houghton K, $T_m = 110°F$	0.25	0.38
Amolite 22, $T_m = 110°F$	0.11	0.34
Beacon 70, $T_m = 190°F$	0.125	0.36
35 % UCON Quenchant A, $T_m = 110°F$	—	0.34
20 % UCON Quenchant E $T_m = 90°F$	—	0.50
5 % UCON Quenchant E $T_m = 90°F$	—	0.60
Water	0.41–1	1.0–1.1

Therefore, Eq 2 can be rewritten as:

$$Kn = \frac{v \cdot K}{\overline{a}\,(T - T_m)} \qquad (3)$$

or

$$Kn = \frac{v \cdot R^2}{5.783 \cdot \overline{a}\,(T - T_m)}. \qquad (4)$$

These expressions will now be used to calculate Kn for various quenchants, including those that exhibit a so-called inverse solubility–those polymer quenchants based on poly-alkyleneglycol (PAG) copolymers such as UCON Quenchant A and UCON Quenchant E shown in Table 2.

The average value $\overline{a}$ at the center of a Type 304 stainless steel cylindrical test specimen for a temperature of 1,300°F is equal to 5.19×10^{-6} m²/s. Cooling rates of these cylindrical specimens with diameters of 0.5 in. (12.7 mm), 1 in. (25.4 mm), and 1.5 in. (38.1 mm) were determined. Using Eq 4 for these three diameters, the following values of Kn are obtained:

- 0.5 in. (12.7 mm): $Kn = 1.235 \times 10^{-3}v$
- 1 in. (25.4 mm): $Kn = 4.94 \times 10^{-3}v$
- 1.5 in. (38.1 mm): $Kn = 11.13 \times 10^{-3}v$

11.3.1 Cooling Capacity of Aqueous Polymer Quenchants

Cooling capacities of aqueous polymer quenchants [4–9] are shown in Tables 3, 4, and 5. Table 3 provides values of Kn for 10 % aqueous solutions of UCON Quenchant A and UCON Quenchant E at 90°F (about 32°C) with an agitation rate of 80 fpm (about 0.4 m/s). These data show that Kn is essentially independent of the sizes of test specimens, which agrees well with the theory presented in Chapter 2. Kn characterizes the cooling capacity of a quenchant, which is dependent on solution temperature and concentration, not part size.

Tables 4 and 5 also confirm this fact: With increasing temperature and concentration, the cooling capacity of a quenchant decreases. The maximum value of Kn that can be achieved in practice is 1. Aqueous solutions of salts of optimal concentration are used for intensive and uniform cooling, and Kn for aqueous solutions of salts and alkalis in water is 0.6. It follows that aqueous polymer solutions exhibiting inverse solubility at their optimal concentration cool as uniformly and intensively as aqueous solutions of salts,

which is due to the formation of a polymer film at the hot metal surface that reduces the heat flux density sufficiently to prevent the development of film boiling, that is, in this case, $q < q_{cr1}$.

The method of using heat-insulated films on the surface of metal to facilitate the intensification of the quench cooling process is described in [10]. Conventional cooling in water leads to the formation of vapor films around the hot metal surface, causing a significant decrease in Kn [9]. Fig. 3 presents the hardness distribution for the cross-section of a part quenched in oil or polymer quenchant or intensively quenched by a spray process [2,7]. Polymer quenchants and intensive spray quenching yield the highest cross-sectional hardness, thus providing good hardenability. When quenching in oil, the hardenability of a part sharply decreases, as shown in Fig. 3 [6].

11.3.2 Cooling Capacity of Oils and Comparison with the Cooling Capacity of Aqueous Polymer Solutions

In the above discussion, values of Kn were calculated for quench cooling processes in aqueous polymer solutions, water, and aqueous salt solutions. It was also emphasized that it is possible to intensify heat transfer by vibromixing or the use of the discrete-impulse energy input (see Chapter 9).

TABLE 3—Kondratjev numbers *Kn* for various size probes in 10 % aqueous solutions of UCON A and UCON E at a temperature of 90°F (~32°C)

Probe diameter	UCON Quenchant A	UCON Quenchant E	$\overline{Kn}$
0.5 in. (12.7 mm)	0.424	0.412	0.415
	0.417	0.408	
1 in. (25.4 mm)	0.546	0.488	0.512
	0.526	0.488	
1.5 in. (38.1 mm)	0.578	0.523	0.543
	0.556	0.514	

Note: The speed of the stream is 80 fpm (~0.4 m/s) and the temperature of the core of the probes is 1,300°F (704°C).

TABLE 4—Kondratjev numbers *Kn* for various size probes in 10 % aqueous solutions of UCON A and UCON E at a temperature 130°F (~43°C)

Probe diameter	UCON Quenchant A	UCON Quenchant E	$\overline{Kn}$
0.5 in. (12.7 mm)	0.365	0.322	0.346
	0.369	0.329	
1 in. (25.4 mm)	0.505	0.477	0.478
	0.472	0.456	
1.5 in. (38.1 mm)	0.512	—	0.52
	0.528		

Note: The speed of the stream is 80 fpm (~0.4 m/s) and the temperature of the core of the probes is 1,300°F (704°C).

TABLE 5—Kondratjev numbers *Kn* for a cylindrical specimen of diameter 1 in. (25.4 mm) versus concentration

Concentration of solution (%)	UCON A	UCON E
5	—	—
10	0.546	0.488
	0.526	0.488
30	0.239	0.372
	0.247	0.376

Note: The temperature of the solution is 90°F (~32°C) and the speed of the stream is 80 fpm (~0.4 m/s).
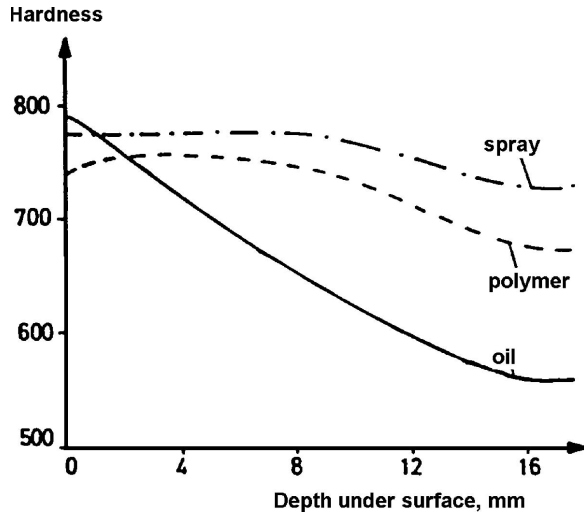
Fig. 3—Hardness distributions for spray, polymer, and oil immersion quenching.

Usually all parts made of alloyed steels, as a rule, are cooled in quench oils. Low-carbon and medium-carbon steels are usually cooled in water. A comparison of cooling times when quenching cylindrical specimens in oils, aqueous polymer solutions, and water is shown in Table 6.

However, it is possible to cool alloyed and high-alloy steels by intensive water streams or intensive jets to prevent cracking. Crack formation during water quenching is due to the occurrence of martensite in the core of parts, which "expands" and results in increased tensile surface stresses. Intensive quenching creates compressive surface stresses, even in case of the formation of 100 % martensite throughout the entire cross-section of the part. This issue was discussed in detail in Chapter 7. As it was noted, during intensive quenching, superstrengthening (additional strengthening) is observed and quench distortion is minimized.

In many cases, when cooling alloyed steels in oil, the part is through-hardened. However, quench cracking is usually not observed, and distortion is decreased relative to quenching in water. The universality of oil quenching may be explained by the high saturation temperature of oil. During the boiling process, the average heat transfer coefficient α within the pearlite range reaches 1,000–3,000 W/m²K, and during the convection cooling, it is typically reduced to 200–300 W/m²K. Since the boiling temperature of many oils is approximately 300–350°C, high values of heat transfer coefficients are observed above the martensite start temperature M_S. At the end of the boiling process, the core is cooled to 400–500°C and with additional cooling convective cooling occurs when $\alpha = 300$–350 W/m²K. Thus, quench oils produce relatively fast cooling at high temperatures, and within the martensite range the cooling process is significantly reduced. Therefore, when quenching steel parts in oil, quench cracks are not usually observed.

When quenching in water and aqueous polymer solutions, at the initial moment of cooling, film boiling may be observed. This transforms into a nucleate boiling process, where the intensity of heat transfer is very high until the surface temperature reaches 100°C. Thus, rapid cooling partially occurs within the martensitic transformation range. Nevertheless, because the intensity of cooling within the martensite range is still insufficient for the formation of high compressive surface stresses, quench cracking and significant distortion may occur.

In the case of intensive cooling, the maximum temperature gradients occur in the cross-sections of the parts. Thus, a martensitic shell is formed surrounding the entire surface of a part. This martensitic shell creates high surface compressive stresses, and distortion of quenched parts is reduced. Therefore, it is important to determine the cooling capacity of oils for comparison with the cooling capacity of aqueous polymer solutions and for intensive cooling processes. This may be done by using average Kondratjev numbers $\overline{Kn}$ to characterize the cooling capacity of all quenchants.

One method of addressing this problem is to use AISI 4140 steel cylindrical probes with diameters of 0.5 in. (12.7 mm), 1 in. (25.4 mm), 1.5 in. (38.1 mm), or 2 in. (50.8 mm). A spring-loaded thermocouple is inserted to the geometric center. All of the probes possessed a length-to-diameter ratio of 4. The probes were heated to the austenitizing temperature of 1,550°F (843°C) and quenched into the desired quench medium with specific cooling conditions (bath temperature and agitation rate). The cooling rate in the core was recorded at temperatures of 1,300°F (704°C), 650°F (343°C), and 400°F (204°C). It was shown above that using these cooling rates, the Kondratjev number Kn is readily calculated, which may then be used to calculate the cooling time of parts to be quenched. This process will now be used to calculate the cooling time of cylindrical probes austenitized at a temperature of 1,550°F (843°C) until the temperature of the core is 400°F (204°C).

Using the generalized dependence described in Chapter 5 (Eq 69), cooling times of cylinders with different diameters from temperature of 1550°F to 400°F were calculated as follows:

$$\tau = \left[0.48 + \ln \frac{1550°F - 110°F}{400°F - 110°F} \right] \frac{K}{\bar{a}\, Kn}$$

or

$$\tau \cong \frac{2K}{\bar{a}\, Kn}.$$

TABLE 6—Cooling time of an AISI 4140 steel cylindrical probe of 1.5-in. (38.1 mm) diameter cooled from 1,550°F (843°C) to 400°F (204°C) by various quenchants

Quenchant and temperature	Cooling time (s)	
	No agitation	Agitation of 100 fpm (0.508 m/s)
Houghton K, 110°F (43°C)	107	75
Amolite 22, 110°F (43°C)	219	84
Beacon 70, 190°F (88°C)	202	80
35 % UCON Quenchant A, 110°F (43°C)	—	84
20 % UCON Quenchant E, 90°F (32°C)	—	63
5 % UCON Quenchant E, 90°F (32°C)	—	50
Water, 70°F (21°C)	55	—

This equation shows that cooling time is directly proportional to the Kondratjev form factor K and inversely proportional to average thermal diffusivity $\bar{a}$ and Kondratjev number $\overline{Kn}$.

Thermal diffusivity a characterizes the thermophysical properties of material, and the Kondratjev number Kn characterizes the cooling capacity of quenchants. For the specific quenching conditions described, the proportionality factor is approximately 2. The value of Kn depends on the physical and chemical properties of the quenchant. Therefore, this number (Kn criterion) is a convenient parameter to describe the cooling capacity of quenchants.

Using the same computational method, the cooling capacity of quench oils will now be illustrated. Table 7 shows that Houghton K quench oil cools relatively faster when the temperature of the core of the heated cylindrical test specimen is equal to 1,300°F (704°C) and slower when the temperature of the core is equal to 650°F (343°C) or 400°F (204°C). This is especially apparent for still (unagitated) oil, as shown in Table 7. When the agitation rate of the oil is increased to 100 fpm (0.508 m/s), the cooling capacity is equalized somewhat with respect to both variation of temperature and probe size, as shown in Table 8. As the size increases, a greater volume of the oil surrounding a part is heated to higher temperature. Small parts (or probes) result in a smaller quantity of heat being transferred to the quenchant medium, and therefore the temperature increase of the oil surrounding the steel is reduced.

With increasing oil temperature, the oil's cooling properties will at first increase and then decrease [8–10]. There is an optimal temperature of oil at which its cooling properties are at a maximum [8]. Therefore, Kn will increase with the section size due to an improvement in the cooling properties of oil surrounding the part. Kn decreases with a decrease in temperature because the viscosity of oil sharply increases and cooling is decreased, especially during convective cooling. Agitation of the oil improves this situation somewhat. Similar behavior was observed for Amolite 22 (see Tables 9–12) and Beacon 70 (see Tables 13–16) quench oils. It should be noted that as the temperature of Beacon 70 oil increases to 190°F, its cooling capacity also increases (see Tables 13–16).

Calculated Kn numbers for various grades of quench oils may be used for not only evaluation of their cooling capacity but also calculations of cooling time for parts to be quenched. Furthermore, these data can be used for designing industrial quenching lines and quenching equipment of any kind.

Tables 17–19 present Kn for 20–35 % aqueous solutions of UCON Quenchant A and UCON Quenchant E, two PAG polymer quenchants. These tables show that high concentrations of aqueous PAG solutions provide approximately the same cooling conditions as oil. With decreasing concentration to 5–10%, Kn is completely stabilized and is essentially independent of the section size of the cylinders (see Table 20). Table 21 provides a comparative summary of Kn values for all of the quenchants evaluated.

TABLE 8—Kondratjev numbers Kn for Houghton K oil at a temperature of 110°F (43.3°C), with agitation of 100 fpm (0.508 m/s), for various sizes of cylindrical probes made of AISI 4140 steel

Probe diameter	Kn at			$\overline{Kn}$
	1,300°F (704°C)	650°F (343°C)	400°F (204°C)	
0.5 in. (12.7 mm)	0.257	0.198	0.170	0.20
	0.244	0.174	0.148	
1 in. (25.4 mm)	0.325	0.287	0.229	0.28
	0.304	0.301	0.227	
1.5 in. (38.1 mm)	0.410	0.275	0.231	0.31
	0.414	0.278	0.226	
2 in. (50.8 mm)	0.424	0.277	0.235	0.31
	0.422	0.273	0.226	

TABLE 7—Kondratjev numbers Kn for Houghton K oil at a temperature of 110°F (43.3°C), with no agitation, for various sizes of cylindrical probes made of AISI 4140 steel

Probe diameter	Kn at			$\overline{Kn}$
	1,300°F (704°C)	650°F (343°C)	400°F (204°C)	
0.5 in. (12.7 mm)	0.230	0.073	0.026	0.106
	0.206	0.073	0.026	
1 in. (25.4 mm)	0.142	0.120	0.046	0.102
	0.139	0.121	0.046	
1.5 in. (38.1 mm)	0.392	0.136	0.071	0.213
	0.407	0.139	0.071	
2 in. (50.8 mm)	0.420	0.158	0.084	0.218
	0.414	0.150	0.084	

TABLE 9—Kondratjev numbers Kn for Amolite 22 oil at a temperature of 110°F (43.3°C), with no agitation, for various sizes of cylindrical probes made of AISI 4140 steel

Probe diameter	Kn at			$\overline{Kn}$
	1,300°F (704°C)	650°F (343°C)	400°F (204°C)	
0.5 in. (12.7 mm)	0.065	0.035	0.026	0.041
	0.056	0.036	0.026	
1 in. (25.4 mm)	0.088	0.063	0.046	0.065
	0.084	0.063	0.048	
1.5 in. (38.1 mm)	0.134	0.092	0.071	0.104
	0.165	0.089	0.071	
2 in. (50.8 mm)	0.306	0.106	0.04	—
	0.288	0.106	0.04	

TABLE 10—Kondratjev numbers *Kn* for Amolite 22 oil at a temperature of 110°F (43.3°C), with agitation of 100 fpm (0.508 m/s), for various sizes of cylindrical probes made of AISI 4140 steel

| Probe diameter | *Kn* at | | | $\overline{Kn}$ |
	1,300°F (704°C)	650°F (343°C)	400°F (204°C)	
0.5 in. (12.7 mm)	0.136	0.169	0.163	0.15
	0.128	0.165	0.143	
1 in. (25.4 mm)	0.184	0.225	0.197	0.205
	0.185	0.233	0.206	
1.5 in. (38.1 mm)	0.275	0.280	0.254	0.27
	0.311	0.273	0.240	
2 in. (50.8 mm)	0.342	0.273	0.251	0.28
	0.319	0.251	0.226	

TABLE 12—Kondratjev numbers *Kn* for Amolite 22 oil at a temperature of 190°F (88°C), with agitation of 100 fpm (0.508 m/s), for various sizes of cylindrical probes made of AISI 4140 steel

| Probe diameter | *Kn* at | | | $\overline{Kn}$ |
	1,300°F (704°C)	650°F (343°C)	400°F (204°C)	
0.5 in. (12.7 mm)	0.167	0.185	0.151	0.17
	0.152	0.192	0.153	
1 in. (25.4 mm)	0.216	0.245	0.211	0.23
	0.210	0.268	0.211	
1.5 in. (38.1 mm)	0.370	0.310	0.273	0.31
	0.373	0.290	0.267	
2 in. (50.8 mm)	0.392	0.305	0.278	0.32
	0.378	0.305	0.266	

During cooling in aqueous polymer solutions, more uniform cooling over the entire surface is achieved. This should be contrasted to quenching in water, where localized vapor films are observed, resulting in cracking and distortion. Interestingly, the cooling capacity of a 5–10 % PAG quenchant solution is greater than that of water. Such aqueous solutions of PAG can be used for implementation of the IQ-2 process (see Chapter 10).

Cooling times for AISI 4140 steel cylinders of 1.5 in. (38.1 mm) in diameter quenched in various media are shown in Table 6. The cooling time is calculated for the temperature range of 1,550°F to 400°F, that is, the duration of cooling from the austenitizing temperature until the temperature at the center of the cylinder reaches 400°F. These data show that the cooling times in water and 5 % UCON differ very little. However, polymer solutions cool more uniformly at high temperatures and reduce the cooling rate more in the convective cooling region.

11.4 CONTINUOUS CONVEYOR LINES AND DESIGN OF THE QUENCHING PROCESSES

In this section, the application of the previously described calculation methodology for various conveyor lines will be described. In particular, the calculation of the conveyor speed with respect to the shape and sizes of steel parts and the cooling capacity of the quenchant will be described.

The most commonly encountered type of conveyor line is illustrated in Fig. 4 [11]. Other examples of continuous lines for quenching steel parts are shown in Figs. 5 and 7. All of these examples utilize special chutes to intensify and stabilize the cooling process (see Fig. 5). The illustration at the top of Fig. 4 shows details of a chute quench [11].

TABLE 11—Kondratjev numbers *Kn* for Amolite 22 oil at a temperature of 190°F (88°C), with no agitation, for various sizes of cylindrical probes made of AISI 4140 steel

| Probe diameter | *Kn* at | | | $\overline{Kn}$ |
	1,300°F (704°C)	650°F (343°C)	400°F (204°C)	
0.5 in. (12.7 mm)	0.068	0.039	0.026	0.044
	0.071	0.037	0.025	
1 in. (25.4 mm)	0.101	0.066	0.046	0.070
	0.100	0.066	0.043	
1.5 in. (38.1 mm)	0.140	0.096	0.072	0.104
	0.161	0.093	0.065	
2 in. (50.8 mm)	0.392	0.114	0.093	—
	0.306	0.114	0.093	

TABLE 13—Kondratjev numbers *Kn* for Beacon 70 oil at a temperature of 110°F (43.3°C), with no agitation, for various sizes of cylindrical probes made of AISI 4140 steel

| Probe diameter | *Kn* at | | | $\overline{Kn}$ |
	1,300°F (704°C)	650°F (343°C)	400°F (204°C)	
0.5 in. (12.7 mm)	0.049	0.057	0.026	0.047
	0.065	0.060	0.027	
1 in. (25.4 mm)	0.085	0.090	0.048	0.074
	0.084	0.090	0.048	
1.5 in. (38.1 mm)	0.154	0.108	0.071	0.118
	0.196	0.108	0.071	
2 in. (50.8 mm)	0.364	0.172	0.084	0.195
	0.297	0.167	0.084	

TABLE 14—Kondratjev numbers *Kn* for Beacon 70 oil at a temperature of 110°F (43.3°C), with agitation of 100 fpm (0.508 m/s), for various sizes of cylindrical probes made of AISI 4140 steel

Probe diameter	*Kn* at			$\overline{Kn}$
	1,300°F (704°C)	650°F (343°C)	400°F (204°C)	
0.5 in. (12.7 mm)	0.144	0.199	0.167	0.166
	0.129	0.195	0.161	
1 in. (25.4 mm)	0.188	0.255	0.221	0.224
	0.191	0.261	0.227	
1.5 in. (38.1 mm)	0.342	0.310	0.268	0.308
	0.367	0.305	0.259	
2 in. (50.8 mm)	0.391	0.290	0.251	0.310
	0.382	0.295	0.251	

TABLE 16—Kondratjev numbers *Kn* for Beacon 70 oil at a temperature of 190°F (88°C), with agitation of 100 fpm (0.508 m/s), for various sizes of cylindrical probes made of AISI 4140 steel

Probe diameter	*Kn* at			$\overline{Kn}$
	1,300°F (704°C)	650°F (343°C)	400°F (204°C)	
0.5 in. (12.7 mm)	0.146	0.177	0.117	0.145
	0.135	0.170	0.125	
1 in. (25.4 mm)	0.221	0.244	0.162	0.205
	0.202	0.235	0.167	
1.5 in. (38.1 mm)	0.361	0.268	0.203	0.284
	0.382	0.283	0.207	
2 in. (50.8 mm)	0.409	0.268	0.201	0.288
	0.384	0.264	0.201	

At the top of Fig. 4, there is a common scheme of a quench tank with a quenchant and devices for agitation. Additional agitation of the quenchant during movement of parts on the conveyor is necessary to provide uniform cooling of the parts and increase the heat transfer coefficient during convective cooling and also to regulate the duration of the nonstationary nucleate boiling stage.

In the examples below, the following quenching media will be considered:

1. Aqueous polymer solutions
2. Aqueous solutions of corrosion-preventing salts
3. Pure cold water

For these examples, the length *L* of the conveyor immersed in the quenchant is 1.5 m. The goal is to determine the conveyor speed that will provide a temperature of 650°F (343°C) at the core of the part when it is removed from the quenchant. For these calculations, the generalized equation 69 from Chapter 5 is used, rewritten as:

$$w = \frac{L}{\tau} = \frac{\bar{a} \, L \, Kn}{\left(\Omega + \ln \dfrac{T_0 - T_m}{T - T_m}\right) K}, \qquad (5)$$

where:

$\bar{a}$ is the average thermal diffusivity of the material for the range of temperatures T_0 to T_m;

Kn is the Kondratjev number (dimensionless);

$\Omega = 0.48$ for cylindrical bodies;

T_0 is the austenitizing temperature or temperature at the time of immersion of the part into the quenchant; and

T_m is the temperature of the medium, if convection prevails, or the temperature of boiling if nucleate boiling prevails.

TABLE 15—Kondratjev numbers *Kn* for Beacon 70 oil at a temperature of 190°F (88°C), with no agitation, for various sizes of cylindrical probes made of AISI 4140 steel

Probe diameter	*Kn* at			$\overline{Kn}$
	1,300°F (704°C)	650°F (343°C)	400°F (204°C)	
0.5 in. (12.7 mm)	0.069	0.047	0.018	0.045
	0.069	0.047	0.018	
1 in. (25.4 mm)	0.089	0.080	0.034	0.068
	0.085	0.085	0.036	
1.5 in. (38.1 mm)	0.147	0.099	0.052	0.113
	0.226	0.102	0.052	
2 in. (50.8 mm)	0.338	0.128	0.067	0.175
	0.338	0.114	0.067	

TABLE 17—Kondratjev numbers *Kn* for a 35 % aqueous UCON A solution at a temperature of 110°F (43.3°C), with agitation of 50 fpm (0.254 m/s), for various sizes of cylindrical probes made of AISI 4140 steel

Probe diameter	*Kn* at			$\overline{Kn}$
	1,300°F (704°C)	650°F (343°C)	400°F (204°C)	
0.5 in. (12.7 mm)	0.046	0.197	0.135	0.128
	0.054	0.190	0.145	
1 in. (25.4 mm)	0.075	0.330	0.218	0.203
	0.074	0.311	0.212	
1.5 in. (38.1 mm)	0.099	0.365	0.377	0.271
	0.120	0.365	0.301	
2 in. (50.8 mm)	0.157	0.546	0.444	0.404
	0.220	0.581	0.478	

TABLE 18—Kondratjev numbers *Kn* for a 20 % aqueous UCON A solution at a temperature of 110°F (43.3°C), with agitation of 100 fpm (0.508 m/s), for various sizes of cylindrical probes made of AISI 4140 steel

Probe diameter	*Kn* at 1,300°F (704°C)	650°F (343°C)	400°F (204°C)	$\overline{Kn}$
0.5 in. (12.7 mm)	0.301	0.347	0.265	0.30
	0.326	0.361	0.201	
1 in. (25.4 mm)	0.452	0.463	0.351	0.42
	0.443	0.449	0.378	
1.5 in. (38.1 mm)	0.497	0.474	0.419	0.46
	0.490	0.471	0.415	
2 in. (50.8 mm)	0.509	0.480	0.470	0.48
	0.509	0.462	0.441	

TABLE 20—Kondratjev numbers *Kn* for a 5 % aqueous UCON E solution at a temperature of 110°F (43.3°C), with agitation of 50 fpm (0.254 m/s), for various sizes of cylindrical probes made of AISI 4140 steel

Probe diameter	*Kn* at 1,300°F (704°C)	650°F (343°C)	400°F (204°C)	$\overline{Kn}$
0.5 in. (12.7 mm)	0.214	0.422	0.304	0.34
	0.356	0.420	0.306	
1 in. (25.4 mm)	0.272	0.461	0.368	0.40
	0.279	0.616	0.397	
1.5 in. (38.1 mm)	0.503	0.513	0.424	0.46
	0.377	0.511	0.424	
2 in. (50.8 mm)	0.516	0.510	0.494	0.51
	0.525	0.506	0.494	

The average thermal diffusivity $\bar{a}$ of the supercooled austenite within the temperature range of 1,550°F (843°C) down to 200°F (93°C) is equal to 5.36 × 10^{-6} m²/s.

From these data, the conveyor speed required to provide a core temperature of 650°F (343°C) for a cylindrical part made of AISI 4140 steel with a diameter of 25 mm and height of 50 mm is calculated. When initially immersed, the part has uniform temperature of 1,550°F (840°C) throughout the cross-section.

The first step is to determine the Kondratjev number *Kn*. For the determination of *Kn*, a database of experimental data is required. Careful quenching experiments have been conducted using AISI 4140 steel cylindrical specimens 0.5 in. (12.7 mm), 1 in. (25.4 mm), 1.5 in. (38.1 mm), and 2 in. (50.8 mm) in diameter. These test specimens were quenched into various polymer quenchants and quench oils. Kondratjev

numbers *Kn* for various quenchants–quench oils, water, aqueous polymer quenchant solutions, water-salt solutions, and other media–were determined. Some results of such calculations are provided in this chapter.

11.4.1 Calculation of the Speed of a Conveyor in a Quench Tank

Having discussed in detail all parameters contained in the equation used for calculation of conveyor speed using Kondratjev numbers *Kn*, consider, for example, a cylindrical steel part of 1 in. (25.4 mm) in diameter and 2 in. (50.8 mm) long, made of AISI 4140 steel. The steel part is to be cooled from 1,550°F (840°C) in a 10 % aqueous PAG-polymer solution at a temperature of 90°F (32.2°C). The agitation rate is 80 fpm (0.4 m/s). It is necessary to establish the speed of the conveyor to deliver the steel part from the quenchant with a core temperature of 650°F (343°C). In this case, there will be

TABLE 19—Kondratjev numbers *Kn* for a 20 % aqueous UCON E solution at a temperature of 110°F (43.3°C), with agitation of 100 fpm (0.508 m/s), for various sizes of cylindrical probes made of AISI 4140 steel

Probe diameter	*Kn* at 1,300°F (704°C)	650°F (343°C)	400°F (204°C)	$\overline{Kn}$
0.5 in. (12.7 mm)	0.288	0.242	0.216	0.23
	0.233	0.228	0.167	
1 in. (25.4 mm)	0.174	0.317	0.346	0.31
	0.152	0.370	0.523	
1.5 in. (38.1 mm)	0.467	0.332	0.259	0.36
	0.473	0.335	0.273	
2 in. (50.8 mm)	0.472	0.348	0.310	0.44
	0.335	0.519	0.670	

TABLE 21—Comparison of cooling capacities of different cooling media on the basis of tests with cylindrical probes of 1.5-inch (38.1-mm) diameter

Cooling medium	$\overline{Kn}$ No agitation	Agitation of 100 fpm (0.508 m/s)
Houghton K, T_m = 110°F	0.213	0.306
Amolite 22, T_m = 110°F	0.104	0.27
Beacon 70, T_m = 190°F	0.118	0.308
35 % UCON A, T_m = 110°F	0.113	0.284
20 % UCON E	—	0.27
5 % UCON E	—	0.36
Water	—	0.46
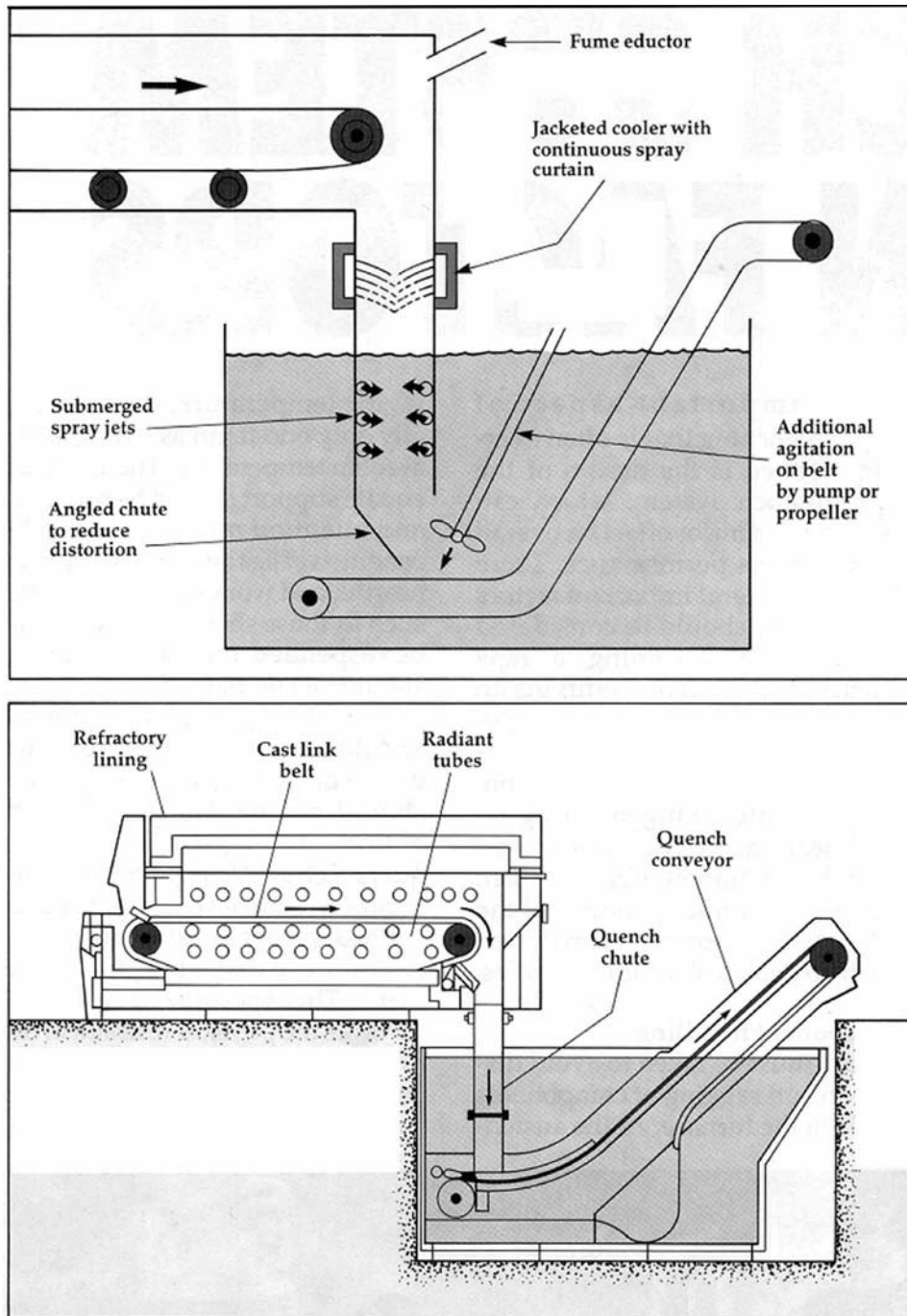
Fig. 4—Typical quenching systems for continuous heat-treating furnaces.

self-tempering of the part and no possibility of quench crack formation.

Substituting the given values into Eq 5, we get:

$$W = \frac{5.36 \cdot 10^{-6} m^2/s \ \cdot 1.5m \ \cdot 0.512}{\left[0.48 + \ln\left(\dfrac{1550°F - 212°F}{650°F - 212°F} \right) \cdot 25.2 \cdot 10^{-6} m^2 \right]}$$

$$= 0.1 \frac{m}{s} \text{ or } 360 \, m/h,$$

where $K = \dfrac{1}{\dfrac{5.783}{R^2} + \dfrac{9.87}{Z^2}} = 25.2 \cdot 10^{-6} m^2.$

11.4.2 Calculation of the Speed of Rotation of Usual and Screw Drums

Besides continuous conveyor lines, rotating apparatus such as screw drums are often used for longitudinal motion of parts to be quenched (see Fig. 6). In some cases, quench tanks are used with devices rotating inside, such as shafts on which supports for parts are fixed. When a part to be quenched is put on the support, the latter moves in a semicircle in the quench tank and then ejects the part into a basket or onto a conveyor. Such devices can be automated and mechanized.

In this case, the speed of rotation of the screw systems and drums depends on the shapes and sizes of the parts, the
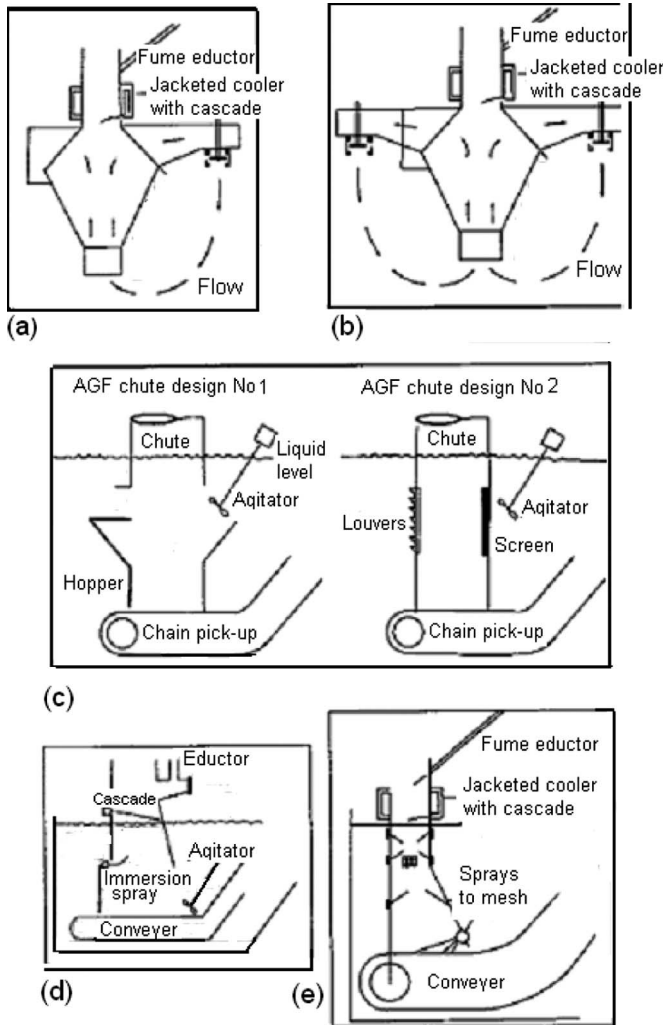
Fig. 5—Examples of possible chute-quench designs.

thermophysical properties of the material, and the cooling capacity of the quenchant. Such operations are often encountered in practice because when the core achieves the martensite start temperature M_S, conventional or intensive cooling must be interrupted immediately to prevent quench crack formation and provide self-tempering of the part.

From the generalized dependences presented in Chapters 2 and 5 for calculation of the cooling time in a

Fig. 6—Illgner continuous chute quench design (From K. Illgner, Harterei-Tech. Mitt. 41(2), 113–120, 1987).

quenchant, simple equations for designing drum-type and screw systems have been derived, such as for the determination of the rotational speed of the screw drum (e.g., the device in Fig. 7). If the length of the screw drum along the circle is L and the quantity of the coils forming the screw conveyor is N, then during one rotation of the drum, the longitudinal motion of a part to be quenched is L/N, and to cover the entire length, it is necessary to make N rotations of the drum.

If the cooling process lasts, for example, for 1 min, it is necessary for the screw conveyor to make N rotations per minute until the part is pushed out from the quenchant. If the process of cooling lasts instead for 3 min or 5 min, the quantity of rotations per minute must decrease by three or five times, respectively. Because the frequency of the screw rotation is directly proportional to the quantity of coils and inversely proportional to the cooling time, then the equation for the frequency n is:

$$n = \frac{N}{\tau} = \frac{N \bar{a} \, Kn}{\left[\Omega + \ln \dfrac{T_0 - T_m}{T - T_m}\right] K}. \tag{6}$$

For another illustration, consider Fig. 7, which illustrates a furnace and quench system consisting of a screw drum and rotating shaft with eight coils forming the screw mechanism. The length of the screw in the quench system is 1.2 m. The quenchant used is a 10 % aqueous solution of sodium carbonate (Na_2CO_3) at a temperature of 20°C. Kn for this solution is 0.6. In the system shown in Fig. 7, 2-in.-diameter (50.8-mm) AISI 52100 steel balls are quenched. The austenitizing temperature is 860°C. It is necessary to calculate the frequency of the screw rotation so that, upon delivery of the part from the quenchant, the temperature at the core of a ball will be 350°C.

The first step is to determine Kondratjev form coefficient K for a ball of diameter 50.8 mm:

$$K = \frac{R^2}{9.87} = \frac{(0.0254m)^2}{9.87} = 65.37 \cdot 10^{-6} m^2.$$

The average thermal diffusivity of material is $\bar{a} = 5.36 \times 10^{-6}$ m^2/s, and $\Omega = 0.24 \times 3 = 0.72$ [11]. Using these values in Eq 5 yields:

$$n = \frac{8 \cdot 5.36 \cdot 10^{-6} m^2/s \cdot 0.6}{\left[0.72 + \ln \dfrac{860°C - 20°C}{350°C - 20°C}\right] \cdot 65.37 \cdot 10^{-6} m^2}$$

$$\approx 0.25 \, rps \text{ or } 15 \, rpm.$$
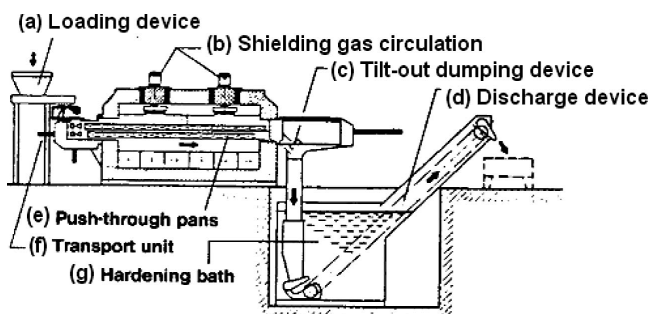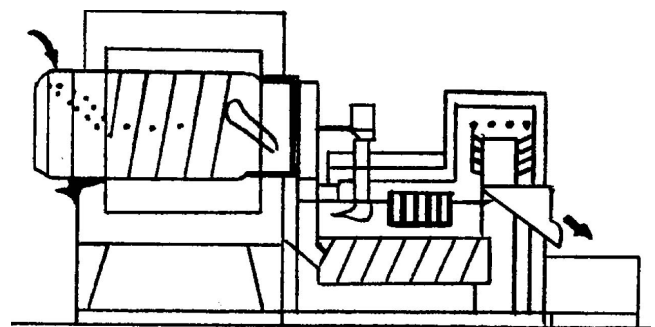
Fig. 7—Schematic of a rotary drum screw conveyor continuous furnace.
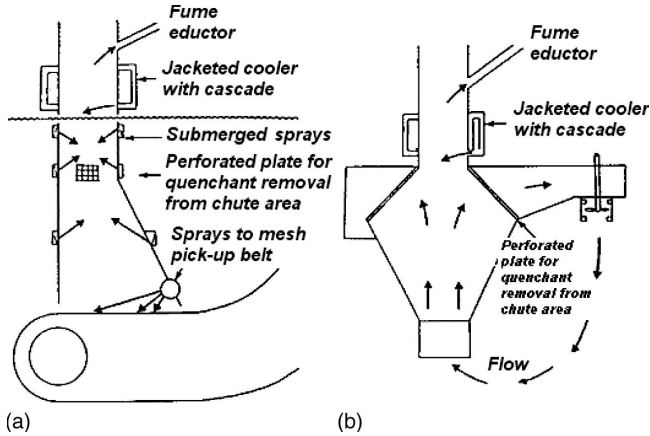
Fig. 8—Chutes with a spray quench system (a) and an impeller agitation system (b).

Thus, the generalized dependence obtained in Chapter 5 can be successfully used for designing quench systems.

These calculations are also necessary for automation of quench cooling processes. The design of quench systems becomes complicated because it is necessary to create intensive agitation of a quenchant at the time of immersion of a hot part into a quench tank. It is also necessary to prevent the penetration of vapor into the furnace. To solve these two problems, special devices have been developed, which are shown in Fig. 5. These devices permit intensive agitation of a quenchant upon immersion of parts into it as well as prevention of vapor ingression into the furnace. Additional details are provided in [12,13] (see Figs. 8 and 9).

Aqueous polymer solutions or salts of optimal concentration can be used for implementation of the IQ-2 process. For the IQ-3 process, water is typically used, because very intensive streams or jets are necessarily applied, which prevents the possibility of the formation of vapor films and even suppresses the process of nucleate boiling.

A specific example of the use of this process will now be provided. For this purpose, consider quenching bolts made of alloyed steels with the complicated configurations shown in Table 22. Quenching of bolts is conducted using volumetric heating in a V-shaped pipe in which intensive streams of water are used, as shown in Fig. 9 [14]. The average diameter of the bolts is 8 mm.

To solve this problem, we must calculate the Biot number Bi for the convective quenching process for bolts of diameters 8 and 10 mm. The equation used is Eq 13 from Chapter 10, for the absence of nucleate boiling:

$$Bi \geq \frac{2(\vartheta_0 - \vartheta_I)}{\vartheta_{uh} + \vartheta_I}, \tag{7}$$

where:
$\vartheta_0 = 920°C - 100°C = 820°C$;
$\vartheta_{uh} = 100°C - 20°C = 80°C$;
$\vartheta_I = 16.5$ for a bolt of diameter of 8 mm; and
$\vartheta_I = 15.4$ for a bolt of diameter of 10 mm (see Chapter 2).

In these cases, the calculation shows that $Bi \geq 16$ and $Kn \approx 0.88$. It is difficult to achieve such conditions of cooling in practice. However, Tkachuk and colleagues [14] cooled bolts by a stream of water at 20 m/s and established that quench cracks were not formed even in the case of superheating the bolts during austenitizing (see Table 22).

If the core temperature desired for the bolts during intensive cooling is 200°C, the cooling time when intensive streams of water are used is calculated as:

$$\tau = \left[0.48 + \ln\frac{920°C - 20°C}{200°C - 20°C}\right]\frac{2.8 \cdot 10^{-6}}{5.65 \cdot 10^{-6} \cdot 0.88} \approx 1.2\,\text{sec},$$

where $K = 2.8 \times 10^{-6}\,\text{m}^2$.

Since Kn was much less, the cooling process for the bolts occurs within 2 s. Daming [16] noted that bolts in a pipe with a turbulent water stream made the cooling process quite efficient. More information can be found in [12–19].

11.5 BATCH QUENCHING

A common view of a quench tank with a propeller for batch quenching is presented in Fig. 10. In this setup, rotating impellers drive water through directing pipes (draft tubes) to the part to be quenched.

The speed of a stream of a quenchant in such systems can achieve 2–3 m/s. Designing similar systems is described in detail in [2] and [15]. Rotating impellers in a draft tube is shown in Fig. 11, and illustrative impeller designs are illustrated in Fig. 12. There are certain requirements for the design of a system with impellers, which can be summarized as follows:

- Draft-tube systems normally use marine propellers for small mixers and airfoil-type impellers for larger units (see Fig. 13).
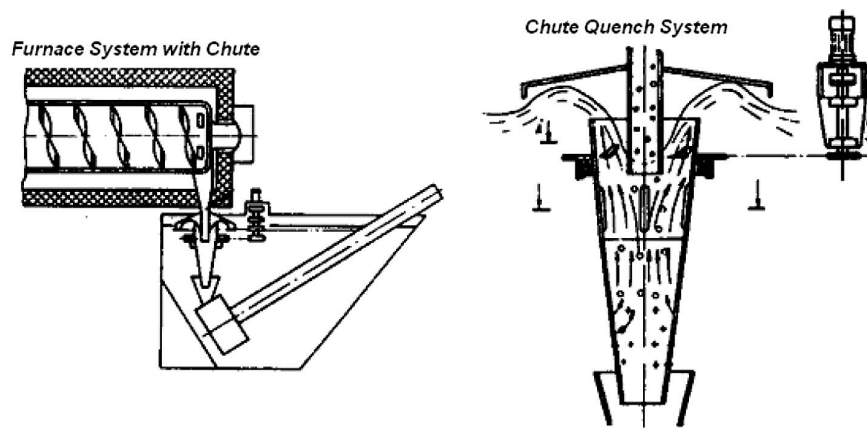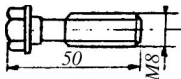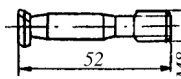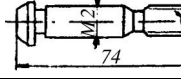
Fig. 9—Mechanically rotated chute quench systems (no pumps or impellers).

TABLE 22—Prevention of quench crack formation by intensive quenching in the V-quenching tank (see Fig. 9)

Sample		Austenitizing temperature (°C)	% of cracked sample during quenching	
Steel	Shape and Size		In moderately agitating caustic solution	In the V-quenching tank
Ck35 (0.35% C)	*(bolt, 50, M8)*	860 920	62 100	0 0
42 CrMo (0.42% C, 1% Cr, 0.2% Mo)	*(bolt, 52, M8)*	920	100	0
40 Cr (0.4% C, 1% Cr)	*(bolt, 74, M2, 2φ)*	920	100	0

- In a draft-tube system, an airfoil-type stirrer will be designed at a lower tip chord angle than that used on a side-entering mixer in order to avoid stalling under conditions of high head resistance.
- The lower weight of the airfoil-type stirrer lowers its cost at diameters greater than 610 mm (24 in.).

It is evident that the total system head resistance should be minimized to maximize the flow developed by the impeller. Although it is not practical to change most of the characteristics of the quench tank system, the draft tube can be designed to minimize head losses. For example, lack of an entrance flare with inadequate liquid coverage over the draft tube can decrease the flow rate by 20 %.

The following characteristics maximize the performance of a draft tube:

- Down-pumping operation takes advantage of the tank bottom as a flow-directing device.
- A 30° entrance flare on the draft tube minimizes entrance head losses and ensures a uniform velocity profile at the inlet.

- Liquid coverage over the draft tube of at least one-half the diameter avoids excessive disruption of the impeller inlet velocity profile.
- Internal flow-straightening vanes prevent fluid rotation or swirl.
- The impeller should be inserted into the draft tube at distance equal to at least one-half the diameter. Inlet velocity profile considerations dictate this dimension.
- A "steady bearing" or limit ring protects the impeller from occasional high deflection. Use of a steady bearing results in a mixer that is lower in cost, but that requires periodic maintenance. For this reason, a limit ring generally is specified as the only protective item. In such case, the mixer manufacturer should be requested to

Fig. 10—Illustration of a typical batch immersion time quenching system. Agitation is provided by two or more continuously variable impeller stirrers [20].
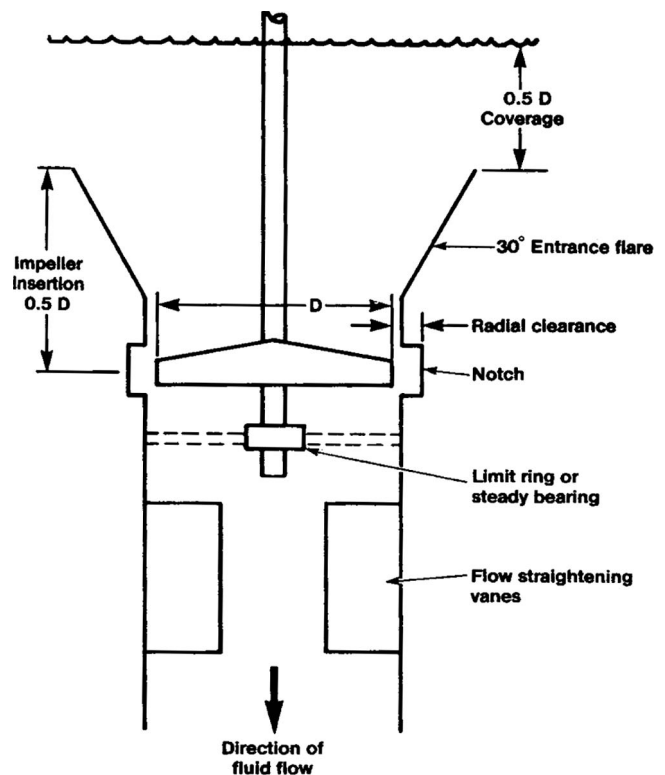
Fig. 11—Typical draft-tube impeller system characteristics.
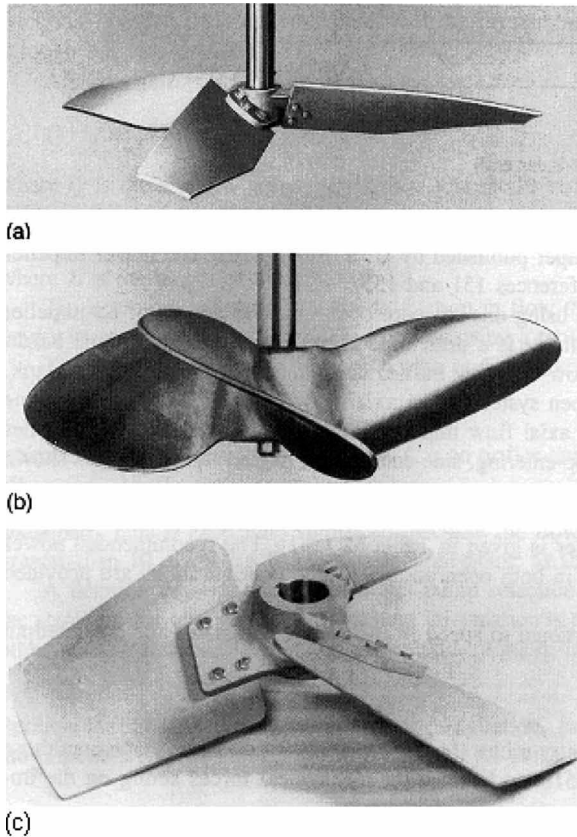
Fig. 12—Types of impellers: (a) high-efficiency airfoil-type impeller; (b) marine propeller; (c) side-entering mixer impeller.
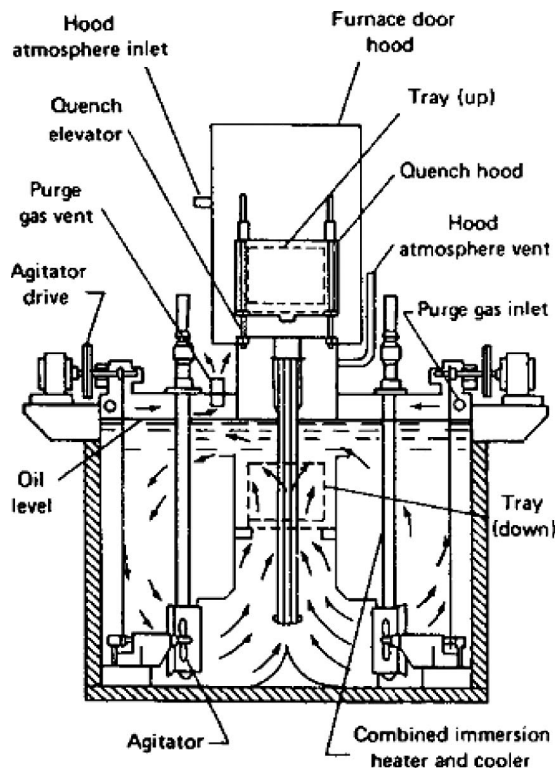
ensure that the total mechanical design of the mixer is safe for operation without a steady bearing. The manufacturer will supply dimensions for the limit ring.

• The impeller normally requires a radial clearance of 25 to 50 mm (1 to 2 in.) between the blade tips and the draft tube. If the size of the draft tube must be minimized, an external notch can be used to reduce the draft-tube diameter by 50 to 74 mm (2 to 3 in.).

11.6 NEW WAYS OF INTENSIFYING PROCESSES OF HEAT TRANSFER DURING QUENCHING

In the previous sections, it has been shown that the optimal concentration of aqueous solutions of polymers and salts can be used for the implementation of intensive quenching methods. This section describes new ways of the intensification of processes of heat transfer during quenching, including the use of rotating magnetic fields and the use of a principle of discrete-impulse energy input. Below they are considered in detail.

11.6.1 The Discrete-Impulse Energy Input Process

The principal approach to the use of discrete-impulse energy input was developed by Dolinskiy and his colleagues [21–23] and lies in the following: Energy is injected into the system and transferred to every bubble of the biphase system. Oscillating bubbles, receiving the injected external energy, essentially create a turbulent flow and thus intensify the cooling processes.

For deeper understanding, consider Fig. 14. The system consists of a quench tank (1) filled with a quenchant; Laval nozzles (2 and 3); a built-in special device (4) that allows rotation of the nozzle upward and downward; and a cylindrical tube (5) connected with the nozzle and forming a type of "penny whistle." The closing and opening of a valve (8) is controlled automatically by means of software (10). Compressed air stored in a tank (9) is connected to the valve. The

Fig. 13—Batch-quenching system with side-entering impellers.
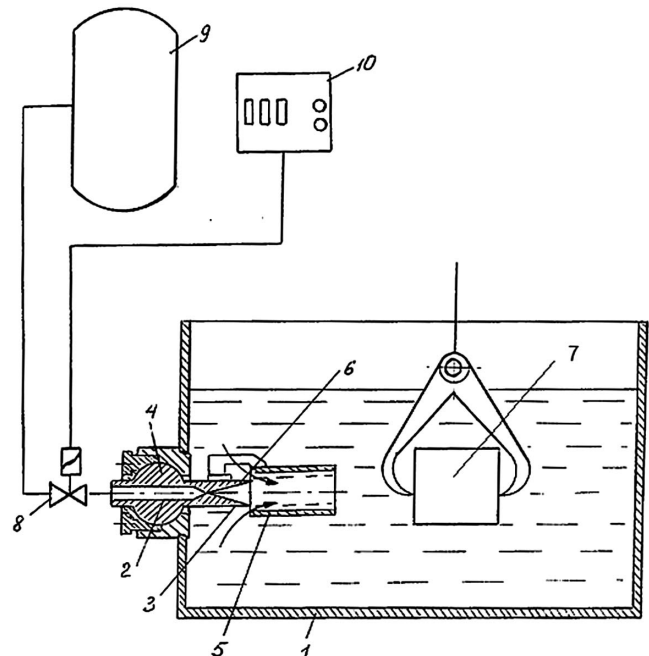
Fig. 14—Special tank for discrete-impulse energy input used for intensive quenching of steel parts [21,22]: 1, quench tank; 2 and 3, Laval nozzles; 4, rotation device; 5, cylindrical tube; 6, taped tube; 7, steel part; 8, valve; 9, compressed air storage tank; 10, computer controller.

valve is periodically turned on and off, forming at the outlet many oscillating bubbles, which provide an intensively turbulent quenchant flow at the surface of a part to be quenched [23]. The part is shown at the center of the tank in Fig. 14, fixed on a hook.

As an example, assume the part is a 220 by 230 by 360-mm bar made of AISI 4140 steel. The convection heat transfer coefficient has been experimentally determined to be 8,000 W/m²K. The objective of this example is to determine the cooling time of a part to be quenched from the austenitizing temperature of 1,550°F (843°C) to a core temperature of 700°F (371°C) at the center of the part.

First of all, determine Biot number Bi_V by the following equation:

$$Bi_V = \frac{\alpha}{\lambda} K \frac{S}{V}.$$

The inputs are determined as follows:

$$K = \frac{1}{9.87 \left[\frac{1}{(0.22)^2} + \frac{1}{(0.23)^2} + \frac{1}{(0.36)^2} \right]} = 2.14 \cdot 10^{-3} m^2; \text{ and}$$

$$\frac{S}{V} = 2 \left(\frac{1}{a} + \frac{1}{b} + \frac{1}{c} \right) = 23.34.$$

Therefore,

$$Bi_V = \frac{8000 W/m^2 K}{23 W/m \cdot K} \cdot 2.14 \cdot 10^{-6} m^2 \cdot 23.34 \approx 17.97.$$

This is equivalent to condition that $Bi \to \infty$. Therefore, the convective flow is immediate, in this case $Kn = 0.96$.

Now calculate the cooling time of the part from temperature of 1,550°F (843°C) to 700°F (371°C) in conditions, when $\alpha_{conv} = 8,000$ W/m²K or $Kn = 0.96$. Using the generalized dependence, Eq 69, yields:

$$\tau = \left[0.48 + \ln \frac{1550°F - 68°F}{700°F - 68°F} \right] \frac{2.14 \cdot 10^{-3} m^2}{5.5 \cdot 10^{-6} \cdot 0.96}$$

$$= 539 \text{ sec or } 9 \text{ minutes}.$$

11.6.2 Use of Rotating Magnetic Fields

Fig. 15 presents a scheme for the use of a rotating magnetic field. The rotating magnetic field is formed by using the stator of a normal electric engine in which, instead of a rotor, parts to be quenched move along a circle of a cylindrical tank inserted into the stator. Parts to be quenched may be ball bearings or balls of spherical mills.

The IQ-2 process can be easily realized by this installation. At the first stage, balls are quenched in an aqueous solution of salts of optimal concentration, for example, 6–8 % sodium carbonate (Na_2CO_3). Balls revolve in the magnetic field until the end of nucleate boiling and are periodically pushed out to the conveyor, which delivers the balls from the quenchant to be self-tempered in air. At the second stage, the parts are washed and at the same time intensively cooled within the martensite range until they are completely cooled down. At the third stage, the parts are dried and tempered by means of induction heating. Heating to the austenitizing temperature can be performed by induction as well.

This is the primary scheme, although it may be implemented in different ways. The advantages of the described technology include the following:
- Magnetic fields improve the mechanical properties of material.
- Alternating magnetic fields result in the destruction of vapor films.
- The process becomes controlled and easily automated.

More particulars on this technology are described in [24].

Examples of designing the industrial processes with regard to this type of installation will now be provided.

Example 11.1

Balls made of AISI 52100 steel, with a diameter of 1 in. (25.4 mm), are cooled in a 6 % sodium carbonate solution from 860°C. The temperature of the quenching solution is 20°C. Balls move in the magnetic field at the speed of 0.5 m/s. The objective is to determine the duration of nonstationary nucleate boiling (self-regulated thermal process) so that, upon the completion of nucleate boiling, the balls are delivered to air cooling.

The Kondratjev number Kn for these conditions of cooling equals 0.6. The convection heat transfer coefficient for
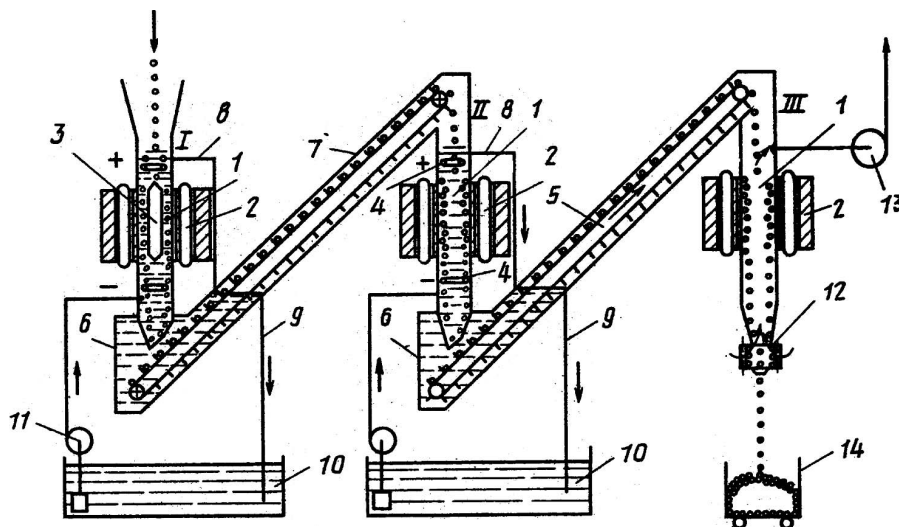
Fig. 15—Line for ball quenching controlled by an electromagnetic field [24].

a speed of 0.5 m/s is equal to about 2,900 W/m²K (see Table 6 in Chapter 10). The Kondratjev form coefficient $K = R^2/5.783 = 16.34 \times 10^{-6}$ m². The average thermal conductivity and thermal diffusivity of material during cooling from 860°C to 100°C are, respectively, 23 W/mK and 5.5×10^{-6} m²/s (see Tables 2 and 3 in Chapter 10).

For the calculation of the duration of nonstationary nucleate boiling, the generalized dependences of Chapter 2–Eqs 37 and 38–will be used. First of all, determine the superficial temperature at the beginning and at the end of nucleate boiling, that is, by computing values of ϑ_I and ϑ_{II}. From Eq 37, we obtain:

$$\vartheta_I = \frac{1}{7.36}\left[\frac{2 \cdot 23(760 - \vartheta_I)}{0.0127}\right]^{0.3},$$

which is valid if $\vartheta_I = 11.6$°C. Similarly, from Eq 38, we get:

$$\vartheta_{II} = \frac{1}{7.36}[2900(\vartheta_{II} + 80°C)]^{0.3}.$$

This equality is valid if $\vartheta_{II} = 5.6$°C.

Using these results, the cooling time is calculated:

$$\tau = \left[3 \cdot 0.24 + 3.21 \cdot \ln\frac{11.6}{5.6}\right]\frac{16.34 \cdot 10^{-6}m^2}{5.5 \cdot 10^{-6}m^2/s \cdot 0.6} \approx 15.2 \text{ sec.}$$

Therefore, the balls in the magnetic field must be rotated for 15 seconds, and then the magnetic field must be disconnected, allowing the balls to fall on the conveyor, which delivers them to air. In air, the balls are self-tempered, and then they come to the second site, where they are washed and completely cooled to room temperature. At the third site, the balls are dried and tempered by induction heating.

Calculations in all examples of this book are presented to illustrate for the reader the simplicity of the calculations, despite the complicated theory of Chapters 2 and 5, where the generalized calculation dependences were obtained that are used here.

11.7 SUMMARY

1. This chapter has presented specific examples of the use of generalized equations for designing manufacturing processes and industrial lines for quench cooling. The technique was developed for calculating conveyor speeds and rotational speeds of screw conveyors with the purpose of controlled cooling of parts to be quenched.
2. Examples explaining how to use the technique have been given.
3. It was shown that the cooling capacity of quenchants is characterized by the main parameter of quenching: Kondratjev number *Kn*.
4. Tables of numbers *Kn* for various quenchants, which form a database of initial data for specific calculations related to quench cooling, were presented. Results of calculations may be used by heat-treating engineers and designers dealing with industrial lines.

References

[1] Lyman, T., Ed., *Metals Handbook: 1948 Edition,* American Society for Metals, Cleveland, OH, 1948.

[2] Totten, G. E., Bates, C. E., and Clinton, M. A., *Handbook of Quenchants and Quenching Technology,* ASM International, Materials Park, OH, 1993.

[3] Kondratjev, G. M., *Teplovye Izmereniya* (Thermal measurements), Mashgiz, Moscow, 1957.

[4] Aronov, M. A., Kobasko, N. I., Powell, J. A., and Hernandez-Morales, J. B., Correlation between Grossmann H-Factor and Generalized Biot Number Bi$_V$, *Proceedings of the 5th WSEAS International Conference on Heat and Mass Transfer (HMT '08),* Acapulco, Mexico, January 25–27, 2008, pp. 122–126.

[5] Hasson, J., Quench System Design Factors, *Advanced Materials & Processes,* Vol. 148, No. 3, 1995, pp. 42S–42U.

[6] Kobasko, N. I., Method of Hardening of Alloy Steels, Ukraine Patent No. 27059, Filed February 17, 1995 under No. 95020715, printed February 28, 2000, Bulletin No 1, Kyiv, Ukraine.

[7] Kobasko, N. I., *Steel Quenching in Liquid Media Under Pressure,* Naukova Dumka, Kyiv, 1980.

[8] Liščič, B., Tensi, H. M., and Luty, W., *Theory and Technology of Quenching,* Springer-Verlag, Berlin, 1992.

[9] Totten, G. E., and Howes, M. A. H., *Steel Heat Treatment Handbook,* Marcel Dekker, New York, 1997.

[10] Kovalenko, G. V., Kobasko, N. I., and Khalatov, A. A., Method of Steel Quenching, Inventor's Certificate 1,355,634 (USSR), *Bulletin of Inventions,* No. 44, 1987.

[11] Kobasko, N. I., Thermal Processes During Steel Quenching, *Metal Science and Heat Treatment,* No. 3, 1968, pp. 2–6.

[12] G. Totten, M. Howes, and T. Inoue, Eds., *Handbook of Residual Stress and Deformation of Steel,* ASM International, Materials Park, OH, 2002.

[13] Kobasko, N. I., and Nikolaev, E. D., Study of Cooling Capacity of Oils MS-20 and I-50. *Technology and Organization of Production,* No. 2, 1977, p. 78.

[14] Tkachuk, T. I., Rudakova, N. Ya., Sheremeta, B. K., and Al'tshuler, M. A., Influence of component composition of quenching oils on the cooling intensity in the bubble boiling period, *Metal Science and Heat Treatment,* No. 10, 1986, pp. 45–47.

[15] Tkachuk, T. I., Rudakova, N. Ya., Sheremeta, B. K., and Novoded, R. D., Possible means of reducing the film period of boiling in hardening in petroleum, *Metal Science and Heat Treatment,* No. 10, 1986, pp. 42–45.

[16] Daming, M., Intense Quenching Method for Preventing Quench Cracking, *Proceedings of the Seventh International Congress on Heat Treatment and Technology of Surface Coating,* December 11–14, 1990, Vneshtorgizdat, Moscow, Vol. 2, pp. 62–71.

[17] Kobasko, N. I., Quenching Apparatus and Method for Hardening Steel Parts, U.S. Patent No. 6,364,974 BI, April 2, 2002.

[18] Ganiev, R. F., Kobasko, N. I., Kulik, V. V., et al., *Vibration Phenomena in Multiphase Media and Their Application in Technology,* Tekhnika, Kyiv, 1980.

[19] Ganiev, R. F., Kobasko, N. I., and Frolov, K. V., On Principally New Ways of Increasing Metal Part Service Life, *Doklady Akademii Nauk* (USSR), Vol. 194, No. 6, 1987, pp. 1369–1373.

[20] Han, S. W., Kang, S. H., Totten, G. E., and Webster, G. M., Immersion Time Quenching, *Advanced Materials & Processes,* Vol. 148, No. 3, 1995, pp. 42AA–42DD.

[21] Dolinskiy, A. A., Kobasko, N. I., Korchinskiy, A. A., and Chayka, A. I., Apparatus for Quenching of Steel Parts, Inventor's Certificate No. 142521, *Bulletin of Inventions,* No. 7, 1988.

[22] Dolinskiy, A. A., Kobasko, N. I., Korchinskiy, A. A., and Chayka, A. I., Setup for Quenching Parts, Inventor's Certificate No. 1,425,221 (USSR), *Bulletin of Inventions,* No. 35, 1988.

[23] Dolinskiy, A. A., Kobasko, N. I., Korchinskiy, A. A., Chayka, A. I., and Garvich, A. P., Setup for Quenching Parts, Inventor's Certificate No. 1,574,648 (USSR), *Bulletin of Inventions,* No. 24, 1990.

[24] Satanovskiy, A. L., Kobasko, N. I., and Khalatov, A. A., Steel Quenching Method and Setup for Its Implementation, Inventor's Certificate No. 1,627,574, *Bulletin of Inventions,* No. 6, 1991.

12

Review of Practical Applications of Intensive Quenching Methods

M. A. Aronov,[1] N. I. Kobasko,[1] and J. A. Powell[1]

12.1 INTRODUCTION

In this chapter, different applications of intensive quenching (IQ) techniques on actual steel products, as well as on steel samples from the part manufacturers, are discussed. Two intensive water quenching methods were applied: the IQ-3 technique, also known as "direct convection cooling," and the IQ-2 technique, a three-step quenching process that initially cools parts under the nucleate boiling mode and then the convection heat transfer mode. Experiments were conducted for a variety of steel products, including automotive parts (coil springs, kingpins, torsion bars, bearing products, ball studs, etc.), fasteners of different types, and tool products (punches, dies, die components, etc.).

For intensive quenching of steel parts, different IQ systems were used. These systems are installed at the Center for Intensive Quenching in Akron, Ohio, and production IQ equipment is also installed at three commercial heat-treating shops.[2] Sections below summarize the test data obtained during the last several years and presented in numerous papers at different heat-treating conferences and forums [1−12]. Prior to discussing these results, however, let us review the relationship between the quench cooling rate and hardened part mechanical properties, and then we will examine the quenching equipment used for the IQ demonstration studies.

12.2 QUENCH COOLING RATE AND PART MECHANICAL PROPERTIES

Metallurgists know that the higher the cooling rate during the quench process, the better the mechanical properties of the steel parts (hardness, hardened depth, tensile and impact strength, etc.) will be. On the other hand, with conventional quenching methods (in water, polymer, oil, or gas), the higher the cooling rate, the more difficult it is to maintain uniform cooling around the part surface, and, therefore, the higher the probability of part distortion or even cracking will be. Therefore, heat treaters have always struggled for a balance between a high quenching rate for its better part properties and a more moderate quenching rate to reduce the probability of part distortion or cracking. With intensive water quenching techniques, the heat treater can have both−better part properties *and* low distortion.

Fig. 1 shows the correlation between part properties and the cooling rate of the part for both conventional quenching and intensive quenching. The curve "breaks" between the conventional and intensive quenching zones. This break illustrates that, in conventional quenching, the part starts experiencing severe distortion (or the ultimate in distortion: cracking) above a certain cooling rate. At that point, it is useless to quench faster in an attempt to obtain any further "improvements" in the steel's mechanical properties on a distorted or broken part.

As also shown in Fig. 1, in the IQ zone, a part's mechanical properties are not only greater compared to the conventional quench zone, but they continuously increase up to a certain "ultimate" level for the given steel type. Once in the intensive quench zone, a faster quench rate on the part surface does not improve the part's properties. This is because at the initiation of the intensive quench, the part's surface temperature almost instantaneously becomes the same as the quenchant temperature. Said another way, after a certain intensity of quench heat extraction, the part cannot give up its heat any faster than the rate of heat conduction through the part. This is why one cannot quench "too fast" during the intensive portion of the quench. Once the part surface layer has reached the temperature of the quenchant, conduction within the part sets a natural limit on the rate of cooling in the subsurface layers and the core of the part. Since conduction is also a very rapid and very uniform form of heat removal, intensive quenching is able to reach the ultimate goal of any quench–the most uniformly rapid removal of heat that yields the least part distortion.

Now, let's consider separately the IQ-2 and IQ-3 quench rate zones shown in Fig. 1. The IQ-2 quenching method is characterized by the nucleate boiling mode of heat transfer on the part surface during the intensive period of the quench. With IQ-2, the film boiling stage is completely absent due to the presence of negative ions in the water-salt solutions used as quenchants and the high (intensive) quenchant agitation rate. In addition, using different water-salt solutions and different rates of agitation, one can control the cooling rate of the part. For example, a water−calcium chloride solution provides a greater intensity of the heat extraction compared to a water−sodium nitrite solution. Special proprietary additives to water-salt solutions can also control the cooling rate of the part. All IQ-2 quenching demonstrations were conducted using a low concentration of sodium nitrite in tap water with no other additives. Therefore, the part properties improvements were not necessarily the maximum achievable for this quenching technique [1−4].

Note that the IQ-2 process is usually conducted in three steps. First, the parts are introduced into the intensively agitated quench. After a certain period of time calculated by the IQ software, the intensive quench is interrupted and the parts continue cooling in the air. At this time, the heat

---

[1] *IQ Technologies, Inc., Akron, Ohio*
[2] Akron Steel Treating Co. of Akron, Ohio; Euclid Heat Treating Co. of Cleveland, Ohio; and HighTemp Furnaces, Ltd., of Bangalore, India.

185
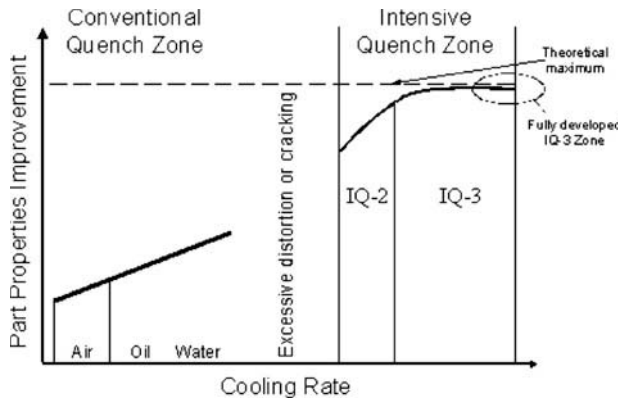
Fig. 1—Steel part properties vs. cooling rate.

coming from the part core tempers the martensitic surface layer (formed during the first step of quenching) and gives the strong surface shell some ductility (tempered martensite). Then, the parts are returned to the intensive quench to complete the phase transformation of the steel in the core.

While the IQ-2 quenching process provides parts with much better properties compared to conventional quenching in water, oil, or air, the ultimate values of steel mechanical properties can be obtained only with a fully developed IQ-3 quenching rate of direct convection cooling. With direct convection cooling, there is no film boiling, and very little, if any, nucleate boiling around the part. The IQ-3 method is said to be "fully developed" IQ-3 quenching when the water flow around the part provides the optimum heat transfer conditions–direct convection cooling–and achieves the highest values for the part's mechanical properties (for the given steel type). Conversely, when as-quenched part properties are below their ultimate values for a given steel type (see Fig. 1), we refer to the IQ-3 method as not being fully developed.

12.3 INTENSIVE QUENCHING AND PART DISTORTION
12.3.1 General Considerations
While there are hundreds of contributing factors for part distortion in the heat treating process, every heat treater knows that part geometry and nonuniform quench cooling are two of the major reasons for part distortion (or cracking) during quenching. Any part distortion that is the same (from quench to quench and from part to part), primarily caused by the part shape, we will categorize as *predictable* or *repeatable* distortion. On the other hand, nonuniform quench cooling will generally cause *unpredictable* distortion. The root cause of this unpredictable distortion is the nonuniform and uncontrollable (and hence unpredictable) cooling from film boiling that usually surrounds the part in the critical early stages of any (traditional) liquid quenching from the austenitizing temperature.

12.3.1.1 DISTORTION DUE TO PART GEOMETRY
If the part has a complex geometry with widely variable thickness, it will distort during quenching even if the heat extraction rate is uniform over the entire part surface area. This is happening, first, because of a nonuniform thermal shrinkage of steel prior to the beginning of the phase transformations and, second, because of a nonuniform expansion of the material due to nonuniform martensite formation

throughout the part. The thin sections of the part cool faster and contract more than the part's thicker sections, inducing thermal stresses and causing plastic deformations in the thick sections. The same happens with the transformation of austenite into martensite: the martensitic transformations take place first in the thin sections of the part and later in the thick sections, regardless of the method of quench cooling on the surface or its uniformity. During phase change, the thin section of the part will swell due to the greater specific volume of the martensite; this swelling during phase change induces internal stresses in the thick sections (which are still hot and plastic) and causes part distortion. However, if the quench cooling rate on the outside of the part is uniform from quench to quench, the distortion due to the part's geometry should be relatively the same each time the part is quenched–again, assuming the part is quenched in a uniform manner. Proper adjustment of the part's "green" size before heat-treating may compensate for this repeatable distortion for the finished part.

12.3.1.2 DISTORTION DUE TO NONUNIFORM COOLING
In practice, it is virtually impossible to provide uniform cooling over the entire part surface area, especially when quenching parts in batches. However, depending on the mode of heat transfer realized during quenching, the distortion caused by nonuniform cooling can be repeatable, too. Let's consider three possible scenarios for the heat transfer modes during quenching:
1. Direct convection cooling
2. Nucleate boiling followed by convection heat transfer
3. Film boiling followed by nucleate boiling and then convection heat transfer

Direct convection cooling takes place when quenching parts intensively in a high-velocity, single-part IQ system, or when quenching relatively large parts (with a thickness of more than about 6 in./150 mm) in an IQ batch water tank. In this case, the boiling process is fully eliminated. The convective mode of heat transfer starts from the very beginning of the quench process.

The heat extraction rate by convection depends on the water flow velocity at the surface of the part and on the water temperature. Note that the water temperature in IQ water tanks is very uniform throughout the tank due to the high ("intensive") quenchant agitation rate. This is in contrast to conventional oil quenching, where the temperature gradient in the quench tank may be significant, especially at the beginning of the quench: relatively slow-moving, thick-viscosity oil does not mix in the quench tank as vigorously as the water mixes in the intensive quench tank.

Assume that the quenchant flow velocity distribution across a quench chamber or a quench tank in the IQ unit is always uniform and does not change from quench to quench for a given part or a load. (Since the quenchant is water, the intensive quench system uniformity can be achieved by maintaining the pump or prop flow rate/amp draw rate; the water temperature; proper baffling of the water flow; proper racking, spacing, and orientation of the parts; etc.) The quenchant velocity may vary from one section of the part to another, but the heat extraction rate distribution will be the same every time for each part in a given load. A nonuniform heat extraction rate throughout the part surface will inevitably result in part distortion. However, this

distortion will be repeatable from load to load as long as the water flow patterns in the tank remain the same.

Note that in the above considerations, we assumed a uniform distribution of water flow velocity throughout the load. In reality, there will always be variations in heat transfer coefficients from part to part throughout a particular load in batch quenching. The water temperature also changes, rising along its way through the load. Due to these variations, the part distortion varies throughout the load, too. But with a proper tank design and correct part racking, these distortion variations can be minimized to an acceptable level. In general, convection heat transfer in water is a quite stable process, depending on factors that can be relatively easily controlled (e.g., the water flow velocity and water temperature).

The second scenario is *nucleate boiling followed by convection heat transfer*. When quenching parts in an IQ tank, the water flow velocity may not be high enough to eliminate the boiling process at the very beginning of the quench. However, a high water agitation rate and the addition of mineral salts to the water can be often used to fully eliminate the nonuniform film-boiling mode of heat transfer and to insure that the nucleate boiling process starts from the very onset of the quench.

Similar to direct convection, nucleate boiling is a very stable mode of heat transfer and therefore a uniform process. The duration of nucleate boiling on the part's surface depends on several factors: the part cross-sectional thickness, the initial part surface temperature, local water flow velocities (convective heat transfer coefficients), and water temperature. However, in contrast to the direct convection cooling that takes place throughout the entire part surface area and over the entire quench period, nucleate boiling may appear only on certain sections of the part. This is because the duration of nucleate boiling will be different depending on the thickness of various part sections.

The heat extraction rate and its distribution throughout the part surface area during the nucleate boiling mode of heat transfer (and during the following convective heat transfer) will affect the rate of martensite formation in the parts. However, if the water temperature and water flow dynamics do not change from load to load, the parameters of the nucleate boiling and convective heat transfer processes will be the same in every quench. Therefore, as with direct convection cooling, nucleate boiling can result in predictable, repeatable part distortion.

The third scenario is *film boiling followed by nucleate boiling and then convection heat transfer*. If at the very beginning of the quench, the initial heat flux from the part surface is very high, the rate of steam bubble formation on the part surface becomes so great that the bubbles merge, creating a vapor blanket, and a film boiling process begins. The heat flux required for the initiation of the film boiling process is called the *first critical heat flux density* or q_{cr1}. Note that at the beginning of quenching, the initial heat flux is greater from the thin sections of the part than from the thicker sections. Therefore, the film boiling process takes place first on the surface of thin sections of the part and as a consequence causes more distortion in these thin sections (e.g., long, thin gear teeth). This phenomenon may appear counterintuitive, but it can be explained as follows.

At the very beginning of the quench, the part surface temperature starts dropping drastically due to the heat transfer from the hot part to the liquid quenchant flowing along the part surface. The temperature of the quenchant layers adjoining the part rises almost instantly to the boiling point of the quenchant. It is intuitively clear that during this very short period of time, the surface temperature of the thin section of the part decreases more than that of the part's thick section. However, during this initial time in the quench, the core temperature of both the thick and thin part sections does not substantially change and remains about equal to the temperature when the part entered the quenchant (the austenitizing temperature). Thus, at the beginning of the quench, the temperature gradient is greater in thin sections of the part compared to that in thick sections (the temperature gradient is equal to a ratio of the temperature difference to the part thickness).

According to Fourier's law, the heat flux from the part surface is directly proportional to the temperature gradient throughout the part cross-section. Because the temperature gradient is greater in thin sections of the part at the very beginning of the quench, the initial heat flux from the surface of the part's thin sections is greater than the heat flux from the surface of the part's thick sections. That is why the film boiling process begins first on the surface of the part's thin sections. Of course, very soon thereafter film boiling (and then nucleate boiling) will also begin on the surface of the thicker sections. As a practical matter, it appears that the vapor blanket engulfs the entire part from the very beginning of the quench.

Note also, that, in contrast to nucleate boiling, the film boiling mode of heat transfer is rather sporadic and unstable. Film boiling usually begins on different spots of the part surface, sporadically creating local vapor blankets. Depending on the quenchant properties (boiling temperature, surface tension, viscosity, etc.) and quench flow rate, these vapor blankets can merge or they can move erratically over the part's surface until the surface cools and the heat flux from the part is not capable of supporting film boiling any more. At this point, the nucleate boiling mode will begin, and once the heat flux from the part surface cannot support nucleate boiling any more, convection cooling will take over as the dominant mode of heat transfer.

The vapor blanket created by the film boiling process insulates the part surface from direct contact with the liquid quenchant, resulting in a relatively low heat transfer coefficient under the vapor blanket during this stage of quenching. The part areas affected by film boiling may experience a slack quench or a delay of the martensite transformations. Both the slack quench and the delayed martensite formation in differing areas of the part may cause an increase in overall part distortion. Since the film boiling process is not predictable, the distortion resulting from film boiling is not predictable, either. Thus, the presence of film boiling creates nonrepeatable part distortion. Conversely, the elimination of film boiling with intensive quenching will reduce part distortion.

12.3.2 Distortion Study on a Keyway Shaft

It is an experimental fact that the IQ process provides less part distortion than conventional oil quenching. In other words, the distortion of a part that was uniformly quenched in oil would be greater than the distortion of the same part quenched intensively in water. The reason for this is a uniform formation of the martensitic layer throughout the entire part surface area and development of high current

Fig. 2—Keyway shaft.
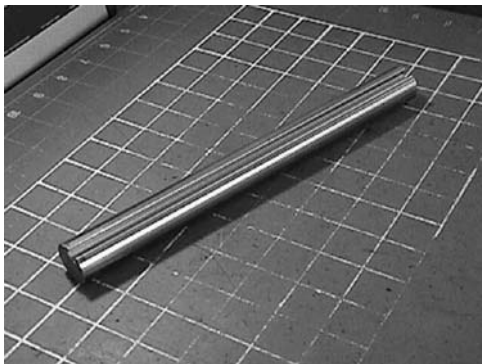
Fig. 3—Keyway shaft distortions.

surface compressive stresses during the IQ process. Both the uniform martensitic layer and high surface compressive stresses reduce the part distortion compared to conventional oil quenching, where the formation of the martensite is not as uniform and the surface compressive stresses are smaller.

To investigate the effect of intensive quenching on part distortion, an experimental study with a set of shafts with a keyway going through the entire shaft length (see Fig. 2) was conducted [7]. The shafts were made of AISI 1045 steel bars of 25.4 mm (1 in.) in diameter and of 254 mm (10 in.) in length. A nominal chemical composition of AISI 1045 steel is 0.43–0.50 % carbon and 0.6–0.9 % manganese. The shafts were ground and polished to within ±0.025 mm (0.001 in.). The keyway size was 6.4 × 6.4 mm (1/4 in. × 1/4 in.). This configuration of part was chosen because of its inclination to distort during quenching. The reason for the part distortion is that martensite forms first along the sharp keyway faces, since these thin sections of the part cool faster to the martensite start temperature. These sections of the part then expand due to the greater specific volume of the martensite (compared to austenite), causing bending in the still-plastic austenite in the core and in the solid wall of the shaft opposite the keyway side.

The shafts were austenitized in a neutral salt bath furnace, then quenched piece by piece, under two different conditions: four shafts were quenched in an open oil tank with "normal" agitation at 27°C (80°F), and four other shafts were quenched in a fast-flowing water stream at 24°C (75°F) using the IQ-3 quench method. A set of eight shafts was also quenched in an integral quench furnace in moderately higher agitated oil. The shafts were placed in various locations within a production load. The oil temperature was 66°C (150°F). As-quenched shaft hardness was measured after oil quenching or intensive quenching.

The intensively quenched shafts proved to have both greater surface hardness and core hardness (see Table 1). For example, intensive quenching improved the core
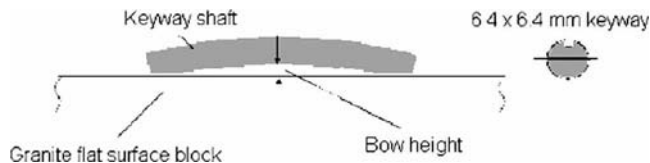
hardness in the 1-in.-diameter (25.4 mm) 1045 bar by about 60 % compared to oil quenching.

To evaluate as-quenched shaft distortion, the parts were placed on the certified flat granite surface block. The height of the shaft bow was measured by using feeler gauges (see Fig. 3); the accuracy of the gauges was ±0.025 mm (±0.001 in.). Table 2 presents the distortion data obtained. As seen from the table, intensive quenching caused much less shaft distortion than did conventional oil quenching.

A finite-element heat-treating-process computer model was used for the detailed comparison of the formation of martensite and distortion in the keyway shafts during conventional and intensive quenching.[3] The model calculates the part temperature and the structural and stress-strain conditions during thermal processing based on the steel phase transformation kinetics, mechanical properties of the material, and heat transfer conditions. Two keyway shafts (one oil quenched and one intensively quenched) were subjected to detailed microstructure and distortion analysis. The results of this analysis were used to compare experimental data with computer simulations.

Figs. 4 and 5 present the temperature and structural changes over time for oil-quenched and intensively quenched keyway shafts, respectively. Figs. 6 and 7 show the dynamics of the stress conditions in the keyway shafts.

As seen from Fig. 4, the temperature lag from the part's core to its surface prior to the martensite transformation is only 30°C in the oil-quenched keyway shaft. This small temperature gradient results in practically simultaneous phase transformation in the surface layer and the core and in minimal austenitic core shrinkage prior to martensite transformation in the core. During intensive quenching, on the other hand, the keyway shaft temperature lag from core to surface is about 500°C prior to the start of martensite transformation. This temperature gradient causes significant austenitic shrinkage of the part's core prior to the start of the martensite transformation in the core, which compensates the subsequent expansion under the surface while transforming into martensite.

As seen from Figs. 6 and 7, within the martensite transformation range (325°C down to 110°C), the current compressive surface stresses (during the IQ process) are much

TABLE 1—Keyway surface and core hardness		
Type of quenching	Surface	Core
Single part oil quenching	53.2 RC	32.1 RC
Batch oil quenching	51.4 RC	31.0 RC
Intensive quenching	57.4 RC	50.0 RC

TABLE 2—Keyway distortion measurements	
Type of quenching	Distortion
Single part oil quenching	0.20–0.36 mm (0.008–0.014 in.)
Batch oil quenching	0.25–0.51 mm (0.010–0.020 in.)
Intensive quenching	0.08–0.12 mm (0.003–0.005 in.)

[3] The study was conducted by Deformation Control Technology, Inc., of Cleveland, Ohio, using its DANTE (Distortion Analysis for Thermal Engineers) software.
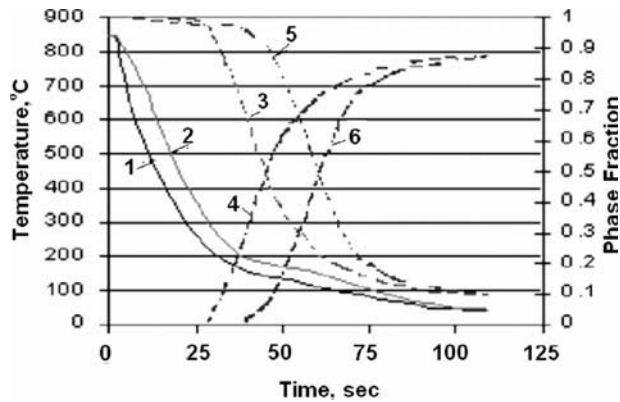
Fig. 4—Keyway shaft temperatures and microstructure (oil-quenched): 1, surface temperature; 2, core temperature; 3, austenite vs. time at the surface; 4, martensite vs. time at the surface; 5, austenite vs. temperature at the core; 6, martensite vs. time at the core.
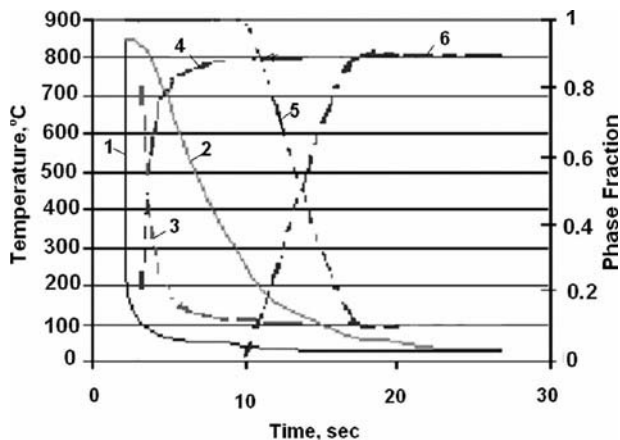
Fig. 5—Keyway shaft temperatures and microstructure (intensively quenched): 1, surface temperature; 2, core temperature; 3, austenite vs. time at the surface; 4, martensite vs. time at the surface; 5, austenite vs. time at the core; 6, martensite vs. time at the core.
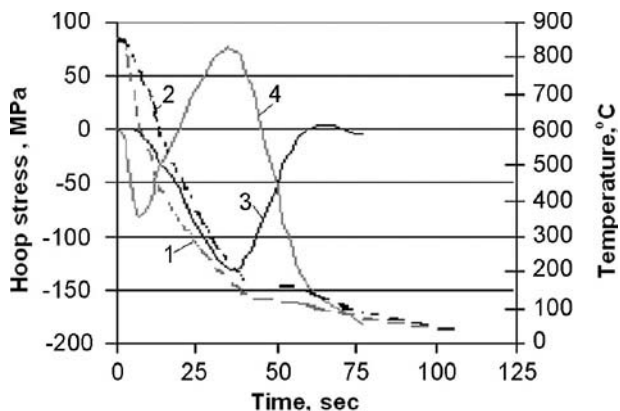
Fig. 6—Keyway shaft stress conditions (oil-quenched): 1, surface temperature; 2, core temperature; 3, hoop stress vs. time at the surface; 4, hoop stress vs. time at the core.

greater than those during the conventional oil quench. Also, the surface residual stresses in the oil-quenched keyway shaft are neutral at the end of quenching, while those in the IQ keyway shaft are compressive (about −100 MPa). As mentioned
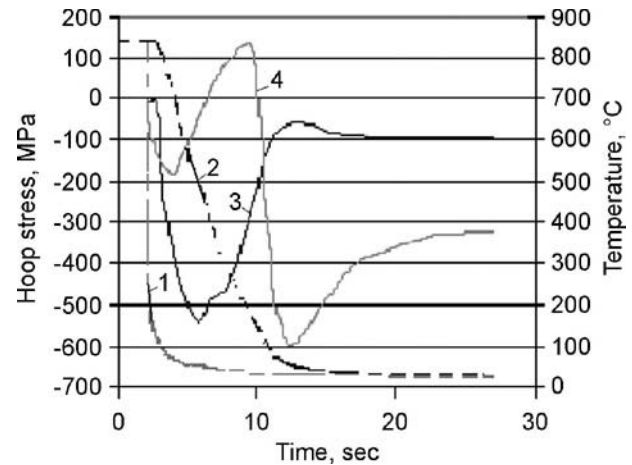
Fig. 7—Keyway shaft stress conditions (intensively quenched): 1, surface temperature; 2, core temperature; 3, hoop stress vs. time at the surface; 4, hoop stress vs. time at the core.

above, high current surface compressive stress is one of the reasons why there is less distortion after intensive quenching.

Table 3 presents experimental data and the results of computer simulations of part structural conditions, hardness, and distortion. As seen from the table, the computer model predicted the keyway shaft microstructure, hardness, and distortion very accurately.

Fig. 8 presents the microstructure in the core of the oil-quenched and intensively quenched keyway shafts. As can be seen, there is a coarse martensite/bainite structure in the core of the oil-quenched keyway shaft and a fine martensite structure in the core of the IQ keyway shaft, which is in agreement with the results of computer simulations.

12.4 INTENSIVE QUENCHING EQUIPMENT USED FOR IQ DEMONSTRATION STUDIES

Two types of IQ equipment were used for IQ trials with actual steel parts: single-part, high-velocity quenching systems; and batch-type quenching units. Single-part quenching systems are characterized by a very high water-flow velocity along the part surface. Usually, no boiling occurs during quenching in this type of IQ equipment–direct convection cooling takes place from the very beginning of the quench. By contrast, in batch-type IQ equipment, quenching starts with a period of boiling on the part surface, followed by convection heat transfer.

12.4.1 Single-Part Quenching IQ Systems

For IQ process demonstrations, two experimental high-velocity IQ systems were used and are described below.

The first experimental high-velocity IQ system (see Fig. 9) includes a 1.9-m^3 (500-gallon) quench tank with a U-shaped tube placed inside the tank. There is a propeller on the one end of the U-tube, rotated by a variable-speed motor. The propeller moves the water from the tank through the U-tube and back into the tank with a velocity of up to 2.5 m/s. There is a loading/unloading mechanism on the other leg of the U-tube that has a diameter of Ø27 cm. The hot part being quenched is placed on the loading/unloading mechanism platform or on the hook and is lowered into the U-tube. A low-concentration sodium nitrite solution in the water was used as the quenchant in this system. Depending on the part size and the propeller speed, this system could

TABLE 3—Keyway shaft experimental and calculation data on distortion, hardness, and microstructure

Parameter	Oil-quenched		Intensively quenched	
	Predicted	Measured	Predicted	Measured
Distortion (mm):				
End diameter	25.32	25.38	25.37	25.40
Middle diameter	25.28	25.37	25.33	25.36
End groove width	6.37	6.39	6.29	6.22
Middle groove width	6.36	6.34	6.33	6.34
End groove depth	5.95	5.97	5.95	5.94
Middle groove depth	5.92	5.92	5.95	6.10
Bow/flatness	0.87	0.89	0.098	0.64
Hardness (HRC)	55–57	53–54	59–60	61–63
Microstructure	81–89 % martensite with mix of pearlite and bainite	Coarse martensite and bainite mixture	89–90 % martensite	Fine martensite with small amount of retained austenite

implement either the IQ-2 or IQ-3 quenching method. Steel parts were austenitized in a neutral salt bath furnace (51 cm in diameter and 61 cm deep) capable of heating parts up to 927°C (1,700°F).

The second experimental high-velocity IQ system was specifically designed for the implementation of the IQ-3

(a) Oil quenched sample, 1000x   (b) Intensively quenched sample, 1000x

Fig. 8—Keyway shaft core metallography (oil and IQ).
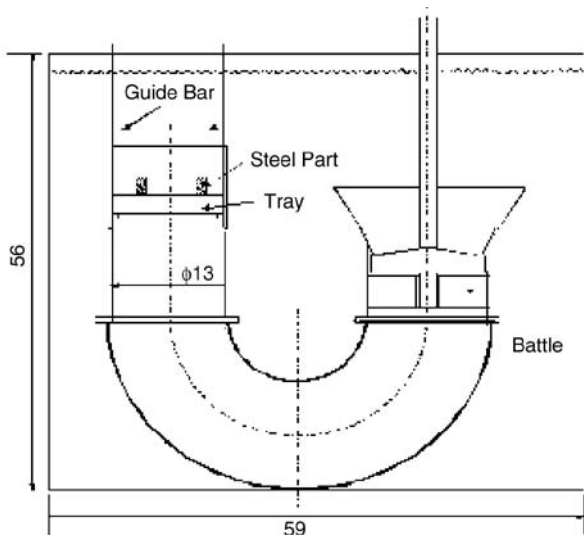
Fig. 9—Experimental 500-gallon IQ system.

quenching process. It differs from the first 500-gallon IQ system by the ability to provide very high water-flow velocity along the part being quenched (up to 20 m/s). The system is able to provide optimum, fully developed IQ-3 quenching conditions for a variety of steel products. The system is capable of intensively quenching steel parts up to 15 cm in diameter and up to 40 cm in length.

Fig. 10 presents a schematic of the second system, while Fig. 11 is a photograph of it. The IQ-3 system consists of the following major components: a water tank (1) of about 3-m^3

Fig. 10—High-velocity experimental IQ system sketch: 1, water tank; 2, pump; 3, stationary upper section of the vertical quench chamber; 4, movable lower section (loading table) of the quench chamber; 5, air cylinders; 6, part to be quenched; 7 and 8, water lines; 9, three-way valve; 10, actuator; 11, control valves; 12, flow meters.

Fig. 11—High-velocity IQ system.

(800-gallon) capacity; a pump (2) with a capacity of about 0.0378 m³/s (600 gpm); a vertical quench chamber that consists of two sections, a stationary upper section (3) and a movable lower section (loading table); four air cylinders (5) that move the loading section (4) up and down with the part to be quenched (6); three water lines, two (7 and 8) that provide the water flow through the quench chamber and one "bypass" water line (not shown on the sketch) that is used in "idle" conditions (immediately before or after the intensive quenching is done); a three-way valve (9), with actuator (10), that provides water flow from the pump either through the quench chamber or through the bypass line; and two control valves (11) and two flow meters (12) installed on the water lines leading to the quench chamber and used for controlling the water flow.

The parts to be quenched in the IQ-3 system are austenitized in a salt bath furnace located next to the quench system. (In practice, any through-heating source may be used for austenitizing the parts: induction, fluid bed, or atmosphere.)

The IQ-3 quench sequence is as follows. With the pump operating and the three-way valve in the bypass position, an austenitized part is placed in the lower section of the quench chamber. The air cylinders move the lower section up to the stationary upper section and lock (seal) the quench chamber in place. The three-way valve switches from the bypass to the quench position, and high-velocity water starts flowing through the quench chamber and over the part. When intensive quenching is completed, the three-way valve switches back to the bypass position, and the water stops flowing through the quench chamber and instead flows through the bypass line. The air cylinders open the quench chamber by moving the lower section down. The part is then removed from the quench chamber lower section.

Note that when the system is in quenching mode, the water flow may be split in two flows after passing the three-way valve. Shutoff valves and a flow meter control each water flow path. The reason for this is that, when quenching bearing rings, it is necessary to control water flows along both the rings' inner-diameter and outer-diameter surfaces. When quenching cylindrical parts (for example, shafts or pins), only one water flow is needed, and therefore one of the above shutoff valves is closed.

One of the key elements of quenching parts in the high-velocity IQ system is providing a uniform water flow along the entire part surface area. No stagnation zones are allowed, since the nonuniformity of cooling could result in local film boiling, which, in turn, can cause excessive part distortion or even cracking. Fluid-dynamics computer simulations can be used to determine the optimum fixture design that provides uniform water flow and heat extraction rate for parts to be quenched in the high-velocity IQ system.

A CFD (computational fluid dynamics) analysis was used for optimizing the quenching process of a helicopter test gear.[4] To intensively quench the gear, the water comes into the quench chamber through a round slot around the outer-diameter gear teeth, and impinges directly on the root area of the gear. After cooling the root of the gear teeth, the water flow splits in two–the continued downward water flow and a reflected upward flow–and then leaves the quench chamber through the gear bore. The fixture provides uniform cooling of the test gear with the required "intensive" heat extraction rate.

12.4.2 Batch-Type IQ Equipment

Two types of IQ units were also used for batch IQ trials: one system equipped with a stand-alone IQ water tank and the other with an IQ structure integrated within the furnace chamber. Fig. 12 presents a schematic of the full-scale production batch-type IQ system.[5] The system includes a radiant tube, an atmosphere furnace having a work zone of 91 by 91 by 122 cm (36 by 36 by 48 in.), and a stand-alone IQ quench tank of 22.7 m³ (6,000 gallons). To ensure that quenchant vapor does not contaminate the furnace atmosphere, a 2.5-m (98-in.) aisle separates the furnace and the quench tank. A cart is used to move the load from the furnace to the quench tank. A fast rear handler mechanism transfers the load from the furnace to the IQ tank in about 10−15 s, minimizing the heat losses by the load during transfer. (Transfer time considerations are no different than in any proper oil
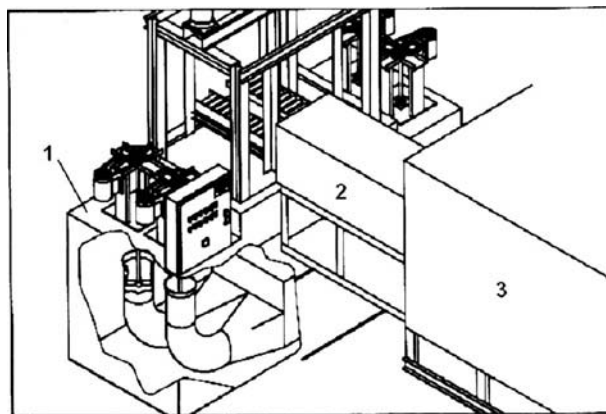
Fig. 12—Diagram of production 6,000-gallon IQ system: 1, quenching system equipped with propellers; 2, load charge car; 3, radiant tube atmosphere batch furnace.

---

[4] Fluid-dynamics computer simulations were conducted by the Air Flow Science Corp. of Livonia, Michigan.
[5] The system is installed at Akron Steel Treating Co. of Akron, Ohio.
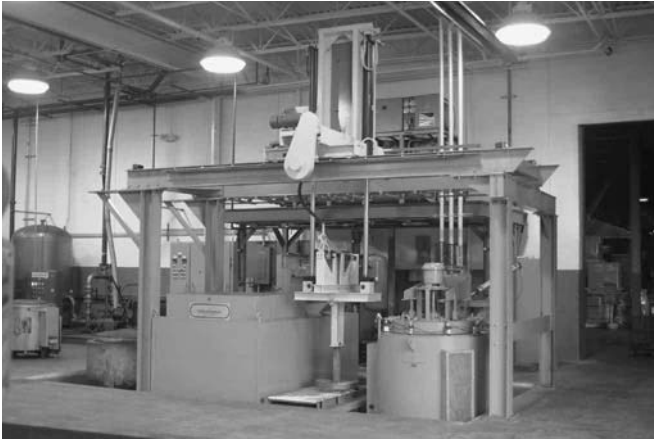
Fig. 13—Fully automated IQ system equipped with a 7.2-m³ IQ water tank, electric atmosphere furnace, and transfer mechanism capable of quenching loads of up to 500 kg.

or air quench practices—the parts must be austenitic when they enter the quench.) The mild steel IQ tank is equipped with four propellers that are rotated by four motors. The tank uses a water–sodium nitrite solution of low concentration (8–10 %) as the quenchant. The quenchant flow velocity in the tank is about 1.5 m/s (5 ft/s) as it passes over the parts. An air-cooling system maintains the quenchant temperature within the required limit. The production IQ system is designed for quenching loads of up to 1,135 kg (2,500 lb).

Fig. 13 presents a photograph of another batch-type IQ unit equipped with a stand-alone IQ water tank. This is a fully automated IQ system installed at the Center for Intensive Quenching in Akron, Ohio. The system includes a pit-type atmosphere furnace, a stand-alone 7.2-m² (1,900-gallon) IQ water tank, and a transfer mechanism to move the load from the furnace into the IQ tank.[6]

Fig. 14 shows a production model of a 91 by 91 by 182-cm (36 by 36 by 72-in.) integral quench atmosphere furnace equipped with an IQ water quench tank of 41.6 m³ (11,000 gallons).[7] The furnace is equipped with an intermediate chamber connecting the heating chamber with the IQ tank

to ensure that quenchant vapor does not contaminate the furnace atmosphere. The furnace atmosphere enters the intermediate chamber through two openings in the furnace door and leaves through the vent. The IQ tank is equipped with four propellers rotated by four motors and with a loading/unloading mechanism that provides a very fast introduction of the load into the quench tank and removal of the load from the tank. The loading/unloading time is within about two or three seconds regardless of the load weight, which ensures a small difference in cooling times between the lower and upper layers of the load.

12.5 INTENSIVE QUENCHING DEMONSTRATION STUDIES

This section summarizes the results of IQ trials obtained for steel samples and actual parts for the following applications:
1. Automotive parts
2. Forgings
3. Tool products
4. Fasteners

Note that in many cases, due to part size considerations, the water-flow velocity in the 500-gallon experimental IQ system and in the production IQ system was not high enough to provide the "ultimate" cooling rate for the particular parts being quenched. Nevertheless, in each case, intensive quenching did provide considerable improvement in the parts' mechanical properties and less distortion compared to oil quenching. Since the above IQ systems were not fully optimized for each different test part, the performance improvements are not necessarily the best attainable with a system designed to achieve fully developed IQ-3.

12.5.1 Automotive Parts
12.5.1.1 COIL SPRINGS
An extensive IQ demonstration study for automotive coil springs was conducted [7].[8] Fig. 15 presents a picture of a typical coil spring. The first intensively quenched coil springs were made of AISI 9259 steel Ø17 mm wire and had an outside diameter of 150 mm and a length of 380 mm. The chemical composition of the AISI 9259 steel was 0.593 %

Fig. 14—Atmosphere furnace equipped with 41-m³ IQ water tank.
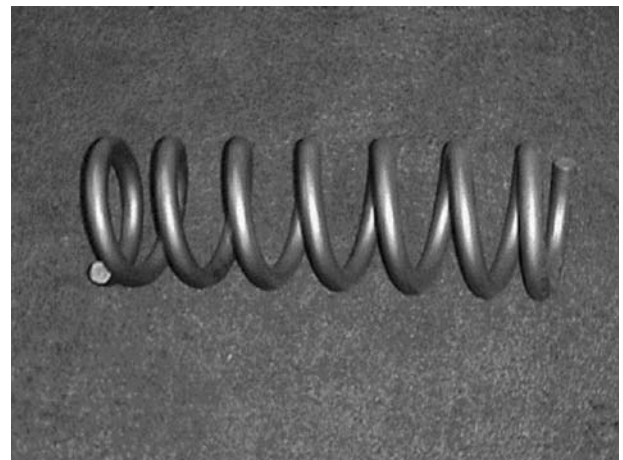
Fig. 15—Automotive coil spring [7].

---

[6] An identical IQ system is installed at HighTemp Furnaces, Ltd., of Bangalore, India.
[7] The furnace is installed at Euclid Heat Treating Co. of Cleveland, Ohio.
[8] The study was conducted together with ArvinMeritor Automotive, Inc., of Detroit.

TABLE 4—Coil spring metallurgical analysis results

Parameter	Oil quench	Intensive quench
Bainite at the surface	5–10 %	0 %
Bainite at the core	15–20 %	2–5 %
Microstructure	Tempered martensite and bainite	Tempered martensite with traces of bainite in the core
Grain size	ASTM8	ASTM9

carbon, 0.87 % manganese, 0.77 % silicon, 0.479 % chromium, 0.006 % molybdenum, 0.01 % nickel, and 0.011 % copper. A set of six of these coil springs was quenched in the original 500-gallon IQ unit. This IQ system could not provide the required cooling rate for these springs. Having a water flow velocity of 2.5 m/s, it was possible to realize only a partially developed IQ-3 process. However, the results of fatigue testing of six intensively quenched and six oil-quenched coil springs made from the same steel heat showed that the fatigue life of IQ springs was about 10 % longer.

The second set of coil springs was quenched in the high-velocity 800-gallon IQ system. These springs were also made of AISI 9259 steel. The springs had the following dimensions: coil outside diameter, 152 mm; spring length, about 547 mm; and spring wire diameter, 21 mm. Eight springs were intensively quenched in the experimental quenching system. The springs were tempered to a required hardness. From the same lot of steel, the customer oil-quenched eight springs in accordance to its regular heat-treating practice. Two springs of each group were destructively tested for residual stress measurements and other metallurgical analysis. Six intensively quenched springs and six oil-quenched springs were tempered and then shot-peened by the customer. The customer then conducted its standardized fatigue test on the two sets of springs. The results of the study are presented below.

The as-quenched microstructure for the intensively quenched spring was superior to that of the oil-quenched spring, as shown in Table 4. The amount of bainite in the intensively quenched sample ranged from none at the surface to 2–5 % in the core, while the amount of bainite in the oil-quenched sample was in the range of 5–10 % at the surface to 15–20% in the core. The intensively quenched spring hardness was approximately 1–3 HRC higher than the oil-quenched hardness. However, the as-tempered hardness was practically the same for both sets of springs.

Figs. 16 through 18 compare the surface residual stresses in the intensively quenched and oil-quenched springs in, respectively, the as-quenched condition, the as-tempered condition, and after shot-peening. Residual surface stresses were measured by the X-ray diffraction method. Compressive residual stresses on the surface of a spring improve the spring's performance, since most of the "work" of the spring is done at the surface, as is most of the fatigue.

As shown in Fig. 16, the oil-quenched coil spring generally exhibited tensile residual stresses, whereas the intensively quenched spring exhibited compressive residual stresses, increasing from −18 MPa on the very surface to −613 MPa at a depth of 0.13 mm. (The lower values of the residual stresses in the thin surface layer of the intensively quenched springs are due to slight decarburization of the spring-wire material during heating in the neutral salt bath furnace prior to quenching.) After tempering, the compressive residual stresses decrease on the intensively quenched coil springs; however, the stresses are still compressive (up to −276 MPa) and not tensile, as shown in Fig. 17. The shot peening provides
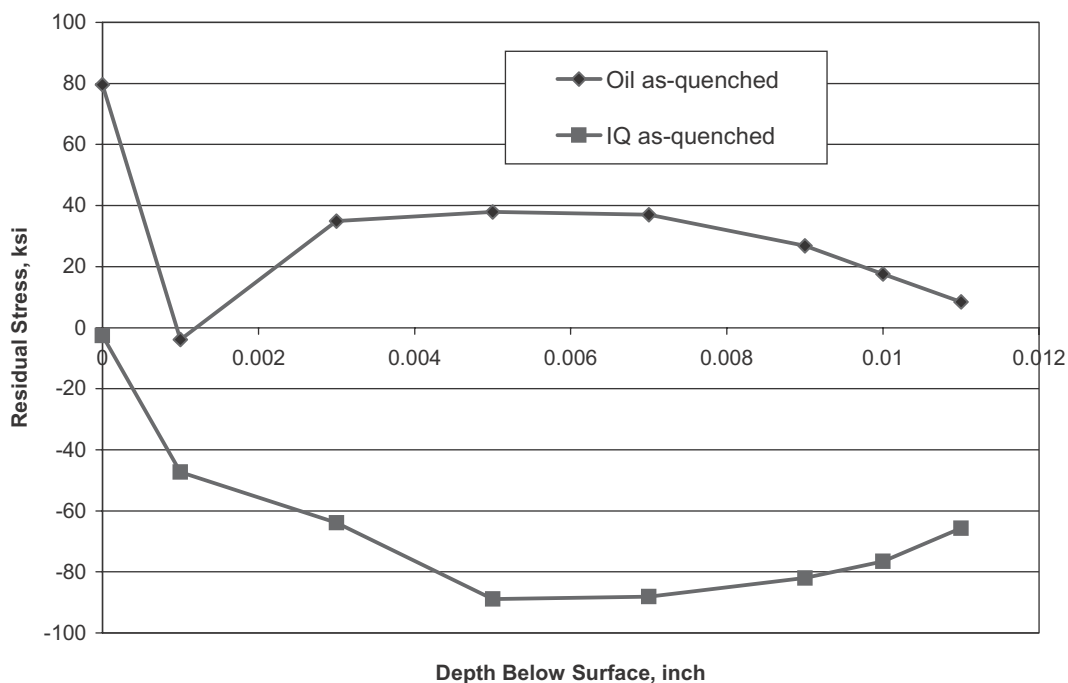
Fig. 16—Coil spring surface residual stresses for as-quenched conditions.
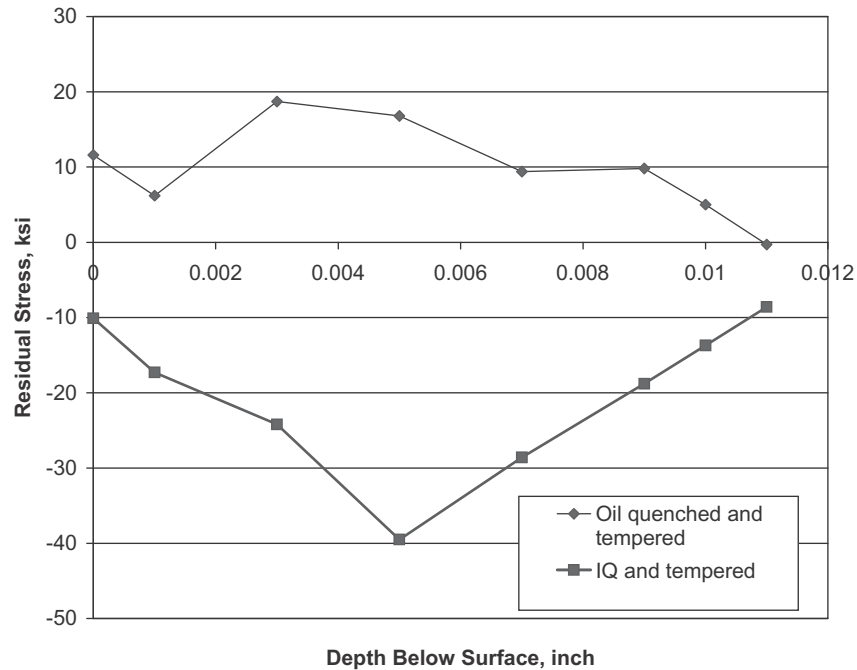
Fig. 17—Coil spring surface residual stresses for as-tempered conditions [7].

compressive stresses on the oil-quenched springs (see Fig. 18), but they are less than the compressive stresses on the intensively quenched springs after shot peening generally by about 138–276 MPa in the measured surface layer of 0.28 mm in depth.

The coil springs were subjected to a standard cyclic fatigue test per the end-user specifications. The fatigue test results revealed that, on average, the intensively quenched springs completed approximately 33 % more cycles than the oil-quenched springs. The Weibull statistical analysis showed that the B10 and B50 life was higher for the intensively quenched springs by about 27 %.

To illustrate a mechanism of the stress formation in the coil spring during both intensive quenching and conventional oil quenching, computer simulations of temperature and of structural and stress-strain conditions for the spring were conducted.[9] The necessary heat transfer boundary conditions that occurred on the coil spring surface in the IQ
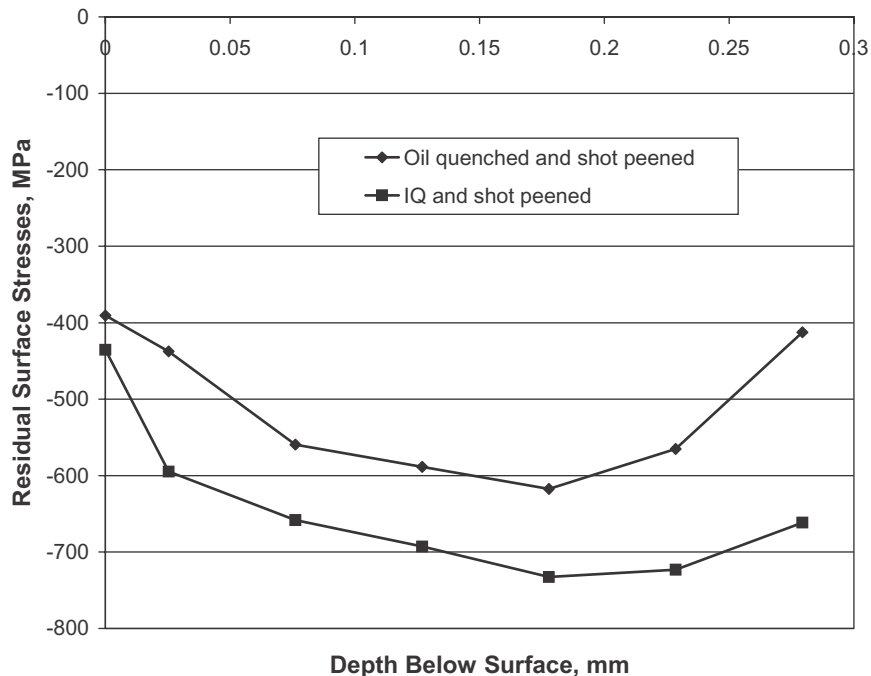
Fig. 18—Coil spring surface residual stresses for as-shot-peened conditions.

[9] Deformation Control Technology, Inc., of Cleveland conducted these calculations using its Dante computer program.

system were specified for the calculations. Results of the computer simulations are presented in Figs. 19–22.

Figs. 19 and 20 show the change of the coil spring surface and core temperatures during intensive quenching and oil quenching. As shown, the surface temperature of the IQ spring cools to the water temperature, which is assumed to be 20°C, within the first 3 s of quenching, creating a temperature gradient throughout the part of 800°C. By contrast, the oil quench takes about 50 s to cool the spring's surface temperature down to the oil temperature (200°C). The

maximum temperature gradient within the oil-quenched springs is about 300°C and occurs 8 s after beginning of quenching.

Figs. 21 and 22 present the dynamics of the formation of the martensite and stress conditions in the spring's surface layer and core. In the IQ spring, the martensitic structure forms first in the surface layer; the martensite starts forming in the spring core in only about 7 s. In the oil-quenched spring, the martensite forms in the surface layer and the core practically simultaneously due to the much smaller temperature gradient in the oil-quenched spring compared to the IQ spring.

The fast formation of the martensitic layer in the IQ spring creates high current surface compressive stresses (up to −1,100 MPa; see Fig. 21). These compressive stresses during the quench diminish slightly when the part core swells (due to the transformation into martensite, which has a

Fig. 19—Intensively quenched coil spring temperatures vs. time.
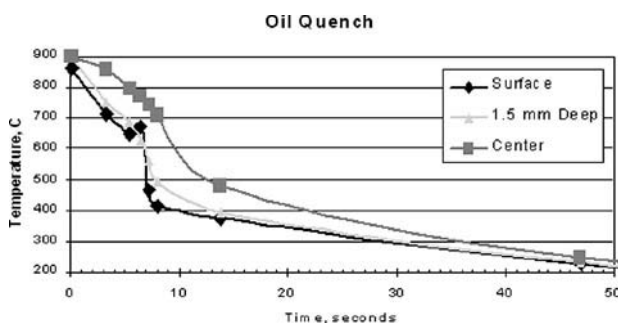
Fig. 20—Oil-quenched coil spring temperature vs. time.
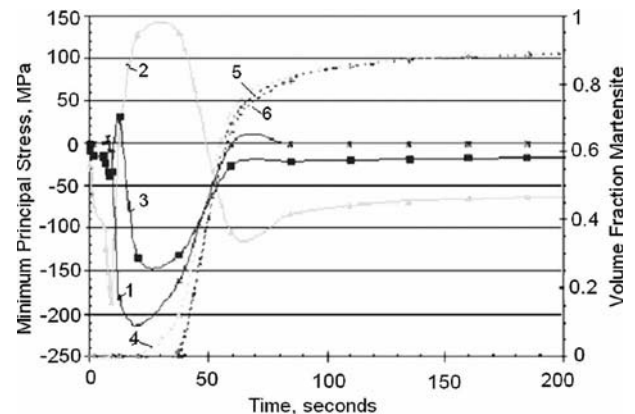
Fig. 22—Oil-quenched coil spring structural and stress conditions: 1, minimum principal stress vs. time at the surface; 2, minimum principal stress vs. time at the core; 3, minimum principal stress vs. time at the midradius; 4, martensite vs. time at the surface; 5, martensite vs. time at the midradius; 6, martensite vs. time at the core.
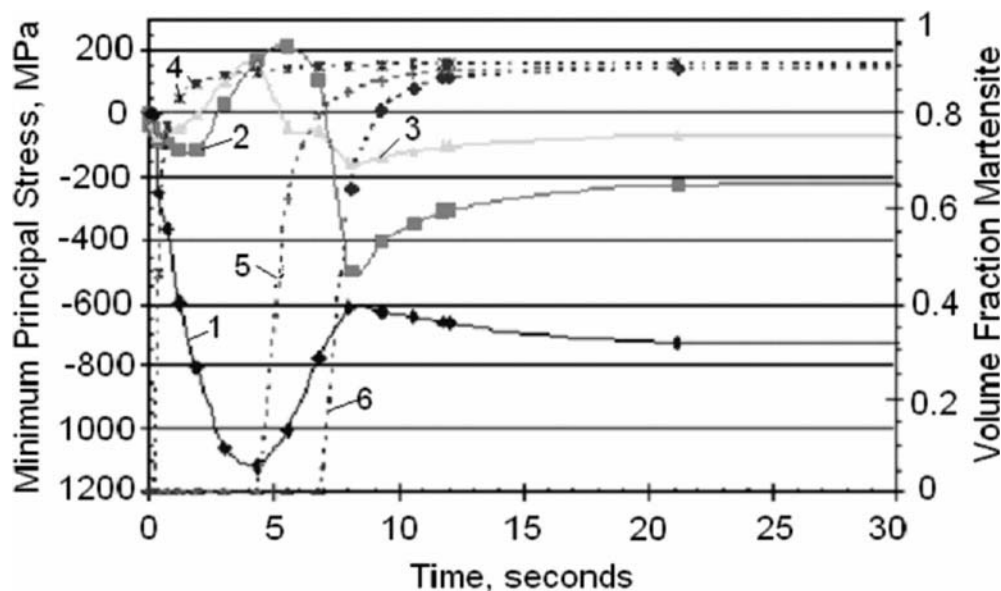
Fig. 21—Intensively quenched coil spring structural and stress conditions: 1, minimum principal stress vs. time at the surface; 2, minimum principal stress vs. time at the core; 3, minimum principal stress vs. time at the midradius; 4, martensite vs. time at the surface; 5, martensite vs. time at the midradius; 6, martensite vs. time at the core.

greater specific volume than the hot austenite). Thus, the 800°C thermal gradient under maximum surface compression compensates (from the core shrinkage) for the later core expansion. There are also surface compressive stresses in the oil-quenched spring; however, the value of these compressive stresses is much less, and they became neutral by the end of quenching due to the swelling of the core. In this case, the core shrinkage is not significant due to a small temperature gradient (only 300°C), and it does not compensate for the subsequent core swelling.

12.5.1.2 LEAF SPRING SAMPLES

An automotive leaf spring manufacturer made twelve samples, 76 mm (3 in.) wide and 16 mm (0.625 in.) thick, with 44-mm (1.75-in.) eyes at each end at a length of 838 mm (33 in.) (to the line of eyes). These samples represented a main leaf of a spring set. Fig. 23 presents a picture of the test strip. The samples were produced with 5160H material, all from the same steel heat. The steel's chemical composition was 0.55−0.65 % carbon, 0.65−1.10 % manganese, 0.150−0.35 % silicon, and 0.60−1.00 % chromium. Six of these samples were heat-treated at a flat condition by the customer with a traditional oil-quenched process. Six other samples were intensively quenched and tempered to the correct hardness. Neither set of samples was shot-peened.

The leaf springs were quenched in the production 6,000-gallon IQ water tank. The water-flow velocity in the quench tank was not enough to create IQ-3 quenching conditions for these parts, so a three-step IQ-2 process was applied. The load of six leaf springs was austenitized at 870°C in the atmosphere furnace, and then the parts were immersed in the water tank for a certain period of time. During this first step of quenching, only the parts' surface layer transformed into martensite. The leaf springs were removed from the quench into the air to allow the temperature to equalize throughout the part's cross-section. The martensitic surface layer was self-tempered during this period of time by the heat coming from the part's core. Then, the leaf springs were put back into the water tank to complete quenching, after which they were tempered to the required hardness.

The spring manufacturer put both sets of leaf springs through cyclic fatigue testing. Each spring was set into spring hangers with one fixed end and one shackle end, as a spring would be mounted into a vehicle. The center section was clamped with 102-mm (4-in.) spacer blocks and the

Fig. 23—Leaf spring sample.

actuator mount assembly. Each leaf was then cycled under a load that was a typical stress range for leaf springs. The average number of cycles performed by the intensively quenched parts was 85 % greater than that performed by the oil-quenched samples. Statistical analysis of the test results showed that the predicted B10 life of the intensively quenched leafs was about 45 % greater than the equivalent spring that was conventionally oil quenched.

12.5.1.3 TORSION BAR SAMPLES

Torsion bar samples were made of AISI 5160 steel and had a diameter of 36 mm and a length of 180 mm.[10] The chemical composition of the steel was similar to the above 5160H steel. Six identical samples were made from the same steel heat and were quenched in oil. The torsion bar samples were quenched intensively in the original 500-gallon experimental system using the IQ-3 method. The results of the study are presented in [5,6]. Note that the cooling rate in this system was less than required for the fully developed IQ-3 process, and therefore the results presented below are not optimum.

Tables 5, 6, and 7 present hardness, microstructure, and residual stress data, respectively, for the intensively quenched and oil-quenched samples. As seen from Table 5, the samples were quenched through in both cases. However, as-quenched hardness of the IQ samples was about two units greater than for the oil-quenched samples. There was also a difference in the microstructure distribution, as seen from Table 6; the IQ samples had fully martensitic structure near the part's surface, only 2 % bainite at the midradius, and 2.5 % bainite in the core. The oil-quenched samples, meanwhile, had 3 % bainite in the surface layers, 12 % at the midradius, and 29 % at the core.

As Table 7 shows, the residual surface stresses in the torsion bar samples were compressive after intensive quenching and were tensile after quenching in oil. For the IQ samples, residual surface stresses were still compressive after tempering. Note that if we could have provided higher cooling rates (from a fully developed IQ-3 process), the residual surface compressive stresses would have been at much greater level.
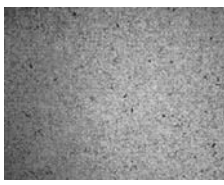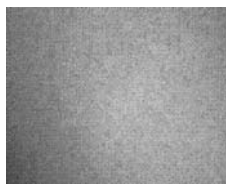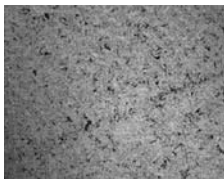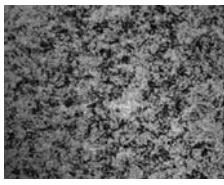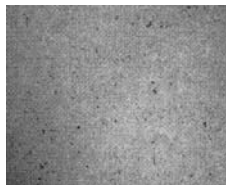
Current compressive stresses on the part surface with seams during quenching prevent part cracking and minimize distortion. Several of the intensively quenched torsion bar samples had small seams on their surface. In field conditions, such seams always develop into cracks during quenching in oil due to current tensile stresses on the part surface during quenching. However, Fig. 24 shows a transverse section of the seam approximately through its center and both ends for one of the intensively quenched and tempered

TABLE 5—Torsion bar sample as-quenched hardness data

Distance from surface	Hardness (HRC)	
	Oil quench	Intensive quench
At surface	61.9	63.6
1/2 radius	59.4	63.2
Core	60.0	63.4

---

[10] ArvinMeritor Automotive, Inc., of Detroit provided torsion bar samples and conducted the metallurgical analysis and X-ray residual stress measurements.

TABLE 6—Torsion bar sample microstructure improvement

Distance from surface	Bainite content (%)	
	Oil quench	Intensive quench
At surface		
	3%	0%
1/2 radius		
	12%	2%
Core		
	29%	2.5%

Fig. 24—Torsion bar samples with seams: transverse sections through one end (a), the center (b), and another end (c) of the seam [5, 6].

Fig. 25—Ball stud.

samples, demonstrating that there was no evidence of quench cracks at these seams after intensive quenching.

12.5.1.4 BALL STUDS

A major goal of the IQ trials conducted for automotive ball studs was to prove that the current steel, AISI 4140 alloy, could be replaced with less expensive, plain-carbon 1040 or 1045 steel. The 4140 steel chemical composition is 0.38–0.43 % carbon, 0.75–1.0 % manganese, 0.20–0.35 % silicon, 0.80–1.10 % chromium, and 0.15–0.25 % molybdenum. Fig. 25 presents a picture of a typical ball stud.

The customer provided two batches of ball studs made of the above steels for intensive quenching in the production 6,000-gallon IQ water tank. The ball stud dimensions were as follows: length, 87 mm; body diameter, 31 mm; ball diameter, 39 mm. The ball studs were austenitized in the atmosphere furnace and were quenched using a three-step IQ-2 method. Ten parts from each batch were checked for surface hardness. A random ball stud from each group was also sectioned for microstructural examination.

Slightly tempered martensite was found in the ball stud surface layer at as-quenched conditions. The reason for this is the following. During the first step of the IQ-2 quenching process, martensite forms in the part's surface layer. Then, after the parts are removed from the quench, the heat coming from the part core tempers the martensite in the surface layer, making it stronger and more ductile and thus preventing part cracking. The phase transformation is completed in the part's core during the third step of quenching in the IQ tank.

The ball stud as-quenched surface hardness was 58–60 HRC, while the interior hardness measured at half the radius was 51–52 HRC. The customer conducted cyclic fatigue testing of the above intensively quenched ball studs. The fatigue life of the ball studs made of plain-carbon steel that was intensively quenched met the customer specifications for 4140 ball studs quenched in oil.

12.5.1.5 UNIVERSAL JOINT CROSSES

Fig. 26 presents a picture of a universal joint cross that was tested.[11] The figure also shows typical universal joint crosses.

TABLE 7—Torsion bar sample as-quenched residual stresses

Distance from surface (mm)	Residual stress (ksi)	
	Oil quench	Intensive quench
0	54.7	−82.2
0.05	17.4	−89.9
0.25	31.3	−134.2

[11] IQ demonstrations for universal joint crosses were conducted in cooperation with HighTemp Furnaces, Ltd., of Bangalore, India.
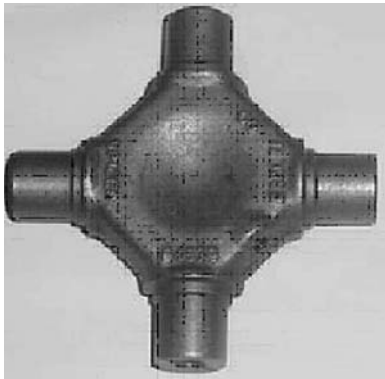
Fig. 26—The universal joint cross.

The crosses were made of carburized alloy steel similar to AISI 8620 steel having the following nominal chemistry: 0.18–0.23 % carbon, 0.70–0.90 % manganese, 0.20–0.35 % silicon, 0.40–0.70 % nickel, 0.40–0.60 % chromium, and 0.15–0.25 % molybdenum.

An IQ study was conducted in two steps [10,11]. First, a limited number of previously carburized universal joint crosses were quenched in the production 6,000-gallon IQ water tank. Second, a full-scale production load containing 500 parts was carburized and quenched in the integral quench furnace equipped with the 11,000-gallon IQ water tank (see Fig. 27).

The following parameters were evaluated after intensive quenching: surface and core hardness, case depth, microstructure, intergranular oxidation, products of nonmartensitic transformation, and part distortion. The results of the metallurgical analysis for the intensively quenched parts were:

- No unacceptable distortion or cracks were observed.
- The case depth was uniform throughout the intensively quenched surface of the cross.
- Intensive water quenching achieved the specified mean case depth of 1.5 mm with only 60 % of the "standard" (oil-quench) carburizing time.
- The core hardness was greater than the required minimum.
- No intergranular oxidation was observed in the intensively quenched crosses.
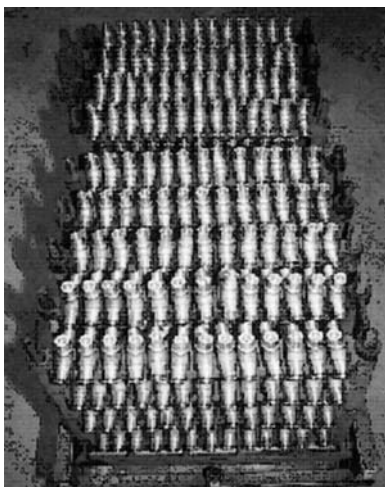
Fig. 27—A full-scale production load containing 500 parts that were carburized and quenched in the integral quench furnace equipped with the 11,000-gallon IQ water tank.

Fig. 28 presents the hardness distribution in the universal joint crosses for different carburization cycle times. The effective case depth is defined as a depth of the part surface layer with a minimum hardness of 50 HRC (513 HV1). As seen from Fig. 28, the case depth is 1.5 mm for standard oil-quenched crosses. Fully carburized crosses that were intensively quenched have a case depth of 1.7 mm—13 % greater than the required standard case depth. The crosses that were carburized for 60 % of the standard carburization time (for 5 hours 10 minutes instead of 8 hours 30 minutes) and intensively quenched had the same case depth as the standard-cycle carburized and oil-quenched parts. Note also that the intensively quenched crosses have a greater core hardness compared to the standard parts by 50–115 HV1 units.

Figs. 29 and 30 present the hardness profiles in the crosses that were carburized for only 50 % and 60 %, respectively, of the standard carburization cycle time. As seen from the figures, the 50 % carburized and 60 % carburized, intensively quenched crosses have a deeper case depth at 50 HRC compared to standard carburized and oil-quenched crosses, by 10% and 32%, respectively.

Fig. 31 presents the uniformity of hardness distribution in the 60 % carburized universal joint crosses. As seen from the figure, the IQ process provides very uniform hardness distribution throughout the part surface. Samples 1, 2, and 3 were taken from different surface areas of the cross journals. The uniformity of hardness throughout the part surface from intensive quenching is mainly due to the absence of the sporadic film boiling on the part surface in the intensively agitated quench; no film boiling equals no soft spots.

Figs. 32 and 33 present photographs of the part microstructure for, respectively, the standard-cycle, carburized, quenched-in-oil cross and the 60 % carburized, intensively quenched cross. For both parts, the case microstructure consists of fine tempered martensite with approximately 5 % retained austenite, no products of nonmartensitic transformation, and no carbide network. However, as seen from the above figures, the martensitic structure of the case was finer in the intensively quenched part compared to the standard oil-quenched part. The intensively quenched cross core consists of low-carbon martensite, while the core of the oil-quenched cross has both low-carbon martensite and bainite.

12.5.2 Forgings
12.5.2.1 RAILROAD PARTS
A railroad part manufacturer provided two types of forged components for IQ trials. Both had quite complicated shapes. The first component was made of AISI 4137 steel (nominal chemical composition: 0.35–0.40 % carbon, 0.70–0.90 % manganese, 0.20–0.35 % silicon, 0.80–1.10 % chromium, and 0.15–0.25 % molybdenum). The part was normally carburized to a case depth of 1.5–2.0 mm (0.060–0.080 in.) and quenched in oil. Its cross-section was about 64 by 114 mm (2.5 by 4.5 in.).

The second part was made of AISI 4130 steel (similar chemistry to 4137 steel except with a carbon content of 0.28–0.33 %). It, too, was normally carburized to the same case depth and oil-quenched. The part cross-sectional area was about 137 by 130 mm (5.4 by 5.1 in.).

As a preliminary test, one of each of the above standard parts that had been carburized only (not quenched in oil) was quenched intensively and tempered (to the required surface hardness). The part manufacturer conducted metallurgical
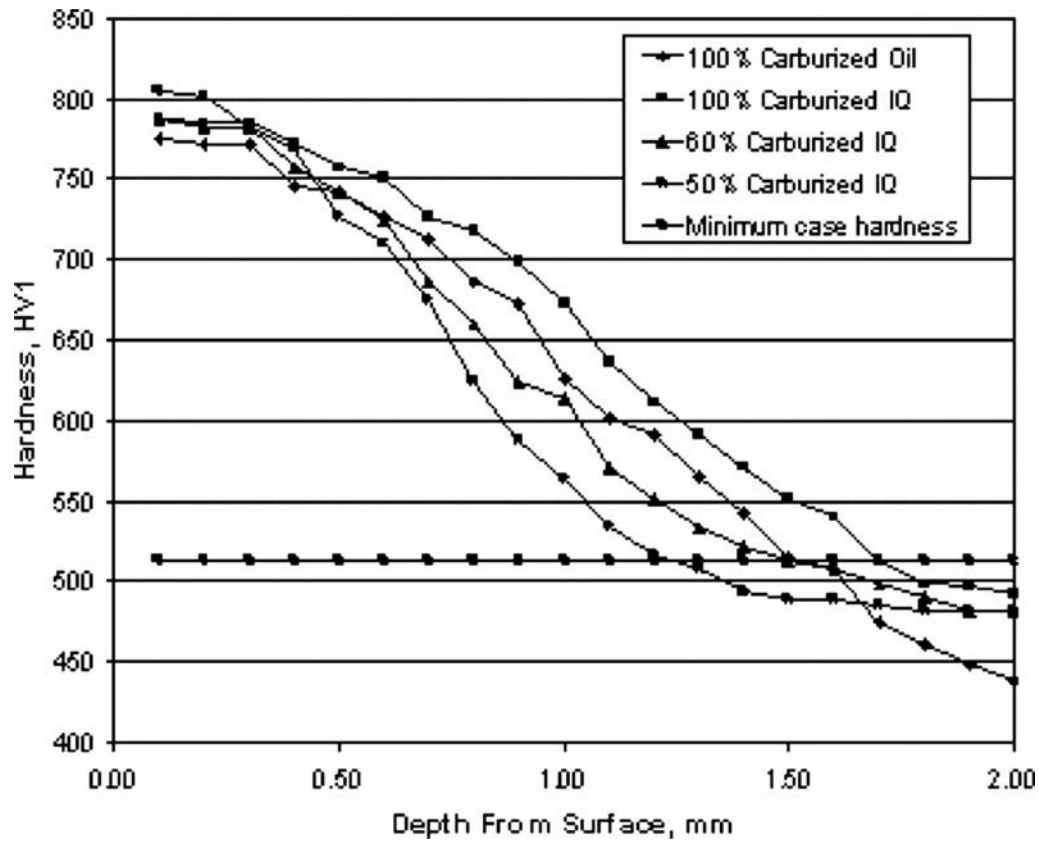
Fig. 28—The hardness distribution in universal joint crosses for different carburization cycle times.
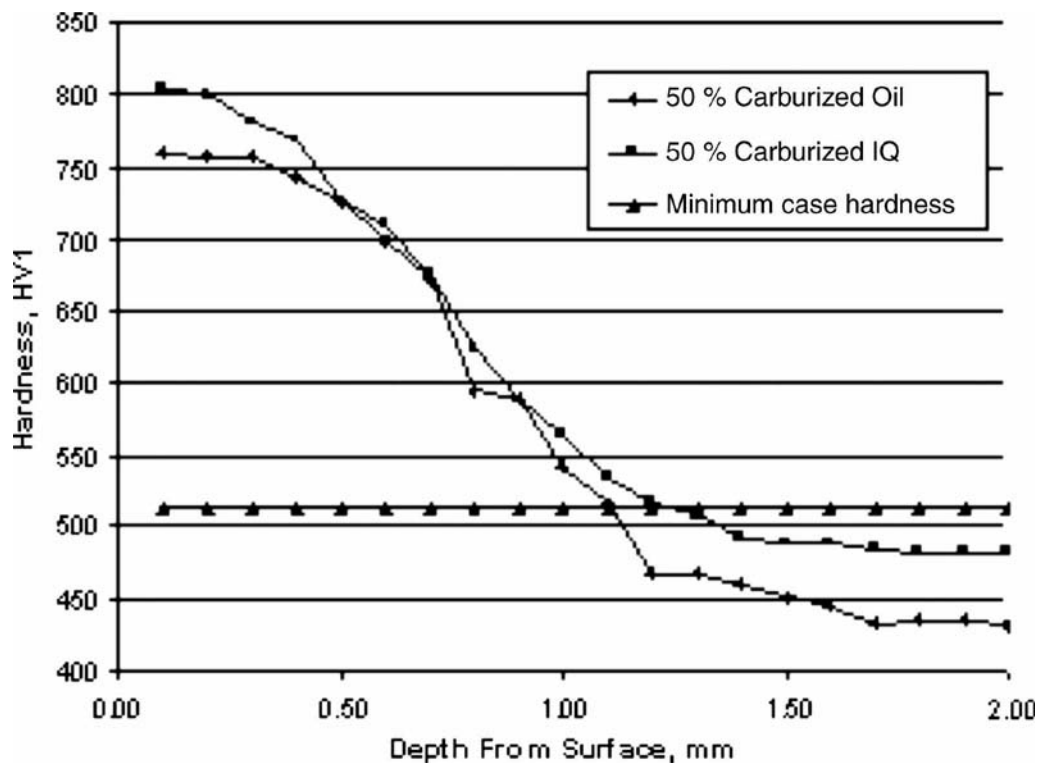
Fig. 29—Hardness profile in 50 % carburized universal joint crosses.
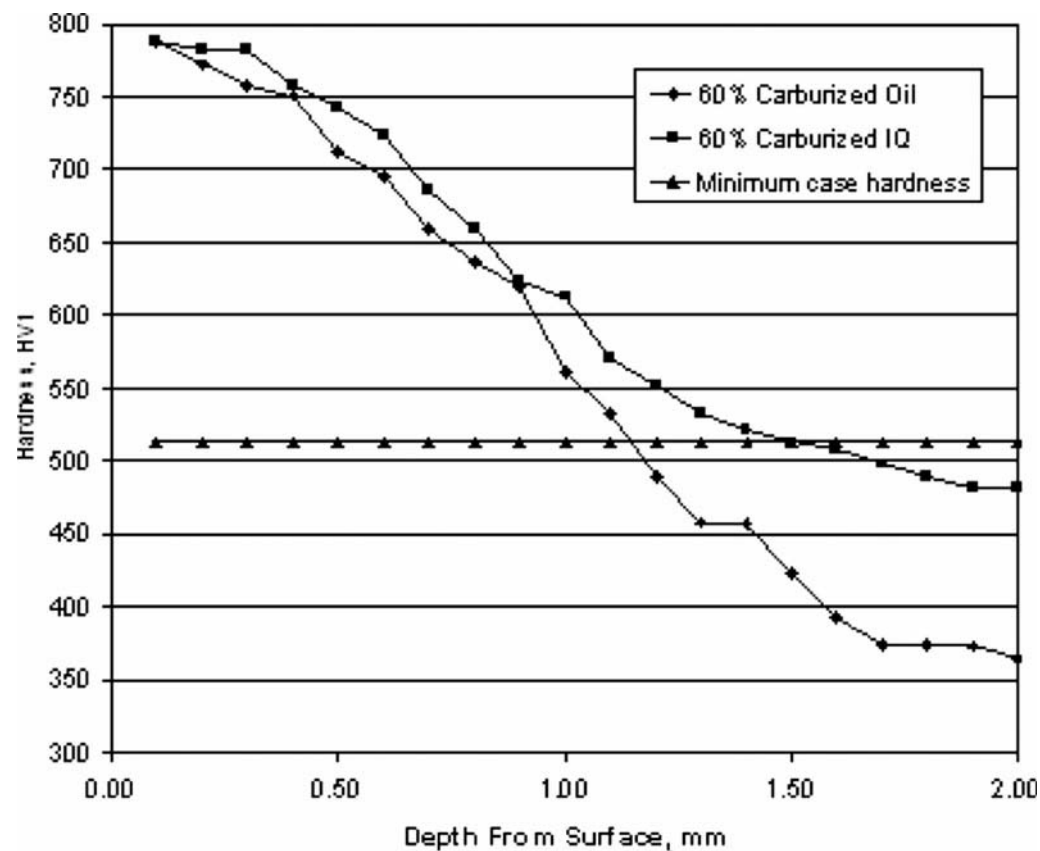
Fig. 30—Hardness profile in 60 % carburized universal joint crosses.
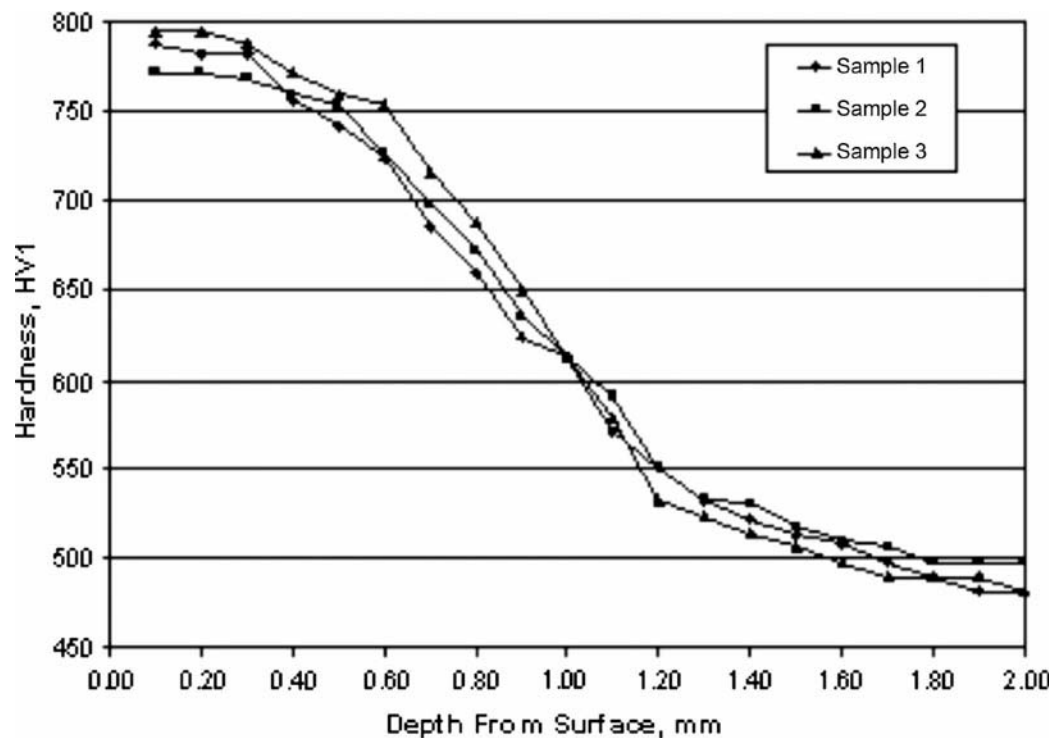
Fig. 31—Uniformity of hardness distribution in 60 % carburized and intensively quenched universal joint crosses.
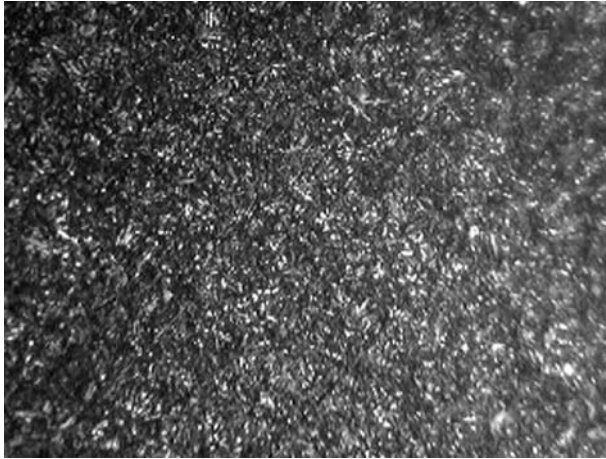
Fig. 32—Case structure of 60 % carburized IQ cross.

analysis and compared the micro hardness distribution and structure throughout the cross-section of these two parts as well as of two similar parts quenched in oil. The results of the study are presented in [8].

A section was removed from each of the above parts at the main contact location for microscopic examination. The samples were metallographically prepared in accordance with ASTM E3-01 and examined in the etched condition at magnifications up to 1,000 times. The results of the examinations are shown in Table 8 and Figs. 34–43.

It was established that the IQ process provided finer martensite for both types of forgings. The metallographic samples were subjected to microhardness testing to determine the hardness profile from the surface to core locations. The testing was performed using a NIST traceable microhardness tester equipped with Knoop diamond indenter and 500-g load in accordance with ASTM E384-99. The resulting

Fig. 33—Case structure of 100 % carburized oil-quenched cross.
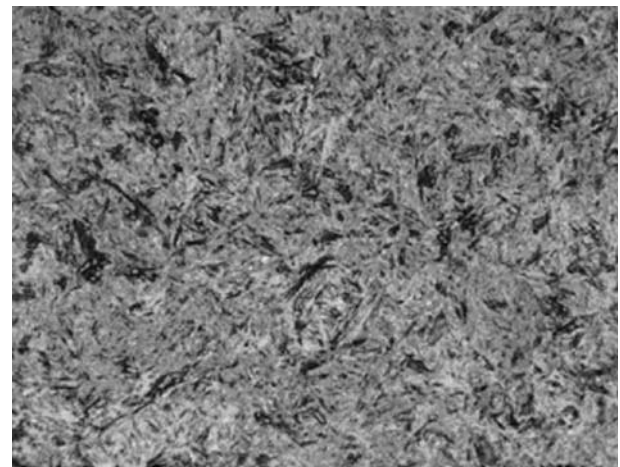
Original Magnification: 800X

Fig. 34—Case macrostructure of oil-quenched 4130 steel forging.

TABLE 8—Metallographic Examination Results for Railroad Parts		
Sample	Case depth	Microstructure
4130 steel part, oil quenched	1.7 mm (0.068 in.)	*Case:* tempered martensite (Fig. 34) *Core:* acicular ferrite/carbide, bainite (Fig. 35)
4130 steel part, intensively quenched	2 mm (0.078 in.)	*Case:* tempered martensite (Fig. 36) *Core:* bainite, acicular ferrite/carbide (Fig. 37) Surface exhibited total decarburization with oxidation to 0.05 mm (0.002 in.) depth and partial decarburization to 0.18 mm (0.007 in.) depth (Fig. 38)*
4137 steel part, oil quenched	2 mm (0.078 in.)	*Case:* tempered martensite (Fig. 39) *Core:* tempered martensite, bainite and small amount of acicular ferrite (Fig. 40)
4137 steel part, intensively quenched	1.8 mm (0.072 in.)	*Case:* finer tempered martensite (Fig. 41) *Core:* finer tempered martensite (Fig. 42) Surface exhibited total decarburization with oxidation to 0.025 mm (0.001 in.) depth and partial decarburization to 0.1 mm (0.004 in.) depth (Fig. 43)*
Note: *Decarburization of the part surface layer was observed in both intensively quenched parts since they were reheated in the atmosphere furnace with a carbon potential of only 0.4.		
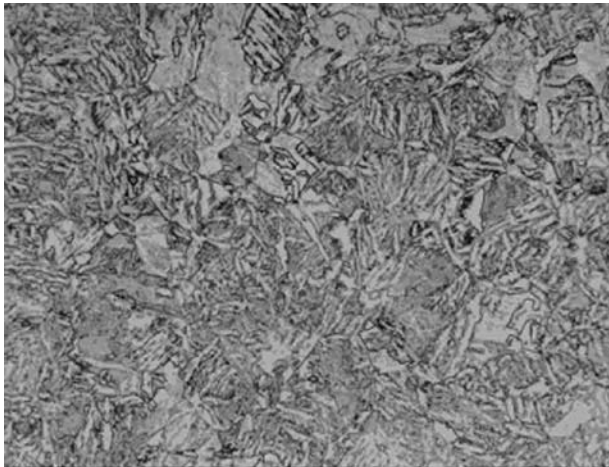
Original Magnification: 800X

Fig. 35—Core macrostructure of oil-quenched 4130 steel forging.
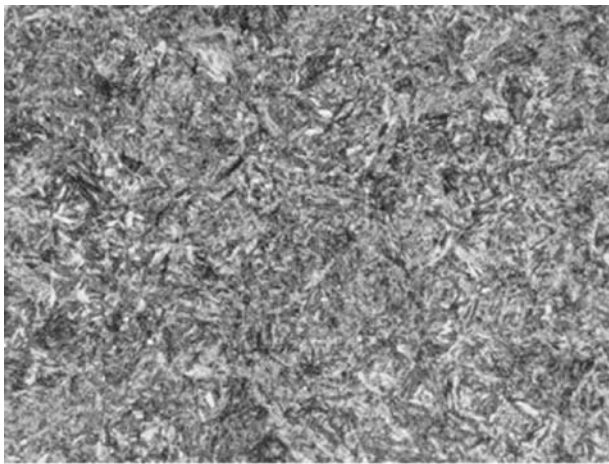
Original Magnification: 800X

Fig. 36—Case macrostructure of intensively quenched 4130 steel forging.

Original Magnification: 800X

Fig. 37—Core macrostructure of intensively quenched 4130 steel forging.
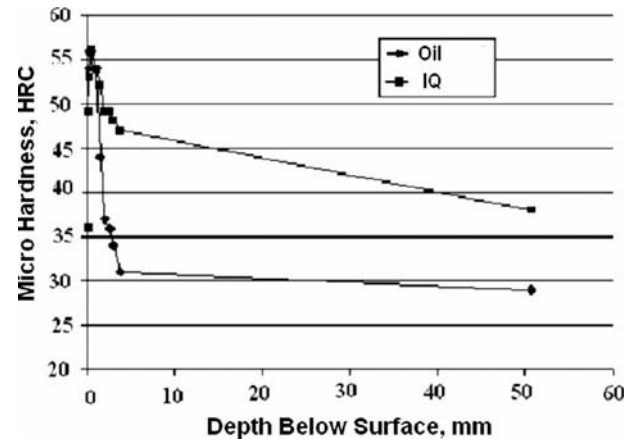
Fig. 38—Macro hardness distribution in 4130 steel forging.
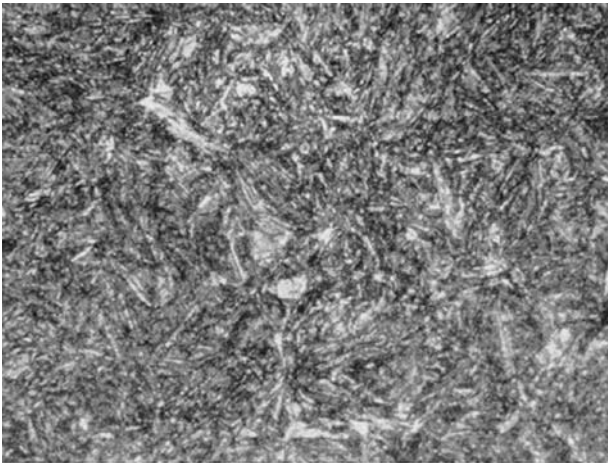
Original Magnification: 800X

Fig. 39—Case macrostructure of oil-quenched 4137 steel forging.
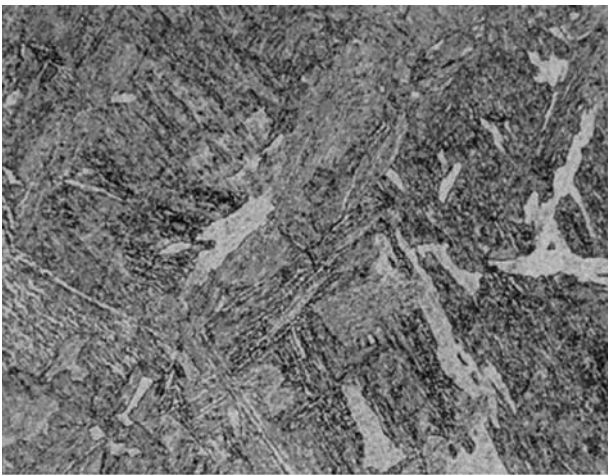
Original Magnification: 800X

Fig. 40—Core macrostructure of oil-quenched 4137 steel forging.

HK values were converted to approximate HRC values. As seen from Table 8, both parts showed microstructural differences within the case and core locations when comparing the standard oil and intensive quenching. For the part made
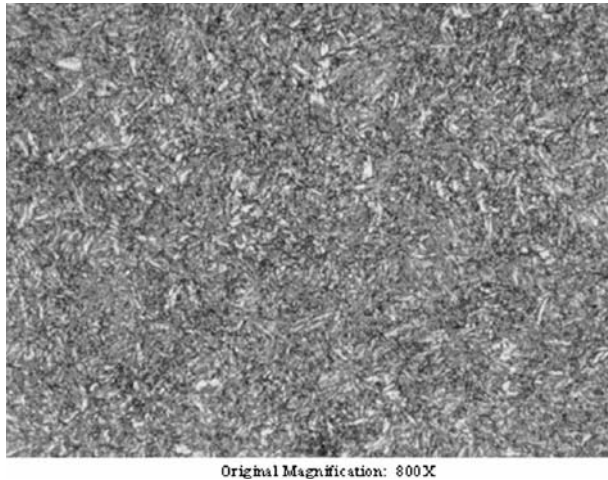
Fig. 41—Case macrostructure of intensively quenched 4137 steel forging.
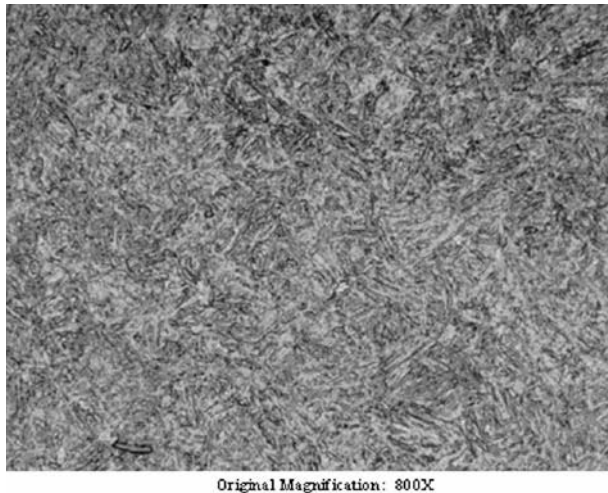
Fig. 42—Core macrostructure of intensively quenched 4137 steel forging.
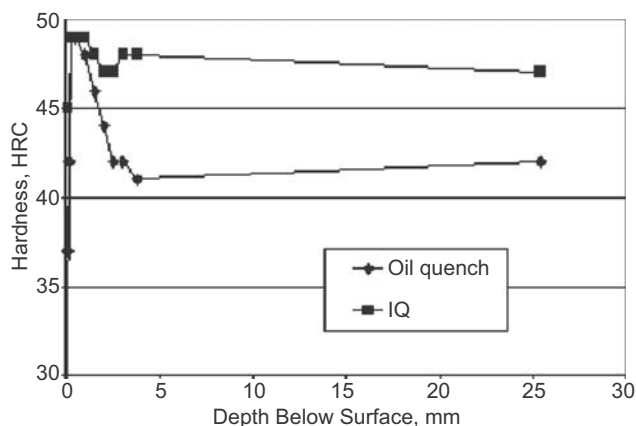
Fig. 43—Macro hardness distribution in 4137 steel forging.

of 4130 steel, both case microstructures exhibited uniform tempered martensite. However, the intensively quenched part exhibited martensite to a greater depth below the surface, which resulted in a greater depth of hardness (i.e., 47 HRC vs. 31 HRC at 4-mm depth).

The oil-quenched 4130 steel part hardness profile exhibited a significant decrease in hardness starting approximately 1.5 mm (0.06 in.) below the surface. Furthermore, the core microstructure exhibited comparatively less bainite, which resulted in a core hardness 9 HRC points lower. The intensively quenched part made of 4130 steel exhibited less drop in hardness profile in the part surface layer. This fact suggested that the part could be carburized less, for a shallower effective case, and still provide the required hardness in the surface layer.

For the part made of 4137 steel (similar to the part made of 4130 steel), both the oil-quenched and intensively quenched case microstructures exhibited uniform tempered martensite. However, the intensively quenched part exhibited a comparatively finer martensite. The intensively quenched part's core microstructure also exhibited primarily tempered martensite, which resulted in relatively uniform hardness values from the case to core locations. By contrast, the oil-quenched core microstructure exhibited tempered martensite and bainite, which resulted in lower core hardness by 5 HRC points. The hardness distribution data obtained for the part made of 4137 steel suggested that this component would not require any carburization when quenched intensively. Elimination of the carburizing cycle with IQ would provide quite an energy savings.

A number of noncarburized parts made of 4137 steel and partially carburized parts made of 4130 steel were quenched for further metallurgical and fatigue/wear evaluation. (Parts made of 4130 steel were processed using a reduced carburization cycle time, to about 50 % of a standard effective case depth). These parts were subjected to both break and fatigue/wear tests.

Fifteen parts made of 4137 steel were break-tested without failure to a load that exceeds the minimum specified break load by about 15 %. Five partially carburized parts made of 4130 steel passed the break test with break loads exceeding the minimum specifications by 55–135 %. Fatigue/wear testing showed that the fatigue and wear resistance of all intensively quenched parts met or exceeded the current specifications for oil-quenched parts.

12.5.2.2 FORKLIFT FORKS

A forklift fork manufacturer provided five forged forklift forks for IQ trials. The incentive to try intensive quenching was the desire to reduce the fork weight and lower fork cost, as well as to eliminate polymer quenching from the heat-treating plant. The forks were made of 15B35H steel having the following chemical composition: 0.32 % carbon, 1.31 % manganese, 0.26 % silicon, and 0.0034 % boron. The fork dimensions were: blade length, 102 cm (40 in.); back length, 55 cm (21.5 in.); cross-sectional area, 130 by 38 mm (5 by 1.5 in.). All five forks were quenched at the same time in the full-scale 6,000-gallon IQ system using a one-step IQ-3 quenching technique. The results of the study are presented in [7].

A metallurgical analysis of the forks showed that they were through-hardened with a very fine martensitic structure. The customer made a number of samples from the intensively quenched forks to measure the steel's mechanical properties. Table 9 shows the mechanical properties' improvements. As shown, both the tensile strength and the yield strength increased by about 40 %, while the impact strength was improved by 200–300 %. The forks were put through a standard cyclic fatigue resistance test, which demonstrated that the intensively

TABLE 9—Improvements of forklift fork mechanical properties

Property	Oil quench	Intensive quench	Improvement (%)*
Yield strength (MPa)	830–1,050	1,400	33.3
Tensile strength (MPa)	950–1,125	1,500	33.3
Impact strength at –20°C (J)	30–60	100–130	66.7–116.7
Elongation (%)	12–18	15	—
Redaction in area (%)	50–65	63	—
Note: *Relative to current practice maximum value.			

quenched fork fatigue life increased by more than 25 % over polymer-quenched forks. Note that in production conditions, forks are clamped when hot and quenched one by one in polymer, while during the IQ trial, five forks were processed in one heat. Single-part intensive quenching, under optimized conditions, will result in even greater improvement in the steel mechanical properties and fork fatigue life.

12.5.3 Tool Products

Tool products are an excellent application for the IQ processes. A number of IQ trials conducted for punches, dies, and die components made of shock-resisting, high-speed, and hot-work tool steels demonstrated a significant improvement in material strength and toughness, resulting in the enhancement of the tool product service life.

12.5.3.1 SHOCK-RESISTING PUNCHES

The main material properties that determine the performance of a punch are toughness, strength, and wear resistance. Strength and toughness are critical in preventing cracking and chipping of the punch under the severe impact of this fabrication process. The wear resistance is required to preserve the cutting edges of the punch, thereby maintaining constant processing parameters and ensuring the dimensional accuracy of the holes punched. All critical properties for punch life are affected by the cooling rate during quenching. A faster cooling rate should permit higher hardness levels without compromising the toughness of the punch.

An experimental program was initiated to evaluate the effect of the IQ process on the properties and performance of S5 steel for punches [3]. Presently, a manufacturer's tool steel punches were being oil-quenched and tempered. While the performance of these punches was satisfactory, the manufacturer was interested in further improving the useful life of the punches by utilizing a faster cooling rate during the quenching process. In addition to the microstructural benefits to the punch from the fast cooling rate, the IQ process should also generate high current and residual compressive stresses at the working surfaces of the punch that minimize the risk of quench cracking and extend the useful life of the punch.

Two commercial heat treaters, a punch manufacturer, and Case Western Reserve University of Cleveland, Ohio (CWRU), joined the program. Cylinders of 38-mm (1.5-in.) diameter and 56 mm (2.2 in.) long and punches machined

from the same steel batch (nominal chemistry: 0.55 % carbon, 0.8 % manganese, 2.0 % silicon) were quenched in oil and by the IQ process. The oil quenching was conducted on batches of punches heated in a vacuum furnace with a rapid transfer mechanism to an integral oil quench tank.

The IQ process was performed in water on individual cylinders and punches in the 500-gallon experimental IQ system using the IQ-3 quenching method. In this process, the part is submersed in a fast flow of water, yielding very fast cooling rates of about 90°C/s at the surface of the cylinder. Quenching is then interrupted when surface compressive stresses reach their maximum value. Charpy V-notch samples were cut from the as-quenched and tempered cylinders and evaluated. Hardness measurements were taken from these samples. The distortion of the cylinders was mapped with a Coordinate Measuring Machine. The depth profile of the residual stresses in the surface region of the cylinders was measured by X-Ray diffraction methods. The X-ray diffraction residual stress measurements were made from the surface to a nominal depth of 0.5 mm in approximate increments of 0.05 mm.

Table 10 presents the hardness measurements of cylindrical punch samples that were intensively water quenched or quenched in oil. The as-quenched hardness of cylinders quenched in oil from 900°C (1,650°F) was 62–63 HRC, while the hardness of intensively quenched cylinders (quenched from the same temperature) was 63–64 HRC. After three hours tempering at 300°F, the hardness of all the cylinders was 60–61

TABLE 10—Hardness of cylindrical punch samples

Cylinder #	V-notch sample #	Hardness (HRC)
Oil quenching		
1	1	60.5; 60.1; 60.1
	2	60.1; 60.2; 60.2
	3	60.0; 60.4; 60.5
	4	60.2; 60.8; 60.7
2	1	60.8; 60.6; 60.8
	2	60.8; 60.7; 60.4
	3	60.8; 60.9; 60.9
Average hardness		60.5
Standard deviation		0.31
Intensive quenching		
3	1	60.6; 61.0; 60.5
	2	61.0; 61.0; 61.2
	3	61.1; 61.4; 61.2
4	1	61.1; 61.3; 61.3
	2	60.4; 60.8; 60.7
	3	60.0; 59.6; 59.9
	4	59.4; 59.5; 59.9
Average hardness		60.6
Standard deviation		0.65

HRC. Hardness measurements were also taken from 14 Charpy V-notch samples cut longitudinally from the cylinders. While the as-tempered average hardness of all the cylinders was practically identical, the oil-quenched specimens were more uniform in hardness from surface to core, with a standard deviation of 0.3 HRC versus 0.6 for the intensively quenched samples. This difference is attributed to the faster heat removal in the IQ process, which generates a faster cooling rate at the surface relative to the center of the cylinders. The hardness at the surface (with the beneficial compressive stresses) therefore tends to be slightly higher than in the center.

The toughness levels measured up to 100°C for the cylinders quenched by the IQ process were higher than the toughness of the oil-quenched cylinders for similar hardness values, although both were relatively low because of the high carbon and hardness values of both sets of punches. The average energy absorbed by the oil-quenched Charpy V-notch sample at room temperature was 1.36 N·m (1 ft·lb) versus 4.08 N·m (3 ft·lb) for the intensively quenched sample. At 100°C, the average energy absorbed by the oil-quenched sample was 3.4 N·m (2.5 ft·lb) versus 6.12 N·m (4.5 ft·lb) for the intensively quenched sample. The higher toughness at similar hardness levels is an indication of superior performance. It means that the intensively quenched punch should have more resistance to chipping. Alternatively, intensively quenched punches could be tempered to higher hardness, while still maintaining acceptable toughness levels. This in turn should improve the wear resistance of the intensively quenched punch relative to an oil-quenched punch.

The difference in quenching rates between the oil and the IQ process also affects the distortion patterns of the cylinders. The distortion map (mapped at CWRU) of an oil-quenched cylinder shows that the cylinder bulges around the center perimeter, with a center diameter about 0.081 mm (0.0032 in.) *larger* than the top and bottom diameters. The distortion map of an intensively quenched cylinder shows that the cylinder has an hourglass shape, with the center diameter being about 0.081 mm (0.0032 in.) *smaller* than the ends.

These differences can be explained by considering the dimensional changes during the phase transformation. The rapid cooling rate during the IQ process quickly forms a hard and stiff "shell" of martensite over the entire surface of the cylinder. The expansion associated with the martensitic transformation causes high compressive stresses at the surface, which are partially accommodated by this change in shape. The top and bottom of the cylinder expand, pushing the adjacent shell outward. At the same time, the longitudinal expansion at the surface is pushing the top and bottom shell perimeters outward.

In the oil-quenched cylinder, the strong martensitic layer does not form as quickly as in the intensively quenched cylinder. When the core transforms and expands, it can still push the surface layer of the cylinder out, causing it to bulge.

These differences are significant in two aspects. The first concerns the dimensional control of the punches, which has to be kept within tolerance. The second aspect relates to the residual stresses. It was anticipated that the IQ process would generate higher compressive stresses in the surface, thus minimizing the risk of cracking during the quench and enhance the performance of the punch in use. The distortion pattern indicates that this is indeed the case.

The axial and circumferential residual stress distributions, measured as functions of depth, are shown graphically
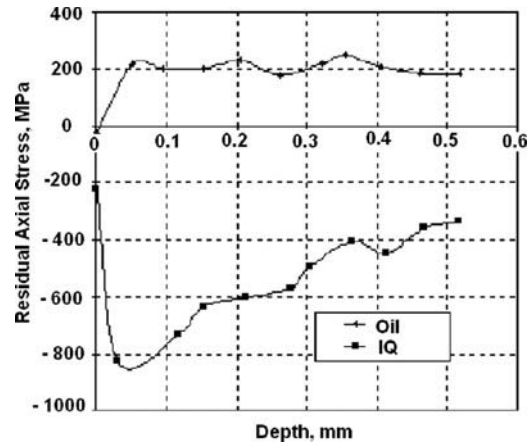
Fig. 44—S5 steel punch sample axial residual stresses.

in Figs. 44 and 45. Compressive stresses are shown as negative values, while tensile stresses are shown as positive, in units of MPa. The X-ray residual stress measurements detected axial and circumferential compressive stresses of −900 MPa at the surface of the intensively quenched cylinders. In the oil-quenched cylinders, tensile residual stresses of about +200 MPa were measured. For cylindrical samples from which complete shells were removed by electropolishing for subsurface measurement, the radial stress was calculated assuming a rotationally symmetrical residual stress distribution. Table 11 below summarizes the punch properties improvements due to the IQ process.
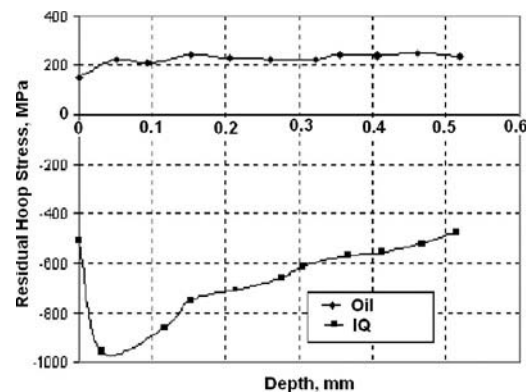
Fig. 45—S5 steel punch sample circumferential residual stresses [3].

TABLE 11—Improvement of S5 steel punch sample properties

Property		Oil quench	Intensive quench
Hardness (HRC)	as quenched	62–63	63–64
	after temper	60–61	60–61
Impact strength (N·m)	at 72°F	1.36	4.08
	at 100°C	3.4	6.12
Residual stresses (MPa)		200	−900
Note: Values as measured by Case Western Reserve University.			

Fig. 46—Square S5 steel punch.

To evaluate punch service life improvement, twelve 17.5-mm (11/16-in.) square S5 steel punches (see Fig. 46) were intensively quenched and put in "production" conditions. The punches were heated to austenite temperature in a neutral salt bath furnace and quenched in batches (six punches per batch) in the IQ experimental system. Twelve identical punches made from the same steel heat were oil-quenched in accordance with the current technology and also put in the field conditions. The oil-quenched punches were heated prior to quenching in a vacuum furnace.

In the field-testing, the punches punched 17.5-mm (11/16-in.) holes through 15.9-mm (5/8-in.) and 19.1-mm (3/4-in.) thick 1085 steel material using a 19.1-mm (3/4-in.) square female die in a single-station 250-ton mechanical press. "Service life" (as defined by the punch user) is when chipping or wear becomes "excessive" and the punched holes are no longer acceptable. The press cycled every 15 seconds. Oil-quenched punches lasted approximately 1 hour and made on the average about 450 holes in the 1085 material. The intensively quenched punches lasted around twice as long, 2 hours, and thus made some 900 holes on average. Thus, the IQ process improved the service life of the S5 punches by about 100 percent, doubling the number of holes per punch.

12.5.3.2 SERVICE LIFE EVALUATION OF HIGH-SPEED PUNCHES AND DIES
Dr. Kobasko conducted a service life evaluation study for high-speed round punches at a tool product manufacturing plant in Bulgaria. The punches were made of R6M5 steel (the material chemistry is very close to the chemical composition of AISI M2 steel: 1.0 % carbon, 1.5 % tungsten, 8.5 % molybdenum, 0.4 % chromium, and 1.0% vanadium). The punches had a diameter of 15.3 mm (0.6 in.) and a length of 126 mm (5 in.) (see Fig. 47). These punches were used at

high loads in an automatic punch press machine with a capacity of 175 strokes per minute.

Seven punches were intensively quenched and seven others (made from the same steel heat) were quenched in accordance with the current technology. Both sets of punches were heated up prior to quenching in a high-temperature salt bath furnace. Table 12 presents the field test data. As the data show, the IQ process improved the average service life by about 2.5 times. This improved performance is attributed to increased material toughness and residual surface compressive stresses from the IQ process.

12.5.3.3 CASE STUDY FOR H-13 STEEL ALUMINUM DIE CASTING DIES
Heat treaters know that the higher the cooling rate is during quenching of "hot-work" die steels, the greater the die's thermal fatigue resistance will be when in service. To prove that the IQ technique provides better thermal fatigue resistance and toughness in die casting dies, CWRU and IQ Technologies intensively quenched standardized 50 by 50 by 178-mm test blocks (see Fig. 48) made of H-13 hot-work die steel [5]. H-13 steel is widely used for aluminum die casting tools in the

TABLE 12—High-speed punch service life improvement

| Test # | Number of strokes* | | Improvement (%) |
	Existing technology	Intensive quenching	
1	6,460	15,600	141
2	6,670	16,500	147
3	3,200	5,300	66
4	4,000	12,075	202
5	6,620	8,110	23
6	2,890	10,500	263
7	2,340	7,300	212

Note: *Until punched holes are no longer functionally acceptable in size or shape.

Fig. 47—Round M2 steel punch.
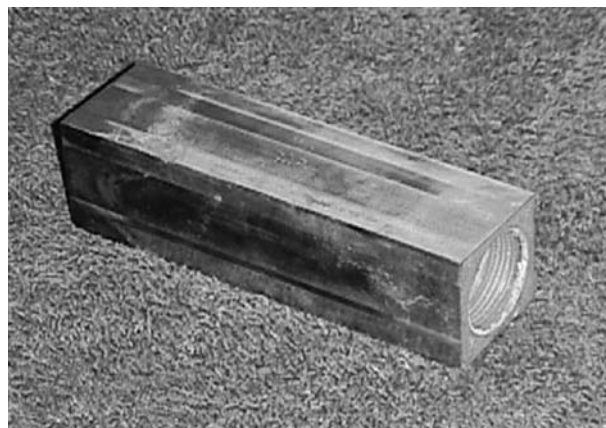
Fig. 48—Square H-13 steel test block.

United States. The steel's nominal chemistry is 0.35 % carbon, 1.5 % molybdenum, 5.0 % chromium, and 1.0 % vanadium.

In die casting of aluminum parts, the dies (and gating for channeling the molten aluminum into the die cavity) must repeatedly withstand temperatures of over 1,000°F with each "shot" of molten aluminum. After taking a shot of molten aluminum, the H-13 tooling undergoes a rapid cooling cycle due to the die's internal water-cooling passages. The water-cooled dies help the aluminum cast part to solidify and become dimensionally stable so the whole process can be repeated. (Since molten aluminum has the viscosity of water, the casting dies must also contain high pressures without distortion.) A duplicate set of test blocks was also made from the same lot of H-13 steel, but quenched in oil. (The usual hardening practice for H-13 steel is to air-quench or to gas-pressure-quench the die in a vacuum furnace.)

The thermal fatigue properties for both the intensively quenched and the oil-quenched H-13 steel test blocks were evaluated by means of a thermal fatigue test methodology developed by CWRU. This test determines the average maximum crack length and total crack area on the four corners of the test block after a certain number of cycles of "in process" heating (by immersion into a bath of molten aluminum at 732°C) and cooling (by coolant flow within the test block's internal water cooling passage). Just like H-13 aluminum casting dies in production situations, the test blocks had a high thermal gradient, repeatedly, every few seconds, throughout the test block cross-section; this high thermal gradient was especially severe at the test blocks' corners. (It should be noted there were no cracks present in any of the intensively or oil-hardened H-13 test blocks at the inception of the cyclic testing.)

Figs. 49 and 50 show the effect of thermal cycles on the average maximum crack length and on total crack area. As shown, there is practically no difference in these two parameters for the test blocks after 5,000 or 10,000 thermal cycles. However, there is a significant difference between these parameters for 15,000 thermal cycles. The average maximum crack length for the intensively quenched test block is about 27 % less than for the oil-quenched test block, and the total crack area for the intensively quenched test block is about 42 % less than for the oil-quenched test block. Since this test correlates with the actual service life of H-13 dies
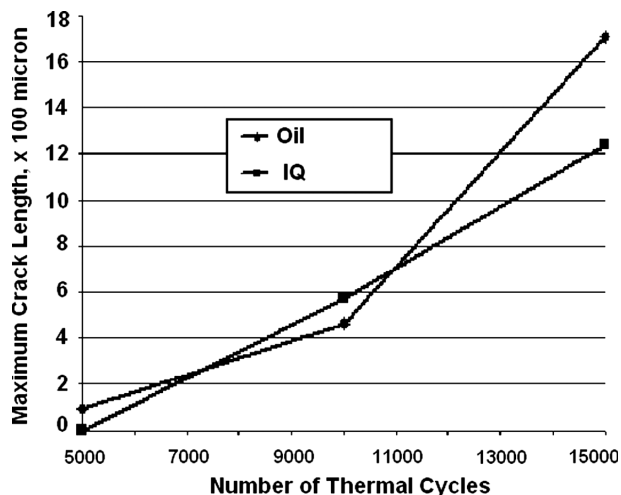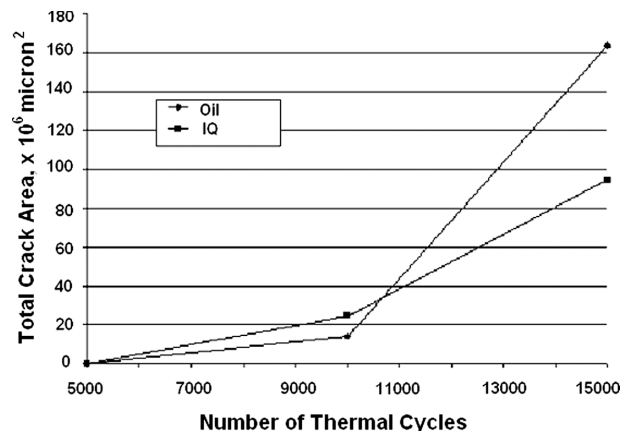
Fig. 50—Total crack surface area vs. number of thermal cycles.

(albeit conventionally air-hardened), the test indicates even greater service life for intensively quenched dies made of H-13 steel.

Over the last several years, a number of different H-13 steel dies and die components were quenched intensively at the Center for Intensive Quenching in Akron, Ohio, using batch-type IQ equipment. All of the quenched dies showed improved service life in the field conditions.

12.5.4 Fasteners

A statistical IQ study was conducted with two fastener manufacturers on the four types of fasteners presented in Fig. 51. The first three types of these fasteners were truck wheel bolts made of 4140 steel (nominal chemistry: 0.38−0.43 % carbon, 0.75−1.0 % manganese, 0.20−0.35 % silicon, 0.80−1.10 % chromium, 0.15−0.25 % molybdenum) and 1340 steel (nominal chemistry: 0.39−0.43 % carbon, 1.6−1.9 % manganese). The fasteners of the fourth group were made of 4037 steel (nominal chemistry: 0.35−0.40 % carbon, 0.70−0.90 % manganese, 0.20−0.35 % silicon, 0.2−0.3 % molybdenum) and were used in a heavy machinery assembly. The goal of this statistical evaluation was to show that the bolts would not have any cracks after intensive quenching in water and the part mechanical properties would be the same or better when compared to the same bolts that were quenched in oil in accordance with the current practice.

Twenty bolts of each of the above groups were intensively quenched, and the same number and type of bolts were quenched in oil in production conditions. Fifteen bolts from each of the samples were subjected to the tensile strength test conducted at the customer's laboratory facilities. Two bolts from each group were cut to measure the core hardness, and three bolts from the fourth group were subjected to impact strength tests.

In all experiments, the same thermal cycles were applied as those used in real production conditions. The parts were heated to austenitizing temperature in a box-type atmosphere furnace in batches of ten bolts per batch. Then they were intensively water quenched one by one in the 500-gallon experimental IQ system using the IQ-3 method. (Note that, due to equipment limitations, the water flow velocity was not optimum; therefore, the IQ-3 process was not fully developed.) No cracks were observed in the intensively quenched bolts.

Table 13 shows the final results for both the intensively quenched bolts and those that were quenched in oil. As seen

Fig. 49—Maximum crack size vs. number of thermal cycles.
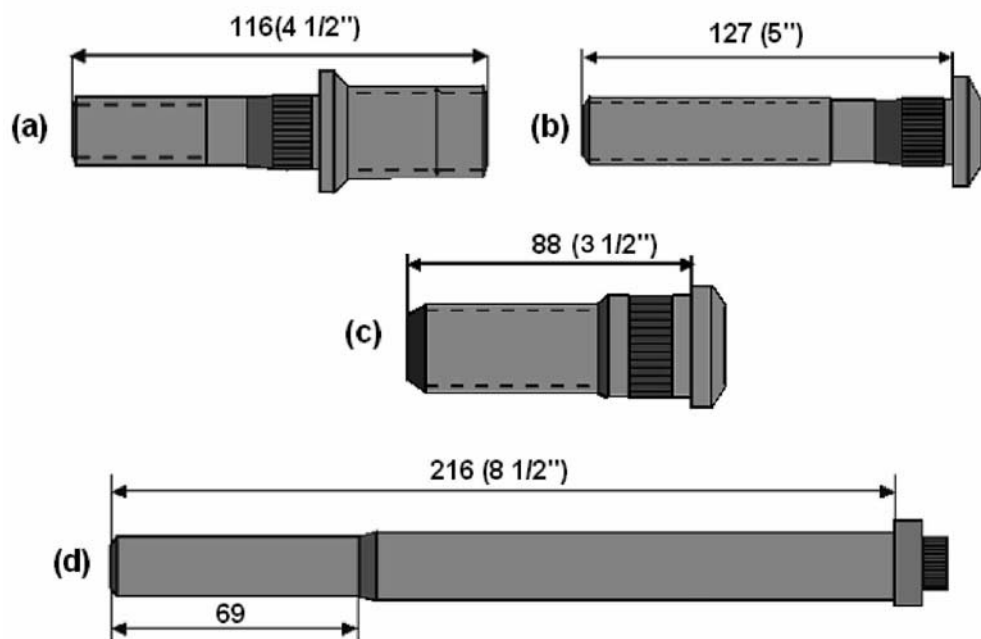
Fig. 51—Tested fasteners: (a) 4140 steel bolt of type 1; (b) 4140 steel bolt of type 2; (c) 1340 steel bolt of type 3; (d) cylinder head bolt sketch.

from the table, the tensile strength for the bolts made of alloy 4140 and 4037 steels did not change dramatically, although there was an improvement of the tensile strength by about 8 % for the bolts made of less alloy 1340 steel. However, there was a significant improvement in impact strength (toughness) for the alloy 4037 steel bolts (see Fig. 52). The impact strength measurements were taken in the temperature range from −100°C to 38°C. As indicated, the impact strength of the bolts improved by about 9–37 %, depending on the temperature range.

12.6 SUMMARY OF INTENSIVE QUENCHING DEMONSTRATION STUDIES

A number of intensive quenching (IQ) demonstrations were conducted for steel products other than the ones described above (bearing rollers, automotive and heavy trucks gears and pinions, industrial gears for different applications, different castings, components of different weapon systems, etc.). The experimental data generated from more than two hundred IQ demonstrations on actual production parts and part samples clearly showed the following benefits of the IQ techniques compared to the conventional oil-quenching method [1–12]:

- Increased surface and core hardness and depth of the hardened layer for parts made of carburized and non-carburized grades of steel
- Reduction of the carburization cycle for the same effective case depth (compared to oil quenching), resulting in the significant reduction of the heat treatment process cost and an increase in the heat-treating equipment production rate

TABLE 13—Mechanical properties of tested fasteners				
	Tensile strength (MPa/m²)		Impact strength at 20°C (N·m)	
Fastener	Oil quenched	Intensively quenched	Oil quenched	Intensively quenched
4140 steel DBL end stud	465.8	474.9	—	—
4140 steel WHL end stud	1,012.9	977.0	—	—
1340 steel M22 bolt	582.3	627.2	—	—
4037 steel bolt	1,202.2	1,187.5	38.7	48.0
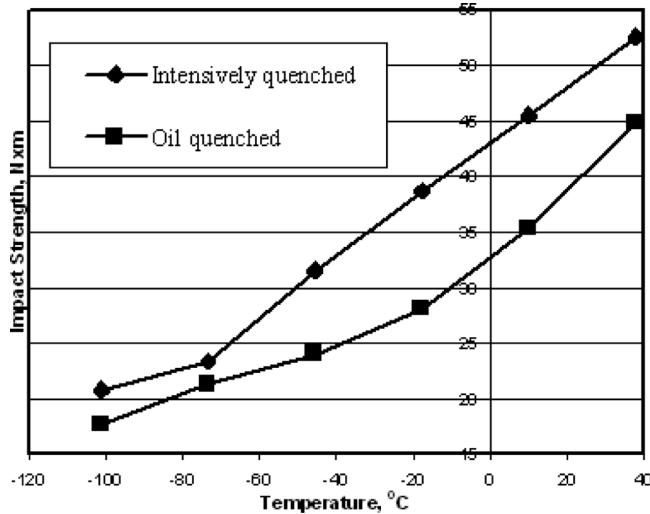
Fig. 52—Impact strength vs. temperature.

- Improved part microstructure (finer grain and "super-strengthened" martensite)
- Higher and deeper residual surface compressive stresses
- Improved material strength and toughness (superstrengthening of steel)
- Substitution of lower-alloy steels for a reduction in part costs and no penalty in part strength or performance
- Possibility of making lighter parts with the same or better performance characteristics and fatigue life as oil-quenched parts due to the strengthening of the material and high residual surface compressive stresses provided by the IQ process
- Less part distortion and no part cracking
- Full elimination of quench oil and its associated costs (cost of the oil, part washing, etc.), resulting in significant reduction of the heat treatment process cost and improved environmental effects
- Possibility of moving heat treatment operations into the manufacturing cell, since the IQ method is an environmentally friendly process

References

[1] Aronov, M. A., Kobasko, N. I., Wallace, J. F., and Schwam, D., Experimental Validation of Intensive Quenching Technology for Steel Parts, *Proceedings of the 18th Heat Treating Conference,* Chicago, 1998, pp. 622–625.

[2] Aronov, M. A., Kobasko, N. I., and Powell, J. A., Practical Application of Intensive Quenching Technology for Steel Parts and Real Time Quench Tank Mapping, *Proceedings of the 19th Heat Treating Conference,* Cincinnati, Midea, S. J., and Paffmann, G. D., Eds., ASM International, Materials Park, OH, 1999, pp. 363–372.

[3] Aronov, M. A., Kobasko, N. I., Powell, J. A., Schwam, D., Wallace, J. F., Vanas, J. H., and Olson, W. R., Experimental Study of Intensive Quenching of Punches, *Proceedings of the 19th Heat Treating Conference,* Cincinnati, Midea, S. J., and Paffmann, G. D., Eds., ASM International, Materials Park, OH, 1999, pp. 382–389.

[4] Aronov, M. A., Kobasko, N. I., Powell, J. A., Wallace, J. F., and Schwam, D., Practical Application of the Intensive Technology for Steel Parts, *Industrial Heating,* No. 4, 1999, pp. 59–63.

[5] Aronov, M. A., Kobasko, N. I., and Powell, J. A., Practical Application of Intensive Quenching Process for Steel Parts, *Proceedings of the 20th Heat Treating Conference,* St. Louis, 2000, pp. 778–784.

[6] Aronov, M. A., Kobasko, N. I., and Powell, J. A., Intensive Quenching Technology for Tool Steels, *IFHTSE 2000 Congress,* Melbourne, Australia, October 29–November 2, 2000.

[7] Aronov, M. A., Kobasko, N. I., and Powell, J. A., Application of Intensive Quenching Methods for Steel Parts, *Proceeding of the 21st Heat Treating Conference,* Indianapolis, 2001 [CD-ROM].

[8] Aronov, M. A., Kobasko, N. I., and Powell, J. A., Review of Practical Applications of Intensive Quenching Methods for Steel Parts, *Proceedings of the 13th IFHTSE Congress,* Columbus, OH. October 7–10, 2002, pp. 410–416.

[9] Kobasko, N. I., Aronov, M. A., Powell, J. A., Canale, L. C. F., and Totten, G. E., Intensive Quenching Process Classification and Applications, *Heat Treatment of Metals,* Vol. 31, No. 3, 2004, pp. 51–58.

[10] Kobasko, N. I., Aronov, M. A., Powell, J. A., and Ghorpade, P., Application of Intensive Quenching Processes for Carburized Parts, *Proceedings of the 25th Heat Treating Conference,* Puna, India, 2005 [CD-ROM].

[11] Kobasko, N. I., Aronov, M. A., Powell, J. A., and Ghorpade, P., Demonstrations of Intensive Quenching Methods for Steel Parts, *Proceedings of the 27th Heat Treating Conference,* Detroit, 2007, pp. 390–397.

[12] Kobasko, N., Aronov, M., Powell, J., and Totten, G., One More Discussion: "What Is Intensive Quenching Process?", *Journal of ASTM International,* Vol. 6, No. 1, 2009, pp. 1–12.

13

Inverse Problems in Quench Process Design

N. I. Kobasko[1] and V. V. Dobryvechir[1]

13.1 INTRODUCTION

A necessity of solving of inverse problems occurs in many branches of industry [1,2]. In general, inverse problems can be defined as problems where the cause is determined based on known results. For example, if four streams join to form a river and four factories are putting known amounts of a pollutant into the streams, it is easy to determine the resultant level of the pollutant in the river. This is a classic *direct problem*. However, a more difficult problem is to determine how much pollutant each factory introduces into each stream by knowing a total amount of the pollutant measured downstream of the place where the streams flow into the river. This is a classical *inverse problem* [3]. Obviously, to solve this inverse problem, it is not enough to know the total resultant pollutant. It is necessary to measure the pollution in the river closer to each of the streams.

Quenching processes where four types of heat transfer modes are taking place represent a similar problem (see Chapters 2 and 3). At present, serious attention is being devoted to solving inverse problems [1,3]. Two international groups, the Inverse Problem International Association and the Finnish Inverse Problems Society, have been established specifically to examine this subject. There are also three academic journals covering inverse problems in general [3]:

- *Journal of Inverse and Ill-posed Problems*
- *Inverse Problems in Science and Engineering*
- *Inverse Problems and Imaging*

There are many methods of solving inverse problems that have been applied to experimental data. However, there are insufficient data relating to boundary conditions during temperature field calculations. There are also insufficient experimental data to develop a universal database for heat treatment and quenching of steel. These problems will be addressed in this chapter.

The boundary conditions (heat transfer coefficients) during quenching of steel parts can be restored by solving inverse heat conduction problems, knowing the temperature field in the part measured experimentally during quenching. Inverse heat conduction problems, unlike traditional direct problems, permit the separation of causes from their effects (which are known from experimental data or measured temperatures). In heat conduction problems, these causes include thermal and physical properties of materials, inner volumetric and surface heat sources (sinks), heat transfer coefficients, coordinates of inner and surface points of a part where experimental data are acquired, time to reach certain thermal conditions, speeds of movement of part boundaries, and heat sources. Solutions of inverse heat conduction problems yield boundary conditions and other determining conditions in industrial or laboratory experiments. For this reason, these methods are often the only way to solve such problems.

At the present time, there is a considerable focus on the design of optimal quenching conditions using aqueous solutions of salts, polymers, air, and water cooling. The optimization of quenching processes by computer simulations is much more efficient with respect to accuracy, time, and cost than experimental optimization. It is an ongoing problem to determine cooling characteristics of quenchants and thermophysical properties of structural components. With these data and appropriate CCT (continuous cooling transformation) diagrams, it is possible to solve thermal problems and to determine temperature fields, and using phase kinetics, it is possible to select the final material structures after quenching and to design proper quenching conditions.

This chapter presents a brief explanation of how inverse heat conduction problems [1,2,4] can be applied to quenching processes. A general approach to solving inverse heat conduction and mass transfer problems and classification of existing methods is provided in [5−7].

13.2 METHODS FOR SOLVING INVERSE HEAT CONDUCTION PROBLEMS

The following inverse heat conduction problems are of interest when studying steel quenching processes:

- Determination of cooling characteristics of quenchants
- Determination of thermal properties of steel during cooling
- Placement of thermocouples in the probes
- Determination of the surface temperature and heat flux densities for specific steel parts

13.2.1 Determination of Cooling Characteristics of Quenchants

Cooling characteristics of quenchants are sufficiently represented by critical heat flux densities q_{cr1} and q_{cr2} or by heat transfer coefficients α (or h), which describe the heat transfer during quenching with good accuracy (see Chapter 3). For bodies of complex shape, accurate computations of the heat transfer between a solid body and a liquid can be performed by solving a coherent heat conduction problem for the solid body and the liquid. Currently, such computations are performed using CFD (computational fluid dynamics) methods [8]. CFD modeling can be applied to convective heat transfer processes, but unfortunately cannot be applied effectively yet to boiling processes, which are the main modes of heat transfer during quenching.

13.2.2 Determination of Thermal Properties of Steel During Cooling

Two major thermal properties of steel affecting the heat conduction and temperature field in the part are thermal conductivity λ (or k) and specific heat capacity C_V. Note that the

---

[1] *IQ Technologies, Inc., Akron, Ohio, and Intensive Technologies Ltd., Kyiv, Ukraine*

210

third material thermal characteristic–thermal diffusivity–can be calculated using values for λ and C_V. The values of material thermal conductivity and specific heat capacity can be determined by solving an inverse heat conduction problem [1,2]. However, there are no data on the above steel thermal properties in the technical literature that were determined by solving the inverse heat conduction problem. For austenitic steels, which have no phase transformations, thermal properties are presented in Chapter 10.

For steels experiencing the phase transformations, thermal conductivity, thermal diffusivity, and specific heat capacity depend on material structure, which changes during the quench process according to CCT or TTT (time-temperature-transformation) diagrams.

13.2.3 Placement of Thermocouples in the Probes

For solving inverse heat conduction problems, it is necessary to gather temperature data, which can be accomplished by using special probes with two or more thermocouples located near the probe surface. The most suitable probe for solving an inverse heat conduction problem is the Liscic probe descried in [9]. Vergana-Hernandez and Hernandez-Morales [10] designed a novel probe to study wetting kinematics during forced convective quenching. This probe was successfully used to solve the inverse heat conduction problem [10].

Typically, cylindrical probes are used for the temperature measurements needed for solving the inverse problem. If the thermocouple is placed at a geometric center of the cylindrical probe and its readings are used for solving the inverse heat conduction problem, the error of calculations will be significant. To restore the temperature at the surface of the probe needed to calculate the heat transfer coefficients, the thermocouple should be placed as close as possible to the surface. The farther the thermocouple is located from the surface of the probe, the greater the error of the calculation of the surface temperature and heat transfer coefficients will be.

For example, for a probe of 20-mm diameter, an error of the placement of the near-surface thermocouple of 0.5 mm will result in the error of 20 % when determining the heat transfer coefficient on the probe surface [5]. To explain this more clearly, let's go back to the four streams and a polluted river. Assume that in the first river the water is blue, in the second the water is yellow, in the third the water is red, and in the fourth the water is green. Near the point where streams merge together, four colors can be seen. By solving the inverse problem of hydrodynamics, one can evaluate how much each plant polluted separately. Farther from this point will be only one color of water. It will be impossible to evaluate how much each plant polluted. The closer the pollution is measured to the place where the streams form the river, the greater the accuracy of the determination of the pollution by each of the factories will be. Measuring the pollution in the river far from the streams allows the calculation of only a cumulative pollution from all four factories.

Another method of locating thermocouples in the probe is to place one thermocouple near the surface and another thermocouple at the probe core. Temperature readings obtained for the probe core are used to compare results of calculations with the experimental data.

13.2.4 Determination of the Surface Temperature and Heat Flux Densities for Specific Steel Parts

To study cooling processes for specific steel parts under specific conditions, it may be necessary to solve two-dimensional or three-dimensional inverse problems for the determination of the surface temperature and heat flux densities. In many situations, this problem may be solved by computer simulation of a coupled heat conduction problem for the solid body and the liquid [1,2,8].

The classification of the methods of solving inverse heat conduction problems is provided in [1,2,4]. More detailed information on solving inverse problems is discussed below.

13.3 VARIOUS METHODS OF SOLVING INVERSE HEAT CONDUCTION PROBLEMS
13.3.1 Computation of Heat Flux Density on the Surface of a Probe

One of the important characteristics of a liquid is a critical heat flux density, which can be derived from the curve of heat flux density versus time. Usually the heat flux density at the part surface is determined based on Fourier's law:

$$q = -\lambda \frac{\partial T}{\partial r} \qquad (1)$$

or

$$q = \lambda \frac{T_{i+1}^k - T_i^k}{\Delta r}.$$

where

q is heat flux density;

λ is thermal conductivity;

T_i^k is surface temperature at k moment of time;

T_{i+1}^k is temperature at the distance Δr from the surface at k moment of time; and

q_c is correction to be evaluated.

The calculation of the heat flux density is more accurate as $\Delta r \to 0$. With an increase of Δr, it is necessary to add a correction term q_c when determining q [11]:

$$q = \lambda \frac{T_{i+1}^k - T_i^k}{\Delta r} + q_c. \qquad (2)$$

If the correction term q_c is disregarded, there will be an error in the heat flux density calculation. At this point, let's look at a proof of Eq 2 and an equation for determining the error when q_c is disregarded.

Any continuous function $f(x)$ can be described in a Taylor series as:

$$f(x) = f(a) + (x-a)f'(a) + \frac{(x-a)^2}{2!}f''(a)$$
$$+ \ldots + \frac{(x-a)^n}{n!}f^n(a) + R_n(x), \qquad (3)$$

where $R_n(x)$ is the remainder term of the Taylor series. Similarly, the temperature at time k, as a function of coordinates, is determined from:

$$T^k(r) \approx T^k(R) + (r-R)\frac{\partial T(R)}{\partial r} + \frac{(r-R)^2}{2!}\frac{\partial^2 T(R)}{\partial r^2} + \ldots, \quad (4)$$

where:

r is the distance from the origin, which is located at the center of the part;

$T^k(r)$ is the temperature at the point with coordinate r at time k;

$T^k(R)$ is the temperature at the surface of the probe at time k; and

$\dfrac{\partial T(R)}{\partial r}$ is the temperature gradient at the surface of the probe. In Eq 4, only the second partial derivative $\dfrac{\partial^2 T}{\partial r^2}$ is unknown, which can be found from the differential equation of heat conductivity (see Chapter 5, Eq 2). Eq 4 may be used for obtaining the equation for determining the heat flux density.

Eq 4 can be transformed into:

$$\frac{T^k(r) - T^k(R)}{\Delta r} = -\frac{\partial T(R)}{\partial r} + \frac{\Delta r}{2!}\frac{\partial^2 T}{\partial r^2} + \dots, \qquad (5)$$

where $r - R = -\Delta r$. Multiplying the right and left parts of the equation by the heat conduction λ produces:

$$\lambda \frac{T^k(r) - T^k(R)}{\Delta r} = -\lambda \frac{\partial T}{\partial r} + \frac{\lambda \Delta r}{2}\frac{\partial^2 T}{\partial r^2}.$$

This is the origin of Eq 1:

$$q \equiv -\lambda \frac{\partial T}{\partial r} = \lambda \frac{T^k(r) - T^k(R)}{\Delta r} - \frac{\lambda \Delta r}{2}\frac{\partial^2 T}{\partial r^2} + \dots. \qquad (6)$$

In Eq 6, the correction factor q_c is the rightmost term:

$$q_c \cong -\lambda \frac{\Delta r}{2}\frac{\partial^2 T}{\partial r^2}. \qquad (7)$$

To find the second partial derivative, transform the differential equation of heat conductivity (see Chapter 5, Eq 2) for the nondimensional case to the form:

$$C_V \frac{\partial T}{\partial \tau} - \frac{n}{r}\lambda\frac{\partial T}{\partial r} - \frac{\partial \lambda}{\partial T}\left(\frac{\partial T}{\partial r}\right)^2 - \lambda\frac{\partial^2 T}{\partial r^2} = 0. \qquad (8)$$

whence we obtain:

$$\lambda\frac{\partial^2 T}{\partial r^2} = C_V \frac{\partial T}{\partial \tau} - \frac{n}{r}\lambda\frac{\partial T}{\partial r} - \frac{\partial \lambda}{\partial T}\left(\frac{\partial T}{\partial r}\right)^2. \qquad (9)$$

Usually, standard probes used for the evaluation of cooling characteristics of quenchants are made of stainless steel, silver, nickel, or other well-known metals. For these materials, a linear correlation of the heat conduction versus temperature may be considered within a small variation of the average temperature, that is,

$$\lambda = a + bT. \qquad (10)$$

Differentiating Eq 10 with respect to T yields:

$$\frac{\partial \lambda}{\partial T} = b.$$

Substituting this expression into Eq 9,

$$\lambda\frac{\partial^2 T}{\partial r^2} = C_V \frac{\partial T}{\partial \tau} - \frac{n}{r}\lambda\frac{\partial T}{\partial r} - b\left(\frac{\partial T}{\partial r}\right)^2.$$

Therefore:

$$q_c \approx -C_V \frac{\partial T}{\partial \tau}\frac{\Delta r}{2} + \frac{n}{r}\lambda\frac{\partial T}{\partial r}\frac{\Delta r}{2} + b\frac{\Delta r}{2}\left(\frac{\partial T}{\partial r}\right)^2.$$

Replacing the partial derivatives by their finite-difference values:

$$\frac{\partial T}{\partial \tau} = \frac{T_i^{k+1} - T_i^k}{\Delta \tau} = -\frac{T_i^k - T_i^{k+1}}{\Delta \tau}$$

and

$$\frac{\partial T}{\partial r} = \frac{T_i^{k+1} - T_i^k}{\Delta r} = -\frac{T_i^k - T_i^{k+1}}{\Delta r}$$

yields:

$$q_c \approx C_v \left(\frac{T_i^k - T_i^{k+1}}{\Delta \tau}\right)\frac{\Delta r}{2} - \frac{n}{2}\frac{\lambda}{r}\left(T_i^k - T_{i+1}^k\right) - \frac{b}{2\Delta r}\left(T_i^k - T_{i+1}^k\right)^2. \qquad (11)$$

Thus, the complete equation for the determination of the heat flux density during cooling of plate-shaped, cylindrical, or spherical bodies can be presented as:

$$q = \lambda\frac{T_i^k - T_{i+1}^k}{\Delta r} + C_V\left(\frac{T_i^k - T_i^{k+1}}{\Delta \tau}\right)\frac{\Delta r}{2} - \frac{n\lambda}{2r}\left(T_i^k - T_{i+1}^k\right) - \frac{b}{2\Delta r}\left(T_i^k - T_{i+1}^k\right)^2. \qquad (12)$$

Now let's find the relative error ε if the value of q_c is disregarded, which is presented as:

$$\varepsilon = \frac{q_c}{q - q_c}\cdot 100\% \qquad (13)$$

or

$$\begin{aligned}
\varepsilon &= \frac{\Delta r}{\lambda\left(T_i^k - T_{i+1}^k\right)}\left[\left(T_i^k - T_i^{k+1}\right)\frac{C_V\Delta r}{2\Delta \tau}\right. \\
&\quad \left. - \frac{n\lambda}{2r}\left(T_i^k - T_{i+1}^k\right) - \frac{b}{2\Delta r}\left(T_i^k - T_{i+1}^k\right)^2\right]\cdot 100\% \\
&= \frac{1}{2}\left[\frac{C_V\Delta r^2}{\lambda\Delta \tau}\left(\frac{T_i^k - T_i^{k+1}}{T_i^k - T_{i+1}^k}\right) - \frac{n\Delta r}{r} - \frac{b}{\lambda}\left(T_i^k - T_{i+1}^k\right)\right]\cdot 100\%. \quad (14)
\end{aligned}$$

Let's analyze Eq 14 for the determination of the relative error ε by evaluation of possible values when probes are cooled under various conditions of heat transfer. When quenching in aqueous polymer solutions and oils, heat transfer coefficients are not large, and therefore the temperature gradient in the part cross-sections is not large, either. This indicates that the third term of Eq 14 can be neglected, since $\left(T_i^k - T_{i+1}^k\right) \to 0$. (For a stainless steel such as Kh18N9T [AISI 304] grade, $b = 0.0157$, and when $Bi \to 0$, the value of $T_i^k - T_{i+1}^k$ also vanishes.) Therefore, for small values of Bi, the main role is played by the first term of Eq 14. The second term of this equation yields the error due to changes in the part shape. The minimum error of this kind is for a plate, because $\dfrac{n\Delta r}{r} = 0$, since $n = 0$. The maximum error is for spheres: because $n = 2$, the second term is $\dfrac{2\Delta r\lambda}{r}$. The shape of the probe has no effect upon the above error only if $\dfrac{\Delta r}{r} \to 0$.

When quenching (cooling) probes with a very intensive heat transfer, for example, in aqueous solutions of salts and alkalis or by an intensive shower or water jets, high values of the heat transfer are reached, and temperature differences are very high. Therefore, when $Bi \to \infty$, the third term of Eq 14 reaches maximum values because $\left(T_i^k - T_{i+1}^k\right)$ can reach large values. Therefore, significant errors appear during intensive cooling, minimum errors during cooling in oils and aqueous polymer solutions.

Using experimental data $\left(\dfrac{\Delta r}{R} = \dfrac{1.5}{25}\right)$, presented in [11,12, 13], the error values presented below were calculated [17,18].

TABLE 1—Values of relative error ε in computations of heat flux density if value of q_c is disregarded, for a cylindrical probe made of Kh18N9T (AISI 304) steel (R = 10 mm), in various conditions of heat transfer [11]								
Cooling conditions	τ (s)	0.1	0.5	1	2	3	4	5
$Bi \rightarrow \infty$	ε (%)	−28	−14	−11	−9	−7.3	−7.1	−6.9
Oil	ε (%)	−3.3	−4.1	—	−4.4	—	—	−4.2

Here R is the radius, and r is a coordinate. The water was strongly agitated. For these computations, the thermal and physical properties of austenitic steel Kh18N9T were taken from Tables 2 and 3 of Chapter 10. Table 1 presents error values that appeared during cooling of a cylindrical probe in oil and in water. The table shows that when $Bi \rightarrow \infty$, the error is maximum.

This analysis provides the evidence that, during computations of heat flux densities, it is necessary to use an equation that includes the heat transfer in the layer near the surface. In Eq 12, the first term takes into account Fourier's law, the second term represents the changes of the heat content in the near-surface layer of Δr thickness, the third term characterizes the shape of the body, and the fourth term takes into account the changes in the material, thermal, and physical properties.

To measure the heat flux density by this method, the Liscic-Nanmac probe (see Fig. 1(a–c)) may be used. This is the most accurate commercially available probe, obtaining the most accurate experimental data.

Some experimental results are provided in Fig. 2. Fig. 2(a) shows the probe surface temperature and the temperature 1.5 mm below the surface versus time. The heat flux density versus time is shown in Fig. 2(b), and the heat flux density versus the surface temperature is shown in Fig. 2(c). Fig. 2(c) indicates that when quenching the probe in the nonagitated oil, film boiling is observed within the range of 600°C to 800°C, and nucleate boiling between 300°C and 600°C. The maximum heat flux density in this experiment is 2.3 MW/m^2.

The following advantages of this probe assembly have been reported [12,13]:
- The response time of the thermocouple is 10^{-5} s, making it sensitive to small and rapid temperature changes.
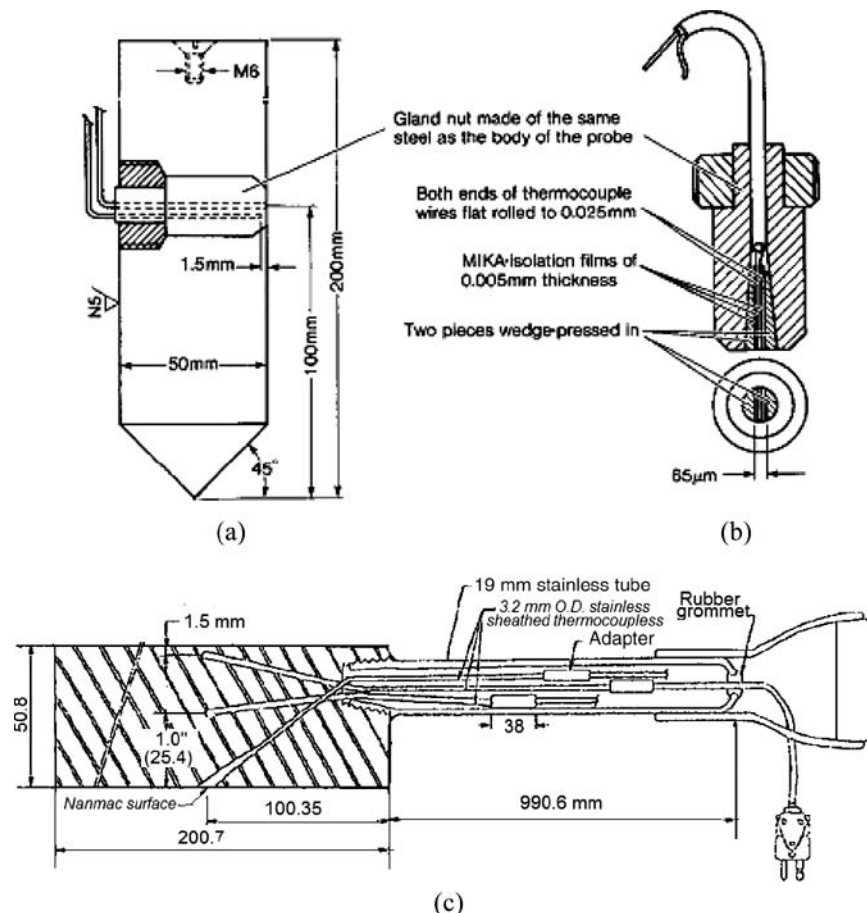
Fig. 1—Liscic-Nanmac steel probes: (a) first version of probe [9]; (b) accurate thermocouple furnishings; (c) second version of probe [12,13].
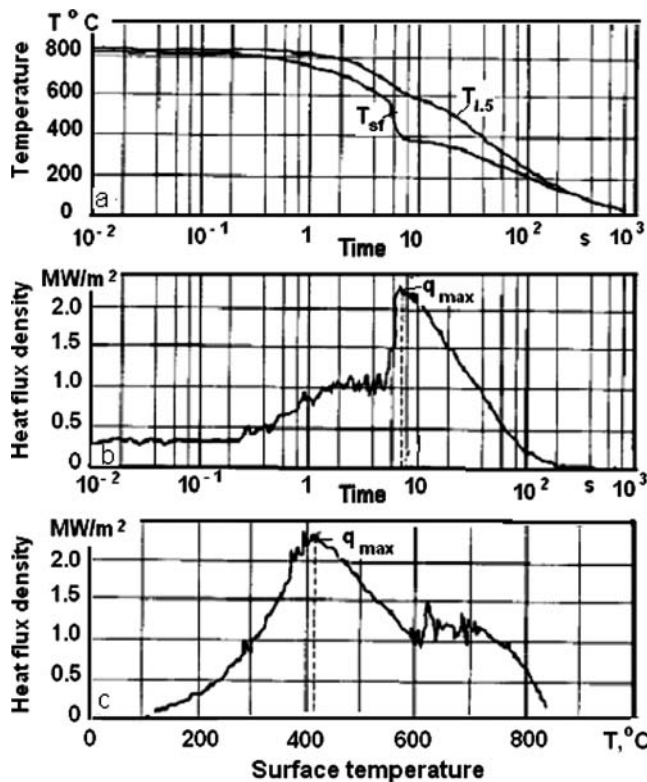
Fig. 2—Experimental data obtained by quenching the Liscic-Nanmac probe in still mineral oil at 20°C [12]: (a) Recorded temperature vs. time for the surface and at a depth of 1.5 mm below the surface; (b) calculated heat flux density vs. time; (c) calculated heat flux density vs. surface temperature.

- The surface condition of the probe can be easily maintained, because only the surface temperature sensor needs to be polished before each measurement.
- The Liscic-Nanmac probe is an excellent tool for investigations of the self-regulated thermal processes reported in Chapter 2.

13.3.2 Tikhonov Regularization Method

Until the middle of the last century, inverse problems were considered to be mathematically incorrectly stated problems, that is, problems that do not meet the principles of correctness [1,2,4]. Nevertheless, inverse problems were posed and solved.

Tikhonov [14,15] proved theoretically that inverse problems could be solved correctly. He also created a new methodology for solving inverse problems (that could not be solved by any other method) by the use of regularizing algorithms. The first works were devoted to inverse problems that are solvable analytically, that is, mainly to linear heat conduction problems. For many problems, theorems of existence and uniqueness of the solution were proved, algorithms to search for the regularization parameter α were suggested, and the convergence of various regularizing algorithms was demonstrated [15,16]. Because thermal processes during quenching are very complicated, more work was needed to develop further improvements in solving inverse heat conduction problems [16–18].

For practical problems related to heating and cooling of steel, it is of an interest to consider the use of the regularizing numerical algorithms for nonlinear heat conduction problems. For these types of problems, the method of regularization is reduced to the introduction of a regularizing term into the error function that is to be minimized:

$$F_\alpha[u] = \|Au - f\|^2_m + \alpha\|u\|^2_C, \qquad (15)$$

where:

u is a vector of required parameters;

F is an error function to be minimized;

f is a vector of experimental data;

A is a matrix of transition from required parameters to estimated values at appropriate points of temperature measurements;

$\|\cdot\|_m$ is a norm in space R^m; and

$\|\cdot\|_C$ is a norm defined as $\|u\| = (Cu, u)^{1/2}$, where C is a positively determined matrix (for example, it is possible to assume $C = E$, where E is a unit matrix.

By the classification presented above, this method is related to the class of extreme methods, a group of minimization with regularization. The next section of this chapter presents specific examples of using the regularization method in practice.

13.3.3 Green Function Method for Solving Nonlinear Inverse Problems

Guseynov [19] used the Green function method for solving linear and nonlinear inverse problems. His approach is especially important for solving nonlinear inverse problems for the hyperbolic heat conductivity equation where some parameters of the mathematical model cannot be derived from the experiment, but are rather determined from exact calculations. Solving a direct classical problem that includes the hyperbolic heat conductivity equation with the nonlinear boundary condition (generated by the boiling process) is an extremely complicated task even for mathematicians. However, solving an inverse problem that includes the hyperbolic heat conductivity equation with the nonlinear boundary condition seems to be even more difficult. Guseynov and his colleagues solved this difficult inverse problem using the Green function method [20–22].

Such solutions are needed for designing new, environmentally safe intensive quenching technologies for strengthening of steel parts. This cycle of analytical and experimental investigations has been carried out under the supervision of the World Scientific and Engineering Academy and Society (WSEAS). The activities of WSEAS include organizing international forums for the discussion of such breakthrough problems.[1]

13.3.4 Statistical Regularization Method

All thermal and physical parameters of the mathematical model (temperature, material properties) as well as spacing (coordinates, time) are stochastic (random) by nature. Thus, their values are always given to some degree of accuracy. The majority of methods of solving inverse problems are based on mathematical models of heat and mass transfer assuming the stochastic nature of temperature measurements only.

---

[1] See the WSEAS website at www.wseas.org; in particular, see www.wseas.org/propose/project/wseas-projects.htm and www.wseas.us/conferences/2010/taipei/hte/.

Krivoshey [23] suggested a stochastic approach of stating and solving inverse heat conduction problems that assumes a stochastic nature of *all* parameters of the mathematical model. Such approach suggests setting the stochasticity of one (or two) parameters while "freezing" (imposing determinacy on) all the others and varying statements of problems depending on the required function. Solving a problem would then consist of two key procedures: first, an introduction into the model (equation) of a stochastically approximated parameter, and second, a subsequent statistical averaging of the obtained stochastic equations with respect to these realizations. With the fulfillment of these two procedures for all parameters, the correctness of the statement of the problem is reached automatically. In terms of the integral equations, this means that the algorithm naturally transforms the incorrect integral equation of the first kind with respect to the required function into the correct equation of the second kind.

On the basis of this approach, the heat conduction equations for statistically averaged values of temperatures, instead of any small regularization parameters, contain the statistical characteristic (dispersion) of the random parameter. The statements of inverse problems on the basis of these equations possess a property of correctness. By the classification presented above, this method is related to the class of extreme methods, a group of minimization with regularization.

This method was used to evaluate temperature and heat flux oscillations in cylindrical steel probes cooled from 800–900°C in aqueous solutions of polymers at 20–30°C [24].

13.3.5 General Approach of Solving Inverse Heat Conduction and Mass Transfer Problems

Krukovskyi [5] used the Newton-Gauss method. He has suggested the estimation of parameters of a nonlinear model combined with the regularization method for solving all inverse heat conduction and mass transfer problems in the most general case. Here, the solving of a direct problem and the parameterization of required values are performed in a specific problem.

Krukovskyi [5] describes a universal computer program called FRIEND (FRee Identification for ENgineers and Designers) that, being linked to a module providing parameterization and solving a direct problem, solves inverse heat and mass transfer problems of any type. To eliminate the instability of the solution, a number of regularizing procedures are suggested, which yield a stable solution of an inverse problem.

By the classification presented above, this method is related to the class of extreme methods, the group of identification and optimal evaluation [4,5].

13.4 COMPARISON OF THE SEQUENTIAL FUNCTION SPECIFICATION TECHNIQUE WITH THE REGULARIZATION METHOD

Authors [7,25–27] suggested to use the sequential function specification technique for solving the inverse heat conduction problem. Let g be a function to be found. Using this algorithm, choose a set of time points $t_0, t_1, \dots t_N$ and determine the values of the function g sequentially. First, at point t_0, determine $g(t_0) = g_0$, then at t_1, iteratively select the best g_1 ($g_1 = g(t_1)$), and so on. At each step, k iterations are used in solving a direct heat transfer problem to minimize the function

$$\left\| F(u) - F(u)_{exper} \right\|,$$

where:

$F(u) = (f(u_0), f(u_1), \dots f(u_k))$, the current solution of the direct heat transfer problem at time points $u_0, u_1, \dots u_k$; and

$F \exp er = (F_0, F_1, \dots F_k)$ is a vector of experimental data at the same time points $u_0, u_1, \dots u_k$, where k is the number of the current step, which constantly increases by 1.

Finally, build a function based on values $g_0, g_1, \dots g_N$, which determines the function g.

For comparison with the regularization method, use the same approach in the selection of time points $u_0, u_1, \dots u_k$, and in building function g based on values $g_0, g_1, \dots g_N$. Assume also that the regularization parameter $\alpha = 0$. The same minimization function as in the sequential function specification technique is thus obtained, with the only difference being that in the sequential function specification technique, the values of g were evaluated sequentially step by step, while in the regularization method, an algebraic matrix to determine g was built and simultaneously found by solving a system of algebraic equations.

In this case, the sequential function specification technique has more advantages: it is simpler in implementation, requires fewer mathematical operations, and therefore consumes less time. At the same time, the inverse heat conduction problem is ill posed, with many solutions. If a different set of time points $t_0, t_1, \dots t_{N1}$ is selected, a different solution, which can be either better or worse, is obtained.

In the regularization method, there is a potential to have more control over this situation. One of the regularization method's most powerful options is the selection of the regularization parameter α. When $\alpha = 0$, the same minimization problem as in the sequential function specification technique is solved. When $\alpha > 0$, a solution with fewer oscillations that is less dependent on temperature measurement errors is obtained. The greater α is, the finer the solution will be. However, the greater α is, the larger the integral difference will be with respect to the values of the experimental data. The problem is to find a compromise where the difference with experimental data is still acceptable with an acceptable solution. More information on this issue can be found in [28] and [29].

Another option in the regularization method is to analyze intermediary solutions at each iteration and add new time points, if necessary, to the originally chosen set of time points $t_0, t_1, \dots t_N$ (which determine splines built on them). One more option in the regularization method is to consider time points $t_0, t_1, \dots t_N$ as variable parameters to be found to minimize the function. Of course, this increases the number of necessary calculations, but it also results in a better solution.

Thus, with regard to the sequential function specification technique, the regularization method has the advantage of automatically getting a finer solution in common practical cases. Its disadvantages are that it is much more complicated to implement in a computer program and that it requires more mathematical operations, and therefore it takes more time to obtain an inverse solution for the same experimental data.

For the problem of determining the cooling characteristics of quenchants (in thousands of experiments that have been conducted), the average computation time for the inverse problem by the regularization method was about one-half minute per experiment. This was acceptable, since it took much more time to prepare the experiments themselves.

13.5 METHOD AND SOFTWARE FOR DETERMINATION OF COOLING CHARACTERISTICS OF QUENCHANTS

For the determination of cooling characteristics of quenchants, the computer program IQLab was developed [30]. The program is based on these and other achievements in this field [5,7,14,16]. It provides cooling characteristics, data acquisition, and processing and generalizes the experimental data. To determine cooling characteristics of a quenchant, the experiments are conducted using probes of a simple shape (cylinder, plate, or ball) with thermocouples inserted inside the probe and near the surface. The data are processed, and then the inverse problem is solved. The solution of the inverse problem determines the temperature field and heat flux density and calculates the heat transfer coefficients, Biot number Bi, generalized Biot number Bi_V, and Kondratjev number Kn for both boiling and convection processes. Results are presented as functions versus time in normal and logarithmic coordinates versus surface temperature and other characteristics in charts and in text form. The temperature field may be viewed superimposed on a CCT diagram, which simplifies the quenching process design.

A preliminary processing of experimental data increases the quality of the solution and in many cases saves computational time. The preliminary processing includes:

1. Removal of erroneous thermocouple data (noise). This operation can be performed automatically or manually by visually editing the data using a built-in text editor. In case of automatic correction, the erroneous thermocouple data are replaced with average values.
2. Narrowing the time range. When performing experiments, the time range is usually selected, and it is preferable to restrict the calculations to the time range of the cooling process to be investigated to save computation time. Narrowing the time range is done by the user based on the visual analysis of the experimental data.
3. Smoothing of the data. Data smoothing eliminates random measurement errors. Although smoothing is not required for solving the inverse problem, since the regularization parameter helps in obtaining a smoothed solution, in some situations, preliminary smoothing improves the solution. To decide whether to smooth the data or not, it is possible to solve the inverse problem both ways and then compare the results.
4. Averaging the data. Averaging the data considerably saves computation time. It is advisable to use data averaging when the cooling process occurs slowly and the data are recorded frequently. The program automatically suggests the optimal rate for the majority of conditions; however, users may change the rate of averaging at their own discretion.

13.6 TESTS OF THE METHOD AND SOFTWARE FOR DETERMINING QUENCHANT COOLING CHARACTERISTICS

The error of the inverse problem solution depends on the experimental data accuracy. For the evaluation of this error, numerical tests have been performed, as described in the examples below.

Example 13.1

An estimate of the method's error is determined in the case where accurate data are available (the calculation error of

TABLE 2—Input of boundary data for a direct problem: time and heat transfer coefficient α (given)	
Time (s)	α (W/m²K)
0.0	0
0.1	4,000
0.2	7,000
0.3	9,000
0.4	10,000
0.5	10,500
0.6	10,400
0.7	10,300
0.8	10,200
0.9	10,100
1.0	10,000

accurate data is 0.01°C). For this purpose, let's solve a direct problem for a 30-mm-diameter steel cylinder made of Ch18N9T (AISI 304) stainless steel. The cylinder is cooled from 800°C, and the heat transfer coefficient is set to smoothly increase from zero up to 10,000 W/m²K, as shown in Table 2. The temperature of the quenching medium is 20°C. For solving the direct and inverse problems, IQLab software was used.

After solving the direct problem, the temperature field is obtained. For testing purposes, the surface temperature and the temperature at 1 mm from the surface are used. These curves are shown in Fig. 3.

The calculation data are saved in a text file, and the inverse problem is solved to calculate the surface temperatures (Tsurf) using the values of the temperature at a distance of 1 mm from the surface as input data. Fig. 4 presents the data used in the inverse problem in column Texp (temperature 1 mm below the surface). The data in columns Tsurf and Alpha conv (given heat transfer coefficient) will be used only for comparison with the data obtained as a result of solving the inverse problem.

The outcome of solving the inverse problem is values for the heat transfer coefficient and surface temperature. Solutions of the inverse problem and the corresponding direct problem are presented in Fig. 5.

The test has shown (see Fig. 5) that the given values of the surface temperature and heat transfer coefficient and those obtained by solving the inverse problem practically coincide (converge). Detailed analysis shows that the maximum temperature error is 9°C (1.2 %) at the moment of the sharp surface temperature drop, and in the other parts of the time range is less than 0.1°C (0.1 %). The maximum error of the heat transfer coefficient is 8 % at the moment of the sharp surface temperature drop; in the remaining time range, the error is less than 0.1 %. Such errors are acceptable.

Example 13.2

Now let's consider the effect of the error of the given experimental data on the solution of an inverse problem. For this
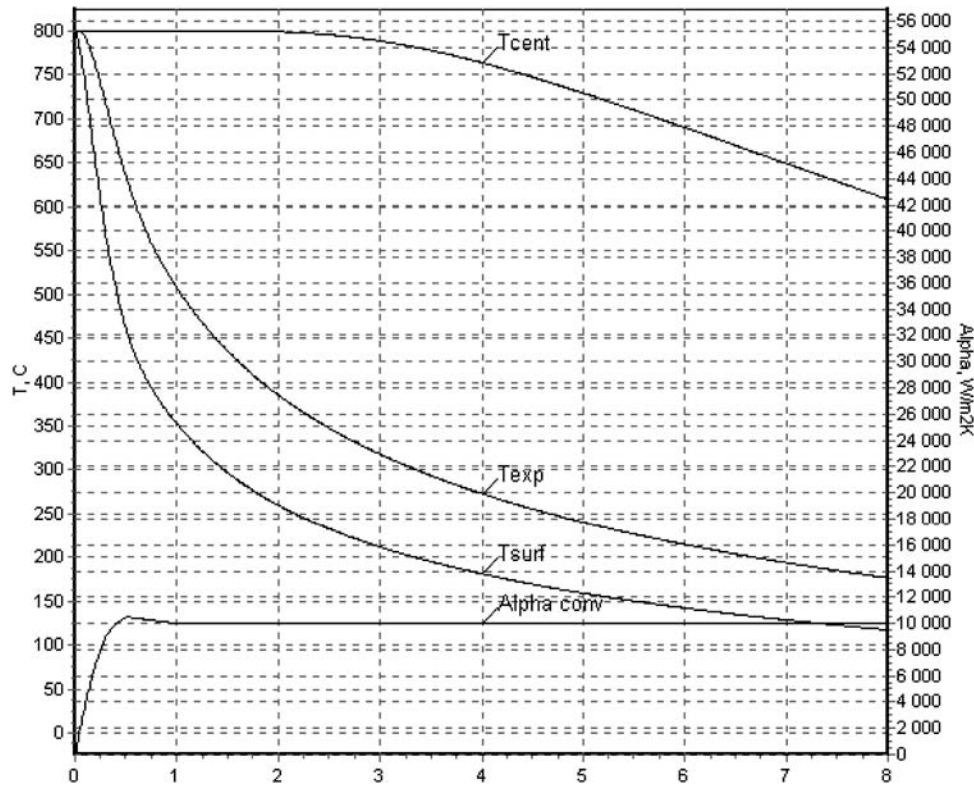
Fig. 3—Results of computations of the direct problem: Tcent is temperature at the center; Tsurf is temperature at the surface; Texp is temperature at the distance of 1 mm from the surface; "Alpha conv" is the given heat transfer coefficient α.
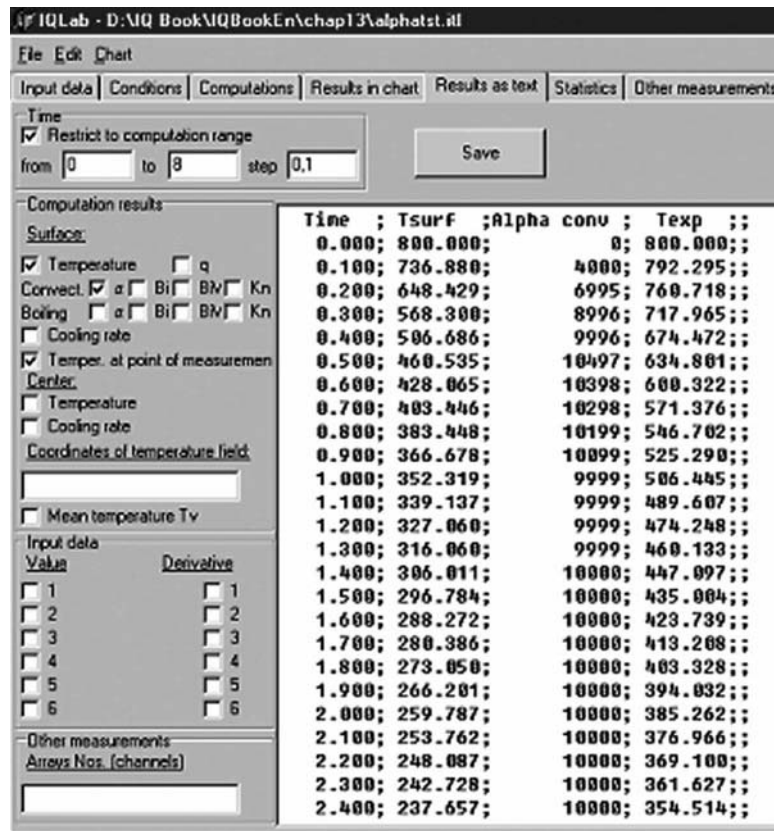
Fig. 4—Sample input to IQLab software, showing the results of solving the direct problem that will be used as the input data for solving the inverse problem.
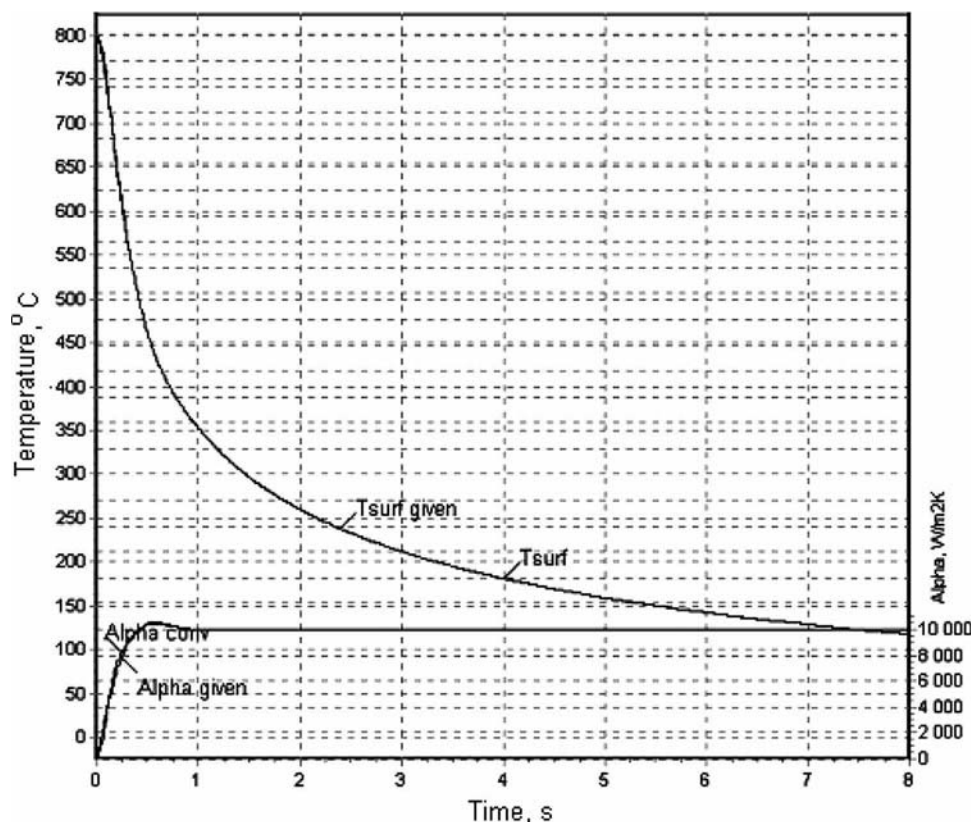
Fig. 5—Results of solving direct and inverse problems: "Alpha given" and "Tsurf given" are given values of the heat transfer coefficient α and the temperature at the surface; "Alpha conv" and Tsurf are the solutions of the inverse problem.

purpose, random numbers having a normal distribution and deviation of 4 are added to the temperature measured at 1 mm from the surface. That is, it is assumed that errors of measurements have a normal distribution and a standard deviation of 4°C. The computations are performed as in Example 13.1. The temperatures obtained with random errors and the results of solving the inverse problem are presented in Fig. 6.

In Fig. 6, the maximum error of the heat transfer coefficient determination is 10 %, and at 75 % of all points, the error is less than 4 %. The maximum temperature determination error is 8°C; at 80 % of all points, the error is less than 2°C.

Example 13.3
The experimental data were shifted by a constant value which was predicted without calculations. It results in the shift of the temperature field by the same value, which has no effect upon the calculation of heat flux densities. However, it can exhibit a significant effect on the calculation of film or nucleate boiling heat transfer coefficients when the temperature approaches the boiling temperature. This error can be easily avoided by performing a calibration before starting the experiment.

Example 13.4
Evaluate the error connected with incorrect positioning of the thermocouple. For this example, assume that the thermocouple to be located at the distance of 1 mm from the surface is actually located at the distance of 1.5 mm from the surface. Also assume that the data are measured with the same random error as in Example 13.2. For the simulation

of these conditions, let's solve the direct problem and use the values of the temperature curve for the point located at 1.5 mm from the surface, add the random errors as in Example 13.2, and then solve the inverse problem specifying the temperature measured at 1 mm from the surface. The solution of the inverse problem is shown in Fig. 7.

The errors in Fig. 7 are not acceptable. The error of the surface temperature determination reaches 100°C and the error of the heat transfer coefficient determination for the majority of points is about 20 %; at the beginning of the cooling process, it exceeds 100 %. This problem may be avoided by placing an additional thermocouple at the center of the test specimen and then determining the position of the thermocouple location by trying different points of the thermocouple placement and solving a direct heat transfer problem. Only after this procedure is it possible to determine the cooling characteristics of quenchants.

13.7 DETERMINATION OF MZM-16 OIL COOLING CAPACITY BASED ON SOLVING THE INVERSE PROBLEM
MZM-16 oil is an accelerated oil that is produced from conventional oil by introducing special additives to eliminate film boiling [31]. Conventional quench oils are typically mineral oils, which may contain antioxidants to reduce the rates of oxidative and thermal degradation. Most of these oils have viscosities in the range of 100 to 110 SUS at 40°C (104°F). Conventional quench oils do not contain additives for increasing the cooling rate [32]. Accelerated quench oils are usually formulated from a mineral oil and contain one or more additives to increase cooling rates [32].
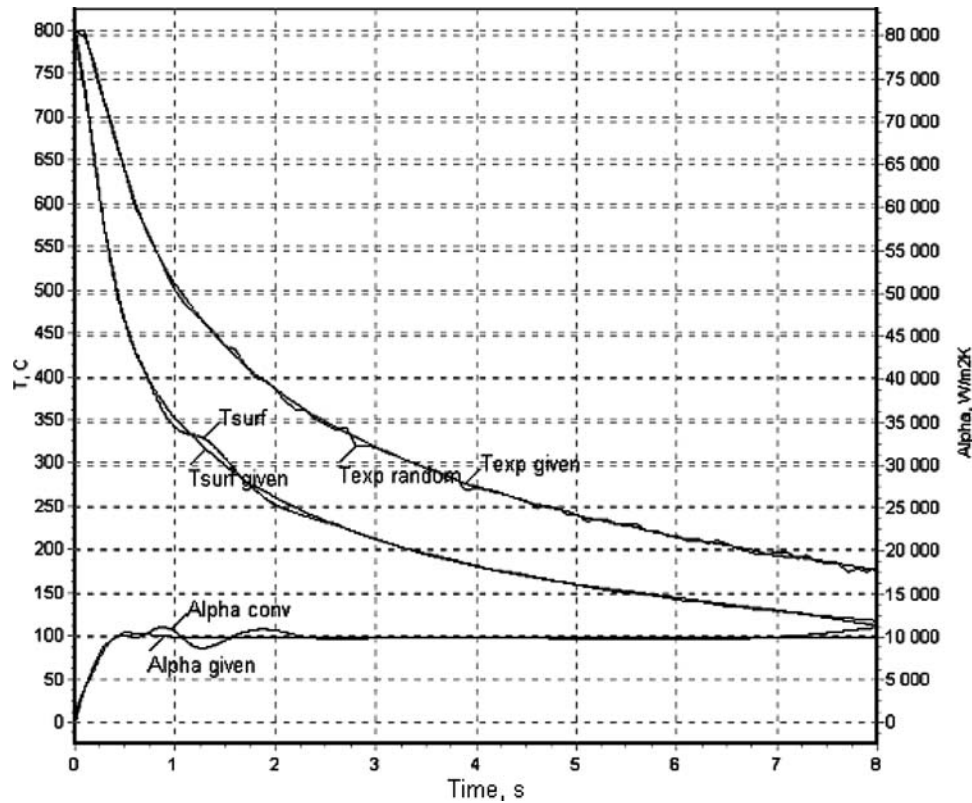
Fig. 6—Temperature versus time at the distance of 1 mm from the surface: "Texp given" is the exact value; "Texp random" is the same, with error having Gaussian distribution and deviation of 4. "Tsurf" and "Alpha conv" are solutions of the inverse problem, "Tsurf given" and "Alpha given" are given values of the temperature at the surface and the heat transfer coefficient α.

To investigate a cooling capacity of MZM-16 oil, cylindrical test specimens of 20 and 30-mm diameter were used. Thin thermocouples were welded onto the surface and at the core of the test specimens [11,31]. The test specimens were made of AISI 304 stainless steel. The thermal properties of austenitic stainless steels are presented in Table 3. The specimens' height H exceeded $4D$, where D is the specimen diameter. The

experimental data obtained by quenching a cylindrical specimen in MZM-16 oil at 61°C are presented in Fig. 8.

The heat flux densities and heat transfer coefficients were calculated by solving a heat conduction inverse problem using IQLab software. The results of these calculations are presented in Figs. 9 and 10.

From Fig. 9, the heat flux density appears to reach its maximum value of 2.3 MW/m^2 when the surface temperature is 450°C. These results are very similar to the data shown in Fig. 2. There, a film boiling process existed when the surface temperature was within the range of 600–800°C, and the heat flux density reached its maximum value when the surface temperature was 420°C. The difference in these surface temperatures (420°C and 450°C) can be explained by the difference in quench oil temperature and size of the test
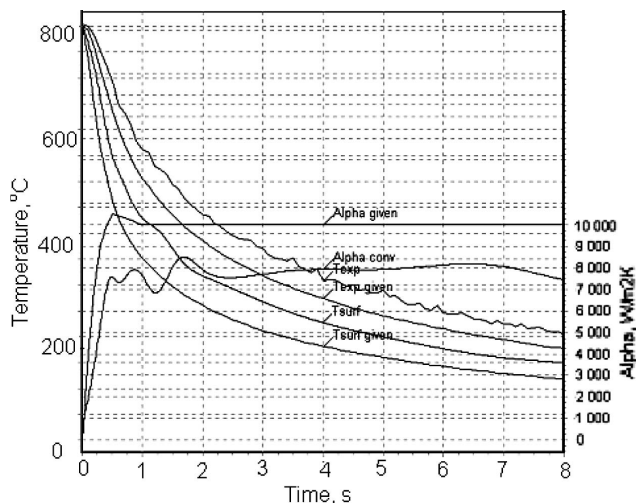
Fig. 7—Given data and results of the computation of the inverse problem in conditions when it is assumed that the thermocouple intended to be located at a distance of 1 mm from the surface is actually located 1.5 mm from the surface.

TABLE 3—Thermal conductivity λ and thermal diffusivity a of austenite versus temperature							
T (°C)	100	200	300	500	600	700	800
$\lambda, \dfrac{W}{mK}$	17.5	18	19.6	23	24.8	26.3	27.8
$\bar{\lambda}, \dfrac{W}{mK}$	17.5	17.7	18.55	20.2	21.1	21.9	22.6
$a \cdot 10^6, \dfrac{m^2}{s}$	4.55	4.6	4.70	5.3	5.6	5.8	6.2
$\bar{a} \cdot 10^6, \dfrac{m^2}{s}$	4.55	4.6	4.63	4.9	5.1	5.2	5.4
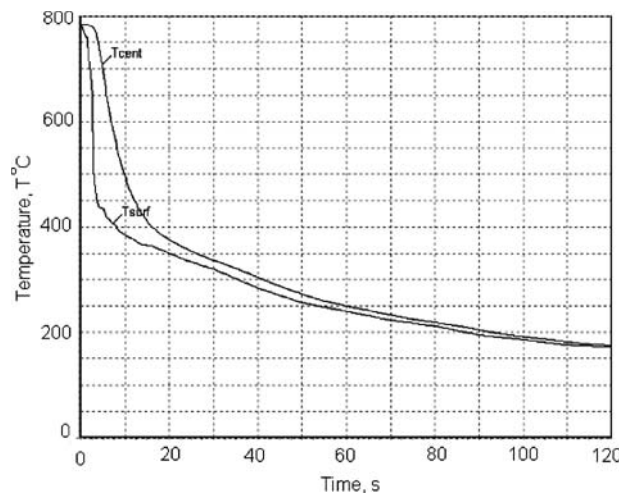
Fig. 8—Temperature at the surface and in the core versus time for MZM-16 oil at 61°C, with a cylindrical test specimen 19.9 mm in diameter and 80 mm in height.

probe. The average heat transfer coefficient during film boiling and nucleate boiling is about 1,800 W/m²K (see Fig. 10).

Film boiling is clearly observed in Figs. 9 and 10. With increasing oil temperature, the first critical heat flux density q_{cr1} increases and achieves its maximum value at 100°C (see Table 4) [31]. This is why it is important to determine the cooling capacity of MZM-16 oil at 100°C. Increasing the temperature of MZM-16 oil to 100°C, the situation changes significantly.

The experimental data (temperature versus time) for the 19.9-mm-diameter probe quenched in MZM-16 oil at 100°C are presented in Fig. 11, where Tsurf is the surface temperature and Tcent is the core temperature of the probe.

From Figs. 12 and 13, it is evident that film boiling is essentially absent when quenching in oil at 100°C. This indicates that the initial heat flux density during immersion of the cylindrical probe into hot MZM-16 oil was less than q_{cr1} (which was equal to 3.4 MW/m²). Very intensive boiling during the probe immersion created an intensive circulation of the oil around the surface of the probe, and therefore the first critical heat flux density exhibited a greater increase.
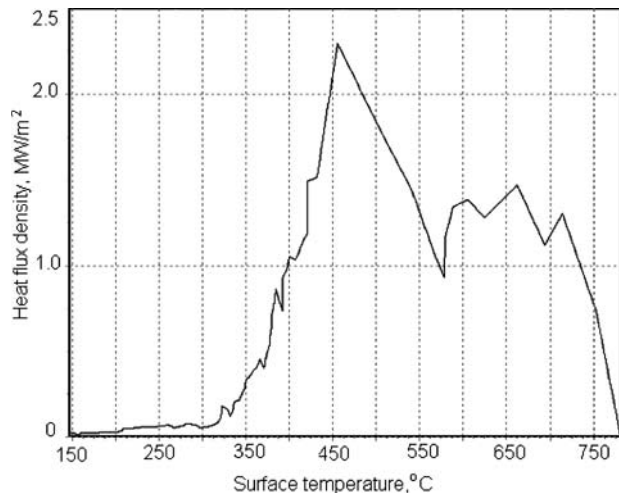
Fig. 9—Heat flux density versus surface temperature for MZM-16 oil at 61°C.

TABLE 4—First critical heat flux density versus temperature for MZM-16 oil

T (°C)	38	40	75	100	150	200
q_{cr1} (MW/m²)	2.8	3.0	3.3	3.4	3.0	2.5

That is why the maximum heat flux density q_{max} increased to 4 MW/m² at a 560°C surface temperature. This result is supported by Eq 13 from Chapter 2, which establishes a correlation between the surface temperature and the heat flux density, that is, $q = f (T_{sf} - T_s)$. Since the heat flux density increased, the surface temperature at which the maximum value of the heat flux density is observed also increased. Compared with Fig. 9, the surface temperature increased from 450°C to 475°C.
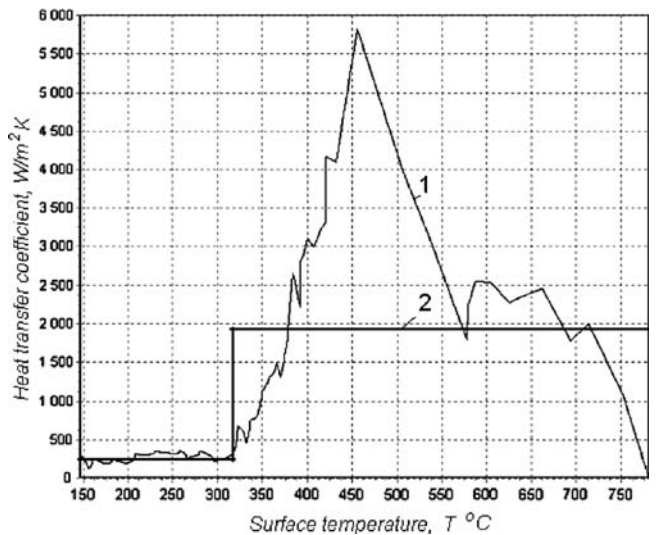
Fig. 10—Heat transfer coefficient versus surface temperature for MZM-16 oil at 61°C, with a cylindrical test specimen of 19.9-mm diameter and 80-mm height: 1, real value; 2, average value.
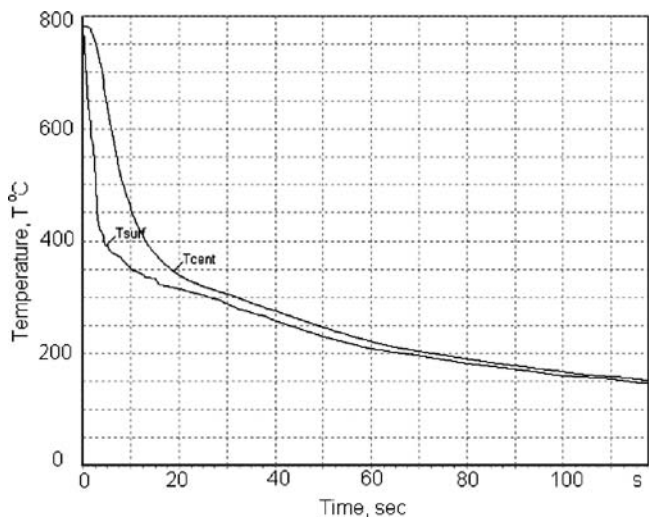
Fig. 11—Experimental temperature at the surface and at the core versus time for MZM-16 oil at 100°C with a cylindrical specimen of 19.9-mm diameter and 80-mm height.
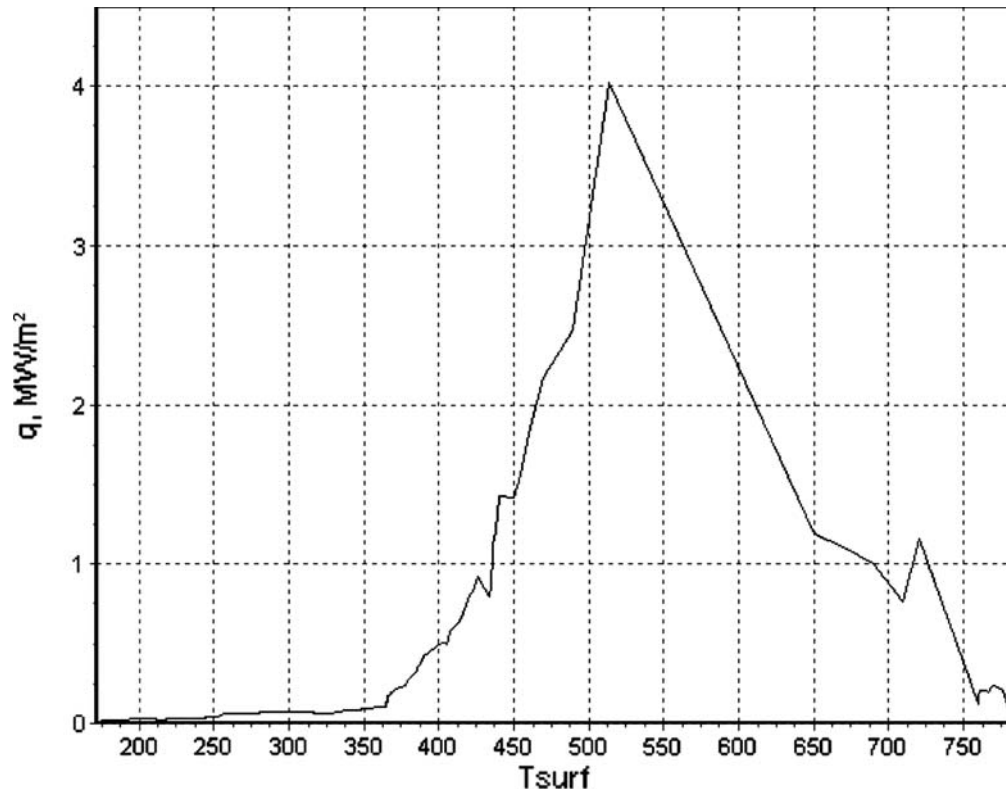
Fig. 12—Heat flux density versus surface temperature for MZM-16 oil at 100°C.

The further increase of the oil temperature above 100°C is connected with the decrease of q_{cr1}. The decrease of heat flux densities and heat transfer coefficients can be anticipated in this case. Some calculation results based on the experimental data are presented in Figs. 14 through 16. From these figures, it is evident that the maximum heat flux density decreased to 2 MW/m² and the average value of the heat transfer coefficient dropped to 1,100−1,200 W/m²K.
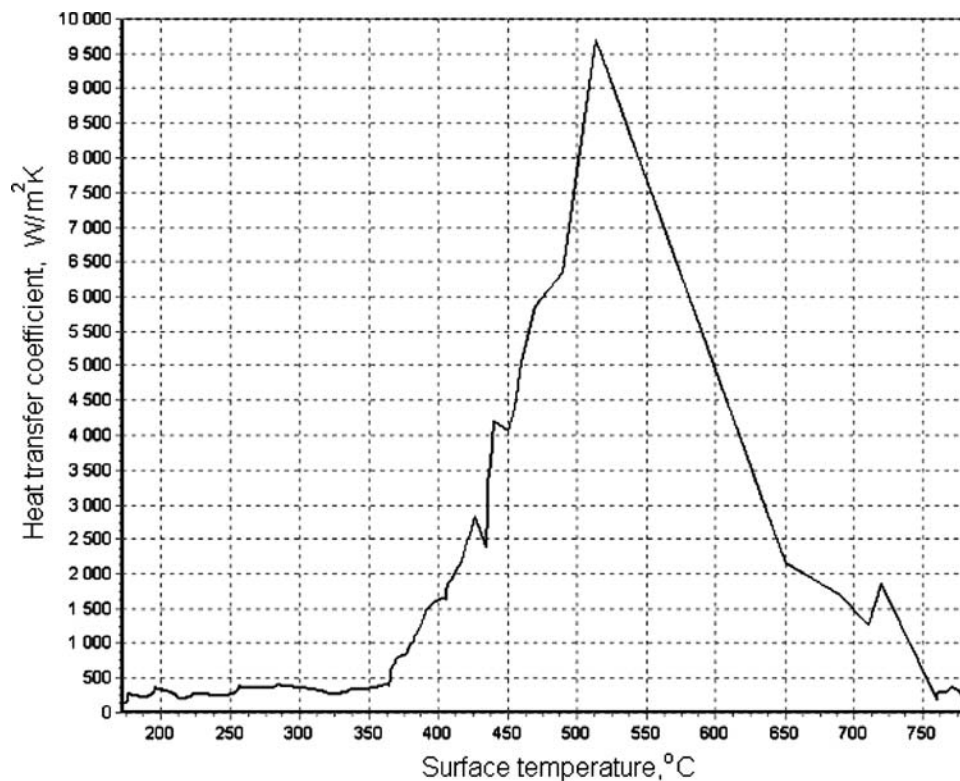
Fig. 13—Heat transfer coefficient versus surface temperature for MZM-16 oil at 100°C, with a cylindrical specimen of 19.9-mm diameter and 80-mm height.
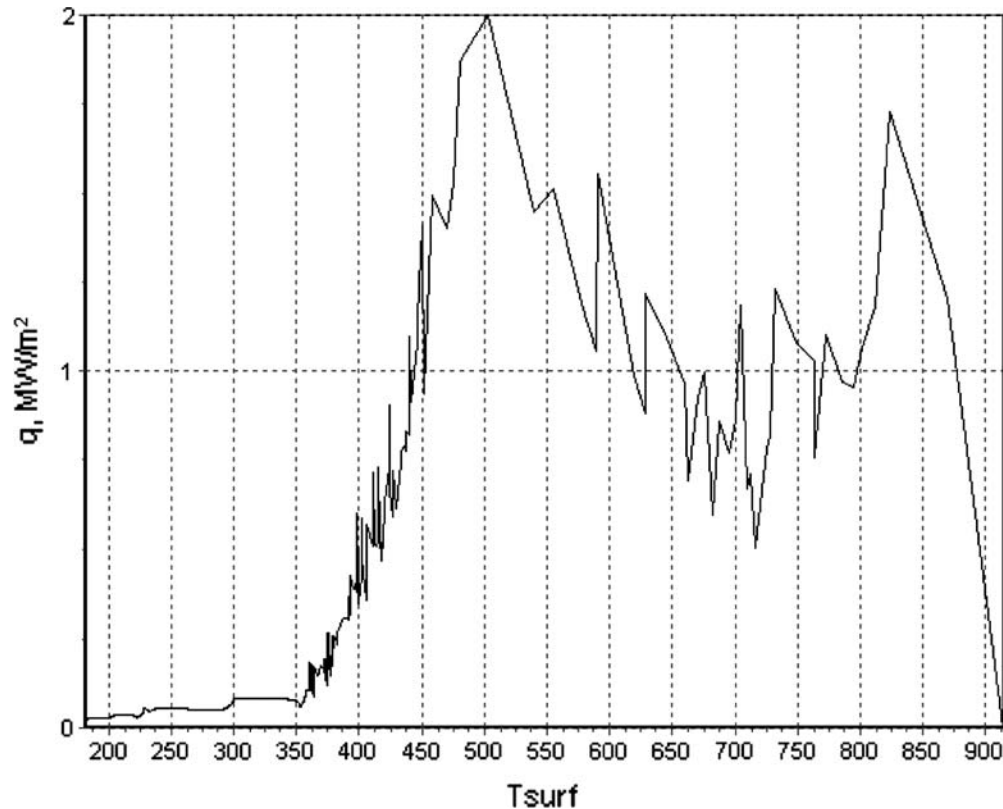
Fig. 14—Heat flux density versus surface temperature for MZM-16 oil at 170°C.

Thus, by solving the inverse heat conduction problem, the same conclusion was drawn that there is an optimal oil temperature where the cooling intensity is maximum and there is no film boiling. This cooling condition is optimal for minimizing the part distortion.

Let's now determine the potential of using average heat transfer coefficients instead of functions of the surface temperature as presented above. In Fig. 17, the heat transfer coefficient as a function of surface temperature and its average values within the boiling process and convection are shown. Within the boiling process, the heat transfer coefficient is 1,100 W/m²K, and during the convection heat transfer, it is approximately 250 W/m²K. The same is true for heat transfer coefficients presented in Figs. 12 and 15. Using the average heat transfer coefficients and taking into account physical properties of oil versus temperature (see
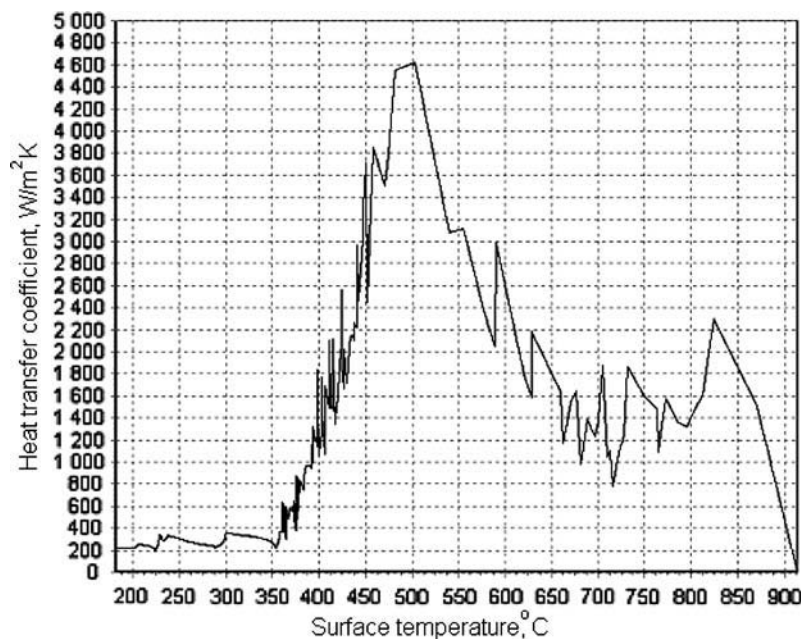
Fig. 15—Heat transfer coefficient versus surface temperature for MZM-16 oil at 170°C.
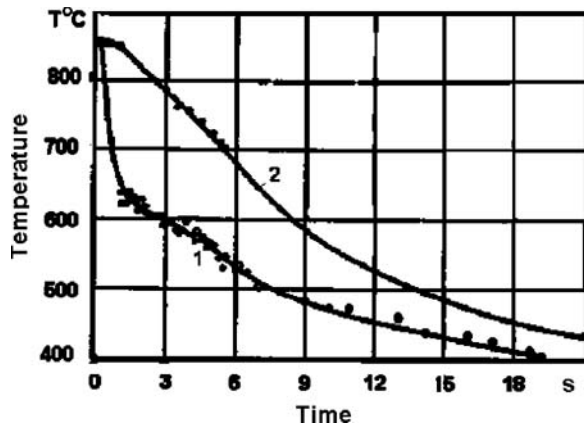
Fig. 16—Cooling curves for cylindrical specimens of 20-mm diameter quenched in MZM-16 oil at room temperature: 1, surface; 2, core.

Table 5), it is possible to calculate the duration of the cooling process during quenching. The results of such calculations, presented in Table 6, show that they are suitable for practical use.

13.8 VERIFICATION OF THE QUENCH PROCESS OF SEMI-AXLES AND CYLINDER-SHAPED STEEL PARTS ON THE BASIS OF CFD ANALYSIS

Recently, considerable attention has been paid to solving inverse problems and computational fluid dynamics (CFD) problems. Both approaches have been used for the analysis and verification of the quenching processes [33–38]. Having accurate experimental data and material thermal properties [39,40], it is possible to determine the boundary condition during quenching by solving the inverse heat conduction problem. CFD analysis provides the means to determine how smoothly the steel part is quenched and how to optimize the cooling fixtures [8]. However, the principal task for both approaches is the initial heat flux density evaluation. By comparing the initial heat flux density with the first critical heat flux, it is possible to predict the future heat transfer modes (these aspects were discussed in Chapter 3).

An important feature has been established: the existence of an optimal concentration of water-salt solutions where

Fig. 17—Temperature at the surface and at the core versus time for MZM-16 oil at 170°C, with a cylindrical specimen of 30-mm diameter and 120-mm height.

q_{cr1} is at a maximum, which provides intensive and smooth cooling of steel parts. In this case, the cooling time of the core of steel parts is evaluated by the generalized equation (Eq 69) presented in Chapter 5. The accuracy of the calculations is acceptable. That is also true when quenching steel parts in a water flow or by water jets. For example, calculation of the process of quenching semi-axles and cylindrical forgings in a water flow has been widely discussed [35–37].

Two approaches were analyzed. The traditional approach for the thermal state analysis during quenching was based on the Newton's boundary condition between the solid surface of the part and the fluid surrounding it. In the second approach, the problem involves the solving of a conjugate heat transfer problem (Navier-Stokes equations full set solution) with CFD computer technology. In this case, it is not necessary to know the heat transfer coefficients at the surface of the part.

Comparisons of both approaches and calculation results show that the generalized correlation can be used for the cooling time calculation. The results of calculations using both approaches agree very well with the experimental results. This means that the generalized equation (Eq 69) from Chapter 5 is suitable for calculations and development of intensive quenching technologies.

Along with verifying the generalized equation, the CFD analysis has allowed the detection of small stagnation zones. The presence of such stagnation zones may cause quench cracks and prevent superstrengthening of the material [8,37].

It has been shown that the initial heat flux density can be evaluated by solving the conjugate problem together with the CFD analysis [33,35,36]. The first critical heat flux density for the water flow in round channels can be calculated as follows:

$$q_{cr1}^{uh} = 2.8\left(0.75W^{0.5} - 1\right) + 0.1(W^{0.35} - 1)\vartheta_{uh}, \qquad (16)$$

where:
W is the water flow rate;
$\vartheta_{uh} = T_S - T_m$ is the underheating temperature;
T_S is the boiling (saturation) temperature; and
T_m is the bath temperature.
Some results of calculations of q_{cr1} for the water flow are presented in Table 7.

The initial heat flux density is evaluated at the moment of immersion of steel part into liquid. The initial heat flux densities for a cylindrical probe quenched in a water flow of 10 m/s, based on CFD simulations, are provided in Table 8 [33,36]. Consider the initial heat flux density at the moment of time when the boundary layer is heated to a saturation temperature and the temperature gradient is already established at the surface of the steel part (see Chapter 4).

Table 8 shows that the maximum initial heat flux density during quenching of the cylindrical test specimen in water flow of 10 m/s is 11.5 MW/m². At the same time, q_{cr1} is 13.74 MW/m² for water at 20° C and a water flow of 10 m/s. This means that, in this case, film boiling will be absent since the initial heat flux density is less than q_{cr1}. For intensive quenching, it is very important to eliminate film boiling in order to provide very high heat transfer during nucleate boiling and forced convection. The nucleate boiling mode is used when designing the IQ-2 process, and the direct forced convection mode of heat transfer is used when designing the IQ-3 process. Direct convection means that film and
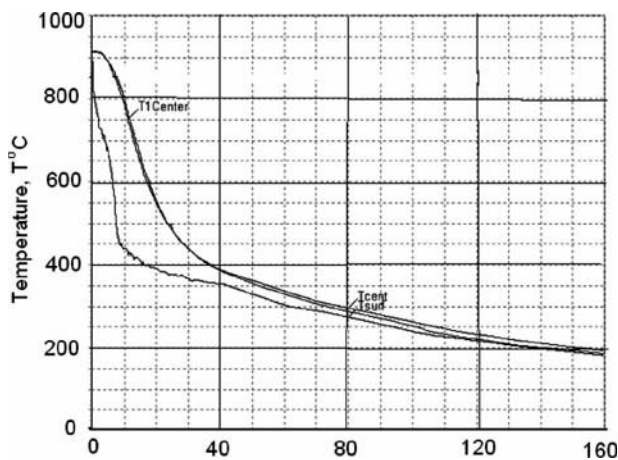
TABLE 5—Physical properties of MK oil versus temperature								
T (°C)	ρ (kg/m³)	c_p (kJ/kg·°C)	λ (W/m·°C)	$\mu \times 10^4$ (Pa·s)	$v \times 10^6$ (m²/s)	$a \times 10^6$ (m²/s)	$\beta \times 10^4$ (1/K)	Pr
10	911.0	1.645	0.1510	35,414	3,883	9.94	8.56	39,000
20	903.0	1.712	0.1485	18,560	1,514	9.58	8.64	15,800
30	894.5	1.758	0.1461	6,180	691.2	9.28	8.71	7,450
40	887.5	1.804	0.1437	3,031	342.0	89.7	87.9	3,810
50	879.0	1.851	0.1413	1,638	186.2	8.69	8.86	2,140
60	871.5	1.897	0.1389	961.4	110.6	8.39	8.95	1,320
70	864.0	1.943	0.1363	603.3	69.3	8.14	9.03	858
80	856.0	1.989	0.1340	399.3	46.6	7.89	9.12	591
90	848.2	2.035	0.1314	273.7	32.3	76.1	9.20	424
100	840.7	2.081	0.1290	202.1	24.0	7.33	9.28	327
110	838.0	2.127	0.1264	145.2	17.4	7.11	9.37	245
120	825.0	2.173	0.1240	110.4	13.4	6.92	9.46	193.5
130	817.0	2.219	0.1214	87.31	10.7	6.69	9.54	160.0
140	809.2	2.265	0.1188	70.34	8.70	6.53	9.65	133.3
150	801.6	2.311	0.1168	56.90	7.10	6.25	9.73	113.5

TABLE 6—Cooling time in seconds for cylindrical specimens of 19.9 and 30-mm diameter quenched in MZM-16 oil from 780°C to 375°C			
		Cooling time (s)	
Dia (mm)	Quenchant	Experiment	Calculation
19.9	Oil MZM-16; 61°C	20	19.5
	$\alpha = 1,800$ W/m²K		
19.9	Oil MZM-16; 100°C	15	15.7
	$\alpha = 2,600$ W/m²K		
30	Oil MZM-16; 170°C	45	47
	$\alpha = 1,100$ W/m²K		

TABLE 7—First critical heat flux density q_{cr1} (MW/m²) versus water temperature and water flow velocity W				
	Water temperature			
W (m/s)	20°C	30°C	40°C	60°C
5	7.94	7.18	6.43	4.91
6	9.32	8.44	7.57	5.83
7	10.57	9.59	8.62	6.66
8	11.70	10.63	9.56	7.42
9	12.76	11.60	10.44	8.13
10	13.74	12.51	11.27	8.79
15	17.97	16.39	14.81	11.65
20	21.40	19.56	17.71	14.00

nucleate boiling are absent and the primary heat transfer mechanism is forced convection.

A CFD analysis has been performed of the IQ-3 process for the cylindrical steel parts shown in Fig. 18 [36,37]. The objective of the CFD modeling was to determine the accuracy of the generalized equation from Chapter 5.

The system (the steel part and the fixture) consists of 16,000 cells [37]. The time step was 0.001 s. The cooling process has been calculated for 50 s. The water flow rate at the entrance of the quench fixture was 10 m/s. To simulate the heat transfer processes, the numerical method of the control volume was used. The study of heat transfer processes during quenching was performed on the basis of the numerical solution of the full system of Navier-Stokes equations determined by Reynolds and differential equations for the two-layer turbulence model [33,36,37]. The CFD technology is not yet able to simulate the nucleate and film boiling processes correctly. At the points where the process of nonstationary nucleate boiling is observed, a CFD simulation will give higher values for the part's surface temperature.

The temperature at the surface (points 1–7) and at the core (point 8) of the steel part versus time is shown in Fig. 19. At points 1, 4, and 7, stagnant areas were observed. At these localized areas, CFD modeling provides incorrect results, since it doesn't take into account nucleate and film boiling. However, the cooling time calculation for the core is correct, because the stagnant areas are very small compared with the entire steel part's surface area.

TABLE 8—Initial heat flux density at the edges and along a semi-axle of 42-mm diameter and 600-mm length (at time = 0.1 s) when cooling in a water flow of 10 m/s (results from CFD modeling [33])

Distance along the specimen (m)	Heat flux density (MW/m^2)
0 (edge)	11.5
0.1	10.14
0.2	10.11
0.3	10.07
0.4	9.95
0.5	9.77
0.6 (edge)	9.78

Fig. 18—Configuration of steel part (*top*) and cross-section (*bottom*) used for meshing and simulating the process of quenching in the flowing water.

To prove this conclusion, the cooling time was compared from the austenitizing temperature T_0 of 870°C to 500 °C at point 8. The Kondratjev form factor K is 171 × 10^{-6} m^2, the Kondratjev number Kn is 0.9 for a water flow 10 m/s, and the thermal diffusivity a is 5.36 × 10^{-6} m^2/s. Using these values, the cooling time, calculated by the generalized equation (Eq 69) from Chapter 5, is 37 s [36,37]:

$$t = \left(0.48 + \ln\left(\frac{870-20}{500-20}\right)\right)\frac{171\times10^{-6}m^2}{5.36\times10^{-6}m^2/s\times0.9} \approx 37s.$$

The cooling time in the same range obtained by CFD simulation was 38 s, which indicates that the impact of the stagnant areas on the cooling time calculation was not significant.

CFD modeling of the quenching process of truck semi-axles of 42-mm diameter made of 40G steel (AISI 1540) was also performed [29,30]. The axles were cooled in a flow of 20°C water from 860°C in a special quench chamber. The inner diameter of the chamber was 80 mm. Some calculation results for the water flow of 10 m/s are presented in Fig. 20.

The calculation results obtained using the generalized equation from Chapter 5 and CFD simulation coincide very well. This means that the generalized equation (Eq 69) from Chapter 5 is a suitable method for such calculations. As an example, the process of quenching of semi-axles is provided in Fig. 20 and Table 9.

The combination of CFD and finite element method (FEM) modeling techniques provides an effective method for the design of quenching processes and related fixtures [37,38]. The CFD simulations assumed that the boiling phenomena were short-lived and had no major impact on the resulting material properties, which is reasonable for high-velocity intensive quenching processes. The results show that the quenchant flow field can exhibit a significant effect on austenite decomposition, internal stress state, and distortion of the finished part. A combination of the Fluent CFD[2] and Dante[3] heat treatment models can be effectively used to develop quench fixtures and processes that have
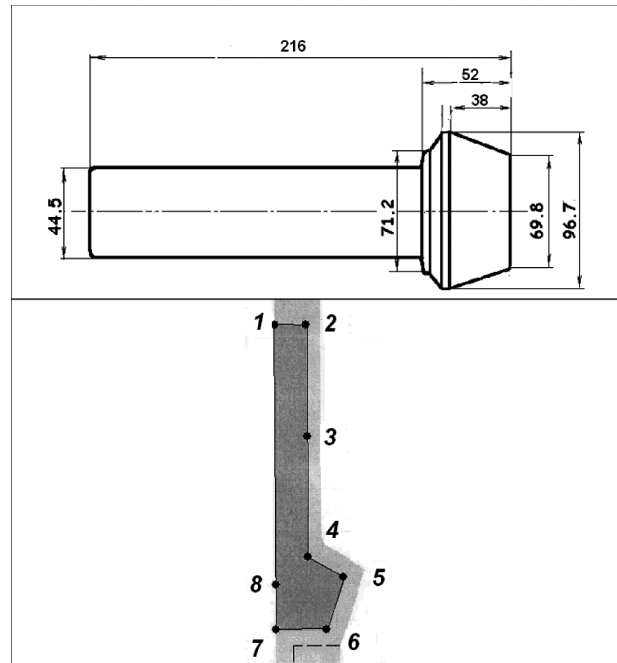
improved uniformity of heat transfer, more desirable residual stress levels, and reduced distortion [8,41]. Dante has been used to investigate quenching processes of complex steel parts such as carburized gears [41].

There is a need to improve CFD programs so that they will include equations governing the film and nucleate boiling processes and will use the values of critical heat flux densities. Without such improvements, it is impossible to perform calculations for nonstationary film and nucleate boiling processes. Furthermore, problems such as the stagnation of the water flow at concave locations of the part, causing a much lower cooling rate than the average [8], are not addressed. Conversely, cooling rates at the outer corners and edges can be much greater than the average which may cause cracking at these locations due to excessive thermal stresses.

As an example of the use of a static CFD analysis, in one published study [42], the oil velocity in a quench tank was predicted using Fluent software. The information was used to predict the cooling uniformity throughout the parts racked in the basket as well as the local cooling differences along the surface of a single part. The heat transfer coefficients were calculated using the quenchant flow velocities obtained from the above CFD model and were used as thermal boundary conditions [8,33,43].

13.9 GENERALIZED EQUATIONS FOR EVALUATION OF CONVEYOR SPEED

Equations for the calculation of the conveyor speed were discussed in Chapters 10 and 11. Here, a generalized

---

[2] Fluent CFD software is available from ANSYS, Inc.; see www.fluent.com/contact/index.htm.
[3] DANTE (Distortion Analysis for Thermal Engineering) is available for licensing from Deformation Control Technology, Inc., 7261 Engle Road, Suite 105, Cleveland, OH 44130; tel: 440-234-8477; fax: 440-234-9140; e-mail: sales@DeformationControl.com; Internet: www.deformationcontrol.com.
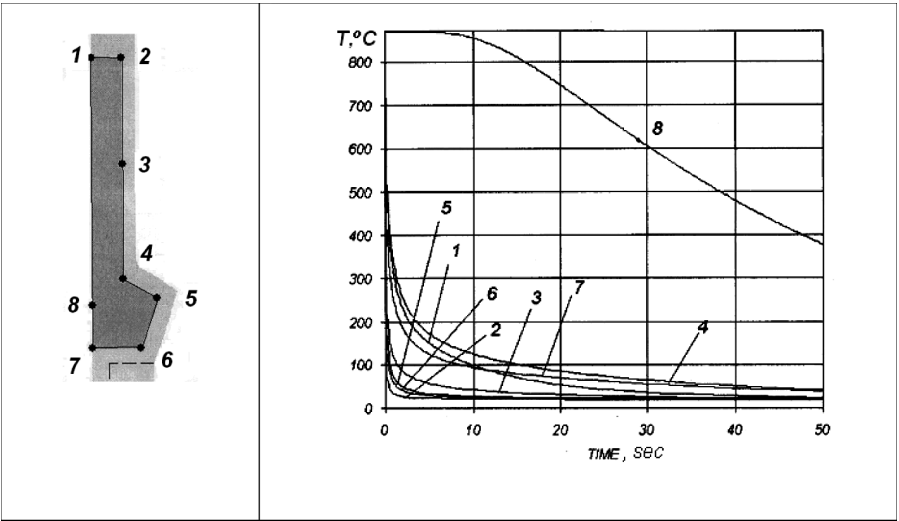
Fig. 19—Temperature versus time at the surface (points 1–7) and at the core (point 8) of forging when quenching in water flow in the fixture.

equation, which takes into account the duration of the nucleate boiling process, is introduced:

$$W = \frac{L}{\tau} = \frac{aL}{(\Omega + b \ln \theta)K}, \qquad (17)$$

where:

W is the conveyor speed;

L is the conveyor's length;

τ is the duration of the transient nucleate boiling process;

a is the thermal diffusivity of steel;

K is the Kondratjev form factor;

$b = 3.21$; and

$\Omega = 0.24k$ (where k = 1, 2, or 3 for plate-shaped, cylindrical, or spherical steel parts, respectively).

Eq 17 is used when quenching parts in water and water-salt solutions. The results can be used for designing a new two-step quenching technology. As the first step, steel parts are cooled in the water-salt solution of optimal concentration.

During the second step, washing and intensive cooling within the martensite range are performed. The cooling time for the first step is regulated by the conveyor speed. This is illustrated by the example below.

Example 13.5

Spheres made of AISI 52100 steel are quenched in water-salt solutions of optimal concentration from 860°C. The temperature of the water-salt solution is 20°C, and it boils at 105°C. For spheres of 50-mm diameter, determine the conveyor speed that provides delivery of the spheres at the end the nucleate boiling process. Assume that the conveyor length is 1.2 m. The average values of thermal conductivity λ and thermal diffusivity a are 22.5 W/mK and 5.3 $\times$ 10^{-6} m^2/s, respectively.

To perform the calculations, it necessary to know the value of

$$\ln \theta = \ln \frac{\vartheta_I}{\vartheta_{II}},$$

where (see Chapter 2):

$$\vartheta_I = \frac{1}{\beta} \left[\frac{2\lambda(\vartheta_0 - \vartheta_I)}{R} \right]^{0.3};$$

$$\vartheta_{II} = \frac{1}{\beta} [\alpha_{conv}(\vartheta_{II} + \vartheta_{uh})]^{0.3};$$

$$\beta = 7.36;$$
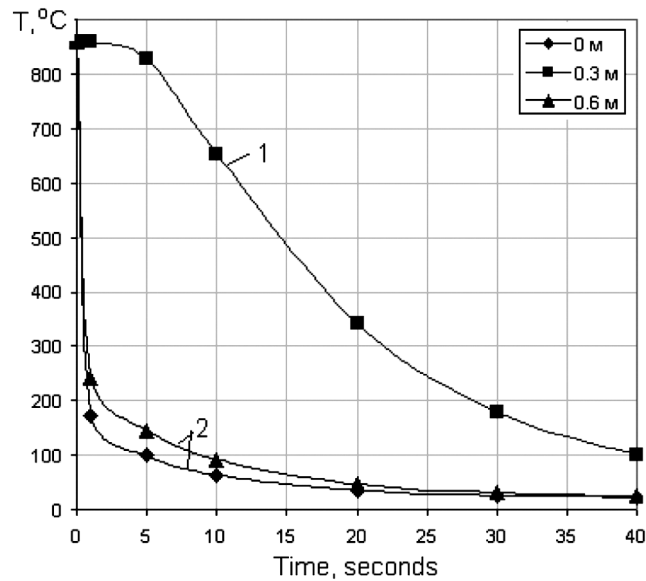
Fig. 20—Temperature versus time at different points of a semi-axle: 1, core; 2, surface at a distance of 0 and 0.6 m [33].

TABLE 9—Comparison of cooling time calculation from 860°C based on both CFD analysis and the generalized equation (Eq 69) of Chapter 5

Core temperature	Cooling time(s)		Error (%)	Av. Error (%)
	Calculated	CFD analysis		
500°C	14.6	14.8	1.4	—
400°C	18	17.7	1.7	3.6
300°C	23.7	22	7.7	—

λ is the thermal conductivity, with an average value of 22.5 W/mK;

$\vartheta_0 = T_0 - T_S$;

T_0 is the austenitizing temperature of 860°C;

T_S is the saturation temperature, 105°C;

T_m is the quenchant temperature;

R is the radius or half the thickness of the plate;

α_{conv} is the convective heat transfer coefficient in W/m²K;

$\vartheta_{uh} = T_S - T_m$;

ϑ_I is the temperature at the beginning of the nucleate boiling process; and

ϑ_{II} is the temperature at the end of the nucleate boiling process.

The results of calculations for Example 13.5 are presented in Table 10.

The following equation is used when quenching parts in oils (see Chapter 11):

$$W = \frac{L}{\tau} = \frac{aLKn}{(\Omega + \ln\theta)K}, \qquad (18)$$

where:

Kn is the Kondratjev number (a dimensionless value); and

$\ln\theta = \ln\dfrac{T_0 - T_m}{T - T_m}$.

The Kondratjev number Kn can be found by solving an inverse heat conduction problem with averaging of the results of calculations, as shown in Table 11 for oil depending on the size of specimens. More information on solving inverse problems is available in [1,2,26,27]. Average values of heat transfer coefficients can be also found experimentally by using ASTM standard probes [44].

TABLE 10—Cooling time and conveyor speed calculation results depending on the size of cylindrical specimens

Dia (mm)	ϑ_I (°C)	τ (s)	W (m/s)	W (m/h)
30	10.93	16.5	0.073	262
40	10	27	0.044	159.6
50	9.38	39.8	0.03	108.5

TABLE 11—Kondratjev number Kn for conventional oils calculated on the basis of experimental data obtained by different authors [45,46]

Cylinder dia (mm)	Malinkina and Lomakin [45]	Kobasko and Totten [46]	Kobasko and Dobryvechir	Average value of Kn
10.0–12.7	0.18	0.15	—	0.165
20–25	0.23	0.205	0.26	0.23
30	0.27	—	0.28	0.275
40	0.30	—	—	0.30
50	0.33	0.28	0.30	0.305
60	0.36	—	—	—

Table 11 shows that Kondratjev numbers during nucleate boiling change very slowly with the changing of the sample diameter. Using these characteristics, it is possible to perform simplified and rapid calculations with an accuracy acceptable for practical use.

Evaluation of Kondratjev numbers for different quenchants are presented in [31,46–48].

13.10 DISCUSSION

Initial heat flux densities and heat transfer coefficients are important parameters to predict the film boiling process, temperature, and residual stress distribution during computer simulation of the quenching processes. That is why it is necessary to create databases of cooling characteristics of quenchants that include critical heat flux densities and heat transfer coefficients. This can be done successfully by the use of computer programs such as IQLab [30].

For determination of critical heat flux densities, it is preferable to use silver cylindrical probes with rounded ends (see Chapter 3), because silver provides film boiling, which is necessary for determining these critical heat flux densities. For determination of heat transfer coefficients, on the other hand, it is preferable to use austenitic steel cylindrical probes (e.g., the Liscic-Nanmac probe of Fig. 1), because no structural transformations are observed during cooling (structural transformations considerably complicate the calculations and demand a knowledge of the thermal and physical properties of each structure).

It has been shown that CFD analysis allows the calculation of initial heat flux densities during immersion of steel parts into a quenchant. By comparison of the initial heat flux density with the first critical heat flux density q_{cr1}, it is possible to predict heat transfer modes: If the initial heat flux density is less than $qcr1$, then full film boiling will be absent; if it is higher than q_{cr1}, then full film boiling will be present. When these values are equal, transition boiling may be observed. This information is very important for engineers and designers. The calculations obtained on the basis of generalized equation and CFD modeling agree very well with the experimental data and with each other.

CFD simulation predicts stagnant areas, which may have an unfavorable effect on the distribution of current and residual stresses and may result in the quench crack formation due to a nonuniform martensite shell over the surface of the steel parts. A nonuniformity of the heat transfer at the part surface is connected with the nonuniform distribution of water flow rates and the appearance of stagnant zones. This information is also very important for engineers and designers. Unfortunately, there is no appropriate database for the cooling capacity of different kinds of quenchants. However, highly developed methods, theoretically and practically, are available now for evaluating boundary conditions on the basis of solving an inverse heat conduction problem and the use of CFD modeling. To start creating such a database for industries, a team of mathematicians, thermal scientists, material scientists, and other specialists has been established [49]. Standard probes for creating the database are needed, which can be developed by ASTM International.

13.11 SUMMARY

1. An overview of the existing methods for solving an inverse heat conduction problem has been provided.

2. Using IQLab software and accurate experiments, the cooling capacity of MZM-16 quench oil has been investigated. It was shown that the optimal temperature for MZM-16 oil is 100°C, which coincides very well with the results provided in Chapter 3.

3. Average heat transfer coefficients can be used for calculating the cooling rate, cooling time, and speed of conveyors during quenching of steel parts.

4. Average Kondratjev numbers Kn for oils change insignificantly with changing of the sizes of steel parts.

5. CFD analysis can predict the time and location where the film boiling first begins, or its absence, over the entire surface and can predict convective heat transfer coefficients.

6. There is no appropriate database for cooling capacities of quenchants to be used by industry.

7. There is a need to develop standard probes to be used for solving inverse heat conduction problems specifically for evaluating quenchants.

References

[1] Aster, R. C., Borchers, B., and Thurber, C. H., *Parameter Estimation and Inverse Problems,* Elsevier, Amsterdam, 2004.

[2] Chadan, K., and Sabatier, P. C., *Inverse Problems in Quantum Scattering Theory,* Springer-Verlag, New York, 1977.

[3] Wikipedia, Inverse Problems, http://en.wikipedia.org/wiki/inverse_problem.

[4] Kozdoba, L. A., and Krukovskyi, P. G., *Methods of Solving Inverse Heat Conduction Problems,* Naukova Dumka, Kyiv, 1982.

[5] Krukovskyi, P. G., *Inverse Heat and Mass Transfer Problems (General Engineering Approach)*, Engineering Thermal-Science Institute, Kyiv, 1998.

[6] Hernandez-Morales, B., Brimacombe, J. K., Hawbolt, E. B., and Gupta, S. M., Determination of Quench Heat-Transfer Coefficients Using Inverse Techniques, *Proceedings of Quenching and Distortion Control Conference,* ASM International, September 22–25, 1992, Chicago, pp. 155–164.

[7] Beck, J. V., and Osman, A. M., Analysis of Quenching and Heat Treating Processes Using Inverse Heat Transfer Method, *Proceedings of Quenching and Distortion Control Conference,* ASM International, September 22–25, 1992, Chicago, pp. 147–154.

[8] Banka, J. F., Li, Z., Ferguson, B. L., and Aronov, M., CFD and FEA Used to Improve the Quenching Process, *Heat Treating Progress,* 2008, pp. 50–56.

[9] Liščić, B., Heat Transfer Control During Quenching, *Materials and Manufacturing Processes,* Vol. 24, 2009, pp. 879–886.

[10] Vergana-Hernandez, H. J., and Hernandez-Morales, B., A Novel Probe Design to Study Wetting Kinematics During Forced Convective Quenching, *Experimental Thermal and Fluid Science,* Vol. 33, No. 5, 2009, pp. 797–807.

[11] Kobasko, N. I., Quenchants, *Metallovedenie i Termicheskaya Obrabotka,* Moscow, VINITI, 1989, pp. 127–166.

[12] Liščić, B., Tensi, H. M., and Luty, W., *Theory and Technology of Quenching,* Springer-Verlag, Berlin, 1992.

[13] Liščić, B., Tensi, H. M., Canale, L. C. F., and Totten, G. E., Eds., *Quenching Theory and Technology,* 2nd Ed., CRC Press, New York, 2010.

[14] Tikhonov, A. N., and Glasko, V. B., Application of Regularization Method in Non-Linear Problems, *Jour. of Comp. Math. and Math. Physics,* Vol. 5, No. 3, 1965, pp. 93–107.

[15] Tikhonov, A. N., and Glasko, V. B., On the Issue of Methods of Determination of the Part's Surface Temperature, *Jour. of Comp. Math. and Math. Physics,* 1967, Vol. 7, No. 4, pp. 910–914.

[16] Alifanov, O. M., Outer Inverse Heat Conduction Problems, *Eng. Phys. Jour.,* Vol. 29, No. 1, 1975, pp. 13–25.

[17] Turchin, V. F., Kozlov, V. P., and Malkevich, M. S., Use of Methods of Mathematical Statistics for Solving Incorrectly-Posed Problems, *Progress of Phys. Sc.,* Vol. 102, No. 3, 1970, pp. 345–386.

[18] Morozov, V. A., On Principle of Error Function at Solving Operation Equations by Regularization Method, *Jour. of Comp. Math. and Math. Physics,* Vol. 8, No. 2, 1968.

[19] Guseynov, Sh. E., Methods of the Solution of Some Linear and Nonlinear Mathematical Physics Inverse Problems, doctoral thesis, University of Latvia, Riga, 2003.

[20] Guseynov, Sh. E., Kobasko, N. I., Buikis, A. A., and Mamedov, A. G., Some Mathematical Models with Nonlinear Boundary Condition and Their Solutions for Intensive Quenching of Steels, *Applied Mathematics and Mathematical Physics (Computer Modeling and New Technology),* Vol. 10, No. 3, 2006, pp. 62–74.

[21] Guseynov, Sh. E., and Kobasko, N. I., On One Nonlinear Mathematical Model for Intensive Steel Quenching and Its Analytical Solution in Closed Form, *Proceedings of the 5th WSEAS International Conference on Heat and Mass Transfer (HMT '08),* Acapulco, Mexico, January 25–27, 2008, pp. 110–115.

[22] Guseynov, Sh. E., Rimshans, J. S., Kobasko, N. I., On One Nonlinear Mathematical Model for Intensive Steel Quenching Method and Its Analytical Solution in Closed Form, *Mathematics in Industry,* Vol. 15, Part 3, 2010, pp. 857–862.

[23] Krivoshey, F. A., Solving Inverse Heat Conduction Problems on the Basis of the Method of Statistical Regularization, doctoral thesis, ITTF of NASU, Kyiv, 1994.

[24] Kobasko, N. I., and Krivoshey, F. A., On the Mechanism of Temperature and Heat Flux Oscillations in Cooling Metallic Specimens in Aqueous Solutions of Polymers, *Reports of Academy of Ukraine (Doklady Akademii Nauk Ukrainy),* No. 11, 1994, pp. 90–94.

[25] Beck, J. V., Blackwell, B., and St. Clair Jr., C. R., *Inverse Heat Conduction: Ill-Posed Problems,* Wiley-Interscience, New York, 1985.

[26] Beck, J. V., Litkouhi, B., and St. Clair Jr., C. R., Efficient Solution of the Nonlinear Inverse Heat Conduction Problem, *Numerical Heat Transfer,* Vol. 5, 1982, pp. 275– 286.

[27] Meekisho, L., Hernández-Morales, B., Téllez-Martínez, J. S., and Chen, X., Computer-Aided Cooling Curve Analysis Using WinProbe, *Int. J. Materials and Product Technology,* Vol. 24, Nos. 1–4, 2005, pp. 155–169.

[28] Temkin, A. G., *Inverse Heat Conduction Problems,* Energiya, Moscow, 1973.

[29] Shumakov, N. V., *Method of Sequential Intervals in Heat Measurement of Non-stationary Processes,* Atomizdat, Moscow, 1979.

[30] Dobryvechir, V. V., Kobasko, N. I., Zotov, E. N., Morhuniuk, W. S., and Sergeyev, Yu. S., *Software IQLab* (commercially available from Intensive Technologies Ltd., Kyiv, Ukraine, iqlab@itl.kiev.ua, www.itl.kiev.ua).

[31] Kobasko, N. I., *Steel Quenching in Liquid Media Under Pressure,* Naukova Dumka, Kyiv, 1980.

[32] Totten, G. E., Bates, C. E., and Clinton, M. A., *Handbook of Quenchants and Quenching Technology,* ASM International, Materials Park, OH, 1993.

[33] Krukovskyi, P., Kobasko, N. I., and Polubinskiy, A., CFD Analysis of a Part Under Quenching as a Transfer Conjugate Problem, *IASME Transactions,* Vol. 2, No. 9, 2005, pp. 1723–1728.

[34] Krukovskyi, P., Kobasko, N. I., and Polubinskiy, A., The Process of Semi-axles Quenching Is Analyzed as Conjugate Heat Transfer Problem, *WSEAS Transactions on Heat and Mass Transfer,* Vol. 1, No. 4, 2006, pp. 563–566.

[35] Krukovskyi, P., Kobasko, N. I., and Yurchenko, D., Analysis of Heat Transfer Processes During Intensive Quenching of Cylinder-Shaped Forgings on the Basis of CFD Simulation, *Proceedings of the 2nd IASME/WSEAS International Conference on Continuum Mechanics (CM '07),* Portoroz, Slovenia, May 15–17, 2007, pp. 7–11.

[36] Kobasko, N. I., Krukovskyi, P., Yurchenko, D., Initial and Critical Heat Flux Densities Evaluated on the Basis of CFD Modeling and Experiments During Intensive Quenching, *Proceedings of the 5th IASME/WSEAS International Conference on Heat Transfer, Thermal Engineering and Environment,* Athens, Greece, August 25–27, 2007, pp. 295–298.

[37] Krukovskyi, P., Kobasko, N. I., and Yurchenko, D., Generalized Equation for Cooling Time Evaluation and Its Verification by CFD Analysis, *JAI,* Vol. 6, Issue 5, 2009, Paper ID JAI101760, epub ahead of print.

[38] Methodology STARCD, Version 3.15, Adapco Group, Computational Dynamics, Ltd., London, 2001.

[39] Chirkin, V. S., *Thermal and Physical Properties of Materials of Nuclear Equipment,* Atomizdat, Moscow, 1968.

[40] Bitkulov, I. Kh., Burkhanov, A. M., Kazantsev, V. A., et al., Effect of Severe Plastic Deformation on the Properties of the Fe−36% Ni Invar Alloy, *Physics of Metals and Metallography,* Vol. 102, No. 1, 2006, pp. 91−96.

[41] Ferguson, B. L., Freborg, A., and Li, Z., Residual Stress and Heat Treatment Process Design for Bending Fatigue Strength Improvement of Carburized Aerospace Gears, *5th International Conference on Heat Treatment: Quenching and Control of Distortion,* 2007, pp. 95−104.

[42] MacKenzie, D. S., Kumar, A., and Metwally, H., Optimizing Agitation and Quench Uniformity Using CFD, *Proceedings of the 23rd ASM Heat Treating Society Conference,* 2005, pp. 271−278.

[43] MacKenzie, D. S., Li, Z., and Ferguson, B. L., Effect of Quenchant Flow on the Distortion of Carburized Automotive Pinion Gears, *5th International Conference on Heat Treatment: Quenching and Control of Distortion,* 2007, pp. 119−129.

[44] ASTM Standard D6200-97: Standard Test Method for Determination of Cooling Characteristics of Quench Oils by Cooling Curve Analysis, *Annual Book of ASTM Standards,* ASTM International, West Conshohocken, PA, 2001.

[45] Malinkina, E. I., and Lomakin, V. N., *Hardenability of Steel,* Mashinostroyenie, Moscow, 1969.

[46] Kobasko, N. I., and Totten, G., Design of Technological Quench Processes and Possible Ways of Their Intensification, *New Processes of Heat Treating,* Neklyudov, I. M., and Shulayev, V. M., Eds., Kontrast, Kharkov, 2004, pp. 93−111.

[47] Kobasko, N. I., Self-Regulated Thermal Process at Steel Quenching, *Promyshlennaya Teplotekhnika,* Vol. 20, No. 5, 1998, pp 10−14.

[48] Kobasko, N. I., and Dobryvechir, V. V., Self-Regulated Thermal Process and Cooling Properties of the Quenchants, *IASME Transactions,* Vol. 2, No. 9, 2005, pp. 1825−1828.

[49] Kobasko, N. I., Database for Cooling Capacities of Various Quenchants to Be Developed with the Modern Computational and Experimental Techniques, 2006, www.worldses.org/projects/Heat_and_Mass_Transfer.doc.

Nikolai I. Kobasko, PhD, FASM

Dr. Kobasko received his Ph.D. from the National Academy of Sciences of Ukraine. He is a leading expert on quenching and heat transfer during the hardening of steels. He was the Head of the laboratory of the Thermal Science Institute of the National Academy of Sciences of Ukraine. He is Director of Technology and Research and Development for IQ Technologies, Inc., Akron, Ohio and President of Intensive Technologies, Ltd, Kyiv, Ukraine. The aim of both companies is material savings, ecological problem-solving, and increasing service life of steel parts. He is an ASM International Fellow (FASM).

Dr. Kobasko is the author and co-author of more than 250 scientific and technical papers, several books and more than 30 patents and certificates. He received the Da Vinci Diamond Award and Certificate in recognition of an outstanding contribution to thermal science. Dr. Nikolai Kobasko was Editor-in-Chief and Co-Editor of the WSEAS Transactions on Heat and Mass Transfer; and is currently a member of the Editorial Board for the International Journal of Mechanics (NAUN) and the Journal of ASTM International (JAI).

Dr. Michael A. Aronov

Dr. Aronov received his B. S. and Masters degrees in Thermal Science and Fluid Dynamics from the St. Petersburg Polytechnic Institute in Russia. Dr. Aronov received his Ph.D. degree in Thermal Science and Engineering from the Institute of Metallurgical Thermal Engineering also in Russia. He is the Chief Executive Officer of IQ Technologies, Inc. of Akron, Ohio.

Dr. Aronov has 37 years of experience in the field of heat and mass transfer, combustion, and thermodynamics in industrial, commercial, and residential heat transfer systems. He has extensive experience in experimental research, mathematical modeling of heat and mass transfer in combustion forging, and heat treating furnaces and quenching machinery. Dr. Aronov also has extensive experience in the design and development of heating and cooling systems for forging and heat-treating applications. Dr. Aronov has published more than 70 technical papers and has ten patents, four of which are related to different types of quenching equipment and technology.

Joseph A. Powell

Joseph A. Powell received his B.S. in Industrial Management from the University of Akron, and was granted a Juris Doctorate from the University of Akron School of Law. Mr. Powell is President, and a principal of IQ Technologies Inc, and of Akron Steel Treating Company (AST), a family business, in Akron, Ohio.

Mr. Powell is a founding member of the Heat Treating Network part of the Metal Treating Institute, a member of the Akron Chapter of ASM, the ASM/Heat Treating Society, and the ASM Quenching and Cooling Committee. He is also a member of the Metal Treating Institute (MTI), an associate member of the National Tooling & Machining Association (NTMA), and the Summit County Machine Shop Group.

Mr. Powell has a patent for "Variable Cooling Rate Quench Media, Cooling Rate Monitoring System and Real Time Computerized Control System for the Quenching of Metals during Heat Treatment or other Controlled Cooling or Solidification Operations."

George E. Totten, Ph.D., FASM

George E. Totten received his B.S. and Masters degrees from Fairleigh Dickinson University in New Jersey and his Ph.D. from New York University. Dr. Totten is past president of the International Federation for Heat Treating and Surface Engineering (IFHTSE) and a fellow of ASM International, SAE International, IFHTSE, and ASTM International. Dr. Totten is a Visiting Research Professor at Portland State University, Portland, Oregon, and he is also president of G.E. Totten and Associates LLC, a research and consulting firm specializing in thermal processing and industrial lubrication problems.

Dr. Totten is the author, coauthor, or editor of over 500 publications, including patents, technical papers, book chapters, and books and sits on several journal editorial boards, including the Journal of ASTM International.

INDEX

Note: Page numbers followed by "*f*" and "*t*" denote figures and tables, respectively.

Index Terms	Links	

This page has been reformatted by Knovel to provide easier navigation.